

Flight Dynamics Principles

A Linear Systems Approach to Aircraft Stability and Control

Flight Dynamics Principles

A Linear Systems Approach to Aircraft Stability and Control

Third Edition

Michael V. Cook BSc, MSc, CEng, FRAeS, CMath, FIMA



AMSTERDAM • BOSTON • HEIDELBERG • LONDON
NEW YORK • OXFORD • PARIS • SAN DIEGO
SAN FRANCISCO • SINGAPORE • SYDNEY • TOKYO

Butterworth-Heinemann is an imprint of Elsevier



Butterworth-Heinemann is an imprint of Elsevier
225 Wyman Street, Waltham, MA 02451, USA
The Boulevard, Langford Lane, Kidlington, Oxford, OX5 1GB, UK

First Edition 1997
Second Edition 2007
Third Edition 2013

Copyright © 2013, 2007 Michael V. Cook. Published by Elsevier Ltd. All rights reserved.

No part of this publication may be reproduced or transmitted in any form or by any means, electronic or mechanical, including photocopying, recording, or any information storage and retrieval system, without permission in writing from the publisher. Details on how to seek permission, further information about the Publisher's permissions policies and our arrangements with organizations such as the Copyright Clearance Center and the Copyright Licensing Agency, can be found at our website: www.elsevier.com/permissions.

This book and the individual contributions contained in it are protected under copyright by the Publisher (other than as may be noted herein).

Notices

Knowledge and best practice in this field are constantly changing. As new research and experience broaden our understanding, changes in research methods, professional practices, or medical treatment may become necessary.

Practitioners and researchers must always rely on their own experience and knowledge in evaluating and using any information, methods, compounds, or experiments described herein. In using such information or methods they should be mindful of their own safety and the safety of others, including parties for whom they have a professional responsibility.

To the fullest extent of the law, neither the Publisher nor the authors, contributors, or editors, assume any liability for any injury and/or damage to persons or property as a matter of products liability, negligence or otherwise, or from any use or operation of any methods, products, instructions, or ideas contained in the material herein.

Library of Congress Cataloging-in-Publication Data

Cook, M. V.

Flight dynamics principles: a linear systems approach to aircraft stability and control / Mike Cook. — 3rd ed.

p. cm.

Includes bibliographical references.

ISBN 978-0-08-098242-7

1. Aerodynamics. I. Title.

TL570.C617 2013

629.132'3—dc23

2012021575

British Library Cataloguing-in-Publication Data

A catalogue record for this book is available from the British Library

For information on all Butterworth-Heinemann publications
visit our website at <http://store.elsevier.com>

Printed in the United States of America

13 14 15 16 17 10 9 8 7 6 5 4 3 2 1

Working together to grow
libraries in developing countries

www.elsevier.com | www.bookaid.org | www.sabre.org

ELSEVIER

BOOK AID
International

Sabre Foundation

Preface

It seems that, in the five years since its publication, the second edition of *Flight Dynamics Principles* has continued to enjoy modest success in the undergraduate marketplace, and there is some limited evidence of its increasing adoption by university courses in North America. So it was not surprising that Elsevier proposed a third edition with the principal objective of enhancing the book's appeal to the American undergraduate market. Central to the objective is the requirement to achieve direct compatibility with American math notation and to link the embedded computational examples with the use of MATLAB or equivalent software tools. In coming to a conclusion about how the book might be developed, Elsevier conducted a review with a fair few universities where relevant courses are taught. Needless to say, every reviewer had a different subjective opinion on the content, structure, and presentation of a text on flight dynamics. However, in general most of the reviews were positive and provided helpful suggestions as to how a third edition might be developed. All of the reviews were carefully analysed, and common areas for attention were identified.

Analysis of the reviews revealed a number of areas for potential improvement, including the substantial addition of new material, the development of existing material, greater emphasis on American notation, and explicit use of MATLAB examples. The most commonly requested addition was more on design of flight control systems. This is a very large subject area indeed, much of which falls outside the scope and intent of this book with the exception of stability augmentation, which has been included from the outset. However, in deference to the requests new material on command augmentation has been added. Some reviewers expressed dissatisfaction with the treatment of some topics in the second edition, and it was agreed that these could be improved. Accordingly, the topics in question have been reorganised and further developed; also, in some instances additional worked examples have been introduced to further enhance the material. The question of the differences between British and American math notations remains a distinguishing feature of all publications on flight dynamics intended for global consumption. Sections explaining the parallel development of the equivalent American notation were introduced in considerable detail in the second edition, and this remains more or less unchanged. Improvements to raise the emphasis, including additional worked examples, have been added where appropriate.

The inclusion of MATLAB examples showing command line entries or passages of programme code have been strenuously avoided. The reason for this is that software tools evolve rather more rapidly than books; in the author's experience most students come to the subject already proficient in the use of MATLAB, and equally capable alternative software tools are available and in use. At least one of the reviewers endorsed this opinion. The solution to this is to set out worked examples in sufficient detail, and in a step-by-step fashion, sufficient to enable direct transfer to the MATLAB environment or to any other similar software environment.

The most important changes introduced in the third edition are summarised as follows. The chapter on longitudinal and lateral-directional static stability has been completely overhauled and revised, mainly to enhance the presentation of the material on lateral-directional static stability. Worked examples have been added to the material on the development of the equations of motion to illustrate the application of American notation. The chapter on manoeuvrability has been

expanded to include new material and worked examples on calculation of the manoeuvring control characteristics of aircraft with stability augmentation. The chapter on design of stability augmentation systems has been expanded to include new material and examples on the design of command augmentation systems for the enhancement of handling qualities. The chapter on aerodynamic stability and control derivatives has been expanded to include a substantial worked example to illustrate estimation of real aircraft derivative data. Chapter 14 is an entirely new chapter that summarises the effect of flight in a nonsteady atmosphere, and is based on the application and interpretation of British and American military flying qualities requirements documents. Finally, a new coursework example is added to Chapter 15 which involves the design of a basic flight control system architecture for an unmanned air vehicle of unconventional layout.

It is proposed that purchasers of this third edition of *Flight Dynamics Principles* will be able to download a computer programme called FDA-CAD, “Flight Dynamics Analysis—Control Augmentation Design,” from the Elsevier website in due course. This is a MATLAB programme developed over a number of years for use by the author’s students. Simple to use, it is based on a graphical user interface and is capable of undertaking all computations and transformations associated with the equations of motion, solution of the equations of motion, control-response plotting, design of simple feedback loops for stability augmentation, and design of command path augmentation for handling qualities enhancement. It is hoped that this software will be available soon after this edition has been launched. Please visit booksite.elsevier.com/9780080982427 for access to the companion software. For instructors using the text as part of their course, additional instructor support material is available by registering at www.textbooks.elsevier.com.

As for the book’s previous editions, it is appropriate to reiterate that *Flight Dynamics Principles* is introductory in its scope and is intended for those coming to the subject for the first time. The intended audience remains unchanged and includes undergraduate and postgraduate students studying aeronautical subjects, avionics, systems engineering, control engineering, mathematics, and so forth. It is also appropriate to include young engineers working in the aerospace industry who are involved in flight dynamics, flight control, and related activities. Most important, in an increasingly automated world the principal objective of the book remains to provide a secure foundation from which to move on to nonlinear flight dynamics, simulation, and advanced flight control system design.

Michael V. Cook
Frinton-on-Sea, Essex
June 2012

Preface to the second edition

It is almost exactly ten years since *Flight Dynamics Principles* was first published, and during that time there has been a modest but steady demand for it. It is apparent that during this period there has been a growing recognition in academic circles that it is more appropriate to teach “aircraft stability and control” in a systems context rather than in the traditional aerodynamic context—a view which is endorsed by industry. This is no doubt due to the considerable increase in application of automatic flight control to all types of aircraft and to the ready availability of excellent computer tools for handling the otherwise complex calculations. Thus the relevance of the book is justified, and this has been supported by positive feedback from readers all over the world.

The publisher was clearly of the same opinion, and a second edition was proposed. It was evident that the first edition had become required reading for many undergraduate courses, but that its original structure was not ideal for the teaching environment. In particular, the lack of examples for students to work was regarded as an omission too far. Consequently, the primary aim of the second edition is to support more generally the requirement of the average undergraduate course, and so it is hoped that it will appeal more widely to students undertaking courses in aeronautical engineering and aeronautical systems engineering at all levels.

The original concept for the book seems to have worked well, so the changes are few. Readers familiar with the book will be aware of rather too many minor errors in the first edition, arising mainly from editing problems in the production process. These have been purged from the second edition, and it is hoped that not so many new errors have been introduced. Apart from editing here and there, the most obvious additions are a versatile computer programme for calculating aircraft trim, introduction of material dealing with the interchangeability of North American notation, new material on lateral-directional control derivatives, and examples for students at the end of most chapters. Once again, the planned chapter on atmospheric disturbance modelling has been omitted because of time constraints. However, an entirely new chapter on coursework studies for students has been added.

It is the opinion of the author that, at the postgraduate level in particular, the assessment of students by means of written examinations tends to trivialise the subject by reducing problems to exercises which can be solved in a few minutes—the real world is not often like that. Consequently, traditional examining was abandoned sometime ago in favour of more realistic, and hence protracted, coursework studies. Each exercise is carefully structured to take the student step by step through the solution of an expansive flight dynamics problem, usually based on real aircraft data. Thus, instead of the short sharp memory test, student assessment becomes an extension and consolidation of the learning process, and equips students with the essential enabling skills appreciated by industry. Feedback from students is generally very positive and it appears that they genuinely enjoy a realistic challenge.

For those who are examined by traditional methods, examples are included at the end of most chapters. These are taken from earlier Cranfield University exam papers set by the author and from more recent exam papers set and kindly provided by Dr Peter Render of Loughborough University. The reader should not assume that chapters without such examples are not examinable. Ready-made questions were simply not available in the very tight time scale applying.

In the last ten years there has been an explosive growth in unmanned air vehicle (UAV) technology, and vehicles of every type, size, and configuration have made headlines on a regular basis. At the simplest level of involvement, many university courses now focus on experimental flight dynamics based on low-cost radio-controlled model technology. The theoretical principles governing the flight dynamics of such vehicles remains unchanged and the content of this book is equally applicable to all UAVs. The only irrelevant material is that concerning piloted aircraft handling qualities since UAVs are, by definition, pilotless. However, the flying qualities of UAVs are just as important as they are for piloted aircraft; although envelope boundaries may not be quite the same, they will be equally demanding. Thus the theory, tools, and techniques described in this book may be applied without modification for analysing the linear flight dynamics of UAVs.

The intended audience for *Flight Dynamics Principles* remains unchanged—that is, undergraduate and postgraduate students studying aeronautical subjects and those students studying avionics, systems engineering, control engineering, mathematics, and the like, with aeronautical application in mind. In view of the take-up by the aerospace industry, it is perhaps appropriate to add young engineers involved in flight dynamics and flight control to the potential readership. It is also appropriate to reiterate that the book is introductory in its scope and is intended for those coming to the subject for the first time. Most important, in an increasingly automated world the principal objective of the book remains to provide a secure foundation from which to move on to nonlinear flight dynamics, simulation, and advanced flight control.

Michael V. Cook
School of Engineering, Cranfield University
May 2007

Preface to the first edition

When I joined the staff of the College of Aeronautics some years ago, I was presented with a well-worn collection of lecture notes and invited to teach a course on aircraft stability and control to postgraduate students. Inspection of the notes revealed the unmistakable signs that their roots reached back to the work of W. J. Duncan, which is perhaps not surprising since Duncan was the first professor of aerodynamics at Cranfield some 50 years ago. It was undoubtedly a privilege and, at first, very daunting to be given the opportunity to follow in the footsteps of such a distinguished academic. From that humble beginning my interpretation of the subject has continuously evolved to its present form, which has provided the basis for this book.

The classical linearised theory of the stability and control of aircraft is timeless, it is brilliant in its relative simplicity, and it is very securely anchored in the domain of the aerodynamicist. What is new? The short answer is, not a great deal. However, today the material is used and applied in ways that have changed considerably, largely because of the advent of the digital computer. The computer is used as the principal tool for analysis and design, and it is also the essential component of the modern flight control system on which all advanced-technology aeroplanes depend. It is the latter development in particular which has had, and continues to have, a major influence on the way in which the material of the subject is now used. It is no longer possible to guarantee good flying and handling qualities simply by tailoring the stability and control characteristics of an advanced-technology aeroplane through aerodynamic design alone. Flight control systems now play an equally important part in determining the flying and handling qualities of an aeroplane by augmenting the stability and control characteristics of the airframe in a beneficial way. Therefore, the subject has had to evolve in order to facilitate integration with flight control, and today the integrated subject is much broader in scope and is more frequently referred to as *flight dynamics*.

The treatment of the material in this book reflects my personal experience of using, applying, and teaching it over a period of many years. My formative experience was gained as a systems engineer in the avionics industry, where the emphasis was on the design of flight control systems. In more recent years, in addition to teaching a formal course in the subject, I have been privileged to have spent many hours teaching the classical material in the College of Aeronautics airborne laboratory aircraft. This experience has enabled me to develop the material from the classical treatment introduced by Duncan in the earliest days of the College of Aeronautics to the present treatment, which is biased towards modern systems applications. However, the vitally important aerodynamic origins of the material remain clear, for which I can take no credit.

Modern flight dynamics tends to be concerned with the wider issues of flying and handling qualities rather than with the traditional, and more limited, issues of stability and control. The former is, of course, largely shaped by the latter, and for this reason the emphasis is on dynamics and their importance to flying and handling qualities. The material is developed using dimensional or normalised dimensional forms of the aircraft equations of motion only. These formulations are in common use, with minor differences, on both sides of the North Atlantic. Understanding of the dimensionless equations of motion has too often been a major stumbling block for many students, and I have never found it necessary, or even preferable, to work with the classical dimensionless equations of motion. These are a creation of the aerodynamicist and are referred to only insofar as

is necessary to explain the origins and interpretation of the dimensionless aerodynamic stability and control derivatives. However, it remains most appropriate to use dimensionless derivatives to describe the aerodynamic properties of an airframe.

It is essential that the modern flight dynamicist have not only a thorough understanding of the classical theory of aircraft stability and control but also some knowledge of the role and structure of flight control systems. Consequently, a basic understanding of the theory of control systems is necessary, and then it becomes obvious that the aircraft may be treated as a *system* that may be manipulated and analysed using the tools of the control engineer. As a result, it is common to find control engineers looking to modern aircraft as an interesting challenge for the application of their skills. Unfortunately, it is also too common to find control engineers who have little or no understanding of the dynamics of their *plant*, which, in my opinion, is unacceptable. It has been my intention to address this problem by developing the classical theory of the stability and control of aircraft in a systems context in order that it become equally accessible to both the aeronautical engineer and the control engineer. This book, then, is an aeronautical text which borrows from the control engineer rather than a control text which borrows from the aeronautical engineer.

Flight Dynamics Principles is primarily intended for undergraduate and postgraduate students studying aeronautical subjects and those studying avionics, systems engineering, control engineering, mathematics, and so forth, who wish to include some flight dynamics in their studies. Of necessity the book's scope is limited to linearised small-perturbation aircraft models since the material is intended for those coming to the subject for the first time. However, a good understanding of the material should give the reader the basic skills and confidence to analyse and evaluate aircraft flying qualities and to initiate preliminary augmentation system design. It should also provide a secure foundation from which to move on to nonlinear flight dynamics, simulation, and advanced flight control.

Michael V. Cook
College of Aeronautics, Cranfield University
January 1997

Acknowledgements

Over the years I have been fortunate to have worked with a number of very able people from whom I have learned a great deal. My own understanding and interpretation of the subject of flight dynamics has benefited enormously from that contact, and it is appropriate to acknowledge the contributions of these individuals.

My own formal education was founded on the text by W.J. Duncan and later on the first text by A. W. Babister. As a result, the structure of the third edition of *Flight Dynamics Principles* has many similarities to those earlier texts. This, I think, is inevitable because the treatment and presentation of the subject have not really been bettered in the intervening years, although the way in which the material is handled today is significantly different.

During my formative years at GEC-Marconi Avionics Ltd (now BAE Systems), I worked with David Sweeting, John Corney, and Richard Smith on various flight control system design projects. This activity also brought me into contact with Brian Gee, John Gibson, and Arthur Barnes at British Aerospace (Military Aircraft Division), all of whom are now retired. Of the many people with whom I worked, these individuals in particular were, in some way, instrumental in helping me to develop a greater understanding of flight dynamics in its widest modern context.

During my early years at Cranfield, my colleagues Angus Boyd, Harry Ratcliffe, Dr Peter Christopher, and Dr Martin Eshelby were especially helpful with advice and guidance at a time when I was establishing my teaching activities. I also consider myself extremely fortunate to have spent hundreds of hours flying with a small but distinguished group of test pilots—Angus McVitie, Ron Wingrove, and Roger Bailey—as we endeavoured to teach and demonstrate the rudiments of flight mechanics to generations of students. My involvement with the experimental flying programme was an invaluable experience which has enhanced my understanding of the subtleties of aircraft behaviour considerably. Later, the development of the postgraduate course in flight dynamics brought me into contact with colleagues Peter Thomasson, Jim Lipscombe, John Lewis, and Dr Sandra Fairs, with all of whom it was a delight to work. Their cooperative interest, and indeed their forbearance during the long preparation of the first edition of this book, provided much appreciated encouragement. In particular, the knowledgeable advice and guidance so freely given by Jim Lipscombe and Peter Thomasson, both now retired, is gratefully acknowledged as it was certainly influential in my development of the material. On a practical note, I am indebted to Chris Daggett, who obtained for me the experimental flight data which has been used to illustrate the examples based on the College of Aeronautics Jetstream aircraft.

After the publication of the first edition of *Flight Dynamics Principles*, a steady stream of constructive comments was received from a very wide audience and all of these were noted in the preparation of the second edition. However, a number of individuals were especially supportive, including Dr David Birdsall of Bristol University, who wrote a very complimentary review shortly after publication; Dr Peter Render of Loughborough University, an enthusiastic user of the book who very kindly provided a selection of his past examination papers for inclusion in the second edition; and my good friend Chris Fielding of BAE Systems, who was particularly helpful by providing continuous industrial liaison and by helping to focus the second edition on industrial applications. I am also most grateful to Dr Stephen Carnduff, also of BAE Systems, who provided

considerable help at the last minute by preparing the solutions manual for the end-of-chapter problems.

In the preparation of the third edition, I am once again indebted to my colleagues at Cranfield, Dr James Whidborne and Dr Alastair Cooke, and to my retired colleague and friend Peter Thomasson, for the opportunity to discuss ideas for development with them and for their helpful comments and suggestions. Once again, I am also especially indebted to my friend and colleague Chris Fielding, recently retired from BAE Systems, for his continuing total support for the book and for his considerable help in developing the new Chapter 14 to better reflect industrial practice.

I am very pleased that Elsevier agreed to retain the second edition front cover photograph for the third edition. I remain indebted to BAE Systems, which kindly provided the photograph, and especially to communications manager Andy Bunce, who arranged permission for it to be reproduced. The splendid photograph shows a Eurofighter Typhoon IPA1, captured by Ray Troll, photographic services manager, just after take-off from Warton for its first flight in the production colour scheme.

The numerous bright young people who have been my students have unwittingly contributed to the material content of *Flight Dynamics Principles* by providing all important “customer feedback”. Since my students represent a large part of the audience to which the work is directed, it is fitting that what has probably been the most important contribution to its continuing development be gratefully acknowledged.

Finally, I am indebted to Joe Hayton of Elsevier, whose belief in the future potential of the book as an undergraduate text convinced me that the time was right for a third edition. I am also grateful to Fiona Geraghty, Heather Tighe, and their colleagues at Elsevier for their help in the production process, and for maintaining the gentle pressure to ensure that I delivered on time.

To the above mentioned I am extremely grateful and to all of them I extend my most sincere thanks.

Elsevier would like to thank the reviewers who contributed to this publication by reviewing the manuscript and/or providing input on the revision plan. They were:

Subodh Bhandari, California State Polytechnic University, Pomona
Riccardo Bonazza, University of Wisconsin
John Cochran, Auburn University
Antonio Filippone, University of Manchester
Jonathan Rogers, Texas A&M University
Rick Lind, University of Florida
Ping Liu, Iowa State University
Kenneth Mease, University of California, Irvine
Praveen Shankar, California State University, Long Beach
Cornel Sultan, Virginia Polytechnic Institute
Douglas Thompson, University of Glasgow
John Valesek, Texas A&M University
Thomas Zeiler, University of Alabama

Nomenclature

Of the very large number of symbols required by the subject, many have more than one meaning. Usually the meaning is clear from the context in which the symbol is used.

a	Wing or wing-body lift curve slope: Acceleration: Local speed of sound
a'	Inertial or absolute acceleration
a_0	Speed of sound at sea level: Tailplane zero-incidence lift coefficient
a_1	Tailplane lift curve slope
a_{1_f}	Canard foreplane lift curve slope
a_{1_F}	Fin lift curve slope
a_2	Elevator lift curve slope
a_{2_A}	Aileron lift curve slope
a_{2_R}	Rudder lift curve slope
a_3	Elevator tab lift curve slope
a_∞	Lift curve slope of infinite-span wing
a_h	Local lift curve slope at coordinate h
a_y	Local lift curve slope at spanwise coordinate y
$a_{z_{cg}}$	Normal acceleration at the cg
a_{z_p}	Normal acceleration at the pilot
ac	Aerodynamic centre
A	Aspect ratio
A_F	Effective aspect ratio of fin
A_T	Effective aspect ratio of tailplane
A	State matrix
b	Wing span
b_1	Elevator hinge moment derivative with respect to α_T
b_2	Elevator hinge moment derivative with respect to η
b_3	Elevator hinge moment derivative with respect to β_η
b_T	Tailplane span
B	Input matrix
c	Chord: Viscous damping coefficient: Command input
\bar{c}	Standard mean chord (<i>smc</i>)
$\overline{\bar{c}}$	Mean aerodynamic chord (<i>mac</i>)
$\overline{\bar{c}}_\eta$	Mean elevator chord aft of hinge line
c_h	Local chord at coordinate h
c_r	Root chord

c_t	Tip chord
c_y	Local chord at spanwise coordinate y
cg	Centre of gravity
cp	Centre of pressure
C	Command path transfer function
\mathbf{C}	Output matrix
C_D	Drag coefficient
C_{D_0}	Zero-lift drag coefficient
C_l	Rolling moment coefficient
C_L	Lift coefficient
C_{L_w}	Wing or wing-body lift coefficient
C_{LT}	Tailplane lift coefficient
C_H	Elevator hinge moment coefficient
C_m	Pitching moment coefficient
C_{m_0}	Pitching moment coefficient about aerodynamic centre of wing or wing-body
C_{m_α}	Slope of C_m - α plot
C_n	Yawing moment coefficient
C_x	Axial force coefficient
C_y	Lateral force coefficient
C_z	Normal force coefficient
C_τ	Thrust coefficient
d	Maximum body width; gust length
D	Drag
D'	Drag in a lateral-directional perturbation
\mathbf{D}	Direction cosine matrix; direct matrix
D_c	Drag due to camber
D_α	Drag due to incidence
e	Exponential function
e	Oswald efficiency factor
\mathbf{E}	Input matrix of gust and turbulence terms
f	Cyclic frequency (Hz)
F	Aerodynamic force: Feed-forward path transfer function: ESDU empirical factor
\mathbf{F}	Direct matrix of gust and turbulence terms
F_c	Aerodynamic force due to camber
F_W	ESDU empirical correction factor
F_α	Aerodynamic force due to incidence
F_η	Elevator control force

g	Acceleration due to gravity
g_η	Elevator stick to surface mechanical gearing constant
G	Controlled system transfer function: ESDU empirical factor: Transfer function gain
G_f	Filter transfer function
h	Height; centre of gravity position on reference chord: Spanwise coordinate along wing sweep line; body height
h_0	Aerodynamic centre position on reference chord
h_F	Fin height coordinate above roll axis
h_m	Controls-fixed manoeuvre point position on reference chord
h'_m	Controls-free manoeuvre point position on reference chord
h_n	Controls-fixed neutral point position on reference chord
h'_n	Controls-free neutral point position on reference chord
H	Elevator hinge moment: Feedback path transfer function
H_F	Fin span measured perpendicular to roll axis
H_m	Controls-fixed manoeuvre margin
H'_m	Controls-free manoeuvre margin
i_x	Dimensionless moment of inertia in roll
i_y	Dimensionless moment of inertia in pitch
i_z	Dimensionless moment of inertia in yaw
i_{xz}	Dimensionless product of inertia about ox and oz axes
I'	Normalised inertia
I_x	Moment of inertia in roll
I_y	Moment of inertia in pitch
I_z	Moment of inertia in yaw
\mathbf{I}	Identity matrix
I_{xy}	Product of inertia about ox and oy axes
I_{xz}	Product of inertia about ox and oz axes
I_{yz}	Product of inertia about oy and oz axes
j	Complex variable ($\sqrt{-1}$)
J	ESDU empirical sideforce correction factor
k	General constant; spring stiffness coefficient
k_q	Pitch rate transfer function gain constant
k_u	Axial velocity transfer function gain constant
k_w	Normal velocity transfer function gain constant
k_θ	Pitch attitude transfer function gain constant
k_τ	Turbo-jet engine gain constant
K	Feedback gain: Constant in drag polar: Gust filter gain constant

K	Feedback gain matrix
K_f	Feel system spring constant
K_n	Controls-fixed static stability margin
K'_n	Controls-free static stability margin
l_f	Fin arm measured between wing and fin quarter-chord points
l_t	Tail arm measured between wing and tailplane quarter-chord points
l_F	Fin arm measured between cg and fin quarter-chord point
l_T	Tail arm measured between cg and tailplane quarter-chord points
L	Lift; rolling moment
L'	Lift in lateral-directional perturbation
L_c	Lift due to camber
L_w	Wing or wing-body lift
L_F	Fin lift
L_T	Tailplane lift
L_α	Lift due to incidence
L	Gust and turbulence scale length
m	Mass
m'	Normalised mass
m_F	ESDU fin moment arm about cg
M	Local Mach number
M_0	Free stream Mach number
M_{crit}	Critical Mach number
M	Pitching moment
\mathbf{M}	“Mass” matrix
M_0	Wing-body pitching moment about wing aerodynamic centre
M_T	Tailplane pitching moment about tailplane aerodynamic centre
n	Total normal load factor
n_α	Normal load factor per unit angle of attack
n'	Inertial normal load factor
n_z	Normal load factor
N	Yawing moment; white noise
o	Origin of axes
p	Roll rate perturbation: Trim reference point; system pole
q	Pitch rate perturbation
Q	Dynamic pressure
r	Yaw rate perturbation: General response variable
R	Radius of turn

s	Wing semi-span; Laplace operator
S	Wing reference area
S_B	Projected body side reference area
S_F	Fin reference area
S_{FR}	Rudder area
S_T	Tailplane reference area
S_η	Elevator area aft of hinge line
t	Time: Maximum aerofoil section thickness
T	Time constant
T_r	Roll mode time constant
T_s	Spiral mode time constant
T_u	Numerator zero in axial velocity transfer function
T_w	Numerator zero in normal velocity transfer function
T_θ	Numerator zero in pitch rate and attitude transfer functions
T_{θ_2}	Incidence lag time constant
T_τ	Turbo-jet engine time constant
T_2	Time to double amplitude
u	Axial velocity perturbation
\mathbf{u}	Input vector
\mathbf{u}_g	Gust and turbulence input vector
U	Total axial velocity
U_e	Axial component of steady equilibrium velocity
U_E	Axial velocity component referred to datum-path earth axes
v	Lateral velocity perturbation: Dummy variable
v_s	Sink rate
\mathbf{v}	Eigenvector; closed-loop system input vector
V	Perturbed total velocity: Total lateral velocity
V_e	Lateral component of steady equilibrium velocity
V_E	Lateral velocity component referred to datum-path earth axes
V_{md}	Minimum drag speed
V_0	Steady equilibrium velocity
\overline{V}_f	Canard foreplane volume ratio
\overline{V}_F	Fin volume ratio
V_{gm}	Maximum gust velocity
\overline{V}_T	Tailplane volume ratio
\mathbf{V}	Eigenvector matrix
w	Normal velocity perturbation

W	Total normal velocity
W_e	Normal component of steady equilibrium velocity
W_E	Normal velocity component referred to datum-path earth axes
x	Longitudinal coordinate in axis system
x_p	Longitudinal coordinate of pilot in axis system
x_τ	Axial coordinate of engine thrust line
\mathbf{x}	State vector
X	Axial force component
y	Lateral coordinate in axis system
y_B	Lateral body "drag" coefficient
y_τ	Lateral coordinate of engine thrust line
\mathbf{y}	Output vector
Y	Lateral force component
z	Normal coordinate in axis system: System zero
z_τ	Normal coordinate of engine thrust line
\mathbf{z}	Transformed state vector
z_p	Normal coordinate of pilot in axis system
Z	Normal force component
α	Angle of attack or incidence perturbation
α'	Incidence perturbation
α_e	Equilibrium incidence
α_0	Zero-lift incidence
α_T	Local tailplane incidence
α_{w_0}	Zero-lift incidence of wing
α_{wr}	Wing rigging angle
β	Sideslip angle perturbation
β_e	Equilibrium sideslip angle
β_η	Elevator trim tab angle
γ	Flight path angle perturbation: Imaginary part of complex number
γ_e	Equilibrium flight path angle
Γ	Wing dihedral angle
δ	Control angle: Increment: Unit impulse function
$\delta\eta$	Elevator angle increment
δ_a	Aileron angle (American)
δ_r	Rudder angle (American)
δ_s	Stabilizer angle (American)
δ_ξ	Roll control stick angle

δ_η	Pitch control stick angle
δ_ζ	Rudder pedal control angle
δm	Mass increment
δn	Normal load factor increment
Δ	Characteristic polynomial; transfer function denominator
ε	Throttle lever angle: Downwash angle at tailplane: Closed-loop system error
ε_0	Zero-lift downwash angle at tail
ζ	Rudder angle perturbation; damping ratio
ζ_d	Dutch roll damping ratio
ζ_p	Phugoid damping ratio
ζ_s	Short-period pitching oscillation damping ratio
η	Elevator angle perturbation
η_d	Elevator angle demand
η_e	Elevator trim angle
η_T	Tailplane setting angle
θ	Pitch angle perturbation; general angle
θ_e	Equilibrium pitch angle
κ	Thrust line inclination to aircraft ox axis
λ	Eigenvalue; taper ratio
Λ	Wing sweep angle
$\boldsymbol{\Lambda}$	Eigenvalue matrix
μ_1	Longitudinal relative density factor
μ_2	Lateral relative density factor
ξ	Aileron angle perturbation
ρ	Air density
σ	Aerodynamic time parameter; real part of complex number; root mean square gust and turbulence intensity
τ	Engine thrust perturbation; time parameter
τ_e	Trim thrust
$\hat{\tau}$	Dimensionless thrust
ϕ	Roll angle perturbation; phase angle; general angle
Φ	Power spectral density
$\boldsymbol{\Phi}$	State transition matrix
ψ	Yaw angle perturbation
ω	Angular frequency (rad/s): Undamped natural frequency
ω_b	Bandwidth frequency
ω_d	Dutch roll undamped natural frequency

ω_n	Damped natural frequency
ω_p	Phugoid undamped natural frequency
ω_s	Short-period pitching oscillation undamped natural frequency
Ω	Spatial frequency

Subscripts

0	Datum axes; normal earth-fixed axes: Wing or wing-body aerodynamic centre: Free stream flow conditions
$\frac{1}{4}$	Quarter-chord
2	Double or twice
∞	Infinite span
<i>a</i>	Aerodynamic
<i>A</i>	Aileron: Aircraft
<i>b</i>	Aeroplane body axes: Bandwidth
<i>B</i>	Body or fuselage
<i>c</i>	Control: Chord: Compressible flow: Camber line
<i>cg</i>	Centre of gravity
<i>d</i>	Atmospheric disturbance: Dutch roll: Control demand
<i>D</i>	Drag
<i>e</i>	Equilibrium, steady or initial condition
<i>E</i>	Datum-path earth axes
<i>f</i>	Canard foreplane: Feel system: Filter
<i>F</i>	Fin; command path filter
<i>g</i>	Gravitational: Gust
<i>H</i>	Elevator hinge moment
<i>i</i>	Incompressible flow
<i>l</i>	Rolling moment
<i>le</i>	Leading edge
<i>L</i>	Lift
<i>m</i>	Pitching moment; manoeuvre: Maximum value
<i>n</i>	Neutral point: Yawing moment
<i>n_z</i>	Normal load factor
<i>N</i>	White noise
<i>p</i>	Power; roll rate; phugoid; pilot
<i>pk</i>	Peak value
<i>q</i>	Pitch rate
<i>r</i>	Yaw rate: Roll mode: Wing root
<i>R</i>	Rudder
<i>s</i>	Short-period pitching oscillation: Spiral mode: Stabiliser (American)
<i>t</i>	Wing tip; aerofoil thickness
<i>T</i>	Tailplane

u	Axial velocity
v	Lateral velocity
w	Aeroplane wind or stability axes: Wing or wing-body: Normal velocity
x	ox axis
y	oy axis
z	oz axis
α	Angle of attack or incidence
ε	Throttle lever
ζ	Rudder
η	Elevator
θ	Pitch
ξ	Ailerons
τ	Thrust

Examples of other symbols and notation

x_u	Shorthand notation to denote concise derivative, dimensional derivative divided by appropriate mass or inertia parameters
X_u	Shorthand notation to denote American normalised dimensional derivative $\frac{\overset{\circ}{X}_u}{m}$
L'_v	Shorthand notation to denote modified American lateral-directional derivative
C_{x_u}	Shorthand coefficient notation to denote American dimensionless derivative
X_u°	Shorthand notation to denote dimensionless derivative $\frac{\partial \dot{X}}{\partial \hat{u}}$
$X_u^{\circ}(t)$	Shorthand notation to denote dimensional derivative $\frac{\partial X}{\partial u}$
$N_u^y(t)$	Shorthand notation to denote transfer function numerator polynomial relating output response y to input u
\hat{u}	Shorthand notation to denote that variable u is dimensionless
\bar{u}	Shorthand notation to denote statistical mean value of u
$(*)$	Superscript to denote complex conjugate: Superscript to denote that derivative includes both aerodynamic and thrust contributions in American notation
$(^{\circ})$	Dressing to denote dimensional derivative in British notation
$(^{\wedge})$	Dressing to denote dimensionless parameter
$(^T)$	Superscript to denote transpose of a matrix

Introduction

1

1.1 Overview

This book is primarily concerned with the provision of good flying and handling qualities in conventional piloted aircraft, although the material is equally applicable to *uninhabited air vehicles* (UAV). Consequently, it is also very much concerned with the stability, control, and dynamic characteristics which are fundamental to the determination of those qualities. Since flying and handling qualities are of critical importance to safety and to the piloting task, it is essential that their origins are properly understood. Here, then, the intention is to set out the basic principles of the subject at an introductory level and to illustrate the application of those principles by means of worked examples.

Following the first flights made by the Wright brothers in December 1903, the pace of aeronautical development quickened and the progress made in the following decade or so was dramatic. However, the stability and control problems that faced early aviators were sometimes considerable since the flying qualities of their aircraft were often less than satisfactory. Many investigators were studying the problems of stability and control at the time, although it is the published works of [Bryan \(1911\)](#) and [Lanchester \(1908\)](#) which are usually credited with laying the first really secure foundations for the subject. By conducting many experiments with flying models, Lanchester was able to observe and successfully describe mathematically some dynamic characteristics of aircraft. The beauty of Lanchester's work was its practicality and theoretical simplicity, which facilitates easy application and interpretation. Bryan, on the other hand, was a mathematician who chose to apply his energies, with the assistance of a Mr. Harper, to the problems of aircraft stability and control. He developed the general equations of motion of a rigid body with six degrees of freedom to successfully describe aircraft motion. His treatment, with very few changes, is still in everyday use. What has changed is the way in which the material is now used, due largely to the advent of the digital computer as an analysis tool. Together, the stability and control of aircraft is a subject which has its origins in aerodynamics, and the classical theory of the subject is traditionally expressed in the language of the aerodynamicist. However, most advanced-technology aircraft may be described as an *integrated system* comprising airframe, propulsion, flight controls, and so on. It is therefore convenient and efficient to utilise powerful computational systems engineering tools to analyse and describe the system's flight dynamics. Thus, the objective of the present work is to revisit the development of the classical theory and to express it in the language of the systems engineer where it is more appropriate to do so.

The subject of *flight dynamics* is concerned with the relatively short-term motion of aircraft in response to controls or to external disturbances such as atmospheric turbulence. The motion of interest can vary from small excursions about trim to very-large-amplitude manoeuvring when normal

aerodynamic behaviour may well become very non-linear. Since the treatment of the subject is introductory, a discussion of large-amplitude dynamics is beyond the scope of the present work.

The dynamic behaviour of an aircraft is shaped significantly by its stability and control properties, which in turn have their roots in the aerodynamics of the airframe. Previously the achievement of aircraft with good stability characteristics usually ensured good flying qualities, all of which depended only on good aerodynamic design. Expanding flight envelopes and the increasing dependence on an *automatic flight control system* (AFCS) for stability augmentation means that good flying qualities are no longer a guaranteed product of good aerodynamic design and good stability-characteristics. The reasons for this apparent inconsistency are now reasonably well understood and, put very simply, result from the addition of flight control system dynamics to those of the airframe. Flight control system dynamics are of course a necessary, but not always desirable, by-product of command and stability augmentation.

Modern flight dynamics is concerned not only with the dynamics, stability, and control of the basic airframe but also with the sometimes complex interaction between the airframe and flight control system. Since the flight control system comprises motion sensors, a control computer, control actuators, and other essential items of control hardware, a study of the subject becomes a multidisciplinary activity. Therefore, it is essential that the modern flight dynamicist has not only a thorough understanding of the classical stability and control theory of aircraft but also a working knowledge of control theory and of the use of computers in *flight-critical* applications. Modern aircraft comprise the airframe together with the flight control equipment and may be treated as a whole *system* using the traditional tools of the aerodynamicist and the analytical tools of the control engineer.

Thus in a modern approach to the analysis of stability and control, it is convenient to treat the airframe as a system component. This leads to the derivation of mathematical models which describe aircraft in terms of aerodynamic *transfer functions*. Described in this way, the stability, control, and dynamic characteristics of aircraft are readily interpreted with the aid of very powerful computational systems engineering tools. It follows that the mathematical model of the aircraft is immediately compatible with, and provides the foundation for integration with, flight control system studies. This is an ideal state of affairs since today it is commonplace to undertake stability and control investigations as a precursor to flight control system development.

The modern flight dynamicist tends to be concerned with the wider issues of flying and handling qualities rather than with the traditional, and more limited, issues of stability and control. The former are, of course, largely determined by the latter. The present treatment of the material is shaped by answering the following questions which a newcomer to the subject might be tempted to ask:

How are the stability and control characteristics of aircraft determined, and how do they influence flying qualities?

The answer to this question involves the establishment of a suitable mathematical framework for the problem, the development of the equations of motion and their solution, investigation of response to controls, and the general interpretation of dynamic behaviour.

What are acceptable flying qualities; how are the requirements defined, interpreted, and applied; and how do they limit flight characteristics?

The answer to this question involves a review of contemporary flying qualities requirements and their evaluation and interpretation in the context of stability and control characteristics.

When an aircraft has unacceptable flying qualities, how may its dynamic characteristics be improved?

The answer to this question involves an introduction to the rudiments of feedback control as the means of augmenting the stability of the basic airframe.

1.2 Flying and handling qualities

The flying and handling qualities of an aircraft are those properties which describe the ease and effectiveness with which the aircraft responds to pilot commands in the execution of a flight task, or *mission task element* (MTE). In the first instance, therefore, flying and handling qualities are described qualitatively and are formulated in terms of *pilot opinion*; consequently, they tend to be rather subjective. The process involved in pilot perception of flying and handling qualities may be interpreted in the form of a signal flow diagram, as shown in Fig. 1.1. The solid lines represent physical, mechanical or electrical signal flow paths; the dashed lines represent sensory feedback information to the pilot. The author's interpretation distinguishes between *flying qualities* and *handling qualities* as indicated. The pilot's perception of flying qualities is considered to be a qualitative description of how well the aeroplane carries out the commanded task. On the other hand, the pilot's perception of handling qualities is considered to be a qualitative description of the adequacy of the short-term dynamic response to controls in the execution of the flight task. The two *qualities* are therefore very much interdependent and in practice are probably inseparable. To summarise, then, flying qualities may be regarded as being task-related whereas the handling qualities may be regarded as being response-related. When the airframe characteristics are augmented by a flight control system, the way in which that system may influence the flying and handling qualities is clearly shown in Fig. 1.1.

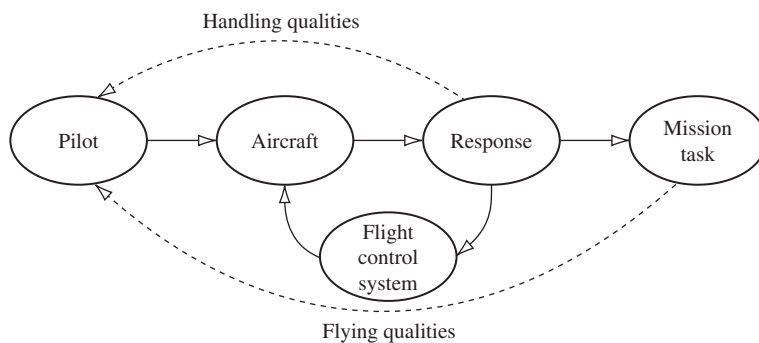


FIGURE 1.1 Flying and handling qualities of conventional aircraft.

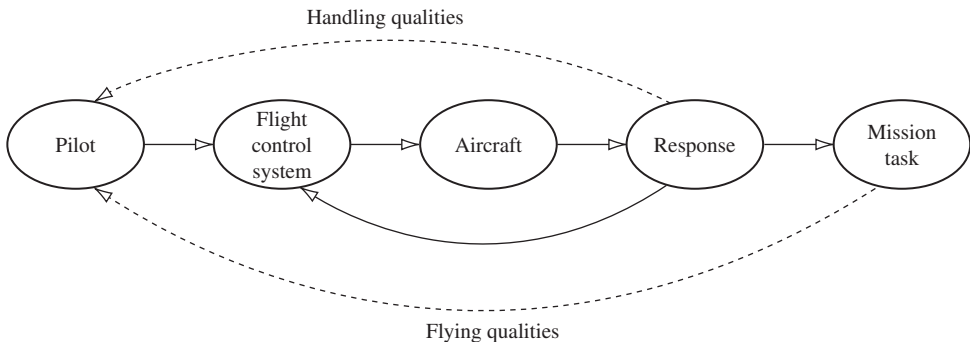


FIGURE 1.2 Flying and handling qualities of FBW aircraft.

Most advanced modern aeroplanes employ *fly-by-wire* (FBW) primary flight controls, and these are usually integrated with the stability augmentation system. In this case, the interpretation of flying and handling qualities is modified to that shown in Fig. 1.2. Here the flight control system becomes an integral part of the primary signal flow path, and the influence of its dynamic characteristics on flying and handling qualities is of critical importance. The need for very careful consideration of the influence of the flight control system in this context cannot be over-emphasised.

The pilot's perception of the flying and handling qualities of an aircraft will be influenced by many factors, among them stability, control, and dynamic characteristics of the airframe; flight control system dynamics; response to atmospheric disturbances; and the less tangible effects of cockpit design. This last factor includes considerations such as control inceptor design, instrument displays, and field of view. Not surprisingly, the quantification of flying qualities is difficult. However, there is an overwhelming necessity for some sort of numerical description of flying and handling qualities for use in engineering design and evaluation. It is well established that the flying and handling qualities of an aircraft are intimately dependent on the stability and control characteristics of the airframe, including the flight control system if one is installed. Since stability and control parameters are readily quantified, these are usually used as indicators and measures of the likely flying qualities of the aeroplane. Therefore, the prerequisite for almost any study of flying and handling qualities is a descriptive mathematical model of the aeroplane which is capable of providing an adequate quantitative indication of its stability, control, and dynamic properties.

1.3 General considerations

In a systematic study of the principles governing the flight dynamics of aircraft, it is convenient to break the problem down into manageable descriptive elements. Thus before attempting to answer the questions posed in Section 1.1, it is useful to consider and define a suitable framework in which the essential mathematical development may take place.

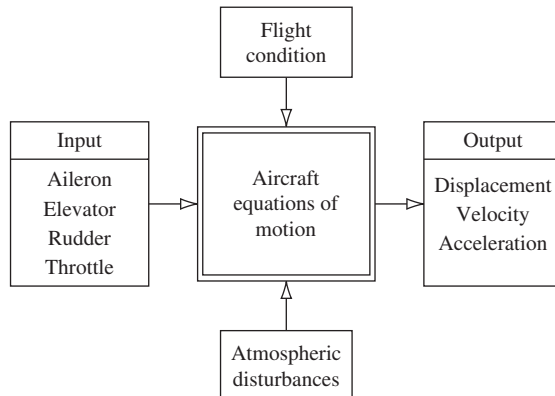


FIGURE 1.3 Basic control-response relationships.

1.3.1 Basic control-response relationships

A description of the basic input-output relationships on which the flying and handling qualities of unaugmented aircraft depend is essential. These relationships are described by the aerodynamic transfer functions which provide the simplest and most fundamental description of airframe dynamics. They describe the control-response relationship as a function of flight condition and may include the influence of atmospheric disturbances when appropriate. These basic relationships are illustrated in Fig. 1.3.

Central to this framework is a mathematical model of the aircraft, usually referred to as *the equations of motion*. The equations of motion provide a complete description of response to controls, subject only to modelling limitations defined at the outset, which is measured in terms of displacement, velocity, and acceleration variables. The flight condition describes the conditions under which the observations are made and includes parameters such as Mach number, altitude, aircraft geometry, mass, and trim state. When the airframe is augmented with a flight control system, the equations of motion are modified to model this configuration. The response transfer functions, derived from the mathematical solution of the equations of motion, are then no longer the basic aerodynamic transfer functions but are obviously the transfer functions of the augmented aeroplane.

1.3.2 Mathematical models

From the foregoing, it is apparent that it is necessary to derive mathematical models to describe the aircraft, its control systems, atmospheric disturbances, and so on. The success of any flight dynamics analysis hinges on the suitability of the models to the problem at hand. Often the temptation is to attempt to derive the most accurate model possible. High-fidelity models are capable of reproducing aircraft dynamics accurately, but they are seldom simple. Their main drawback is the lack of *functional visibility*. In very complex aircraft and system models, it may be difficult, or even impossible, to relate response to the simple physical aerodynamic properties of the airframe or to the properties of the control system components. For the investigation of flying and handling

qualities, it is frequently adequate to use simple approximate models, which have the advantage of maximising functional visibility and thereby drawing attention to the dominant characteristics. Such models have the potential to enhance the visibility of the physical principles involved, greatly facilitating the interpretation of flying and handling qualities. Often the deterioration in fidelity of the response resulting from the use of approximate models may be relatively insignificant. For a given problem, it is necessary to develop a model which balances the desire for response fidelity against the requirement to maintain functional visibility. As is so often the case in many fields of engineering, simplicity is a most desirable virtue.

1.3.3 Stability and control

Flying and handling qualities are substantially dependent on, and are usually described in terms of, the stability and control characteristics of an aircraft. It is therefore essential to be able to completely describe and quantify stability and control parameters. Analysis may then be performed using the stability parameters. Static stability analysis enables the *control displacement* and *control force* characteristics to be determined for both steady and manoeuvring flight conditions. Dynamic stability analysis enables the temporal *response to controls* and reponse to atmospheric disturbances to be determined for various flight conditions.

1.3.4 Stability and control augmentation

When an aircraft has flying and handling deficiencies it becomes necessary to correct, or *augment*, the aerodynamic characteristics which give rise to them. To a limited extent, this could be achieved by modification of the aerodynamic design of the aircraft. In this event, it is absolutely essential to understand the relationship between the aerodynamics of the airframe and controls and the stability and control characteristics of that airframe. However, many aircraft today are designed with their aerodynamics optimised for performance over a very large flight envelope, and a consequence of this is that their flying qualities are often deficient. The intent at the outset is to rectify those deficiencies with a stability augmentation system. Therefore, the alternative to aerodynamic design modification is the introduction of a flight control system. In this case it becomes essential to understand how feedback control techniques may be used to artificially modify the apparent aerodynamic characteristics of the airframe. So once again, but for different reasons, it is absolutely essential to understand the relationship between the aerodynamics of the airframe and its stability and control characteristics. Further, it becomes very important to appreciate the effectiveness of servo-systems for autostabilisation whilst acknowledging the attendant advantages, disadvantages, and limitations introduced by the system hardware. At this stage of consideration it is beginning to become obvious why flight dynamics is now a complex multidisciplinary subject. However, since this work is introductory, the subject of stability augmentation is treated only at the most elementary level.

1.4 Aircraft equations of motion

The equations of motion of an aeroplane are the foundation on which the framework for flight dynamics studies is built; they provide the key to a proper understanding of flying and handling

qualities. At their simplest, the equations of motion can describe small-perturbation motion about trim only. At their most complex, they can be completely descriptive, simultaneously embodying static stability, dynamic stability, aero-elastic effects, atmospheric disturbances, and control system dynamics for a given aeroplane configuration. The equations of motion enable the rather intangible description of flying and handling qualities to be related to quantifiable stability and control parameters, which in turn may be related to identifiable aerodynamic characteristics of the airframe. For initial studies the theory of small perturbations is applied to the equations to facilitate their analytical solution and to enhance their functional visibility. However, for more advanced applications, which are beyond the scope of the present work, the fully descriptive non-linear form of the equations might be retained. In this case the equations are difficult to solve analytically and computer simulation techniques become necessary to obtain a numerical solution.

1.5 Aerodynamics

The aerodynamics of the airframe and its controls make a fundamental contribution to the stability and control characteristics of the aircraft. It is usual to incorporate aerodynamic descriptions in the equations of motion in the form of *aerodynamic stability and control derivatives*. Since it is necessary to constrain the motion to well-defined limits to obtain the derivatives, the scope of the resulting aircraft model is similarly constrained in its application. However, it is quite common to find aircraft models constrained in this way being used to predict flying and handling qualities at conditions well beyond the imposed limits. This is not recommended practice! An important aspect of flight dynamics concerns the proper definition of aerodynamic derivatives as functions of common aerodynamic parameters. It is also most important that the values of the derivatives are compatible with the scope of the problem to which the model is to be applied. The processes involved in the estimation or measurement of aerodynamic derivatives provide an essential contribution to a complete understanding of aircraft behaviour.

1.5.1 Small perturbations

The aerodynamic properties of an aircraft vary considerably over the flight envelope, and their mathematical descriptions are approximations at best. The limit of the approximations is determined either by the ability of mathematics to describe the physical phenomena involved or by the acceptable complexity of the description. The aim is to obtain the simplest approximation consistent with adequate physical representation. In the first instance this aim is best met when the motion of interest is constrained to *small perturbations* about a steady flight condition, which is usually, but not necessarily, trimmed equilibrium. This means that the aerodynamic characteristics can be approximated by *linearising* about the chosen flight condition. Simple approximate mathematical descriptions of aerodynamic stability and control derivatives then follow relatively easily. This is the approach pioneered by [Bryan \(1911\)](#), and it usually works extremely well provided the limitations of the model are recognised from the outset.

1.6 Computers

No discussion of flight dynamics would be complete without mention of the very important role played by the computer in all aspects of the subject. It is probably true to say that the development of today's very advanced aircraft would not have been possible without parallel developments in computer technology. In fact, there is ample evidence to suggest that the demands of aeronautics have forced the pace of computer development. Computers are used for two main functions: as a general-purpose tool for design and analysis and to provide "intelligence" in flight control systems.

1.6.1 Analytical computers

In the past, all electronic computation, whether for analysis, simulation, or airborne flight control, would have been analogue. Analogue computer technology developed rapidly during and immediately after World War II and by the late 1960s had reached its highest level of development following the introduction of the electronic integrated operational amplifier. The principal role of the analogue computer was that of simulation, and its main advantages were its ability to run in real time, its continuous electrical signals, and its high level of functional visibility. Its main disadvantage was that the electronic hardware required was directly proportional to the functional complexity of the problem to be simulated. This meant that complex aircraft models with complex flight control systems required physically large and very costly hardware. During the 1960s and 1970s electronic digital computing technology advanced rapidly and soon displaced the analogue computer as the primary tool for design and analysis. However, it took somewhat longer before the digital computer acquired the capacity and speed necessary to meet the demands of simulation. Today most of the computational requirements for design, analysis, and simulation can be provided by a modest personal computer.

1.6.2 Flight control computers

In the present context, flight control is taken to mean *flight-critical stability augmentation*, where a computer malfunction or failure might hazard the continued safe operation of the aircraft. In the case of a FBW computer, a total failure would mean total loss of control. Therefore, hardware integrity is a very serious issue in flight control computer design. The modern aircraft may also have an autopilot computer, air data computer, navigation computer, energy management computer, weapon systems computer, and more. Many of these additional computers may be capable of exercising some degree of control over the aircraft, but none is quite as critical as the stability augmentation computer in the event of a malfunction.

For the last 70 years or more, computers have been used in aircraft for flight control. For much of that time the dedicated analogue electronic computer was unchallenged because of its relative simplicity, its easy interface engineering with mechanical flying controls, and its excellent safety record. Toward the end of the 1970s the digital computer had reached the stage of development where its use in flight-critical applications became a viable proposition, with the promise of vastly expanded control capability. The pursuit of increasingly sophisticated performance goals led to an increase in complexity of the aerodynamic design of aircraft. This in turn placed greater demands on the flight control system for the maintenance of good flying and handling qualities. The attraction of the digital computer for flight control is its capability for handling very complex control

functions easily. The disadvantage is its lack of functional visibility and the consequent difficulty of ensuring safe trouble-free operation. Nevertheless, the digital flight-critical computer is here to stay and is now used in all advanced-technology aircraft. Research continues to improve hardware, software, and applications. Confidence in digital flight control systems is now such that applications include full-FBW civil transport aeroplanes.

Functionally complex flight control systems have given the modern aeroplane hitherto unobtainable performance benefits. But nothing is free! The consequence of using such systems is the unavoidable introduction of unwanted control system dynamics. These usually manifest themselves as control phase lag and can intrude on the piloting task in an unacceptable way, resulting in an aircraft with poor flying and handling qualities. This problem is still a subject of research and is very much beyond the scope of this book. However, the essential foundation material on which such studies are built is set out in the following chapters.

1.6.3 Computer software tools

Many computer software tools are now available which are suitable for flight dynamics analysis. Most packages are intended for control systems applications, but they are ideal for handling aeronautical system problems and may be installed on a modest PC. Software tools used regularly by the author are listed here, but it must be appreciated that the list is by no means exhaustive, nor is it implied that the programs listed are the best or necessarily the most appropriate.

MATLAB

MATLAB is a very powerful control system design and analysis tool which is intended for systems configured in state-space format. As a result, all computation is handled in matrix format. MATLAB's screen graphics are good. All of the examples and problems in this book can be solved with the aid of MATLAB.

Simulink

Simulink is a continuous simulation supplementary addition to MATLAB, on which it depends for its mathematical modelling. It is also a powerful tool and is easy to apply using a block diagram format for model building. Simulink is not strictly necessary for application to the material in this book, although it can be used with advantage for some examples. Its main disadvantage is its limited functional visibility since models are built using interconnecting blocks whose functions are not always immediately obvious to the user. Nevertheless, Simulink enjoys widespread use throughout industry and academia.

MATLAB and Simulink, Student Version Release 14

MATLAB and Simulink, Student Version Release 14 is a combined package available to registered students at low cost.

Program CC, Version 5

Program CC, Version 5 is also a very powerful control system design and analysis tool. It is capable of handling classical control problems in transfer function format as well as modern state-space control problems in matrix format. The current version is very similar in use to MATLAB to the

extent that many procedures are identical. This is not entirely surprising since the source of the underlying mathematical routines is the same for both programs. An advantage of Program CC is that it was written by flight dynamicists for flight dynamicists; as a result, its use is intuitive once the commands have been learned. The screen graphics are good and have some flexibility of presentation. A downloadable low-cost student version is available which is suitable for solving all examples and problems in this book.

Mathcad

Mathcad Prime 2 is a very powerful general-purpose tool for mathematical problem solving. It is useful for repetitive calculations, but it comes into its own for solving difficult non-linear equations. It is also capable of undertaking complex algebraic computations. The screen graphics are generally very good and are very flexible. In particular, Mathcad is a valuable tool for aircraft trim and performance computations where the requirement is to solve simultaneous non-linear algebraic equations. Its use in this role is illustrated in Chapter 3. A low-cost student version of this software is available to registered students.

20-sim

20-sim is a modern version of the traditional simulation language and has been written to capitalise on the functionality of the PC. Models can be built up from the equations of motion, from the equivalent matrix equations, or from both. Common modules can be assigned icons of the user's design, and the simulation can then be constructed in a manner similar to the block diagram format of Simulink. The versatility of 20-sim is enhanced by its direct compatibility with MATLAB. Significant advantages are excellent functional visibility, model-building flexibility, and the infinitely variable control of the model structure. The screen graphics are excellent, and there is the additional facility for direct visualisation of the modelled system in real time. At the time of writing, the main disadvantage of 20-sim is the lack of a library of aerospace simulation components; however, this will no doubt be addressed as the language matures.

1.7 Summary

An attempt has been made in this chapter to provide a broad appreciation of what flight dynamics is all about. To produce a comprehensive text on the subject would require many volumes, assuming that it were even possible. The present intention is therefore to set out fundamental principles only. However, where appropriate, comments are included in the text to indicate the direction in which the material in question might be developed for more advanced studies.

References

- Bryan, G. H. (1911). *Stability in aviation*. London: Macmillan.
Lanchester, F. W. (1908). *Aerodonetics*. London: Constable.

Sources

- Mathcad. Adept Scientific, Amor Way, Letchworth, Herts, SG6 1ZA. <www.adeptscience.co.uk>.
- MATLAB and Simulink. The Mathworks Ltd., Matrix House, Cowley Park, Cambridge, CB4 0HH. <www.mathworks.co.uk/store>. The Mathworks, Inc., 3 Apple Hill drive, Natick, MA 01760-2098, USA. <www.mathworks.com>.
- Program CC. Systems Technology Inc., 13766 South Hawthorne Boulevard, Hawthorne, CA 90250-7083. <www.programcc.com>.
- 20-sim. Controllab Products B.V., Drienerlolaan 5 HO-8266, 7522 NB Enschede, The Netherlands. <www.20sim.com>.

Systems of Axes and Notation

2

Before commencing the main task of developing mathematical models of the aircraft, it is first necessary to put in place an appropriate and secure foundation on which to build the models. This foundation comprises a mathematical framework in which the equations of motion can be developed in an orderly and consistent way. Since aircraft have six degrees of freedom, the description of their motion can be relatively complex. Therefore, motion is usually described by a number of variables which are related to a suitably chosen system of axes. In the United Kingdom, the scheme of notation and nomenclature in common use is based on that developed by [Hopkin \(1970\)](#), and a simplified summary may be found in the appropriate [ESDU \(1987\)](#) data item. As far as is reasonably possible, the notation and nomenclature used throughout this book corresponds with Hopkin's.

By making the appropriate choice of axis systems, order and consistency may be introduced to the process of model building. The importance of order and consistency in the definition of the mathematical framework cannot be overemphasised because, without either, misunderstanding and chaos will surely follow. Only the most basic commonly used axis systems appropriate to aircraft are discussed in the following sections. In addition to the above named references, a more expansive treatment may be found in [Etkin \(1972\)](#) or in [McRuer et al. \(1973\)](#), for example.

2.1 Earth axes

Since only normal atmospheric flight is considered, it is usual to measure aircraft motion with reference to an earth-fixed framework. The accepted convention for defining earth axes determines that a reference point o_0 on the surface of the earth is the origin of a right-handed orthogonal system of axes $(o_0x_0y_0z_0)$, where o_0x_0 points to the north, o_0y_0 points to the east, and o_0z_0 points vertically "down" along the gravity vector. Conventional earth axes are illustrated in [Fig. 2.1](#).

Clearly, the plane $(o_0x_0y_0)$ defines the local horizontal plane which is tangential to the surface of the earth. The flight path of an aircraft flying in the atmosphere in the vicinity of the reference point o_0 may thus be completely described by its coordinates in the axis system. This assumes a *flat earth* where the vertical is "tied" to the gravity vector. For localised flight this model is quite adequate, although it is best suited to navigation and performance applications where flight path trajectories are of primary interest.

For investigations involving trans-global navigation, the axis system described is inappropriate; a spherical coordinate system is preferred. Similarly, for trans-atmospheric flight involving the launch and reentry of space vehicles, a spherical coordinate system is more appropriate. However, since in such an application the angular velocity of the earth becomes important, it is necessary to define a fixed spatial axis system to which the spherical earth axis system may be referenced.

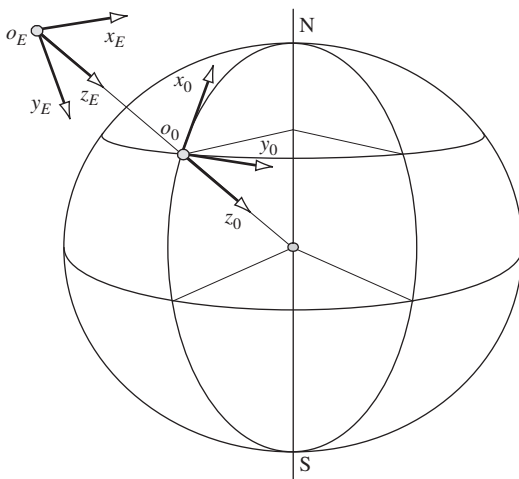


FIGURE 2.1 Conventional earth axes.

For flight dynamics applications a simpler definition of earth axes is preferred. Since only short-term motion is of interest, it is perfectly adequate to assume flight above a flat earth. The most common consideration is that of motion about *straight and level* flight. Straight and level flight assumes flight in a horizontal plane at a constant altitude; whatever the subsequent motion of the aircraft might be, the *attitude* is determined with respect to the horizontal. Referring again to Fig. 2.1, the horizontal plane is defined by $(o_Ex_Ey_E)$ and is parallel to the plane $(o_0x_0y_0)$ at the surface of the earth. The only difference is that the o_Ex_E axis points in the arbitrary direction of the flight of the aircraft rather than to the north. The o_Ez_E axis points vertically down as before. Therefore, it is only necessary to place the origin o_E in the atmosphere at the most convenient point, which is frequently coincident with the origin of the aircraft body-fixed axes. Earth axes $(o_Ex_Ey_Ez_E)$ defined in this way are called *datum-path earth axes*; they are “tied” to the earth by means of the gravity vector and provide the inertial reference frame for short-term aircraft motion.

2.2 Aircraft body-fixed axes

A number of aircraft body-fixed axis systems are in common use. However, for small perturbation analysis only the generalised body axes and wind, or stability, axes need be considered.

2.2.1 Generalised body axes

It is usual practice to define a right-handed orthogonal axis system fixed in the aircraft and constrained to move with it. Thus, when the aircraft is disturbed from its initial flight condition, the axes move with the airframe and the motion is quantified in terms of perturbation variables referred to the moving axes. The way in which the axes may be fixed in the airframe is arbitrary, although it is preferable to use an accepted standard orientation. The most general axis system is known as a

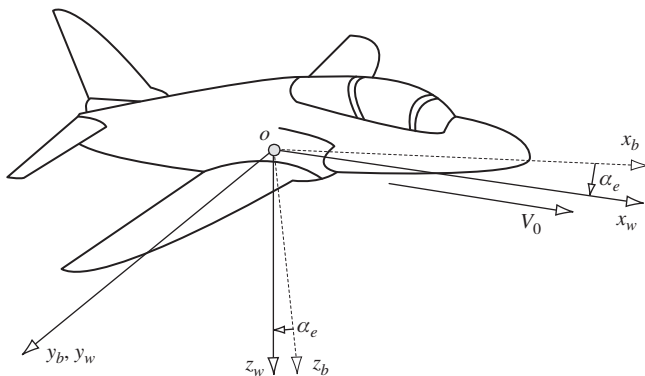


FIGURE 2.2 Moving-axis systems.

body axis system ($ox_b y_b z_b$), which is fixed in the aircraft as shown in Fig. 2.2. The ($ox_b z_b$) plane defines the plane of symmetry of the aircraft, and it is convenient to arrange the ox_b axis such that it is parallel to the geometrical *horizontal fuselage datum*. Thus in normal flight attitudes the oy_b axis is directed to starboard and the oz_b axis is directed “downward.” The origin o of the axes is fixed at a convenient reference point in the airframe, which is usually, but not necessarily, coincident with the centre of gravity (cg).

2.2.2 Aerodynamic, wind, or stability axes

It is often convenient to define a set of aircraft fixed axes such that the ox axis is parallel to the total velocity vector V_0 , as shown in Fig. 2.2. Such axes are called *aerodynamic, wind, or stability axes*. In steady symmetric flight, wind axes ($ox_w y_w z_w$) are just a particular version of body axes which are rotated about the oy_b axis through the steady body incidence angle α_e until the ox_w axis aligns with the velocity vector. Thus the plane ($ox_w z_w$) remains the plane of symmetry of the aircraft and the oy_w and the oy_b axes are coincident. There is a unique value of body incidence angle α_e for every flight condition; therefore, for every flight condition, the wind axes orientation in the airframe is different. However, for any given flight condition this orientation is defined and fixed in the aircraft at the outset and is constrained to move with it in subsequent disturbed flight. Typically, the body incidence might vary in the range $-10^\circ \leq \alpha_e \leq 20^\circ$ over a normal flight envelope.

2.2.3 Perturbation variables

The motion of the aircraft is described in terms of force, moment, linear and angular velocities, and attitude resolved into components with respect to the chosen aircraft fixed axis system. For convenience, it is preferable to assume a generalised *body axis* system in the first instance. Thus the aircraft is initially assumed to be in steady rectilinear, but not necessarily level, flight when the body incidence is α_e and the steady velocity V_0 resolves into components U_e , V_e , and W_e as indicated in Fig. 2.3. In steady nonaccelerating flight the aircraft is in equilibrium and the forces and moments acting on the airframe are in balance and sum to zero. This initial condition is usually referred to as *trimmed equilibrium*.

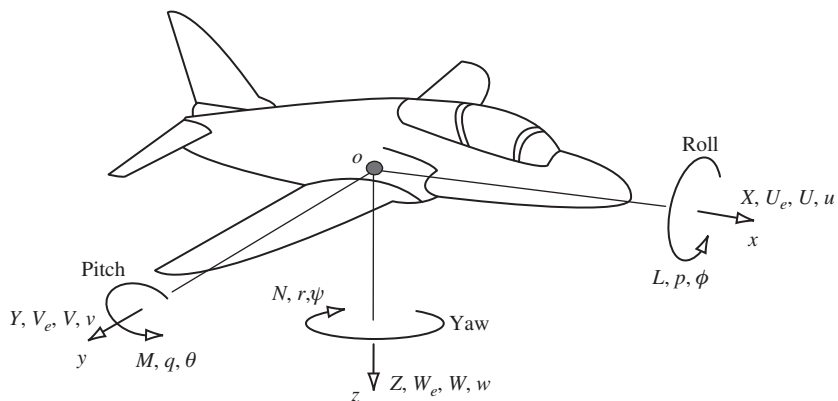


FIGURE 2.3 Motion variables notation.

Whenever the aircraft is disturbed from equilibrium, the force and moment balance is upset and the resulting transient motion is quantified in terms of the perturbation variables. The perturbation variables are shown in Fig. 2.3 and summarised in Table 2.1.

The positive sense of the variables is determined by the choice of a right-handed axis system. Components of linear quantities, force, velocity, and so forth are positive when their direction of action is the same as the direction of the axis to which they relate. The positive sense of the components of rotary quantities, moment, velocity, attitude, and so forth is a right-handed rotation and may be determined as follows. Positive *roll* about the ox axis is such that the oy axis moves toward the oz axis; positive *pitch* about the oy axis is such that the oz axis moves toward the ox axis; and positive *yaw* about the oz axis is such that the ox axis moves toward the oy axis. Therefore, positive roll is right wing down, positive pitch is nose up, and positive yaw is nose to the right as seen by the pilot.

A simple description of the perturbation variables is given in Table 2.2. The intention is to provide some insight into the physical meaning of the many variables used in the model. Note that the components of the total linear velocity perturbations (U, V, W) are given by the sum of the steady equilibrium components and the transient perturbation components (u, v, w); thus

$$\begin{aligned} U &= U_e + u \\ V &= V_e + v \\ W &= W_e + w \end{aligned} \tag{2.1}$$

2.2.4 Angular relationships in symmetric flight

Since it is assumed that the aircraft is in steady rectilinear, but not necessarily level, flight and that the axes fixed in the aircraft are body axes, it is useful to relate the steady and perturbed angles as shown in Fig. 2.4.

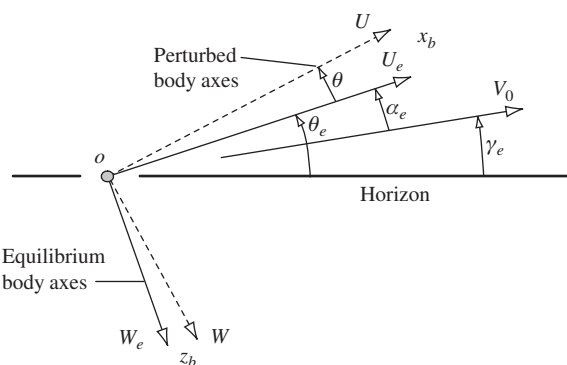
With reference to Fig. 2.4, the steady velocity vector V_0 defines the flight path and γ_e is the steady flight path angle. As before, α_e is the steady body incidence and θ_e is the steady pitch

Table 2.1 Summary of Motion Variables

	Trimmed Equilibrium			Perturbed		
Aircraft axis	ox	oy	oz	ox	oy	oz
Force	0	0	0	X	Y	Z
Moment	0	0	0	L	M	N
Linear velocity	U_e	V_e	W_e	U	V	W
Angular velocity	0	0	0	p	q	r
Attitude	0	θ_e	0	ϕ	θ	ψ

Table 2.2 Perturbation Variables

X	Axial “drag” force	Sum of the components of aerodynamic, thrust and weight forces
Y	Side force	
Z	Normal “lift” force	
L	Rolling moment	Sum of the components of aerodynamic, thrust and weight moments
M	Pitching moment	
N	Yawing moment	
p	Roll rate	Components of angular velocity
q	Pitch rate	
r	Yaw rate	
U	Axial velocity	Total linear velocity components of the <i>cg</i>
V	Lateral velocity	
W	Normal velocity	

**FIGURE 2.4** Generalised body axes in symmetric flight.

attitude of the aircraft. The relative angular change in a perturbation is also shown in Fig. 2.4, where it is implied that the axes have moved with the airframe and the motion is viewed at some instant during the disturbance. Thus the steady flight path angle is given by

$$\gamma_e = \theta_e - \alpha_e \quad (2.2)$$

In the case when the aircraft-fixed axes are wind axes rather than body axes, then

$$\alpha_e = 0 \quad (2.3)$$

and in the special case when the axes are wind axes and the initial condition is level flight,

$$\alpha_e = \theta_e = 0 \quad (2.4)$$

It is also useful to note that the perturbation in pitch attitude θ and the perturbation in body incidence α are the same, so it is convenient to write

$$\tan(\alpha_e + \theta) \equiv \tan(\alpha_e + \alpha) = \frac{W}{U} \equiv \frac{W_e + w}{U_e + u} \quad (2.5)$$

2.2.5 Choice of axes

Having reviewed the definition of aircraft-fixed axis systems, an obvious question must be: *When is it appropriate to use wind axes and when is it appropriate to use body axes?* The answer to this question depends on the use to which the equations of motion are to be put. The best choice of axes simply facilitates the analysis of the equations of motion. When starting from first principles, it is preferable to use generalised body axes since the resulting equations can serve for most applications. It is then reasonably straightforward to simplify the equations to a wind axis form if the application warrants it. On the other hand, to extend wind axis-based equations to serve the more general case is not as easy.

When dealing with numerical data for an existing aircraft, it is not always obvious which axis system has been used in the derivation of the model. However, by reference to equation (2.3) or (2.4) and the quoted values of α_e and θ_e , the system used should become clear.

When it is necessary to make experimental measurements in an actual aircraft, or in a model, which are to be used subsequently in the equations of motion, it is preferable to use a generalised body axis system. Since the measuring equipment is installed in the aircraft, its location is precisely known in terms of body axis coordinates, which therefore determines the best choice of axis system. In a similar way, most aerodynamic measurements and computations are referenced to the free stream velocity vector. For example, in wind tunnel work the obvious reference is the tunnel axis which is coincident with the velocity vector. Thus, for aerodynamic investigations involving the equations of motion, a wind axis reference is preferred. Traditionally, all aerodynamic data for use in the equations of motion are referenced to wind axes.

To summarise, it is not particularly important which axis system is chosen provided it models the flight condition to be investigated; the end result does not depend on this choice. However, when compiling data for use in the aircraft equations of motion, it is quite common for some data to be referred to wind axes and for some to be referred to body axes. It therefore becomes necessary to have available the mathematical tools for transforming data between different reference axes.

2.3 Euler angles and aircraft attitude

The angles defined by the right-handed rotation about the three axes of a right-handed system of axes are called *Euler angles*. The sense of the rotations and the order in which they are considered about the three axes are, in turn, very important because angles do not obey the commutative law. The attitude of an aircraft is defined as the angular orientation of the airframe-fixed axes with respect to earth axes. Attitude angles are therefore a particular application of Euler angles. With reference to Fig. 2.5, $(ox_0y_0z_0)$ are datum or reference axes and $(ox_3y_3z_3)$ are aircraft-fixed axes, either generalised body axes or wind axes. The attitude of the aircraft, with respect to the datum axes, may be established by considering the rotation about each axis in turn required to bring $(ox_3y_3z_3)$ into coincidence with $(ox_0y_0z_0)$. Thus, first rotate about ox_3 through the *roll* angle ϕ to $(ox_2y_2z_2)$. Second, rotate about oy_2 through the *pitch* angle θ to $(ox_1y_1z_1)$. Third, rotate about oz_1 through the *yaw* angle ψ to $(ox_0y_0z_0)$. Clearly, when the attitude of the aircraft is considered with respect to earth axes, $(ox_0y_0z_0)$ and $(ox_Ey_Ez_E)$ are coincident.

2.4 Axes transformations

It is frequently necessary to transform motion variables and other parameters from one system of axes to another. Clearly, the angular relationships used to describe attitude may be generalised to describe the angular orientation of one set of axes with respect to another. A typical example might be to transform components of linear velocity from wind axes to body axes. Thus, with reference to Fig. 2.5, $(ox_0y_0z_0)$ may be used to describe the velocity components in wind axes and $(ox_3y_3z_3)$ may be used to describe the components of velocity in body axes; the angles (ϕ, θ, ψ) then describe the generalised angular orientation of one set of axes with respect to the other. It is usual to retain the

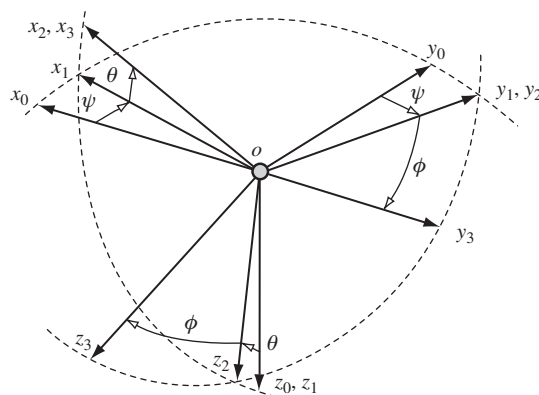


FIGURE 2.5 Euler angles.

angular description of *roll*, *pitch*, and *yaw*, although the angles do not necessarily describe attitude strictly in accordance with the definition given in [Section 2.3](#).

2.4.1 Linear quantities transformation

As an example, let (ox_3, oy_3, oz_3) represent components of a linear quantity in the axis system $(ox_3y_3z_3)$, and let (ox_0, oy_0, oz_0) represent components of the same linear quantity transformed into the axis system $(ox_0y_0z_0)$. The linear quantities of interest might be acceleration, velocity, displacement, and so forth. Resolving through each rotation in turn and in the correct order, then, with reference to [Fig. 2.5](#) it may be shown that, after *rolling* about ox_3 through the angle ϕ ,

$$\begin{aligned} ox_3 &= ox_2 \\ oy_3 &= oy_2 \cos \phi + oz_2 \sin \phi \\ oz_3 &= -oy_2 \sin \phi + oz_2 \cos \phi \end{aligned} \quad (2.6)$$

Alternatively, writing [equations \(2.6\)](#) in the more convenient matrix form,

$$\begin{bmatrix} ox_3 \\ oy_3 \\ oz_3 \end{bmatrix} = \begin{bmatrix} 1 & 0 & 0 \\ 0 & \cos \phi & \sin \phi \\ 0 & -\sin \phi & \cos \phi \end{bmatrix} \begin{bmatrix} ox_2 \\ oy_2 \\ oz_2 \end{bmatrix} \quad (2.7)$$

Similarly, after *pitching* about oy_2 through the angle θ ,

$$\begin{bmatrix} ox_2 \\ oy_2 \\ oz_2 \end{bmatrix} = \begin{bmatrix} \cos \theta & 0 & -\sin \theta \\ 0 & 1 & 0 \\ \sin \theta & 0 & \cos \theta \end{bmatrix} \begin{bmatrix} ox_1 \\ oy_1 \\ oz_1 \end{bmatrix} \quad (2.8)$$

and after *yawing* about oz_1 through the angle ψ ,

$$\begin{bmatrix} ox_1 \\ oy_1 \\ oz_1 \end{bmatrix} = \begin{bmatrix} \cos \psi & \sin \psi & 0 \\ -\sin \psi & \cos \psi & 0 \\ 0 & 0 & 1 \end{bmatrix} \begin{bmatrix} ox_0 \\ oy_0 \\ oz_0 \end{bmatrix} \quad (2.9)$$

By repeated substitution, [equations \(2.7\), \(2.8\), and \(2.9\)](#) may be combined to give the required transformation relationship:

$$\begin{bmatrix} ox_3 \\ oy_3 \\ oz_3 \end{bmatrix} = \begin{bmatrix} 1 & 0 & 0 \\ 0 & \cos \phi & \sin \phi \\ 0 & -\sin \phi & \cos \phi \end{bmatrix} \begin{bmatrix} \cos \theta & 0 & -\sin \theta \\ 0 & 1 & 0 \\ \sin \theta & 0 & \cos \theta \end{bmatrix} \begin{bmatrix} \cos \psi & \sin \psi & 0 \\ -\sin \psi & \cos \psi & 0 \\ 0 & 0 & 1 \end{bmatrix} \begin{bmatrix} ox_0 \\ oy_0 \\ oz_0 \end{bmatrix} \quad (2.10)$$

or

$$\begin{bmatrix} ox_3 \\ oy_3 \\ oz_3 \end{bmatrix} = \mathbf{D} \begin{bmatrix} ox_0 \\ oy_0 \\ oz_0 \end{bmatrix} \quad (2.11)$$

where the *direction cosine matrix* \mathbf{D} is given by

$$\mathbf{D} = \begin{bmatrix} \cos \theta \cos \psi & \cos \theta \sin \psi & -\sin \theta \\ \sin \phi \sin \theta \cos \psi & \sin \phi \sin \theta \sin \psi & \sin \phi \cos \theta \\ -\cos \phi \sin \psi & +\cos \phi \cos \psi & \\ \cos \phi \sin \theta \cos \psi & \cos \phi \sin \theta \sin \psi & \cos \phi \cos \theta \\ +\sin \phi \sin \psi & -\sin \phi \cos \psi & \end{bmatrix} \quad (2.12)$$

As shown, equation (2.11) transforms linear quantities from $(ox_0y_0z_0)$ to $(ox_3y_3z_3)$. By inverting the direction cosine matrix \mathbf{D} , the transformation from $(ox_3y_3z_3)$ to $(ox_0y_0z_0)$ is obtained:

$$\begin{bmatrix} ox_0 \\ oy_0 \\ oz_0 \end{bmatrix} = \mathbf{D}^{-1} \begin{bmatrix} ox_3 \\ oy_3 \\ oz_3 \end{bmatrix} \quad (2.13)$$

EXAMPLE 2.1

To illustrate the use of equation (2.11), consider the very simple example in which it is required to resolve the velocity of the aircraft through both the incidence angle and the sideslip angle into aircraft axes. The situation prevailing is assumed to be steady and is shown in Fig. 2.6.

The axes $(oxyz)$ are generalised aircraft body axes with velocity components U_e , V_e , and W_e , respectively. The free stream velocity vector is V_0 , and the angles of incidence and sideslip are α_e and β_e , respectively. With reference to equation (2.11), axes $(oxyz)$ correspond with axes $(ox_3y_3z_3)$ and V_0 corresponds with ox_0 of axes $(ox_0y_0z_0)$. Therefore, the following vector substitutions may be made:

$$(ox_0, oy_0, oz_0) = (V_0, 0, 0) \text{ and } (ox_3, oy_3, oz_3) = (U_e, V_e, W_e)$$

The angular correspondence means that the following substitution may be made:

$$(\phi, \theta, \psi) = (0, \alpha_e, -\beta_e)$$

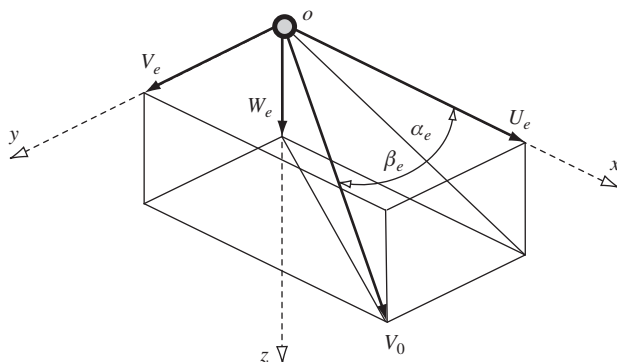


FIGURE 2.6 Resolution of velocity through incidence and sideslip angles.

Note that a positive sideslip angle is equivalent to a negative yaw angle. Thus, making the substitutions in [equation \(2.9\)](#),

$$\begin{bmatrix} U_e \\ V_e \\ W_e \end{bmatrix} = \begin{bmatrix} \cos \alpha_e \cos \beta_e & -\cos \alpha_e \sin \beta_e & -\sin \alpha_e \\ \sin \beta_e & \cos \beta_e & 0 \\ \sin \alpha_e \cos \beta_e & -\sin \alpha_e \sin \beta_e & \cos \alpha_e \end{bmatrix} \begin{bmatrix} V_0 \\ 0 \\ 0 \end{bmatrix} \quad (2.14)$$

Whence, equivalently,

$$\begin{aligned} U_e &= V_0 \cos \alpha_e \cos \beta_e \\ V_e &= V_0 \sin \beta_e \\ W_e &= V_0 \sin \alpha_e \cos \beta_e \end{aligned} \quad (2.15)$$

EXAMPLE 2.2

Another very useful application of the direction cosine matrix is to calculate height perturbations in terms of aircraft motion. [Equation \(2.13\)](#) may be used to relate the velocity components in aircraft axes to the corresponding components in earth axes as follows:

$$\begin{bmatrix} U_E \\ V_E \\ W_E \end{bmatrix} = \mathbf{D}^{-1} \begin{bmatrix} U \\ V \\ W \end{bmatrix} = \begin{bmatrix} \cos \psi \cos \theta & \cos \psi \sin \theta \sin \phi & \cos \psi \sin \theta \cos \phi \\ -\sin \psi \cos \phi & +\sin \psi \sin \phi & \\ \sin \psi \cos \theta & \sin \psi \sin \theta \sin \phi & \sin \psi \sin \theta \cos \phi \\ +\cos \psi \cos \phi & -\cos \psi \sin \phi & \\ -\sin \theta & \cos \theta \sin \phi & \cos \theta \cos \phi \end{bmatrix} \begin{bmatrix} U \\ V \\ W \end{bmatrix} \quad (2.16)$$

where, U_E , V_E , and W_E are the perturbed total velocity components referred to earth axes. Now, since height is measured positive in the “upward” direction, the rate of change of height due to the perturbation in aircraft motion is given by

$$\dot{h} = -W_E$$

Whence, from [equation \(2.16\)](#),

$$\dot{h} = U \sin \theta - V \cos \theta \sin \phi - W \cos \theta \cos \phi \quad (2.17)$$

2.4.2 Angular velocities transformation

Probably the most useful angular quantities transformation relates the angular velocities p, q, r of the aircraft-fixed axes to the resolved components of angular velocity, the attitude rates $\dot{\phi}, \dot{\theta}, \dot{\psi}$ with respect to datum axes. The easiest way to deal with the algebra of this transformation whilst retaining a good grasp of the physical implications is to superimpose the angular rate vectors onto the axes shown in [Fig. 2.5](#); the result of this is shown in [Fig. 2.7](#).

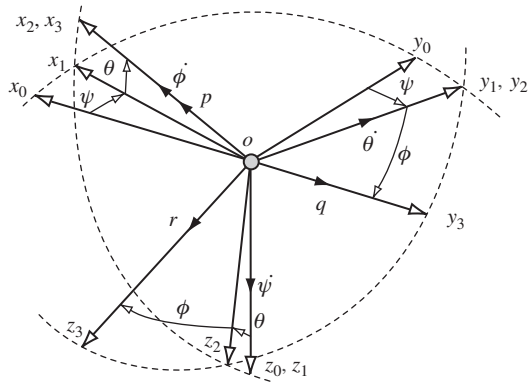


FIGURE 2.7 Angular rates transformation.

The angular *body rates* p, q, r are shown in the aircraft axes ($ox_3y_3z_3$), then, considering each rotation in turn necessary to bring the aircraft axes into coincidence with the datum axes ($ox_0y_0z_0$). First, *roll* about ox_3 through the angle ϕ with angular velocity $\dot{\phi}$. Second, *pitch* about oy_2 through the angle θ with angular velocity $\dot{\theta}$. Third, *yaw* about oz_1 through the angle ψ with angular velocity $\dot{\psi}$. Again, it is most useful to refer the attitude rates to earth axes, in which case datum axes ($ox_0y_0z_0$) are coincident with earth axes ($o_{EX}E_yE_zE$). The *attitude rate* vectors are clearly shown in Fig. 2.7. The relationship between the aircraft body rates and the attitude rates, referred to datum axes, is readily established as follows:

Roll rate p is equal to the sum of the components of $\dot{\phi}, \dot{\theta}, \dot{\psi}$ resolved along ox_3 :

$$p = \dot{\phi} - \dot{\psi} \sin \theta \quad (2.18)$$

Pitch rate q is equal to the sum of the components of $\dot{\phi}, \dot{\theta}, \dot{\psi}$ resolved along oy_3 :

$$q = \dot{\theta} \cos \phi + \dot{\psi} \sin \phi \cos \theta \quad (2.19)$$

Yaw rate r is equal to the sum of the components of $\dot{\phi}, \dot{\theta}, \dot{\psi}$ resolved along oz_3 :

$$r = \dot{\psi} \cos \phi \cos \theta - \dot{\theta} \sin \phi \quad (2.20)$$

Equations (2.18), (2.19), and (2.20) may be combined into the convenient matrix notation

$$\begin{bmatrix} p \\ q \\ r \end{bmatrix} = \begin{bmatrix} 1 & 0 & -\sin \theta \\ 0 & \cos \phi & \sin \phi \cos \theta \\ 0 & -\sin \phi & \cos \phi \cos \theta \end{bmatrix} \begin{bmatrix} \dot{\phi} \\ \dot{\theta} \\ \dot{\psi} \end{bmatrix} \quad (2.21)$$

and the inverse of equation (2.21) is

$$\begin{bmatrix} \dot{\phi} \\ \dot{\theta} \\ \dot{\psi} \end{bmatrix} = \begin{bmatrix} 1 & \sin \phi \tan \theta & \cos \phi \tan \theta \\ 0 & \cos \phi & -\sin \phi \\ 0 & \sin \phi \sec \theta & \cos \phi \sec \theta \end{bmatrix} \begin{bmatrix} p \\ q \\ r \end{bmatrix} \quad (2.22)$$

When the aircraft perturbations are small, such that (ϕ, θ, ψ) may be treated as small angles, equations (2.21) and (2.22) may be approximated by

$$\begin{aligned} p &= \dot{\phi} \\ q &= \dot{\theta} \\ r &= \dot{\psi} \end{aligned} \quad (2.23)$$

EXAMPLE 2.3

To illustrate the use of the angular velocities transformation, consider the situation when an aircraft is flying in a steady level coordinated turn at a speed of 250 m/s at a bank angle of 60° . It is required to calculate the turn rate $\dot{\psi}$, the yaw rate r , and the pitch rate q . The forces acting on the aircraft are shown in Fig. 2.8.

By resolving the forces acting on the aircraft vertically and horizontally, and eliminating the lift L between the two resulting equations, it is easily shown that the radius of turn is given by

$$R = \frac{V_0^2}{g \tan \phi} \quad (2.24)$$

The time to complete one turn is given by

$$t = \frac{2\pi R}{V_0} = \frac{2\pi V_0}{g \tan \phi} \quad (2.25)$$

Therefore, the rate of turn is given by

$$\dot{\psi} = \frac{2\pi}{t} = \frac{g \tan \phi}{V_0} \quad (2.26)$$

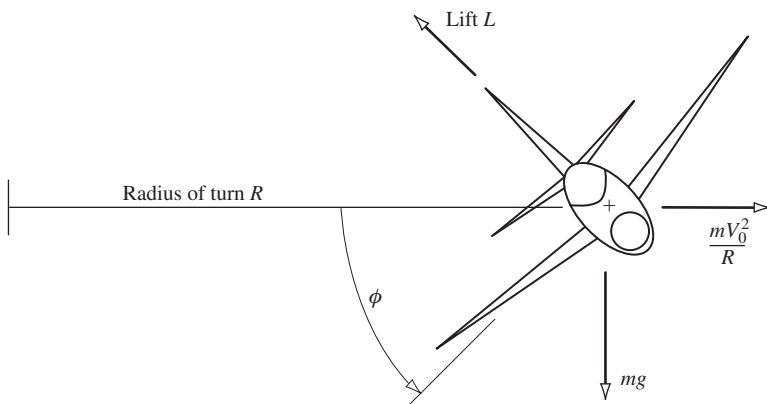


FIGURE 2.8 Aircraft in a steady banked turn.

Thus $\dot{\psi} = 0.068 \text{ rad/s}$. For the conditions applying to the turn, $\dot{\phi} = \dot{\theta} = \theta = 0$ and thus [equation \(2.21\)](#) may now be used to find the values of r and q :

$$\begin{bmatrix} p \\ q \\ r \end{bmatrix} = \begin{bmatrix} 1 & 0 & 0 \\ 0 & \cos 60^\circ & \sin 60^\circ \\ 0 & -\sin 60^\circ & \cos 60^\circ \end{bmatrix} \begin{bmatrix} 0 \\ 0 \\ \dot{\psi} \end{bmatrix}$$

Therefore, $p = 0$, $q = 0.059 \text{ rad/s}$, and $r = 0.034 \text{ rad/s}$. Note that p , q , and r are the angular velocities that would be measured by rate gyros fixed in the aircraft with their sensitive axes aligned with the ox , oy , and oz aircraft axes, respectively.

2.5 Aircraft reference geometry

A description of the geometric layout of an aircraft is an essential part of the mathematical modelling process. For the purposes of flight dynamics analysis, it is convenient that the geometry of the aircraft can be adequately described by a small number of dimensional reference parameters, which are defined next and illustrated in [Fig. 2.9](#).

2.5.1 Wing area

The reference area is usually the gross plan area of the wing, including that part within the fuselage, and is denoted S , where

$$S = b\bar{c} \quad (2.27)$$

b is the wing span, and \bar{c} is the standard mean chord of the wing.

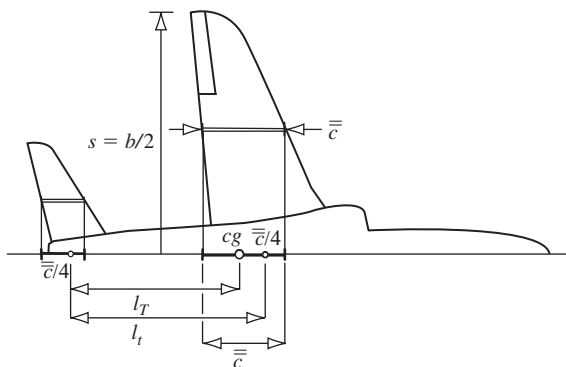


FIGURE 2.9 Longitudinal reference geometry.

2.5.2 Mean aerodynamic chord

The *mean aerodynamic chord* of the wing (*mac*) is denoted \bar{c} and is defined as

$$\bar{c} = \frac{\int_{-s}^s c_y^2 dy}{\int_{-s}^s c_y dy} \quad (2.28)$$

The reference *mac* is located on the centre line of the aircraft by projecting \bar{c} from its spanwise location as shown in Fig. 2.9.

For a swept wing, then, the leading edge of the *mac* lies aft of the leading edge of the root chord of the wing. The *mac* represents the location of the root chord of a rectangular wing that has the same aerodynamic influence on the aircraft as the actual wing. Traditionally, the *mac* is used in stability and control studies since a number of important aerodynamic reference centres are located on it.

2.5.3 Standard mean chord

The *standard mean chord* of the wing (*smc*) is effectively the same as the geometric mean chord and is denoted \bar{c} . For a wing of symmetric planform it is defined as

$$\bar{c} = \frac{\int_{-s}^s c_y dy}{\int_{-s}^s dy} \quad (2.29)$$

where $s = b/2$ is the semi-span and c_y is the local chord at spanwise coordinate y . For a straight tapered wing, equation (2.29) simplifies to

$$\bar{c} = \frac{S}{b} \quad (2.30)$$

The reference *smc* is located on the centre line of the aircraft by projecting \bar{c} from its spanwise location in the same way that the *mac* is located. Thus for a swept wing the leading edge of the *smc* also lies aft of the leading edge of the root chord of the wing. The *smc* is the mean chord preferred by aircraft designers since it relates very simply to the geometry of the aircraft. For most aircraft the *smc* and *mac* are sufficiently similar in length and location to be practically interchangeable. It is quite common to find references that quote a mean chord without specifying *smc* or *mac*. This is not good practice, although the error incurred by assuming the wrong chord is rarely serious. However, the reference chord used in any application should always be clearly defined at the outset.

2.5.4 Aspect ratio

The aspect ratio of the aircraft wing is a measure of its spanwise slenderness and is denoted A . It is defined as follows:

$$A = \frac{b^2}{S} = \frac{b}{\bar{c}} \quad (2.31)$$

2.5.5 Location of centre of gravity

The centre of gravity of an aircraft, cg , is usually located on the reference chord as indicated in Fig. 2.9. Its position is quoted as a fraction of \bar{c} (or c), denoted h , and is measured from the leading edge of the reference chord as shown. The cg position varies as a function of aircraft loading; the typical variation is in the range of 10% to 40% of \bar{c} or, equivalently, $0.1 \leq h \leq 0.4$.

2.5.6 Tail moment arm and tail volume ratio

The *mac* of the horizontal tailplane, or foreplane, is defined and located in the airframe in the same way as the *mac* of the wing, as indicated in Fig. 2.9. The wing and tailplane aerodynamic forces and moments are assumed to act at their respective aerodynamic centres, which, to a good approximation, lie at the quarter-chord points of the *mac* of the wing and tailplane, respectively. The tail moment arm l_T is defined as the longitudinal distance between the centre of gravity and the aerodynamic centre of the tailplane, as shown in Fig. 2.9. The *tail volume ratio* \bar{V}_T is an important geometric parameter and is defined as

$$\bar{V}_T = \frac{S_T l_T}{\bar{S} \bar{c}} \quad (2.32)$$

where S_T is the gross area of the tailplane and *mac* \bar{c} is the longitudinal reference length. Typically, the tail volume ratio has a value in the range $0.5 \leq \bar{V}_T \leq 1.3$ and is a measure of the aerodynamic effectiveness of the tailplane as a stabilising device.

Sometimes, especially in stability and control studies, it is convenient to measure the longitudinal tail moment about the aerodynamic centre of the wing *mac*. In this case the tail moment arm is denoted l_t , as shown in Fig. 2.9, and a slightly modified tail volume ratio is defined.

2.5.7 Fin moment arm and fin volume ratio

The *mac* of the fin is defined and located in the airframe in the same way as the *mac* of the wing, as indicated in Fig. 2.10. As for the tailplane, the fin moment arm l_F is defined as the longitudinal distance between the centre of gravity and the aerodynamic centre of the fin, as shown in Fig. 2.10. The *fin volume ratio* \bar{V}_F is an important geometric parameter and is defined as

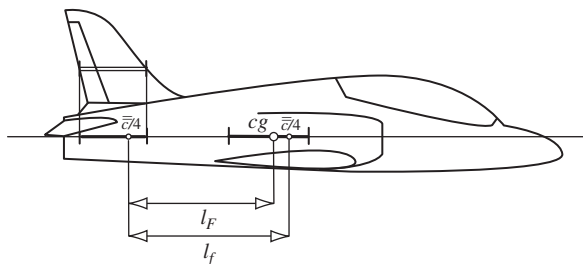


FIGURE 2.10 Fin moment arm.

$$\overline{V}_F = \frac{S_F l_F}{Sb} \quad (2.33)$$

where S_F is the gross area of the fin and the wing span b is the lateral-directional reference length. Again, the fin volume ratio is a measure of the aerodynamic effectiveness of the fin as a directional stabilising device.

As stated previously, it is sometimes convenient to measure the longitudinal moment of the aerodynamic forces acting at the fin about the aerodynamic centre of the wing *mac*. In this case the fin moment arm is denoted l_f , as shown in Fig. 2.10.

2.6 Controls notation

The definition of the sense of controls and pilot control actions is often vague at best, and so it is appropriate to review the commonly accepted notation for aerodynamic and propulsion controls.

2.6.1 Aerodynamic controls

Sometimes there appears to be some confusion with respect to the correct notation for aerodynamic controls, especially when unconventional control surfaces are used. Hopkin (1970) defines a notation which is intended to be generally applicable, but, since a very large number of combinations of control motivators are possible, the notation relating to control interceptors may become ill defined and hence application-dependent. However, for the conventional aircraft there is a universally accepted notation, which accords with Hopkin, and it is simple to apply. Generally, a positive *control action* by the pilot gives rise to a positive aircraft response, whereas a positive *control surface displacement* gives rise to a negative aircraft response. Thus

In roll: positive right push force on the stick \Rightarrow positive stick displacement \Rightarrow right aileron up and left aileron down (negative mean) \Rightarrow right wing down roll response (positive).

In pitch: positive pull force on the stick \Rightarrow positive aft stick displacement \Rightarrow elevator trailing edge up (negative) \Rightarrow nose-up pitch response (positive).

In yaw: positive push force on the right rudder pedal \Rightarrow positive rudder bar displacement \Rightarrow rudder trailing edge displaced to the right (negative) \Rightarrow nose to the right yaw response (positive).

Roll and pitch control stick displacements are denoted δ_ξ and δ_η , respectively, and rudder pedal displacement is denoted δ_ζ . Aileron, elevator, and rudder surface displacements are denoted ξ , η , and ζ , respectively, as indicated in Fig. 2.11. It should be noted that since ailerons act differentially, the displacement ξ is usually taken as the mean value of the separate displacements of each aileron.

2.6.2 Engine control

Engine thrust τ is controlled by throttle lever displacement ε . Positive throttle lever displacement is usually in the forward push sense and results in a positive increase in thrust. For a turbojet engine the relationship between thrust and throttle lever angle is approximated by a simple first-order lag transfer function,

$$\frac{\tau(s)}{\varepsilon(s)} = \frac{k_\tau}{(1 + sT_\tau)} \quad (2.34)$$

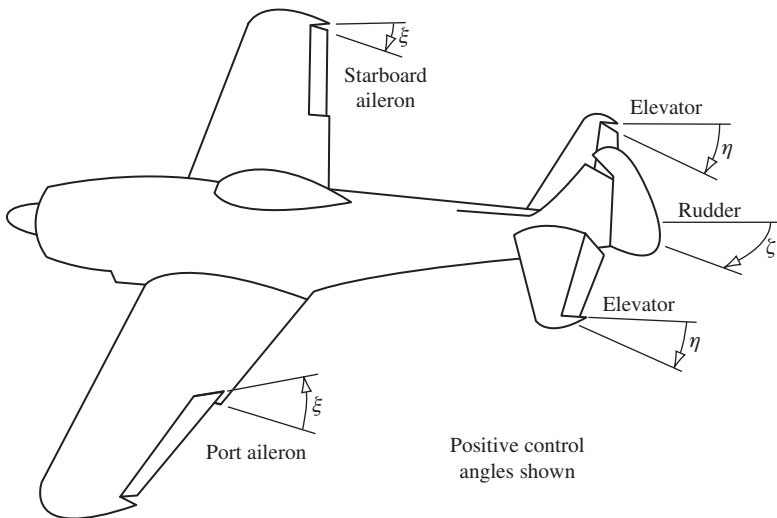


FIGURE 2.11 Aerodynamic controls notation.

where k_τ is a suitable gain constant and T_τ is the lag time constant, which is typically of the order of two to three seconds.

2.7 Aerodynamic reference centres

With reference to Fig. 2.12, the *centre of pressure* of an aerofoil, wing, or complete aircraft, cp , is the point at which the resultant aerodynamic force F acts. It is usual to resolve the force into the *lift* component perpendicular to the velocity vector and the *drag* component parallel to the velocity vector, denoted L and D , respectively, in the usual way. The cp is located on the *mac* and thereby determines an important aerodynamic reference centre.

Simple theory establishes that the resultant aerodynamic force F generated by an aerofoil comprises two components—that due to camber F_c and that due to angle of attack F_α —both of which resolve into lift and drag forces as indicated. The aerodynamic force due to camber is constant and acts at the midpoint of the aerofoil chord; for a symmetric aerofoil section this force is zero. The aerodynamic force due to angle of attack acts at the quarter-chord point and varies directly with angle of attack at angles below the stall. This also explains why the zero-lift angle of attack of a cambered aerofoil is usually a small negative value because, in this condition, the lift due to camber is equal and opposite to the lift due to angle of attack. Thus at low speeds, when the angle of attack is generally large, most of the aerodynamic force is due to the angle of attack-dependent contribution and cp is nearer to the quarter-chord point.

On the other hand, at high speeds, when the angle of attack is generally small, a larger contribution to the aerodynamic force is due to the camber-dependent component and cp is nearer to the

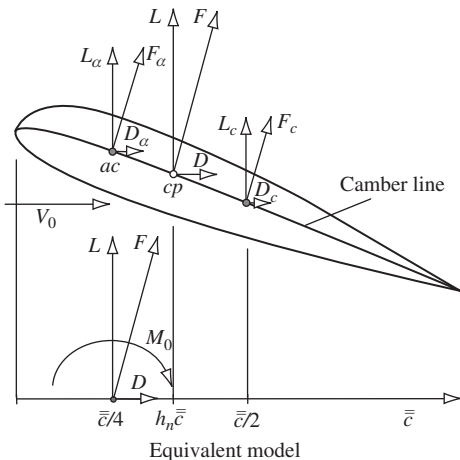


FIGURE 2.12 Aerodynamic reference centres.

midpoint of the chord. Thus, in the limit, the aerofoil *cp* generally lies between the quarter-chord and mid-chord points. More generally, the interpretation for an aircraft recognises that *cp* moves as a function of angle of attack, Mach number, and configuration. For example, at low angles of attack and high Mach numbers, *cp* tends to move aft and vice versa. Consequently, *cp* is of limited use as an aerodynamic reference point in stability and control studies. It should be noted that the *cp* of the complete aircraft in trimmed-equilibrium flight corresponds to the *controls-fixed neutral point* $h_n \bar{c}$, which is discussed in Chapter 3.

If, instead of *cp*, another *fixed* point on the *mac* is chosen as an aerodynamic reference point, at this point the total aerodynamic force remains the same but is accompanied by a pitching moment about the point. Clearly, the most convenient reference point on the *mac* is the quarter-chord point since the pitching moment is the moment of the aerodynamic force due to camber and remains constant with variation in angle of attack. This point is called the *aerodynamic centre*, denoted *ac*, which at low Mach numbers lies at, or very close to, the quarter-chord point $\bar{c}/4$. It is for this reason that *ac*, or equivalently the quarter-chord point of the reference chord, is preferred as a reference point. The corresponding equivalent aerofoil model is shown in Fig. 2.12. Since *ac* remains essentially fixed in position during small perturbations about a given flight condition, and since the pitching moment is nominally constant about the *ac*, it is used as a reference point in stability and control studies. It is important to appreciate the fact that, as the flight condition Mach number is increased, the *ac* moves aft; in supersonic-flow conditions it is located at, or very near, $\bar{c}/2$.

The definition of aerodynamic centre given above applies most strictly to the location of the *ac* on the chord of an aerofoil. However, it also applies reasonably well to the location of the *ac* on the *mac* of a wing and is used extensively for locating the *ac* on the *mac* of a wing-body combination without too much loss of validity. It should be appreciated that the complex aerodynamics of a wing-body combination might result in an *ac* location which is not at the quarter-chord point, although typically it would not be too far removed from that point.

References

- ESDU (1987). *Introduction to aerodynamic derivatives, equations of motion and stability*, Stability of Aircraft. Engineering Sciences Data (Vol. 9a, Data Item No. 86021, Aerodynamics Series). Bracknell, UK: ESDU International Ltd. London. www.esdu.com.
- Etkin, B. (1972). *Dynamics of atmospheric flight*. New York: John Wiley and Sons, Inc.
- Hopkin, H. R. (1970). *A scheme of notation and nomenclature for aircraft dynamics and associated aerodynamics*. Aeronautical Research Council, Reports and Memoranda No. 3562. Her Majesty's Stationery Office, London.
- McRuer, D., Ashkenas, I., & Graham, D. (1973). *Aircraft dynamics and automatic control*. Princeton, NJ: Princeton University Press.

PROBLEMS

- 2.1** A tailless aircraft of 9072 kg mass has a delta wing with aspect ratio 1 and area 37 m^2 . Show that the aerodynamic mean chord of a delta wing,

$$\bar{c} = \frac{\int_0^{\frac{b}{2}} c^2 dy}{\int_0^{\frac{b}{2}} c dy}$$

is two-thirds of its root chord and that for this wing it is 5.73 m.

(CU 1983)

- 2.2** With the aid of a diagram, describe the axis systems used in aircraft stability and control analysis. State the conditions under which each axis system might be preferred.

(CU 1982)

- 2.3** Show that, in a longitudinal symmetric small perturbation, the components of aircraft weight resolved into the ox and oz axes are given by

$$\begin{aligned} X_g &= -mg\theta \cos \theta_e - mg \sin \theta_e \\ Z_g &= mg \cos \theta_e - mg\theta \sin \theta_e \end{aligned}$$

where θ is the perturbation in pitch attitude and θ_e is the equilibrium pitch attitude.

(CU 1982)

- 2.4** With the aid of a diagram showing a generalised set of aircraft body axes, define the parameter notation used in the mathematical modelling of aircraft motion.

(CU 1982)

- 2.5** In the context of aircraft motion, what are the Euler angles? If the standard right-handed aircraft axis set is rotated through pitch θ and yaw ψ angles only, show that the initial vector quantity (x_0, y_0, z_0) is related to the transformed vector quantity (x, y, z) as follows:

$$\begin{bmatrix} x \\ y \\ z \end{bmatrix} = \begin{bmatrix} \cos \theta \cos \psi & \cos \theta \sin \psi & -\sin \theta \\ -\sin \psi & \cos \psi & 0 \\ \sin \theta \cos \psi & \sin \theta \sin \psi & \cos \theta \end{bmatrix} \begin{bmatrix} x_0 \\ y_0 \\ z_0 \end{bmatrix}$$

(CU 1982)

- 2.6** Define the span, gross area, aspect ratio, and mean aerodynamic chord of an aircraft wing.
(CU 2001)
- 2.7** Distinguish between the centre of pressure and the aerodynamic centre of an aerofoil. Explain why the pitching moment about the quarter-chord point of an aerofoil is nominally constant in subsonic flight.
(CU 2001)

3

Static Equilibrium and Trim

3.1 Trim equilibrium

When considering the short term dynamic stability and control characteristics of an aircraft it is usual to refer the motion to a steady trimmed flight condition. An essential prerequisite, therefore, is to define trim and to set out the conditions for the aircraft to remain in stable equilibrium.

3.1.1 Preliminary considerations

In normal flight it is usual for the pilot to adjust the controls of an aircraft such that on release of the controls it continues to fly steadily at the chosen flight condition. By this means the pilot is relieved of the tedium of constantly adjusting control inputs to maintain equilibrium and of holding the associated control forces, which may be tiring. The aircraft is then said to be *trimmed*, and the trim state defines the initial equilibrium condition about which the dynamics of interest may be studied. All aircraft are equipped with a means for presetting, or adjusting, the *datum*, *equilibrium*, or *trim* setting of the primary control surfaces. The ailerons, elevator, and rudder are all fitted with *trim tabs* for this purpose, which in all but the simplest aircraft may be adjusted from the cockpit in flight. However, all aircraft are fitted with a continuously adjustable elevator trim tab for the maintenance of longitudinal trim, which is continuously variable with flight condition.

It is an essential requirement that an aircraft must be stable if it is to remain in equilibrium following trimming. In particular, the static stability characteristics about all three axes largely determine the *trimmability* of an aircraft, and the *degree* of static stability determines, in part, the pilot control actions required to establish trimmed equilibrium. Thus *stability* characteristics and *control* characteristics are completely interdependent and both are determined by the aerodynamic design of the aircraft and by the action of a control and stability augmentation system when fitted. Dynamic stability is also important, of course, and largely determines the characteristics of the transient motion following a disturbance about a trimmed flight condition.

The object of trimming is to bring the forces and moments acting on the aircraft into a state of balance, or equilibrium. That is the condition when the net axial, normal, and side forces, and the net roll, pitch, and yaw moments are all zero. The force balance is often expressed approximately as the requirement that the lift equal the weight and the thrust equal the drag since, by definition, the net side force must be zero in trimmed symmetric flight. Provided the aircraft is stable, it will then remain in equilibrium until it is disturbed by pilot control inputs or by external influences such as turbulence. The transient motion following such a disturbance is characterised by the dynamic stability characteristics, and the stable aircraft will eventually settle into its equilibrium state once more.

The maintenance of trimmed equilibrium requires the correct simultaneous adjustment of the main flight variables in all six degrees of freedom and is dependent on airspeed, or Mach number, flight path angle, airframe configuration, weight, and *cg* position. As these parameters change during the course of a typical flight, trim adjustments are made as necessary. Fortunately, the task of trimming an aircraft is not as challenging as it might at first seem. The symmetry of a typical airframe confers symmetric aerodynamic properties on the airframe, which usually reduces the task to that of longitudinal trim only. Lateral-directional trim adjustments are only likely to be required when the aerodynamic symmetry is lost as a result, for example, of loss of an engine in a multi-engined aircraft.

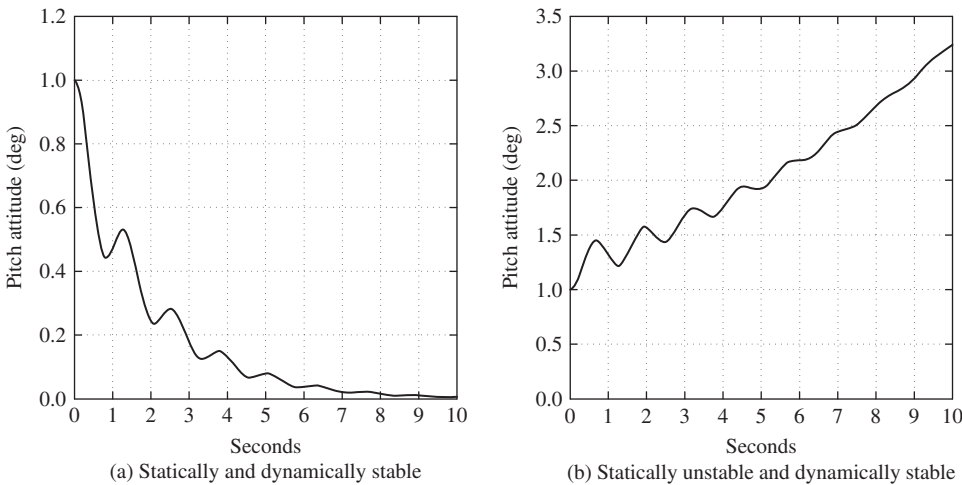
Lateral-directional stability is designed into most aircraft and ensures that in roll the aircraft remains *wings-level* and that in yaw it tends to *weathercock* into wind when the ailerons and rudder are at their zero or datum positions. Thus, under normal circumstances, the aircraft will naturally seek lateral-directional equilibrium without interference by the pilot. This applies even when significant changes are made to airspeed, configuration, weight, and *cg* position, for example, since the symmetry of the airframe is retained throughout. However, such variations in flight condition can lead to dramatic changes in longitudinal trim.

Longitudinal trim involves the simultaneous adjustment of elevator angle and thrust to give the required airspeed and flight path angle for a given airframe configuration. Equilibrium is achievable only if the aircraft is longitudinally stable, and the magnitude of the control action to trim depends on the *degree* of longitudinal static stability. Since the longitudinal flight condition is continuously variable, it is very important that trimmed equilibrium is possible at all conditions. For this reason, considerable emphasis is given to the problems of ensuring adequate longitudinal static stability and adequate longitudinal aerodynamic trim control. Because of its importance, the generic description *static stability and trim* is often interpreted to mean *longitudinal static stability and trim*.

The commonly used theory of longitudinal static stability was developed by [Gates and Lyon \(1944\)](#) and derives from a full static and dynamic stability analysis of the equations of motion of an aircraft. An excellent and accessible summary of the findings of Gates and Lyon is given in [Duncan \(1959\)](#) and in [Babister \(1961\)](#). In the interest of understanding and physical interpretation, the theory is often reduced to a linearised form that retains only the principal aerodynamic and configuration parameters. It is in this simplest form that the theory is reviewed here since it is only required as the basis on which to build the small-perturbation dynamics model. It is important to appreciate that, although the longitudinal static stability model is described only in terms of the aerodynamic properties of the airframe, the control and trim properties as seen by the pilot must conform to the same physical interpretation even when they are augmented by a flight control system. It is also important to recognise that static and dynamic stability are, in reality, inseparable. However, the separate treatment of static stability is a useful means for introducing the concept of stability insofar as it determines the control and trim characteristics of the aircraft.

3.1.2 Conditions for stability

The static stability of an aircraft is commonly interpreted to describe its tendency to converge on the initial equilibrium condition following a small disturbance from trim. Dynamic stability, on the other hand, describes the transient motion involved in the process of recovering equilibrium following the disturbance. [Fig. 3.1](#) includes two illustrations showing the effects of static stability and static instability in an otherwise dynamically stable aircraft. Following an initial disturbance

**FIGURE 3.1 Stability.**

displacement, in pitch for example, at time $t = 0$, the subsequent response time history is shown and is clearly dependent on the stability of the aircraft. It should be noted that damping of the dynamic oscillatory component of the responses shown was deliberately chosen to be low in order to best illustrate the static and dynamic stability characteristics.

In establishing trim equilibrium, the pilot adjusts the elevator angle and thrust to obtain a lift force sufficient to support the weight and thrust sufficient to balance the drag at the desired speed and flight path angle. Since the airframe is symmetric, the equilibrium side force is, of course, zero. Provided that the speed is above the minimum drag speed, the force balance will remain stable with speed. Therefore, the static stability of the aircraft reduces to a consideration of the effects of angular disturbances about the three axes. Following such a disturbance the aerodynamic forces and moments will no longer be in equilibrium, and in a statically stable aircraft the resultant moments will cause the aircraft to converge on its initial condition. The condition for an aircraft to be statically stable is therefore easily deduced.

Consider a positive incidence disturbance from equilibrium. This is in the nose-up sense and results in an increase in incidence α and hence in lift coefficient C_L . In a stable aircraft the resulting pitching moment must be restoring—that is, in the negative or nose-down sense. And, of course, the converse must be true following a nose-down disturbance. Thus the condition for longitudinal static stability may be determined by plotting the total aircraft pitching moment M or, equivalently, pitching moment coefficient C_m for variation in incidence α about the trim value α_e , as shown in Fig. 3.2. The nose-up disturbance increases α and takes the aircraft to the out-of-trim point p where the pitching moment coefficient becomes negative and is therefore restoring. This property describes the *pitch stiffness* of an aircraft. Clearly, a nose-down disturbance leads to a similar conclusion. As indicated, the aircraft is stable when the slope of this plot is negative. Thus the condition for stable longitudinal trim at incidence α_e may be expressed as

$$C_m = 0 \quad (3.1)$$

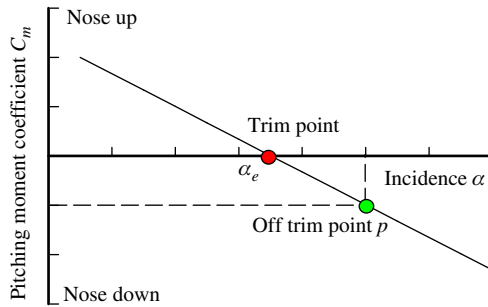


FIGURE 3.2 Pitching moment variation with incidence for a stable aircraft.

and

$$\frac{dC_m}{d\alpha} < 0 \quad (3.2)$$

The previous observation is strictly valid only when it is assumed that the aerodynamic force and moment coefficients are functions of incidence only. This is usually an acceptable approximation for subsonic aircraft and, indeed, the plot of total aircraft pitching moment coefficient against incidence may well be very nearly linear as shown in Fig. 3.2. However, this argument becomes increasingly inappropriate with increasing Mach number. As compressibility effects become significant, the aerodynamic force and moment coefficients become functions of both incidence and Mach number. When this occurs equation (3.2) may not always guarantee that stable trim can be achieved.

The rather more complex analysis by Gates and Lyon (1944) takes speed effects into account and defines a general requirement for longitudinal static stability as

$$\frac{dC_m}{dC_L} < 0 \quad (3.3)$$

For subsonic aircraft equations (3.2) and (3.3) are completely interchangeable since α and C_L are linearly, or very nearly linearly, related by the lift curve slope a .

Inspection of Fig. 3.2 indicates that it is not possible to achieve trim unless the zero-incidence ($\alpha = 0$) pitching moment coefficient for the aircraft is positive, which determines the additional constraint for a stable trimmable aircraft:

$$C_{m(\alpha=0)} > 0 \quad (3.4)$$

More generally, it is a requirement that the zero-lift ($C_L = 0$) pitching moment coefficient be positive as well for a trimmable aircraft:

$$C_{m(C_L=0)} > 0 \quad (3.5)$$

Now it is important to recognise that the pitching moment referred to in equations (3.4) and (3.5) is the *whole-aircraft* pitching moment, not to be confused with the *wing-body* zero-lift

($C_L = 0$) pitching moment coefficient, C_{m_0} , referred to in later sections of this chapter. The wing-body zero-lift pitching moment is assumed to be dominated by the aerodynamic properties of the wing, and for a typical wing having an aerofoil section with positive camber, C_{m_0} is negative. Thus, in order that the whole aircraft zero-lift pitching moment coefficient is positive, a tailplane is added and set at a local angle of attack sufficient to ensure stable trim over the operational flight envelope. An actual application is discussed in Example 3.1. Typically, a tailplane has a symmetric uncambered aerofoil section which contributes zero pitching moment at zero tail lift. Consequently, the tailplane contribution to total aircraft pitching moment is determined by its local angle of attack and by deflection of the elevator control surface only, and its magnitude is determined by the aerodynamic design choices relating to tail moment arm about the c_g and by tailplane area. This concept defines the basis for the detailed analysis of pitching moment set out in [Section 3.2](#).

The special case of tailless aircraft poses challenges if longitudinal static stability is to be achieved. Since a lifting wing requires an aerofoil section with positive camber, the problem of negative pitching moment remains. Without a tail surface it is possible, by careful placement of the c_g , to use the weight-lift moment to balance the inherent negative pitching moment, but it is usually only possible to achieve a satisfactory arrangement for a limited range of operating conditions. A more flexible arrangement involves the use of special aerofoil sections with reflex camber toward the trailing edge, which can significantly reduce the magnitude of the section pitching moment.

Alternative arrangements are sometimes encountered in which trailing edge flaps are used to provide the reflex camber aerodynamics. Variable reflex camber is exploited to the limit in the hang glider, and pilot weight-lift moment is used to trim the pitching moment using weight shift control. A comprehensive analysis of the longitudinal static stability of the flexible tailless hang glider is given by [Cook \(1994\)](#). In more advanced-technology aircraft an easier solution is to utilise the advantages of command and stability augmentation systems to establish a stable controllable vehicle. However, in this case it remains a fundamental requirement that the longitudinal aerodynamic controls are capable of generating the longitudinal pitching moment for trim, stability augmentation, and control.

3.1.3 Degree of longitudinal stability

It was shown earlier that the condition for an aircraft to possess longitudinal static stability at a given trim condition is that the gradient of the $C_m - \alpha$ plot be negative. Obviously, a very large range of values of the gradient is possible, and the magnitude of the gradient determines the *degree of stability* possessed by the aircraft. Variation in the degree of longitudinal static stability is illustrated in [Fig. 3.3](#). The degree of stability is described in terms of *stability margin*, which quantifies how much stability the aircraft has over and above zero or neutral stability. Thus, for example, the longitudinal static stability margin is directly related to the gradient of the $C_m - \alpha$ plot.

With reference to [Fig. 3.3](#), and for a given disturbance in α , it is clear that the corresponding restoring pitching moment C_m is greatest for a very stable aircraft. The magnitude of the restoring moment decreases as the degree of stability, or stability margin, is reduced and becomes zero at neutral stability. When the aircraft is unstable the moment is clearly of the opposite sign and is therefore divergent. Thus the higher the degree of stability, the greater the restoring moment following a disturbance. This means that a very stable aircraft has significant pitch stiffness and will

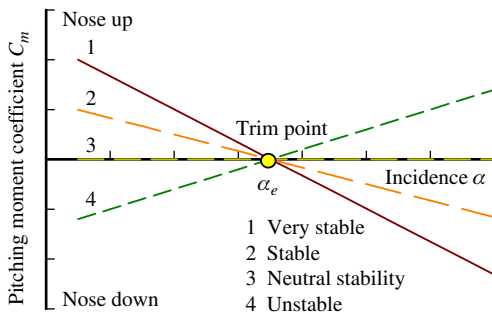


FIGURE 3.3 Degree of longitudinal static stability.

be very resistant to upset, which in turn means that greater control actions will be needed to encourage the aircraft to change its trim state or to manoeuvre. It follows, then, that the stability margins determine the magnitude of the control actions, quantified in terms of displacement and force, required to trim the aircraft. It is easy to appreciate that a consequence of this is that too much stability can be as hazardous as too little stability since the available control power is limited.

3.1.4 Variation in stability

Changes in the aerodynamic operating conditions of an aircraft which result in pitching moment changes inevitably lead to variation in longitudinal static stability. Such variation in stability is normally manifest as a nonlinear version of the C_m - C_L characteristic shown in Fig. 3.2. For the subsonic classical aircraft such changes are usually small and may result in some nonlinearity of the pitching moment characteristic with a change in trim. In general, the variation in the degree of stability is acceptably small. For the modern supersonic high-performance aircraft, the situation is not so well defined. Large flight envelopes and significant variation in flight condition can lead to dramatic changes in static stability. For example, it is possible for such an aircraft to be stable at some conditions and unstable at others. It is easy to see how such variations might arise in a physical sense, but it is much more difficult to describe the variations in mathematical terms. A brief review of some of the more obvious sources of variation in stability follows.

Power effects

Probably the most significant variation in longitudinal static stability arises from the effects of power. Direct effects result from the point of application and line of action of the thrust forces with respect to the *cg*. Clearly, as illustrated in Fig. 3.4, a high thrust line results in a nose-down pitching moment and vice versa. In normal trimmed flight the thrust moment is additive to the aerodynamic moment, and the total pitching moment is trimmed to zero by adjustment of the elevator. However, any aerodynamic perturbation about trim which results in a thrust perturbation is potentially capable of giving rise to a nonlinear stability characteristic. The precise nature of the

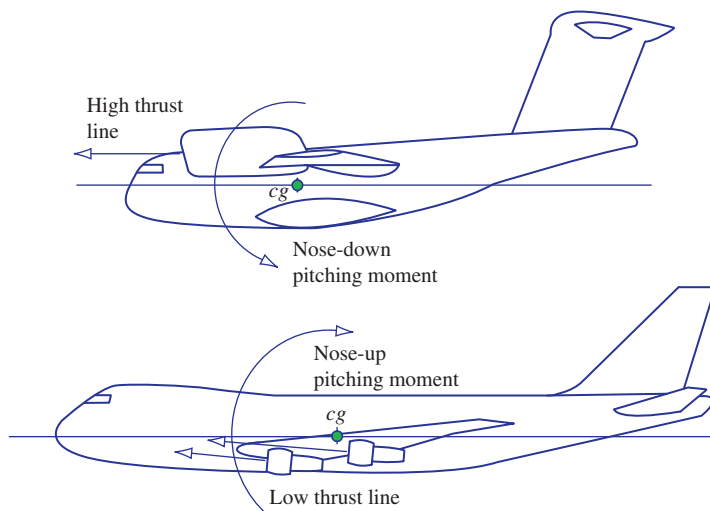


FIGURE 3.4 Typical thrust line effects on pitching moment.

variation in stability is dependent on the operating characteristics of the installed power unit, which may not be easy to identify.

Indirect power effects are caused by the induced flow associated with a propeller and its wake or the intake and exhaust of a gas turbine engine. Some of the more obvious induced-flow effects are illustrated in Fig. 3.5. The process of turning the incident flow through the body incidence angle into the propeller disc or into the engine intake creates a normal force at the propeller or engine intake as shown. In general, this effect gives rise to a nose-up pitching moment. The magnitude of the normal force is dependent on the body incidence angle and on the increase in flow energy at the propeller disc or engine intake. The force therefore varies considerably with trim condition. It is also sensitive to aerodynamic perturbations about trim, so it is easy to appreciate its contribution to pitching moment nonlinearity.

The wake behind a propeller is a region of high-energy flow, which modifies the aerodynamic operating conditions over parts of the wing and tailplane. The greatest effect on pitching moment arises from the tailplane. The effectiveness of the tailplane is enhanced simply because of increased flow velocity and reduced downwash angle. These two effects together increase the nose-down pitching moment available and hence increase the degree of stability of the aircraft. The induced-flow effects associated with propeller-driven aircraft can have a significant influence on longitudinal static stability. These effects also change with aerodynamic conditions, especially at high angles of attack. It is therefore quite common to see some nonlinearity in the pitching moment trim plot for such an aircraft at high values of lift coefficient. It should also be noted that the propeller wake rotates about the longitudinal axis. Although less significant, the rotating flow has some influence on the aircraft's lateral-directional static stability.

The exhaust from a jet engine, being a region of very high velocity and reduced pressure, creates an inflow field, as indicated in Fig. 3.5. Clearly, the influence on pitching moment depends on

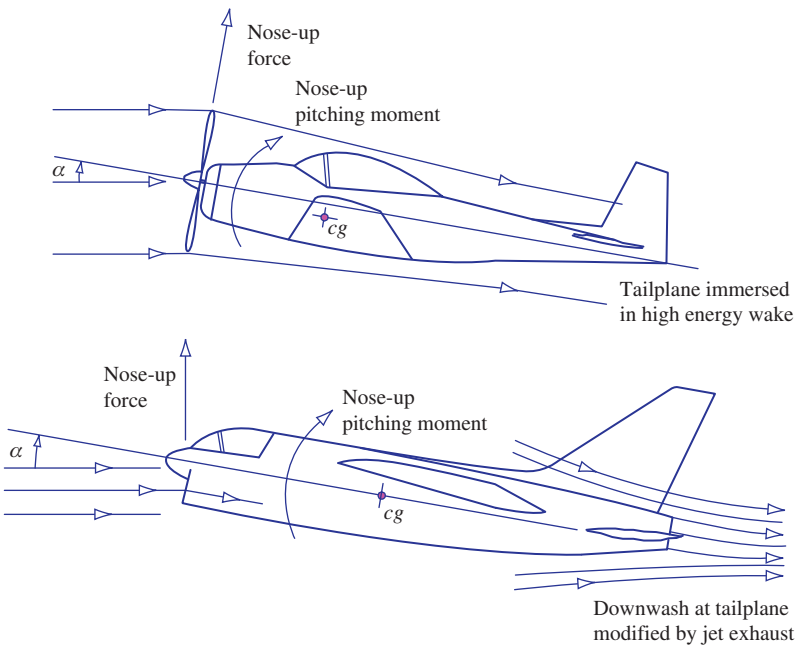


FIGURE 3.5 Typical induced-flow effects on pitching moment.

the relative location of the aerodynamic surfaces of the aircraft and the engine exhaust. When the tailplane is immersed in this induced-flow field, there is a change in the downwash angle. Thus the effect is to increase static stability when the downwash angle is reduced and vice versa. In general, this effect is not very significant, except perhaps for aircraft with engines mounted in pods on the rear fuselage and in which the tailplane is very close to the exhaust wake.

Other effects

Although power effects generally make the most significant contribution to variation in longitudinal static stability, other potentially important contributory sources also exist. For example, wing sweep back and aircraft geometry, which result in significant variation in downwash at the tailplane, generally tend to reduce the available stability, an effect which is clearly dependent on the aerodynamic trim condition. The fuselage alone is usually unstable, and the condition worsens with increasing Mach number. On the other hand, at high subsonic and supersonic Mach numbers the aerodynamic centres of the wing and tailplane move aft. This has the effect of increasing the available nose-down pitching moment, which is a stabilising characteristic. Finally, since all airframes have some degree of flexibility, the structure distorts under the influence of aerodynamic loads. Today aeroelastic distortion of the structure is carefully controlled by design and is not usually significant in influencing static stability. However, in very large civil transport aircraft the relative geometric disposition of the wing and tailplane changes with loading conditions; some contribution to the variation in pitching moment is therefore inevitable but is usually small.

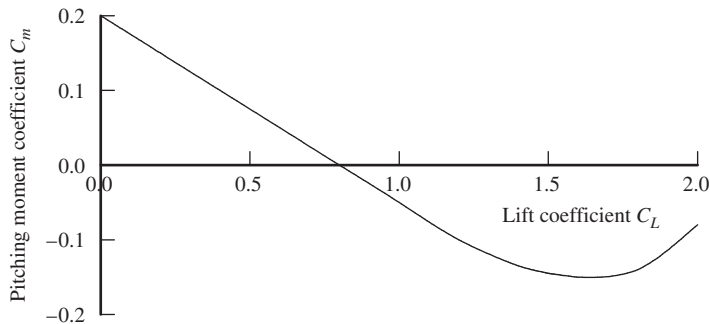


FIGURE 3.6 Stability reversal at a high lift coefficient.

Taking all of these effects together, the prospect of ever being able to quantitatively define the longitudinal static stability of an aircraft may seem daunting. Fortunately, these effects are well understood and can be minimised by design. The result for most aircraft is a pitching moment trim characteristic with some nonlinear tendency at higher values of trim lift coefficient. In extreme cases the stability of the aircraft can actually reverse at high values of lift coefficient, resulting in an unstable pitch-up characteristic. A typical pitching moment trim plot for an aircraft with a pitch-up characteristic is shown in Fig. 3.6.

EXAMPLE 3.1

To illustrate the variation in the pitching moment characteristic for a typical subsonic aircraft, the relevant data obtained from wind tunnel experiments on a 1/6th-scale model of the Handley Page HP-137 are plotted in Fig. 3.7. The data, extracted from a report by [Storey \(1966\)](#), were obtained at a tunnel speed of 200 ft/s, and the Reynolds number was $\text{Re} = 1.2 \times 10^6$ based on mean aerodynamic chord \bar{c} . The HP-137 is in fact the well-known Jetstream; however, it is not known if the data shown are representative of the actual aircraft flying today.

The plots show the characteristic for the aircraft without tail and for the aircraft with tail at various combinations of setting angle η_T and elevator angle η . Clearly, all of the plots are reasonably linear at all values of lift coefficient up to the stall. Without a tailplane the aircraft is unstable since the slope of the plot is positive. With tailplane the slope, and hence the degree of stability, is more or less constant. Assuming that the trim ($C_m = 0$) range of lift coefficient is approximately $-0.2 \leq C_L \leq 1.0$, by interpolation it can be seen that this can be obtained with an elevator angle range of approximately $-0.6^\circ \leq \eta \leq 0^\circ$. This is clearly well within the control capability of the tailplane and elevator configuration shown in this example.

This kind of experimental analysis is used to confirm the geometric design of the tailplane and elevator. In particular, it is essential to establish that the aircraft has an adequate stability margin across the trim envelope, that the elevator angle required to trim the aircraft is within its aerodynamic capability, and that a sufficient margin of elevator control range remains for manoeuvring.

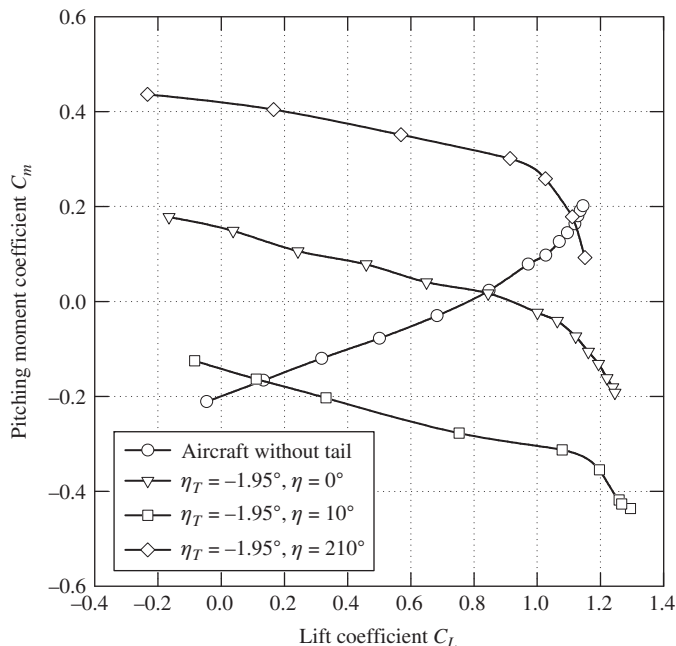


FIGURE 3.7 $C_m-\alpha$ plots for a 1/6th scale model of the Handley Page Jetstream.

3.2 The pitching moment equation

Having established the importance of pitching moment in the determination of longitudinal static stability, further analysis of stability requires the development of the pitching moment equation. A fully representative general pitching moment equation is difficult to develop since it is very dependent on the geometry of the aircraft. However, it is possible to develop a simple approximation which is sufficiently representative for most preliminary studies and which provides considerable insight into the basic requirements for static stability and trim.

3.2.1 Simple development of the pitching moment equation

For the development of the simplest possible pitching moment equation, it is usual to define a model showing only the normal forces and pitching moments acting on the aircraft. It is assumed that in steady level flight the thrust and drag are in equilibrium and act through the *cg*; it is further assumed that, for small disturbances in incidence, changes in this equilibrium are insignificant. These assumptions therefore imply that small disturbances in incidence cause significant changes in lift forces and pitching moments only. The model defined in these terms is shown in Fig. 3.8.

For the purposes of modelling pitching behaviour the model comprises two parts: the wing-fuselage combination and the tailplane. It is thus assumed that the wing-fuselage combination behave

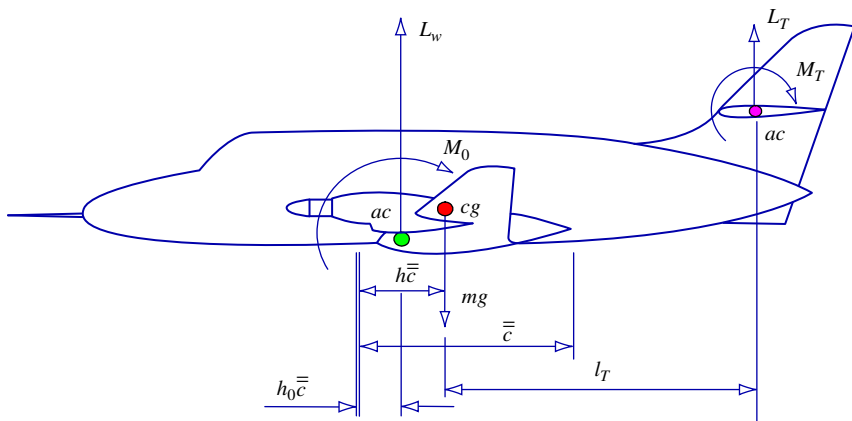


FIGURE 3.8 Simple pitching moment model.

aerodynamically like a wing alone. However, this is not strictly true since the fuselage may make significant aerodynamic contributions and, in any event, its presence interferes with the aerodynamic properties of the wing to a greater or lesser extent. However, for conventional subsonic aircraft with a wing of reasonably high aspect ratio this is a very satisfactory approximation. The tailplane is treated as a separate component since it provides the principal aerodynamic mechanism for controlling longitudinal static stability and trim. The following analysis establishes the fundamental importance of the tailplane parameters to longitudinal static stability.

Referring to Fig. 3.8, the wing-fuselage lift L_w and residual pitching moment M_0 act at the aerodynamic centre ac of the combination, which is assumed to be coincident with the aerodynamic centre of the wing alone. In a similar way the lift L_T and pitching moment M_T of the tailplane are assumed to act at its aerodynamic centre. The longitudinal geometry of the model is entirely related to the mean aerodynamic chord mac as shown in Fig. 3.8. An expression for the total pitching moment M about the cg may therefore be written as

$$M = M_0 + L_w(h - h_0)\bar{c} - L_T l_T + M_T \quad (3.6)$$

If, as is usual, it is assumed that the tailplane aerofoil section is symmetric, then M_T becomes zero. Thus, in the more convenient coefficient form, equation (3.6) may be written as

$$C_m = C_{m_0} + C_{L_w}(h - h_0) - C_{L_T} \bar{V}_T \quad (3.7)$$

To facilitate further analysis of pitching moment it is necessary to express the tailplane lift coefficient C_{L_T} in terms of more accessible tailplane parameters. The tailplane lift coefficient may be expressed as

$$C_{L_T} = a_0 + a_1 \alpha_T + a_2 \eta + a_3 \beta_\eta \quad (3.8)$$

where, a_0 , a_1 , a_2 , and a_3 are constant aerodynamic coefficients, α_T is the local incidence, η is the elevator angle, and β_η is the elevator trim tab angle. Note that, since a symmetric tailplane aerofoil

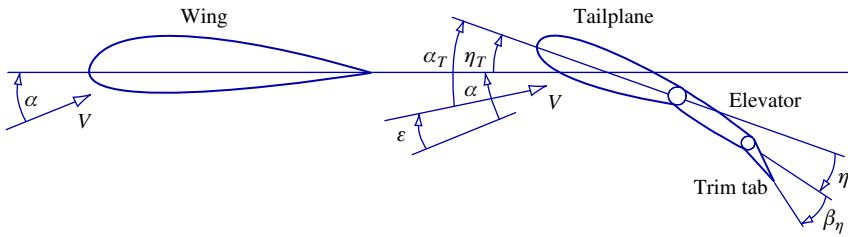


FIGURE 3.9 Wing-tailplane flow geometry.

section is assumed, a_0 is also zero. The local tailplane incidence is influenced by the *tailplane setting angle* η_T and the local flow distortion due to the effect of the downwash field behind the wing. The flow geometry is shown in Fig. 3.9.

Clearly, the angle of attack of the tailplane is given by

$$\alpha_T = \alpha - \varepsilon + \eta_T \quad (3.9)$$

where ε is the downwash angle at the tailplane. Since, to a good approximation, for small disturbances the downwash angle is a function of wing-body incidence α only,

$$\alpha - \varepsilon = \alpha \left(1 - \frac{d\varepsilon}{d\alpha} \right) = \frac{C_{L_w}}{a} \left(1 - \frac{d\varepsilon}{d\alpha} \right) \quad (3.10)$$

whence

$$\alpha_T = \frac{C_{L_w}}{a} \left(1 - \frac{d\varepsilon}{d\alpha} \right) + \eta_T \quad (3.11)$$

Now, substituting the expression for α_T given by equation (3.11) into equation (3.8), substituting the resulting expression for C_{L_T} into equation (3.7), and noting that a_0 is zero, the pitching moment equation in its simplest and most general form is obtained:

$$C_m = C_{m_0} + C_{L_w}(h - h_0) - \bar{V}_T \left(C_{L_w} \frac{a_1}{a} \left(1 - \frac{d\varepsilon}{d\alpha} \right) + a_2 \eta + a_3 \beta_\eta + a_1 \eta_T \right) \quad (3.12)$$

A simple computational algorithm for estimating the rate of change in downwash with angle of attack $d\varepsilon/d\alpha$ is given in [Stribling \(1984\)](#) and its use is illustrated in the Mathcad trim program listed in Appendix 1.

3.2.2 Elevator angle to trim

It has already been shown, in equation (3.1), that the condition for trim is that the total pitching moment be adjustable to zero (i.e., $C_m = 0$). Applying this condition to equation (3.12), the elevator angle required to trim the aircraft is given by

$$\eta = \frac{1}{\bar{V}_T a_2} (C_{m_0} + C_{L_w}(h - h_0)) - \frac{C_{L_w}}{a} \left(\frac{a_1}{a_2} \right) \left(1 - \frac{d\varepsilon}{d\alpha} \right) - \frac{a_3}{a_2} \beta_\eta - \frac{a_1}{a_2} \eta_T \quad (3.13)$$

When the elevator tab is set at its neutral position, $\beta_\eta = 0$, and for a given *cg* position h , the elevator angle to trim varies only with lift coefficient. For any other tab setting a different elevator angle is required to trim. Therefore, the elevator and elevator tab to an extent provide interchangeable means for achieving longitudinal trim.

3.2.3 Condition for longitudinal static stability

The basic requirement for an aircraft to be statically stable at a given trim condition is stated in equation (3.2). By differentiating equation (3.12) with respect to C_L or, equivalently, C_{L_w} , and noting that η_T and, by definition, C_{m_0} , are constants, the condition for the aircraft to be stable is given by

$$\frac{dC_m}{dC_{L_w}} < 0$$

where

$$\frac{dC_m}{dC_{L_w}} = (h - h_0) - \bar{V}_T \left(\frac{a_1}{a} \left(1 - \frac{d\varepsilon}{d\alpha} \right) + a_2 \frac{d\eta}{dC_{L_w}} + a_3 \frac{d\beta_\eta}{dC_{L_w}} \right) \quad (3.14)$$

Thus, at a given *cg* position h , the longitudinal static stability of the aircraft and the aerodynamic control characteristics—that is, *elevator angle to trim*, $d\eta/dC_{L_w}$, and *elevator tab angle to trim*, $d\beta_\eta/dC_{L_w}$ —are interdependent. Further analysis is usually carried out by separating the effects of elevator angle and tab angle in equation (3.14). *Controls-fixed stability* is concerned with the interdependence of elevator angle to trim and stability, whereas *controls-free stability* is concerned with the interdependence of elevator tab angle to trim and stability.

3.3 Longitudinal static stability

A more detailed analysis of longitudinal static stability leads to a description of pilot control actions to trim. In particular, control displacement is determined by controls-fixed stability and control force to trim is determined by controls-free stability.

3.3.1 Controls-fixed stability

The condition described as *controls-fixed* is taken to mean the condition when the elevator and elevator tab are held at constant settings corresponding to the prevailing trim condition. In practice, this means that the pilot is flying the aircraft with his hands on the controls and is holding the controls at the *fixed* setting required to trim. This, of course, assumes that the aircraft is stable and remains in trim.

Since the controls are fixed,

$$\frac{d\eta}{dC_{L_w}} = \frac{d\beta_\eta}{dC_{L_w}} = 0 \quad (3.15)$$

and equation (3.14) may be written as

$$\frac{dC_m}{dC_{L_w}} = (h - h_0) - \bar{V}_T \frac{a_1}{a} \left(1 - \frac{d\varepsilon}{d\alpha} \right) \quad (3.16)$$

or as

$$K_n = -\frac{dC_m}{dC_{L_w}} = h_n - h \quad (3.17)$$

where K_n is the *controls-fixed stability margin*, the slope of the $C_m - C_L$ plot. The location of the *controls-fixed neutral point* h_n on the mean aerodynamic chord \bar{c} is therefore given by

$$h_n = h_0 + \bar{V}_T \frac{a_1}{a} \left(1 - \frac{d\varepsilon}{d\alpha} \right) \quad (3.18)$$

For a statically stable aircraft the stability margin K_n is positive, and the greater its value the greater the degree of stability. With reference to [equation \(3.17\)](#), it is clear that the aircraft is stable when the *cg* position h is ahead of the controls-fixed neutral point h_n . The acceptable margins of stability therefore determine the permitted range of *cg* position in a given aircraft. The aft limit often corresponds with the controls-fixed neutral point, whereas the forward limit is determined by the maximum permissible stability margin. Recall from [Section 3.1.3](#) that too much stability can be as hazardous as too little.

The meaning of controls-fixed stability is easily interpreted by considering the pilot actions required to trim an aircraft in a controls-fixed sense. It is assumed at the outset that the aircraft is in fact stable and hence can be trimmed to an equilibrium flight condition. When the aircraft is in a trimmed initial equilibrium state the pitching moment is zero and [equation \(3.12\)](#) may be written as

$$0 = C_{m_0} + C_{L_w}(h - h_0) - \bar{V}_T \left(C_{L_w} \frac{a_1}{a} \left(1 - \frac{d\varepsilon}{d\alpha} \right) + a_2\eta + a_3\beta_\eta + a_1\eta_T \right) \quad (3.19)$$

It is assumed that the pilot is holding the controls at the required elevator angle, the power is set to give steady level flight, and the elevator tab is set at its datum, $\beta_\eta = 0$. Now, to retrim the aircraft at a new flight condition in a controls-fixed sense it is necessary for the pilot to move the controls to the new elevator setting and then to hold the controls at that setting. For example, to retrim at a higher speed in a more nose-down attitude, the pilot moves the control column forward until his new condition is established and then to simply hold the column at that position. This of course leaves the aircraft in a descending condition unless the power is increased sufficient to maintain level flight at the higher speed. However, power variations are not allowed for in the simple model reviewed here.

Thus trimming a stable aircraft at any condition in its speed envelope simply requires the selection of the correct elevator angle, all other parameters remaining constant. The variable in controls-fixed stability analysis is therefore elevator angle to trim. Differentiating [equation \(3.19\)](#) with respect to C_{L_w} and making the same assumptions as before, but allowing elevator angle η to vary with trim, it may be shown, after some rearrangement, that

$$\frac{d\eta}{dC_{L_w}} = \frac{-1}{\bar{V}_T a_2} (h_n - h) = \frac{-1}{\bar{V}_T a_2} K_n \quad (3.20)$$

Since \bar{V}_T and a_2 are constants, the *elevator angle to trim* characteristic $d\eta/dC_{L_w}$ is thus proportional to the controls-fixed stability margin K_n . Measurements of elevator angle to trim for a range of flight conditions, subject to the assumptions described, provide a practical means for determining

controls-fixed stability characteristics from flight experiments. However, in such experiments it is not generally possible to completely eliminate the effects of power on the results.

EXAMPLE 3.2

The practical evaluation of controls-fixed static stability centres on the application of [equations \(3.13\), \(3.19\), and \(3.20\)](#) to a stable aircraft. It is relatively straightforward to obtain measurements of the elevator angle η required to trim an aircraft at a chosen value of lift coefficient C_L . Provided that the power and elevator trim tab angle β_η are maintained at constant settings throughout the measurement process, the equations apply directly. A flight test exercise conducted in a Handley Page Jetstream by the author under these conditions provided the trim data plotted in [Fig. 3.10](#) for three different cg positions. At any given value of lift coefficient C_L the corresponding value of elevator angle to trim η is given by the solution of [equation \(3.13\)](#) or, alternatively, [equation \(3.19\)](#). The plots are clearly nonlinear and the nonlinearity in this aircraft is almost entirely due to the effects of power.

Since the gradients of the plots shown in [Fig. 3.10](#) are all negative, the aircraft is statically stable in accordance with [equation \(3.20\)](#). However, for any given cg position the gradient varies with lift coefficient, indicating a small variation in stability margin. In a detailed analysis the stability margin would be evaluated at each value of trimmed lift coefficient in order to quantify

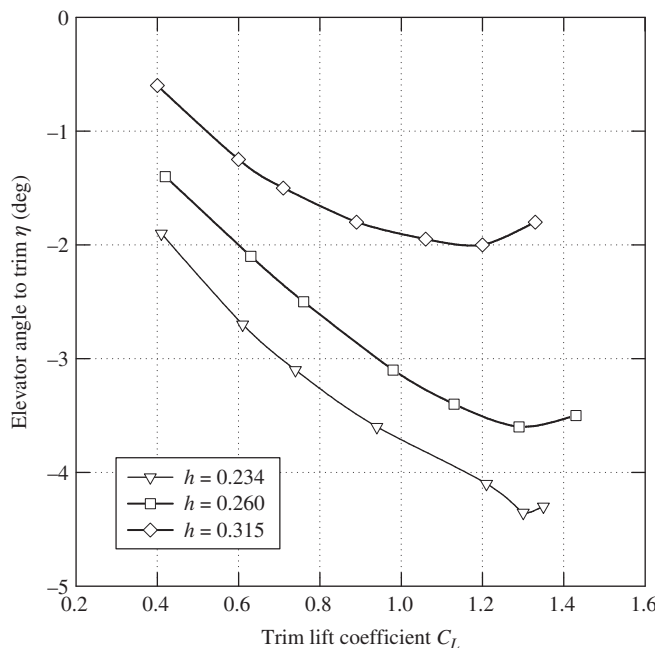


FIGURE 3.10 Plot of elevator angle to trim.

the variation in stability. In the present example the quality of the data was not good enough to allow such a complete analysis. To establish the location of the controls-fixed neutral point h_n , equation (3.20) must be solved at each value of trim lift coefficient. This is most easily done graphically, as shown in Fig. 3.11.

Equation (3.20) is solved by plotting $d\eta/dC_L$ against cg position h as shown. In this example the mean gradient for each cg position, rather than the value at each trim point, is plotted. Since equation (3.20) represents a linear plot, a straight line may be fitted to the three data points as shown. Extrapolation to the neutral stability point at which $d\eta/dC_L = 0$ corresponds with a cg position of approximately $h = 0.37$. Clearly, three data points through which to draw a line is barely adequate for this kind of evaluation. A controls-fixed neutral point h_n at 37% of mac correlates well with the known properties of the aircraft. The most aft cg position permitted is in fact at 37% of mac . With the location of the controls-fixed neutral point established, the controls-fixed stability margin K_n for each cg position follows from the application of equation (3.20).

In a more searching stability evaluation, rather more data points would be required and data of much better quality would be essential. Although limited, the present example does illustrate the typical controls-fixed longitudinal static stability characteristics of a well-behaved classical aircraft.

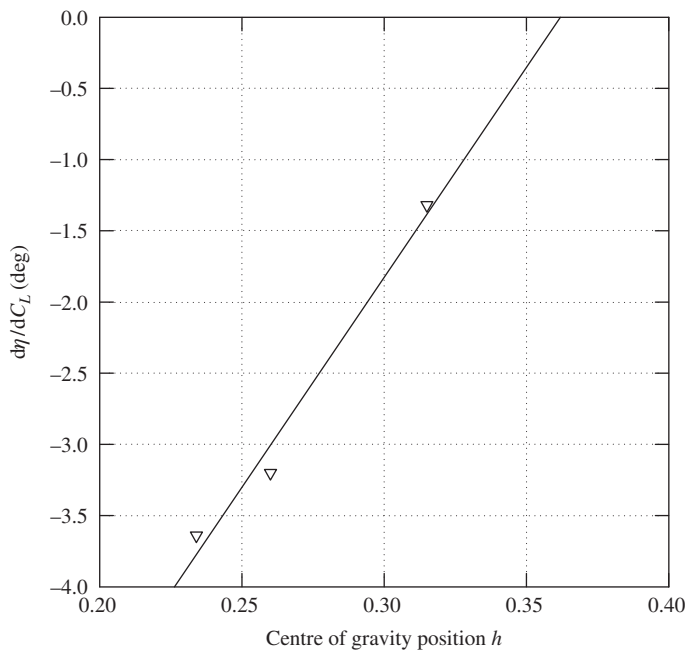


FIGURE 3.11 Determination of controls-fixed neutral point.

3.3.2 Controls-free stability

The condition described as *controls-free* is taken to mean the condition when the elevator is free to float at an angle corresponding to the prevailing trim condition. In practice this means that the pilot can fly the aircraft with his hands off the controls whilst the aircraft remains in its trimmed flight condition. Again, it is assumed that the aircraft is stable; otherwise, it would diverge when the controls were released. Now this situation can only be obtained if the controls can be adjusted such that the elevator floats at the correct angle for the desired *hands-off* trim condition. This is arranged by adjusting the elevator trim tab until the required trim is obtained. Thus controls-free stability is concerned with the trim tab and its control characteristics.

When the controls are free, the elevator hinge moment H is zero and the elevator floats at an indeterminate angle η . It is therefore necessary to eliminate elevator angle from the pitching moment equation (3.12) in order to facilitate analysis of controls-free stability. The elevator hinge moment coefficient is given by the expression

$$C_H = b_1 \alpha_T + b_2 \eta + b_3 \beta_\eta \quad (3.21)$$

where, b_1 , b_2 , and b_3 are constants determined by the design of the elevator and trim tab control circuitry. Substituting for local tailplane incidence α_T as given by equation (3.11), equation (3.21) may be rearranged to determine the angle at which the elevator floats. Thus

$$\eta = \frac{1}{b_2} C_H - \frac{C_{L_w}}{a} \frac{b_1}{b_2} \left(1 - \frac{d\varepsilon}{d\alpha} \right) - \frac{b_3}{b_2} \beta_\eta - \frac{b_1}{b_2} \eta_T \quad (3.22)$$

To eliminate elevator angle from the pitching moment equation, substitute equation (3.22) into equation (3.12) to obtain

$$C_m = C_{m_0} + C_{L_w}(h - h_0) - \bar{V}_T \left(\begin{array}{l} C_{L_w} \frac{a_1}{a} \left(1 - \frac{d\varepsilon}{d\alpha} \right) \left(1 - \frac{a_2 b_1}{a_1 b_2} \right) + a_3 \beta_\eta \left(1 - \frac{a_2 b_3}{a_3 b_2} \right) \\ + a_1 \eta_T \left(1 - \frac{a_2 b_1}{a_1 b_2} \right) + \frac{a_2}{b_2} C_H \end{array} \right) \quad (3.23)$$

Now, in the controls-free condition $C_H = 0$, and noting that η_T , C_{m_0} and, since the tab is set at the trim value, β_η are constants, differentiating equation (3.23) with respect to C_{L_w} gives

$$\frac{dC_m}{dC_{L_w}} = (h - h_0) - \bar{V}_T \frac{a_1}{a} \left(1 - \frac{d\varepsilon}{d\alpha} \right) \left(1 - \frac{a_2 b_1}{a_1 b_2} \right) \quad (3.24)$$

Or, writing,

$$K'_n = - \frac{dC_m}{dC_{L_w}} = h'_n - h \quad (3.25)$$

where K'_n is the *controls-free stability margin*, the slope of the $C_m - C_L$ plot with the controls free. The location of the *controls-free neutral point* h'_n on the mean aerodynamic chord \bar{c} is given by

$$\begin{aligned} h'_n &= h_0 + \bar{V}_T \frac{a_1}{a} \left(1 - \frac{d\varepsilon}{d\alpha} \right) \left(1 - \frac{a_2 b_1}{a_1 b_2} \right) \\ &= h_n - \bar{V}_T \frac{a_2 b_1}{a b_2} \left(1 - \frac{d\varepsilon}{d\alpha} \right) \end{aligned} \quad (3.26)$$

As before, for a statically stable aircraft the controls-free stability margin K'_n is positive and the greater its value, the greater the degree of stability possessed by the aircraft. With reference to equation (3.25), it is clear that for controls-free stability the *cg* position h must be ahead of the controls-free neutral point h'_n . Equation (3.26) shows the relationship between the controls-fixed and controls-free neutral points. The numerical values of the elevator and tab constants are such that usually $h'_n > h_n$, which means that it is common for the controls-free neutral point to lie aft of the controls-fixed neutral point. Thus an aircraft that is stable controls-fixed is also usually stable controls-free, and it follows that the controls-free stability margin K'_n is greater than the controls-fixed stability margin K_n .

The meaning of controls-free stability is readily interpreted by considering the pilot actions required to trim the aircraft in a controls-free sense. It is assumed that the aircraft is stable and is initially in a hands-off trim condition. In this condition the pitching moment is zero and hence equation (3.23) may be written as

$$0 = C_{m_0} + C_{L_w}(h - h_0) - \bar{V}_T \left(C_{L_w} \frac{a_1}{a} \left(1 - \frac{d\varepsilon}{d\alpha} \right) \left(1 - \frac{a_2 b_1}{a_1 b_2} \right) + a_3 \beta_\eta \left(1 - \frac{a_2 b_3}{a_3 b_2} \right) + a_1 \eta_T \left(1 - \frac{a_2 b_1}{a_1 b_2} \right) \right) \quad (3.27)$$

To retrim the aircraft it is necessary for the pilot to grasp the control column and move it to the position corresponding with the elevator angle required for the new trim condition. However, if he releases the control it will simply move back to its original trim position since an out-of-trim elevator hinge moment, and hence stick force, exists at the new position. To rectify the problem the pilot must use the trim tab. Having moved the control to the position corresponding with the new trim condition, he will be holding a force on the control. By adjusting the trim tab he can null the force and following which, he can release the control and it will remain in the new hands-off position as required. Thus trim tab adjustment is equivalent to control force adjustment, which in turn is directly related to elevator hinge moment adjustment in a mechanical flying control system.

To reiterate the previous illustration, consider the situation when the pilot wishes to retrim the aircraft at a higher speed in a more nose-down attitude. As before, he will *push* the control column forward until the desired condition is obtained, which will leave him holding an out-of-trim force and descending. Elevator tab adjustment will enable him to reduce the control force to zero, whereupon the pilot can release the control to enjoy his new hands-off trim condition. Since he is descending it is normally necessary to increase power in order to regain level flight. However, as already stated, thrust variations are not allowed in this model; if they were, the analysis would be considerably more complex.

Thus to trim a stable aircraft at any hands-off flight condition in its speed envelope simply requires the correct selection of elevator tab angle. The variable in controls-free stability analysis is therefore elevator tab angle to trim. Differentiating [equation \(3.27\)](#) with respect to C_{L_w} and making the same assumptions as previously but allowing elevator tab angle β_η to vary with trim, after some rearrangement it may be shown that

$$\frac{d\beta_\eta}{dC_{L_w}} = \frac{-(h'_n - h)}{a_3 \bar{V}_T \left(1 - \frac{a_2 b_3}{a_3 b_2} \right)} = \frac{-K'_n}{a_3 \bar{V}_T \left(1 - \frac{a_2 b_3}{a_3 b_2} \right)} \quad (3.28)$$

Since it is usual for

$$-a_3 \bar{V}_T \left(1 - \frac{a_2 b_3}{a_3 b_2} \right) > 0 \quad (3.29)$$

the *elevator tab angle to trim* characteristic $d\beta_\eta/dC_{L_w}$ is positive and proportional to the controls-free stability margin K'_n . Measurement of the tab angles required to trim a range of flight conditions, subject to the assumptions described, provides a practical means for determining controls-free stability characteristics from flight experiments. However, since tab angle, elevator hinge moment, and control force are all equivalent, it is often more meaningful to investigate control force to trim directly since this is the parameter of direct concern to the pilot.

To determine the equivalence between elevator tab angle to trim and control force to trim, consider the aircraft in a stable hands-off trim state with the tab set at its correct trim value. If the pilot moves the controls in this condition, the elevator hinge moment, and hence control force, will vary. [Equation \(3.23\)](#) is applicable and may be written as

$$0 = C_{m_0} + C_{L_w}(h - h_0) - \bar{V}_T \left(C_{L_w} \frac{a_1}{a} \left(1 - \frac{d\varepsilon}{d\alpha} \right) \left(1 - \frac{a_2 b_1}{a_1 b_2} \right) + a_3 \beta_\eta \left(1 - \frac{a_2 b_3}{a_3 b_2} \right) + a_1 \eta_T \left(1 - \frac{a_2 b_1}{a_1 b_2} \right) + \frac{a_2}{b_2} C_H \right) \quad (3.30)$$

where β_η is set at its datum trim position and is assumed constant, and hinge moment coefficient C_H is allowed to vary with trim condition. Differentiate [equation \(3.30\)](#) with respect to C_{L_w} subject to these conditions, and rearrange to obtain

$$\frac{dC_H}{dC_{L_w}} = \frac{-1}{\bar{V}_T \frac{a_2}{b_2}} (h'_n - h) = \frac{-1}{\bar{V}_T \frac{a_2}{b_2}} K'_n \quad (3.31)$$

Comparison of [equation \(3.31\)](#) with [equation \(3.28\)](#) demonstrates the equivalence of tab angle to trim and hinge moment to trim. Further, if the elevator control force is denoted F_η and g_η denotes the mechanical gearing between the control column and elevator, then

$$F_\eta = g_\eta H = \frac{1}{2} \rho V_0^2 S_\eta \bar{c}_\eta g_\eta C_H \quad (3.32)$$

where S_η is the elevator area aft of the hinge line and \bar{c}_η is the mean aerodynamic chord of the elevator aft of the hinge line. This therefore demonstrates the relationship between control force and hinge moment, although [equation \(3.32\)](#) shows that the relationship also depends on the square of the speed.

EXAMPLE 3.3

The practical evaluation of controls-free static stability is undertaken in much the same way as the evaluation of controls-fixed stability discussed in Example 3.2. In this case the evaluation centres on the application of [equations \(3.30\), \(3.31\), and \(3.32\)](#) to a stable aircraft. It is relatively straightforward to obtain measurements of the elevator stick force F_η , and hence the hinge moment coefficient C_H , required to trim an aircraft at a chosen value of lift coefficient C_L . Provided that the power and elevator trim tab angle β_η are maintained at constant settings throughout the measurement process, the above mentioned equations apply directly.

As before, a flight test exercise conducted in a Handley Page Jetstream under these conditions provided the trim data plotted in [Fig. 3.12](#) for three different cg positions. At any given value of lift coefficient C_L , the corresponding value of elevator hinge moment to trim C_H is given by the solution of [equation \(3.30\)](#). Again, the plots are nonlinear primarily because of the effects of

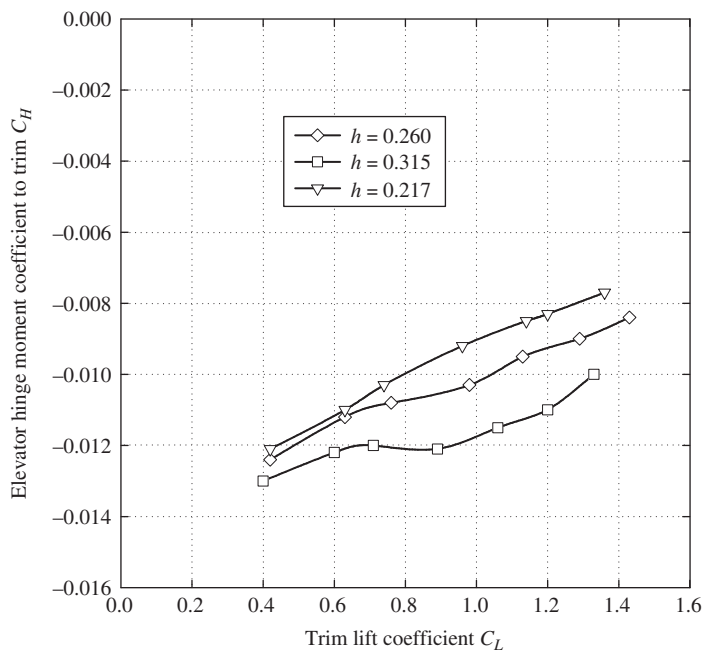


FIGURE 3.12 Plot of hinge moment coefficient to trim.

power. However, since force measurements are involved, the influence of friction in the mechanical control runs is significant and inconsistent. The result of this is data with rather too many spurious points. To provide a meaningful example, the obviously spurious data points have been “adjusted” to correlate with the known characteristics of the aircraft.

Since the gradients of the plots shown in Fig. 3.12 are all positive, the aircraft is statically stable in accordance with equation (3.31). However, for any given cg position the gradient varies with lift coefficient, indicating rather inconsistent variations in stability margin. However, in this case the variations are more likely to be the result of poor-quality data rather than orderly changes in the aerodynamic properties of the aircraft. Again, in a detailed analysis the stability margin would be evaluated at each value of trimmed lift coefficient in order to quantify the variation in stability. In the present example the data were clearly not good enough to allow such a complete analysis. To establish the location of the controls-free neutral point h'_n , equation (3.31) must be solved at each value of trim lift coefficient. This is most easily done graphically as shown in Fig. 3.13.

Equation (3.31) is solved by plotting dC_H/dC_L against cg position h as shown. In this example the mean gradient for each cg position is plotted rather than the value at each trim point. Since equation (3.31) represents a linear plot, a straight line may be fitted to the three data points as

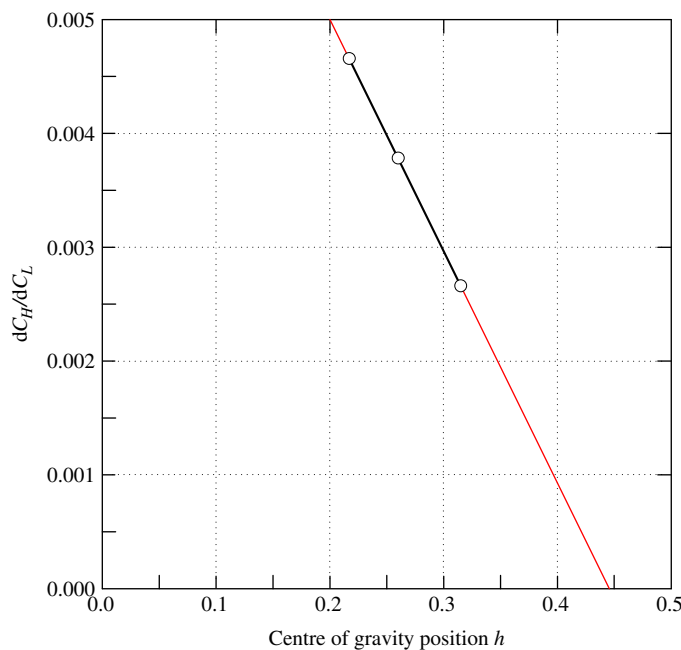


FIGURE 3.13 Determination of the controls-free neutral point.

shown. Extrapolation to the neutral stability point at which $dC_H/dC_L = 0$ corresponds with a *cg* position of approximately $h = 0.44$. A controls-free neutral point h'_n at 44% of *mac* correlates reasonably well with the known properties of the aircraft. Having established the location of the controls-free neutral point, the controls-free stability margin K'_n for each *cg* position follows from the application of [equation \(3.25\)](#).

3.3.3 Summary of longitudinal static stability

A physical interpretation of the meaning of longitudinal static stability may be brought together in the summary shown in [Fig. 3.14](#). The important parameters are neutral point positions and their relationship to the *cg* position, which in turn determines the stability margins of the aircraft. The stability margins determine literally how much stability the aircraft has in hand, in the controls-fixed and controls-free senses, over and above neutral stability. The margins therefore indicate how safe the aircraft is. Equally important, however, the stability margins provide a measure of the control actions required to trim the aircraft. In particular, the controls-fixed stability margin is a measure of the control displacement required to trim and the controls-free stability margin is a measure of the control force required to trim.

From a flying and handling qualities point of view, it is the interpretation of stability in terms of control characteristics which is by far the most important consideration. In practice, the assessment of longitudinal static stability is frequently concerned only with the measurement of control characteristics, as illustrated by Examples 3.2 and 3.3.

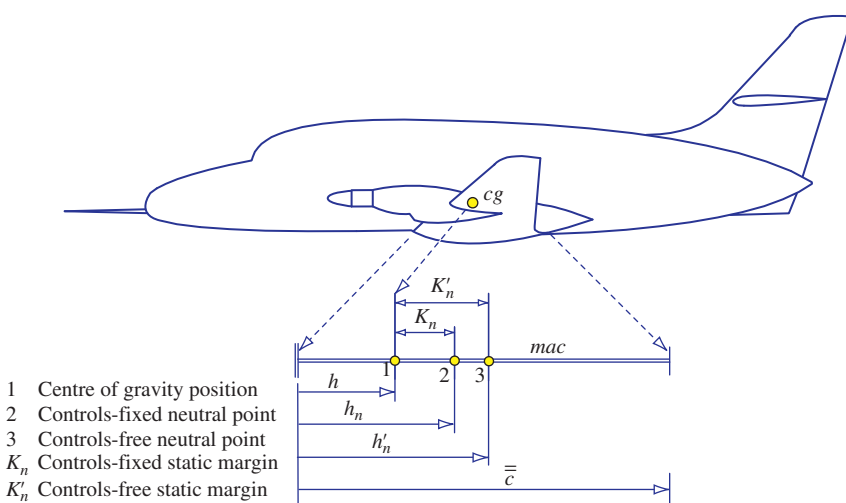


FIGURE 3.14 Longitudinal stability margins.

3.4 Lateral-directional static stability

Lateral-directional static stability is concerned with the ability of the aircraft to recover equilibrium following a sideslip disturbance; it is the lateral-directional equivalent to longitudinal static stability in its interpretation. As discussed in [Section 3.1.1](#), the lateral-directional equilibrium trim state is determined by the condition when the net side force and the net roll and yaw moments are all zero. Since conventional aircraft are geometrically symmetric, the side force is zero in trimmed rectilinear flight; whenever the aircraft experiences a sideslip disturbance, the resulting out-of-trim side force always acts in a sense to oppose the disturbance. Such a condition is always stable, so the lateral-directional stability properties of the aircraft reduce to a consideration of roll and yaw moment response to a sideslip disturbance. As for longitudinal stability, the transient motion following such a disturbance is characterised by the dynamic stability properties, and the stable aircraft will eventually settle to its equilibrium state once more.

A positive sideslip disturbance is shown in [Fig. 3.15](#), in which the aircraft slips to the right with velocity v . Thus the disturbed aircraft velocity vector V is displaced to the right through the sideslip angle β , and it is easily determined that

$$\tan \beta = \frac{v}{U} \quad (3.33)$$

where U is the axial component of velocity in the disturbance. Since the disturbance is assumed to be small, and in reality a sideslip angle greater than 10° would be considered excessive, it is usual to write

$$\beta \approx \frac{v}{U} \approx \frac{v}{V_0} \quad (3.34)$$

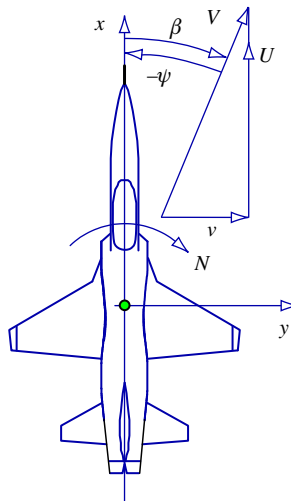


FIGURE 3.15 Sideslip disturbance.

where V_0 is the undisturbed equilibrium velocity of the aircraft. As shown in Fig. 3.15, in the disturbance the nose of the aircraft is displaced to the left of the velocity vector and the sideslip angle β is equivalent to the yaw angle $-\psi$ since the disturbance is assumed small.

Because the lateral-directional static stability of the aircraft is usually fixed by design, it usually remains more or less constant throughout the flight envelope. The lateral-directional stability margins therefore remain nominally constant for all flight conditions. This situation may well break down when large-amplitude manoeuvring is considered. Under such circumstances normally linear aerodynamic behaviour may well become very nonlinear and cause dramatic changes to observed lateral-directional stability and control characteristics. Although of considerable interest to the flight dynamicist, nonlinear behaviour is beyond the scope of this book. Nominally constant lateral-directional static stability is assumed throughout.

In general, the degree of lateral-directional static stability is quantified by the aerodynamic stability derivatives L_v and N_v or, equivalently, L_β and N_β , and a full analytical derivation and discussion of the derivatives is given in Section 13.3.2.

3.4.1 Lateral static stability

Lateral static stability is concerned with the ability of the aircraft to maintain wings-level equilibrium in the roll sense. Wing dihedral is the most visible parameter which confers lateral static stability on an aircraft, although there are many other contributions, some of which are destabilising. Since all aircraft are required to fly with their wings level in the steady trim state, lateral static stability is designed in from the outset. Dihedral is the easiest parameter to adjust in the design process in order to “tune” the degree of stability to an acceptable level. Remember that too much lateral static stability results in an aircraft that is reluctant to manoeuvre in roll, so it is important to obtain the correct degree of stability in order not to compromise aileron control power. A more detailed analysis of lateral control derivatives is given in Section 13.4.2.

The effect of dihedral as a means for providing lateral static stability is easily appreciated by considering the situation depicted in Fig. 3.16. Following a small positive disturbance in sideslip β , the right wing tends to drop and the aircraft slides “downhill” to the right with a sideslip velocity v . Consider the resulting change in the aerodynamic conditions on the leading right wing, which has dihedral angle Γ . Since the wing has dihedral, the sideslip velocity has a small component v' resolved perpendicular to the plane of the wing panel, where

$$v' = v \sin \Gamma \quad (3.35)$$

The velocity component v' combines with the axial velocity component U_e to increase the angle of attack of the leading wing by α' . Since $v' \ll U_e$, the change in angle of attack α' is small and the total disturbed axial velocity component $U \cong U_e$. The increase in angle of attack on the leading wing gives rise to an increase in lift, which in turn gives rise to a restoring rolling moment $-L$. The corresponding aerodynamic change on the left wing trailing into the sideslip results in a small decrease in lift, which also produces a restoring rolling moment. The net effect is therefore to create a negative rolling moment which causes the aircraft to recover its zero sideslip wings-level

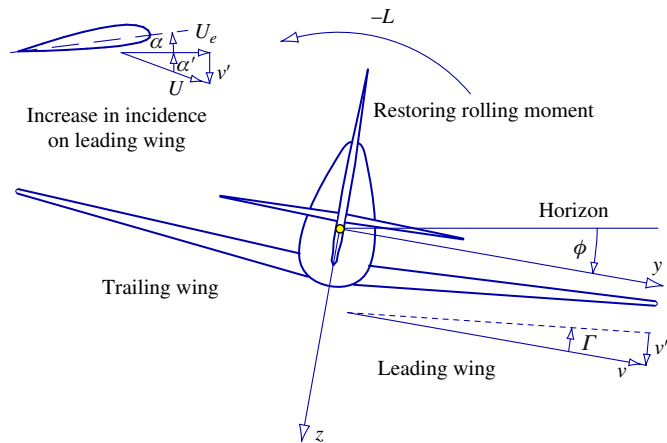


FIGURE 3.16 Dihedral effect.

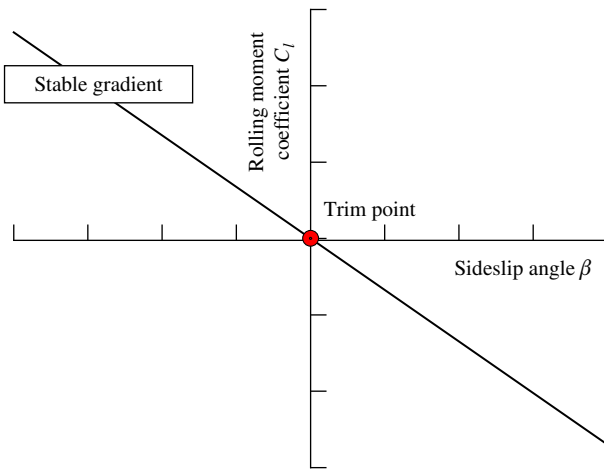


FIGURE 3.17 $C_l - \beta$ plot for a stable aircraft.

equilibrium. Thus the condition for an aircraft to be laterally stable is that the rolling moment resulting from a positive disturbance in sideslip be negative, or, in mathematical terms,

$$\frac{dC_l}{d\beta} < 0 \quad (3.36)$$

where C_l is the rolling moment coefficient. This is shown graphically in Fig. 3.17 and may be interpreted in a similar way to the pitching moment plot shown in Fig. 3.2.

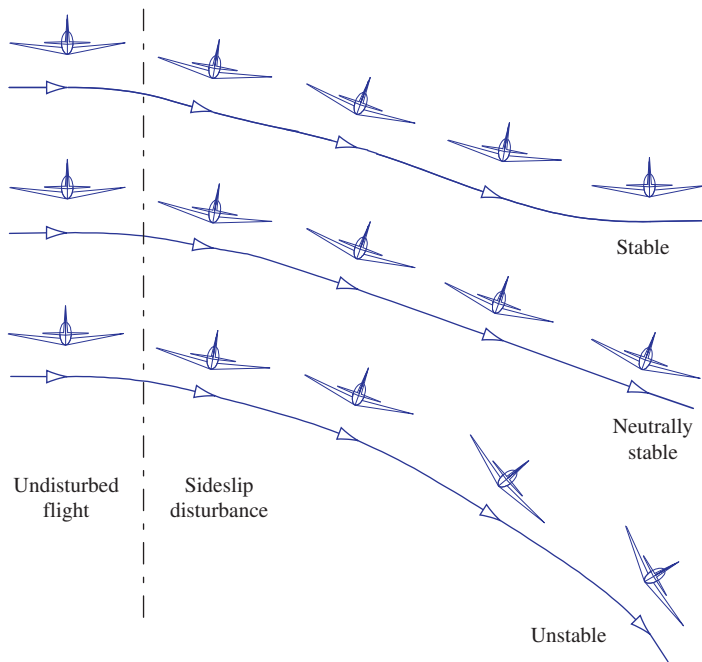


FIGURE 3.18 Effect of dihedral on lateral stability.

Note that the trim point for all flight conditions corresponds with zero sideslip angle, and that the gradient of the rolling moment against sideslip plot must be negative for stability. As in the case of longitudinal static stability, the magnitude of the gradient determines the degree of lateral static stability; the correct value provides a satisfactory balance between stability and roll control of the aircraft.

The sequence of events following a sideslip disturbance are shown for a laterally stable, neutrally stable, and unstable aircraft in Fig. 3.18. However, it must be remembered that, once disturbed, the subsequent motion will be determined by the lateral dynamic stability characteristics as well.

Wing sweep can also make a significant positive contribution to lateral static stability. For this reason dihedral is not commonly seen on swept-wing combat aircraft in order to avoid an excessive level of lateral stability, which would compromise roll manoeuvre performance. Indeed, anhedral (negative dihedral), which is destabilising, is used on some swept-wing combat aircraft as a means of “tuning” lateral static stability to an acceptable level.

With reference to Fig. 3.15, a wing in sideslip is effectively yawed through the sideslip angle such that $\psi = -\beta$. A swept wing in sideslip is therefore treated as a yawed wing, and it must be remembered that the disturbed aircraft tends to roll in the direction of sideslip. Now the lift on a

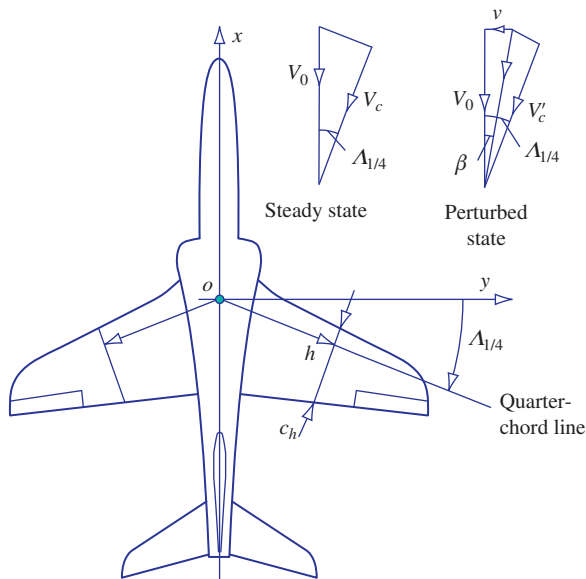


FIGURE 3.19 Swept wing in sideslip.

yawed wing is determined by the component of velocity normal to the quarter-chord line in subsonic flight and normal to the leading edge in supersonic flight.

With reference to Fig. 3.19, consider a chordwise section c_h on the right wing panel which is perpendicular to the quarter-chord line. Subsonic flow conditions are assumed, and the flow direction is parallel to the chord line. In the steady equilibrium flight condition the chordwise component of velocity is given by

$$V_c = V_0 \cos \Lambda_{1/4} \quad (3.37)$$

In the presence of a positive sideslip disturbance this becomes

$$V'_c = \frac{V_0}{\cos \beta} \cos(\Lambda_{1/4} - \beta) \cong V_0 \cos(\Lambda_{1/4} - \beta) \quad (3.38)$$

where β is the sideslip angle, which is small by definition. Since $V'_c > V_c$, the lift on the right wing panel is increased in sideslip, which creates a negative rolling moment to restore the aircraft to wings-level flight. On the left wing panel there is a corresponding reduction in chordwise velocity in sideslip, which also creates a negative rolling moment. It is therefore evident that wing sweep gives rise to a positive contribution to the lateral static stability of an aircraft.

The fin also contributes to lateral static stability, but its contribution can be stabilising, destabilising, or neutral depending on the steady trim condition when sideslip is experienced. With

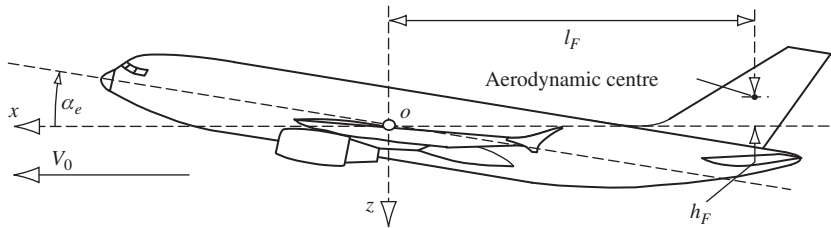


FIGURE 3.20 Fin in sideslip.

reference to Fig. 3.15, when in a sideslip the fin is at incidence to the flow direction equal to the sideslip angle, which causes the fin to generate lift perpendicular to the flow direction. As shown in Fig. 3.20, the fin lift in sideslip acts at the aerodynamic centre of the fin, which may be above or below the roll axis, thereby giving rise to a rolling moment.

With reference to Chapter 13 (Section 13.3.2), it is shown from equation (13.108) that the lateral static stability contribution due to the fin is given by

$$\frac{dC_l}{d\beta_{fin}} = -\bar{V}_F \frac{h_F}{l_F} a_{l_F} \quad (3.39)$$

where a_{l_F} is the fin lift curve slope and the *fin volume ratio* is given by

$$\bar{V}_F = \frac{S_F l_F}{Sb} \quad (3.40)$$

When the aerodynamic centre of the fin is above the roll axis, h_F is positive and the expression given by equation (3.39) is negative and hence stabilising. However, it is evident that, depending on aircraft geometry, h_F may be small and may even change sign at extreme aircraft attitude. Thus the fin contribution to lateral static stability varies with trimmed aircraft attitude and may become positive and hence destabilising at low-speed flight conditions.

A number of additional aerodynamic properties of an aircraft can be identified which contribute to lateral static stability in both stabilising and destabilising senses. However, these contributions are often difficult to quantify in terms of simple aerodynamic properties and can only be evaluated by experiment or by complex analysis. For example, a significant contribution arises from the geometry since, in a sideslip disturbance, the lateral cross-flow in the vicinity of the wing root gives rise to differential wing lift, which in turn gives rise to rolling moment. In particular, a high-wing configuration makes a stabilising contribution to lateral static stability whereas a low-wing configuration makes a destabilising contribution. This explains why many high-wing aircraft have little or no dihedral while low-wing configurations often have significant dihedral. Once again, this is an example of how dihedral is used to “tune” the overall lateral static stability of an aircraft. This topic is discussed in a little more detail in Chapter 13 (Section 13.3.2).

As can be seen, the lateral static stability of an aircraft is the sum total of all the contributions. It is extremely important in determining the roll control characteristics of the aircraft and is probably one of the most difficult derivative characteristics to estimate reliably by means of simple analysis alone.

3.4.2 Directional static stability

Directional static stability is concerned with the ability of the aircraft to yaw or *weathercock* into wind in order to maintain directional equilibrium. Since all aircraft are required to fly with zero sideslip in the yaw sense, positive directional stability is designed in from the outset. The fin is the most visible contributor to directional static stability, although, as in the case of lateral stability, there are many other contributions, some of which are destabilising. Again, it is useful to remember that too much directional static stability results in an aircraft that is reluctant to manoeuvre directionally, so obtaining the correct degree of stability is important.

Consider an aircraft that is subject to a positive sideslip disturbance as shown in Fig. 3.21. The combination of sideslip velocity v and axial velocity component U results in a positive sideslip angle β . Note that a positive sideslip angle equates to a negative yaw angle since the nose of the aircraft has swung to the left of the resultant total velocity vector V . In the disturbance, as shown in Fig. 3.21, the fin is at a nonzero angle of attack equivalent to the sideslip angle β . It therefore generates lift L_F , which acts in the sense shown, thereby creating a positive yawing moment N . The yawing moment is stabilising since it causes the aircraft to yaw to the right until the sideslip angle

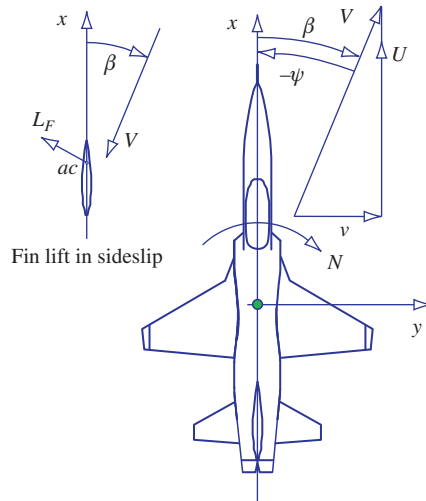


FIGURE 3.21 Directional weathercock effect.

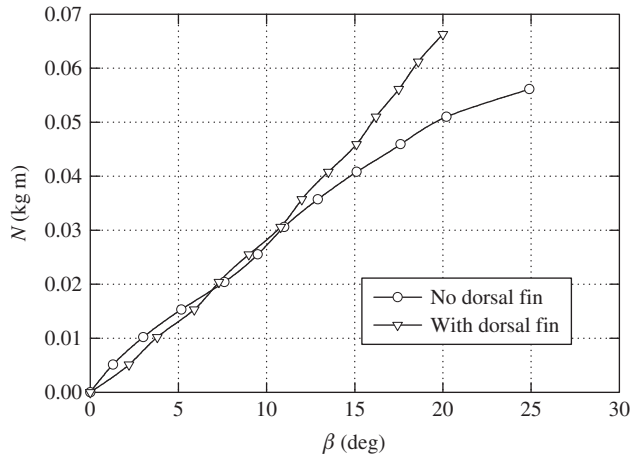


FIGURE 3.22 Plot of yawing moment against sideslip for a stable aircraft.

is reduced to zero. The condition for an aircraft to be directionally stable is thus readily established:

$$\frac{dC_n}{d\beta} > 0 \text{ or, equivalently, } \frac{dC_n}{d\psi} < 0 \quad (3.41)$$

where C_n is the yawing moment coefficient.

A typical plot of yawing moment against sideslip angle for a directionally stable aircraft is given in Fig. 3.22. It shows the results of a wind tunnel test on a simple conventional aircraft model. For small disturbances in yaw the plot is reasonably linear since it is dominated by the lifting properties of the fin. However, as the fin approaches the stall its lifting properties deteriorate and other influences begin to dominate, resulting ultimately in loss of directional stability. The main destabilising contribution comes from the fuselage, which at small yaw angles is masked by the powerful fin effect. The addition of a dorsal fin significantly delays the onset of fin stall, thereby enabling directional static stability to be maintained to higher yaw disturbance angles as indicated in Fig. 3.22.

Fin effectiveness also deteriorates with increasing body incidence angle since the base of the fin becomes increasingly immersed in the fuselage wake, which reduces its effectiveness. This problem has become particularly evident in a number of modern combat aircraft. Such aircraft typically have two engines mounted side by side in the rear fuselage. This results in a broad flat fuselage ahead of the fin, creating a substantial wake which dramatically reduces fin effectiveness at moderate to high angles of incidence. For this reason, many aircraft of this type have noticeably large fins and in some cases have two fins attached to the outer edges of the upper rear fuselage.

Additional sources of yawing moment in sideslip that contribute to the overall directional static stability of the aircraft may be identified, although they may not be so easy to quantify. For

example, as shown in Fig. 3.16 and Fig. 3.19, dihedral effect gives rise to differential lift across the wing span when in a sideslip disturbance. The associated differential-induced drag generates a yawing moment which usually gives rise to a contribution to directional static stability. The side area of the fuselage, especially in very large aircraft, also makes some contribution to directional static stability. The side area ahead of and aft of the *cg* generates yawing moment in sideslip, and the magnitude and sign depend on the distribution of side area about the *cg*. Typically, the yawing moment due to sideslip arising from the side area is often negative and hence destabilising. These contributions to directional static stability are also discussed in more detail in Chapter 13 (Section 13.3.2).

Once again, the directional static stability of an aircraft is the sum total of all contributions. It is extremely important in determining the ability of the aircraft to fly straight and to manoeuvre in yaw, and it is also difficult to estimate reliably by means of simple analysis.

3.5 Calculation of aircraft trim condition

As described in Section 3.1, the condition for an aircraft to remain in steady trimmed flight requires that the forces and moments acting on it sum to zero and that it is stable. Thus in calculating the trim condition of an aircraft it is convenient to assume straight, or symmetric, flight and to apply the principles described earlier in this chapter. For a given aircraft mass, *cg* position, altitude, and airspeed, symmetric trim is described by the aerodynamic operating condition—namely, angle of attack, thrust, pitch attitude, elevator angle, and flight path angle. Other operating condition parameters can then be derived as required.

The forces and moments acting on an aeroplane in the general case of steady symmetric climbing flight are shown in Fig. 3.23, where the symbols have their usual meanings. Since the aircraft is symmetric, the lateral-directional forces and moments are assumed to remain in equilibrium throughout, so the problem reduces to the establishment of longitudinal equilibrium only. Thus, the reference axes are aircraft body axes which define the plane of symmetry *oxz*, with the origin *o* located at the aircraft *cg* as shown.

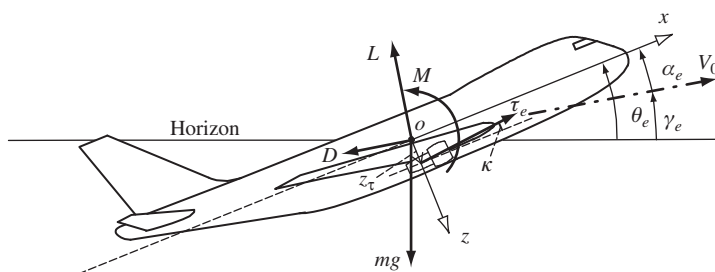


FIGURE 3.23 Symmetric forces and moments acting on a trimmed aircraft.

3.5.1 Defining the trim condition

The total axial force X is given by resolving the total lift L , total drag D , weight mg , and thrust τ_e into the ox axis; these components must sum to zero in trim. Whence

$$X = L \sin\alpha_e + \tau_e \cos\kappa - D \cos\alpha_e - mg \sin(\alpha_e + \gamma_e) = 0 \quad (3.42)$$

where α_e is the equilibrium body incidence, γ_e is the steady flight path angle, and κ is the inclination of the thrust line to the ox body axis (positive nose up). Similarly, the total normal force Z is given by resolving the forces into the oz axis which must also sum to zero in trim. Whence

$$Z = mg \cos(\alpha_e + \gamma_e) - L \cos\alpha_e - D \sin\alpha_e - \tau_e \sin\kappa = 0 \quad (3.43)$$

The development of the aerodynamic pitching moment about the cg is described in [Section 3.2](#) and is given by [equation \(3.6\)](#). However, since the total pitching moment is required, [equation \(3.6\)](#) must be modified to include the thrust and any other significant moment contributions. As before, the total drag moment is assumed insignificant since the normal displacement between the cg and aerodynamic centre is typically small for most aircraft configurations. Also, the tailplane zero-lift pitching moment M_T is assumed small since the aerofoil section is usually symmetrical; and the tailplane drag moment is also very small since the tailplane setting would be designed to trim at a small local incidence angle. Thus the total pitching moment about the cg is given by the sum of the wing-body, tailplane, and thrust moments, which must sum to zero in trim. Whence

$$M = M_0 + L_w(h - h_0)\bar{\bar{c}} - L_T l_T + \tau_e z_\tau = 0 \quad (3.44)$$

where L_w is the wing-body lift and L_T is the tailplane lift. The other symbols are evident from [Fig. 3.23](#).

It is convenient to write [equations \(3.42\) through \(3.44\)](#) in coefficient form:

$$\frac{mg}{\frac{1}{2}\rho V_0^2 S} \sin(\alpha_e + \gamma_e) = C_\tau \cos\kappa + C_L \sin\alpha_e - C_D \cos\alpha_e \quad (3.45)$$

$$\frac{mg}{\frac{1}{2}\rho V_0^2 S} \cos(\alpha_e + \gamma_e) = C_L \cos\alpha_e + C_D \sin\alpha_e + C_\tau \sin\kappa \quad (3.46)$$

$$C_m = C_{m_0} + (h - h_0)C_{L_w} - \bar{V}_T C_{L_T} + \frac{z_\tau}{\bar{\bar{c}}} C_\tau = 0 \quad (3.47)$$

where the thrust coefficient is given by

$$C_\tau = \frac{\tau_e}{\frac{1}{2}\rho V_0^2 S} \quad (3.48)$$

the total lift coefficient is given by

$$C_L = C_{L_w} + \frac{S_T}{S} C_{L_T} \quad (3.49)$$

and the total drag coefficient is given by

$$C_D = C_{D_0} + \frac{1}{\pi A e} C_L^2 \equiv C_{D_0} + K C_L^2 \quad (3.50)$$

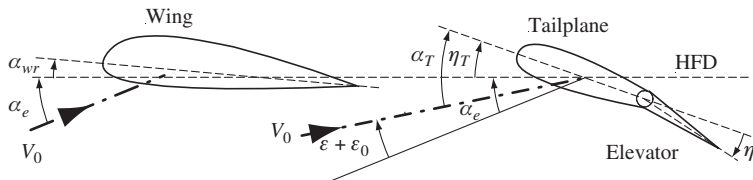


FIGURE 3.24 Practical wing-tailplane aerodynamic geometry.

The wing-body lift coefficient, which is assumed to comprise wing aerodynamic properties only, is given by

$$C_{L_w} = a(\alpha_w - \alpha_{w0}) \equiv a(\alpha_e + \alpha_{wr} - \alpha_{w0}) \quad (3.51)$$

where α_{wr} is the wing rigging angle as shown in Fig. 3.24 and α_{w0} is the zero-lift angle of attack of the wing.

Simultaneous solution of equations (3.45) through (3.51) for a given flight condition determines the values of the aerodynamic coefficients and the body incidence defining the aircraft trim state.

3.5.2 Elevator angle to trim

Once the trim condition is determined, the important elevator angle to trim can be derived along with other useful trim variables. However, the basic aerodynamic relationships described earlier represent the simplest possible definitions in the interests of functional visibility. For a practical aircraft application, it is necessary to take additional contributions into account when assembling the defining equations. For example, the wing-tail aerodynamic relationship is modified by the constraints of a practical layout as illustrated in Fig. 3.24, which is of course a modified version of Fig. 3.9 that includes the wing rigging angle α_{wr} and a zero-lift downwash term ε_0 .

The aircraft-fixed reference for the angle definitions is the *horizontal fuselage datum* (HFD), which is usually a convenient *base line*, or *centre line*, for the aircraft geometric layout. It is convenient to define the aircraft *ox* body axis parallel to the HFD, with its origin located at the *cg*; this is shown in Fig. 3.25.

With reference to Fig. 3.24, wing angle of attack is given by

$$\alpha_w = \alpha_e + \alpha_{wr} \quad (3.52)$$

and tailplane angle of attack is given by

$$\alpha_T = \eta_T + \alpha_e - \varepsilon - \varepsilon_0 = \eta_T + \alpha_w - \alpha_{wr} - \varepsilon - \varepsilon_0 \quad (3.53)$$

With reference to equation (3.10),

$$\alpha_w - \varepsilon = \alpha_w \left(1 - \frac{d\varepsilon}{d\alpha} \right) \quad (3.54)$$

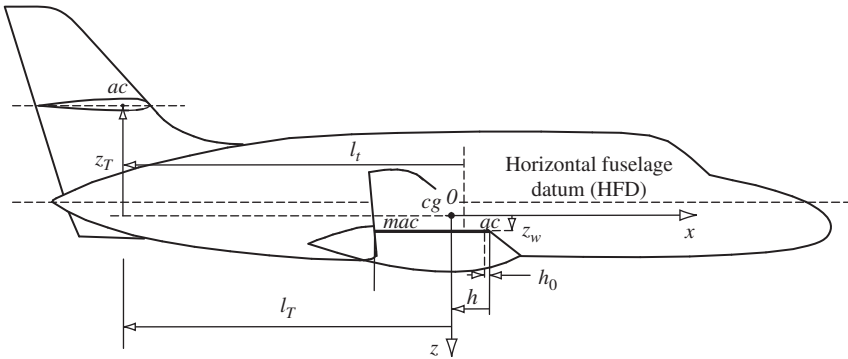


FIGURE 3.25 Practical aircraft longitudinal geometry.

and [equation \(3.53\)](#) may be written as

$$\alpha_T = \eta_T + \alpha_w \left(1 - \frac{d\varepsilon}{d\alpha} \right) - \alpha_{wr} - \varepsilon_0 \quad (3.55)$$

It is assumed that the elevator trim tab angle is zero and that aircraft trim is determined by the elevator angle to trim η_e . As before, it is assumed that $a_0 = 0$ since the tailplane aerofoil section is typically symmetrical. The tailplane lift coefficient given by [equation \(3.8\)](#) may therefore be restated with the appropriate substitution of [equation \(3.55\)](#):

$$C_{L_T} = a_1 \alpha_T + a_2 \eta_e = a_1 \left(\eta_T + \alpha_w \left(1 - \frac{d\varepsilon}{d\alpha} \right) - \alpha_{wr} - \varepsilon_0 \right) + a_2 \eta_e \quad (3.56)$$

The elevator angle to trim thus follows by rearrangement of [equation \(3.56\)](#):

$$\eta_e = \frac{C_{L_T}}{a_2} - \frac{a_1}{a_2} \left(\eta_T + \alpha_w \left(1 - \frac{d\varepsilon}{d\alpha} \right) - \alpha_{wr} - \varepsilon_0 \right) \quad (3.57)$$

Note that [equation \(3.57\)](#) is equivalent to [equation \(3.13\)](#).

3.5.3 Controls-fixed static stability

The location of the controls-fixed neutral point on the mean aerodynamic chord and the controls-fixed static margin are very important parameters in any aircraft trim assessment, since they both influence the aerodynamic, thrust, and control requirements for achieving trim. In practice, the achievement of a satisfactory range of elevator angles to trim over the flight envelope is determined by the static margin, and this in turn places constraints on the permitted range of cg positions. The neutral point usually determines the most aft cg limit in a stable aircraft. Fortunately, the simple

expressions given by [equations \(3.17\) and \(3.18\)](#) are sufficient for most practical assessment, and they are repeated here for convenience. The neutral point location h_n is given by

$$h_n = h_0 + \bar{V}_T \frac{a_1}{a} \left(1 - \frac{d\varepsilon}{d\alpha} \right) \quad (3.58)$$

and the static margin K_n is given by

$$K_n = h_n - h \quad (3.59)$$

Estimation of the wing-body aerodynamic centre location h_0 on the mean aerodynamic chord requires careful consideration. For a subsonic wing, typically $h_0 = 0.25$. For the purpose of illustrating the simple theory in [Section 3.3](#), this value is often assumed, incorrectly, to apply to a wing-body combination. However, the presence of the fuselage usually causes a forward shift of the combined wing-body aerodynamic centre to a value more like $h_0 = 0.1$ or less. Clearly, this has an impact on the requirements for trim, and it is important to obtain the best estimate of its location. This can be done by wind tunnel tests on a wing-body combination or, more conveniently, by reference to empirical data sources. Estimation of h_0 is described in ESDU 92024, Volume 4b ([ESDU, 2006](#)).

Estimation of the rate of change of downwash angle at the tail with wing angle of attack is another parameter that requires careful estimation, and for the same reasons. Typical values are in the region of $d\varepsilon/d\alpha \approx 0.5$, but the geometric location of the tailplane with respect to the wing strongly influences the actual value. Again, a value can be estimated by wind tunnel testing of a suitable model. Alternatively, $d\varepsilon/d\alpha$ can be estimated with the aid of ESDU 80020, Volume 9a ([ESDU, 2006](#)). A simple computer program for estimating $d\varepsilon/d\alpha$ may be found in [Stribling \(1984\)](#), and the use of this program is illustrated in the next section.

3.5.4 “AeroTrim”: A Mathcad trim program

A computer program called “AeroTrim” has been written by the author in the Mathcad language to implement the trim calculations described previously; a listing is given in Appendix 1. Since Mathcad permits the development of programs in the format of a mathematical document, the listing is easy to read and is self-explanatory. Because of its computational visibility, Mathcad is an ideal tool for programs of this type, although the program could be written in a number of alternative languages.

AeroTrim is a simple generic trim calculator limited to subsonic flight at altitudes up to 36,000 ft. However, it is very easy for the user to modify the program to suit particular requirements, and it should be regarded as a foundation for such further development. Indeed, the author has produced versions of the program to deal with transonic flight conditions and aircraft performance, and versions can be substantially extended to include aerodynamic derivative estimation.

As listed in Appendix 1, AeroTrim includes numerical data for the Cranfield University National Flying Laboratory Centre (NFLC) Jetstream 31 aircraft. To use it for other aircraft applications it is necessary only to delete and replace the numerical data where prompted to do so. Although based on simple mathematical models, the program produces plausible estimates for the known trim characteristics of the Jetstream, but the small differences from observed practice are thought to be due mainly to propeller effects, which are notoriously difficult to model adequately.

With the program loaded into Mathcad, operation is as simple as clicking on the Calculate button. The impact on trim of changing one or more of the numerical input values can thus be evaluated instantaneously. Points to note include the following:

- Section 1.** The user inputs flight condition data for which a trim evaluation is required.
- Section 2.** The program calculates atmospheric temperature, air density, and density ratio for the chosen altitude based on the ISA model. It is currently limited to the troposphere, but is easily modified to include the stratosphere.
- Section 3.** The user defines the velocity range over which the trim conditions are required, bearing in mind that the computations are valid only for subsonic flight conditions. The counter sets the number of velocity steps through the range, currently set at 10. The range expression sets the starting velocity, currently set at 100 knots, and the increment, currently set at 15 knots.
- Section 4.** The user inserts values for the aircraft geometry constants, taking care to observe the body axis system used. All of this information would be readily available in a three-dimensional drawing of the aircraft.
- Section 5.** The user inputs values for the principal wing-body aerodynamic parameters for the aircraft. Unknowns obviously have to be estimated by whatever means are available.
- Section 6.** The user inputs values for the tailplane aerodynamic parameters. Again, unknowns have to be estimated by whatever means are available.
- Section 7.** The program calculates some basic wing-body-tail parameters.
- Section 8.** The program estimates $d\varepsilon/d\alpha$ for the given aircraft geometry using a simple algorithm described by [Stribling \(1984\)](#). Since the model does not include fuselage interference effects or thrust effects, it may underestimate the parameter by a small amount. However, results obtained with the algorithm seem to be plausible and appropriate.
- Section 9.** The program estimates the induced-drag factor K in the drag polar $C_D = C_{D_0} + KC_L^2$ using an empirical method described in Shevell (1983), which is based on industrial flight test experience. The very limited data for the fuselage drag factor s_d and the empirical constant k_D were plotted and curves were fitted to give expressions suitable for inclusion in the computation. Results obtained for the Jetstream compare very favourably with the known drag properties of the aircraft.
- Section 10.** The program calculates some useful standard performance and stability parameters.
- Section 11.** The program calculates the trim conditions, solving [equations \(3.45\) through \(3.51\)](#) simultaneously for each velocity step defined in [Section 3](#).
- Section 12.** The program calculates the dependent trim variables, including elevator angle, for the velocity steps defined in [Section 3](#) and using the results of Section 11.
- Sections 13 and 14.** These are self-explanatory auxiliary computations.
- Section 15.** Results: The program gives a summary of the flight condition parameters for the chosen application.
- Section 16.** Results: The program gives a tabulated summary of the trim values of all variables at each velocity step in the range chosen.
- Section 17.** Results: the program shows some plotted variables to illustrate the kind of output Mathcad can provide. It is very easy to edit this section to include plots of any variables from the table in Section 16.

EXAMPLE 3.4

To illustrate the use of AeroTrim the program is applied to the NFLC Jetstream 31 aircraft. Since a comprehensive flight simulation model of the aircraft has been assembled and matched to observed flight behaviour, the numerical data are believed to be reasonably representative. The sources of data used include manufacturers' published technical information, the flight manual, limited original wind tunnel test data, and data obtained from flight experiments. Aerodynamic data not provided by any of these sources were estimated using the ESDU Aerodynamics Series ([ESDU, 2006](#)) and refined by reference to observed flight behaviour. The numerical data are not listed here since they are illustrated in the Mathcad listing in Appendix 1.

The chosen operating condition is typical for the aircraft, and the speed range was chosen to vary from the stall, at around 100 knots, to 250 knots in 15-knot increments. Good-quality data for the remaining input parameters were available, with the possible exception of the values for wing-body aerodynamic centre position h_0 and the rate of change of downwash at the tail with wing angle of attack $d\varepsilon/d\alpha$. Both parameters were estimated for the aircraft, although the actual

Flight Condition	Units	Value
Aircraft weight	kN	61.8
Altitude	ft	6562
Flight path angle	deg	0
cg position		0.29
Neutral point		0.412
Static margin		0.122
Minimum drag speed	knots	150
Stall speed	knots	116

Example Trim Data									
V_{true} (knots)	C_L	C_D	C_τ	L/D	α_e (deg)	η_e (deg)	L (kN)	D (kN)	τ_e (kN)
100	1.799	0.174	0.181	9.409	15.105	-1.208	60.23	5.834	6.042
115	1.374	0.114	0.116	11.017	10.885	-0.460	60.83	5.053	5.146
130	1.081	0.082	0.083	12.106	7.970	0.100	61.15	4.643	4.688
145	0.872	0.064	0.064	12.603	5.885	0.521	61.34	4.494	4.518
160	0.717	0.053	0.053	12.573	4.346	0.842	61.46	4.535	4.548
175	0.600	0.046	0.046	12.154	3.181	1.091	61.54	4.722	4.729
190	0.510	0.042	0.042	11.496	2.277	1.287	61.60	5.025	5.029
205	0.438	0.039	0.039	10.720	1.564	1.444	61.65	5.424	5.426
220	0.381	0.036	0.036	9.912	0.990	1.572	61.70	5.907	5.908
235	0.334	0.035	0.035	9.123	0.523	1.677	61.74	6.465	6.465
250	0.295	0.034	0.034	8.383	0.136	1.764	61.79	7.089	7.089

value for $d\varepsilon/d\alpha$ is thought to be larger than that estimated by the program. Using the value $d\varepsilon/d\alpha = 0.279$ as calculated, the value of $h_0 = -0.08$ was estimated since it returned values for the neutral point position h_n and static margin K_n close to their known values. It is likely that this places the aerodynamic centre too far forward in the aircraft. However, with a value of $d\varepsilon/d\alpha$ nearer to its probable value, $d\varepsilon/d\alpha \approx 0.4$, a more aft aerodynamic centre position would return the known stability properties. This illustrates one of the difficulties of gathering reliable aerodynamic data for an aircraft. For unconventional configurations the difficulties are generally greater. Running the program returns trim data for the chosen operating flight condition, of which a reduced selection is shown.

For the purpose of trim analysis, the data can be graphed as required, and some examples are given in the Mathcad program listing. It follows that the effect of any aerodynamic variable on aircraft design performance can be evaluated quickly using the program. Indeed, this approach was used to identify plausible values for some of the more uncertain values in the model definition.

References

- Babister, A. W. (1961). *Aircraft stability and control*. London: Pergamon Press.
- Cook, M. V. (1994). The theory of the longitudinal static stability of the hang-glider. *Aeronautical Journal*, 98, 978.
- Duncan, W. J. (1959). *The principles of the control and stability of aircraft*. Cambridge, UK: Cambridge University Press.
- ESDU (2006). *ESDU aerodynamics series*. London: IHS ESDU International, www.esdu.com.
- Gates, S. B., & Lyon, H. M. (1944). *A continuation of longitudinal stability and control analysis: Part 1, general theory*, Reports and Memoranda No. 2027, Aeronautical Research Council. Her Majesty's Stationery Office, London.
- Shevell, R. S. (1989). *Fundamentals of flight* (2nd ed.). Englewood Cliffs, NJ: Prentice Hall, USA.
- Storey, R. F. R. (1966). *H.P.137. Longitudinal and lateral stability measurements on a 1/6th scale model*, W.T. Report No. 3021. Weybridge: Surrey: BAC (Operating) Ltd.
- Stribling, C. B. (1984). *Basic aerodynamics*. London: Butterworth & Co.

Source

Mathcad. Adept Scientific, Amor Way, Letchworth, Herts, SG6 1ZA. <www.adeptscience.co.uk>.

PROBLEMS

- 3.1** Explain why the pitching moment coefficient $C_{m_{ac}}$ about the aerodynamic centre of an aerofoil is constant. What is the special condition for $C_{m_{ac}}$ to be zero?

The NACA 64-412 is a cambered aerofoil with lift coefficient given by

$$C_L = 0.11\alpha + 0.3$$

where α is in degree units. What is the value of the constant pitching moment coefficient about the aerodynamic centre? Estimate the position of the centre of pressure for the aerofoil at an angle of attack of 5 deg. State all assumptions made in answering this question.

(CU 1998)

- 3.2** What are the conditions for the stable longitudinal trim equilibrium of an aircraft? The pitching moment coefficient about the *cg* for a stable aircraft is given by

$$C_m = C_{m_0} + C_{L_w}(h - h_0) - \bar{V}_T \left(C_{L_w} \frac{a_1}{a} \left(1 - \frac{d\varepsilon}{d\alpha} \right) + a_2 \eta \right)$$

where the symbols have the usual meaning. Derive expressions for the controls-fixed static margin K_n and the elevator angle to trim as a function of static margin. Explain the physical meaning of the controls-fixed neutral point.

(CU 1998)

- 3.3** State the conditions required for an aircraft to remain in longitudinal trimmed equilibrium in steady level flight. The pitching moment equation, referred to the centre of gravity (*cg*), for a canard-configured combat aircraft is given by

$$C_m = C_{m_0} + (h - h_0)C_{L_{wb}} + \bar{V}_f \left(\frac{a_{1_f}}{a_{wb}} C_{L_{wb}} + a_{1_f} \delta \right)$$

where the symbols have the usual meaning; additionally, \bar{V}_f is the foreplane volume ratio, a_{1_f} is the foreplane lift curve slope, and δ is the control angle of the all-moving foreplane.

- (a) Derive expressions for the controls-fixed static margin and for the controls-fixed neutral point. State any assumptions made.
 (b) Given that the mean aerodynamic chord (*mac*) is 4.7 m, the wing-body aerodynamic centre is located at 15% of *mac*, the foreplane volume ratio is 0.12, and the lift curve slopes of the wing-body and foreplane are 3.5 rad^{-1} and 4.9 rad^{-1} , respectively, calculate the aft *cg* limit for the aircraft to remain stable with controls fixed. Calculate also the *cg* location for the aircraft to have a controls-fixed static margin of 15%.

(CU 1999)

- 3.4** Sketch a typical $C_m - \alpha$ plot and explain the condition for trim, the requirement for static stability, and the concept of stability margin. Why is too much stability as hazardous as too little?

(CU 2001)

The Equations of Motion

4

4.1 The equations of motion for a rigid symmetric aircraft

As stated in Chapter 1, the first formal derivation of the equations of motion for a rigid symmetric aircraft is usually attributed to [Bryan \(1911\)](#). Bryan's treatment, with very few changes, remains in use today and provides the basis for the following development. The derivation of the equations of motion is based on the application of Newton's second law of motion, which states,

The acceleration of a particle acted on by a force is proportional to and in the direction of the force, the factor of proportionality being independent of the force and the time.

Generalisation of Newton's second law to a rigid body, rather than a particle, together with analytical consideration of momentum, leads to the *principles of linear and angular momentum*, which state,

The rate of change of linear momentum of a rigid body in any direction equals the sum of the components of the external forces acting on the body in that direction.

The rate of change of angular momentum of a rigid body about any fixed axis is equal to the sum of the moments of the external forces acting on the body about that axis.

With the appropriate definitions and choice of units, these principles are commonly interpreted as

$$\begin{aligned} \text{Force} &= \text{Mass} \times \text{Inertial Acceleration} \\ \text{Moment} &= \text{Moment of Inertia} \times \text{Angular Acceleration} \end{aligned} \quad (4.1)$$

Thus the derivation of the equations of motion requires that [equations \(4.1\)](#) be developed and expressed in terms of the motion variables defined in Chapter 2. The derivation is *classical* in the sense that the equations of motion are differential equations derived from first principles. However, a number of equally valid alternatives for deriving these equations are in common use—for example, methods based on the use of vector algebra. The classical approach is retained here since, in the author's opinion, maximum physical visibility is maintained throughout.

4.1.1 The components of inertial acceleration

The first task in realising [equations \(4.1\)](#) is to define the inertial acceleration components that result from application of the components of external force acting on the aircraft. Consider the motion referred to an orthogonal axis set ($oxyz$) with the origin o coincident with the *cg* of the arbitrary and, in the first instance, not necessarily rigid body shown in [Fig. 4.1](#). The body, and hence the

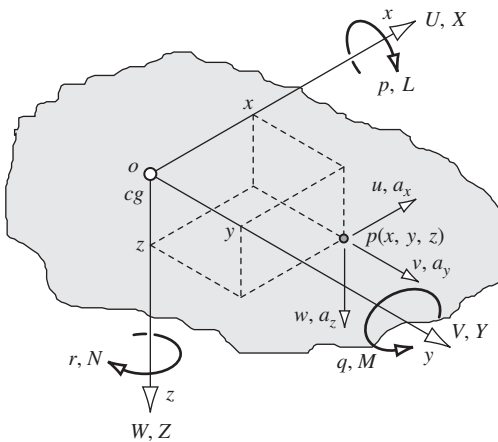


FIGURE 4.1 Motion referred to generalised body axes.

axes, is assumed to be in motion with respect to an external reference frame such as earth (or *inertial*) axes. The components of velocity and force along the axes ox , oy , and oz are denoted (U, V, W) and (X, Y, Z) , respectively. The components of angular velocity and moment about the same axes are denoted (p, q, r) and (L, M, N) , respectively. The point p is an arbitrarily chosen point within the body with coordinates (x, y, z) . The local components of velocity and acceleration at p relative to the body axes are denoted (u, v, w) and (a_x, a_y, a_z) , respectively.

The velocity components at $p(x, y, z)$ relative to o are given by

$$\begin{aligned} u &= \dot{x} - ry + qz \\ v &= \dot{y} - pz + rx \\ w &= \dot{z} - qx + py \end{aligned} \quad (4.2)$$

It will be seen that they each comprise a linear term and two additional terms due to rotary motion. The origin of the terms due to rotary motion in the component u , for example, is illustrated in Fig. 4.2. Both $-ry$ and qz represent *tangential velocity* components acting along a line through $p(x, y, z)$ parallel to the ox axis. The rotary terms in the remaining two components of velocity are determined in a similar way. Now, since the generalised body shown in Fig. 4.1 represents the aircraft, which is assumed to be rigid,

$$\dot{x} = \dot{y} = \dot{z} = 0 \quad (4.3)$$

and equations (4.2) reduce to

$$\begin{aligned} u &= qz - ry \\ v &= rx - pz \\ w &= py - qx \end{aligned} \quad (4.4)$$

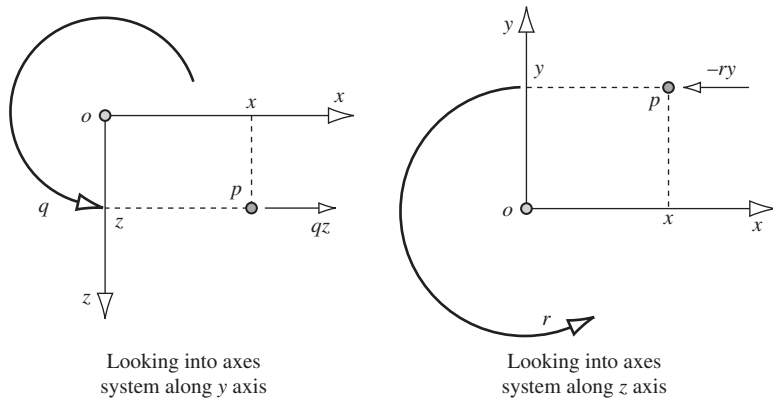


FIGURE 4.2 Velocity terms due to rotary motion.

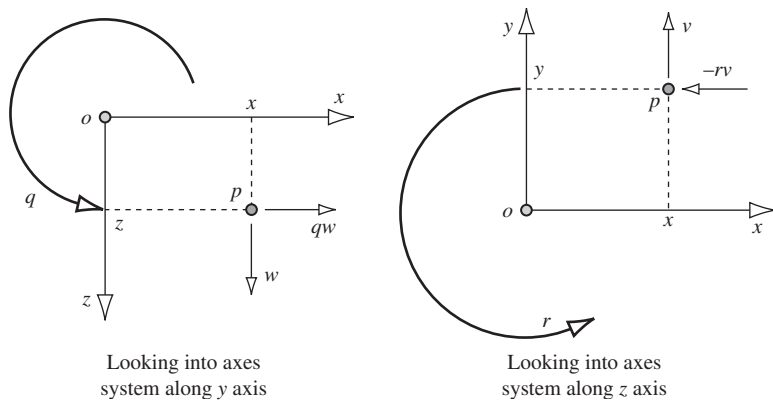


FIGURE 4.3 Acceleration terms due to rotary motion.

The corresponding components of acceleration at $p(x, y, z)$ relative to o are given by

$$\begin{aligned} a_x &= \dot{u} - rv + qw \\ a_y &= \dot{v} - pw + ru \\ a_z &= \dot{w} - qu + pv \end{aligned} \quad (4.5)$$

Again, it will be seen that the acceleration components each comprise a linear term and two additional terms due to rotary motion. The origin of the terms due to rotary motion in the component a_x , for example, is illustrated in Fig. 4.3. Both $-rv$ and qw represent *tangential acceleration* components acting along a line through $p(x, y, z)$ parallel to the ox axis. The accelerations arise from the mutual interaction of the linear components of velocity with the components of angular velocity. The acceleration terms due to rotary motion in the remaining two components of acceleration are determined in a similar way.

By superimposing the velocity components of the *cg* (U, V, W) on the local velocity components (u, v, w), the absolute, or inertial, velocity components (u', v', w') of the point $p(x, y, z)$ are obtained. Thus

$$\begin{aligned} u' &= U + u = U - ry + qz \\ v' &= V + v = V - pz + rx \\ w' &= W + w = W - qx + py \end{aligned} \quad (4.6)$$

where the expressions for (u, v, w) are substituted from [equations \(4.4\)](#). Similarly, the components of inertial acceleration (a'_x, a'_y, a'_z) at the point $p(x, y, z)$ are obtained simply by substituting the expressions for (u', v', w'), [equations \(4.6\)](#) for (u, v, w) in [equations \(4.5\)](#). Whence

$$\begin{aligned} a'_x &= \dot{u}' - rv' + qw' \\ a'_y &= \dot{v}' - pw' + ru' \\ a'_z &= \dot{w}' - qu' + pv' \end{aligned} \quad (4.7)$$

Differentiate [equations \(4.6\)](#) with respect to time and note that since a rigid body is assumed, [equation \(4.3\)](#) applies. Then

$$\begin{aligned} \dot{u}' &= \dot{U} - \dot{r}y + \dot{q}z \\ \dot{v}' &= \dot{V} - \dot{p}z + \dot{r}x \\ \dot{w}' &= \dot{W} - \dot{q}x + \dot{p}y \end{aligned} \quad (4.8)$$

Thus, by substituting from [equations \(4.6\)](#) and [\(4.8\)](#) into [equations \(4.7\)](#), the inertial acceleration components of the point $p(x, y, z)$ in the rigid body are obtained, which, after some rearrangement, may be written as

$$\begin{aligned} a'_x &= \dot{U} - rV + qW - x(q^2 + r^2) + y(pq - \dot{r}) + z(pr + \dot{q}) \\ a'_y &= \dot{V} - pW + rU + x(pq + \dot{r}) - y(p^2 + r^2) + z(qr - \dot{p}) \\ a'_z &= \dot{W} - qU + pV + x(pr - \dot{q}) + y(qr + \dot{p}) - z(p^2 + q^2) \end{aligned} \quad (4.9)$$

EXAMPLE 4.1

To illustrate the usefulness of [equations \(4.9\)](#), consider the following simple example.

A pilot in an aerobatic aircraft performs a loop in 20 s at a steady velocity of 100 m/s. His seat is located 5 m ahead of, and 1 m above the *cg*. What total normal load factor does he experience at the top and at the bottom of the loop?

Assuming that the motion is in the plane of symmetry only, then $V = \dot{p} = p = r = 0$ and, since the pilot's seat is also in the plane of symmetry, $y = 0$. The expression for normal acceleration is, from [equations \(4.9\)](#),

$$a'_z = \dot{W} - qU + x\dot{q} - zq^2$$

Since the manoeuvre is steady, a further simplification can be made, $\dot{W} = \dot{q} = 0$, and the expression for the normal acceleration at the pilot's seat reduces to

$$a'_z = -qU - zq^2$$

Now,

$$q = \frac{2\pi}{20} = 0.314 \text{ rad/s}$$

$$U = 100 \text{ m/s}$$

$$x = 5 \text{ m}$$

$$z = -1 \text{ m (above cg hence negative)}$$

whence $a'_z = -31.30 \text{ m/s}^2$. Now, by definition, the corresponding incremental normal load factor due to the manoeuvre is given by

$$n' = \frac{-a'_z}{g} = \frac{31.30}{9.81} = 3.19$$

The total normal load factor n comprises that due to the manoeuvre n' plus that due to gravity n_g . At the top of the loop $n_g = -1$; thus the total normal load factor is given by

$$n = n' + n_g = 3.19 - 1 = 2.19$$

and at the bottom of the loop $n_g = 1$ and in this case the total normal load factor is given by

$$n = n' + n_g = 3.19 + 1 = 4.19$$

It is interesting that the normal acceleration measured by an accelerometer mounted at the pilot's seat corresponds with the total normal load factor. The accelerometer therefore gives the following readings:

At the top of the loop $a_z = ng = 2.19 \times 9.81 = 21.48 \text{ m/s}^2$.

At the bottom of the loop $a_z = ng = 4.19 \times 9.81 = 41.10 \text{ m/s}^2$.

Equations (4.9) can therefore be used to determine the accelerations that would be measured by suitably aligned accelerometers located at any point in the airframe and defined by the coordinates (x, y, z) .

4.1.2 The generalised force equations

Consider now an incremental mass δm at point $p(x, y, z)$ in the rigid body. Applying the first of **equations (4.1)** to the incremental mass, the incremental components of force acting on the mass are given by $(\delta ma'_x, \delta ma'_y, \delta ma'_z)$. Thus the total force components (X, Y, Z) acting on the body are given by summing the force increments over the whole body; whence

$$\begin{aligned}\Sigma \delta ma'_x &= X \\ \Sigma \delta ma'_y &= Y \\ \Sigma \delta ma'_z &= Z\end{aligned}\tag{4.10}$$

Substitute the expressions for the components of inertial acceleration (a'_x, a'_y, a'_z) from [equations \(4.9\)](#) into [equations \(4.10\)](#) and note that since the origin of axes coincides with the *cg*,

$$\Sigma\delta mx = \Sigma\delta my = \Sigma\delta mz = 0 \quad (4.11)$$

Therefore, the resultant components of total force acting on the rigid body are given by

$$\begin{aligned} m(\dot{U} - rV + qW) &= X \\ m(\dot{V} - pW + rU) &= Y \\ m(\dot{W} - qU + pV) &= Z \end{aligned} \quad (4.12)$$

where m is the total mass of the body.

[Equations \(4.12\)](#) represent the force equations of a generalised rigid body and describe the motion of its *cg* since the origin of the axis system is co-located with the *cg* in the body. In some applications, the airship for example, it is often convenient to locate the origin of the axis system at some point other than the *cg*. In such cases the condition described by [equation \(4.11\)](#) does not apply and [equations \(4.12\)](#) would include rather more terms.

4.1.3 The generalised moment equations

Consider now the moments produced by the forces acting on the incremental mass δm at point $p(x, y, z)$ in the rigid body. The incremental force components create an incremental moment component about each of the three body axes, and by summing these over the whole body the moment equations are obtained. The moment equations are, of course, the realisation of the angular equation of motion given in [equations \(4.1\)](#).

For example, the total moment L about the *ox* axis is given by summing the incremental moments over the whole body:

$$\Sigma\delta m(ya'_z - za'_y) = L \quad (4.13)$$

Substituting in [equation \(4.13\)](#) for a'_y and a'_z obtained from [equations \(4.9\)](#), and noting that [equation \(4.11\)](#) applies, after some rearrangement [equation \(4.13\)](#) may be written as

$$\left(\dot{p}\Sigma\delta m(y^2 + z^2) + qr\Sigma\delta m(y^2 - z^2) + (r^2 - q^2)\Sigma\delta myz - (pq + \dot{r})\Sigma\delta mxz + (pr - \dot{q})\Sigma\delta mxy \right) = L \quad (4.14)$$

Terms under the summation sign Σ in [equation \(4.14\)](#) have the units of moment of inertia; thus it is convenient to define the moments and products of inertia as set out in [Table 4.1](#).

[Equation \(4.14\)](#) may therefore be rewritten as

$$I_x\ddot{p} - (I_y - I_z)qr + I_{xy}(pr - \dot{q}) - I_{xz}(pq + \dot{r}) + I_{yz}(r^2 - q^2) = L \quad (4.15)$$

Table 4.1 Moments and Products of Inertia

$I_x = \Sigma \delta m(y^2 + z^2)$	Moment of inertia about ox axis
$I_y = \Sigma \delta m(x^2 + z^2)$	Moment of inertia about oy axis
$I_z = \Sigma \delta m(x^2 + y^2)$	Moment of inertia about oz axis
$I_{xy} = \Sigma \delta m xy$	Product of inertia about ox and oy axes
$I_{xz} = \Sigma \delta m xz$	Product of inertia about ox and oz axes
$I_{yz} = \Sigma \delta m yz$	Product of inertia about oy and oz axes

In a similar way the total moments M and N about the oy and oz axes, respectively, are given by summing the incremental moment components over the whole body:

$$\begin{aligned}\Sigma \delta m(z a'_x - x a'_z) &= M \\ \Sigma \delta m(x a'_y - y a'_x) &= N\end{aligned}\quad (4.16)$$

Substituting a'_x , a'_y and a'_z from [equations \(4.9\)](#) into [equations \(4.16\)](#), noting again that [equation \(4.11\)](#) applies, and making use of the inertia definitions given in [Table 4.1](#), the moment M about the oy axis is given by

$$I_y \dot{q} + (I_x - I_z)pr + I_{yz}(pq - \dot{r}) + I_{xz}(p^2 - r^2) - I_{xy}(qr + \dot{p}) = M \quad (4.17)$$

and the moment N about the oz axis is given by

$$I_z \dot{r} - (I_x - I_y)pq - I_{yz}(pr + \dot{q}) + I_{xz}(qr - \dot{p}) + I_{xy}(q^2 - p^2) = N \quad (4.18)$$

[Equations \(4.15\), \(4.17\), and \(4.18\)](#) represent the moment equations of a generalised rigid body and describe the rotational motion about the orthogonal axes through its cg since the origin of the axis system is co-located with the cg in the body.

When the generalised body represents an aircraft, the moment equations may be simplified since it is assumed that the aircraft is symmetric about the oxz plane and that the mass is uniformly distributed. As a result, the products of inertia $I_{xy} = I_{yz} = 0$. Thus the moment equations simplify to the following:

$$\begin{aligned}I_x \dot{p} - (I_y - I_z)qr - I_{xz}(pq + \dot{r}) &= L \\ I_y \dot{q} + (I_x - I_z)pr + I_{xz}(p^2 - r^2) &= M \\ I_z \dot{r} - (I_x - I_y)pq + I_{xz}(qr - \dot{p}) &= N\end{aligned}\quad (4.19)$$

[Equations \(4.19\)](#) describe rolling motion, pitching motion, and yawing motion, respectively. A further simplification can be made if it is assumed that the aircraft body axes are aligned to be *principal inertia axes*. In this special case the remaining product of inertia I_{xz} is also zero. This simplification is not often used owing to the difficulty of precisely determining the principal inertia axes. However, the symmetry of the aircraft determines that I_{xz} is generally very much smaller than I_x , I_y , and I_z and can often be neglected.

4.1.4 Perturbation forces and moments

Together, [equations \(4.12\)](#) and [\(4.19\)](#) comprise the generalised six degrees of freedom equations of motion of a rigid symmetric airframe having a uniform mass distribution. Further development of the equations of motion requires that the terms on the right hand side of the equations adequately describe the perturbation or disturbing forces and moments. The traditional approach, after [Bryan \(1911\)](#), is to assume that the disturbing forces and moments are due to aerodynamic effects, gravitational effects, movement of aerodynamic controls, power effects, and the effects of atmospheric disturbances. Thus, bringing together [equations \(4.12\)](#) and [\(4.19\)](#), they may be written to include these contributions as follows:

$$\begin{aligned} m(\dot{U} - rV + qW) &= X_a + X_g + X_c + X_p + X_d \\ m(\dot{V} - pW + rU) &= Y_a + Y_g + Y_c + Y_p + Y_d \\ m(\dot{W} - qU + pV) &= Z_a + Z_g + Z_c + Z_p + Z_d \\ I_x \dot{p} - (I_y - I_z)qr - I_{xz}(pq + \dot{r}) &= L_a + L_g + L_c + L_p + L_d \\ I_y \dot{q} + (I_x - I_z)pr + I_{xz}(p^2 - r^2) &= M_a + M_g + M_c + M_p + M_d \\ I_z \dot{r} - (I_x - I_y)pq + I_{xz}(qr - \dot{p}) &= N_a + N_g + N_c + N_p + N_d \end{aligned} \quad (4.20)$$

Now [equations \(4.20\)](#) describe the generalised motion of the aeroplane without regard for the magnitude of the motion and subject to the assumptions applying. The equations are *non-linear*, and their solution by analytical means is not generally practicable. Further, the terms on the right hand side of the equations must be replaced with suitable expressions, which are particularly difficult to determine for the most general motion. Typically, the continued development of the non-linear equations of motion and their solution is most easily accomplished using computer modelling or simulation techniques which are beyond the scope of this book.

To proceed with the development of the equations of motion for analytical purposes, the equations must be linearised. Linearisation is very simply accomplished by constraining the motion of the aeroplane to small perturbations about the trim condition.

4.2 The linearised equations of motion

Initially the aeroplane is assumed to be flying in steady trimmed rectilinear flight with zero roll, sideslip, and yaw angles. Thus the plane of symmetry of the aeroplane oxz is *vertical* with respect to the earth reference frame. At this flight condition the velocity of the aeroplane is V_0 , the components of linear velocity are (U_e, V_e, W_e) , and the angular velocity components are all zero. Since there is no sideslip, $V_e = 0$. A stable undisturbed atmosphere is also assumed such that

$$X_d = Y_d = Z_d = L_d = M_d = N_d = 0 \quad (4.21)$$

If now the aeroplane experiences a small perturbation about trim, the components of the linear disturbance velocities are (u, v, w) and the components of the angular disturbance velocities

are (p, q, r) with respect to the undisturbed aeroplane axes ($oxyz$). Thus the total velocity components of the cg in the disturbed motion are given by

$$\begin{aligned} U &= U_e + u \\ V &= V_e + v = v \\ W &= W_e + w \end{aligned} \quad (4.22)$$

By definition, (u, v, w) and (p, q, r) are small quantities such that terms involving their products and squares are insignificantly small and may be ignored. Thus, substituting [equations \(4.21\)](#) and [\(4.22\)](#) into [equations \(4.20\)](#), note that (U_e, V_e, W_e) are steady and hence constant, and eliminating the insignificantly small terms, the linearised equations of motion are obtained:

$$\begin{aligned} m(\dot{u} + qW_e) &= X_a + X_g + X_c + X_p \\ m(\dot{v} - pW_e + rU_e) &= Y_a + Y_g + Y_c + Y_p \\ m(\dot{w} - qU_e) &= Z_a + Z_g + Z_c + Z_p \\ I_x\ddot{p} - I_{xz}\dot{r} &= L_a + L_g + L_c + L_p \\ I_y\ddot{q} &= M_a + M_g + M_c + M_p \\ I_z\ddot{r} - I_{xz}\dot{p} &= N_a + N_g + N_c + N_p \end{aligned} \quad (4.23)$$

The development of expressions to replace the terms on the right hand side of [equations \(4.23\)](#) is now much simpler since it is only necessary to consider small disturbances about trim.

4.2.1 Gravitational terms

The weight force mg acting on the aeroplane may be resolved into components acting in each of the three aeroplane axes. When the aeroplane is disturbed these components vary according to the perturbations in attitude, thereby making a contribution to the disturbed motion. The gravitational contribution to [equations \(4.23\)](#) is thus obtained by resolving the aeroplane weight into the disturbed body axes. Since the origin of the aeroplane body axes is coincident with the cg , there is no weight moment about any axis. Therefore,

$$L_g = M_g = N_g = 0 \quad (4.24)$$

Since the aeroplane is flying wings level in the initial symmetric flight condition, the components of weight appear only in the plane of symmetry, as shown in [Fig. 4.4](#). Thus, in the steady state, the components of weight resolved into aeroplane axes are

$$\begin{bmatrix} X_{g_e} \\ Y_{g_e} \\ Z_{g_e} \end{bmatrix} = \begin{bmatrix} -mg \sin \theta_e \\ 0 \\ mg \cos \theta_e \end{bmatrix} \quad (4.25)$$

During the disturbance the aeroplane attitude perturbation is (ϕ, θ, ψ) and the components of weight in the disturbed aeroplane axes may be derived with the aid of the transformation

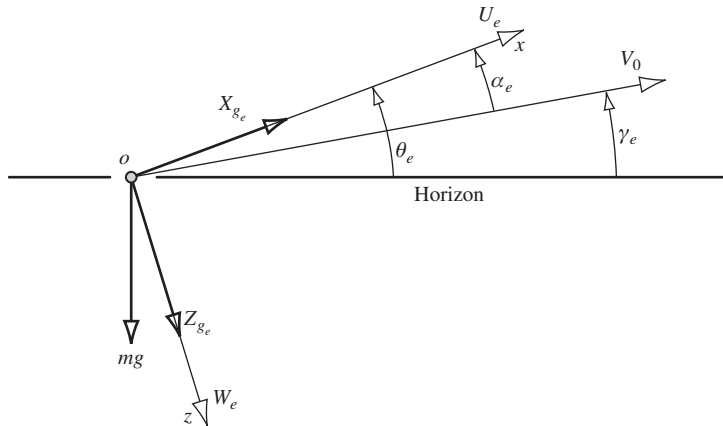


FIGURE 4.4 Steady state weight components in the plane of symmetry.

equation (2.11). Since, by definition, the angular perturbations are small, small angle approximations may be used in the direction cosine matrix to give the following relationship:

$$\begin{bmatrix} X_g \\ Y_g \\ Z_g \end{bmatrix} = \begin{bmatrix} 1 & \psi & -\theta \\ -\psi & 1 & \phi \\ \theta & -\phi & 1 \end{bmatrix} \begin{bmatrix} X_{g_e} \\ Y_{g_e} \\ Z_{g_e} \end{bmatrix} = \begin{bmatrix} 1 & \psi & -\theta \\ -\psi & 1 & \phi \\ \theta & -\phi & 1 \end{bmatrix} \begin{bmatrix} -mg \sin \theta_e \\ 0 \\ mg \cos \theta_e \end{bmatrix} \quad (4.26)$$

Again, the products of small quantities have been neglected on the grounds that they are insignificantly small. Thus, the gravitational force components in the small perturbation equations of motion are given by

$$\begin{aligned} X_g &= -mg \sin \theta_e - mg \theta \cos \theta_e \\ Y_g &= mg \psi \sin \theta_e + mg \phi \cos \theta_e \\ Z_g &= mg \cos \theta_e - mg \theta \sin \theta_e \end{aligned} \quad (4.27)$$

4.2.2 Aerodynamic terms

Whenever the aeroplane is disturbed from its equilibrium, the aerodynamic balance is obviously upset. To describe explicitly the aerodynamic changes occurring during a disturbance is a considerable challenge in view of the subtle interactions present in the motion. However, although limited in scope, the method first described by [Bryan \(1911\)](#) works extremely well for classical aeroplanes when the motion of interest is limited to (relatively) small perturbations. Although the approach is unchanged, the rather more modern notation of [Hopkin \(1970\)](#) is adopted.

The usual procedure is to assume that the aerodynamic force and moment terms in [equations \(4.20\)](#) are dependent only on the disturbed motion variables and their derivatives. Mathematically, this is conveniently expressed as a function comprising the sum of a number of Taylor series,

each series involving one motion variable or one derivative of a motion variable. Since the motion variables are (u, v, w) and (p, q, r) , the aerodynamic term X_a in the axial force equation, for example, may be expressed as

$$\begin{aligned}
 X_a = & X_{a_e} + \left(\frac{\partial X}{\partial u} u + \frac{\partial^2 X}{\partial u^2} \frac{u^2}{2!} + \frac{\partial^3 X}{\partial u^3} \frac{u^3}{3!} + \frac{\partial^4 X}{\partial u^4} \frac{u^4}{4!} + \dots \right) \\
 & + \left(\frac{\partial X}{\partial v} v + \frac{\partial^2 X}{\partial v^2} \frac{v^2}{2!} + \frac{\partial^3 X}{\partial v^3} \frac{v^3}{3!} + \frac{\partial^4 X}{\partial v^4} \frac{v^4}{4!} + \dots \right) \\
 & + \left(\frac{\partial X}{\partial w} w + \frac{\partial^2 X}{\partial w^2} \frac{w^2}{2!} + \frac{\partial^3 X}{\partial w^3} \frac{w^3}{3!} + \frac{\partial^4 X}{\partial w^4} \frac{w^4}{4!} + \dots \right) \\
 & + \left(\frac{\partial X}{\partial p} p + \frac{\partial^2 X}{\partial p^2} \frac{p^2}{2!} + \frac{\partial^3 X}{\partial p^3} \frac{p^3}{3!} + \frac{\partial^4 X}{\partial p^4} \frac{p^4}{4!} + \dots \right) \\
 & + \left(\frac{\partial X}{\partial q} q + \frac{\partial^2 X}{\partial q^2} \frac{q^2}{2!} + \frac{\partial^3 X}{\partial q^3} \frac{q^3}{3!} + \frac{\partial^4 X}{\partial q^4} \frac{q^4}{4!} + \dots \right) \\
 & + \left(\frac{\partial X}{\partial r} r + \frac{\partial^2 X}{\partial r^2} \frac{r^2}{2!} + \frac{\partial^3 X}{\partial r^3} \frac{r^3}{3!} + \frac{\partial^4 X}{\partial r^4} \frac{r^4}{4!} + \dots \right) \\
 & + \left(\frac{\partial X}{\partial \dot{u}} \dot{u} + \frac{\partial^2 X}{\partial \dot{u}^2} \frac{\dot{u}^2}{2!} + \frac{\partial^3 X}{\partial \dot{u}^3} \frac{\dot{u}^3}{3!} + \dots \right) \\
 & + \left(\frac{\partial X}{\partial \dot{v}} \dot{v} + \frac{\partial^2 X}{\partial \dot{v}^2} \frac{\dot{v}^2}{2!} + \frac{\partial^3 X}{\partial \dot{v}^3} \frac{\dot{v}^3}{3!} + \dots \right) \\
 & + \text{series terms in } \dot{w}, \dot{p}, \dot{q}, \text{ and } \dot{r} \\
 & + \text{series terms in higher order derivatives}
 \end{aligned} \tag{4.28}$$

where X_{a_e} is a constant term. Since the motion variables are small, for all practical aeroplanes only the first term in each of the series functions is significant. Further, the only significant higher order derivative terms commonly encountered are those involving \dot{w} . Thus equation (4.28) is dramatically simplified to

$$X_a = X_{a_e} + \frac{\partial X}{\partial u} u + \frac{\partial X}{\partial v} v + \frac{\partial X}{\partial w} w + \frac{\partial X}{\partial p} p + \frac{\partial X}{\partial q} q + \frac{\partial X}{\partial r} r + \frac{\partial X}{\partial \dot{w}} \dot{w} \tag{4.29}$$

Using an alternative shorthand notation for the derivatives, [equation \(4.29\)](#) may be written as

$$X_a = X_{a_e} + \overset{\circ}{X}_u u + \overset{\circ}{X}_v v + \overset{\circ}{X}_w w + \overset{\circ}{X}_p p + \overset{\circ}{X}_q q + \overset{\circ}{X}_r r + \overset{\circ}{X}_{\dot{w}} \dot{w} \quad (4.30)$$

The coefficients $\overset{\circ}{X}_u, \overset{\circ}{X}_v, \overset{\circ}{X}_w$, and so on, are called *aerodynamic stability derivatives*, and the dressing (\circ) denotes them to be *dimensional*. Since [equation \(4.30\)](#) has the units of force, the units of each of the aerodynamic stability derivatives are self-evident. In a similar way the force and moment terms in the remaining [equations \(4.20\)](#) are determined. For example, the aerodynamic term in the rolling-moment equation is given by

$$L_a = L_{a_e} + \overset{\circ}{L}_u u + \overset{\circ}{L}_v v + \overset{\circ}{L}_w w + \overset{\circ}{L}_p p + \overset{\circ}{L}_q q + \overset{\circ}{L}_r r + \overset{\circ}{L}_{\dot{w}} \dot{w} \quad (4.31)$$

4.2.3 Aerodynamic control terms

The primary aerodynamic controls are the elevator, ailerons, and rudder. Since the forces and moments created by control deflections arise from changes in aerodynamic conditions, it is usual to quantify their effect in terms of *aerodynamic control derivatives*. The assumptions applied to the aerodynamic terms are also applied to the control terms; thus, for example, the pitching moment due to aerodynamic controls may be expressed as

$$M_c = \frac{\partial M}{\partial \xi} \xi + \frac{\partial M}{\partial \eta} \eta + \frac{\partial M}{\partial \zeta} \zeta \quad (4.32)$$

where aileron angle, elevator angle, and rudder angle are denoted ξ , η , and ζ , respectively. Since [equation \(4.32\)](#) describes the effect of the aerodynamic controls with respect to the prevailing trim condition, it is important to realise that the control angles, ξ , η , and ζ , are measured relative to the trim settings ξ_e , η_e , and ζ_e , respectively. Again, the shorthand notation may be used and [equation \(4.32\)](#) may be written as

$$\overset{\circ}{M}_c = \overset{\circ}{M}_\xi \xi + \overset{\circ}{M}_\eta \eta + \overset{\circ}{M}_\zeta \zeta \quad (4.33)$$

The aerodynamic control terms in the remaining equations of motion are assembled in a similar way. If it is required to study the response of an aeroplane to other aerodynamic controls, for example, flaps, spoilers, leading edge devices, etc., additional terms may be appended to [equation \(4.33\)](#) and the remaining equations of motion as required.

4.2.4 Power terms

Power, and hence thrust τ , is usually controlled by throttle lever angle ε , and the relationship between the two variables for a simple turbojet engine is given by [equation \(2.34\)](#) in Chapter 2. Movement of the throttle lever causes a thrust change, which in turn gives rise to a change in the components of force and moment acting on the aeroplane. It is mathematically convenient to

describe these effects in terms of engine thrust derivatives. For example, normal force due to thrust may be expressed in the usual shorthand notation:

$$Z_p = \dot{Z}_\tau \tau \quad (4.34)$$

The contributions to the remaining equations of motion are expressed in a similar way. As for the aerodynamic controls, power changes are measured with respect to the prevailing trim setting. Therefore, τ quantifies the thrust perturbation relative to the trim setting τ_e .

4.2.5 The equations of motion for small perturbations

To complete the development of the linearised equations of motion, it only remains to substitute the appropriate expressions for the aerodynamic, gravitational, aerodynamic control, and thrust terms into [equations \(4.23\)](#). The aerodynamic terms are exemplified by expressions like [equations \(4.30\) and \(4.31\)](#), expressions for the gravitational terms are given in [equations \(4.27\)](#), the aerodynamic control terms are exemplified by expressions like [equation \(4.33\)](#), and the thrust terms are exemplified by expressions like [equation \(4.34\)](#). Bringing all of these together, the following equations are obtained:

$$\begin{aligned} m(\dot{u} + qW_e) &= X_{a_e} + \dot{X}_u u + \dot{X}_v v + \dot{X}_w w + \dot{X}_p p + \dot{X}_q q + \dot{X}_r r + \dot{X}_{\dot{w}} \dot{w} \\ &\quad - mg \sin \theta_e - mg \theta \cos \theta_e + \dot{X}_\xi \xi + \dot{X}_\eta \eta + \dot{X}_\zeta \zeta + \dot{X}_\tau \tau \\ m(\dot{v} - pW_e + rU_e) &= Y_{a_e} + \dot{Y}_u u + \dot{Y}_v v + \dot{Y}_w w + \dot{Y}_p p + \dot{Y}_q q + \dot{Y}_r r + \dot{Y}_{\dot{w}} \dot{w} \\ &\quad + mg \psi \sin \theta_e + mg \phi \cos \theta_e + \dot{Y}_\xi \xi + \dot{Y}_\eta \eta + \dot{Y}_\zeta \zeta + \dot{Y}_\tau \tau \\ m(\dot{w} - qU_e) &= Z_{a_e} + \dot{Z}_u u + \dot{Z}_v v + \dot{Z}_w w + \dot{Z}_p p + \dot{Z}_q q + \dot{Z}_r r + \dot{Z}_{\dot{w}} \dot{w} \\ &\quad + mg \cos \theta_e - mg \theta \sin \theta_e + \dot{Z}_\xi \xi + \dot{Z}_\eta \eta + \dot{Z}_\zeta \zeta + \dot{Z}_\tau \tau \\ I_x \dot{p} - I_{xz} \dot{r} &= L_{a_e} + \dot{L}_u u + \dot{L}_v v + \dot{L}_w w + \dot{L}_p p + \dot{L}_q q + \dot{L}_r r \\ &\quad + \dot{L}_{\dot{w}} \dot{w} + \dot{L}_\xi \xi + \dot{L}_\eta \eta + \dot{L}_\zeta \zeta + \dot{L}_\tau \tau \\ I_y \dot{q} &= M_{a_e} + \dot{M}_u u + \dot{M}_v v + \dot{M}_w w + \dot{M}_p p + \dot{M}_q q + \dot{M}_r r \\ &\quad + \dot{M}_{\dot{w}} \dot{w} + \dot{M}_\xi \xi + \dot{M}_\eta \eta + \dot{M}_\zeta \zeta + \dot{M}_\tau \tau \\ I_z \dot{r} - I_{xz} \dot{p} &= N_{a_e} + \dot{N}_u u + \dot{N}_v v + \dot{N}_w w + \dot{N}_p p + \dot{N}_q q + \dot{N}_r r \\ &\quad + \dot{N}_{\dot{w}} \dot{w} + \dot{N}_\xi \xi + \dot{N}_\eta \eta + \dot{N}_\zeta \zeta + \dot{N}_\tau \tau \end{aligned} \quad (4.35)$$

Now, in the steady trimmed flight condition, all of the perturbation variables and their derivatives are, by definition, zero. Thus, the steady state equations (4.35) reduce to

$$\begin{aligned} X_{a_e} &= mg \sin \theta_e \\ Y_{a_e} &= 0 \\ Z_{a_e} &= -mg \cos \theta_e \\ L_{a_e} &= 0 \\ M_{a_e} &= 0 \\ N_{a_e} &= 0 \end{aligned} \quad (4.36)$$

Equations (4.36) therefore identify the constant trim terms which may be substituted into equations (4.35) and, following rearrangement, they may be written as

$$\begin{aligned} m\dot{u} - \overset{\circ}{X}_u u - \overset{\circ}{X}_v v - \overset{\circ}{X}_{\dot{w}} \dot{w} - \overset{\circ}{X}_w w \\ - \overset{\circ}{X}_p p - \left(\overset{\circ}{X}_q - mW_e \right) q - \overset{\circ}{X}_r r + mg \theta \cos \theta_e = \overset{\circ}{X}_\xi \xi + \overset{\circ}{X}_\eta \eta + \overset{\circ}{X}_\zeta \zeta + \overset{\circ}{X}_\tau \tau \\ - \overset{\circ}{Y}_u u + m\dot{v} - \overset{\circ}{Y}_v v - \overset{\circ}{Y}_{\dot{w}} \dot{w} - \overset{\circ}{Y}_w w - \left(\overset{\circ}{Y}_p + mW_e \right) p \\ - \overset{\circ}{Y}_q q - \left(\overset{\circ}{Y}_r - mU_e \right) r - mg \phi \cos \theta_e - mg \psi \sin \theta_e = \overset{\circ}{Y}_\xi \xi + \overset{\circ}{Y}_\eta \eta + \overset{\circ}{Y}_\zeta \zeta + \overset{\circ}{Y}_\tau \tau \\ - \overset{\circ}{Z}_u u - \overset{\circ}{Z}_v v + \left(m - \overset{\circ}{Z}_{\dot{w}} \right) \dot{w} - \overset{\circ}{Z}_w w \\ - \overset{\circ}{Z}_p p - \left(\overset{\circ}{Z}_q + mU_e \right) q - \overset{\circ}{Z}_r r + mg \theta \sin \theta_e = \overset{\circ}{Z}_\xi \xi + \overset{\circ}{Z}_\eta \eta + \overset{\circ}{Z}_\zeta \zeta + \overset{\circ}{Z}_\tau \tau \quad (4.37) \\ - \overset{\circ}{L}_u u - \overset{\circ}{L}_v v - \overset{\circ}{L}_{\dot{w}} \dot{w} - \overset{\circ}{L}_w w \\ + I_x \dot{p} - \overset{\circ}{L}_p p - \overset{\circ}{L}_q q - I_x \dot{r} - \overset{\circ}{L}_r r = \overset{\circ}{L}_\xi \xi + \overset{\circ}{L}_\eta \eta + \overset{\circ}{L}_\zeta \zeta + \overset{\circ}{L}_\tau \tau \\ - \overset{\circ}{M}_u u - \overset{\circ}{M}_v v - \overset{\circ}{M}_{\dot{w}} \dot{w} \\ - \overset{\circ}{M}_w w - \overset{\circ}{M}_p p + I_y \dot{q} - \overset{\circ}{M}_q q - \overset{\circ}{M}_r r = \overset{\circ}{M}_\xi \xi + \overset{\circ}{M}_\eta \eta + \overset{\circ}{M}_\zeta \zeta + \overset{\circ}{M}_\tau \tau \\ - \overset{\circ}{N}_u u - \overset{\circ}{N}_v v - \overset{\circ}{N}_{\dot{w}} \dot{w} - \overset{\circ}{N}_w w \\ - I_x \dot{p} - \overset{\circ}{N}_p p - \overset{\circ}{N}_q q + I_z \dot{r} - \overset{\circ}{N}_r r = \overset{\circ}{N}_\xi \xi + \overset{\circ}{N}_\eta \eta + \overset{\circ}{N}_\zeta \zeta + \overset{\circ}{N}_\tau \tau \end{aligned}$$

Equations (4.37) are the small perturbation equations of motion, referred to body axes, which describe the transient response of an aeroplane about the trimmed flight condition following a small input disturbance. They comprise six simultaneous linear differential equations written in the traditional manner with the forcing, or input, terms on the right hand side. As written, and subject to the assumptions made in their derivation, the equations of motion are perfectly general and describe motion in which longitudinal and lateral dynamics may be fully coupled. However, for the vast majority of aeroplanes when only small-perturbation transient motion is considered, as

is the case here, longitudinal-lateral coupling is usually negligible. Consequently, it is convenient to simplify the equations by assuming that longitudinal and lateral motion is in fact fully decoupled.

4.3 The decoupled equations of motion

4.3.1 The longitudinal equations of motion

Decoupled longitudinal motion is motion in response to a disturbance which is constrained to the longitudinal plane of symmetry, the oxz plane, only. The motion is therefore described by the axial force X , the normal force Z , and the pitching moment M equations only. Since no lateral-directional motion is involved, the motion variables v , p , and r and their derivatives are all zero. Also, decoupled longitudinal-lateral motion means that the aerodynamic coupling derivatives are negligibly small and may be taken as zero, whence

$$\ddot{X}_v = \ddot{X}_p = \ddot{X}_r = \ddot{Z}_v = \ddot{Z}_p = \ddot{Z}_r = \ddot{M}_v = \ddot{M}_p = \ddot{M}_r = 0 \quad (4.38)$$

Similarly, since aileron or rudder deflections do not usually cause motion in the longitudinal plane of symmetry, the coupling aerodynamic control derivatives may also be taken as zero, thus

$$\ddot{X}_\xi = \ddot{X}_\zeta = \ddot{Z}_\xi = \ddot{Z}_\zeta = \ddot{M}_\xi = \ddot{M}_\zeta = 0 \quad (4.39)$$

The equations of longitudinal symmetric motion are therefore obtained by extracting the axial force, normal force, and pitching moment equations from [equations \(4.37\)](#) and substituting [equations \(4.38\)](#) and [\(4.39\)](#) as appropriate. Whence

$$\begin{aligned} m\dot{u} - \ddot{X}_u u - \ddot{X}_w \dot{w} - \ddot{X}_w w - (\ddot{X}_q - mW_e) q + mg \theta \cos \theta_e &= \ddot{X}_\eta \eta + \ddot{X}_\tau \tau \\ -\ddot{Z}_u u + (m - \ddot{Z}_w) \dot{w} - \ddot{Z}_w w - (\ddot{Z}_q + mU_e) q + mg \theta \sin \theta_e &= \ddot{Z}_\eta \eta + \ddot{Z}_\tau \tau \\ -\ddot{M}_u u - \ddot{M}_w \dot{w} - \ddot{M}_w w + I_y \dot{q} - \ddot{M}_q q &= \ddot{M}_\eta \eta + \ddot{M}_\tau \tau \end{aligned} \quad (4.40)$$

[Equations \(4.40\)](#) are the most general form of the dimensional decoupled equations of longitudinal symmetric motion referred to aeroplane body axes. If it is assumed that the aeroplane is in level flight and that the reference axes are wind or stability axes, then

$$\theta_e = W_e = 0 \quad (4.41)$$

and the equations simplify further to

$$\begin{aligned} m\dot{u} - \ddot{X}_u u - \ddot{X}_w \dot{w} - \ddot{X}_w w - \ddot{X}_q q + mg \theta &= \ddot{X}_\eta \eta + \ddot{X}_\tau \tau \\ -\ddot{Z}_u u + (m - \ddot{Z}_w) \dot{w} - \ddot{Z}_w w - (\ddot{Z}_q + mU_e) q &= \ddot{Z}_\eta \eta + \ddot{Z}_\tau \tau \\ -\ddot{M}_u u - \ddot{X}_w \dot{w} - \ddot{M}_w w + I_y \dot{q} - \ddot{M}_q q &= \ddot{M}_\eta \eta + \ddot{M}_\tau \tau \end{aligned} \quad (4.42)$$

Equations (4.42) represent the simplest possible form of the decoupled longitudinal equations of motion. Further simplification is only generally possible when the numerical values of the coefficients in the equations are known, since some coefficients are often negligibly small.

EXAMPLE 4.2

Longitudinal derivative and other data for the McDonnell F-4C Phantom aeroplane were obtained from [Heffley and Jewell \(1972\)](#) for a flight condition of Mach 0.6 at an altitude of 35,000 ft. The original data are presented in imperial units and in a format preferred in the United States. Normally, it is advisable to work with the equations of motion and the data in the format and units as given; otherwise, conversion can be tedious in the extreme and is easily subject to error. However, for the purposes of illustration, the derivative data have been converted to a form compatible with the equations developed previously, and the units have been changed to the more familiar SI format. The data are quite typical; they would normally be supplied in this, or in a similar, form by aerodynamicists and, as such, represent the starting point in any flight dynamics analysis.

Flight path angle	$\gamma_e = 0^\circ$	Air density	$\rho = 0.3809 \text{ kg/m}^3$
Body incidence	$\alpha_e = 9.4^\circ$	Wing area	$S = 49.239 \text{ m}^2$
Velocity	$V_0 = 178 \text{ m/s}$	Mean aerodynamic chord	$\bar{c} = 4.889 \text{ m}$
Mass	$m = 17642 \text{ kg}$	Acceleration due to gravity	$g = 9.81 \text{ m/s}^2$
Pitch moment of inertia	$I_y = 165669 \text{ kgm}^2$		

Since the flight path angle $\gamma_e = 0$ and the body incidence α_e is non-zero, it may be deduced that the following derivatives are referred to a body axes system and that $\theta_e \equiv \alpha_e$. The dimensionless longitudinal derivatives are given, and any missing aerodynamic derivatives must be assumed insignificant and hence zero. On the other hand, missing control derivatives may not be assumed insignificant, although their absence will prohibit analysis of response to those controls.

$$\begin{array}{lll} X_u = 0.0076 & Z_u = -0.7273 & M_u = 0.0340 \\ X_w = 0.0483 & Z_w = -3.1245 & M_w = -0.2169 \\ X_{\dot{w}} = 0 & Z_{\dot{w}} = -0.3997 & M_{\dot{w}} = -0.5910 \\ X_q = 0 & Z_q = -1.2109 & M_q = -1.2732 \\ X_\eta = 0.0618 & Z_\eta = -0.3741 & M_\eta = -0.5581 \end{array}$$

Equations (4.40) are compatible with the data, although the dimensional derivatives must first be calculated according to the definitions given in Appendix 2, Tables A2.1 and A2.2. Thus the dimensional longitudinal equations of motion, referred to body axes, are obtained by substituting the appropriate values into [equations \(4.40\)](#) to give

$$\begin{aligned} 17642\dot{u} - 12.67u - 80.62w + 512852.94q + 170744.06\theta &= 18362.32\eta \\ 1214.01u + 17660.33\dot{w} + 5215.44w - 3088229.7q + 28266.507\theta &= -111154.41\eta \\ -277.47u + 132.47\dot{w} + 1770.07w + 165669\dot{q} + 50798.03q &= -810886.19\eta \end{aligned}$$

where $W_e = V_0 \sin \theta_e = 29.07$ m/s, and $U_e = V_0 \cos \theta_e = 175.61$ m/s. Note that angular variables in the equations of motion have radian units. When written like this, it is clear that the equations of motion are unwieldy. They can be simplified a little by dividing through by the mass or inertia as appropriate. Thus the first equation is divided by 17642, the second equation by 17660.33, and the third equation by 165669. After some rearrangement the following rather more convenient version is obtained.

$$\begin{aligned}\dot{u} &= 0.0007u + 0.0046w - 29.0700q - 9.6783\theta + 1.0408\eta \\ \dot{w} &= -0.0687u - 0.2953w + 174.8680q - 1.6000\theta - 6.2940\eta \\ \dot{q} + 0.0008\dot{w} &= 0.0017u - 0.0107w - 0.3066q - 4.8946\eta\end{aligned}$$

It must be remembered that, when written in this form, the equations have the units of acceleration. Their most striking feature, however written, is the large variation in the values of the coefficients. Terms which may at first sight appear insignificant are frequently important in the solution of the equations. It is therefore prudent to maintain sensible levels of accuracy when manipulating the equations by hand. Fortunately, this activity is not often required.

4.3.2 The lateral-directional equations of motion

Decoupled lateral-directional motion involves roll, yaw, and sideslip only. It is therefore described by the equations for side force Y , rolling moment L , and yawing moment N . Since no longitudinal motion is involved, the longitudinal motion variables u , w , and q and their derivatives are all zero. Also, decoupled longitudinal-lateral motion means that the aerodynamic coupling derivatives are negligibly small and may be taken as zero, whence

$$\dot{Y}_u = \dot{Y}_{\dot{w}} = \dot{Y}_w = \dot{Y}_q = \dot{L}_u = \dot{L}_{\dot{w}} = \dot{L}_w = \dot{L}_q = \dot{N}_u = \dot{N}_{\dot{w}} = \dot{N}_w = \dot{N}_q = 0 \quad (4.43)$$

Similarly, since the airframe is symmetric, elevator deflection and thrust variation do not usually cause lateral-directional motion, and the coupling aerodynamic control derivatives may also be taken as zero, thus

$$\dot{Y}_\eta = \dot{Y}_\tau = \dot{L}_\eta = \dot{L}_\tau = \dot{N}_\eta = \dot{N}_\tau = 0 \quad (4.44)$$

The equations of lateral asymmetric motion are therefore obtained by extracting the side-force, rolling-moment, and yawing-moment equations from [equations \(4.37\)](#) and substituting [equations \(4.43\) and \(4.44\)](#) as appropriate:

$$\begin{aligned}\left(m\dot{v} - \dot{Y}_v - (\dot{Y}_p + mW_e)p - (\dot{Y}_r - mU_e)r \right) &= \dot{Y}_\xi\xi + \dot{Y}_\zeta\zeta \\ -mg\phi\cos\theta_e - mg\psi\sin\theta_e &\\ -\dot{L}_v v + I_x\dot{p} - \dot{L}_p p - I_{xz}\dot{r} - \dot{L}_r r &= \dot{L}_\xi\xi + \dot{L}_\zeta\zeta \\ -\dot{N}_v v - I_{xz}\dot{p} - N_p p + I_z\dot{r} - N_r r &= \dot{N}_\xi\xi + \dot{N}_\zeta\zeta\end{aligned} \quad (4.45)$$

Equations (4.45) are the most general form of the dimensional decoupled equations of lateral-directional asymmetric motion referred to aeroplane body axes. If it is assumed that the aeroplane is in level flight and that the reference axes are wind or stability axes, then, as before,

$$\theta_e = W_e = 0 \quad (4.46)$$

and the equations simplify further to

$$\begin{aligned} m\dot{v} - \dot{Y}_v v - p\dot{Y}_p - \left(\dot{Y}_r - mU_e \right)r - mg\phi &= \dot{Y}_\xi\xi + \dot{Y}_\zeta\zeta \\ -\dot{L}_v v + I_x\dot{p} - \dot{L}_p p - I_{xz}\dot{r} - \dot{L}_r r &= \dot{L}_\xi\xi + \dot{L}_\zeta\zeta \\ -\dot{N}_v v - I_{xz}\dot{p} - N_p p + I_z\dot{r} - N_r r &= \dot{N}_\xi\xi + \dot{N}_\zeta\zeta \end{aligned} \quad (4.47)$$

Equations (4.47) represent the simplest possible form of the decoupled lateral-directional equations of motion. As for the longitudinal equations of motion, further simplification is only generally possible when the numerical values of their coefficients are known since some coefficients are often negligibly small.

4.4 Alternative forms of the equations of motion

4.4.1 The dimensionless equations of motion

Traditionally, the development of the equations of motion and investigations of stability and control involving their use have been securely resident in the domain of the aerodynamicist. Many aerodynamic phenomena are most conveniently explained in terms of *dimensionless aerodynamic coefficients*—for example, lift coefficient, Mach number, Reynolds number, etc., and often this mechanism provides the only practical means for making progress. The advantage of this approach is that the aerodynamic properties of an aeroplane can be completely described in terms of dimensionless parameters which are independent of airframe geometry and flight condition. A lift coefficient of 0.5, for example, has precisely the same meaning whether it applies to a Boeing 747 or to a Cessna 150. It is thus not surprising to discover that historically, the small perturbation equations of motion of an aeroplane were treated in the same way. This in turn leads to the concept of the *dimensionless derivative*, which is just another aerodynamic coefficient and may be interpreted in much the same way. However, the dimensionless equations of motion are of little use to the modern flight dynamicist other than as a means for explaining the origin of the dimensionless derivatives. The development of the dimensionless decoupled small perturbation equations of motion is outlined below solely for this purpose.

As formally described by Hopkin (1970), the equations of motion are rendered dimensionless by dividing each one by a generalised force or moment parameter as appropriate. Sometimes the dimensionless equations of motion are referred to as *aero-normalised* and the corresponding derivative coefficients are referred to as *aero-normalised derivatives*. To illustrate the procedure consider the axial force equation taken from the decoupled longitudinal equations of motion (4.42):

$$m\dot{u} - \dot{X}_u u - \dot{X}_{\dot{w}} \dot{w} - \dot{X}_w w - q\dot{X}_q + mg\theta = \dot{X}_\eta\eta + \dot{X}_\tau\tau \quad (4.48)$$

Since [equation \(4.48\)](#) has the units of force, it may be rendered dimensionless by dividing, or normalising, each term by the aerodynamic force parameter $\frac{1}{2}\rho V_0^2 S$, where S is the reference wing area. The following parameters are defined:

Dimensionless time:

$$\hat{t} = \frac{t}{\sigma} \quad \text{where} \quad \sigma = \frac{m}{\frac{1}{2}\rho V_0 S} \quad (4.49)$$

Longitudinal relative density factor:

$$\mu_1 = \frac{m}{\frac{1}{2}\rho S \bar{c}} \quad (4.50)$$

where the longitudinal reference length is \bar{c} , the mean aerodynamic chord.

Dimensionless velocities:

$$\begin{aligned} \hat{u} &= \frac{u}{V_0} \\ \hat{w} &= \frac{w}{V_0} \\ \hat{q} &= q\sigma = \frac{qm}{\frac{1}{2}\rho V_0 S} \end{aligned} \quad (4.51)$$

Since level flight is assumed the lift and weight are equal thus:

$$mg = \frac{1}{2}\rho V_0^2 S C_L \quad (4.52)$$

Thus, dividing [equation \(4.48\)](#) through by the aerodynamic force parameter and making use of the parameters defined in [equations \(4.49\) through \(4.52\)](#), the following is obtained:

$$\begin{pmatrix} \frac{\dot{u}}{V_0} \sigma - \left(\frac{\overset{\circ}{X}_u}{\frac{1}{2}\rho V_0 S} \right) \frac{u}{V_0} - \left(\frac{\overset{\circ}{X}_{\dot{w}}}{\frac{1}{2}\rho S \bar{c}} \right) \frac{\dot{w}\sigma}{V_0 \mu_1} \\ - \left(\frac{\overset{\circ}{X}_w}{\frac{1}{2}\rho V_0 S} \right) \frac{w}{V_0} - \left(\frac{\overset{\circ}{X}_q}{\frac{1}{2}\rho V_0 S \bar{c}} \right) \frac{q\sigma}{\mu_1} + \frac{mg}{\frac{1}{2}\rho V_0^2 S} \theta \end{pmatrix} = \left(\frac{\overset{\circ}{X}_\eta}{\frac{1}{2}\rho V_0^2 S} \right) \eta + \overset{\circ}{X}_\tau \left(\frac{\tau}{\frac{1}{2}\rho V_0^2 S} \right) \quad (4.53)$$

which is more conveniently written as

$$\hat{u} - X_u \hat{u} - X_{\dot{w}} \frac{\hat{w}}{\mu_1} - X_w \hat{w} - X_q \frac{\hat{q}}{\mu_1} + C_L \theta = X_\eta \eta + X_\tau \hat{\tau} \quad (4.54)$$

The derivatives denoted $X_u, X_w, X_v, X_q, X_\eta$ and X_τ are the *dimensionless or aero-normalised derivatives* and their definitions follow from [equation \(4.53\)](#). It is in this form that the aerodynamic stability and control derivatives are usually provided for an aeroplane by aerodynamicists.

In a similar way the remaining longitudinal equations of motion may be rendered dimensionless. Note that the aerodynamic moment parameter used to divide the pitching moment equation is $\frac{1}{2}\rho V_0^2 S \bar{C}$. Whence

$$\begin{aligned} -Z_u \hat{u} + \hat{w} - Z_w \frac{\hat{w}}{\mu_1} - Z_w \hat{w} - Z_q \frac{\hat{q}}{\mu_1} - \hat{q} &= Z_\eta \eta + Z_\tau \tau \\ -M_u \hat{u} - M_w \frac{\hat{w}}{\mu_1} - M_w \hat{w} + i_y \frac{\hat{q}}{\mu_1} - M_q \frac{\hat{q}}{\mu_1} &= M_\eta \eta + M_\tau \tau \end{aligned} \quad (4.55)$$

where i_y , the dimensionless pitch inertia, and is given by

$$i_y = \frac{I_y}{\frac{mc^2}{2}} \quad (4.56)$$

Similarly, the lateral-directional equations of motion [\(4.47\)](#) may be rendered dimensionless by dividing the side force equation by the aerodynamic force parameter $\frac{1}{2}\rho V_0^2 S$ and the rolling- and yawing-moment equations by the aerodynamic moment parameter $\frac{1}{2}\rho V_0^2 S b$, where for lateral motion the reference length is the wing span b . Additional parameter definitions required to deal with the lateral-directional equations are as follows:

Lateral relative density factor:

$$\mu_2 = \frac{m}{\frac{1}{2}\rho S b} \quad (4.57)$$

Dimensionless inertias:

$$i_x = \frac{I_x}{mb^2}, \quad i_z = \frac{I_z}{mb^2} \quad \text{and} \quad i_{xz} = \frac{I_{xz}}{mb^2} \quad (4.58)$$

Since the equations of motion are referred to wind axes and since level flight is assumed, [equations \(4.47\)](#) may be written in dimensionless form as follows:

$$\begin{aligned} \hat{v} - Y_v \hat{v} - Y_p \frac{\hat{p}}{\mu_2} - Y_r \frac{\hat{r}}{\mu_2} - \hat{r} - C_L \phi &= Y_\xi \xi + Y_\zeta \zeta \\ -L_v \hat{v} + i_x \frac{\hat{p}}{\mu_2} - L_p \frac{\hat{p}}{\mu_2} - i_{xz} \frac{\hat{r}}{\mu_2} - L_r \frac{\hat{r}}{\mu_2} &= L_\xi \xi + L_\zeta \zeta \\ -N_v \hat{v} - i_{xz} \frac{\hat{p}}{\mu_2} - N_p \frac{\hat{p}}{\mu_2} + i_z \frac{\hat{r}}{\mu_2} - N_r \frac{\hat{r}}{\mu_2} &= N_\xi \xi + N_\zeta \zeta \end{aligned} \quad (4.59)$$

For convenience, the definitions of all of the dimensionless aerodynamic stability and control derivatives are given in [Appendix 2](#).

4.4.2 The equations of motion in state space form

The solution of the equations of motion poses few problems today since very powerful computational tools are readily available. Because computers are very good at handling numerical matrix calculations, the use of matrix methods for solving linear dynamic system problems has become an important topic in modern applied mathematics. In particular, matrix methods together with the digital computer have led to the development of the relatively new field of modern control system theory. For small perturbations, the aeroplane is a classical example of a linear dynamic system, and frequently the solution of the aircraft equations of motion is a prelude to flight control system design and analysis. It is therefore convenient and straightforward to use multivariable system theory tools in the solution of the equations of motion, but it is first necessary to arrange them in a suitable format.

The motion, or *state*, of any linear dynamic system may be described by a minimum set of variables called the *state variables*. The number of state variables required to completely describe the motion of the system is dependent on the number of degrees of freedom the system has. Thus the motion of the system is described in a multidimensional vector space called the *state space*, the number of state variables being equal to the number of dimensions. The equation of motion, or *state equation*, of the *linear time invariant* (LTI) multivariable system is written as

$$\dot{\mathbf{x}}(t) = \mathbf{A}\mathbf{x}(t) + \mathbf{B}\mathbf{u}(t) \quad (4.60)$$

where

$\mathbf{x}(t)$ is the column vector of n state variables, called the *state vector*

$\mathbf{u}(t)$ is the column vector of m input variables, called the *input vector*

\mathbf{A} is the $(n \times n)$ *state matrix*

\mathbf{B} is the $(n \times m)$ *input matrix*

Since the system is LTI, the matrices \mathbf{A} and \mathbf{B} have constant elements. Equation (4.60) is the matrix equivalent of a set of n simultaneous linear differential equations, and it is a straightforward matter to configure the small perturbation equations of motion for an aeroplane in this format.

For many systems some of the state variables may be inaccessible or their values may not be determined directly. Thus a second equation is required to determine the system output variables. The *output equation* is written in the general form

$$\mathbf{y}(t) = \mathbf{C}\mathbf{x}(t) + \mathbf{D}\mathbf{u}(t) \quad (4.61)$$

where

$\mathbf{y}(t)$ is the column vector of r output variables, called the *output vector*

\mathbf{C} is the $(r \times n)$ *output matrix*

\mathbf{D} is the $(r \times m)$ *direct matrix*

and, typically, $r \leq n$. Again, for a LTI system the matrices \mathbf{C} and \mathbf{D} have constant elements. Together, equations (4.60) and (4.61) provide a complete description of the system. A complete description of the formulation of the general state model and the mathematics required in its analysis may be found in Barnett (1975).

For most aeroplane problems it is convenient to choose the output variables to be the state variables. Thus

$$\mathbf{y}(t) = \mathbf{x}(t) \quad \text{and} \quad r = n$$

and consequently

$\mathbf{C} = \mathbf{I}$, the $(n \times n)$ identity matrix

$\mathbf{D} = \mathbf{0}$, the $(n \times m)$ zero matrix

As a result, the output equation simplifies to

$$\mathbf{y}(t) = \mathbf{Ix}(t) \equiv \mathbf{x}(t) \quad (4.62)$$

and it is only necessary to derive the state equation from the aeroplane equations of motion.

Consider, for example, the longitudinal equations of motion (4.40) referred to aeroplane body axes. These may be rewritten with the acceleration terms on the left hand side as follows:

$$\begin{aligned} \dot{m}\dot{u} - \dot{X}_{\dot{w}}\dot{w} &= \ddot{X}_u u + \ddot{X}_w w + (\ddot{X}_q - mW_e)q - mg\theta \cos \theta_e + \ddot{X}_\eta \eta + \ddot{X}_\tau \tau \\ m\dot{w} - \dot{Z}_{\dot{w}}\dot{w} &= \ddot{Z}_u u + \ddot{Z}_w w + (\ddot{Z}_q + mU_e)q - mg\theta \sin \theta_e + \ddot{Z}_\eta \eta + \ddot{Z}_\tau \tau \\ I_y \dot{q} - \dot{M}_{\dot{w}}\dot{w} &= \ddot{M}_u u + \ddot{M}_w w + \ddot{M}_q q + \ddot{M}_\eta \eta + \ddot{M}_\tau \tau \end{aligned} \quad (4.63)$$

Since the longitudinal motion of the aeroplane is described by four state variables u , w , q , and θ , four differential equations are required. Thus the additional equation is the auxiliary equation relating pitch rate to attitude rate, which for small perturbations is

$$\dot{\theta} = q \quad (4.64)$$

Equations (4.63) and (4.64) may be combined and written in matrix form:

$$\mathbf{M}\dot{\mathbf{x}}(t) = \mathbf{A}'\mathbf{x}(t) + \mathbf{B}'\mathbf{u}(t) \quad (4.65)$$

where

$$\mathbf{x}^T(t) = [u \quad w \quad q \quad \theta] \quad \mathbf{u}^T(t) = [\eta \quad \tau]$$

$$\mathbf{M} = \begin{bmatrix} m & -\dot{X}_{\dot{w}} & 0 & 0 \\ 0 & (m - \dot{Z}_{\dot{w}}) & 0 & 0 \\ 0 & -\dot{M}_{\dot{w}} & I_y & 0 \\ 0 & 0 & 0 & 1 \end{bmatrix}$$

$$\mathbf{A}' = \begin{bmatrix} \ddot{X}_u & \ddot{X}_w & (\ddot{X}_q - mW_e) & -mg \cos \theta_e \\ \ddot{Z}_u & \ddot{Z}_w & (\ddot{Z}_q + mU_e) & -mg \sin \theta_e \\ \ddot{M}_u & \ddot{M}_w & \ddot{M}_q & 0 \\ 0 & 0 & 1 & 0 \end{bmatrix} \quad \mathbf{B}' = \begin{bmatrix} \ddot{X}_\eta & \ddot{X}_\tau \\ \ddot{Z}_\eta & \ddot{Z}_\tau \\ \ddot{M}_\eta & \ddot{M}_\tau \\ 0 & 0 \end{bmatrix}$$

The longitudinal state equation is derived by pre-multiplying equation (4.65) by the inverse of the *mass matrix* \mathbf{M} ; whence

$$\dot{\mathbf{x}}(t) = \mathbf{Ax}(t) + \mathbf{Bu}(t) \quad (4.66)$$

where

$$\mathbf{A} = \mathbf{M}^{-1}\mathbf{A}' = \begin{bmatrix} x_u & x_w & x_q & x_\theta \\ z_u & z_w & z_q & z_\theta \\ m_u & m_w & m_q & m_\theta \\ 0 & 0 & 1 & 0 \end{bmatrix} \quad \mathbf{B} = \mathbf{M}^{-1}\mathbf{B}' = \begin{bmatrix} x_\eta & x_\tau \\ z_\eta & z_\tau \\ m_\eta & m_\tau \\ 0 & 0 \end{bmatrix}$$

The elements of the state matrix \mathbf{A} are the aerodynamic stability derivatives, referred to aeroplane body axes, in *concise form*; the elements of the input matrix \mathbf{B} are the control derivatives, also in concise form. The definitions of the concise derivatives follow directly from the above relationships and are given in full in Appendix 2. Thus the longitudinal state equation may be written out in full as

$$\begin{bmatrix} \dot{u} \\ \dot{w} \\ \dot{q} \\ \dot{\theta} \end{bmatrix} = \begin{bmatrix} x_u & x_w & x_q & x_\theta \\ z_u & z_w & z_q & z_\theta \\ m_u & m_w & m_q & m_\theta \\ 0 & 0 & 1 & 0 \end{bmatrix} \begin{bmatrix} u \\ w \\ q \\ \theta \end{bmatrix} + \begin{bmatrix} x_\eta & x_\tau \\ z_\eta & z_\tau \\ m_\eta & m_\tau \\ 0 & 0 \end{bmatrix} \begin{bmatrix} \eta \\ \tau \end{bmatrix} \quad (4.67)$$

and the output equation is, very simply,

$$\mathbf{y}(t) = \mathbf{Ix}(t) = \begin{bmatrix} 1 & 0 & 0 & 0 \\ 0 & 1 & 0 & 0 \\ 0 & 0 & 1 & 0 \\ 0 & 0 & 0 & 1 \end{bmatrix} \begin{bmatrix} u \\ w \\ q \\ \theta \end{bmatrix} \quad (4.68)$$

Clearly, the longitudinal small-perturbation motion of the aeroplane is completely described by the four state variables u , w , q , and θ . Equation (4.68) determines that, in this instance, the output variables are chosen to be the same as the four state variables.

EXAMPLE 4.3

Consider the requirement to write the longitudinal equations of motion for the McDonnell F-4C Phantom of Example 4.2 in state form. As the derivatives are given in dimensionless form, it is convenient to express the matrices \mathbf{M} , \mathbf{A}' , and \mathbf{B}' in terms of the dimensionless derivatives.

Substituting appropriately for the dimensional derivatives and, after some rearrangement, the matrices may be written as

$$\mathbf{M} = \begin{bmatrix} m' & -\frac{X_{\dot{w}}\bar{c}}{V_0} & 0 & 0 \\ 0 & \left(m' - \frac{Z_{\dot{w}}\bar{c}}{V_0}\right) & 0 & 0 \\ 0 & -\frac{M_{\dot{w}}\bar{c}}{V_0} & I'_y & 0 \\ 0 & 0 & 0 & 1 \end{bmatrix}$$

$$\mathbf{A}' = \begin{bmatrix} X_u & X_w & (X_q\bar{c} - m'W_e) & -m'g \cos \theta_e \\ Z_u & Z_w & (Z_q\bar{c} + m'U_e) & -m'g \sin \theta_e \\ M_u & M_w & M_q\bar{c} & 0 \\ 0 & 0 & 1 & 0 \end{bmatrix} \quad \mathbf{B}' = \begin{bmatrix} V_0X_\eta \\ V_0Z_\eta \\ V_0M_\eta \\ 0 \end{bmatrix}$$

where

$$m' = \frac{m}{\frac{1}{2}\rho V_0 S} \quad \text{and} \quad I'_y = \frac{I_y}{\frac{1}{2}\rho V_0 S \bar{c}}$$

and, in steady symmetric flight, $U_e = V_0 \cos \theta_e$ and $W_e = V_0 \sin \theta_e$.

Substituting the derivative values given in Example 4.2, the longitudinal state [equation \(4.65\)](#) may be written as

$$\begin{bmatrix} 10.569 & 0 & 0 & 0 \\ 0 & 10.580 & 0 & 0 \\ 0 & 0.0162 & 20.3 & 0 \\ 0 & 0 & 0 & 1 \end{bmatrix} \begin{bmatrix} \dot{u} \\ \dot{w} \\ \dot{q} \\ \dot{\theta} \end{bmatrix} = \begin{bmatrix} 0.0076 & 0.0483 & -307.26 & -102.29 \\ -0.7273 & -3.1245 & 1850.10 & -16.934 \\ 0.034 & -0.2169 & -6.2247 & 0 \\ 0 & 0 & 1 & 0 \end{bmatrix} \begin{bmatrix} u \\ w \\ q \\ \theta \end{bmatrix} + \begin{bmatrix} 11.00 \\ -66.5898 \\ -99.341 \\ 0 \end{bmatrix} \eta$$

which may be reduced to the standard form by pre-multiplying each term by the inverse of \mathbf{M} , as indicated previously, to obtain the longitudinal state equation, referred to body axes, in concise form:

$$\begin{bmatrix} \dot{u} \\ \dot{w} \\ \dot{q} \\ \dot{\theta} \end{bmatrix} = \begin{bmatrix} 7.181 \times 10^{-4} & 4.570 \times 10^{-3} & -29.072 & -9.678 \\ -0.0687 & -0.2953 & 174.868 & -1.601 \\ 1.73 \times 10^{-3} & -0.0105 & -0.4462 & 1.277 \times 10^{-3} \\ 0 & 0 & 1 & 0 \end{bmatrix} \begin{bmatrix} u \\ w \\ q \\ \theta \end{bmatrix} + \begin{bmatrix} 1.041 \\ -6.294 \\ -4.888 \\ 0 \end{bmatrix} \eta$$

This computation was carried out with the aid of Program CC, and it should be noted that the resulting equation compares with the final equations given in Example 4.2. The elements of the matrices could equally well have been calculated using the concise derivative definitions given in Appendix 2, Tables A2.5 and A2.6.

For the purpose of illustration, some of the elements in the matrices have been rounded to a more manageable number of decimal places. Normally this is not good practice since the rounding errors may lead to accumulated computational errors in any subsequent computer analysis involving the use of these equations. However, once the basic matrices have been entered into a computer program at the level of accuracy given, all subsequent computations can be carried out using computer generated data files. In this way computational errors are minimized, although it is prudent to be aware that not all computer algorithms for handling matrices can cope with those that are poorly conditioned. Aeroplane computer models occasionally fall into this category.

The lateral-directional small perturbation [equations \(4.45\)](#), referred to body axes, may be treated in exactly the same way to obtain the lateral state equation:

$$\begin{bmatrix} \dot{v} \\ \dot{p} \\ \dot{r} \\ \dot{\phi} \\ \dot{\psi} \end{bmatrix} = \begin{bmatrix} y_v & y_p & y_r & y_\phi & y_\psi \\ l_v & l_p & l_r & l_\phi & l_\psi \\ n_v & n_p & n_r & n_\phi & n_\psi \\ 0 & 1 & 0 & 0 & 0 \\ 0 & 0 & 1 & 0 & 0 \end{bmatrix} \begin{bmatrix} v \\ p \\ r \\ \phi \\ \psi \end{bmatrix} + \begin{bmatrix} y_\xi & y_\zeta \\ l_\xi & l_\zeta \\ n_\xi & n_\zeta \\ 0 & 0 \\ 0 & 0 \end{bmatrix} \begin{bmatrix} \xi \\ \zeta \end{bmatrix} \quad (4.69)$$

Note that when the lateral equations of motion are referred to wind axes, [equations \(4.47\)](#), the lateral-directional state [equation \(4.69\)](#) is reduced from fifth order to fourth order to become

$$\begin{bmatrix} \dot{v} \\ \dot{p} \\ \dot{r} \\ \dot{\phi} \end{bmatrix} = \begin{bmatrix} y_v & y_p & y_r & y_\phi \\ l_v & l_p & l_r & l_\phi \\ n_v & n_p & n_r & n_\phi \\ 0 & 1 & 0 & 0 \end{bmatrix} \begin{bmatrix} v \\ p \\ r \\ \phi \end{bmatrix} + \begin{bmatrix} y_\xi & y_\zeta \\ l_\xi & l_\zeta \\ n_\xi & n_\zeta \\ 0 & 0 \end{bmatrix} \begin{bmatrix} \xi \\ \zeta \end{bmatrix} \quad (4.70)$$

However, in this case the derivatives are referred to aeroplane wind axes rather than to body axes and generally have slightly different values. The definitions of the concise lateral stability and control derivatives referred to aeroplane body axes are also given in Appendix 2.

Examples of the more general procedures used to create the state descriptions of various dynamic systems may be found in many books on control systems. [Shinners \(1980\)](#) and [Friedland \(1987\)](#) both contain useful aeronautical examples.

EXAMPLE 4.4

Lateral-directional derivative data for the McDonnell F-4C Phantom, referred to body axes, were obtained from [Heffley and Jewell \(1972\)](#) and are used to illustrate the formulation of the lateral

state equation. The data relate to the same flight condition as the previous example, Mach 0.6, and an altitude of 35,000 ft. As before, the leading aerodynamic variables have the following values:

Flight path angle	$\gamma_e = 0^\circ$	Inertia product	$I_{xz} = 2952 \text{ kgm}^2$
Body incidence	$\alpha_e = 9.4^\circ$	Air density	$\rho = 0.3809 \text{ kg/m}^3$
Velocity	$V_0 = 178 \text{ m/s}$	Wing area	$S = 49.239 \text{ m}^2$
Mass	$m = 17642 \text{ kg}$	Wing span	$b = 11.787 \text{ m}$
Roll moment of inertia	$I_x = 33898 \text{ kgm}^2$	Acceleration due to gravity	$g = 9.81 \text{ m/s}^2$
Yaw moment of inertia	$I_z = 189496 \text{ kgm}^2$		

The dimensionless lateral derivatives, referred to body axes, are given and, as before, any missing aerodynamic derivatives must be assumed insignificant and hence zero. Note that, in accordance with American notation, the roll control derivative L_ξ is positive.

$$\begin{aligned} Y_v &= -0.5974 & L_v &= -0.1048 & N_v &= 0.0987 \\ Y_p &= 0 & L_p &= -0.1164 & N_p &= -0.0045 \\ Y_r &= 0 & L_r &= 0.0455 & N_r &= -0.1132 \\ Y_\xi &= -0.0159 & L_\xi &= 0.0454 & N_\xi &= 0.00084 \\ Y_\zeta &= 0.1193 & L_\zeta &= 0.0086 & N_\zeta &= -0.0741 \end{aligned}$$

As for the longitudinal equations of motion, the lateral-directional state equation (4.65) may be written in terms of the more convenient dimensionless derivatives:

$$\mathbf{M}\dot{\mathbf{x}}(t) = \mathbf{A}'\mathbf{x}(t) + \mathbf{B}'\mathbf{u}(t)$$

where

$$\begin{aligned} \mathbf{x}^T(t) &= [v \quad p \quad r \quad \phi \quad \psi] \quad \mathbf{u}^T(t) = [\xi \quad \zeta] \\ \mathbf{M} &= \begin{bmatrix} m' & 0 & 0 & 0 & 0 \\ 0 & I'_x & -I'_{xz} & 0 & 0 \\ 0 & -I'_{xz} & I'_z & 0 & 0 \\ 0 & 0 & 0 & 1 & 0 \\ 0 & 0 & 0 & 0 & 1 \end{bmatrix} \\ \mathbf{A}' &= \begin{bmatrix} Y_v & (Y_p b + m' W_e) & (Y_r b - m' U_e) & m' g \cos \theta_e & m' g \sin \theta_e \\ L_v & L_p b & L_r b & 0 & 0 \\ N_v & N_p b & N_r b & 0 & 0 \\ 0 & 1 & 0 & 0 & 0 \\ 0 & 0 & 1 & 0 & 0 \end{bmatrix} \quad \mathbf{B}' = \begin{bmatrix} V_0 Y_\xi & V_0 Y_\zeta \\ V_0 L_\xi & V_0 L_\zeta \\ V_0 N_\xi & V_0 N_\zeta \\ 0 & 0 \\ 0 & 0 \end{bmatrix} \end{aligned}$$

where

$$m' = \frac{m}{\frac{1}{2}\rho V_0 S}, \quad I'_x = \frac{I_x}{\frac{1}{2}\rho V_0 S b}, \quad I'_z = \frac{I_z}{\frac{1}{2}\rho V_0 S b} \text{ and } I'_{xz} = \frac{I_{xz}}{\frac{1}{2}\rho V_0 S b}$$

and, as before, $U_e = V_0 \cos \theta_e$ and $W_e = V_0 \sin \theta_e$ in steady symmetric flight.

Substituting the appropriate values into these matrices and premultiplying the matrices \mathbf{A}' and \mathbf{B}' by the inverse of the mass matrix \mathbf{M} , the concise lateral-directional state [equation \(4.69\)](#), referred to body axes, is obtained:

$$\begin{bmatrix} \dot{v} \\ \dot{p} \\ \dot{r} \\ \dot{\phi} \\ \dot{\psi} \end{bmatrix} = \begin{bmatrix} -0.0565 & 29.072 & -175.610 & 9.6783 & 1.6022 \\ -0.0601 & -0.7979 & -0.2996 & 0 & 0 \\ 9.218 \times 10^{-3} & -0.0179 & -0.1339 & 0 & 0 \\ 0 & 1 & 0 & 0 & 0 \\ 0 & 0 & 1 & 0 & 0 \end{bmatrix} \begin{bmatrix} v \\ p \\ r \\ \phi \\ \psi \end{bmatrix}$$

$$+ \begin{bmatrix} -0.2678 & 2.0092 \\ 4.6982 & 0.7703 \\ 0.0887 & -1.3575 \\ 0 & 0 \\ 0 & 0 \end{bmatrix} \begin{bmatrix} \xi \\ \zeta \end{bmatrix}$$

Again, the matrix computation was undertaken with the aid of Program CC. However, the elements of the matrices could equally well have been calculated using the expressions for the concise derivatives given in Appendix 2, Tables A2.7 and A2.8.

4.4.3 The equations of motion in American normalised form

The preferred North American form of the equations of motion expresses the axial equations of motion in units of linear acceleration rather than force, and the angular equations of motion in terms of angular acceleration rather than moment. This is easily achieved by *normalising* the force and moment equations by dividing by mass or moment of inertia as appropriate. Restating the linear equations of motion [\(4.23\)](#),

$$\begin{aligned} m(\ddot{u} + qW_e) &= X \\ m(\ddot{v} - pW_e + rU_e) &= Y \\ m(\ddot{w} - qU_e) &= Z \\ I_x \ddot{p} - I_{xz} \ddot{r} &= L \\ I_y \ddot{q} &= M \\ I_z \ddot{r} - I_{xz} \ddot{p} &= N \end{aligned} \tag{4.71}$$

The normalised form of the decoupled longitudinal equations of motion from [equations \(4.71\)](#) are written as

$$\begin{aligned}\dot{u} + qW_e &= \frac{X}{m} \\ \dot{w} - qU_e &= \frac{Z}{m} \\ \dot{q} &= \frac{M}{I_y}\end{aligned}\tag{4.72}$$

and the normalised form of the decoupled lateral-directional equations of motion may also be obtained from [equations \(4.71\)](#):

$$\begin{aligned}\dot{v} - pW_e + rU_e &= \frac{Y}{m} \\ \dot{p} - \frac{I_{xz}}{I_x} \dot{r} &= \frac{L}{I_x} \\ \dot{r} - \frac{I_{xz}}{I_z} \dot{p} &= \frac{N}{I_z}\end{aligned}\tag{4.73}$$

Further, both the rolling and yawing moment [equations in \(4.73\)](#) include roll and yaw acceleration terms, \dot{p} and \dot{r} , respectively, and it is usual to eliminate \dot{r} from the rolling moment equation and \dot{p} from the yawing moment equation. This reduces [equations \(4.73\)](#) to the alternative form:

$$\begin{aligned}\dot{v} - pW_e + rU_e &= \frac{Y}{m} \\ \dot{p} &= \left(\frac{L}{I_x} + \frac{N I_{xz}}{I_z I_x} \right) \left(\frac{1}{1 - I_{xz}^2/I_x I_z} \right) \\ \dot{r} &= \left(\frac{N}{I_z} + \frac{L I_{xz}}{I_x I_z} \right) \left(\frac{1}{1 - I_{xz}^2/I_x I_z} \right)\end{aligned}\tag{4.74}$$

Now the decoupled longitudinal force and moment expressions as derived in [Section 4.2](#) may be obtained from [equations \(4.40\)](#):

$$\begin{aligned}X &= \ddot{X}_u u + \ddot{X}_{\dot{w}} \dot{w} + \ddot{X}_w w + \ddot{X}_q q + \ddot{X}_\eta \eta + \ddot{X}_\tau \tau - mg \theta \cos \theta_e \\ Z &= \ddot{Z}_u u + \ddot{Z}_{\dot{w}} \dot{w} + \ddot{Z}_w w + \ddot{Z}_q q + \ddot{Z}_\eta \eta + \ddot{Z}_\tau \tau - mg \theta \sin \theta_e \\ M &= \ddot{M}_u u + \ddot{M}_{\dot{w}} \dot{w} + \ddot{M}_w w + \ddot{M}_q q + \ddot{M}_\eta \eta + \ddot{M}_\tau \tau\end{aligned}\tag{4.75}$$

Substituting [equations \(4.75\)](#) into [equations \(4.72\)](#), and after some rearrangement, the longitudinal equations of motion may be written as

$$\begin{aligned}\dot{u} &= \frac{\dot{X}_u}{m} u + \frac{\dot{X}_{\dot{w}}}{m} \dot{w} + \frac{\dot{X}_w}{m} w + \left(\frac{\dot{X}_q}{m} - W_e \right) q - g \theta \cos \theta_e + \frac{\dot{X}_\eta}{m} \eta + \frac{\dot{X}_\tau}{m} \tau \\ \dot{w} &= \frac{\dot{Z}_u}{m} u + \frac{\dot{Z}_{\dot{w}}}{m} \dot{w} + \frac{\dot{Z}_w}{m} w + \left(\frac{\dot{Z}_q}{m} + U_e \right) q - g \theta \sin \theta_e + \frac{\dot{Z}_\eta}{m} \eta + \frac{\dot{Z}_\tau}{m} \tau \\ \dot{q} &= \frac{\dot{M}_u}{I_y} u + \frac{\dot{M}_{\dot{w}}}{I_y} \dot{w} + \frac{\dot{M}_w}{I_y} w + \frac{\dot{M}_q}{I_y} q + \frac{\dot{M}_\eta}{I_y} \eta + \frac{\dot{M}_\tau}{I_y} \tau\end{aligned}\quad (4.76)$$

Alternatively, [equations \(4.76\)](#) may be expressed in terms of American normalised derivatives as follows:

$$\begin{aligned}\dot{u} &= X_u u + X_{\dot{w}} \dot{w} + X_w w + (X_q - W_e) q - g \theta \cos \theta_e + X_{\delta_e} \delta_e + X_{\delta_{th}} \delta_{th} \\ \dot{w} &= Z_u u + Z_{\dot{w}} \dot{w} + Z_w w + (Z_q + U_e) q - g \theta \sin \theta_e + Z_{\delta_e} \delta_e + Z_{\delta_{th}} \delta_{th} \\ \dot{q} &= M_u u + M_{\dot{w}} \dot{w} + M_w w + M_q q + M_{\delta_e} \delta_e + M_{\delta_{th}} \delta_{th}\end{aligned}\quad (4.77)$$

with the control inputs stated in American notation, elevator angle $\delta_e \equiv \eta$, and thrust $\delta_{th} \equiv \tau$.

In a similar way, the decoupled lateral-directional force and moment expressions may be obtained from [equations \(4.45\)](#):

$$\begin{aligned}Y &= \overset{\circ}{Y}_v v + \overset{\circ}{Y}_p p + \overset{\circ}{Y}_r r + \overset{\circ}{Y}_\xi \xi + \overset{\circ}{Y}_\zeta \zeta + mg \phi \cos \theta_e + mg \psi \sin \theta_e \\ L &= \overset{\circ}{L}_v v + \overset{\circ}{L}_p p + \overset{\circ}{L}_r r + \overset{\circ}{L}_\xi \xi + \overset{\circ}{L}_\zeta \zeta \\ N &= \overset{\circ}{N}_v v + \overset{\circ}{N}_p p + \overset{\circ}{N}_r r + \overset{\circ}{N}_\xi \xi + \overset{\circ}{N}_\zeta \zeta\end{aligned}\quad (4.78)$$

Substituting [equations \(4.78\)](#) into [equations \(4.74\)](#), and after some rearrangement, the lateral-directional equations of motion may be written as

$$\begin{aligned}\dot{v} &= \frac{\overset{\circ}{Y}_v}{m} v + \left(\frac{\overset{\circ}{Y}_p}{m} + W_e \right) p + \left(\frac{\overset{\circ}{Y}_r}{m} - U_e \right) r + \frac{\overset{\circ}{Y}_\xi}{m} \xi + \frac{\overset{\circ}{Y}_\zeta}{m} \zeta + g \phi \cos \theta_e + g \psi \sin \theta_e \\ \dot{p} &= \left(\left(\frac{\overset{\circ}{L}_v}{I_x} + \frac{\overset{\circ}{N}_v}{I_z} \frac{I_{xz}}{I_x} \right) v + \left(\frac{\overset{\circ}{L}_p}{I_x} + \frac{\overset{\circ}{N}_p}{I_z} \frac{I_{xz}}{I_x} \right) p + \left(\frac{\overset{\circ}{L}_r}{I_x} + \frac{\overset{\circ}{N}_r}{I_z} \frac{I_{xz}}{I_x} \right) r \right) \left(\frac{1}{1 - I_{xz}^2/I_x I_z} \right) \\ &\quad + \left(\frac{\overset{\circ}{L}_\xi}{I_x} + \frac{\overset{\circ}{N}_\xi}{I_z} \frac{I_{xz}}{I_x} \right) \xi + \left(\frac{\overset{\circ}{L}_\zeta}{I_x} + \frac{\overset{\circ}{N}_\zeta}{I_z} \frac{I_{xz}}{I_x} \right) \zeta \\ \dot{r} &= \left(\left(\frac{\overset{\circ}{N}_v}{I_z} + \frac{\overset{\circ}{L}_v}{I_x} \frac{I_{xz}}{I_z} \right) v + \left(\frac{\overset{\circ}{N}_p}{I_z} + \frac{\overset{\circ}{L}_p}{I_x} \frac{I_{xz}}{I_z} \right) p + \left(\frac{\overset{\circ}{N}_r}{I_z} + \frac{\overset{\circ}{L}_r}{I_x} \frac{I_{xz}}{I_z} \right) r \right) \left(\frac{1}{1 - I_{xz}^2/I_x I_z} \right) \\ &\quad + \left(\frac{\overset{\circ}{N}_\xi}{I_z} + \frac{\overset{\circ}{L}_\xi}{I_x} \frac{I_{xz}}{I_z} \right) \xi + \left(\frac{\overset{\circ}{N}_\zeta}{I_z} + \frac{\overset{\circ}{L}_\zeta}{I_x} \frac{I_{xz}}{I_z} \right) \zeta\end{aligned}\quad (4.79)$$

As before, [equations \(4.79\)](#) may be expressed in terms of American normalised derivatives as follows:

$$\begin{aligned}\dot{v} &= Y_v v + (Y_p + W_e)p + (Y_r - U_e)r + Y_{\delta_a} \delta_a + Y_{\delta_r} \delta_r + g \phi \cos \theta_e + g \psi \sin \theta_e \\ \dot{p} &= \left(\left(L_v + N_v \frac{I_{xz}}{I_x} \right) v + \left(L_p + N_p \frac{I_{xz}}{I_x} \right) p + \left(L_r + N_r \frac{I_{xz}}{I_x} \right) r \right) \left(\frac{1}{1 - I_{xz}^2 / I_x I_z} \right) \\ &\quad + \left(L_{\delta_a} + N_{\delta_a} \frac{I_{xz}}{I_x} \right) \delta_a + \left(L_{\delta_r} + N_{\delta_r} \frac{I_{xz}}{I_x} \right) \delta_r \\ \dot{r} &= \left(\left(N_v + L_v \frac{I_{xz}}{I_z} \right) v + \left(N_p + L_p \frac{I_{xz}}{I_z} \right) p + \left(N_r + L_r \frac{I_{xz}}{I_z} \right) r \right) \left(\frac{1}{1 - I_{xz}^2 / I_x I_z} \right) \\ &\quad + \left(N_{\delta_a} + L_{\delta_a} \frac{I_{xz}}{I_z} \right) \delta_a + \left(N_{\delta_r} + L_{\delta_r} \frac{I_{xz}}{I_z} \right) \delta_r\end{aligned}\tag{4.80}$$

with the control inputs stated in American notation, aileron angle $\delta_a \equiv \xi$, and rudder angle $\delta_r \equiv \zeta$.

Clearly, the formulation of the rolling and yawing moment [equations in \(4.80\)](#) is very cumbersome, so it is usual to modify the definitions of the rolling and yawing moment derivatives to reduce [equations \(4.80\)](#) to the more manageable format,

$$\begin{aligned}\dot{v} &= Y_v v + (Y_p + W_e)p + (Y_r - U_e)r + Y_{\delta_a} \delta_a + Y_{\delta_r} \delta_r + g \phi \cos \theta_e + g \psi \sin \theta_e \\ \dot{p} &= L'_v v + L'_p p + L'_r r + L'_{\delta_a} \delta_a + L'_{\delta_r} \delta_r \\ \dot{r} &= N'_v v + N'_p p + N'_r r + N'_{\delta_a} \delta_a + N'_{\delta_r} \delta_r\end{aligned}\tag{4.81}$$

where, for example, the modified normalised derivatives are given by expressions like

$$\begin{aligned}L'_v &= \left(L_v + N_v \frac{I_{xz}}{I_x} \right) \left(\frac{1}{1 - I_{xz}^2 / I_x I_z} \right) \equiv \left(\frac{\overset{\circ}{L}_v}{I_x} + \frac{\overset{\circ}{N}_v I_{xz}}{I_z I_x} \right) \left(\frac{1}{1 - I_{xz}^2 / I_x I_z} \right) \\ N'_r &= \left(N_r + L_r \frac{I_{xz}}{I_z} \right) \left(\frac{1}{1 - I_{xz}^2 / I_x I_z} \right) \equiv \left(\frac{\overset{\circ}{N}_r}{I_z} + \frac{\overset{\circ}{L}_r I_{xz}}{I_x I_z} \right) \left(\frac{1}{1 - I_{xz}^2 / I_x I_z} \right)\end{aligned}\tag{4.82}$$

and the remaining modified derivatives are defined in a similar way with reference to [equations \(4.79\)](#), [\(4.80\)](#), and [\(4.81\)](#).

Thus the small perturbation equations of motion in American normalised notation, referred to aircraft body axes, are given by [equations \(4.77\)](#) and [\(4.81\)](#). A full list of the American normalised derivatives and their British equivalents is given in Appendix 7.

A common alternative formulation of the longitudinal equations of motion [\(4.77\)](#) is frequently used when thrust is assumed to have a velocity or Mach number dependency. The normalised derivatives X_u , Z_u , and M_u , as stated in [equations \(4.77\)](#), denote the *aerodynamic* derivatives only,

and thrust is assumed to remain constant for small perturbations in velocity or Mach number. However, the notation X_u^* , Z_u^* , and M_u^* , as shown in [equations \(4.83\)](#), denote that the normalised derivatives include both the *aerodynamic and thrust* dependencies on small perturbations in velocity or Mach number.

$$\begin{aligned}\dot{u} &= X_u^* u + X_{\dot{w}} \dot{w} + X_w w + (X_q - W_e) q - g \theta \cos \theta_e + X_{\delta_e} \delta_e + X_{\delta_{th}} \delta_{th} \\ \dot{w} &= Z_u^* u + Z_{\dot{w}} \dot{w} + Z_w w + (Z_q + U_e) q - g \theta \sin \theta_e + Z_{\delta_e} \delta_e + Z_{\delta_{th}} \delta_{th} \\ \dot{q} &= M_u^* u + M_{\dot{w}} \dot{w} + M_w w + M_q q + M_{\delta_e} \delta_e + M_{\delta_{th}} \delta_{th}\end{aligned}\quad (4.83)$$

It is also common to express the lateral velocity perturbation v in [equations \(4.81\)](#) in terms of sideslip angle β since, for small disturbances, $v = \beta V_0$:

$$\begin{aligned}\dot{\beta} &= Y_v \beta + \frac{1}{V_0} (Y_p + W_e) p + \frac{1}{V_0} (Y_r - U_e) r + Y_{\delta_a}^* \delta_a + Y_{\delta_r}^* \delta_r + \frac{g}{V_0} (\phi \cos \theta_e + \psi \sin \theta_e) \\ \dot{p} &= L'_\beta \beta + L'_p p + L'_r r + L'_{\delta_a} \delta_a + L'_{\delta_r} \delta_r \\ \dot{r} &= N'_\beta \beta + N'_p p + N'_r r + N'_{\delta_a} \delta_a + N'_{\delta_r} \delta_r\end{aligned}\quad (4.84)$$

where

$$Y_{\delta_a}^* = \frac{Y_{\delta_a}}{V_0} \quad Y_{\delta_r}^* = \frac{Y_{\delta_r}}{V_0}$$

$$L'_\beta = L'_v V_0 \quad N'_\beta = N'_v V_0$$

[Equations \(4.83\) and \(4.84\)](#) probably represent the most commonly encountered form of the American normalised equations of motion.

EXAMPLE 4.5

To illustrate application of the longitudinal equations of motion [\(4.83\)](#), consider the Boeing B-747 large civil transport aeroplane, data for which are given in [Heffley and Jewell \(1972\)](#). A typical level flight cruise configuration was chosen and corresponds with Mach 0.8 at an altitude of 40,000 ft. The relevant flight condition data as given are

Flight path angle	$\gamma_e = 0^\circ$
Body incidence	$\alpha_e = 4.6^\circ$
Velocity	$V_0 = 774 \text{ ft/s}$
Mass	$m = 1.9771 \times 10^4 \text{ slug}$
Pitch moment of inertia	$I_y = 3.31 \times 10^7 \text{ slugft}^2$
Acceleration due to gravity	$g = 32.2 \text{ ft/s}^2$

The normalised longitudinal aerodynamic and control derivatives, referred to body axes, are given, and, as before, any missing aerodynamic derivatives must be assumed insignificant and hence zero. Note that, since the derivatives are normalised, they have units as shown and are consistent with the standard imperial system of units used in North America. Note also that, to preserve computational consistency, the thrust control derivatives assume that the thrust control

variable is dimensionless and varies in the range $0 \leq \delta_{th} \leq 1$, where 1 corresponds to maximum thrust with all four engines operating symmetrically.

$$\begin{aligned} X_u^* &= -0.00276 \text{ 1/s} & M_w &= -0.000116 \text{ 1/ft} \\ Z_u^* &= -0.0650 \text{ 1/s} & M_q &= -0.339 \text{ 1/s} \\ M_u^* &= 0.000193 \text{ 1/sft} & X_{\delta_e} &= 1.44 \text{ ft/s}^2 \text{ rad} \\ X_w &= 0.0389 \text{ 1/s} & Z_{\delta_e} &= -17.9 \text{ ft/s}^2 \text{ rad} \\ Z_w &= -0.317 \text{ 1/s} & M_{\delta_e} &= -1.16 \text{ 1/s}^2 \\ M_w &= -0.00105 \text{ 1/sft} & X_{\delta_{th}} &= 5.05 \times 10^{-5} \text{ ft/s}^2 \\ Z_{\dot{w}} &= 0.00666 & Z_{\delta_{th}} &= -2.20 \times 10^{-6} \text{ ft/s}^2 \\ Z_q &= -5.16 \text{ ft/s} & M_{\delta_{th}} &= 3.02 \times 10^{-7} \text{ 1/s}^2 \end{aligned}$$

In steady level symmetric flight, $U_e = V_0 \cos \theta_e$, $W_e = V_0 \sin \theta_e$, and $\theta_e \equiv \alpha_e$. Substituting numerical values into equations (4.83) gives

$$\begin{aligned} \dot{u} &= -0.00276u + 0.0389w - 62.1\theta + 1.44\delta_e + 5.05 \times 10^{-5}\delta_{th} \\ \dot{w} &= -0.0650u + 0.00666\dot{w} - 0.317w + 766.34q - 2.582\theta - 17.9\delta_e - 2.20 \times 10^{-6}\delta_{th} \\ \dot{q} &= 0.000193u - 0.000116\dot{w} - 0.00105w - 0.339q - 1.16\delta_e + 3.02 \times 10^{-7}\delta_{th} \end{aligned} \quad (4.85)$$

Equations (4.85) may be assembled in the matrix form defined by (4.65), with the addition of small perturbation auxiliary equation (2.23), $\dot{\theta} = q$, to give

$$\begin{bmatrix} 1 & 0 & 0 & 0 \\ 0 & 0.9933 & 0 & 0 \\ 0 & 0.000116 & 1 & 0 \\ 0 & 0 & 0 & 1 \end{bmatrix} \begin{bmatrix} \dot{u} \\ \dot{w} \\ \dot{q} \\ \dot{\theta} \end{bmatrix} = \begin{bmatrix} -0.00276 & 0.0389 & -62.1 & -32.1 \\ -0.0650 & -0.317 & 766.34 & -2.582 \\ 0.000193 & -0.00105 & -0.339 & 0 \\ 0 & 0 & 1 & 0 \end{bmatrix} \begin{bmatrix} u \\ w \\ q \\ \theta \end{bmatrix} + \begin{bmatrix} 1.44 & 5.05 \times 10^{-5} \\ -17.9 & -2.20 \times 10^{-6} \\ -1.16 & 3.02 \times 10^{-7} \\ 0 & 0 \end{bmatrix} \begin{bmatrix} \delta_e \\ \delta_{th} \end{bmatrix} \quad (4.86)$$

Multiplying equation (4.86) by the inverse of the mass matrix gives the longitudinal state equation in the standard formulation:

$$\begin{bmatrix} \dot{u} \\ \dot{w} \\ \dot{q} \\ \dot{\theta} \end{bmatrix} = \begin{bmatrix} -0.00276 & 0.0389 & -62.1 & -32.1 \\ -0.0654 & -0.3191 & 771.51 & -2.5994 \\ 0.0002 & -0.001013 & -0.4285 & 0.0003 \\ 0 & 0 & 1 & 0 \end{bmatrix} \begin{bmatrix} u \\ w \\ q \\ \theta \end{bmatrix} + \begin{bmatrix} 1.44 & 5.05 \times 10^{-5} \\ -18.021 & -2.215 \times 10^{-6} \\ -1.1579 & 3.0226 \times 10^{-7} \\ 0 & 0 \end{bmatrix} \begin{bmatrix} \delta_e \\ \delta_{th} \end{bmatrix} \quad (4.87)$$

Equation (4.87) is quite independent of the notation and style of the original equations of motion, with the exception of the units of the variables, which remain consistent with the original model. In this simple example, velocities u and w have units ft/s, pitch rate q has units rad/s, pitch attitude θ and elevator angle δ_e have units rad, and the thrust variable δ_{th} is dimensionless, as explained previously. Analysis of the longitudinal flight dynamics of the B-747 at this flight condition may now be carried out using equation (4.87) and the methods described in later chapters.

EXAMPLE 4.6

The lateral-directional equations of motion of the Boeing B-747 are also given in Heffley and Jewell (1972) and may be used to illustrate the application of equations (4.84). At the same typical flight condition of Mach 0.8 at an altitude of 40,000 ft, the relevant flight condition data as given are

Flight path angle	$\gamma_e = 0^\circ$
Body incidence	$\alpha_e = 4.6^\circ$
Velocity	$V_0 = 774 \text{ ft/s}$
Mass	$m = 1.9771 \times 10^4 \text{ slug}$
Roll moment of inertia	$I_x = 1.82 \times 10^7 \text{ slugft}^2$
Yaw moment of inertia	$I_z = 4.97 \times 10^7 \text{ slugft}^2$
Inertia product	$I_{xz} = 970,056 \text{ slugft}^2$
Acceleration due to gravity	$g = 32.2 \text{ ft/s}^2$

The *modified* normalised lateral-directional aerodynamic and control derivatives, referred to body axes, are given and, as before, any missing aerodynamic derivatives must be assumed insignificant and hence zero. Since the derivatives are normalised, they have units as shown and are consistent with the standard imperial system of units used in North America.

$$\begin{aligned}
 Y_v &= -0.0558 \text{ 1/s} & N'_r &= -0.115 \text{ 1/s} \\
 Y_\beta &= -43.2 \text{ ft/s}^2 & Y_{\delta_a}^* &= 0 \text{ 1/s} \\
 L'_\beta &= -3.05 \text{ 1/s}^2 & L'_{\delta_a} &= 0.143 \text{ 1/s}^2 \\
 N'_\beta &= 0.598 \text{ 1/s}^2 & N'_{\delta_a} &= 0.00775 \text{ 1/s}^2 \\
 L'_p &= -0.465 \text{ 1/s} & Y_{\delta_r}^* &= 0.00729 \text{ 1/s} \\
 N'_p &= -0.0318 \text{ 1/s} & L'_{\delta_r} &= 0.153 \text{ 1/s}^2 \\
 L'_r &= 0.388 \text{ 1/s} & N'_{\delta_r} &= -0.475 \text{ 1/s}^2
 \end{aligned}$$

As before, $U_e = V_0 \cos \theta_e$, $W_e = V_0 \sin \theta_e$, and $\theta_e \equiv \alpha_e$; substituting numerical values into equations (4.84) gives

$$\begin{aligned}
 \dot{\beta} &= -0.0558\beta + 0.08p - 0.997r + 0.0415\phi + 0.0033\psi + 0.00729\delta_r \\
 \dot{p} &= -3.05\beta - 0.465p + 0.388r + 0.143\delta_a + 0.153\delta_r \\
 \dot{r} &= 0.598\beta - 0.0318p - 0.115r + 0.00775\delta_a - 0.475\delta_r
 \end{aligned} \tag{4.88}$$

Equations (4.88) may also be assembled in the matrix form defined by equation (4.65), with the addition of small perturbation auxiliary equations (2.23), $\dot{\phi} = p$ and $\dot{\psi} = r$, to give the lateral-directional state equation directly:

$$\begin{bmatrix} \dot{\beta} \\ \dot{p} \\ \dot{r} \\ \dot{\phi} \\ \dot{\psi} \end{bmatrix} = \begin{bmatrix} -0.0558 & 0.08 & -0.997 & 0.0415 & 0.0033 \\ -3.05 & -0.465 & 0.388 & 0 & 0 \\ 0.598 & -0.318 & -0.115 & 0 & 0 \\ 0 & 1 & 0 & 0 & 0 \\ 0 & 0 & 1 & 0 & 0 \end{bmatrix} \begin{bmatrix} \beta \\ p \\ r \\ \phi \\ \psi \end{bmatrix} + \begin{bmatrix} 0 & 0.00729 \\ 0.143 & 0.153 \\ 0.00775 & -0.475 \\ 0 & 0 \\ 0 & 0 \end{bmatrix} \begin{bmatrix} \delta_a \\ \delta_r \end{bmatrix} \quad (4.89)$$

Again, it is evident that equation (4.89) is quite independent of the notation and style of the original equations of motion, with the exception of the units of the variables, which remain consistent with the original model.

References

- Barnett, S. (1975). *Introduction to mathematical control theory*. Oxford, UK: Clarendon Press.
- Bryan, G. H. (1911). *Stability in aviation*. London: Macmillan.
- Friedland, B. (1987). *Control system design*. New York: McGraw-Hill.
- Heffley, R. K., & Jewell, W. F. (1972). *Aircraft handling qualities data*. NASA Contractor Report, NASA CR-2144, Washington, DC: National Aeronautics and Space Administration.
- Hopkin, H. R. (1970). *A scheme of notation and nomenclature for aircraft dynamics and associated aerodynamics*. London: Aeronautical Research Council, Reports and Memoranda No. 3562. Her Majesty's Stationery Office.
- Shinners, S. M. (1980). *Modern control system theory and application*. Boston: Addison-Wesley.

PROBLEMS

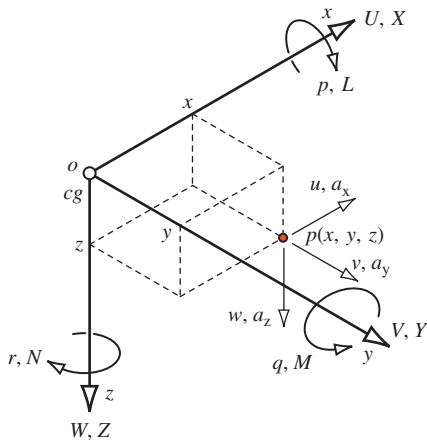
- 4.1** Consider the dimensional longitudinal equations of motion of an aircraft in the following format:

$$\begin{aligned} m\ddot{u} - \dot{X}_u u - \dot{X}_w w - (\dot{X}_q - mW_e)q + mg\theta \cos\theta_e &= \dot{X}_\eta \eta \\ -\dot{Z}_u u + m\dot{w} - \dot{Z}_w w - (\dot{Z}_q + mU_e)q + mg\theta \sin\theta_e &= \dot{Z}_\eta \eta \\ -\dot{M}_u u - \dot{M}_w w - \dot{M}_q q + I_y \dot{q} &= \dot{M}_\eta \eta \end{aligned}$$

Rearrange them in dimensionless form, referred to wind axes. Discuss the relative merits of using the equations of motion in dimensional, dimensionless, and concise forms.

(CU 1982)

- 4.2** The right handed orthogonal axis system ($oxyz$) shown in the following figure is fixed in a rigid airframe such that o is coincident with the centre of gravity.



- a.** The components of velocity and force along ox , oy , and oz are U , V , W and X , Y , Z , respectively. The components of angular velocity about ox , oy , and oz are p , q , r , respectively. The point $p(x, y, z)$ in the airframe has local velocity and acceleration components u , v , w and a_x , a_y , a_z , respectively. Show that by superimposing the motion of the axes ($oxyz$) on to the motion of the point $p(x, y, z)$, the absolute acceleration components of $p(x, y, z)$ are given by

$$\begin{aligned} a'_x &= \dot{U} - rV + qW - x(q^2 + r^2) + y(pq - \dot{r}) + z(pr + \dot{q}) \\ a'_y &= \dot{V} - pW + rU + x(pq + \dot{r}) - y(p^2 + r^2) + z(qr - \dot{p}) \\ a'_z &= \dot{W} - qU + pV + x(pr - \dot{q}) + y(qr + \dot{p}) - z(p^2 + q^2) \end{aligned}$$

- b.** Further, assuming the mass of the aircraft to be uniformly distributed, show that the total body force components are given by

$$\begin{aligned} X &= m(\dot{U} - rV + qW) \\ Y &= m(\dot{V} - pW + rU) \\ Z &= m(\dot{W} - qU + pV) \end{aligned}$$

where m is the mass of the aircraft.

(CU 1986)

- 4.3 The linearised longitudinal equations of motion of an aircraft describing small perturbations about a steady trimmed rectilinear flight condition are given by

$$\begin{aligned} m(\dot{u}(t) + q(t)W_e) &= X(t) \\ m(\dot{w}(t) - q(t)U_e) &= Z(t) \\ I_y\dot{q}(t) &= M(t) \end{aligned}$$

Develop expressions for $X(t)$, $Z(t)$, and $M(t)$ and thus complete the equations of motion referred to generalised aircraft body axes. What simplifications may be made if a wind axes reference and level flight are assumed?

(CU 1987)

- 4.4 State the assumptions made in deriving the small perturbation longitudinal equations of motion for an aircraft. For each assumption give a realistic example of an aircraft type, or configuration, which may make the assumption invalid.

(LU 2002)

- 4.5 Show that, when the product of inertia I_{xz} is much smaller than the moments of inertia in roll and yaw, I_x and I_z , respectively, the lateral-directional derivatives in modified American normalised form may be approximated by the unmodified American normalised form.

The Solution of the Equations of Motion

5

5.1 Methods of solution

The primary reason for solving the equations of motion is to obtain a mathematical, and hence graphical, description of the time histories of all motion variables in response to a control input, or atmospheric disturbance, and to enable an assessment of stability. It is also important that the chosen method of solution provides good insight into the way in which the physical properties of the airframe influence the responses. Since the evolution of the development of the equations of motion and their solution followed in the wake of observation of aeroplane behaviour, it was no accident that practical constraints were applied which resulted in the decoupled small-perturbation equations. The longitudinal and lateral-directional decoupled equations of motion are each represented by a set of three simultaneous linear differential equations which have traditionally been solved using classical mathematical analysis methods. Although laborious to apply, the advantage of the traditional approach is that it is capable of providing excellent insight into the nature of aircraft stability and response. However, since traditional methods invariably involve the use of the dimensionless equations of motion, considerable care in the interpretation of the numerical results is required if confusion is to be avoided. A full discussion of these methods can be found in many of the earlier books on the subject, for example, Duncan (1952).

Operational methods have also enjoyed some popularity as a means for solving the equations of motion. In particular, the Laplace transform method has been, and continues to be, used extensively. By transforming the differential equations, they become algebraic equations expressed in terms of the Laplace operator s . Their manipulation to obtain a solution then becomes a relatively straightforward exercise in algebra. The problem is thus transformed into one of solving a set of simultaneous linear algebraic equations, a process that is readily accomplished by computational methods. Further, the input-output response relationship or transfer characteristic is described by a simple algebraic *transfer function* in terms of the Laplace operator. The time response then follows by finding the inverse Laplace transform of the transfer function for the input of interest.

Now, the transfer function as a means for describing the characteristics of a linear dynamic system is the principal tool of the control systems engineer, and a vast array of mathematical tools is available for transfer function analysis. With relative ease, analysis of the transfer function of a system enables a complete picture of its dynamic behaviour to be drawn. In particular, stability, time response, and frequency response information is readily obtained. Furthermore, obtaining the system transfer function is usually the prelude to design of a feedback control system, and an

additional array of mathematical tools is available to support this task. Since most modern aeroplanes are dependent, to a greater or lesser extent, on feedback control for their continued proper operation, it would seem particularly advantageous to be able to describe them in terms of transfer functions. Fortunately, this is easily accomplished. The Laplace transform of the linearised small-perturbation equations of motion is readily obtained, and by the subsequent application of the appropriate mathematical tools the *response transfer functions* may be derived. An analysis of the dynamic properties of the aeroplane may then be made using control engineering tools as an alternative to the traditional methods of the aerodynamicist. Indeed, as described in Chapter 1, many computer software packages are available which facilitate the rapid and accurate analysis of linear dynamic systems and the design of automatic control systems. Today, access to computer software of this type is essential for the flight dynamicist.

The process of solution requires that the equations of motion be assembled in the appropriate format, numerical values for the derivatives and other parameters substituted, and then the whole model input to a suitable computer program. The output, which is usually obtained instantaneously, is most conveniently arranged in terms of response transfer functions. The objective can thus usually be achieved relatively easily, with great rapidity and good accuracy. A significant shortcoming of such computational methods is the lack of *visibility*; that is, the functional steps in the solution process are hidden from the investigator. Consequently, considerable care, and some skill, is required to analyse the solution correctly, which can be greatly facilitated if the investigator has a good understanding of the computational solution process. Indeed, it is considered essential to have an understanding of the steps involved in the solution of the equations of motion using the operational methods common to most computer software packages.

Much of the remainder of this chapter is concerned with the use of the Laplace transform for solving the small-perturbation equations of motion to obtain the response transfer functions. This is followed by a description of the computational process involving matrix methods which is normally undertaken with the aid of a suitable computer software package.

5.2 Cramer's rule

Cramer's rule describes a mathematical process for solving sets of simultaneous linear algebraic equations. It may be used to solve the equations of motion algebraically and is found in many degree-level mathematical texts, and in books devoted to the application of computational methods to linear algebra (e.g., [Goult et al. \(1974\)](#)). Since Cramer's rule involves the use of matrix algebra it is easily implemented in a digital computer.

To solve the system of n simultaneous linear algebraic equations described in matrix form as

$$\mathbf{y} = \mathbf{Ax} \quad (5.1)$$

where \mathbf{x} and \mathbf{y} are column vectors and \mathbf{A} is a matrix of constant coefficients, Cramer's rule states that

$$\mathbf{x} = \mathbf{A}^{-1}\mathbf{y} \equiv \left(\frac{\text{Adjoint}\mathbf{A}}{\text{Det}\mathbf{A}} \right) \mathbf{y} \quad (5.2)$$

where the solution for x_i , the i th row of [equation \(5.2\)](#), is given by

$$x_i = \frac{1}{|\mathbf{A}|} (A_{1i}y_1 + A_{2i}y_2 + A_{3i}y_3 + \dots + A_{ni}y_n) \quad (5.3)$$

The significant observation is that the numerator of [equation \(5.3\)](#) is equivalent to the determinant of \mathbf{A} , with the i th column replaced by the vector \mathbf{y} . Thus the solution of [equations \(5.1\)](#) to find all the x_i reduces to the relatively simple problem of evaluating $n+1$ determinants.

EXAMPLE 5.1

To illustrate the use of Cramer's rule, consider the trivial example in which it is required to solve the simultaneous linear algebraic equations

$$\begin{aligned} y_1 &= x_1 + 2x_2 + 3x_3 \\ y_2 &= 2x_2 + 4x_2 + 5x_3 \\ y_3 &= 3x_1 + 5x_2 + 6x_3 \end{aligned}$$

or, in matrix notation,

$$\begin{bmatrix} y_1 \\ y_2 \\ y_3 \end{bmatrix} = \begin{bmatrix} 1 & 2 & 3 \\ 2 & 4 & 5 \\ 3 & 5 & 6 \end{bmatrix} \begin{bmatrix} x_1 \\ x_2 \\ x_3 \end{bmatrix}$$

Applying Cramer's rule to solve for x_i ,

$$x_1 = \frac{\begin{vmatrix} y_1 & 2 & 3 \\ y_2 & 4 & 5 \\ y_3 & 5 & 6 \end{vmatrix}}{\begin{vmatrix} 1 & 2 & 3 \\ 2 & 4 & 5 \\ 3 & 5 & 6 \end{vmatrix}} = \frac{y_1 \begin{vmatrix} 4 & 5 \\ 5 & 6 \end{vmatrix} - y_2 \begin{vmatrix} 2 & 3 \\ 5 & 6 \end{vmatrix} + y_3 \begin{vmatrix} 2 & 3 \\ 4 & 5 \end{vmatrix}}{-1} = y_1 - 3y_2 + 2y_3$$

$$x_2 = \frac{\begin{vmatrix} 1 & y_1 & 3 \\ 2 & y_2 & 5 \\ 3 & y_3 & 6 \end{vmatrix}}{\begin{vmatrix} 1 & 2 & 3 \\ 2 & 4 & 5 \\ 3 & 5 & 6 \end{vmatrix}} = \frac{-y_1 \begin{vmatrix} 2 & 5 \\ 3 & 6 \end{vmatrix} + y_2 \begin{vmatrix} 1 & 3 \\ 3 & 6 \end{vmatrix} - y_3 \begin{vmatrix} 1 & 3 \\ 2 & 5 \end{vmatrix}}{-1} = -3y_1 + 3y_2 - y_3$$

and

$$x_3 = \frac{\begin{vmatrix} 1 & 2 & y_1 \\ 2 & 4 & y_2 \\ 3 & 5 & y_3 \end{vmatrix}}{\begin{vmatrix} 1 & 2 & 3 \\ 2 & 4 & 5 \\ 3 & 5 & 6 \end{vmatrix}} = \frac{y_1 \begin{vmatrix} 2 & 4 \\ 3 & 5 \end{vmatrix} - y_2 \begin{vmatrix} 1 & 2 \\ 3 & 5 \end{vmatrix} + y_3 \begin{vmatrix} 1 & 2 \\ 2 & 4 \end{vmatrix}}{-1} = 2y_1 - y_2$$

Clearly, in this example, the numerator determinants are found by expanding about the column containing \mathbf{y} . The denominator determinant may be found by expanding about the first row; thus

$$\begin{vmatrix} 1 & 2 & 3 \\ 2 & 4 & 5 \\ 3 & 5 & 6 \end{vmatrix} = 1 \begin{vmatrix} 4 & 5 \\ 5 & 6 \end{vmatrix} - 2 \begin{vmatrix} 2 & 5 \\ 3 & 6 \end{vmatrix} + 3 \begin{vmatrix} 2 & 4 \\ 3 & 5 \end{vmatrix} = -1 + 6 - 6 = -1$$

5.3 Aircraft response transfer functions

Aircraft response transfer functions describe the dynamic relationships between the input variables and the output variables. The relationships are indicated diagrammatically in Fig. 5.1 and it is clear that a number of possible input-output relationships exist. When the mathematical model of the aircraft comprises the decoupled small-perturbation equations of motion, transfer functions relating longitudinal input variables to lateral-directional output variables do not exist and vice versa. This may not necessarily be the case when the aircraft is described by a fully coupled set of small-perturbation equations of motion. For example, such a description is quite usual when modelling the helicopter.

All transfer functions are written as a ratio of two polynomials in the Laplace operator s . All *proper* transfer functions have a numerator polynomial which is at least one order less than the denominator polynomial, although occasionally *improper* transfer functions crop up in aircraft applications. For example, the transfer function describing acceleration response to an input variable is improper; the numerator and denominator polynomials are of the same order. Care is needed when working with improper transfer functions, as sometimes the computational tools are unable to deal with them correctly. Obviously, this is a situation where some understanding of the physical meaning of the transfer function can be of considerable advantage. A shorthand notation is used to represent aircraft response transfer functions in this book. For example, pitch attitude $\theta(s)$ response to elevator $\eta(s)$ is denoted

$$\frac{\theta(s)}{\eta(s)} \equiv \frac{N_\eta^\theta(s)}{\Delta(s)} \quad (5.4)$$

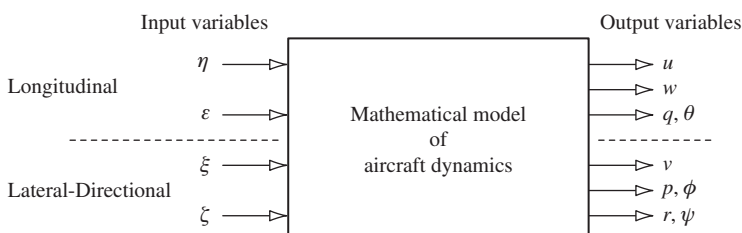


FIGURE 5.1 Aircraft input-output relationships.

where $N_\eta^\theta(s)$ is the unique numerator polynomial in s relating pitch attitude response to elevator input, and $\Delta(s)$ is the denominator polynomial in s which is common to all longitudinal response transfer functions. Similarly, for example, roll rate response to aileron is denoted

$$\frac{p(s)}{\xi(s)} \equiv \frac{N_\xi^p(s)}{\Delta(s)} \quad (5.5)$$

where in this instance $\Delta(s)$ is the denominator polynomial which is common to all of the lateral-directional response transfer functions. Since $\Delta(s)$ is context-dependent its correct identification does not usually present problems.

The denominator polynomial $\Delta(s)$ is called the *characteristic polynomial* and, when equated to zero, defines the *characteristic equation*. Thus $\Delta(s)$ completely describes the longitudinal or lateral-directional stability characteristics of the aeroplane as appropriate, and the roots, or *poles*, of $\Delta(s)$ describe its *stability modes*. Thus the stability characteristics of an aeroplane can be determined simply on inspection of the response transfer functions.

5.3.1 The longitudinal response transfer functions

The Laplace transforms of the differential quantities $\dot{x}(t)$ and $\ddot{x}(t)$, for example, are given by

$$\begin{aligned} L\{\dot{x}(t)\} &= sx(s) - x(0) \\ L\{\ddot{x}(t)\} &= s^2x(s) - sx(0) - \dot{x}(0) \end{aligned} \quad (5.6)$$

where $x(0)$ and $\dot{x}(0)$ are the initial values of $x(t)$ and $\dot{x}(t)$, respectively, at $t = 0$. Now, taking the Laplace transform of the longitudinal equations of motion (4.40), referred to body axes, assuming zero initial conditions, and since small-perturbation motion only is considered, write

$$\dot{\theta}(t) = q(t) \quad (5.7)$$

then

$$\begin{aligned} (ms - \dot{X}_u)u(s) - (\dot{X}_{\dot{w}}s + \dot{X}_w)w(s) - ((\dot{X}_q - mW_e)s - mg \cos \theta_e)\theta(s) &= \dot{X}_\eta \eta(s) + \dot{X}_\tau \tau(s) \\ - \dot{Z}_u u(s) - ((\dot{Z}_{\dot{w}} - m)s + \dot{Z}_w)w(s) - ((\dot{Z}_q + mU_e)s - mg \sin \theta_e)\theta(s) &= \dot{Z}_\eta \eta(s) + \dot{Z}_\tau \tau(s) \\ - \dot{M}_u u(s) - (\dot{M}_{\dot{w}}s + \dot{M}_w)w(s) + (I_y s^2 - \dot{M}_q s)\theta(s) &= \dot{M}_\eta \eta(s) + \dot{M}_\tau \tau(s) \end{aligned} \quad (5.8)$$

Writing equations (5.8) in matrix format,

$$\begin{bmatrix} (ms - \dot{X}_u) & -(\dot{X}_{\dot{w}}s + \dot{X}_w) & -((\dot{X}_q - mW_e)s - mg \cos \theta_e) \\ -\dot{Z}_u & -((\dot{Z}_{\dot{w}} - m)s + \dot{Z}_w) & -((\dot{Z}_q + mU_e)s - mg \sin \theta_e) \\ -\dot{M}_u & -(\dot{M}_{\dot{w}}s + \dot{M}_w) & (I_y s^2 - \dot{M}_q s) \end{bmatrix} \begin{bmatrix} u(s) \\ w(s) \\ \theta(s) \end{bmatrix} = \begin{bmatrix} \dot{X}_\eta & \dot{X}_\tau \\ \dot{Z}_\eta & \dot{Z}_\tau \\ \dot{M}_\eta & \dot{M}_\tau \end{bmatrix} \begin{bmatrix} \eta(s) \\ \tau(s) \end{bmatrix} \quad (5.9)$$

Cramer's rule can now be applied to obtain the longitudinal response transfer functions—for example, those describing response to elevator. Assume, therefore, that the thrust remains constant,

which means that the throttle is fixed at its trim setting τ_e , and $\tau(s) = 0$. Therefore, after dividing through by $\eta(s)$ equation, (5.9) may be simplified to

$$\begin{bmatrix} \left(ms - \dot{\bar{X}}_u\right) & -\left(\dot{\bar{X}}_{\dot{w}}s + \dot{\bar{X}}_w\right) & -\left(\left(\dot{\bar{X}}_q - mW_e\right)s - mg \cos \theta_e\right) \\ -\dot{\bar{Z}}_u & -\left(\left(\dot{\bar{Z}}_{\dot{w}} - m\right)s + \dot{\bar{Z}}_w\right) & -\left(\left(\dot{\bar{Z}}_q + mU_e\right)s - mg \sin \theta_e\right) \\ -\dot{\bar{M}}_u & -\left(\dot{\bar{M}}_{\dot{w}}s + \dot{\bar{M}}_w\right) & \left(I_y s^2 - \dot{\bar{M}}_q s\right) \end{bmatrix} \begin{bmatrix} \frac{u(s)}{\eta(s)} \\ \frac{w(s)}{\eta(s)} \\ \frac{\theta(s)}{\eta(s)} \end{bmatrix} = \begin{bmatrix} \dot{\bar{X}}_\eta \\ \dot{\bar{Z}}_\eta \\ \dot{\bar{M}}_\eta \end{bmatrix} \quad (5.10)$$

Equation (5.10) is of the same form as equation (5.1). Cramer's rule may be applied directly, and the elevator response transfer functions are given by

$$\frac{u(s)}{\eta(s)} \equiv \frac{N_\eta^u(s)}{\Delta(s)} \quad \frac{w(s)}{\eta(s)} \equiv \frac{N_\eta^w(s)}{\Delta(s)} \quad \frac{\theta(s)}{\eta(s)} \equiv \frac{N_\eta^\theta(s)}{\Delta(s)} \quad (5.11)$$

Since the Laplace transform of equation (5.7) is $s\theta(s) = q(s)$, the pitch rate response transfer function follows directly:

$$\frac{q(s)}{\eta(s)} \equiv \frac{N_\eta^q(s)}{\Delta(s)} = \frac{sN_\eta^\theta(s)}{\Delta(s)} \quad (5.12)$$

The numerator polynomials are given by the following determinants:

$$N_\eta^u(s) = \begin{vmatrix} \dot{\bar{X}}_\eta & -\left(\dot{\bar{X}}_{\dot{w}}s + \dot{\bar{X}}_w\right) & -\left(\left(\dot{\bar{X}}_q - mW_e\right)s - mg \cos \theta_e\right) \\ \dot{\bar{Z}}_\eta & -\left(\left(\dot{\bar{Z}}_{\dot{w}} - m\right)s + \dot{\bar{Z}}_w\right) & -\left(\left(\dot{\bar{Z}}_q + mU_e\right)s - mg \sin \theta_e\right) \\ \dot{\bar{M}}_\eta & -\left(\dot{\bar{M}}_{\dot{w}}s + \dot{\bar{M}}_w\right) & \left(I_y s^2 - \dot{\bar{M}}_q s\right) \end{vmatrix} \quad (5.13)$$

$$N_\eta^w(s) = \begin{vmatrix} \left(ms - \dot{\bar{X}}_u\right) & \dot{\bar{X}}_\eta & -\left(\left(\dot{\bar{X}}_q - mW_e\right)s - mg \cos \theta_e\right) \\ -\dot{\bar{Z}}_u & \dot{\bar{Z}}_\eta & -\left(\left(\dot{\bar{Z}}_q + mU_e\right)s - mg \sin \theta_e\right) \\ -\dot{\bar{M}}_u & \dot{\bar{M}}_\eta & \left(I_y s^2 - \dot{\bar{M}}_q s\right) \end{vmatrix} \quad (5.14)$$

$$N_\eta^\theta(s) = \begin{vmatrix} \left(ms - \dot{\bar{X}}_u\right) & -\left(\dot{\bar{X}}_{\dot{w}}s + \dot{\bar{X}}_w\right) & \dot{\bar{X}}_\eta \\ -\dot{\bar{Z}}_u & -\left(\left(\dot{\bar{Z}}_{\dot{w}} - m\right)s + \dot{\bar{Z}}_w\right) & \dot{\bar{Z}}_\eta \\ -\dot{\bar{M}}_u & -\left(\dot{\bar{M}}_{\dot{w}}s + \dot{\bar{M}}_w\right) & \dot{\bar{M}}_\eta \end{vmatrix} \quad (5.15)$$

and the common denominator polynomial is given by the determinant

$$\Delta(s) = \begin{vmatrix} \left(ms - \dot{\bar{X}}_u\right) & -\left(\dot{\bar{X}}_{\dot{w}}s + \dot{\bar{X}}_w\right) & -\left(\left(\dot{\bar{X}}_q - mW_e\right)s - mg \cos \theta_e\right) \\ -\dot{\bar{Z}}_u & -\left(\left(\dot{\bar{Z}}_{\dot{w}} - m\right)s + \dot{\bar{Z}}_w\right) & -\left(\left(\dot{\bar{Z}}_q + mU_e\right)s - mg \sin \theta_e\right) \\ -\dot{\bar{M}}_u & -\left(\dot{\bar{M}}_{\dot{w}}s + \dot{\bar{M}}_w\right) & \left(I_y s^2 - \dot{\bar{M}}_q s\right) \end{vmatrix} \quad (5.16)$$

The thrust response transfer functions may be derived by assuming the elevator to be fixed at its trim value; thus $\eta(s) = 0$, and $\tau(s)$ is written in place of $\eta(s)$. Then the derivatives \dot{X}_η , \dot{Z}_η , and \dot{M}_η in [equations \(5.13\), \(5.14\), and \(5.15\)](#) are replaced by \dot{X}_τ , \dot{Z}_τ , and \dot{M}_τ , respectively. Since the polynomial expressions given by the determinants are substantial, they are set out in full in Appendix 3.

5.3.2 The lateral-directional response transfer functions

The lateral-directional response transfer functions may be obtained by exactly the same means as the longitudinal transfer functions. The Laplace transform, assuming zero initial conditions, of the lateral-directional equations of motion referred to body axes, [equation \(4.45\)](#), may be written in matrix form as follows:

$$\begin{bmatrix} \left(ms - \dot{Y}_v\right) & -\left(\left(\dot{Y}_p + mW_e\right)s + mg \cos \theta_e\right) & -\left(\left(\dot{Y}_r - mU_e\right)s + mg \sin \theta_e\right) \\ -\dot{L}_v & \left(I_x s^2 - \dot{L}_p s\right) & -\left(I_{xz} s^2 + \dot{L}_r s\right) \\ -\dot{N}_v & -\left(I_{xz} s^2 + \dot{N}_p s\right) & \left(I_z s^2 - \dot{N}_r s\right) \end{bmatrix} \begin{bmatrix} v(s) \\ \phi(s) \\ \psi(s) \end{bmatrix} = \begin{bmatrix} \dot{Y}_\xi & \dot{Y}_\zeta \\ \dot{L}_\xi & \dot{L}_\zeta \\ \dot{N}_\xi & \dot{N}_\zeta \end{bmatrix} \begin{bmatrix} \xi(s) \\ \zeta(s) \end{bmatrix} \quad (5.17)$$

where $s\phi(s) = p(s)$ and $s\psi(s) = r(s)$. By holding the rudder at its trim setting, $\zeta(s) = 0$, the aileron response transfer functions may be obtained by applying Cramer's rule to [equation \(5.17\)](#). Similarly, by holding the ailerons at the trim setting, $\xi(s) = 0$, the rudder response transfer functions may be obtained. For example, roll rate response to aileron is given by

$$\frac{N_\xi^p(s)}{\Delta(s)} \equiv \frac{p(s)}{\xi(s)} = \frac{s\phi(s)}{\xi(s)} \equiv \frac{sN_\xi^\phi(s)}{\Delta(s)} \quad (5.18)$$

where the numerator polynomial is given by

$$N_\xi^p(s) = s \begin{vmatrix} \left(ms - \dot{Y}_v\right) & \dot{Y}_\xi & -\left(\left(\dot{Y}_r - mU_e\right)s + mg \sin \theta_e\right) \\ -\dot{L}_v & \dot{L}_\xi & -\left(I_{xz} s^2 + \dot{L}_r s\right) \\ -\dot{N}_v & \dot{N}_\xi & \left(I_z s^2 - \dot{N}_r s\right) \end{vmatrix} \quad (5.19)$$

and the denominator polynomial is given by

$$\Delta(s) = \begin{vmatrix} \left(ms - \dot{Y}_v\right) & -\left(\left(\dot{Y}_p + mW_e\right)s + mg \cos \theta_e\right) & -\left(\left(\dot{Y}_r - mU_e\right)s + mg \sin \theta_e\right) \\ -\dot{L}_v & \left(I_x s^2 - \dot{L}_p s\right) & -\left(I_{xz} s^2 + \dot{L}_r s\right) \\ -\dot{N}_v & -\left(I_{xz} s^2 + \dot{N}_p s\right) & \left(I_z s^2 - \dot{N}_r s\right) \end{vmatrix} \quad (5.20)$$

Again, since the polynomial expressions given by the determinants are substantial, they are also set out in full in Appendix 3.

EXAMPLE 5.2

We wish to obtain the transfer function describing pitch attitude response to elevator for the Lockheed F-104 Starfighter. The data were obtained from Teper (1969) and describe a sea-level flight condition. Inspection of the data revealed that $\theta_e = 0$; thus it was concluded that the equations of motion to which the data relate are referred to wind axes.

Air density ρ	= 0.00238 slug/ft ³
Axial velocity component U_e	= 305 ft/s
Aircraft mass m	= 746 slugs
Moment of inertia in pitch I_y	= 65000 slug ft ²
Gravitational constant g	= 32.2 ft/s ²

The dimensional aerodynamic stability and control derivatives follow. Derivatives which are not quoted are assumed to be insignificant and are given a zero value; whence

$$\begin{array}{lll} \dot{\bar{X}}_u = -26.26 \text{ slug/s} & \dot{\bar{Z}}_u = -159.64 \text{ slug/s} & \dot{\bar{M}}_u = 0 \\ \dot{\bar{X}}_w = 79.82 \text{ slug/s} & \dot{\bar{Z}}_w = -328.24 \text{ slug/s} & \dot{\bar{M}}_w = -1014.0 \text{ slug ft/s} \\ \dot{\bar{X}}_{\dot{w}} = 0 & \dot{\bar{Z}}_{\dot{w}} = 0 & \dot{\bar{M}}_{\dot{w}} = -36.4 \text{ slug ft} \\ \dot{\bar{X}}_q = 0 & \dot{\bar{Z}}_q = 0 & \dot{\bar{M}}_q = -18,135 \text{ slug ft}^2/\text{s} \\ \dot{\bar{X}}_\eta = 0 & \dot{\bar{Z}}_\eta = -16,502 \text{ slug ft/s}^2/\text{rad} & \dot{\bar{M}}_\eta = -303,575 \text{ slug ft/s}^2/\text{rad} \end{array}$$

The American imperial units are retained in this example since it is preferable to work with the equations of motion in the dimensional units appropriate to the source material. Conversion from one system of units to another often leads to confusion and error and is therefore not recommended. However, for information, factors for conversion from American imperial units to SI units are given in Appendix 4.

These numerical values are substituted into equation (5.10) to obtain

$$\begin{bmatrix} 746s + 26.26 & -79.82 & 24021.2 \\ 159.64 & 746s + 328.24 & -227530s \\ 0 & 36.4s + 1014 & 65000s^2 + 18135s \end{bmatrix} \begin{bmatrix} u(s) \\ w(s) \\ \theta(s) \end{bmatrix} = \begin{bmatrix} 0 \\ -16502 \\ -303575 \end{bmatrix} \eta(s) \quad (5.21)$$

Cramer's rule may be applied directly to equation (5.21) to obtain the transfer function of interest:

$$\frac{N_\eta^\theta(s)}{\Delta(s)} = \frac{\begin{vmatrix} 746s + 26.26 & -79.82 & 0 \\ 159.64 & 746s + 328.24 & -16502 \\ 0 & 36.4s + 1014 & -303575 \end{vmatrix}}{\begin{vmatrix} 746s + 26.26 & -79.82 & 24021.2 \\ 159.64 & 746s + 328.24 & -227530s \\ 0 & 36.4s + 1014 & 65000s^2 + 18135s \end{vmatrix}} \text{ rad/rad} \quad (5.22)$$

Whence

$$\frac{N_\eta^\theta(s)}{\Delta(s)} = \frac{-16.850 \times 10^{10}(s^2 + 0.402s + 0.036)}{3.613 \times 10^{10}(s^4 + 0.925s^3 + 4.935s^2 + 0.182s + 0.108)} \text{ rad/rad} \quad (5.23)$$

Or, in the preferable factorised form,

$$\frac{N_\eta^\theta(s)}{\Delta(s)} = \frac{-4.664(s + 0.135)(s + 0.267)}{(s^2 + 0.033s + 0.022)(s^2 + 0.893s + 4.884)} \text{ rad/rad} \quad (5.24)$$

The denominator of [equation \(5.24\)](#) factorises into two pairs of complex roots (*poles*), each of which describes a longitudinal stability mode. The factors describing the modes may be written alternatively $(s^2 + 2\zeta\omega s + \omega^2)$, which is clearly the characteristic polynomial describing damped harmonic motion. The stability of each mode is determined by the damping ratio ζ ; the undamped natural frequency, by ω . The lower-frequency mode is called the *phugoid* and the higher-frequency mode is called the *short-period pitching oscillation*. For the aeroplane to be completely longitudinally stable, the damping ratio of both modes must be positive.

The units of the transfer function given in [equation \(5.24\)](#) are rad/rad or, equivalently deg/deg. Angular measure is usually, and correctly, quantified in radians, and care must be applied when interpreting transfer functions since the radian is a very large angular quantity in the context of aircraft small-perturbation motion. This becomes especially important when dealing with transfer functions in which the input and output variables have different units. For example, the transfer function describing speed response to elevator for the F-104 has units ft/s/rad, and one radian of elevator input is impossibly large! It is therefore very important to remember that one radian is equivalent to 57.3 degrees. It is also important to remember that all transfer functions have units, which should always be indicated if confusion is to be avoided.

The transfer function given by [equation \(5.24\)](#) provides a complete description of the longitudinal stability characteristics and the dynamic pitch response to elevator of the F-104 at the flight condition in question. It is interesting that the transfer function has a negative sign. This means that a positive elevator deflection results in a negative pitch response, which is completely in accordance with the notation defined in Chapter 2. Clearly, the remaining longitudinal response transfer functions can be obtained by applying Cramer's rule to [equation \(5.21\)](#) for each of the remaining motion variables. A comprehensive review of aeroplane dynamics based on transfer function analysis can be found in Chapters 6 and 7.

The complexity of this example is such that, although tedious, the entire computation is easily undertaken manually to produce a result of acceptable accuracy. Alternatively, transfer function (5.23) can be calculated merely by substituting the values of the derivative and other data into the appropriate polynomial expressions given in Appendix 3.

5.4 Response to controls

Time histories for the aircraft response to controls are readily obtained by finding the inverse Laplace transform of the appropriate transfer function expression. For example, the roll rate response to aileron is given by [equation \(5.5\)](#) as

$$p(s) = \frac{N_\xi^p(s)}{\Delta(s)} \xi(s) \quad (5.25)$$

assuming that the aeroplane is initially in trimmed flight. The numerator polynomial $N_\xi^p(s)$ and denominator polynomial $\Delta(s)$ are given in Appendix 3. The aileron input $\xi(s)$ is simply the Laplace transform of the required input function. For example, two commonly used inputs are the *impulse* and *step* functions, where

Impulse of magnitude k is given by $\xi(s) = k$

Step of magnitude k is given by $\xi(s) = k/s$

Other useful input functions include the *ramp*, *pulse* (or step) of finite length, *doublet*, and *sinusoid*. However, the Laplace transform of these functions is not quite so straightforward. Fortunately, most computer programs for handling transfer function problems have the most commonly used functions “built in.”

To continue with the example, the roll rate response to an aileron step input of magnitude k is given by

$$p(t) = L^{-1} \left\{ \frac{k N_\xi^p(s)}{s \Delta(s)} \right\} \quad (5.26)$$

Solution of equation (5.26) to obtain the time response involves finding the inverse Laplace transform of the expression on the right-hand side, which may be accomplished manually with a table of standard transforms. However, this calculation is painlessly achieved with an appropriate computer software package such as MATLAB or Program CC, for example. Even so, it is instructive to review the mathematical procedure since this provides valuable insight into the correct interpretation of a computer solution, and this is most easily achieved by example, as follows.

EXAMPLE 5.3

To obtain the pitch response of the F-104 aircraft to a unit step elevator input at the flight condition evaluated in Example 5.2. Assuming the unit step input to be in degree units, then from equation (5.24),

$$\theta(t) = L^{-1} \left\{ \frac{-4.664(s + 0.135)(s + 0.267)}{s(s^2 + 0.033s + 0.022)(s^2 + 0.893s + 4.884)} \right\} \text{ deg} \quad (5.27)$$

Before the inverse Laplace transform of the expression in parentheses can be found, it is first necessary to reduce it to partial fractions. Thus

$$\frac{-4.664(s^2 + 0.402s + 0.036)}{s(s^2 + 0.033s + 0.022)(s^2 + 0.893s + 4.884)} = -4.664 \left(\begin{array}{l} \frac{A}{s} + \frac{Bs + C}{(s^2 + 0.033s + 0.022)} \\ + \frac{Ds + E}{(s^2 + 0.893s + 4.884)} \end{array} \right) \quad (5.28)$$

To determine the values for A , B , C , D , and E , multiply out the fractions on the right-hand side and equate the numerator coefficients from both sides of the equation for like powers of s to obtain

$$\begin{aligned} 0 &= (A + B + D)s^4 \\ 0 &= (0.925A + 0.893B + C + 0.033D + E)s^3 \\ s^2 &= (4.935A + 4.884B + 0.893C + 0.022D + 0.033E)s^2 \\ 0.402s &= (0.182A + 4.884C + 0.022E)s \\ 0.036 &= 0.108A \end{aligned}$$

These simultaneous linear algebraic equations are easily solved using Cramer's rule if they are first written in matrix form:

$$\begin{bmatrix} 1 & 1 & 0 & 1 & 0 \\ 0.925 & 0.893 & 1 & 0.033 & 1 \\ 4.935 & 4.884 & 0.893 & 0.022 & 0.033 \\ 0.182 & 0 & 4.884 & 0 & 0.022 \\ 0.108 & 0 & 0 & 0 & 0 \end{bmatrix} \begin{bmatrix} A \\ B \\ C \\ D \\ E \end{bmatrix} = \begin{bmatrix} 0 \\ 0 \\ 1 \\ 0.402 \\ 0.036 \end{bmatrix} \quad (5.29)$$

Thus $A = 0.333$, $B = -0.143$, $C = 0.071$, $D = -0.191$, $E = -0.246$ and [equation \(5.27\)](#) may be written as

$$\theta(t) = L^{-1} \left\{ -4.664 \left(\frac{0.333}{s} - \frac{(0.143s - 0.071)}{(s^2 + 0.033s + 0.022)} - \frac{(0.191s + 0.246)}{(s^2 + 0.893s + 4.884)} \right) \right\} \text{deg} \quad (5.30)$$

A very short table of Laplace transforms relevant to this problem is given in Appendix 5. Inspection of the table of transforms determines that [equation \(5.30\)](#) needs some rearrangement before its inverse transform can be found. When solving problems of this type, it is useful to appreciate that the solution contains terms describing damped harmonic motion; the required form of the terms in [equation \(5.30\)](#) is thus more easily established. With reference to Appendix 5, transform pairs 1, 5, and 6 appear to be most applicable. Therefore, rearranging [equation \(5.30\)](#) to suit,

$$\theta(t) = L^{-1} \left\{ -4.664 \left(\frac{0.333}{s} - \left(\frac{0.143(s + 0.017)}{(s + 0.017)^2 + 0.148^2} - \frac{0.496(0.148)}{(s + 0.017)^2 + 0.148^2} \right) \right) - \left(\frac{0.191(s + 0.447)}{(s + 0.447)^2 + 2.164^2} + \frac{0.074(2.164)}{(s + 0.447)^2 + 2.164^2} \right) \right\} \text{deg} \quad (5.31)$$

Using transform pairs 1, 5, and 6, [equation \(5.31\)](#) may be evaluated to give the time response:

$$\begin{aligned} \theta(t) &= -1.553 + 0.667e^{-0.017t}(\cos 0.148t - 3.469 \sin 0.148t) \\ &\quad + 0.891e^{-0.447t}(\cos 2.164t + 0.389 \sin 2.164t) \text{ deg} \end{aligned} \quad (5.32)$$

The solution given by [equation \(5.32\)](#) comprises three terms which may be interpreted as follows:

The first term, -1.553 deg, is the constant steady-state pitch attitude (gain) of the aeroplane. The second term describes the contribution made by the phugoid dynamics, the undamped natural frequency $\omega_p = 0.148$ rad/s, and since $\zeta_p \omega_p = 0.017$ rad/s, the damping ratio is $\zeta_p = 0.115$.

The third term describes the contribution made by the short-period pitching oscillation dynamics, the undamped natural frequency $\omega_s = 2.164$ rad/s, and since $\zeta_s \omega_s = 0.447$ rad/s, the damping ratio is $\zeta_s = 0.207$.

The time response described by [equation \(5.32\)](#) is shown in [Fig. 5.2](#), in which the two dynamic modes are clearly visible. It is also clear that the pitch attitude eventually settles to the steady-state value predicted previously.

Example 5.3 illustrates that it is not necessary to have a complete time response solution merely to obtain the characteristics of the dynamic modes. The principal mode characteristics, damping ratio and natural frequency, are directly obtainable on inspection of the characteristic polynomial $\Delta(s)$ in any aircraft transfer function. The steady-state gain is also readily established by application of the *final value theorem*, which states that

$$f(t)_{t \rightarrow \infty} = \lim_{s \rightarrow 0} (sf(s)) \quad (5.33)$$

The corresponding *initial value theorem*, also a valuable tool, states that

$$f(t)_{t \rightarrow 0} = \lim_{s \rightarrow \infty} (sf(s)) \quad (5.34)$$

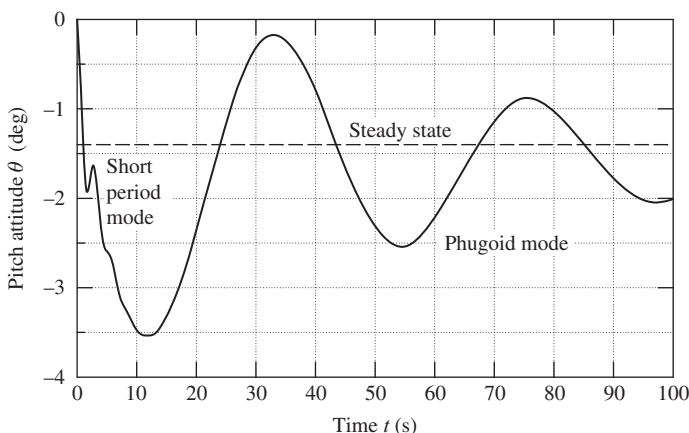


FIGURE 5.2 F-104 pitch attitude response to a 1° step of elevator.

A complete discussion of these theorems may be found in most books on control theory—for example, [Shinners \(1980\)](#).

EXAMPLE 5.4

Applying the initial value and final value theorems to find the initial and steady values of the pitch attitude response of the F-104 of the previous examples. From [equation \(5.27\)](#), the Laplace transform of the unit step response is given by

$$\theta(s) = \frac{-4.664(s + 0.135)(s + 0.267)}{s(s^2 + 0.033s + 0.022)(s^2 + 0.893s + 4.884)} \text{ deg} \quad (5.35)$$

Applying the final value theorem, we obtain

$$\theta(t)_{t \rightarrow \infty} = \lim_{s \rightarrow 0} \left(\frac{-4.664(s + 0.135)(s + 0.267)}{(s^2 + 0.033s + 0.022)(s^2 + 0.893s + 4.884)} \right) \text{ deg} = -1.565 \text{ deg} \quad (5.36)$$

and applying the initial value theorem, we obtain

$$\theta(t)_{t \rightarrow 0} = \lim_{s \rightarrow \infty} \left(\frac{-4.664(s + 0.135)(s + 0.267)}{(s^2 + 0.033s + 0.022)(s^2 + 0.893s + 4.884)} \right) \text{ deg} = 0 \text{ deg} \quad (5.37)$$

The values given by [equations \(5.36\)](#) and [\(5.37\)](#) clearly correlate reasonably well with the known pitch attitude response calculated in Example 5.3. Bear in mind that, in all calculations, numbers have been rounded to three decimal places for convenience.

5.5 Acceleration response transfer functions

Acceleration response transfer functions are frequently required but are not given directly by the solution of the equations of motion described previously. Expressions for the components of inertial acceleration are given in [equations \(4.9\)](#) and clearly comprise a number of motion variable contributions. Assuming small-perturbation motion such that the usual simplifications can be made, [equations \(4.9\)](#) may be restated as

$$\begin{aligned} a_x &= \dot{u} - rV_e + qW_e - y\dot{r} + z\dot{q} \\ a_y &= \dot{v} - pW_e + rU_e + x\dot{r} - z\dot{p} \\ a_z &= \dot{w} - qU_e + pV_e - x\dot{q} + y\dot{p} \end{aligned} \quad (5.38)$$

If, for example, the normal acceleration response to elevator referred to the *cg* is required ($x = y = z = 0$) and if fully decoupled motion is assumed ($pV_e = 0$), then the equation for normal acceleration simplifies to

$$a_z = \dot{w} - qU_e \quad (5.39)$$

The Laplace transform of [equation \(5.39\)](#), assuming zero initial conditions, may be written as

$$a_z(s) = sw(s) - s\theta(s)U_e \quad (5.40)$$

Or, expressing equation (5.40) in terms of elevator response transfer functions,

$$a_z(s) = s \frac{N_\eta^w(s)}{\Delta(s)} \eta(s) - s U_e \frac{N_\eta^\theta(s)}{\Delta(s)} \eta(s) = \frac{s(N_\eta^w(s) - U_e N_\eta^\theta(s))\eta(s)}{\Delta(s)} \quad (5.41)$$

Thus the required normal acceleration response transfer function may be written as

$$\frac{N_\eta^{a_z}(s)}{\Delta(s)} \equiv \frac{a_z(s)}{\eta(s)} = \frac{s(N_\eta^w(s) - U_e N_\eta^\theta(s))}{\Delta(s)} \quad (5.42)$$

Transfer functions for the remaining acceleration response components may be derived in a similar manner.

Another useful transfer function which is often required in handling qualities studies gives the normal acceleration response to elevator measured at the pilot's seat. In this special case, x in equations (5.38) represents the distance measured from the *cg* to the pilot's seat; the normal acceleration is therefore given by

$$a_z = \dot{w} - q U_e - x \dot{q} \quad (5.43)$$

As before, the transfer function is easily derived:

$$\left. \frac{N_\eta^{a_z}(s)}{\Delta(s)} \right|_{\text{pilot}} = \frac{s(N_\eta^w(s) - (U_e + xs)N_\eta^\theta(s))}{\Delta(s)} \quad (5.44)$$

EXAMPLE 5.5

To calculate the normal acceleration response to elevator at the *cg* for the F-104 Starfighter at the flight condition defined in Example 5.2. At this flight condition the steady axial velocity component $U_e = 305$ ft/s and the pitch attitude and normal velocity transfer functions describing response to elevator are given by

$$\frac{N_\eta^\theta(s)}{\Delta(s)} = \frac{-4.664(s + 0.135)(s + 0.267)}{(s^2 + 0.033s + 0.022)(s^2 + 0.893s + 4.884)} \text{ rad/rad} \quad (5.45)$$

and

$$\frac{N_\eta^w(s)}{\Delta(s)} = \frac{-22.147(s^2 + 0.035s + 0.022)(s + 64.675)}{(s^2 + 0.033s + 0.022)(s^2 + 0.893s + 4.884)} \text{ ft/s/rad} \quad (5.46)$$

Substitute equations (5.45) and (5.46) together with U_e into equation (5.42), paying particular attention to the units, and multiply out the numerator and factorise the result to obtain the required transfer function:

$$\frac{N_\eta^{a_z}(s)}{\Delta(s)} = \frac{-22.147s(s + 0.037)(s - 4.673)(s + 5.081)}{(s^2 + 0.033s + 0.022)(s^2 + 0.893s + 4.884)} \text{ ft/s}^2/\text{rad} \quad (5.47)$$

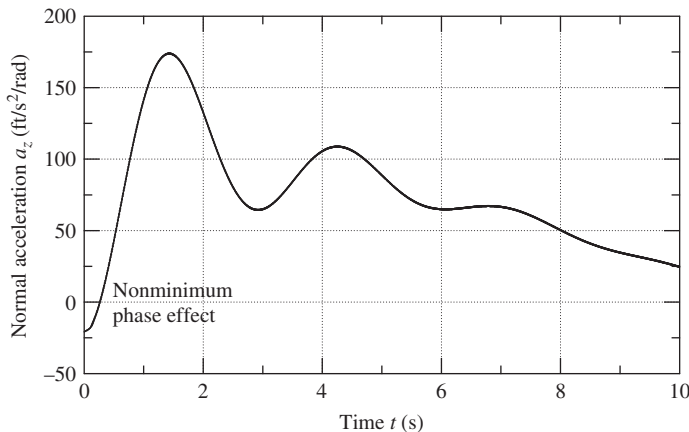


FIGURE 5.3 Normal acceleration response at the *cg* to an elevator unit step input.

Note that, since the numerator and denominator are of the same order, the acceleration transfer function from equation (5.47) is *improper*. The positive numerator root, or *zero*, implies that the transfer function is *nonminimum phase*, which is typical of aircraft acceleration transfer functions. The nonminimum phase effect is illustrated in the unit (1 rad) step response time history shown in Fig. 5.3 and causes the initial response to be in the wrong sense. Only the first few seconds of the response are shown and, as may be determined by application of the final value theorem, the steady-state acceleration is zero.

5.6 The state-space method

The use of the state-space method greatly facilitates solution of the small-perturbation equations of motion. Since the computational mechanism is based on the use of matrix algebra, it is most conveniently handled by a digital computer and, as already indicated, many suitable software packages are available. Most commercial software is intended for problems in modern control, so some care is needed to ensure that the aircraft equations of motion are correctly assembled before a solution is computed using these tools. However, the available tools are generally very powerful, and their use for the solution of the equations of motion of aircraft is particularly simple.

5.6.1 The transfer function matrix

The general state equations, (4.60) and (4.61), describing a linear dynamic system may be written as

$$\begin{aligned}\dot{\mathbf{x}}(t) &= \mathbf{A}\mathbf{x}(t) + \mathbf{B}\mathbf{u}(t) \\ \mathbf{y}(t) &= \mathbf{C}\mathbf{x}(t) + \mathbf{D}\mathbf{u}(t)\end{aligned}\tag{5.48}$$

The assembly of the equations of motion in this form, for the particular application to aircraft, was explained in Section 4.4.2. Since \mathbf{A} , \mathbf{B} , \mathbf{C} , and \mathbf{D} are matrices of constant coefficients, the Laplace transform of [equations \(5.48\)](#), assuming zero initial conditions, is

$$\begin{aligned}s\mathbf{x}(s) &= \mathbf{Ax}(s) + \mathbf{Bu}(s) \\ \mathbf{y}(s) &= \mathbf{Cx}(s) + \mathbf{Du}(s)\end{aligned}\quad (5.49)$$

The state equation may be rearranged and written as

$$\mathbf{x}(s) = (s\mathbf{I} - \mathbf{A})^{-1} \mathbf{Bu}(s) \quad (5.50)$$

where \mathbf{I} is the identity matrix and is the same order as \mathbf{A} . Thus, eliminating $\mathbf{x}(s)$, the state vector, by combining the output equation and [equation \(5.50\)](#), the output vector $\mathbf{y}(s)$ is given by

$$\mathbf{y}(s) = [\mathbf{C}(s\mathbf{I} - \mathbf{A})^{-1} \mathbf{B} + \mathbf{D}] \mathbf{u}(s) = \mathbf{G}(s) \mathbf{u}(s) \quad (5.51)$$

where $\mathbf{G}(s)$ is called the *transfer function matrix*. In general, the transfer function matrix has the form

$$\mathbf{G}(s) = \frac{1}{\Delta(s)} \mathbf{N}(s) \quad (5.52)$$

and $\mathbf{N}(s)$ is a polynomial matrix whose elements are all of the response transfer function numerators. The denominator $\Delta(s)$ is the characteristic polynomial and is common to all transfer functions. Thus the application of the state-space method to the solution of the equations of motion enables all response transfer functions to be obtained in a single computation.

Now, as explained in Section 4.4.2, when dealing with the solution of the equations of motion it is usually required that $\mathbf{y}(s) = \mathbf{x}(s)$, that is, the output vector and state vector are chosen to be the same. In this case [equation \(5.51\)](#) may be simplified since $\mathbf{C} = \mathbf{I}$ and $\mathbf{D} = 0$; therefore,

$$\mathbf{G}(s) = (s\mathbf{I} - \mathbf{A})^{-1} \mathbf{B} = \frac{\text{Adj}(s\mathbf{I} - \mathbf{A}) \mathbf{B}}{|s\mathbf{I} - \mathbf{A}|} \quad (5.53)$$

and [equation \(5.53\)](#) is equivalent to the multivariable application of Cramer's rule as discussed in Section 5.3.

Comparing [equation \(5.53\)](#) with [equation \(5.52\)](#), it is evident that the polynomial numerator matrix is given by

$$\mathbf{N}(s) = \text{Adj}(s\mathbf{I} - \mathbf{A}) \mathbf{B}$$

and the characteristic polynomial is given by

$$\Delta(s) = |s\mathbf{I} - \mathbf{A}|$$

5.6.2 The longitudinal transfer function matrix

The concise longitudinal state equations were given by equations (4.67) and (4.68). Substituting for \mathbf{A} , \mathbf{B} , and \mathbf{I} in equation (5.53), the longitudinal transfer function matrix is thus given by

$$\mathbf{G}(s) = \begin{bmatrix} s-x_u & -x_w & -x_q & -x_\theta \\ -z_u & s-z_w & -z_q & -z_\theta \\ -m_u & -m_w & s-m_q & -m_\theta \\ 0 & 0 & -1 & s \end{bmatrix}^{-1} \begin{bmatrix} x_\eta & x_\tau \\ z_\eta & z_\tau \\ m_\eta & m_\tau \\ 0 & 0 \end{bmatrix} \quad (5.54)$$

Algebraic manipulation of equation (5.54) leads to

$$\mathbf{G}(s) = \frac{1}{\Delta(s)} \begin{bmatrix} N_\eta^u(s) & N_\tau^u(s) \\ N_\eta^w(s) & N_\tau^w(s) \\ N_\eta^q(s) & N_\tau^q(s) \\ N_\eta^\theta(s) & N_\tau^\theta(s) \end{bmatrix} \quad (5.55)$$

In this case the numerator and denominator polynomials are expressed in terms of the concise derivatives. A complete listing of the longitudinal algebraic transfer functions in this form is given in Appendix 3.

5.6.3 The lateral-directional transfer function matrix

The lateral-directional state equation is given in terms of normalised derivatives by equation (4.69). Thus substituting for \mathbf{A} , \mathbf{B} , and \mathbf{I} in equation (5.53), the lateral transfer function matrix is given by

$$\mathbf{G}(s) = \begin{bmatrix} s-y_v & -y_p & -y_r & -y_\phi & -y_\psi \\ -l_v & s-l_p & -l_r & -l_\phi & -l_\psi \\ -n_v & -n_p & s-n_r & -n_\phi & -n_\psi \\ 0 & -1 & 0 & s & 0 \\ 0 & 0 & -1 & 0 & s \end{bmatrix}^{-1} \begin{bmatrix} y_\xi & y_\zeta \\ l_\xi & l_\zeta \\ n_\xi & n_\zeta \\ 0 & 0 \\ 0 & 0 \end{bmatrix} \quad (5.56)$$

As for the longitudinal solution, the lateral-directional transfer function matrix may be written as

$$\mathbf{G}(s) = \frac{1}{\Delta(s)} \begin{bmatrix} N_\xi^v(s) & N_\zeta^v(s) \\ N_\xi^p(s) & N_\zeta^p(s) \\ N_\xi^r(s) & N_\zeta^r(s) \\ N_\xi^\phi(s) & N_\zeta^\phi(s) \\ N_\xi^\psi(s) & N_\zeta^\psi(s) \end{bmatrix} \quad (5.57)$$

Again, the numerator and denominator polynomials are expressed in terms of the concise derivatives. A complete listing of the lateral algebraic transfer functions in this form is given in Appendix 3.

EXAMPLE 5.6

This example illustrates the use of the state space method for obtaining the lateral-directional transfer function matrix. Data for the Lockheed C-5A were obtained from [Heffley and Jewell \(1972\)](#). The data relate to a flight condition at an altitude of 20,000 ft and a Mach number of 0.6, and are referred to aircraft body axes. Although the data are given in American imperial units, they are converted to SI units simply for illustration. The normalised derivatives were derived from the data, great care being exercised to ensure the correct units. The derivatives are listed here, and, as in previous examples, missing derivatives are assumed to be insignificant and made equal to zero.

$$\begin{aligned} y_v &= -0.1060 \text{ 1/s} & l_v &= -0.0070 \text{ 1/m/s} & n_v &= 0.0023 \text{ 1/m/s} \\ y_p &= 0 & l_p &= -0.9880 \text{ 1/s} & n_p &= -0.0921 \text{ 1/s} \\ y_r &= -189.586 \text{ m/s} & l_r &= 0.2820 \text{ 1/s} & n_r &= -0.2030 \text{ 1/s} \\ y_\phi &= 9.8073 \text{ m/s}^2 & l_\phi &= 0 & n_\phi &= 0 \\ y_\psi &= 0.3768 \text{ m/s}^2 & l_\psi &= 0 & n_\psi &= 0 \\ y_\xi &= -0.0178 \text{ m/s}^2 & l_\xi &= 0.4340 \text{ 1/s}^2 & n_\xi &= 0.0343 \text{ 1/s}^2 \\ y_\zeta &= 3.3936 \text{ m/s}^2 & l_\zeta &= 0.1870 \text{ 1/s}^2 & n_\zeta &= -0.5220 \text{ 1/s}^2 \end{aligned}$$

The lateral-directional state equation is obtained by substituting the derivative values into equation (4.69):

$$\begin{bmatrix} \dot{v} \\ \dot{p} \\ \dot{r} \\ \dot{\phi} \\ \dot{\psi} \end{bmatrix} = \begin{bmatrix} -0.106 & 0 & -189.586 & 9.8073 & 0.3768 \\ -0.007 & -0.988 & 0.282 & 0 & 0 \\ 0.0023 & -0.0921 & -0.203 & 0 & 0 \\ 0 & 1 & 0 & 0 & 0 \\ 0 & 0 & 1 & 0 & 0 \end{bmatrix} \begin{bmatrix} v \\ p \\ r \\ \phi \\ \psi \end{bmatrix} + \begin{bmatrix} -0.0178 & 3.3936 \\ 0.434 & 0.187 \\ 0.0343 & -0.522 \\ 0 & 0 \\ 0 & 0 \end{bmatrix} \begin{bmatrix} \xi \\ \zeta \end{bmatrix} \quad (5.58)$$

The output equation, written out in full, is

$$\begin{bmatrix} v \\ p \\ r \\ \phi \\ \psi \end{bmatrix} = \begin{bmatrix} 1 & 0 & 0 & 0 & 0 \\ 0 & 1 & 0 & 0 & 0 \\ 0 & 0 & 1 & 0 & 0 \\ 0 & 0 & 0 & 1 & 0 \\ 0 & 0 & 0 & 0 & 1 \end{bmatrix} \begin{bmatrix} v \\ p \\ r \\ \phi \\ \psi \end{bmatrix} + \begin{bmatrix} 0 & 0 \\ 0 & 0 \\ 0 & 0 \\ 0 & 0 \\ 0 & 0 \end{bmatrix} \begin{bmatrix} \xi \\ \zeta \end{bmatrix} \quad (5.59)$$

The transfer function matrix was calculated using Program CC. The matrices **A**, **B**, **C**, and **D** are input to the program, and the command for finding the transfer function matrix is invoked. A printout of the result produces the following:

$$\mathbf{G}(s) = \frac{1}{\Delta(s)} \mathbf{N}(s) \quad (5.60)$$

where equation (5.60) is the shorthand version of equation (5.57) and

$$\mathbf{N}(s) = \begin{bmatrix} -0.018s(s+0.15)(s-0.98)(s+367.35) & 3.394s(s-0.012)(s+1.05)(s+2.31) \\ 0.434s(s-0.002)(s^2+0.33s+0.57) & 0.187s(s-0.002)(s+1.55)(s-2.16) \\ 0.343s(s+0.69)(s^2-0.77s+0.51) & -0.522s(s+1.08)(s^2+0.031s+0.056) \\ 0.434(s-0.002)(s^2+0.33s+0.57) & 0.187(s-0.002)(s+1.55)(s-2.16) \\ 0.343(s+0.69)(s^2-0.77s+0.51) & -0.522(s+1.08)(s^2+0.031s+0.056) \end{bmatrix} \quad (5.61)$$

The common denominator, the lateral characteristic polynomial, is given by

$$\Delta(s) = s(s+0.01)(s+1.11)(s^2+0.18s+0.58) \quad (5.62)$$

The lateral-directional characteristic polynomial factorises into three real roots and a complex pair of roots. Its roots, or poles, provide a complete description of the lateral-directional stability characteristics of the aeroplane. The zero root indicates *neutral stability* in yaw, the first non-zero real root describes the *spiral mode*, the second real root describes the *roll subsidence mode*, and the complex pair of roots describe the *oscillatory dutch roll mode*.

It is very important to remember the units of the transfer functions comprising the transfer function matrix, which are

$$\text{units of } \mathbf{G}(s) = \frac{1}{\Delta(s)} \begin{bmatrix} N_\xi^v(s) & N_\zeta^v(s) \\ N_\xi^p(s) & N_\zeta^p(s) \\ N_\xi^r(s) & N_\zeta^r(s) \\ N_\xi^\phi(s) & N_\zeta^\phi(s) \\ N_\xi^\psi(s) & N_\zeta^\psi(s) \end{bmatrix} = \begin{bmatrix} \text{m/s/rad} & \text{m/s/rad} \\ \text{rad/s/rad} & \text{rad/s/rad} \\ \text{rad/s/rad} & \text{rad/s/rad} \\ \text{rad/rad} & \text{rad/rad} \\ \text{rad/rad} & \text{rad/rad} \end{bmatrix} \quad (5.63)$$

Thus the transfer functions of interest can be obtained from inspection of equation (5.61) together with equation (5.62). For example, the transfer function describing sideslip velocity response to rudder is given by

$$\frac{v(s)}{\zeta(s)} = \frac{N_\zeta^v(s)}{\Delta(s)} = \frac{3.394(s-0.012)(s+1.05)(s+29.31)}{(s+0.01)(s+1.11)(s^2+0.18s+0.58)} \text{ m/s/rad} \quad (5.64)$$

Comparison of these results with those of the original source material in Heffley and Jewell (1972) reveals a number of small numerical discrepancies. These are due in part to the numerical rounding employed to keep this illustration to a reasonable size and in part to the differences in the computational algorithms used to obtain the solutions. However, in both cases the accuracy is adequate for most practical purposes.

It is worth noting that many matrix inversion algorithms introduce numerical errors which accumulate rapidly with increasing matrix order, and it is possible to obtain seriously inaccurate results with some poorly conditioned matrices. The typical aircraft state matrix has a tendency to fall into this category, so it is advisable to check the result of a transfer function matrix computation for reasonableness when accuracy is in doubt. This may be done, for example, by making a test

calculation using the expressions given in Appendix 3. For this reason, Program CC includes two algorithms for calculating the transfer function matrix. In Example 5.6 it was found that the *Generalised Eigenvalue Problem* algorithm gave obviously incorrect values for some transfer function numerators, whereas the *Faddeeva* algorithm gave the entirely correct solution. Thus when using computer tools for handling aircraft stability and control problems, it is advisable to input the aircraft derivative and other data at the accuracy given.

5.6.4 Response in terms of state description

The main reasons for the use of state-space modelling tools are the extreme power and convenience of machine solution of the equations of motion and the fact that the solution is obtained in a form which readily lends itself to further analysis in the context of flight control. The solution process is usually completely hidden from the investigator. However, it is important to be aware of the mathematical procedures implemented in the software algorithms for the reasons mentioned previously. A description of the methods of solution of the state equations describing a general system may be found in many books on modern control or system theory. For example, descriptions may be found in Barnett (1975), Shinnars (1980), and Owens (1981). The following description is a summary of the solution of the aircraft state equations and includes only those aspects of the process which are most relevant to the aircraft application. For a more comprehensive review, the reader should consult the references.

The Laplace transform of the state [equations \(5.49\)](#) may be restated for the general case in which non-zero initial conditions are assumed:

$$\begin{aligned} s\mathbf{x}(s) - \mathbf{x}(0) &= \mathbf{Ax}(s) + \mathbf{Bu}(s) \\ \mathbf{y}(s) &= \mathbf{Cx}(s) + \mathbf{Du}(s) \end{aligned} \quad (5.65)$$

Thus the state equation may be written as

$$\mathbf{x}(s) = [s\mathbf{I} - \mathbf{A}]^{-1}\mathbf{x}(0) + [s\mathbf{I} - \mathbf{A}]^{-1}\mathbf{Bu}(s) \quad (5.66)$$

or

$$\mathbf{x}(s) = \Phi(s)\mathbf{x}(0) + \Phi(s)\mathbf{Bu}(s) \quad (5.67)$$

where $\Phi(s)$ is called the *resolvent* of \mathbf{A} . The most general expression for the state vector $\mathbf{x}(t)$ is determined by finding the inverse Laplace transform of [equation \(5.67\)](#), which is written as

$$\mathbf{x}(t) = \Phi(t - t_0)\mathbf{x}(t_0) + \int_{t_0}^t \Phi(t - \tau)\mathbf{Bu}(\tau)d\tau \quad (5.68)$$

The *state transition matrix* $\Phi(t - t_0)$ is defined as

$$\Phi(t - t_0) = \mathcal{L}^{-1}\{[s\mathbf{I} - \mathbf{A}]^{-1}\} = e^{\mathbf{A}(t-t_0)} \quad (5.69)$$

It is equivalent to the *matrix exponential* and describes the transition in the state response $x(t)$ from time t_0 to time t . The state transition matrix has the following special properties:

$$\Phi(0) = e^{\mathbf{At}=0} = \mathbf{I}$$

$$\begin{aligned}
 \Phi(\infty) &= \underset{t=\infty}{e^{\mathbf{A}t}} = \mathbf{0} \\
 \Phi(t + \tau) &= \Phi(t)\Phi(\tau) = e^{\mathbf{A}t}e^{\mathbf{A}\tau} \\
 \Phi(t_2 - t_0) &= \Phi(t_2 - t_1)\Phi(t_1 - t_0) = e^{\mathbf{A}(t_2-t_1)}e^{\mathbf{A}(t_1-t_0)} \\
 \Phi^{-1}(t) &= \Phi(-t) = e^{-\mathbf{A}t}
 \end{aligned} \tag{5.70}$$

The integral term in [equation \(5.68\)](#) is a *convolution integral* whose properties are well known and discussed in most texts on linear systems theory. A very accessible explanation of the role of the convolution integral in determining system response may be found in [Auslander et al. \(1974\)](#).

For aircraft applications it is usual to measure time from $t_0 = 0$, so [equation \(5.68\)](#) may be written as

$$\begin{aligned}
 \mathbf{x}(t) &= \Phi(t)\mathbf{x}(0) + \int_0^t \Phi(t-\tau)\mathbf{B}\mathbf{u}(\tau)d\tau \\
 &= e^{\mathbf{A}t}\mathbf{x}(0) + \int_0^t e^{\mathbf{A}(t-\tau)}\mathbf{B}\mathbf{u}(\tau)d\tau
 \end{aligned} \tag{5.71}$$

The output response vector $\mathbf{y}(t)$ is determined by substituting the state vector $\mathbf{x}(t)$, obtained from [equation \(5.71\)](#), into the output equation:

$$\begin{aligned}
 \mathbf{y}(t) &= \mathbf{C}\mathbf{x}(t) + \mathbf{D}\mathbf{u}(t) \\
 &= \mathbf{C}e^{\mathbf{A}t}\mathbf{x}(0) + \mathbf{C} \int_0^t e^{\mathbf{A}(t-\tau)}\mathbf{B}\mathbf{u}(\tau)d\tau + \mathbf{D}\mathbf{u}(t)
 \end{aligned} \tag{5.72}$$

Analytical solution of the state [equation \(5.71\)](#) is only possible when the form of the input vector $\mathbf{u}(t)$ is known; therefore, further limited progress can be made only for specified applications. Three solutions are of particular interest in aircraft applications: the *unforced* or *homogeneous* response, the *impulse* response, and the *step* response.

Eigenvalues and eigenvectors

The characteristic equation is given by equating the characteristic polynomial to zero:

$$\Delta(s) = |s\mathbf{I} - \mathbf{A}| = 0 \tag{5.73}$$

The roots or *zeros* of this equation, denoted λ_i , are the *eigenvalues* of the state matrix \mathbf{A} . An eigenvalue λ_i and its corresponding non-zero *eigenvector* \mathbf{v}_i are such that

$$\mathbf{A}\mathbf{v}_i = \lambda_i\mathbf{v}_i \tag{5.74}$$

whence

$$[\lambda_i\mathbf{I} - \mathbf{A}]\mathbf{v}_i = 0 \tag{5.75}$$

Since $\mathbf{v}_i \neq 0$, $[\lambda_i\mathbf{I} - \mathbf{A}]$ is singular. The eigenvectors \mathbf{v}_i are always linearly independent provided the eigenvalues λ_i are *distinct*—that is, the characteristic [equation \(5.73\)](#) has no repeated roots. When an eigenvalue is complex its corresponding eigenvector is also complex, and the complex conjugate λ_i^* corresponds with the complex conjugate \mathbf{v}_i^* .

The *eigenvector* or *modal matrix* comprises all of the eigenvectors and is defined as

$$\mathbf{V} = [\mathbf{v}_1 \quad \mathbf{v}_2 \quad \cdots \quad \mathbf{v}_m] \quad (5.76)$$

It follows directly from [equation \(5.74\)](#) that

$$\mathbf{AV} = \mathbf{V} \begin{bmatrix} \lambda_1 & & & \\ & \lambda_2 & & \mathbf{0} \\ & & \ddots & \\ \mathbf{0} & & & \ddots & \\ & & & & \lambda_m \end{bmatrix} \equiv \mathbf{V}\Lambda \quad (5.77)$$

where Λ is the diagonal *eigenvalue matrix*. Thus

$$\mathbf{V}^{-1}\mathbf{AV} = \Lambda \quad (5.78)$$

and \mathbf{A} is said to be *similar* to the diagonal eigenvalue matrix Λ . The mathematical operation on the state matrix \mathbf{A} described by [equation \(5.78\)](#) is referred to as a *similarity transform*. Similar matrices possess the special property that their eigenvalues are the same. When the state equations are transformed into a similar form such that the state matrix \mathbf{A} is replaced by the diagonal eigenvalue matrix Λ , their solution is greatly facilitated. Presented in this way, the state equations are said to be in *modal form*.

Eigenvectors may be determined as follows. By definition,

$$[\lambda_i \mathbf{I} - \mathbf{A}]^{-1} = \frac{\text{Adj}[\lambda_i \mathbf{I} - \mathbf{A}]}{|\lambda_i \mathbf{I} - \mathbf{A}|} \quad (5.79)$$

and since, for any eigenvalue λ_i , $|\lambda_i \mathbf{I} - \mathbf{A}| = \mathbf{0}$, [equation \(5.79\)](#) may be rearranged and written as

$$[\lambda_i \mathbf{I} - \mathbf{A}] \text{Adj}[\lambda_i \mathbf{I} - \mathbf{A}] = |\lambda_i \mathbf{I} - \mathbf{A}| \mathbf{I} = \mathbf{0} \quad (5.80)$$

Comparing [equation \(5.80\)](#) with [equation \(5.75\)](#), the eigenvector \mathbf{v}_i corresponding to the eigenvalue λ_i is defined as

$$\mathbf{v}_i = \text{Adj}[\lambda_i \mathbf{I} - \mathbf{A}] \quad (5.81)$$

Any nonzero column of the adjoint matrix is an eigenvector, and if there is more than one column they differ only by a constant factor. Eigenvectors are therefore unique in direction only, not in magnitude. However, the dynamic characteristics of a system determine the unique relationship between each of its eigenvectors.

The modal equations

Define the transform

$$\mathbf{x}(t) = \mathbf{V}\mathbf{z}(t) \equiv \mathbf{v}_1 z_1(t) + \mathbf{v}_2 z_2(t) + \dots + \mathbf{v}_m z_m(t) = \sum_{i=1}^{i=m} \mathbf{v}_i z_i(t) \quad (5.82)$$

Then the state equations (5.48) may be rewritten in modal form as

$$\begin{aligned}\dot{\mathbf{z}}(t) &= \Lambda\mathbf{z}(t) + \mathbf{V}^{-1}\mathbf{B}\mathbf{u}(t) \\ \mathbf{y}(t) &= \mathbf{C}\mathbf{V}\mathbf{z}(t) + \mathbf{D}\mathbf{u}(t)\end{aligned}\quad (5.83)$$

Unforced response

With reference to equation (5.71), the solution to the state equation in modal form, equation (5.83), is given by

$$\mathbf{z}(t) = e^{\Lambda t}\mathbf{z}(0) + \int_0^t e^{\Lambda(t-\tau)}\mathbf{V}^{-1}\mathbf{B}\mathbf{u}(\tau)d\tau \quad (5.84)$$

The *matrix exponential* $e^{\Lambda t}$ in diagonal form is defined as

$$e^{\Lambda t} = \begin{bmatrix} e^{\lambda_1 t} & & & \\ & e^{\lambda_2 t} & & \mathbf{0} \\ & & \ddots & \\ \mathbf{0} & & & \ddots & e^{\lambda_m t} \end{bmatrix} \quad (5.85)$$

and since it is diagonal, the solution of the transformed state variables $z_i(t)$ given by equation (5.84) are uncoupled, which is the principal advantage of the transform. Thus

$$z_i(t) = e^{\lambda_i t} z_i(0) + \int_0^t e^{\lambda_i(t-\tau)} \mathbf{V}^{-1} \mathbf{B} u_i(\tau) d\tau \quad (5.86)$$

The unforced response is given by equation (5.84) when $\mathbf{u}(t) = 0$; whence

$$\mathbf{z}(t) = e^{\Lambda t}\mathbf{z}(0) \quad (5.87)$$

Or, substituting equation (5.87) into equation (5.82), the unforced state trajectory $\mathbf{x}(t)$ may be derived:

$$\mathbf{x}(t) = \mathbf{V} e^{\Lambda t} \mathbf{z}(0) = \sum_{i=1}^{i=m} \mathbf{v}_i e^{\lambda_i t} z_i(0) = \sum_{i=1}^{i=m} \mathbf{v}_i e^{\lambda_i t} \mathbf{V}^{-1} x_i(0) \quad (5.88)$$

or

$$\mathbf{x}(t) = \mathbf{V} e^{\Lambda t} \mathbf{V}^{-1} \mathbf{x}(0) \equiv e^{\Lambda t} \mathbf{x}(0) \quad (5.89)$$

From equation (5.72) the output response follows:

$$\mathbf{y}(t) = \mathbf{C}\mathbf{x}(t) = \mathbf{C}\mathbf{V} e^{\Lambda t} \mathbf{V}^{-1} \mathbf{x}(0) \equiv \mathbf{C} e^{\Lambda t} \mathbf{x}(0) \quad (5.90)$$

Clearly the system behaviour is governed by the *system modes* $e^{\lambda_i t}$, the *eigenfunctions* $\mathbf{v}_i e^{\lambda_i t}$, and the *initial state* $\mathbf{z}(0) = \mathbf{V}^{-1} \mathbf{x}(0)$.

Impulse response

The *unit impulse function* or *Dirac delta function*, denoted $\delta(t)$, is usually taken to mean a rectangular pulse of unit area, and in the limit the width of the pulse tends to zero whilst its magnitude tends to infinity. Thus the special property of the unit impulse function is

$$\int_{-\infty}^{+\infty} \delta(t - t_0) dt = 1 \quad (5.91)$$

where t_0 is the time at which the impulse commences.

The solution of the modal state equation in response to a unit impulse follows from [equation \(5.84\)](#):

$$\mathbf{z}(t) = e^{\Lambda t} \mathbf{z}(0) + \int_0^t e^{\Lambda(t-\tau)} \mathbf{V}^{-1} \mathbf{B} \mathbf{u}_\delta(\tau) d\tau \quad (5.92)$$

where $\mathbf{u}_\delta(\tau)$ is a unit impulse vector. The property of the unit impulse function enables the convolution integral to be solved, and

$$\mathbf{z}(t) = e^{\Lambda t} \mathbf{z}(0) + e^{\Lambda t} \mathbf{V}^{-1} \mathbf{B} = e^{\Lambda t} [\mathbf{z}(0) + \mathbf{V}^{-1} \mathbf{B}] \quad (5.93)$$

Thus the transform, [equation \(5.82\)](#), enables the state vector to be determined:

$$\mathbf{x}(t) = \mathbf{V} e^{\Lambda t} \mathbf{V}^{-1} [\mathbf{x}(0) + \mathbf{B}] \equiv e^{\Lambda t} [\mathbf{x}(0) + \mathbf{B}] \quad (5.94)$$

The corresponding output response vector is given by

$$\begin{aligned} \mathbf{y}(t) &= \mathbf{C} \mathbf{V} e^{\Lambda t} \mathbf{V}^{-1} [\mathbf{x}(0) + \mathbf{B}] + \mathbf{D} \mathbf{u}_\delta(t) \\ &\equiv \mathbf{C} e^{\Lambda t} [\mathbf{x}(0) + \mathbf{B}] + \mathbf{D} \mathbf{u}_\delta(t) \end{aligned} \quad (5.95)$$

For application to aeroplanes, it was established in Chapter 4 (Section 4.4.2) that the direct matrix \mathbf{D} is zero. Comparing [equations \(5.95\)](#) and [\(5.90\)](#), it is seen that the impulse response is the same as the unforced response with initial condition $[\mathbf{x}(0) + \mathbf{B}]$.

Step response

When the vector input to the system is a step of constant magnitude, denoted \mathbf{u}_k , applied at time $t_0 = 0$, the state [equation \(5.84\)](#) may be written as

$$\mathbf{z}(t) = e^{\Lambda t} \mathbf{z}(0) + \int_0^t e^{\Lambda(t-\tau)} \mathbf{V}^{-1} \mathbf{B} \mathbf{u}_k d\tau \quad (5.96)$$

Since the input is constant, the convolution integral is easily evaluated and

$$\mathbf{z}(t) = e^{\Lambda t} \mathbf{z}(0) + \Lambda^{-1} [e^{\Lambda t} - I] \mathbf{V}^{-1} \mathbf{B} \mathbf{u}_k \quad (5.97)$$

Thus the transform, [equation \(5.82\)](#), enables the state vector to be determined:

$$\begin{aligned} \mathbf{x}(t) &= \mathbf{V} e^{\Lambda t} [\mathbf{V}^{-1} \mathbf{x}(0) + \Lambda^{-1} \mathbf{V}^{-1} \mathbf{B} \mathbf{u}_k] - \Lambda^{-1} \mathbf{B} \mathbf{u}_k \\ &\equiv e^{\Lambda t} [\mathbf{x}(0) + \Lambda^{-1} \mathbf{B} \mathbf{u}_k] - \Lambda^{-1} \mathbf{B} \mathbf{u}_k \end{aligned} \quad (5.98)$$

The derivation of [equation \(5.98\)](#) makes use of the following property of the matrix exponential:

$$\Lambda^{-1} e^{\Lambda t} \equiv e^{\Lambda t} \Lambda^{-1} \quad (5.99)$$

It also draws on the similarity transform:

$$\mathbf{A}^{-1} = \mathbf{V}\Lambda^{-1}\mathbf{V}^{-1} \quad (5.100)$$

Again, the output response is obtained by substituting the state vector $\mathbf{x}(t)$, equation (5.98), into the output equation to give

$$\begin{aligned} \mathbf{y}(t) &= \mathbf{C}\mathbf{V}\mathbf{e}^{\Lambda t}[\mathbf{V}^{-1}\mathbf{x}(0) + \Lambda^{-1}\mathbf{V}^{-1}\mathbf{B}\mathbf{u}_k] - [\mathbf{C}\mathbf{A}^{-1}\mathbf{B} - \mathbf{D}]\mathbf{u}_k \\ &\equiv \mathbf{C}\mathbf{e}^{\Lambda t}[\mathbf{x}(0) + \mathbf{A}^{-1}\mathbf{B}\mathbf{u}_k] - [\mathbf{C}\mathbf{A}^{-1}\mathbf{B} - \mathbf{D}]\mathbf{u}_k \end{aligned} \quad (5.101)$$

Since the direct matrix \mathbf{D} is zero for aeroplanes, comparing equations (5.101) and (5.95) shows that the step response is the same as the impulse response with initial condition $[\mathbf{x}(0) + \mathbf{A}^{-1}\mathbf{B}\mathbf{u}_k]$ superimposed on the constant output $-\mathbf{C}\mathbf{A}^{-1}\mathbf{B}\mathbf{u}_k$.

Response shapes

With reference to equations (5.90), (5.95), and (5.101), it is clear that, irrespective of the input, the transient output response shapes are governed by the system eigenfunctions $\mathbf{V}\mathbf{e}^{\Lambda t}$ or, alternatively, by the eigenvectors and eigenvalues. Most computer solutions of the state equations produce output response in the form of time history data together with the eigenvalues and eigenvectors. Thus, in aircraft response analysis, the system modes and eigenfunctions may be calculated if required. The value of this facility is that it provides a very effective means for gaining insight into the key physical properties governing the response. In particular, it enables the mode content in any response variable to be assessed merely by inspection of the corresponding eigenvectors.

The output response to other input functions may also be calculated algebraically provided the input function can be expressed in a suitable analytic form. Typical examples include the ramp function and various sinusoidal functions. Computer software packages intended for analysing system response always include a number of common input functions and usually provide a means for creating others. However, in aircraft response analysis input functions other than those discussed in detail previously are generally of less interest.

EXAMPLE 5.7

The longitudinal equations of motion for the Lockheed F-104 Starfighter given in Example 5.2 may be written in state form as described in Chapter 4 (Section 4.4.2). Thus

$$\begin{bmatrix} 746 & 0 & 0 & 0 \\ 0 & 746 & 0 & 0 \\ 0 & 36.4 & 65000 & 0 \\ 0 & 0 & 0 & 1 \end{bmatrix} \begin{bmatrix} \dot{u} \\ \dot{w} \\ \dot{q} \\ \dot{\theta} \end{bmatrix} = \begin{bmatrix} -26.26 & 79.82 & 0 & -24021.2 \\ -159.64 & -328.24 & 227530 & 0 \\ 0 & -1014 & -18135 & 0 \\ 0 & 0 & 1 & 0 \end{bmatrix} \begin{bmatrix} u \\ w \\ q \\ \theta \end{bmatrix} + \begin{bmatrix} 0 \\ -16502 \\ -303575 \\ 0 \end{bmatrix} \eta \quad (5.102)$$

Premultiplying this equation by the inverse of the mass matrix results in the usual form of the state equation in terms of the concise derivatives:

$$\begin{bmatrix} \dot{u} \\ \dot{w} \\ \dot{q} \\ \dot{\theta} \end{bmatrix} = \begin{bmatrix} -0.0352 & 0.1070 & 0 & -32.2 \\ -0.2140 & -0.4400 & 305 & 0 \\ 1.198E-04 & -0.0154 & -0.4498 & 0 \\ 0 & 0 & 1 & 0 \end{bmatrix} \begin{bmatrix} u \\ w \\ q \\ \theta \end{bmatrix} + \begin{bmatrix} 0 \\ -22.1206 \\ -4.6580 \\ 0 \end{bmatrix} \eta \quad (5.103)$$

or, in algebraic form,

$$\dot{\mathbf{x}}(t) = \mathbf{Ax}(t) + \mathbf{Bu}(t) \quad (5.104)$$

which defines the matrices \mathbf{A} and \mathbf{B} and the vectors $\mathbf{x}(t)$ and $\mathbf{u}(t)$. Using the computer software package MATLAB interactively, the diagonal eigenvalue matrix is calculated:

$$\begin{aligned} \Lambda &= \begin{bmatrix} -0.4459 + 2.1644j & 0 & 0 & 0 \\ 0 & -0.4459 - 2.1644j & 0 & 0 \\ 0 & 0 & -0.0166 + 0.1474j & 0 \\ 0 & 0 & 0 & -0.0166 - 0.1474j \end{bmatrix} \quad (5.105) \\ &\equiv \begin{bmatrix} \lambda_s & 0 & 0 & 0 \\ 0 & \lambda_s^* & 0 & 0 \\ 0 & 0 & \lambda_p & 0 \\ 0 & 0 & 0 & \lambda_p^* \end{bmatrix} \end{aligned}$$

and the corresponding eigenvector matrix is calculated:

$$\mathbf{V} = \begin{bmatrix} 0.0071 - 0.0067j & 0.0071 + 0.0067j & -0.9242 - 0.3816j & -0.9242 + 0.3816j \\ 0.9556 - 0.2944j & 0.9556 + 0.2944j & 0.0085 + 0.0102j & 0.0085 - 0.0102j \\ 0.0021 + 0.0068j & 0.0021 - 0.0068j & -0.0006 - 0.0002j & -0.0006 + 0.0002j \\ 0.0028 - 0.0015j & 0.0028 + 0.0015j & -0.0012 + 0.0045j & -0.0012 - 0.0045j \end{bmatrix} \quad (5.106)$$

λ_s , λ_p , and their complex conjugates, λ_s^* , λ_p^* , are the eigenvalues corresponding to the short-period pitching oscillation and the phugoid, respectively. The corresponding matrix exponential is given by

$$\mathbf{e}^{\Lambda t} = \begin{bmatrix} e^{(-0.4459+2.1644j)t} & 0 & 0 & 0 \\ 0 & e^{(-0.4459-2.1644j)t} & 0 & 0 \\ 0 & 0 & e^{(-0.0166+0.1474j)t} & 0 \\ 0 & 0 & 0 & e^{(-0.0166-0.1474j)t} \end{bmatrix} \quad (5.107)$$

The eigenfunction matrix $\mathbf{Ve}^{\Lambda t}$ therefore has complex nonzero elements, and each row describes the dynamic content of the state variable to which it relates. For example, the *first row* describes the dynamic content of the velocity perturbation u and comprises the following four elements:

$$\begin{aligned}
 & (0.0071 - 0.0067j)e^{(-0.4459+2.1644j)t} \\
 & (0.0071 + 0.0067j)e^{(-0.4459-2.1644j)t} \\
 & (-0.9242 - 0.3816j)e^{(-0.0166+0.1474j)t} \\
 & (-0.9242 + 0.3816j)e^{(-0.0166-0.1474j)t}
 \end{aligned} \tag{5.108}$$

The first two elements in (5.108) describe the short-period pitching oscillation content in a velocity perturbation, and the second two elements describe the phugoid content. The relative *magnitudes* of the eigenvectors, the terms in parentheses, associated with the phugoid dynamics are the largest and clearly indicate that the phugoid dynamics are dominant in a velocity perturbation. The short-period pitching oscillation, on the other hand, is barely visible. Obviously, this kind of observation can be made for all of the state variables simply by inspection of the eigenvector and eigenvalue matrices only. This is a very useful facility for investigating the response properties of an aeroplane, especially when the behaviour is not conventional, when stability modes are obscured, or when a significant degree of mode coupling is present.

When it is recalled that

$$e^{j\pi t} = \cos \pi t + j \sin \pi t \tag{5.109}$$

where π represents an arbitrary scalar variable, the velocity eigenfunctions, (5.108), may be written alternatively as

$$\begin{aligned}
 & (0.0071 - 0.0067j)e^{-0.4459t}(\cos 2.1644t + j \sin 2.1644t) \\
 & (0.0071 + 0.0067j)e^{-0.4459t}(\cos 2.1644t - j \sin 2.1644t) \\
 & (-0.9242 - 0.3816j)e^{-0.0166t}(\cos 0.1474t + j \sin 0.1474t) \\
 & (-0.9242 + 0.3816j)e^{-0.0166t}(\cos 0.1474t - j \sin 0.1474t)
 \end{aligned} \tag{5.110}$$

Since the elements in (5.110) include sine and cosine functions of time, the origins of the oscillatory response characteristics in the overall solution of the equations of motion are identified.

As described in Examples 5.2 and 5.3, the damping ratio and undamped natural frequency characterise the stability modes. This information comprises the eigenvalues, included in the matrix equation (5.105), and is interpreted as follows:

For the short-period pitching oscillation, the higher frequency mode

$$\begin{aligned}
 \text{Undamped natural frequency } \omega_s &= 2.1644 \text{ rad/s} \\
 \zeta_s \omega_s &= 0.4459 \text{ rad/s} \\
 \text{Damping ratio } \zeta_s &= 0.206
 \end{aligned}$$

For the phugoid oscillation, the lower frequency mode

$$\text{Undamped natural frequency } \omega_p = 0.1474 \text{ rad/s}$$

$$\zeta_p \omega_p = 0.0166 \text{ rad/s}$$

$$\text{Damping ratio } \zeta_p = 0.1126$$

It is instructive to calculate the pitch attitude response to a unit elevator step input using the state-space method for comparison with the method described in Example 5.3. The step response is given by [equation \(5.101\)](#), which, for zero initial conditions, a zero direct matrix **D**, and output matrix **C** replaced with the identity matrix **I**, reduces to

$$\begin{aligned} \mathbf{y}(t) &= \mathbf{IVe}^{\Lambda t} \mathbf{\Lambda}^{-1} \mathbf{V}^{-1} \mathbf{Bu}_k - \mathbf{IA}^{-1} \mathbf{Bu}_k \\ &= \mathbf{Ve}^{\Lambda t} \mathbf{\Lambda}^{-1} \mathbf{V}^{-1} \mathbf{b} - \mathbf{A}^{-1} \mathbf{b} \end{aligned} \quad (5.111)$$

Since the single elevator input is a unit step, $\mathbf{u}_k = 1$ and the input matrix **B** becomes the column matrix **b**. The expression on the right-hand side of [equation \(5.111\)](#) is a (4×1) column matrix, the elements of which describe u , w , q , and θ responses to the input. With the aid of MATLAB the following were calculated:

$$\mathbf{\Lambda}^{-1} \mathbf{V}^{-1} \mathbf{b} = \begin{bmatrix} 147.36 + 19.07j \\ 147.36 - 19.07j \\ 223.33 - 133.29j \\ 223.33 + 133.29j \end{bmatrix} \quad \mathbf{A}^{-1} \mathbf{b} = \begin{bmatrix} -512.2005 \\ 299.3836 \\ 0 \\ 1.5548 \end{bmatrix} \quad (5.112)$$

The remainder of the calculation of the first term on the right-hand side of [equation \(5.111\)](#) was completed by hand, an exercise which is definitely not recommended! Pitch attitude response is given by the fourth row of the resulting column matrix $\mathbf{y}(t)$ and is

$$\begin{aligned} \theta(t) &= 0.664e^{-0.017t}(\cos 0.147t - 3.510 \sin 0.147t) \\ &\quad + 0.882e^{-0.446t}(\cos 2.164t + 0.380 \sin 2.164t) - 1.5548 \end{aligned} \quad (5.113)$$

This equation compares very favourably with [equation \(5.32\)](#) and may be interpreted in exactly the same way.

This example is intended to illustrate the role of the various elements contributing to the solution and, as such, are not normally undertaken on a routine basis. Machine computation simply produces the result in the most accessible form, which is usually graphical, although the investigator can obtain additional information in much the same way as shown in this example.

5.7 State-space model augmentation

It is frequently necessary to obtain response characteristics for variables which are not included in the aeroplane equations of motion. Provided that the variables of interest can be expressed as functions of the basic aeroplane motion variables, then response transfer functions can be derived in the same way as the acceleration response transfer functions described in Section 5.5. However, when the additional transfer functions of interest are strictly proper, they can also be obtained by

extending, or *augmenting*, the state description of the aeroplane and solving in the usual way as described. This latter course of action is extremely convenient as it extends the usefulness of the aeroplane state-space model and requires little additional effort on behalf of the investigator.

For some additional variables, such as height, it is necessary to create a new state variable and to augment the state equation accordingly. For others, such as flight path angle, which may be expressed as the simple sum of basic aeroplane state variables, it is only necessary to create an additional output variable and to augment the output equation accordingly. It is also a straightforward matter to augment the state description to include the additional dynamics of components such as engines and control surface actuators. In this case all of the response transfer functions obtained in the solution of the equations of motion implicitly include the effects of the additional dynamics.

5.7.1 Height response transfer function

An expression for height rate was given by equation (2.17), which for small perturbations may be written as

$$\dot{h} = U\theta - V\phi - W \quad (5.114)$$

Substitute for (U, V, W) from equation (2.1) and note that, for symmetric flight, $V_e = 0$. Since the products of small quantities are insignificantly small, they may be ignored and [equation \(5.114\)](#) may be written as

$$\dot{h} = U_e\theta - W_e - w \quad (5.115)$$

With reference to Fig. 2.4, assuming α_e to be small, $U_e \approx V_0$, $W_e \approx 0$, and [equation \(5.114\)](#) may be written, to a good approximation, as

$$\dot{h} = V_0\theta - w \quad (5.116)$$

The decoupled longitudinal state equation in concise form, equation (4.67), may be augmented to include the height variable by the inclusion of [equation \(5.116\)](#):

$$\begin{bmatrix} \dot{u} \\ \dot{w} \\ \dot{q} \\ \dot{\theta} \\ \dot{h} \end{bmatrix} = \begin{bmatrix} x_u & x_w & x_q & x_\theta & 0 \\ z_u & z_w & z_q & z_\theta & 0 \\ m_u & m_w & m_q & m_\theta & 0 \\ 0 & 0 & 1 & 0 & 0 \\ 0 & -1 & 0 & V_0 & 0 \end{bmatrix} \begin{bmatrix} u \\ w \\ q \\ \theta \\ h \end{bmatrix} + \begin{bmatrix} x_\eta & x_\tau \\ z_\eta & z_\tau \\ m_\eta & m_\tau \\ 0 & 0 \\ 0 & 0 \end{bmatrix} \begin{bmatrix} \eta \\ \tau \end{bmatrix} \quad (5.117)$$

Alternatively, this may be written in a more compact form:

$$\begin{bmatrix} \dot{\mathbf{x}}(t) \\ \dot{h}(t) \end{bmatrix} = \begin{bmatrix} \mathbf{A} & \mathbf{0} \\ \dots & \dots \\ 0 & -1 & 0 & V_0 & 0 \end{bmatrix} \begin{bmatrix} \mathbf{x}(t) \\ h(t) \end{bmatrix} + \begin{bmatrix} \mathbf{B} \\ \dots \\ 0 & 0 \end{bmatrix} \mathbf{u}(t) \quad (5.118)$$

where $\mathbf{x}(t)$ and $\mathbf{u}(t)$ are the state and input vectors, respectively, and \mathbf{A} and \mathbf{B} are the state and input matrices, respectively, of the basic aircraft state equation (4.67). Solution of [equation \(5.118\)](#) to obtain the longitudinal response transfer functions now results in two additional transfer functions describing the height response to an elevator perturbation and the height response to a thrust perturbation.

5.7.2 Incidence and sideslip response transfer functions

Dealing first with the inclusion of incidence angle in the longitudinal decoupled equations of motion. It follows from equation (2.5) that for small-perturbation motion incidence, α is given by

$$\alpha \cong \tan \alpha = \frac{w}{V_0} \quad (5.119)$$

since $U_e \rightarrow V_0$ as the perturbation tends to zero. Thus incidence α is equivalent to normal velocity w divided by the steady free stream velocity. Incidence can be included in the longitudinal state equations in two ways. Either it can be added to the output vector $\mathbf{y}(t)$ without changing the state vector or it can replace normal velocity w in the state vector. When the output equation is augmented, the longitudinal state equations (4.67) and (4.68) are written as

$$\begin{aligned} \dot{\mathbf{x}}(t) &= \mathbf{A}\mathbf{x}(t) + \mathbf{B}\mathbf{u}(t) \\ \mathbf{y}(t) &= \begin{bmatrix} u \\ w \\ q \\ \theta \\ \alpha \end{bmatrix} = \begin{bmatrix} 1 & 0 & 0 & 0 \\ 0 & 1 & 0 & 0 \\ 0 & 0 & 1 & 0 \\ 0 & 0 & 0 & 1 \\ 0 & 1/V_0 & 0 & 0 \end{bmatrix} \begin{bmatrix} u \\ w \\ q \\ \theta \end{bmatrix} = \begin{bmatrix} \dots & \mathbf{I} & \dots \\ \dots & \dots & \dots \\ 0 & 1/V_0 & 0 & 0 \end{bmatrix} \mathbf{x}(t) \end{aligned} \quad (5.120)$$

When incidence replaces normal velocity, it is first necessary to note that equation (5.119) may be differentiated to give $\dot{\alpha} = \dot{w}/V_0$. Thus the longitudinal state equation (4.67) may be rewritten as

$$\begin{bmatrix} \dot{u} \\ \dot{\alpha} \\ \dot{q} \\ \dot{\theta} \end{bmatrix} = \begin{bmatrix} x_u & x_w V_0 & x_q & x_\theta \\ z_u/V_0 & z_w & z_q/V_0 & z_\theta/V_0 \\ m_u & m_w V_0 & m_q & m_\theta \\ 0 & 0 & 1 & 0 \end{bmatrix} \begin{bmatrix} u \\ \alpha \\ q \\ \theta \end{bmatrix} + \begin{bmatrix} x_\eta & x_\tau \\ z_\eta/V_0 & z_\tau/V_0 \\ m_\eta & m_\tau \\ 0 & 0 \end{bmatrix} \begin{bmatrix} \eta \\ \tau \end{bmatrix} \quad (5.121)$$

The output equation (4.68) remains unchanged except that the output vector $\mathbf{y}(t)$ now includes α instead of w ; thus

$$\mathbf{y}^T(t) = [u \quad \alpha \quad q \quad \theta] \quad (5.122)$$

In a similar way it is easily shown that in a lateral perturbation the sideslip angle β is given by

$$\beta \cong \tan \beta = \frac{v}{V_0} \quad (5.123)$$

and the lateral small-perturbation equations can be modified in the same way as the longitudinal equations in order to incorporate sideslip angle β in the output equation; alternatively, it may replace lateral velocity v in the state equation. When the output equation is augmented, the lateral-directional state equations may be written as

$$\begin{aligned} \dot{\mathbf{x}}(t) &= \mathbf{A}\mathbf{x}(t) + \mathbf{B}\mathbf{u}(t) \\ \mathbf{y}(t) &= \begin{bmatrix} v \\ p \\ r \\ \phi \\ \beta \end{bmatrix} = \begin{bmatrix} 1 & 0 & 0 & 0 \\ 0 & 1 & 0 & 0 \\ 0 & 0 & 1 & 0 \\ 0 & 0 & 0 & 1 \\ 1/V_0 & 0 & 0 & 0 \end{bmatrix} \begin{bmatrix} v \\ p \\ r \\ \phi \end{bmatrix} = \begin{bmatrix} \dots & \mathbf{I} & \dots \\ \dots & \dots & \dots \\ 1/V_0 & 0 & 0 & 0 \end{bmatrix} \mathbf{x}(t) \end{aligned} \quad (5.124)$$

where the lateral-directional state equation is given by equation (4.70). When sideslip angle β replaces lateral velocity v in the lateral-directional state equation (4.70), it is written as

$$\begin{bmatrix} \dot{\beta} \\ \dot{p} \\ \dot{r} \\ \dot{\phi} \end{bmatrix} = \begin{bmatrix} y_v & y_p/V_0 & y_r/V_0 & y_\phi/V_0 \\ l_v V_0 & l_p & l_r & l_\phi \\ n_v V_0 & n_p & n_r & n_\phi \\ 0 & 1 & 0 & 0 \end{bmatrix} \begin{bmatrix} \beta \\ p \\ r \\ \phi \end{bmatrix} + \begin{bmatrix} y_\xi/V_0 & y_\zeta/V_0 \\ l_\xi & l_\zeta \\ n_\xi & n_\zeta \\ 0 & 0 \end{bmatrix} \begin{bmatrix} \xi \\ \zeta \end{bmatrix} \quad (5.125)$$

Again, for this alternative the lateral-directional output vector $\mathbf{y}(t)$ remains unchanged except that sideslip angle β replaces lateral velocity v ; thus

$$\mathbf{y}^T(t) = [\beta \ p \ r \ \phi] \quad (5.126)$$

Solution of the longitudinal or lateral-directional state equations will produce the transfer function matrix in the usual way. In every case, transfer functions are calculated to correspond with the particular set of variables that make up the output vector.

5.7.3 Flight path angle response transfer function

Sometimes flight path angle γ response to controls is required, especially when handling qualities in the approach flight condition are under consideration. Perturbations in flight path angle γ may be expressed in terms of perturbations in pitch attitude θ and incidence α , as indicated for the steady-state case by equation (2.2). Whence

$$\gamma = \theta - \alpha \cong \theta - \frac{w}{V_0} \quad (5.127)$$

Thus the longitudinal output equation (4.68) may be augmented to include flight path angle as an additional output variable. The form of the longitudinal state equations is then similar to that of equations (5.120), and

$$\begin{aligned} \dot{\mathbf{x}}(t) &= \mathbf{A}\mathbf{x}(t) + \mathbf{B}\mathbf{u}(t) \\ \mathbf{y}(t) &= \begin{bmatrix} u \\ w \\ q \\ \theta \\ \gamma \end{bmatrix} = \begin{bmatrix} \mathbf{I} \\ \dots \\ 0 & -1/V_0 & 0 & 1 \end{bmatrix} \mathbf{x}(t) \end{aligned} \quad (5.128)$$

where the state vector $\mathbf{x}(t)$ remains unchanged:

$$\mathbf{x}^T(t) = [u \ w \ q \ \theta] \quad (5.129)$$

5.7.4 Addition of engine dynamics

Provided that the thrust-producing devices can be modelled by a linear transfer function then, in general, it can be integrated into the aircraft state description. This then enables the combined

engine and airframe dynamics to be modelled by the overall system response transfer functions. A very simple engine thrust model was described by equation (2.34), with transfer function

$$\frac{\tau(s)}{\varepsilon(s)} = \frac{k_\tau}{(1 + sT_\tau)} \quad (5.130)$$

where $\tau(t)$ is the thrust perturbation in response to a perturbation in throttle lever angle $\varepsilon(t)$. The transfer function [equation \(5.130\)](#) may be rearranged thus:

$$s\tau(s) = \frac{k_\tau}{T_\tau} \varepsilon(s) - \frac{1}{T_\tau} \tau(s) \quad (5.131)$$

This is the Laplace transform, assuming zero initial conditions, of the following time domain equation:

$$\dot{\tau}(t) = \frac{k_\tau}{T_\tau} \varepsilon(t) - \frac{1}{T_\tau} \tau(t) \quad (5.132)$$

The longitudinal state equation (4.67) may be augmented to include the engine dynamics described by [equation \(5.132\)](#), which, after some rearrangement, may be written as

$$\begin{bmatrix} \dot{u} \\ \dot{w} \\ \dot{q} \\ \dot{\theta} \\ \dot{\tau} \end{bmatrix} = \begin{bmatrix} x_u & x_w & x_q & x_\theta & x_\tau \\ z_u & z_w & z_q & z_\theta & z_\tau \\ m_u & m_w & m_q & m_\theta & m_\tau \\ 0 & 0 & 1 & 0 & 0 \\ 0 & 0 & 0 & 0 & -1/T_\tau \end{bmatrix} \begin{bmatrix} u \\ w \\ q \\ \theta \\ \tau \end{bmatrix} + \begin{bmatrix} x_\eta & 0 \\ z_\eta & 0 \\ m_\eta & 0 \\ 0 & 0 \\ 0 & k_\tau/T_\tau \end{bmatrix} \begin{bmatrix} \eta \\ \varepsilon \end{bmatrix} \quad (5.133)$$

Thus the longitudinal state equation has been augmented to include thrust as an additional state, and the second input variable is now throttle lever angle ε . The output equation (4.68) remains unchanged except that the C matrix is increased in order to the (5×5) identity matrix I to provide the additional output variable corresponding to the extra state variable τ .

The procedure described above, in which a transfer function model of engine dynamics is converted to a form suitable for augmenting the state equation, is known as *system realisation*. More generally, relatively complex higher-order transfer functions can be *realised* as state equations, although the procedure for so doing is rather more involved than that illustrated here for a particularly simple example. The mathematical methods required are described in most books on modern control theory. The advantage and power of this relatively straightforward procedure is considerable since it literally enables the state equation describing a very complex system, such as an aircraft with advanced flight controls, to be built by repeated augmentation. The state descriptions of the various system components are simply added to the matrix state equation until the overall system dynamics are fully represented. Typically, this might mean, for example, that the basic longitudinal or lateral-directional (4×4) airframe state matrix is augmented to a much higher order of perhaps (12×12) or more, depending on the complexity of the engine model, control system, surface actuators, and so on. Whatever the result, the equations are easily solved using the tools described.

EXAMPLE 5.8

To illustrate the procedure for augmenting an aeroplane state model, let the longitudinal model for the Lockheed F-104 Starfighter of Example 5.2 be augmented to include height h and flight path angle γ and to replace normal velocity w with incidence α . The longitudinal state equation expressed in terms of concise derivatives is given by [equation \(5.103\)](#), which is modified in accordance with [equation \(5.121\)](#) to replace normal velocity w with incidence α :

$$\begin{bmatrix} \dot{u} \\ \dot{\alpha} \\ \dot{q} \\ \dot{\theta} \end{bmatrix} = \begin{bmatrix} -0.0352 & 32.6342 & 0 & -32.2 \\ -7.016E-04 & -0.4400 & 1 & 0 \\ 1.198E-04 & -4.6829 & -0.4498 & 0 \\ 0 & 0 & 1 & 0 \end{bmatrix} \begin{bmatrix} u \\ \alpha \\ q \\ \theta \end{bmatrix} + \begin{bmatrix} 0 \\ -0.0725 \\ -4.6580 \\ 0 \end{bmatrix} \eta \quad (5.134)$$

[Equation \(5.134\)](#) is now augmented by the addition of [equation \(5.116\)](#), the height equation expressed in terms of incidence α and pitch attitude θ :

$$\dot{h} = V_0(\theta - \alpha) = 305\theta - 305\alpha \quad (5.135)$$

Thus the augmented state equation is written as

$$\begin{bmatrix} \dot{u} \\ \dot{\alpha} \\ \dot{q} \\ \dot{\theta} \\ \dot{h} \end{bmatrix} = \begin{bmatrix} -0.0352 & 32.6342 & 0 & -32.2 & 0 \\ -7.016E-04 & -0.4400 & 1 & 0 & 0 \\ 1.198E-04 & -4.6829 & -0.4498 & 0 & 0 \\ 0 & 0 & 1 & 0 & 0 \\ 0 & -305 & 0 & 305 & 0 \end{bmatrix} \begin{bmatrix} u \\ \alpha \\ q \\ \theta \\ h \end{bmatrix} + \begin{bmatrix} 0 \\ -0.0725 \\ -4.6580 \\ 0 \\ 0 \end{bmatrix} \eta \quad (5.136)$$

The corresponding output equation is augmented to included flight path angle γ as given by [equation \(5.127\)](#) and is then written as

$$\begin{bmatrix} u \\ \alpha \\ q \\ \theta \\ h \\ \gamma \end{bmatrix} = \begin{bmatrix} 1 & 0 & 0 & 0 & 0 \\ 0 & 1 & 0 & 0 & 0 \\ 0 & 0 & 1 & 0 & 0 \\ 0 & 0 & 0 & 1 & 0 \\ 0 & 0 & 0 & 0 & 1 \\ 0 & -1 & 0 & 1 & 0 \end{bmatrix} \begin{bmatrix} u \\ \alpha \\ q \\ \theta \\ h \end{bmatrix} \quad (5.137)$$

This, of course, assumes the direct matrix \mathbf{D} to be zero, as discussed earlier. [Equations \(5.136\)](#) and [\(5.137\)](#) together provide the complete state description of the Lockheed F-104 as required. Solving these equations with the aid of Program CC results in the six transfer functions describing the response to elevator.

The common denominator polynomial (the characteristic polynomial) is given by

$$\Delta(s) = s(s^2 + 0.033s + 0.022)(s^2 + 0.892s + 4.883) \quad (5.138)$$

The numerator polynomials are given by

$$\begin{aligned}
 N_{\eta}^u(s) &= -2.367s(s - 4.215)(s + 5.519) \text{ ft/s/rad} \\
 N_{\eta}^{\alpha}(s) &= -0.073s(s + 64.675)(s^2 + 0.035s + 0.023) \text{ rad/rad} \\
 N_{\eta}^q(s) &= -4.658s^2(s + 0.134)(s + 0.269) \text{ rad/s/rad} \\
 N_{\eta}^{\theta}(s) &= -4.658s(s + 0.134)(s + 0.269) \text{ rad/rad} \\
 N_{\eta}^h(s) &= 22.121(s + 0.036)(s - 4.636)(s + 5.085) \text{ ft/rad} \\
 N_{\eta}^{\gamma}(s) &= 0.073s(s + 0.036)(s - 4.636)(s + 5.085) \text{ rad/rad}
 \end{aligned} \tag{5.139}$$

Note that the additional zero pole in the denominator is due to the increase in order of the state equation from four to five; it represents the *height integration*. This is easily interpreted since an elevator step input will cause the aeroplane to climb or descend steadily after the transient has died away, at which point the response becomes similar to that of a simple integrator. Note also that the denominator zero cancels with a zero in all numerator polynomials except that describing the height response. Thus the response transfer functions describing the basic aircraft motion variables u , α , q , and θ are identical to those obtained from the basic fourth-order state equations. The reason for the similarity between the height and flight path angle response numerators becomes obvious if the expression for the height, [equation \(5.135\)](#), is compared with the expression for flight path angle, [equation \(5.127\)](#).

References

- Auslander, D. M., Takahashi, Y., & Rabins, M. J. (1974). *Introducing systems and control*. Kogakusha Ltd, Tokyo: McGraw Hill.
- Barnett, S. (1975). *Introduction to mathematical control theory*. Oxford, UK: Clarendon Press.
- Duncan, W. J. (1959). *The principles of the control and stability of aircraft*. Cambridge, UK: Cambridge University Press.
- Goult, R. J., Hoskins, R. F., Milner, J. A., & Pratt, M. J. (1974). *Computational methods in linear algebra*. London: Stanley Thorne (Publishers) Ltd.
- Heffley, R. K., and Jewell, W. F. (1972). *Aircraft handling qualities data*. NASA Contractor Report, NASA CR-2144.
- Owens, D. H. (1981). *Multivariable and optimal systems*. Boston: Academic Press.
- Shinnars, S. M. (1980). *Modern control system theory and application*. Boston: Addison-Wesley.
- Teper, G. L. (1969). *Aircraft stability and control data*. Systems Technology, Inc., STI Technical Report 176-1. NASA Contractor Report, National Aeronautics and Space Administration, Washington D.C. 20546

PROBLEMS

- 5.1** The free response $x(t)$ of a linear second-order system after release from an initial displacement A is given by

$$x(t) = \frac{1}{2}Ae^{-\omega\zeta t}\left(\left(1 + \frac{\zeta}{\sqrt{\zeta^2 - 1}}\right)e^{-\omega t\sqrt{\zeta^2 - 1}} + \left(1 - \frac{\zeta}{\sqrt{\zeta^2 - 1}}\right)e^{\omega t\sqrt{\zeta^2 - 1}}\right)$$

where ω is the undamped natural frequency and ζ is the damping ratio.

- (a) With the aid of sketches, show the possible forms of the motion as ζ varies from zero to a value greater than 1.
- (b) How is the motion dependent on the sign of ζ ?
- (c) How do the time response shapes relate to the solution of the equations of motion of an aircraft?
- (d) Define the damped natural frequency and explain how it depends on damping ratio ζ .

(CU 1982)

- 5.2** For an aircraft in steady rectilinear flight, describe flight path angle, incidence, and attitude, and show how they are related.

(CU 1986)

- 5.3** Write the Laplace transform of the longitudinal small-perturbation equations of motion of an aircraft for the special case when the phugoid motion is suppressed. It may be assumed that the equations are referred to wind axes and that the influence of the derivatives \dot{Z}_q , $\dot{Z}_{\dot{w}}$, and $\dot{M}_{\dot{w}}$ is negligible. State all other assumptions made.

- (a) By the application of Cramer's rule, obtain algebraic expressions for the pitch rate response and incidence angle response to elevator transfer functions.
- (b) Derivative data for the Republic Thunderchief F-105B aircraft flying at an altitude of 35,000 ft and a speed of 518 kt are

$$\frac{\dot{Z}_w}{m} = -0.4 \text{ s}^{-1} \quad \frac{\dot{M}_w}{I_y} = -0.0082 \text{ ft}^{-1} \text{ s}^{-1} \quad \frac{\dot{M}_q}{I_y} = -0.485 \text{ s}^{-1}$$

$$\frac{\dot{M}_\eta}{I_y} = -12.03 \text{ s}^{-2} \quad \frac{\dot{Z}_\eta}{m} = -65.19 \text{ ft.s}^{-2}$$

Evaluate the transfer functions for this aircraft and calculate values for the longitudinal short-period frequency and damping.

- (c) Sketch the pitch rate response to a 1 deg step of elevator angle and indicate the significant features of the response.

(CU 1990)

- 5.4** The roll response to aileron control of the Douglas DC-8 airliner in an approach flight condition is given by the following transfer function:

$$\frac{\phi(s)}{\xi(s)} = \frac{-0.726(s^2 + 0.421s + 0.889)}{(s - 0.013)(s + 1.121)(s^2 + 0.22s + 0.99)}$$

Realise the transfer function in terms of its partial fractions and, by calculating the inverse Laplace transform, obtain an expression for the roll time history in response to a unit aileron impulse. State all assumptions.

- 5.5** Describe the methods by which the normal acceleration response to elevator transfer function may be calculated. Using the Republic Thunderchief F-105B model given in Problem 5.3, calculate the transfer function $a_z(s)/\eta(s)$.
- (a) With the aid of MATLAB, Program CC, or a similar software tool, obtain a normal acceleration time history response plot for a unit elevator step input. Choose a time scale of about 10 s.
- (b) Calculate the inverse Laplace transform of $a_z(s)/\eta(s)$ for a unit step elevator input. Plot the time history given by the response function and compare with that obtained in Problem 5.5(a).

- 5.6** The lateral-directional equations of motion for the Boeing B-747 cruising at Mach 0.8 at 40,000 ft are given by [Heffley and Jewell \(1972\)](#) as follows:

$$\begin{bmatrix} (s + 0.0558) & -\frac{(62.074s + 32.1)}{774} & \frac{(771.51s - 2.576)}{774} \\ \dots & \dots & \dots \\ 3.05 & s(s + 0.465) & -0.388 \\ \dots & \dots & \dots \\ -0.598 & 0.0318s & (s + 0.115) \end{bmatrix} \begin{bmatrix} \beta \\ p \\ r \end{bmatrix} = \begin{bmatrix} 0 \\ \dots \\ 0.143 \\ \dots \\ 0.00775 \end{bmatrix} \begin{bmatrix} 0.00729 \\ \dots \\ 0.153 \\ \dots \\ -0.475 \end{bmatrix} \begin{bmatrix} \xi \\ \zeta \end{bmatrix}$$

where s is the Laplace operator and all angles are in radians. Using Cramer's rule, calculate all of the response transfer functions and factorise the numerators and common denominator. What are the stability mode characteristics at this flight condition?

- 5.7** The longitudinal equations of motion as given by [Heffley and Jewell \(1972\)](#) are

$$\begin{bmatrix} (1 - X_{\dot{u}})s - X_u^* & -X_{\dot{w}}s - X_w^* & (-X_q + W_e)s + g \cos \theta_e \\ \dots & \dots & \dots \\ -Z_{\dot{u}}s - Z_u^* & (1 - Z_w)s - Z_w & (-Z_q - U_e)s + g \sin \theta_e \\ \dots & \dots & \dots \\ -M_{\dot{u}}s - M_u^* & -(M_{\dot{w}}s + M_w) & s^2 - M_q s \end{bmatrix} \begin{bmatrix} u \\ w \\ \theta \end{bmatrix} = \begin{bmatrix} X_\eta \\ Z_\eta \\ M_\eta \end{bmatrix} \eta$$

$$q = s\theta$$

$$\dot{h} = -w \cos \theta_e + u \sin \theta_e + (U_e \cos \theta_e + W_e \sin \theta_e)$$

$$a_z = sw - U_e q + (g \sin \theta_e) \theta$$

Note that the derivatives are in American notation and represent the mass- or inertia-divided dimensional derivatives as appropriate. The * symbol on the speed-dependent derivatives indicates that they include thrust effects as well as the usual aerodynamic characteristics.

All other symbols have their usual meanings. Rearrange these equations into the state space format:

$$\mathbf{M}\dot{\mathbf{x}}(t) = \mathbf{A}'\mathbf{x}(t) + \mathbf{B}'\mathbf{u}(t)$$

$$\mathbf{y}(t) = \mathbf{C}\mathbf{x}(t) + \mathbf{D}\mathbf{u}(t)$$

with state vector $\mathbf{x} = [u \ w \ q \ \theta \ h]$, input vector $\mathbf{u} = \eta$, and output vector $\mathbf{y} = [u \ w \ q \ \theta \ h \ a_z]$. State all assumptions made.

- 5.8** Longitudinal data for the Douglas A-4D Skyhawk flying at Mach 1.0 at 15,000 ft are given in [Teper \(1969\)](#) as follows:

Trim Pitch Attitude	0.4°		
Speed of Sound at 15,000 ft	1058 ft/s		
X_w	-0.0251 1/s	$M_{\dot{w}}$	-0.000683 1/ft
X_u	-0.1343 1/s	M_q	-2.455 1/s
Z_w	-1.892 1/s	X_η	-15.289 ft/rad s ²
Z_u	-0.0487 1/s	Z_η	-94.606 ft/rad s ²
M_w	-0.1072 1/ft s	M_η	-31.773 1/s ²
M_u	0.00263 1/ft s		

Using the state-space model derived in Problem 5.7, obtain the state equations for the Skyhawk in the following format:

$$\begin{aligned}\dot{\mathbf{x}}(t) &= \mathbf{Ax}(t) + \mathbf{Bu}(t) \\ \mathbf{y}(t) &= \mathbf{Cx}(t) + \mathbf{Du}(t)\end{aligned}$$

Using MATLAB or Program CC, solve the state equations to obtain the response transfer functions for all output variables. What are the longitudinal stability characteristics of the Skyhawk at this flight condition?

Longitudinal Dynamics

6

6.1 Response to controls

The solution of the longitudinal equations of motion by, for example, the methods described in Chapter 5 enables the response transfer functions to be obtained. These completely describe the linear dynamic response to a control input in the plane of symmetry. Implicit in the response are the dynamic properties determined by the stability characteristics of the aeroplane. The transfer functions and the response variables described by them are linear, since the entire modelling process is based on the assumption that the motion is constrained to small disturbances about an equilibrium trim state. However, it is common practice to assume that the response to controls is valid when the magnitude of the response can hardly be described as “a small perturbation.” For many conventional aeroplanes the error incurred by so doing is generally acceptably small, as such aeroplanes tend to have substantially linear aerodynamic characteristics over their flight envelopes. For aeroplanes with very large flight envelopes, significant aerodynamic nonlinearity, and, or, dependence on sophisticated flight control systems, it is advisable not to use the linearised equations of motion for analysis of response other than that which can justifiably be described as being of small magnitude.

It is convenient to review the longitudinal response to elevator about a trim state in which thrust is held constant. The longitudinal state equation (4.67) may then be written as

$$\begin{bmatrix} \dot{u} \\ \dot{w} \\ \dot{q} \\ \dot{\theta} \end{bmatrix} = \begin{bmatrix} x_u & x_w & x_q & x_\theta \\ z_u & z_w & z_q & z_\theta \\ m_u & m_w & m_q & m_\theta \\ 0 & 0 & 1 & 0 \end{bmatrix} \begin{bmatrix} u \\ w \\ q \\ \theta \end{bmatrix} + \begin{bmatrix} x_\eta \\ z_\eta \\ m_\eta \\ 0 \end{bmatrix} \eta \quad (6.1)$$

The four response transfer functions obtained in the solution of [equation \(6.1\)](#) may conveniently be written as

$$\frac{u(s)}{\eta(s)} \equiv \frac{N_\eta^u(s)}{\Delta(s)} = \frac{k_u(s + 1/T_u)(s^2 + 2\zeta_u\omega_u s + \omega_u^2)}{(s^2 + 2\zeta_p\omega_p s + \omega_p^2)(s^2 + 2\zeta_s\omega_s s + \omega_s^2)} \quad (6.2)$$

$$\frac{w(s)}{\eta(s)} \equiv \frac{N_\eta^w(s)}{\Delta(s)} = \frac{k_w(s + 1/T_\alpha)(s^2 + 2\zeta_\alpha\omega_\alpha s + \omega_\alpha^2)}{(s^2 + 2\zeta_p\omega_p s + \omega_p^2)(s^2 + 2\zeta_s\omega_s s + \omega_s^2)} \quad (6.3)$$

$$\frac{q(s)}{\eta(s)} \equiv \frac{N_\eta^q(s)}{\Delta(s)} = \frac{k_qs(s + 1/T_{\theta_1})(s + 1/T_{\theta_2})}{(s^2 + 2\zeta_p\omega_p s + \omega_p^2)(s^2 + 2\zeta_s\omega_s s + \omega_s^2)} \quad (6.4)$$

$$\frac{\theta(s)}{\eta(s)} \equiv \frac{N_\eta^\theta(s)}{\Delta(s)} = \frac{k_\theta(s + 1/T_{\theta_1})(s + 1/T_{\theta_2})}{(s^2 + 2\zeta_p\omega_p s + \omega_p^2)(s^2 + 2\zeta_s\omega_s s + \omega_s^2)} \quad (6.5)$$

The solution of the equations of motion results in polynomial descriptions of the transfer function numerators and common denominator, as set out in Appendix 3. The polynomials factorise into real and complex pairs of roots, which are most explicitly quoted in the style of [equations \(6.2\) through \(6.5\)](#). Since the roots are interpreted as time constants, damping ratios, and natural frequencies, this style of writing makes the essential information instantly available. It should also be noted that the numerator and denominator factors are typical for a conventional aeroplane. Sometimes complex pairs of roots may become two real roots and vice versa. However, this does not usually mean that the dynamic response characteristics of the aeroplane become dramatically different. Differences in the interpretation of response may be evident but will not necessarily be large.

As has already been indicated, the common denominator of the transfer functions describes the characteristic polynomial, which in turn describes the stability characteristics of the aeroplane. Thus the response of all variables to an elevator input is dominated by the denominator parameters: damping ratios and natural frequencies. The differences between the individual responses are entirely determined by their respective numerators. It is therefore important to fully appreciate the role of the numerator in determining response dynamics. The *response shapes* of the individual variables are determined by the common denominator and “coloured” by their respective numerators. The numerator plays no part in determining stability in a linear system, which is how the aeroplane is modelled here.

EXAMPLE 6.1

The equations of motion and aerodynamic data for the Ling-Temco-Vought A-7A Corsair II aircraft were obtained from [Teper \(1969\)](#). The flight condition corresponds to level cruising flight at an altitude of 15,000 ft at Mach 0.3. The equations of motion, referred to a body axis system, are arranged in state space format:

$$\begin{bmatrix} \dot{u} \\ \dot{w} \\ \dot{q} \\ \dot{\theta} \end{bmatrix} = \begin{bmatrix} 0.00501 & 0.00464 & -72.90000 & -31.34000 \\ -0.08570 & -0.54500 & 309.00000 & -7.40000 \\ 0.00185 & -0.00767 & -0.39500 & 0.00132 \\ 0 & 0 & 1 & 0 \end{bmatrix} \begin{bmatrix} u \\ w \\ q \\ \theta \end{bmatrix} + \begin{bmatrix} 5.63000 \\ -23.80000 \\ -4.51576 \\ 0 \end{bmatrix} \eta \quad (6.6)$$

Since incidence α and flight path angle γ are useful variables in the evaluation of handling qualities, it is convenient to augment the corresponding output equation, as was described in Section 5.7, in order to obtain their response transfer functions in the solution of the equations of motion. The output equation is therefore

$$\begin{bmatrix} u \\ w \\ q \\ \theta \\ \alpha \\ \gamma \end{bmatrix} = \begin{bmatrix} 1 & 0 & 0 & 0 \\ 0 & 1 & 0 & 0 \\ 0 & 0 & 1 & 0 \\ 0 & 0 & 0 & 1 \\ 0 & 0.00316 & 0 & 0 \\ 0 & -0.00316 & 0 & 1 \end{bmatrix} \begin{bmatrix} u \\ w \\ q \\ \theta \\ \alpha \\ \gamma \end{bmatrix} + \begin{bmatrix} 0 \\ 0 \\ 0 \\ 0 \\ 0 \\ 0 \end{bmatrix} \eta \quad (6.7)$$

Note that all elements in the matrices in [equations \(6.6\) and \(6.7\)](#) have been rounded to five decimal places simply to keep the equations to a reasonable physical size. This should not be done with equations used in actual computation.

Solution of the equations of motion using Program CC determines the following response transfer functions:

$$\begin{aligned}
 \frac{u(s)}{\eta(s)} &= \frac{5.63(s + 0.369)(s + 0.587)(s + 58.437)}{(s^2 + 0.033s + 0.020)(s^2 + 0.902s + 2.666)} \text{ ft/s/rad} \\
 \frac{w(s)}{\eta(s)} &= \frac{-23.8(s^2 - 0.0088s + 0.0098)(s + 59.048)}{(s^2 + 0.033s + 0.020)(s^2 + 0.902s + 2.666)} \text{ ft/s/rad} \\
 \frac{q(s)}{\eta(s)} &= \frac{-4.516s(s - 0.008)(s + 0.506)}{(s^2 + 0.033s + 0.020)(s^2 + 0.902s + 2.666)} \text{ rad/s/rad (deg/s/deg)} \\
 \frac{\theta(s)}{\eta(s)} &= \frac{-4.516(s - 0.008)(s + 0.506)}{(s^2 + 0.033s + 0.020)(s^2 + 0.902s + 2.666)} \text{ rad/rad (deg/deg)} \\
 \frac{\alpha(s)}{\eta(s)} &= \frac{-0.075(s^2 - 0.0088s + 0.0098)(s + 59.048)}{(s^2 + 0.033s + 0.020)(s^2 + 0.902s + 2.666)} \text{ rad/rad (deg/deg)} \\
 \frac{\gamma(s)}{\eta(s)} &= \frac{0.075(s - 0.027)(s + 5.004)(s - 6.084)}{(s^2 + 0.033s + 0.020)(s^2 + 0.902s + 2.666)} \text{ rad/rad (deg/deg)}
 \end{aligned} \tag{6.8}$$

All coefficients have again been rounded to a convenient number of decimal places, and the previous caution should be noted.

The characteristic equation is given by equating the common denominator polynomial to zero:

$$\Delta(s) = (s^2 + 0.033s + 0.020)(s^2 + 0.902s + 2.666) = 0$$

The first pair of complex roots describes the phugoid stability mode with the following characteristics:

Damping ratio $\zeta_p = 0.11$

Undamped natural frequency $\omega_p = 0.14 \text{ rad/s}$

The second pair of complex roots describes the short-period pitching oscillation, or short-period stability mode, with the following characteristics:

Damping ratio $\zeta_s = 0.28$

Undamped natural frequency $\omega_s = 1.63 \text{ rad/s}$

These mode characteristics indicate that the airframe is aerodynamically stable, although it will be shown later that the short-period mode damping ratio is unacceptably low.

The response of the aircraft to a unit step (1°) elevator input is shown in [Fig. 6.1](#). All of the variables in the solution of the equations of motion are shown, the responses being characterised by the transfer functions, [equations \(6.8\)](#).

The responses clearly show both dynamic stability modes, the short-period pitching oscillation and the phugoid. However, the magnitude of each stability mode differs in each response

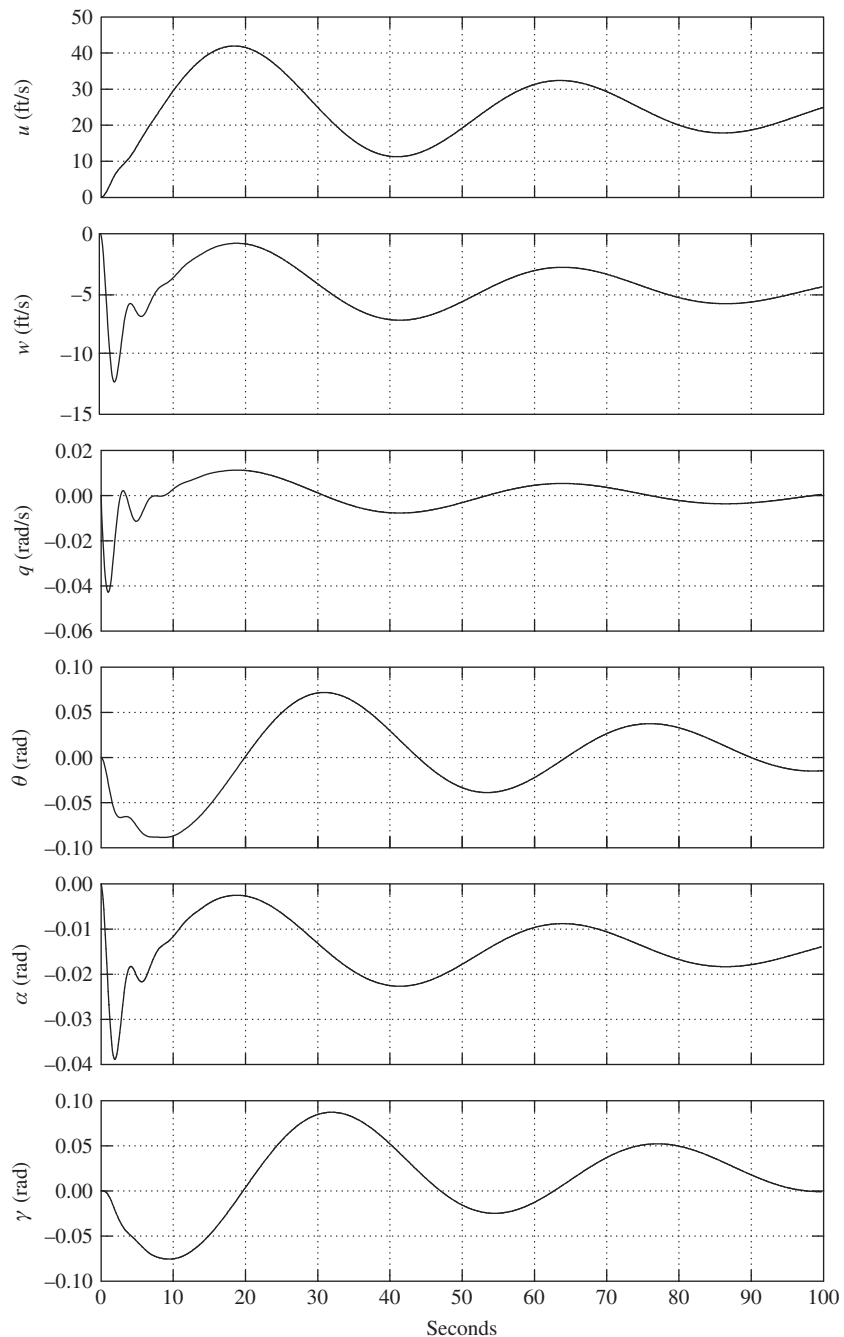


FIGURE 6.1 Aircraft response to a 1° elevator step input.

variable. For example, the short-period pitching oscillation is most visible as the initial transient in the variables w , q , and α whereas the phugoid mode is visible in all variables, although the relative magnitudes vary considerably. Clearly, the stability of the responses is the same, as determined by the common denominator of the transfer functions, [equations \(6.8\)](#), but the differences between the response variables are determined by the unique numerator of each response transfer function.

The mode content in each of the motion variables is given most precisely by the eigenvectors. The analytical procedure described in [Example 5.7](#) is applied to the equations of motion for the A-7A. With the aid of MATLAB the eigenvector matrix \mathbf{V} is determined as follows:

$$\mathbf{V} = \begin{bmatrix} & \text{short-period mode} & & \text{phugoid mode} \\ \begin{array}{cc|cc} -0.1682 - 0.1302j & -0.1682 + 0.1302j & 0.1467 + 0.9677j & 0.1467 - 0.9677j \\ 0.2993 + 0.9301j & 0.2993 - 0.9301j & 0.0410 + 0.2008j & 0.0410 - 0.2008j \\ -0.0046 + 0.0018j & -0.0046 - 0.0018j & 0.0001 + 0.0006j & 0.0001 - 0.0006j \\ 0.0019 + 0.0024j & 0.0019 - 0.0024j & 0.0041 - 0.0013j & 0.0041 + 0.0013j \end{array} \end{bmatrix} : \begin{array}{l} u \\ w \\ q \\ \theta \end{array} \quad (6.9)$$

To facilitate interpretation of the eigenvector matrix, the magnitude of each component eigenvector is calculated as follows:

$$\begin{bmatrix} 0.213 & 0.213 & 0.979 & 0.979 \\ 0.977 & 0.977 & 0.204 & 0.204 \\ 0.0049 & 0.0049 & 0.0006 & 0.0006 \\ 0.0036 & 0.0036 & 0.0043 & 0.0043 \end{bmatrix} : \begin{array}{l} u \\ w \\ q \\ \theta \end{array}$$

The phugoid mode is clearly dominant in u since $0.979 \gg 0.213$; the short-period mode is dominant in w since $0.977 \gg 0.204$; the short-period mode is dominant in q since $0.0049 \gg 0.0006$; and the contents of the short-period and phugoid modes in θ are of similar order. These observations accord very well with the responses shown in [Fig. 6.1](#).

The steady-state values of the variables following a unit step (1°) elevator input may be determined by application of the final value theorem, [equation \(5.33\)](#). The transfer functions, [equations \(6.8\)](#), assume a unit elevator displacement to mean 1 rad, and this has transfer function

$$\eta(s) = \frac{1}{s} \text{rad}$$

For a unit step input of 1° the transfer function becomes

$$\eta(s) = \frac{1}{57.3s} = \frac{0.0175}{s} \text{rad}$$

Thus, for example, the Laplace transform of the speed response to a 1° elevator step input is given by

$$u(s) = \frac{5.63(s + 0.369)(s + 0.587)(s + 58.437)}{(s^2 + 0.033s + 0.020)(s^2 + 0.902s + 2.666)} \frac{0.0175}{s} \text{ ft/s}$$

Applying the final value theorem, equation (5.33),

$$u(t)|_{ss} = \lim_{s \rightarrow 0} \left(s \frac{5.63(s + 0.369)(s + 0.587)(s + 58.437)}{(s^2 + 0.033s + 0.020)(s^2 + 0.902s + 2.666)} \frac{0.0175}{s} \right) \text{ ft/s} = 23.39 \text{ ft/s}$$

Since the step input is positive in the nose-down sense, the response eventually settles to the small steady increase in speed indicated.

In a similar way the steady-state response of all the motion variables may be calculated to give

$$\begin{bmatrix} u \\ w \\ q \\ \theta \\ \alpha \\ \gamma \end{bmatrix}_{\text{steady state}} = \begin{bmatrix} 23.39 \text{ ft/s} \\ -4.53 \text{ ft/s} \\ 0 \\ 0.34^\circ \\ -0.81^\circ \\ 1.15^\circ \end{bmatrix} \quad (6.10)$$

It is important to remember that the steady-state values given in [equation \(6.10\)](#) represent the *changes* with respect to the initial equilibrium trim state following the 1° elevator step input. Although the initial response is applied in the nose-down sense, inspection of [equation \(6.10\)](#) indicates that after the mode transients have damped out, the aircraft is left with a small reduction in incidence and a small increase in pitch attitude, and is climbing steadily at a flight path angle of 1.15° . This apparent anomaly is due to the fact that at the chosen flight condition the aircraft is operating close to the stall boundary on the *back side* of the drag speed curve—that is, below the minimum drag speed. Thus the disturbance results in a significant decrease in drag, leaving the aircraft with sufficient excess power to climb gently. It is for the same reason that a number of the transfer functions, [equations \(6.8\)](#), have non-minimum phase numerator terms where these would not normally be expected.

6.1.1 The characteristic equation

The longitudinal characteristic polynomial for a classical aeroplane is fourth order; it determines the common denominator in the longitudinal response transfer functions and, when equated to zero, defines the characteristic equation, which may be written as

$$As^4 + Bs^3 + Cs^2 + Ds + E = 0 \quad (6.11)$$

The characteristic [equation \(6.11\)](#) most commonly factorises into two pairs of complex roots, which are most conveniently written as

$$(s^2 + 2\zeta_p\omega_ps + \omega_p^2)(s^2 + 2\zeta_s\omega_ss + \omega_s^2) = 0 \quad (6.12)$$

As already explained, the second-order characteristics in [equation \(6.12\)](#) describe the phugoid and short-period stability modes, respectively. The stability modes that make up [equation \(6.12\)](#) provide a *complete description* of the longitudinal stability properties of the aeroplane subject to the constraint of small-perturbation motion. Interpretation of the characteristic equation written in

this way is most readily accomplished if reference is first made to the properties of the classical mechanical mass-spring-damper system, which are summarised in Appendix 6.

Thus the longitudinal dynamics of the aeroplane may be likened to a pair of loosely coupled mass-spring-damper systems, and the interpretation of the motion of the aeroplane following a disturbance from equilibrium may be made by direct comparison with the behaviour of the mechanical mass-spring-damper. However, the damping and frequency characteristics of the aeroplane are obviously not mechanical in origin; they derive entirely from the aerodynamic properties of the airframe. The connection between the observed dynamics of the aeroplane and its aerodynamic characteristics is made by comparing [equation \(6.12\)](#) with [equation \(6.11\)](#) and then referring to Appendix 3 for the definitions of the coefficients in [equation \(6.11\)](#) in terms of aerodynamic stability derivatives. Clearly, the relationships between the damping ratios and the undamped frequencies of [equation \(6.12\)](#), and their aerodynamic *drivers*, are neither obvious nor simple. Means for dealing with this difficulty are described in the following sections; simplifying approximations are made based on the observation and understanding of the physical behaviour of aeroplane dynamics.

6.2 The dynamic stability modes

Both longitudinal dynamic stability modes are excited whenever the aeroplane is disturbed from its equilibrium trim state. A disturbance may be initiated by pilot control inputs, by a change in power setting, by airframe configuration changes, such as flap deployment, and by external atmospheric influences such as gusts and turbulence.

6.2.1 The short-period pitching oscillation

The short-period mode is typically a damped oscillation in pitch about the oy axis. Whenever an aircraft is disturbed from its pitch equilibrium state, the mode is excited and manifests itself as a classical second-order oscillation in which the principal variables are incidence $\alpha(w)$, pitch rate q , and pitch attitude θ . This observation is easily confirmed by reference to the eigenvectors in the solution of the equations of motion; it may be seen in Example 6.1 and in [Fig. 6.1](#). Typically, the undamped natural frequency of the mode is in the range 1 rad/s to 10 rad/s, and the damping is usually stabilizing, although the damping ratio is often lower than desired. A significant feature of the mode is that the speed remains approximately constant ($u = 0$) during a disturbance. As the period of the mode is short, inertia and momentum effects ensure that speed response in the time scale of the mode is negligible.

The physical situation applying can be interpreted by comparison with a torsional mass-spring-damper system. The aircraft behaves as if it were restrained by a torsional spring about the oy axis, as indicated in [Fig. 6.2](#). A pitch disturbance from trim equilibrium causes the “spring” to produce a restoring moment, thereby giving rise to an oscillation in pitch. The oscillation is damped and this can be interpreted as a viscous damper as suggested in [Fig. 6.2](#). Of course, the spring and viscous damping effects are not mechanical. In reality, they are produced entirely by aerodynamic mechanisms with contributions from all parts of the airframe, not all of which are necessarily stabilising. However, in the interests of promoting understanding, the stiffness and damping effects are assumed to be dominated by the aerodynamics of the tailplane. The spring stiffness arises from the

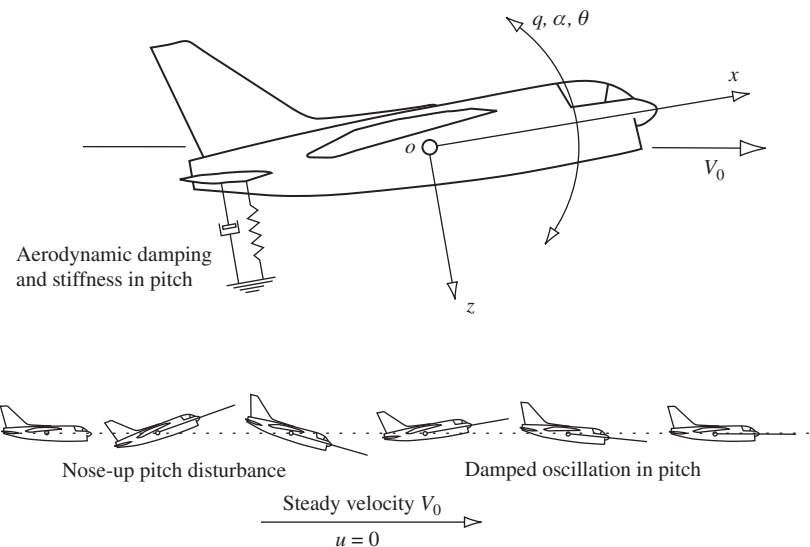


FIGURE 6.2 Stable short-period pitching oscillation.

natural *weathercock* tendency of the tailplane to align with the incident flow. The damping arises from the motion of the tailplane during the oscillation when, clearly, it behaves as a kind of viscous paddle damper. The total observed mode dynamics depend not only on the tailplane contribution but also on the magnitudes of the additional contributions from other parts of the airframe. When the overall stability is marginal, it is implied that the additional contributions are significant, which makes it much more difficult to identify and quantify the principal aerodynamic mode drivers.

6.2.2 The phugoid

The phugoid mode is most commonly a lightly damped low-frequency oscillation in speed u , which couples into pitch attitude θ and height h . A significant feature of this mode is that the incidence $\alpha(w)$ remains substantially constant during a disturbance. Again, these observations are easily confirmed by reference to the eigenvectors in the solution of the equations of motion, which may be seen in Example 6.1 and in Fig. 6.1. However, it is clear that the phugoid appears, to a greater or lesser extent, in all of the longitudinal motion variables; however, the relative magnitudes of the phugoid components in incidence $\alpha(w)$ and in pitch rate q are very small. Typically, the undamped natural frequency of the phugoid is in the range 0.1 rad/s to 1 rad/s and the damping ratio is very low. However, the apparent damping characteristics of the mode may be substantially influenced by power effects in some aeroplanes.

Consider the development of classical phugoid motion following a small disturbance in speed, as illustrated in Fig. 6.3. Initially the aeroplane is in trimmed level equilibrium flight with steady velocity V_0 such that lift L and weight mg are equal. Let the aeroplane be disturbed (Fig 6.3a) such

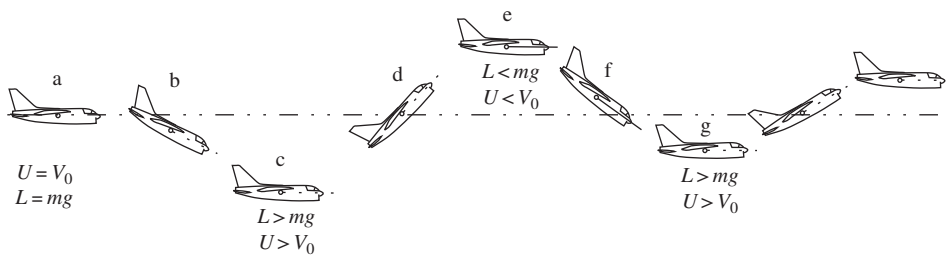


FIGURE 6.3 Development of a stable phugoid.

that the velocity is reduced by a small amount u . Since the incidence remains substantially constant, this results in a small reduction in lift such that the aeroplane is no longer in vertical equilibrium. It therefore starts to lose height and, since it is flying “downhill,” starts to accelerate (Fig. 6.3b). The speed continues to build up to a value in excess of V_0 , which is accompanied by a build up in lift which eventually exceeds the weight by a significant margin. The build up in speed and lift causes the aircraft to pitch up steadily until it starts to climb (Fig. 6.3c). Since it now has an excess of kinetic energy, inertia and momentum effects cause it to fly up through the nominal trimmed height datum (Fig. 6.3d), losing speed and lift as it goes because it is now flying “uphill.” As it decelerates it pitches down steadily until its lift is significantly less than the weight and the accelerating descent starts again (Fig. 6.3e). Inertia and momentum effects cause the aeroplane to continue flying down through the nominal trimmed height datum (Fig. 6.3f), and, as speed and lift continue to build up, it pitches up steadily until it starts climbing again to commence the next cycle of oscillation (Fig. 6.3g). As the motion progresses the effects of drag cause the motion variable maxima and minima at each peak to reduce gradually in magnitude until the motion eventually damps out.

Thus the phugoid is classical damped harmonic motion resulting in the aircraft flying a gentle sinusoidal flight path about the nominal trimmed height datum. As large inertia and momentum effects are involved, the motion is necessarily relatively slow such that the angular accelerations, \dot{q} and $\dot{\alpha}(w)$, are insignificantly small. Consequently, the natural frequency of the mode is low and, since drag is designed to be low, the damping is also low. Typically, once excited, many cycles of the phugoid may be visible before it eventually damps out. Since the rate of energy loss is low, a consequence of low drag damping effects, the motion is often approximated by undamped harmonic motion, in which potential and kinetic energy are exchanged as the aircraft flies the sinusoidal flight path. This in fact was the basis on which [Lanchester \(1908\)](#) first successfully analysed the motion.

6.3 Reduced-order models

Thus far the emphasis has been on the exact solution of the longitudinal equations of motion which results in an exact description of the stability and response characteristics of the aircraft. Although this is usually the object of a flight dynamics investigation, it has two disadvantages. First, a computational facility is required if a very tedious manual solution is to be avoided; second, it is

difficult, if not impossible, to establish the relationships between the stability characteristics and their aerodynamic drivers. Both of these disadvantages can be avoided by seeking approximate solutions, which can also provide considerable insight into the physical phenomena governing the dynamic behaviour of the aircraft.

For example, an approximate solution of the longitudinal characteristic [equation, \(6.11\)](#), is based on the fact that the coefficients A , B , C , D , and E have relative values which do not change very much for conventional aeroplanes. Generally A , B , and C are significantly larger than D and E such that the quartic has the following approximate factors:

$$A \left(s^2 + \frac{(CD - BE)}{C^2} s + \frac{E}{C} \right) \left(s^2 + \frac{B}{A} s + \frac{C}{A} \right) = 0 \quad (6.13)$$

[Equation \(6.13\)](#) is in fact the first step in the classical manual iterative solution of the quartic; the first pair of complex roots describes the phugoid mode, and the second pair describes the short-period mode. Algebraic expressions, in terms of aerodynamic derivatives, mass and inertia parameters, etc. for the coefficients A , B , C , D , and E are given in [Appendix 3](#). Since these expressions are relatively complex, further physical insight is not particularly revealing unless simplifying assumptions are made. However, the approximate solution given by [equation \(6.13\)](#) is often useful for preliminary mode evaluations, or as a check of computer solutions, when the numerical values of the coefficients A , B , C , D , and E are known. For conventional aeroplanes the approximate solution is often surprisingly close to the exact solution of the characteristic equation.

6.3.1 The short-period mode approximation

The short-term response characteristics of an aircraft are of particular importance in consideration of flying and handling qualities for the reasons discussed in [Section 6.5](#). Since short-term behaviour is dominated by the short-period mode, it is convenient to obtain the *reduced-order* equations of motion in which the phugoid is suppressed or omitted. By observing the nature of the short-period pitching oscillation, sometimes called *rapid incidence adjustment*, it is possible to simplify the longitudinal equations of motion to describe short-term dynamics only. The terms remaining in the reduced-order equations of motion are therefore the terms which dominate short-term dynamics, thereby providing insight into the important aerodynamic drivers governing physical behaviour.

It has already been established that the short-period pitching oscillation is almost exclusively an oscillation in which the principal variables are pitch rate q and incidence α , with the speed remaining essentially constant; thus $u = 0$. Therefore, the speed equation and the speed-dependent terms may be removed from the longitudinal equations of motion, (6.1); since they are all approximately zero in short-term motion, the revised equations may be written as

$$\begin{bmatrix} \dot{w} \\ \dot{q} \\ \dot{\theta} \end{bmatrix} = \begin{bmatrix} z_w & z_q & z_\theta \\ m_w & m_q & m_\theta \\ 0 & 1 & 0 \end{bmatrix} \begin{bmatrix} w \\ q \\ \theta \end{bmatrix} + \begin{bmatrix} z_\eta \\ m_\eta \\ 0 \end{bmatrix} \eta \quad (6.14)$$

Further, assuming that the equations of motion are referred to aircraft wind axes and that the aircraft is initially in steady level flight, then

$$\theta_e \equiv \alpha_e = 0 \quad \text{and} \quad U_e = V_0$$

and, with reference to Appendix 2, it follows that

$$z_\theta = m_\theta = 0$$

Equation (6.14) then reduces to its simplest possible form:

$$\begin{bmatrix} \dot{w} \\ \dot{q} \end{bmatrix} = \begin{bmatrix} z_w & z_q \\ m_w & m_q \end{bmatrix} \begin{bmatrix} w \\ q \end{bmatrix} + \begin{bmatrix} z_\eta \\ m_\eta \end{bmatrix} \eta \quad (6.15)$$

where now the derivatives are referred to a wind axes system. Equation (6.15) is sufficiently simple that the transfer function matrix may be calculated manually by the application of equation (5.53):

$$\mathbf{G}(s) = \frac{\mathbf{N}(s)}{\Delta(s)} = \frac{\begin{bmatrix} s - m_q & z_q \\ m_w & s - z_w \end{bmatrix} \begin{bmatrix} z_\eta \\ m_\eta \end{bmatrix}}{\begin{vmatrix} s - z_w & -z_q \\ -m_w & s - m_q \end{vmatrix}} = \frac{\begin{bmatrix} z_\eta \left(s + \left(m_q + z_w \frac{m_\eta}{z_\eta} \right) \right) \\ m_\eta \left(s + \left(m_w \frac{z_\eta}{m_\eta} - z_w \right) \right) \end{bmatrix}}{(s^2 - (m_q + z_w)s + (m_q z_w - m_w z_q))} \quad (6.16)$$

The transfer functions may be further simplified by noting that

$$z_q \frac{m_\eta}{z_\eta} > > m_q \quad \text{and} \quad -z_w > > m_w \frac{z_\eta}{m_\eta}$$

and, with reference to Appendix 2,

$$z_q = \frac{\overset{\circ}{Z}_q + mU_e}{m - \overset{\circ}{Z}_{\dot{w}}} \cong U_e$$

since

$$\overset{\circ}{Z}_q < < mU_e \quad \text{and} \quad m > > \overset{\circ}{Z}_{\dot{w}}$$

Thus the two short-term transfer functions describing response to elevator may be written as

$$\frac{w(s)}{\eta(s)} = \frac{z_\eta \left(s + U_e \frac{m_\eta}{z_\eta} \right)}{(s^2 - (m_q + z_w)s + (m_q z_w - m_w U_e))} \equiv \frac{k_w (s + 1/T_\alpha)}{(s^2 + 2\zeta_s \omega_s s + \omega_s^2)} \quad (6.17)$$

$$\frac{q(s)}{\eta(s)} = \frac{m_\eta (s - z_w)}{(s^2 - (m_q + z_w)s + (m_q z_w - m_w U_e))} \equiv \frac{k_q (s + 1/T_{\theta_2})}{(s^2 + 2\zeta_s \omega_s s + \omega_s^2)} \quad (6.18)$$

where now it is understood that $k_w, k_q, T_\alpha, T_{\theta_2}, \zeta_s$, and ω_s represent approximate values. Clearly, it is now very much easier to relate the most important parameters describing the aircraft's longitudinal short-term transient dynamics to the aerodynamic properties of the airframe, represented in equations (6.17) and (6.18) by the concise derivatives.

The reduced-order characteristic equation may be written on inspection of [equation \(6.17\)](#) or [\(6.18\)](#) as

$$\Delta(s) = s^2 + 2\zeta_s \omega_s s + \omega_s^2 = s^2 - (m_q + z_w)s + (m_q z_w - m_w U_e) = 0 \quad (6.19)$$

and, by analogy with the classical mass-spring-damper system described in Appendix 6, the damping and natural frequency of the short-period mode are given, to a good approximation, by

$$\begin{aligned} 2\zeta_s \omega_s &= -(m_q + z_w) \\ \omega_s &= \sqrt{m_q z_w - m_w U_e} \end{aligned} \quad (6.20)$$

It is instructive to write the damping and natural frequency expressions (6.20) in terms of the dimensional derivatives. The appropriate conversions are obtained from Appendix 2, and the assumptions made previously are applied to give

$$\begin{aligned} 2\zeta_s \omega_s &= -\left(\frac{\dot{M}_q}{I_y} + \frac{\dot{Z}_w}{m} + \frac{\dot{M}_w U_e}{I_y}\right) \\ \omega_s &= \sqrt{\frac{\dot{M}_q \dot{Z}_w}{I_y m} - \frac{\dot{M}_w \dot{U}_e}{I_y}} \end{aligned} \quad (6.21)$$

Note that the terms on the right-hand side of expressions (6.21) comprise aerodynamic derivatives divided either by mass or by moment of inertia in pitch. These terms may be interpreted in exactly the same way as those of the classical mass-spring-damper, so it becomes apparent that the aerodynamic derivatives are providing stiffness and viscous damping in pitch, although there is more than one term contributing to damping and to natural frequency. Therefore, the aerodynamic origins of the short-period dynamics are a little more complex than those of the classical mass-spring-damper, and the various contributions do not always act in the most advantageous way. However, for conventional aeroplanes the overall dynamic characteristics usually describe a stable short-period mode.

For a typical conventional aeroplane, the relative magnitudes of the aerodynamic derivatives are such that, to a crude approximation,

$$\begin{aligned} 2\zeta_s \omega_s &= \frac{-\dot{M}_q}{I_y} \\ \omega_s &= \sqrt{\frac{-\dot{M}_w \dot{U}_e}{I_y}} \end{aligned} \quad (6.22)$$

which serves only to indicate what are usually regarded as the dominant terms governing the short-period mode. Normally, the derivative \dot{Z}_w , which is dependent on the lift curve slope of the wing, and the derivative \dot{M}_q , which is determined largely by the viscous “paddle” damping properties of the tailplane, are both negative numbers. The derivative \dot{M}_w is a measure of the aerodynamic stiffness in pitch and is also dominated by the aerodynamics of the tailplane. The sign of \dot{M}_w depends on the position of the *cg*, becoming increasingly negative as the *cg* moves forward in the airframe. Thus the short-period mode is stable if the *cg* is far enough forward in the airframe. The *cg* position

in the airframe where \dot{M}_w changes sign is called the *controls-fixed neutral point*; \dot{M}_w is therefore also a measure of the *controls-fixed stability margin* of the aircraft. With reference to [equation \(6.19\)](#) and expressions (6.20), the corresponding *cg* position where $(m_q z_w - m_w U_e)$ changes sign is called the *controls-fixed manoeuvre point* and $(m_q z_w - m_w U_e)$ is a measure of the *controls-fixed manoeuvre margin* of the aircraft. The subject of manoeuvrability is discussed in Chapter 8.

6.3.2 The phugoid mode approximation

A reduced-order model of the aircraft retaining only the phugoid dynamics is very rarely required in flight dynamics studies. However, the greatest usefulness of such a model is to identify the aerodynamic properties of the airframe that govern the characteristics of the mode.

The Lanchester model

Probably the first successful analysis of aeroplane dynamics was carried out by [Lanchester \(1908\)](#), who devised a mathematical model to describe phugoid motion based on his observations of the behaviour of gliding model aeroplanes. His analysis gives an excellent insight into the physical nature of the mode and may be applied to modern aeroplanes by interpreting and restating his original assumptions as follows:

- The aircraft is initially in steady level flight.
- The total energy of the aircraft remains constant.
- The incidence α remains constant at its initial trim value.
- The thrust τ balances the drag D .
- The motion is sufficiently slow that pitch rate q effects may be ignored.

Referring to [Fig. 6.4](#), the aircraft is initially in trimmed straight level flight with velocity V_0 . Following a disturbance in speed which excites the phugoid mode, the disturbed speed, pitch

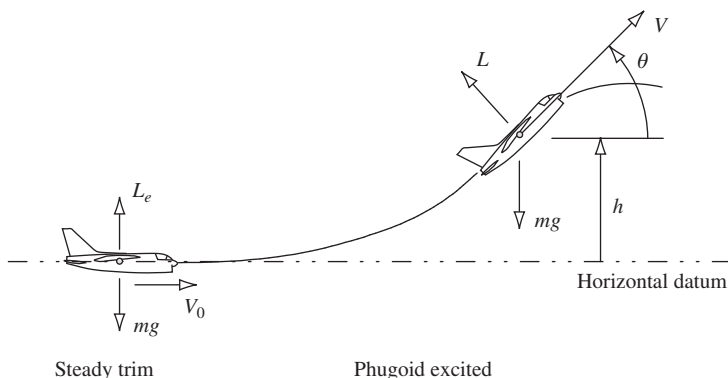


FIGURE 6.4 Phugoid oscillation.

attitude, and height are denoted V , θ , and h , respectively. Then, based on Lanchester's second assumption,

$$\frac{1}{2}mV_0^2 = \frac{1}{2}mV^2 + mgh = \text{constant}$$

whence

$$V^2 = V_0^2 - 2gh \quad (6.23)$$

which describes the exchange of kinetic and potential energy as the aeroplane flies the sinusoidal flight path.

In the initial steady trim state, the lift and weight are in balance; thus

$$L_e = \frac{1}{2}\rho V_0^2 SC_L = mg \quad (6.24)$$

and in disturbed flight the lift is given by

$$L = \frac{1}{2}\rho V^2 SC_L \quad (6.25)$$

As a consequence of Lanchester's third assumption, the lift coefficient C_L also remains constant and [equations \(6.23\), \(6.24\), and \(6.25\)](#) may be combined to give

$$L = mg - \rho gh SC_L \quad (6.26)$$

Since simple undamped oscillatory motion is assumed as a consequence of Lanchester's second assumption, the single degree of freedom equation of motion in height may be written as

$$\ddot{m}h = L \cos \theta - mg \cong L - mg \quad (6.27)$$

since, by definition, θ is a small angle. Substituting for lift L from [equation \(6.26\)](#) into [equation \(6.27\)](#),

$$\ddot{h} + \left(\frac{\rho g SC_L}{m} \right) h = \ddot{h} + \omega_p^2 h = 0 \quad (6.28)$$

Thus the frequency of the phugoid mode is given approximately by

$$\omega_p = \sqrt{\frac{\rho g SC_L}{m}} = \frac{g\sqrt{2}}{V_0} \quad (6.29)$$

when [equation \(6.24\)](#) is used to eliminate the mass.

To a reasonable approximation, then, Lanchester's model shows that the phugoid frequency is inversely proportional to the steady trimmed speed about which the mode oscillates and that its damping is zero.

A reduced-order model

A more detailed approximate model of the phugoid mode may be derived from the equations of motion by making simplifications based on assumptions about the nature of the motion. Following

a disturbance, the variables $w(\alpha)$ and q respond in the time scale associated with the short-period mode; thus it is reasonable to assume that $w(\alpha)$ and q are quasi-steady in the longer time scale associated with the phugoid. It follows that

$$\dot{w} = \dot{q} = 0$$

Once again, it is assumed that the equations of motion are referred to aircraft wind axes and, since the disturbance takes place about steady level flight,

$$\theta_e \equiv \alpha_e = 0 \quad \text{and} \quad U_e = V_0$$

With reference to Appendix 2, it follows that

$$x_\theta = -g \quad \text{and} \quad z_\theta = m_\theta = 0$$

As for the reduced-order short-period model and with reference to Appendix 2,

$$z_q = \frac{\overset{\circ}{Z}_q + mU_e}{m - \overset{\circ}{Z}_{\dot{w}}} \cong U_e$$

since

$$\overset{\circ}{Z}_q < < mU_e \quad \text{and} \quad m > > \overset{\circ}{Z}_{\dot{w}}$$

Additionally, it is usually assumed that the aerodynamic derivative x_q is insignificantly small. Thus the equations of motion (6.1) may be simplified accordingly:

$$\begin{bmatrix} \dot{u} \\ 0 \\ 0 \\ \dot{\theta} \end{bmatrix} = \begin{bmatrix} x_u & x_w & 0 & -g \\ z_u & z_w & U_e & 0 \\ m_u & m_w & m_q & 0 \\ 0 & 0 & 1 & 0 \end{bmatrix} \begin{bmatrix} u \\ w \\ q \\ \theta \end{bmatrix} + \begin{bmatrix} x_\eta \\ z_\eta \\ m_\eta \\ 0 \end{bmatrix} \eta \quad (6.30)$$

The second and third rows of equation (6.30) may be written as

$$\begin{aligned} z_u u + z_w w + U_e q + z_\eta \eta &= 0 \\ m_u u + m_w w + m_q q + m_\eta \eta &= 0 \end{aligned} \quad (6.31)$$

Equations (6.31) may be solved algebraically to obtain expressions for w and q in terms of u and η :

$$\begin{aligned} w &= \left(\frac{m_u U_e - m_q z_u}{m_q z_w - m_w U_e} \right) u + \left(\frac{m_\eta U_e - m_q z_\eta}{m_q z_w - m_w U_e} \right) \eta \\ q &= \left(\frac{m_w z_u - m_u z_w}{m_q z_w - m_w U_e} \right) u + \left(\frac{m_w z_\eta - m_\eta z_w}{m_q z_w - m_w U_e} \right) \eta \end{aligned} \quad (6.32)$$

The expressions for w and q are substituted into rows 1 and 4 of equation (6.30) and after some rearrangement, the reduced-order state equation is obtained:

$$\begin{bmatrix} \dot{u} \\ \dot{\theta} \end{bmatrix} = \begin{bmatrix} x_u - x_w \left(\frac{m_u U_e - m_q z_u}{m_w U_e - m_q z_w} \right) & -g \\ \left(\frac{m_u z_w - m_w z_u}{m_w U_e - m_q z_w} \right) & 0 \end{bmatrix} \begin{bmatrix} u \\ \theta \end{bmatrix} + \begin{bmatrix} x_\eta - x_w \left(\frac{m_\eta U_e - m_q z_\eta}{m_w U_e - m_q z_w} \right) \\ \left(\frac{m_\eta z_w - m_w z_\eta}{m_w U_e - m_q z_w} \right) \end{bmatrix} \eta \quad (6.33)$$

or

$$\dot{\mathbf{x}} = \mathbf{A}_p \mathbf{x} + \mathbf{B}_p \mathbf{u} \quad (6.34)$$

Equation (6.33) may be solved algebraically to obtain the response transfer functions for the phugoid variables u and θ . However, it is not very meaningful to analyse long-term dynamic response to elevator in this way. The characteristic equation describing the reduced-order phugoid dynamics is considerably more useful and is given by

$$\Delta(s) = \det[s\mathbf{I} - \mathbf{A}_p] = 0$$

whence

$$\begin{aligned} \Delta(s) &= s^2 + 2\zeta_p \omega_p s + \omega_p^2 \\ &= s^2 - \left(x_u - x_w \left(\frac{m_u U_e - m_q z_u}{m_w U_e - m_q z_w} \right) \right) s + g \left(\frac{m_u z_w - m_w z_u}{m_w U_e - m_q z_w} \right) \end{aligned} \quad (6.35)$$

Thus the approximate damping and natural frequency of the phugoid mode are given in terms of a limited number of aerodynamic derivatives. More explicit, but rather more approximate, insight into the aerodynamic properties of the aeroplane that dominate the mode characteristics may be obtained by making some further assumptions. Typically, for conventional aeroplanes in subsonic flight,

$$m_u \rightarrow 0, \quad |m_u z_w| < < |m_w z_u| \quad \text{and} \quad |m_w U_e| > > |m_q z_w|$$

then the corresponding expressions for the damping and natural frequency become

$$\begin{aligned} 2\zeta_p \omega_p &= -x_u \\ \omega_p &= \sqrt{\frac{-g z_u}{U_e}} \end{aligned} \quad (6.36)$$

Now, with reference to Appendix 2,

$$x_u \underset{\text{def}}{\cong} \frac{\overset{\circ}{X_u}}{m} = \frac{\rho V_0 S X_u}{2m} \quad \text{and} \quad z_u \underset{\text{def}}{\cong} \frac{\overset{\circ}{Z_u}}{m} = \frac{\rho V_0 S Z_u}{2m} \quad (6.37)$$

since $\overset{\circ}{X_w}$ is negligibly small and $m > > \overset{\circ}{Z_w}$. Expressions for the dimensionless aerodynamic derivatives are given in Appendix 8 and may be approximated as shown in expressions (6.38) when the

basic aerodynamic properties are assumed to be independent of speed. This follows from the assumption that the prevailing flight condition is subsonic such that the aerodynamic properties of the airframe are not influenced by compressibility effects:

$$\begin{aligned} X_u &= -2C_D - V_0 \frac{\partial C_D}{\partial V} + \left(\frac{1}{\frac{1}{2}\rho V_0 S} \right) \frac{\partial \tau}{\partial V} \cong -2C_D \\ Z_u &= -2C_L - V_0 \frac{\partial C_L}{\partial V} \cong -2C_L \end{aligned} \quad (6.38)$$

Expressions (6.36) may therefore be restated in terms of aerodynamic parameters, assuming again that the trimmed lift is equal to the aircraft weight:

$$\begin{aligned} \zeta_p \omega_p &= \frac{g C_D}{C_L V_0} \\ \omega_p &= \sqrt{\frac{2g^2}{U_e V_0}} \equiv \frac{g\sqrt{2}}{V_0} \end{aligned} \quad (6.39)$$

A simplified approximate expression for the damping ratio follows:

$$\zeta_p \cong \frac{1}{\sqrt{2}} \left(\frac{C_D}{C_L} \right) \quad (6.40)$$

The expressions for damping ratio and natural frequency of the phugoid mode are obviously very approximate because they are the result of many simplifying assumptions. Note that the expression for ω_p is the same as that derived by Lanchester, [equation \(6.29\)](#), which indicates that the natural frequency of the phugoid mode is approximately inversely proportional to the trimmed speed. It is also interesting and important to note that the damping ratio of the phugoid mode is approximately inversely proportional to the *lift-to-drag ratio* of the aeroplane, [equation \(6.40\)](#). Since one of the main objectives of aeroplane design is to achieve a high lift-to-drag ratio it is easy to see why the damping of the phugoid mode is usually very low.

EXAMPLE 6.2

To illustrate the use of reduced-order models, consider the A-7A Corsair II aircraft of Example 6.1, at the same flight condition as in that example. Now the equations of motion in Example 6.1 are referred to a body axis system, and the use of the reduced-order models described previously requires the equations of motion referred to a wind, or stability, axis system. Using the axis transformation relationships given in Appendices 9 and 10, the stability and control derivatives and

inertia parameters referred to wind axes were calculated from the original values, which of course refer to body axes. The longitudinal state equation was then recalculated to give

$$\begin{bmatrix} \dot{u} \\ \dot{w} \\ \dot{q} \\ \dot{\theta} \end{bmatrix} = \begin{bmatrix} -0.04225 & -0.11421 & 0 & -32.2 \\ -0.20455 & -0.49774 & 317.48 & 0 \\ 0.00003 & -0.00790 & -0.39499 & 0 \\ 0 & 0 & 1 & 0 \end{bmatrix} \begin{bmatrix} u \\ w \\ q \\ \theta \end{bmatrix} + \begin{bmatrix} 0.00381 \\ -24.4568 \\ -4.51576 \\ 0 \end{bmatrix} \eta \quad (6.41)$$

The reduced-order model corresponding to the short-period approximation, as given by [equation \(6.15\)](#), is simply taken out of [equation \(6.41\)](#) and written as

$$\begin{bmatrix} \dot{w} \\ \dot{q} \end{bmatrix} = \begin{bmatrix} -0.49774 & 317.48 \\ -0.00790 & -0.39499 \end{bmatrix} \begin{bmatrix} w \\ q \end{bmatrix} + \begin{bmatrix} -24.4568 \\ -4.51576 \end{bmatrix} \eta \quad (6.42)$$

Solution of the equations of motion (6.42) using Program CC determines the following reduced-order response transfer functions:

$$\begin{aligned} \frac{w(s)}{\eta(s)} &= \frac{-24.457(s + 59.015)}{(s^2 + 0.893s + 2.704)} \text{ ft/s/rad} \\ \frac{q(s)}{\eta(s)} &= \frac{-4.516(s + 0.455)}{(s^2 + 0.893s + 2.704)} \text{ rad/s/rad (deg/s/deg)} \\ \frac{\alpha(s)}{\eta(s)} &= \frac{-0.077(s + 59.015)}{(s^2 + 0.893s + 2.704)} \text{ rad/rad (deg/deg)} \end{aligned} \quad (6.43)$$

It is important to remember that these transfer functions describe, approximately, the short-term response of those variables which are dominant in short-period motion. The corresponding short-term pitch attitude response transfer function follows since, for small-perturbation motion,

$$\frac{\theta(s)}{\eta(s)} = \frac{1}{s} \frac{q(s)}{\eta(s)} = \frac{-4.516(s + 0.455)}{s(s^2 + 0.893s + 2.704)} \text{ rad/rad (deg/deg)} \quad (6.44)$$

From the pitch rate response transfer function in [equations \(6.43\)](#), it is readily determined that the steady-state pitch rate following a positive unit step elevator input is -0.76 rad/s , which implies that the aircraft pitches continuously until the input is removed. The pitch attitude response transfer function confirms this because, after the short-period transient has damped out, the aircraft behaves like a perfect integrator in pitch. This is indicated by the presence of the s term in the denominator of [equation \(6.44\)](#). In reality, the phugoid dynamics usually prevent this situation unless the input is very large and accompanied by a thrust increase which results in a vertical loop manoeuvre. The model described here would be most inappropriate for the analysis of such large-amplitude motion.

The common denominator of transfer functions (6.43) represents the approximate reduced-order short-period characteristic polynomial, [equation \(6.19\)](#). Thus approximate values of the damping ratio and undamped natural frequency of the short-period mode are easily calculated:

$$\text{Damping ratio } \zeta_s = 0.27$$

$$\text{Undamped natural frequency } \omega_s = 1.64 \text{ rad/s}$$

It will be seen that these values compare very favourably with the exact values given in Example 6.1.

Interpretation of the reduced-order model is probably best illustrated by observing short-term response to an elevator input. The responses to a 1° elevator step input of the variables given in [equations \(6.43\)](#) are shown in [Fig. 6.5](#). Also shown in the same plots are the corresponding responses of the full aircraft model derived from [equation \(6.41\)](#). It is clear that the responses diverge with time, as expected, as no phugoid dynamics are present in the reduced-order model. However, for the first ten seconds or so the comparison is favourable, indicating that the reduced-order model is acceptable for most short-term response studies.

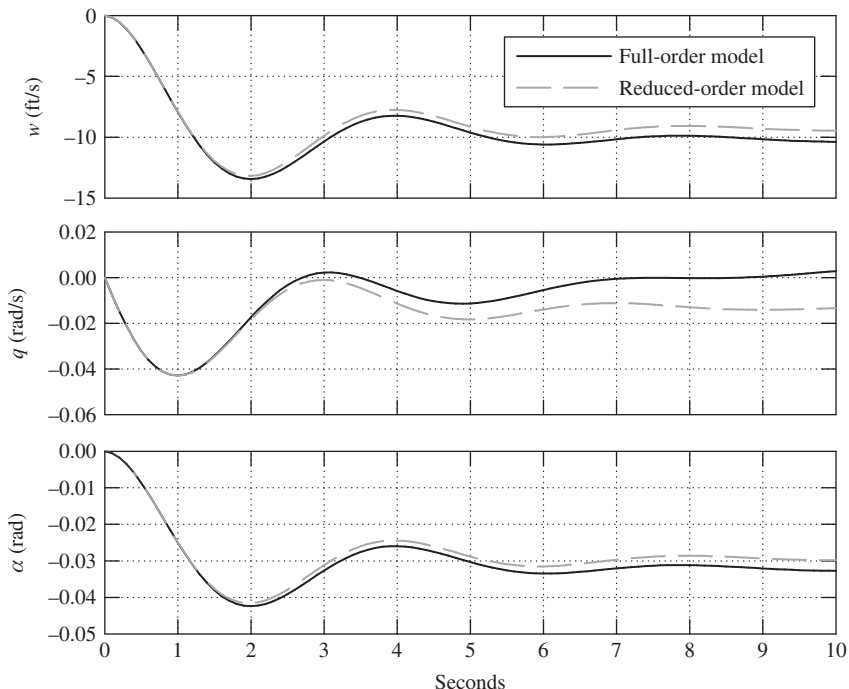


FIGURE 6.5 Reduced-order longitudinal response to a 1° elevator step input.

Turning now to the approximate reduced-order phugoid mode characteristics. From the state equation referred to wind axes, [equation \(6.41\)](#), the required numerical parameters are

$$\begin{aligned}x_u &= -0.04225 \text{ 1/s} \\z_u &= -0.20455 \text{ 1/s} \\m_u &= 0.00003 \text{ rad/ft s} \\U_e \equiv V_0 &= 317.48 \text{ ft/s}\end{aligned}$$

The simple Lanchester model determines that the damping of the phugoid is zero and that the undamped natural frequency is given by [equation \(6.29\)](#). Thus the approximate characteristics of the phugoid mode calculated according to this model are

Damping ratio $\zeta_p = 0$
Undamped natural frequency $\omega_p = 0.143 \text{ rad/s}$

The approximate phugoid mode characteristics determined according to the rather more detailed reduced-order model are given by [equation \(6.36\)](#). Since the chosen flight condition is genuinely subsonic, the derivative m_u is very small indeed, which matches the constraints of the model well. The approximate characteristics of the phugoid mode calculated according to this model are

Damping ratio $\zeta_p = 0.147$
Undamped natural frequency $\omega_p = 0.144 \text{ rad/s}$

Again, comparing these approximate values of the phugoid mode characteristics with the exact values in Example 6.1 indicates good agreement, especially for the undamped natural frequency. Since the phugoid damping ratio is always small (near zero), it is very sensitive to computational rounding errors and to the approximating assumptions, which makes a really good approximate match difficult to achieve. The goodness of the match here is enhanced by the very subsonic flight condition which correlates well with assumptions made in the derivation of the approximate models.

6.4 Frequency response

For the vast majority of flight dynamics investigations, time domain analysis is usually adequate, especially when the subject is the classical unaugmented aeroplane. The principal graphical tool used in time domain analysis is, of course, the time history plot showing the response of the aeroplane to controls or to some external disturbance. However, when the subject aeroplane is an advanced modern aircraft fitted with a flight control system, flight dynamics analysis in the frequency domain can provide additional valuable insight into its behaviour. In recent years frequency domain analysis has made an important contribution to the understanding of the sometimes unconventional handling qualities of aeroplanes whose flying qualities are largely shaped by a flight control system. It is for this reason that a brief review of simple frequency response concepts is considered here. Because frequency response analysis tools are fundamental to classical control

engineering, their description can be found in almost every book on the subject. Very accessible material can be found in [Shinners \(1980\)](#) and [Friedland \(1987\)](#), for example.

Consider the hypothetical situation in which the elevator of an otherwise trimmed aeroplane is operated sinusoidally with constant amplitude k and variable frequency ω . The longitudinal input to the aeroplane may therefore be expressed as

$$\eta(t) = k \sin \omega t \quad (6.45)$$

It is reasonable to expect that each of the output variables describing aircraft motion will respond sinusoidally to the input. However, the amplitudes of the output variables will not necessarily be the same, and they will not necessarily be in phase with one another or with the input. Thus the general expression describing any output response variable may be written as

$$y(t) = K \sin(\omega t + \phi) \quad (6.46)$$

where both output amplitude K and phase shift ϕ are functions of excitation frequency ω . As excitation frequency ω is increased from zero so, initially, at low frequencies, the sinusoidal response is clearly visible in all output variables. As it is increased further, the sinusoidal response starts to diminish in magnitude and eventually becomes imperceptible in the outputs. Simultaneously, phase shift ϕ indicates an increasingly large lag between input and output.

The reason for the observations just given is that, at sufficiently high frequencies, the mass and inertia properties of the aeroplane simply prevent it from responding quickly enough to follow the input. The limiting frequency at which the response commences to diminish rapidly is referred to as the *bandwidth* of the aeroplane with respect to the output variable of interest. A more precise definition of bandwidth is given later. Since aeroplanes respond only to frequencies below the bandwidth frequency, they have the frequency response properties of a *low-pass system*. At exciting frequencies corresponding to the damped natural frequencies of the phugoid and short-period modes, peaks in output magnitude K are seen together, with significant changes in phase shift ϕ . The mode frequencies are described as *resonant*, and the magnitudes of the output parameters K and ϕ at *resonance* are determined by the damping ratios of the modes. The system (or aeroplane) *gain* in any particular response variable is defined as

$$\text{System gain} = \left| \frac{K(\omega)}{k} \right| \quad (6.47)$$

where, in normal control system applications, it is usually assumed that the input and output variables have the same units. This is often not the case in aircraft applications, and care must be exercised in the interpretation of gain.

A number of graphical tools have been developed for the frequency response analysis of linear systems; these include the Nyquist diagram, the Nichols chart, and the Bode diagram. All are intended to simplify analytical procedures, the mathematical calculation of which is tedious without a computer, and all plot input-output gain and phase as functions of frequency. Perhaps the simplest of the graphical tools to use and interpret is the Bode diagram, although the information it is capable of providing is limited. Nevertheless, the Bode diagram is used extensively for flight dynamics analysis, especially in advanced studies of handling qualities.

6.4.1 The Bode diagram

The intention here is not to describe construction of a Bode diagram but to describe its application to the aeroplane and to explain its correct interpretation. For an explanation of Bode diagram construction, the reader should consult a suitable control engineering text, such as either of those referenced in the previous section.

To illustrate the application of the Bode diagram to a typical classical aeroplane, consider the pitch attitude response to elevator transfer function as given by [equation \(6.5\)](#):

$$\frac{\theta(s)}{\eta(s)} = \frac{k_\theta(s + 1/T_{\theta_1})(s + 1/T_{\theta_2})}{(s^2 + 2\zeta_p\omega_p s + \omega_p^2)(s^2 + 2\zeta_s\omega_s s + \omega_s^2)} \quad (6.48)$$

This function is of particular relevance to longitudinal handling studies and has the simplifying advantage that both input and output variables have the same units. In frequency response calculation it is usual to assume a sinusoidal input signal of unit magnitude. Also, it is important that, whenever the response transfer function is negative, which is often the case in aircraft applications, a negative input is assumed which ensures the correct computation of phase. Therefore, in this particular application, since k_θ is usually a negative number, a sinusoidal elevator input of unit magnitude, $\eta(t) = -1 \sin \omega t$ is assumed. The pitch attitude frequency response is calculated by writing $s = j\omega$ in [equation \(6.48\)](#); the right-hand side then becomes a complex number whose magnitude and phase can be evaluated for a suitable range of frequency ω . Since the input magnitude is unity, the *system gain*, [equation \(6.47\)](#), is given simply by the absolute value of the magnitude of the complex number representing the right-hand side of [equation \(6.48\)](#) and is, of course, a function of frequency ω .

Because the calculation of gain and phase involves the products of several complex numbers, it is preferred to work in terms of the logarithm of the complex number representing the transfer function. The total gain and phase then become the simple sums of the gain and phase of each transfer function factor. For example, each factor in parentheses on the right-hand side of [equation \(6.48\)](#) may have its gain and phase characteristics calculated separately as a function of frequency; total gain and phase are then given by summing the contributions from each factor. However, the system gain is now expressed as a logarithmic function of the gain ratio, [equation \(6.47\)](#), defined as

$$\text{Logarithmic Gain} = 20 \log_{10} \left| \frac{K(\omega)}{k} \right| \text{ dB} \quad (6.49)$$

with units of *decibels* (dB). Fortunately, it is no longer necessary to calculate frequency response by hand since many computer software packages, such as MATLAB, have this facility and can also provide the desired graphical output. However, some knowledge of the analytical procedure for obtaining frequency response is, as always, essential so that the computer output may be correctly interpreted.

The Bode diagram comprises the corresponding *gain plot* and *phase plot*. The gain plot shows the logarithmic gain (decibels), plotted against $\log_{10}(\omega)$, and the phase plot shows the phase (degrees), also plotted against $\log_{10}(\omega)$. To facilitate interpretation, the two plots are often superimposed on a common frequency axis. The Bode diagram showing the typical pitch attitude frequency response, as given by transfer function (6.48), is shown in [Fig. 6.6](#).

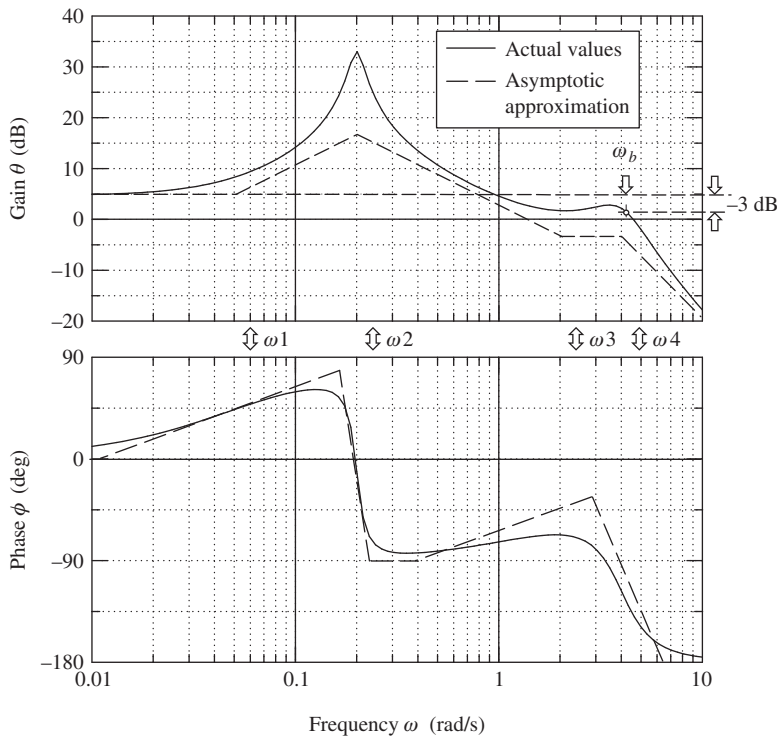


FIGURE 6.6 Bode diagram showing the classical pitch attitude frequency response.

Also shown in Fig. 6.6 are the asymptotic approximations to the actual gain and phase plots as functions of frequency. The asymptotes can be drawn in simply from inspection of the transfer function, equation (6.48), and serve as an aid to interpretation. Quite often the asymptotic approximation is sufficient for the evaluation in hand, thereby dispensing with the need to compute the actual frequency response entirely.

The shape of the gain plot is characterised by the *break frequencies* ω_1 to ω_4 , which determine the locations of the discontinuities in the asymptotic gain plot. Each break frequency is defined by a key frequency parameter in the transfer function:

$$\omega_1 = \frac{1}{T_{\theta 1}} \quad \text{with first-order phase lead } (+45^\circ)$$

$$\omega_2 = \omega_p \quad \text{with second-order phase lag } (-90^\circ)$$

$$\omega_3 = \frac{1}{T_{\theta 2}} \quad \text{with first-order phase lead } (+45^\circ)$$

$$\omega_4 = \omega_s \quad \text{with second-order phase lag } (-90^\circ)$$

Since the transfer function is classical minimum phase, the corresponding phase shift at each break frequency is either a *lead*, if it arises from a numerator term, or a *lag*, if it arises from a denominator term. If, as is often the case in aircraft studies, non-minimum phase terms appear in the transfer function, their frequency response properties are unchanged except that the sign of the phase is reversed. Further, a first-order term gives rise to a total phase shift of 90 deg and a second-order term gives rise to a total phase shift of 180 deg. The characteristic phase response is such that half the total phase shift associated with any particular transfer function factor occurs at the corresponding break frequency. Armed with this limited information, a modest interpretation of the pitch attitude frequency response of the aeroplane is possible. The frequency response of the other motion variables may be dealt with in a similar way.

6.4.2 Interpretation of the Bode diagram

With reference to Fig. 6.6, it is seen that at very low frequencies, $\omega < 0.01$ rad/s, there is no phase shift between the input and output and the gain remains constant—a little below 5 dB in this illustration. In other words, the pitch attitude follows the stick movement more or less precisely. As the input frequency is increased through ω_1 , the pitch response leads the input in phase, the output magnitude increases rapidly, and the aeroplane appears to behave like an *amplifier*. At the phugoid frequency the output reaches a substantial peak, consistent with the low damping, and thereafter the gain drops rapidly, accompanied by a rapid increase in phase lag. As the input frequency is increased further, the gain continues to reduce gently and the phase settles at -90 deg until the influence of break frequency ω_3 comes into play. The reduction in gain is arrested, and the effect of the phase lead may be clearly seen. However, when the input frequency reaches the short-period break frequency, a small peak in gain is seen, consistent with the higher damping ratio, and at higher frequencies the gain continues to reduce steadily. Meanwhile, the phase lag associated with the short-period mode results in a constant total phase lag of -180 deg at higher frequencies.

Once the output-input gain ratio drops below unity, or 0 dB, the aeroplane appears to behave like an *attenuator*. The frequency at which the gain becomes small enough for the magnitude of the output response to become insignificant is called the *bandwidth frequency*, denoted ω_b . There are various definitions of bandwidth, but the one used here is probably the most common and defines bandwidth frequency as the frequency at which the gain first drops to -3 dB below the zero-frequency, or steady-state, gain. The bandwidth frequency is indicated in Fig. 6.6, and it is commonly a little higher than the short-period frequency. A gain of -3 dB corresponds with a gain ratio of $1/\sqrt{2} = 0.707$. Thus, by definition, the gain at the bandwidth frequency is 0.707 times the steady-state gain. Since the pitch attitude bandwidth frequency is close to the short-period frequency, the latter may sometimes be substituted for the bandwidth frequency, which is often good enough for most practical purposes.

The peaks in the gain plot are determined by the characteristics of the stability modes. A very pronounced peak indicates low mode damping and vice versa, an infinite peak corresponding with zero damping. The magnitude of the changes in gain and phase occurring in the vicinity of a peak indicates the significance of the mode in the response variable in question. Fig. 6.6 indicates that the magnitude of the phugoid is much greater than the magnitude of the short-period mode in the pitch response of the aeroplane. This is in fact confirmed by response time histories and inspection of the corresponding eigenvectors.

In the classical application of the Bode diagram, as used by the control engineer, inspection of the gain and phase properties in the vicinity of the bandwidth frequency enables conclusions to be made about the stability of the system. Typically, stability is quantified in terms of *gain margin* and *phase margin*. However, such evaluations are only appropriate when the system transfer function is *minimum phase*. Since aircraft transfer functions that are non-minimum phase are frequently encountered, and many also have the added complication that they are negative, it is not usual for aircraft stability to be assessed in the Bode diagram. It is worth noting that, for aircraft augmented with flight control systems, the behaviour of the phase plot in the vicinity of the bandwidth frequency is now known to be linked to the susceptibility of the aircraft to *pilot-induced oscillations*, a particularly nasty handling deficiency.

The foregoing summary interpretation of frequency response assumes a sinusoidal elevator input to the aircraft. Clearly, this is never likely to occur as a result of normal pilot action, but normal pilot actions may be interpreted to comprise a mix of many different frequency components. For example, in gentle manoeuvring the frequency content of the input is generally low whilst in aggressive or high-workload situations the frequency content is higher and may even exceed the bandwidth of the aeroplane. In such a limiting condition the pilot is certainly aware that the aeroplane cannot follow his demands quickly enough and, depending in detail on the gain and phase response properties of the aeroplane, he may well encounter hazardous handling problems. For this reason, bandwidth is a measure of the *quickness of response* achievable in a given aeroplane. As a general rule, it is desirable that flight control system designers seek the highest-response bandwidth consistent with the dynamic capabilities of the airframe.

EXAMPLE 6.3

The longitudinal frequency response of the A-7A Corsair II aircraft is evaluated for the same flight condition as in Examples 6.1 and 6.2. However, the longitudinal response transfer functions used for the evaluations are referred to wind axes and were obtained in the solution of the full-order state [equation \(6.41\)](#). The transfer functions of primary interest are

$$\begin{aligned}\frac{u(s)}{\eta(s)} &= \frac{0.00381(s + 0.214)(s + 135.93)(s + 598.3)}{(s^2 + 0.033s + 0.02)(s^2 + 0.902s + 2.666)} \text{ ft/s/rad} \\ \frac{\theta(s)}{\eta(s)} &= \frac{-4.516(s - 0.008)(s + 0.506)}{(s^2 + 0.033s + 0.02)(s^2 + 0.902s + 2.666)} \text{ rad/rad} \\ \frac{\alpha(s)}{\eta(s)} &= \frac{-0.077(s^2 + 0.042s + 0.02)(s + 59.016)}{(s^2 + 0.033s + 0.02)(s^2 + 0.902s + 2.666)} \text{ rad/rad}\end{aligned}\quad (6.50)$$

It will be noticed that the values of the various numerator terms in the velocity and incidence transfer functions differ significantly from the values in the corresponding transfer functions in Example 6.1, [equations \(6.8\)](#). This is due to the different reference axes used and to the fact that the angular difference between body and wind axes is a significant body incidence angle of 13.3 deg. Such a large angle is consistent with the very low speed flight condition. The frequency response of each transfer function was calculated with the aid of Program CC, and the Bode

diagrams are shown, in Figs. 6.7 through 6.9 respectively. Interpretation of the diagrams for the three variables is straightforward and follows the general interpretation discussed earlier. However, important or significant differences are commented on as follows.

The frequency response of axial velocity u to elevator input η is shown in Fig. 6.7, and it is clear, as might be expected, that it is dominated by the phugoid. The very large low-frequency gain values are due entirely to the transfer function units, which are in ft/s/rad, and a unit radian elevator input is of course unrealistically large! The peak gain of 75 dB at the phugoid frequency corresponds with a gain ratio of approximately 5600 ft/s/rad. However, since the aircraft model is linear, this may be interpreted equivalently as approximately 98 ft/s/deg, which is much easier to appreciate physically. Since the gain drops away rapidly as the frequency increases beyond the phugoid frequency, the velocity bandwidth frequency is only a little higher than the phugoid frequency. This accords well with practical observation: Velocity perturbations at frequencies in the vicinity of the short-period mode are usually insignificantly small. The phase plot indicates that there is no appreciable phase shift between input and output until the frequency exceeds the

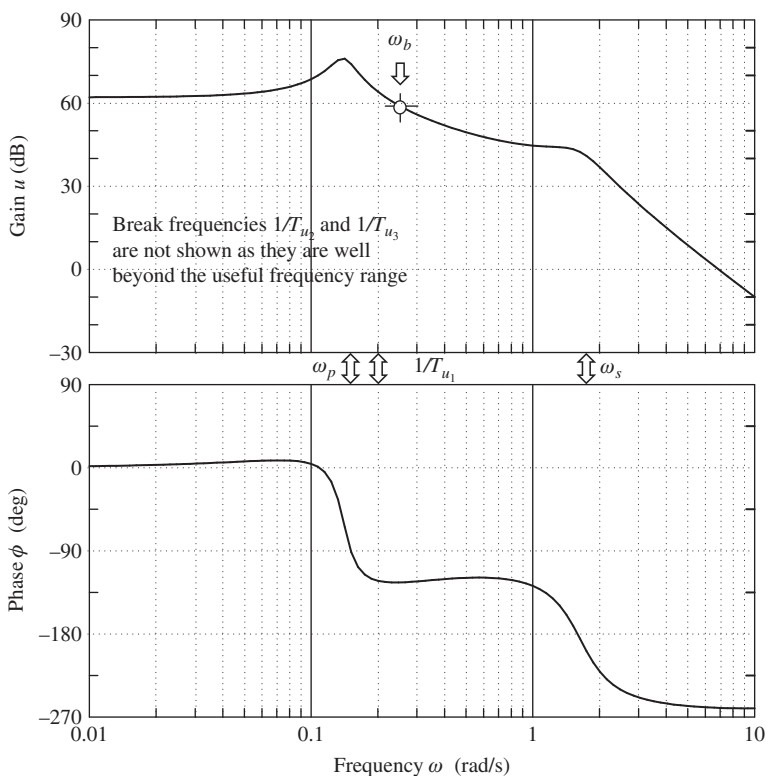


FIGURE 6.7 A-7A velocity frequency response.

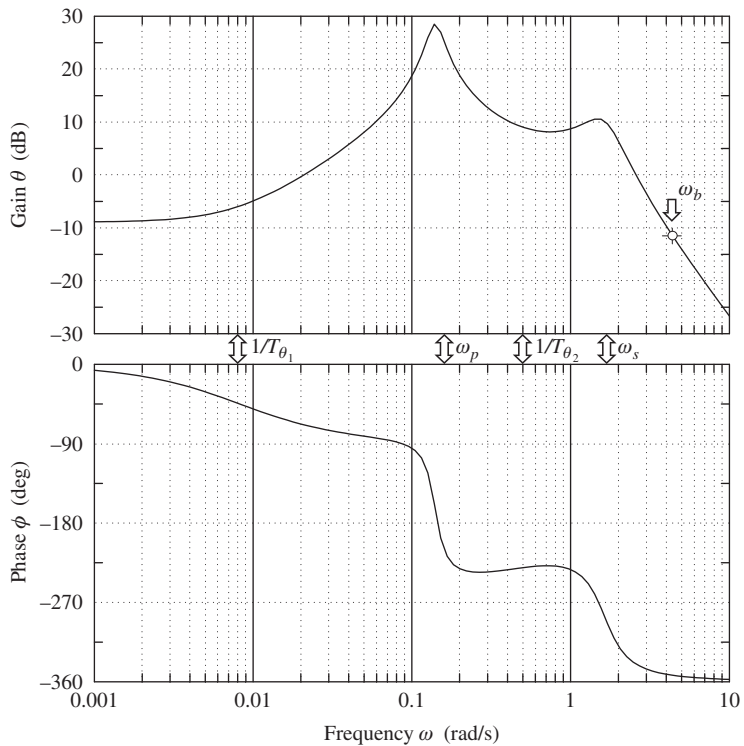


FIGURE 6.8 A-7A pitch attitude frequency response.

phugoid frequency, when there is a rapid increase in phase lag. This means that, for all practical purposes, speed changes demanded by the pilot follow the stick in the usable frequency band.

The pitch attitude θ frequency response to elevator input η is shown in Fig. 6.8. General interpretation of this figure follows the discussion of Fig. 6.6 and is not repeated here. However, there are some significant differences which must not be overlooked. These differences are due to the fact that the transfer function is non-minimum phase, a consequence of selecting a very-low-speed flight condition for the example. Referring to equations (6.50), this means that the numerator zero $1/T_{\theta_1}$ is negative, and the reasons for this are discussed in Example 6.1.

The non-minimum phase effects do not influence the gain plot in any significant way, so its interpretation is quite straightforward. However, the effect of the nonminimum phase numerator zero is to introduce phase lag at very low frequencies rather than the usual phase lead. It is likely that, in manoeuvring at this flight condition, the pilot is aware of the pitch attitude lag in response to his stick input.

The body incidence α frequency response to elevator input η is shown in Fig. 6.9, and it is clear, as might be expected, that this is dominated by the short-period mode. For all practical purposes,

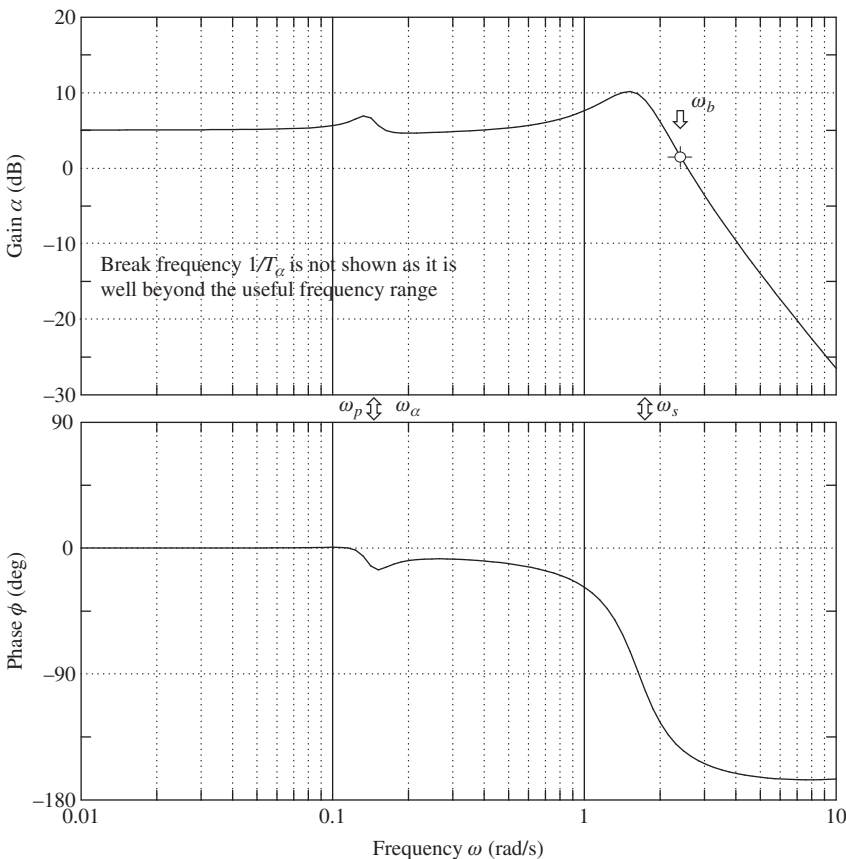


FIGURE 6.9 A-7A body incidence frequency response.

the influence of the phugoid on both gain and phase frequency responses is insignificant, which may be confirmed by reference to the appropriate transfer function in [equations \(6.50\)](#). There it is seen that the second-order numerator term very nearly cancels the phugoid term in the denominator. This is an important observation since it is quite usual to cancel approximately equal numerator and denominator terms in any response transfer function to simplify it.

Simplified transfer functions often provide adequate response models in both the time and frequency domains, and can be extremely useful for explaining and interpreting aircraft dynamic behaviour. In modern control parlance the phugoid dynamics are said to be *not observable* in this illustration. The frequency response in both gain and phase is more or less *flat* at frequencies up to the short-period frequency, or for most of the usable frequency range. In practical terms, this means that incidence follows the stick at constant gain and without appreciable phase lag, obviously a desirable state of affairs.

6.5 Flying and handling qualities

The longitudinal stability modes play a fundamental role in determining the longitudinal flying and handling qualities of an aircraft and it is essential that their characteristics must be “correct” if the aircraft is to be flown by a human pilot. A simplistic view of the human pilot suggests that he behaves like an adaptive dynamic system and will adapt his dynamics to harmonise with those of the controlled vehicle. Since his dynamics interact and couple with those of the aircraft, he will adapt, within human limits, to produce the best *closed-loop* system dynamics compatible with the piloting task. His adaptability enables him to cope with an aircraft with less than desirable flying qualities.

However, the problems of coupling between incompatible dynamic systems can be disastrous no stop and it is this latter aspect of the piloting task that has attracted much attention in recent years. Every time the aircraft is disturbed in response to control commands, the stability modes are excited and it is not difficult to appreciate why their characteristics are so important. Similarly, the stability modes are equally important in determining *ride quality* when the main concern is response to atmospheric disturbances. In military combat aircraft, ride quality determines the effectiveness of the airframe as a weapons platform; in the civil transport aircraft, it determines the comfort of passengers.

In general, it is essential that the short-period mode, which has a natural frequency close to human pilot natural frequency, is adequately damped. Otherwise, dynamic coupling with the pilot may occur under certain conditions, leading to severe, or even catastrophic, handling problems. On the other hand, as the phugoid mode is much lower in frequency, its impact on the piloting task is much less demanding. The average human pilot can easily control the aircraft even when the phugoid is mildly unstable. The phugoid mode can, typically, manifest itself as a minor trimming problem when poorly damped. Although not in itself hazardous, this can lead to increased pilot workload, and for this reason it is desirable to ensure adequate phugoid damping. It is also important that the natural frequencies of the stability modes should be well separated in order to avoid interaction, or coupling, between the modes. Mode coupling may give rise to unusual handling characteristics and is generally regarded as an undesirable feature in longitudinal dynamics. The subject of aircraft handling qualities is discussed in rather more detail in Chapter 10.

6.6 Mode excitation

Because the longitudinal stability modes are usually well separated in frequency, it is possible to excite them more or less independently for purposes of demonstration or measurement. Indeed, it is a general flying qualities requirement that the modes be well separated in frequency to avoid handling problems arising from dynamic mode coupling. The modes may be excited selectively by a sympathetic elevator input to the trimmed aircraft. The methods developed for in-flight mode excitation reflect an intimate understanding of the dynamics involved and are generally easily adapted to the analytical environment. Because the longitudinal modes are usually well separated in frequency, the form of the input disturbance is not, in practice, very critical. However, some consistency in the flight test analytical procedures adopted is desirable if meaningful comparative studies are to be made.

The short-period pitching oscillation may be excited by applying a short-duration disturbance in pitch to the trimmed aircraft. This is best achieved with an elevator pulse with a duration of a second or less. Analytically, this is adequately approximated by a unit impulse applied to the elevator. The essential feature of the disturbance is that it must be sufficiently short so as not to significantly excite the phugoid. However, as the phugoid damping is usually very low it is almost impossible not to excite the phugoid at the same time but, it does not usually develop fast enough to obscure observation of the short-period mode.

An example of a short-period response recorded during a flight test exercise in a Handley Page Jetstream aircraft is shown in Fig. 6.10. In fact, two excitations are shown, the first in the nose-up

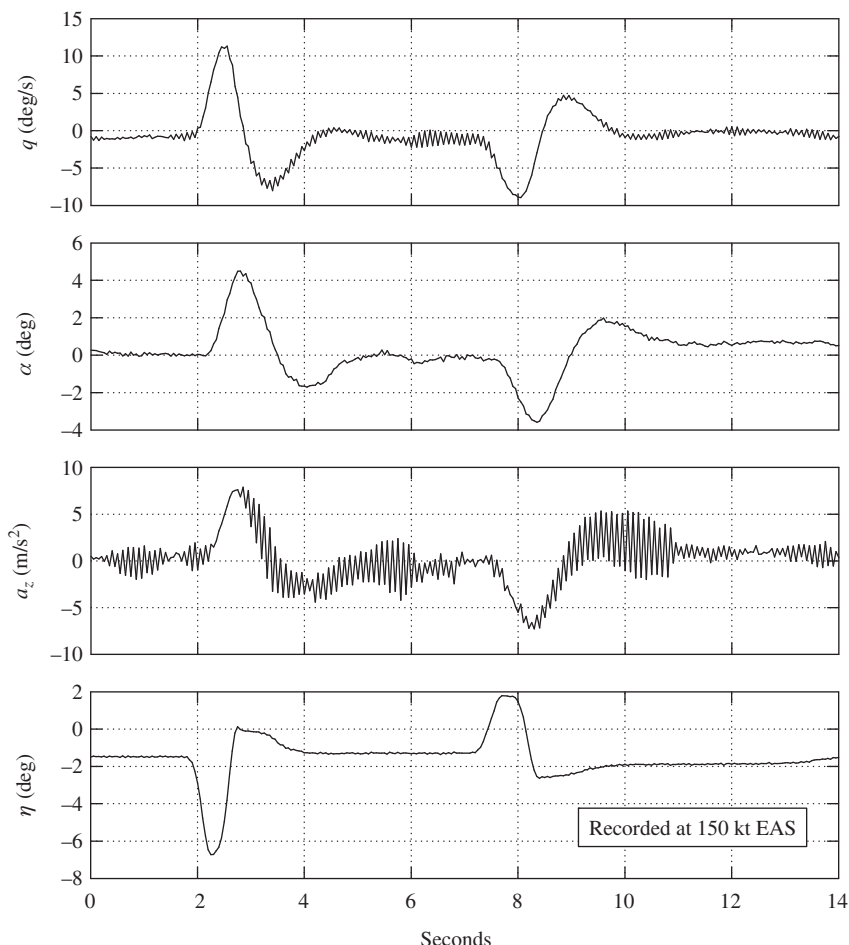


FIGURE 6.10 Flight recording of the short-period pitching oscillation.

sense and the second in the nose-down sense. The pilot input “impulse” is clearly visible and represents his best attempt at achieving a clean impulse-like input; some practice is required before consistently good results are obtained. Immediately following the input the pilot released the controls to obtain the controls-free dynamic response, which explains why the elevator angle does not recover its equilibrium trim value until the short-period transient has settled. During this short elevator free period, its motion is driven by oscillatory aerodynamic loading and is also coloured by the control circuit dynamics, which can be noticeably intrusive. Otherwise the response is typical of a well damped aeroplane.

The phugoid mode may be excited by applying a small speed disturbance to the aircraft in trimmed flight. This is best achieved by applying a small step input to the elevator which causes the aircraft to fly up or down according to the sign of the input. If the power is left at its trimmed setting, the speed will decrease or increase accordingly. When the speed has diverged from its steady trimmed value by about 5%, the elevator is returned to its trim setting. This provides the disturbance, and a stable aircraft will then execute a phugoid oscillation as it recovers its trim equilibrium. Analytically, the input is equivalent to an elevator pulse of several seconds’ duration. The magnitude and length of the pulse would normally be established by trial and error since its effect is very aircraft dependent. However, it should be remembered that for proper interpretation of the resulting response, the disturbance should be small in magnitude since a small-perturbation model is implied.

An example of a phugoid response recorded during a flight test exercise in a Handley Page Jetstream aircraft is shown in Fig. 6.11. The pilot input “pulse” is clearly visible and, as for the short-period mode, some practice is required before consistently good results are obtained. Again, the controls are released following the input to obtain the controls-free dynamic response, and the subsequent elevator motion is caused by the sinusoidal aerodynamic loading on the surface itself. The leading and trailing edge “steps” of the input elevator pulse may excite the short-period mode, but the short-period mode transient normally decays to zero well before the phugoid has properly developed and therefore would not obscure the observation of interest.

It is clear from inspection of Fig. 6.11 that the phugoid damping is significantly higher than might be expected from the previous discussion of mode characteristics. What is in fact shown is the aerodynamic, or basic airframe, phugoid modified by the inseparable effects of power. The Astazou engines of the Jetstream are governed to run at constant rpm, and thrust changes are achieved by varying the propeller blade pitch. Thus, as the aircraft flies the sinusoidal flight path during a phugoid disturbance, the sinusoidal propeller loading causes the engine to automatically adjust its power to maintain constant propeller rpm. This very effectively increases the apparent phugoid damping. It is possible to operate the aircraft at a constant power condition when the “power damping” effect is suppressed. Under these circumstances, the aerodynamic phugoid is found to be much less stable, as predicted by the simple theoretical model, and at some flight conditions is unstable.

The above flight recording of the longitudinal stability modes illustrates the *controls-free* dynamic stability characteristics. The same exercise could of course be repeated with the controls held fixed following the disturbing input; then the *controls-fixed* dynamic stability characteristics would be observed. In general, the differences between responses would be small and not too significant. Now controls-free dynamic response is only possible in aeroplanes with reversible controls, which includes most small classical aeroplanes. Virtually all larger modern aircraft have

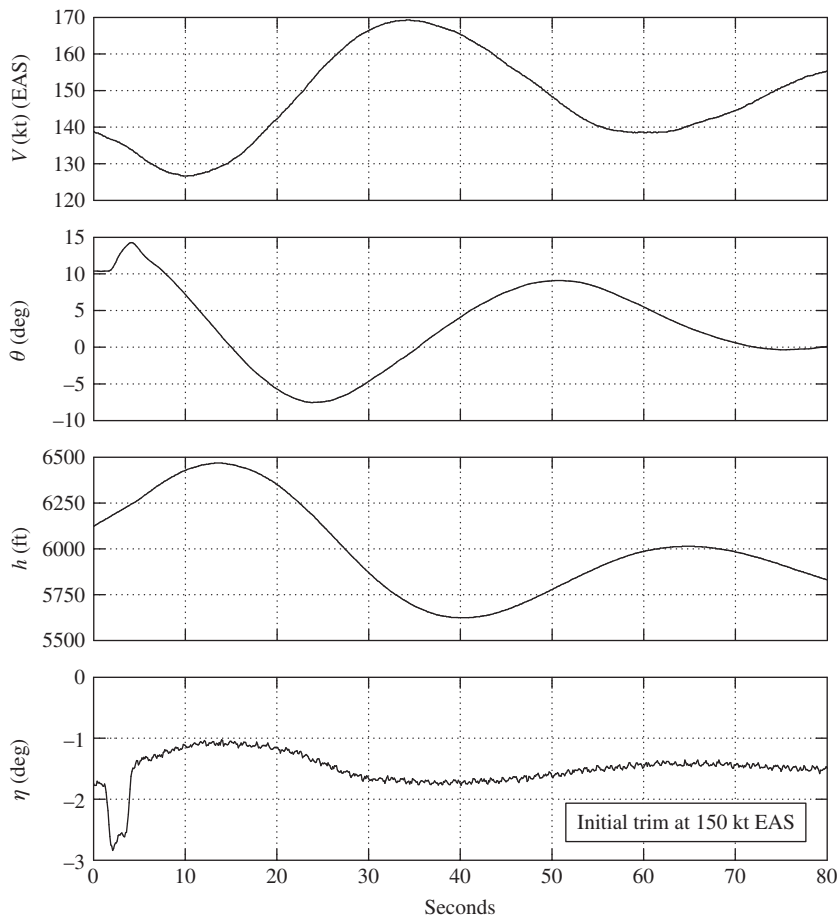


FIGURE 6.11 Flight recording of the phugoid.

powered controls, driven by electronic flight control systems, which are effectively irreversible. This means that such aircraft are only capable of controls-fixed dynamic response. For this reason, most current theoretical modelling and analysis is concerned with controls-fixed dynamics only, as is the case throughout this book. However, a discussion of the differences between controls-fixed and controls-free aeroplane dynamics may be found in Hancock (1995).

When it is required to analyse the dynamics of a single mode in isolation, the best approach is to emulate flight test practice as far as that is possible. It is necessary to choose the most appropriate transfer functions to show the dominant response variables in the mode of interest. For example, as illustrated in Figures 6.10 and 6.11, the short-period mode is best observed in the dominant response variables q and $w(\alpha)$ whereas the phugoid is best observed in its dominant response

variables u , h , and θ . It is necessary to apply a control input disturbance sympathetic to the mode dynamics, and it is also necessary to observe the response for an appropriate period of time. For example, Fig. 6.1 shows both longitudinal modes, but the time scale of the illustration reveals the phugoid mode in much greater detail than the short-period mode. Whereas, the time scale of Fig. 6.5 was chosen to reveal the short-period mode in detail since that is the mode of interest. The form of the control input is not usually difficult to arrange in analytical work because most software packages have built-in impulse, step, and pulse functions, whilst more esoteric functions can usually be programmed by the user. This kind of informed approach to analysis is required if the best possible visualisation of the longitudinal modes and their associated dynamics is to be obtained.

References

- Friedland, B. (1987). *Control system design*. New York: McGraw-Hill.
 Hancock, G. J. (1995). *An introduction to the flight dynamics of rigid aeroplanes*. Hemel Hempstead: Ellis Horwood Ltd.
 Lanchester, F. W. (1908). *Aerodonetics*. London: Constable and Co. Ltd.
 Shinners, S. M. (1980). *Modern control system theory and application*. Boston: Addison-Wesley.
 Teper, G. L. (1969). *Aircraft stability and control data*. Systems Technology, Inc., STI Technical Report 176-1. NASA Contractor Report, National Aeronautics and Space Administration, Washington D.C. 20546.

PROBLEMS

- 6.1** A tailless aeroplane of 9072 kg mass has an aspect ratio 1 delta wing of area 37 m². The longitudinal short-period motion of the aeroplane is described by the characteristic quadratic

$$\lambda^2 + B\lambda + C = 0$$

where

$$B = \frac{1}{2} \left(\frac{dC_L}{d\alpha} \right) \cos^2 \alpha$$

and

$$C = -\frac{1}{2} \left(\frac{\mu_1}{i_y} \right) \left(\frac{dC_m}{d\alpha} \right) \cos \alpha$$

α is the wing incidence, $\mu_1 = m/\frac{1}{2}\rho S \bar{c}$ is the longitudinal relative density parameter, and $i_y = I_y/m \bar{c}^2$ is the dimensionless moment of inertia in pitch. The aeroplane's moment of inertia in pitch is 1.356×10^5 kg/m². The variation of C_L and C_m with incidence $\alpha > 0$ is non-linear for the aspect ratio 1 delta wing:

$$C_L = \frac{1}{2} \pi \alpha + 2\alpha^2$$

$$C_m = C_{m_0} - 0.025\pi\alpha - 0.1\alpha^2$$

Describe and compare the short-period motions when the aeroplane is flying straight and level at 152 m/s at sea level and at 35,000 ft.

$$\rho_0 = 1.225 \text{ kg/m}^3 \text{ at sea level; } \rho/\rho_0 = 0.310 \text{ at 35,000 ft; characteristic time } \sigma = m/\frac{1}{2}\rho V_0 S. \quad (\text{CU 1983})$$

- 6.2 (a) List the characteristics of the longitudinal phugoid stability mode.
 (b) List the characteristics of the longitudinal short-period pitching stability mode.
 (c) The transfer function for the unaugmented McDonnell F-4C Phantom describing the pitch attitude response to elevator when flying at Mach 1.2 at an altitude of 35,000 ft is given by

$$\frac{\theta(s)}{\eta(s)} = \frac{-20.6(s + 0.013)(s + 0.62)}{(s^2 + 0.017s + 0.002)(s^2 + 1.74s + 29.49)} \text{ rad/rad}$$

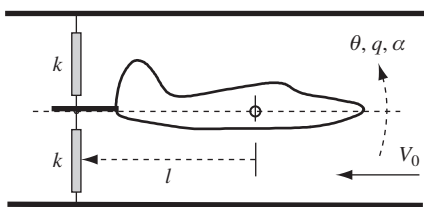
Write down the longitudinal characteristic equation and state whether the aeroplane is stable, or not.

- (d) What are the numerical parameters describing the longitudinal stability modes of the McDonnell F-4C Phantom?

(CU 1999)

- 6.3 Describe the longitudinal short-period pitching oscillation. On what parameters do its characteristics depend?

A model aircraft is mounted in a wind tunnel such that it is free to pitch about an axis through its *cg* as shown. The model is restrained by two springs attached at a point on a fuselage aft extension which is at a distance $l = 0.5 \text{ m}$ from the *cg*. The model has wing span $b = 0.8 \text{ m}$, mean aerodynamic chord $\bar{c} = 0.15 \text{ m}$ and the air density may be taken as $\rho = 1.225 \text{ kg/m}^3$.



With the wind off, the model is displaced in pitch and released. The frequency of the resulting oscillation is 10 rad/s, and the damping ratio is 0.1. The experiment is repeated with a wind velocity $V_0 = 30 \text{ m/s}$, the frequency is now found to be 12 rad/s, and the damping ratio is 0.3. Given that the spring stiffness $k = 16 \text{ N/m}$, calculate the moment of inertia in pitch and the values for the dimensionless stability derivatives M_q and M_w . It may be assumed that the influence of the derivative $M_{\dot{w}}$ is negligible. State all assumptions made.

(CU 1987)

- 6.4** (a) Show that the period of the phugoid is given approximately by $T_p = \sqrt{2\pi} \frac{V_0}{g}$, and state all assumptions used during the derivation.
 (b) State which aerodynamic parameters introduce damping into a phugoid, and discuss how varying forward speed whilst on approach to landing may influence phugoid characteristics.

(LU 2001)

- 6.5** (a) Using a simple physical model, show that the short-period pitching oscillation can be approximated by

$$I_y \ddot{\theta} + \frac{1}{2} \rho V_0^2 a_1 S_T l_T^2 \dot{\theta} - \frac{1}{2} \rho V_0^2 S \bar{c} \frac{dC_m}{d\alpha} \theta = 0$$

- (b) The aircraft described here is flying at sea level at 90 m/s. Determine the centre of gravity location at which the short-period pitching oscillation ceases to be oscillatory.

Wing lift curve slope = 5.7 1/rad

Tailplane lift curve slope = 3.7 1/rad

Horizontal tail arm = 6 m

Tailplane area = 5 m²

$d\varepsilon/d\alpha = 0.30$

$I_y = 40,000 \text{ kg/m}^2$

Wing area = 30 m²

Mean aerodynamic chord = 1.8 m

Aerodynamic centre = 0.18 \bar{c}

Hint: Modify the equation in part (a) to include tailplane lag effects.

- (c) Determine the period of the short-period pitching oscillation if the *cg* location is moved 0.2 \bar{c} forward of the position calculated in part (b).

(LU 2001)

- 6.6** For a conventional aircraft on approach to landing, discuss how the aircraft's aerodynamics may influence longitudinal stability.

(LU 2002)

- 6.7** Determine the time to half-amplitude and the period of the short-period pitching oscillation. Assume that the short-period pitching oscillation can be approximated by

$$I_y \ddot{\theta} - \frac{\partial M}{\partial q} \dot{\theta} - \frac{\partial M}{\partial w} V \theta = 0 \text{ and } M_w = \partial C_m / \partial \alpha$$

(LU 2003)

Lateral-Directional Dynamics

7

7.1 Response to controls

The procedures for investigating and interpreting the lateral-directional dynamics of an aeroplane are much the same as those used to deal with the longitudinal dynamics; thus they are not repeated at the same level of detail in this chapter. However, some aspects of lateral-directional dynamics, and their interpretation, differ significantly from those of longitudinal dynamics, and the procedures for interpreting the differences are dealt with appropriately. The lateral-directional response transfer functions are obtained in the solution of the lateral equations of motion using, for example, the methods described in Chapter 5. The transfer functions completely describe the linear dynamic asymmetric response in sideslip, roll, and yaw to aileron and rudder inputs. As in the longitudinal solution, implicit in the response are the dynamic properties determined by the lateral-directional stability characteristics of the aeroplane. As before, the transfer functions and the response variables described by them are linear since the entire modelling process is based on the assumption that the motion is constrained to small disturbances about an equilibrium trim state. The equilibrium trim state is assumed to mean steady level flight in the first instance, and the previously stated caution concerning the magnitude of a small lateral-directional perturbation applies.

The most obvious difference between the solutions of the longitudinal equations of motion and the lateral—directional equations of motion is that there is more algebra to deal with. Since two aerodynamic inputs are involved, the ailerons and the rudder, two sets of input-output response transfer functions are produced in the solution of the equations of motion. However, these are no more difficult to deal with than a single input-output set of transfer functions; there are just more of them! The most significant difference between the longitudinal and lateral-directional dynamics of the aeroplane concerns interpretation. In general, the lateral-directional stability modes are not so distinct and tend to exhibit dynamic coupling to a greater extent. Thus some care is needed in the choice of assumptions made to facilitate their interpretation. A mitigating observation is that, unlike longitudinal dynamics, lateral-directional dynamics do not change much with flight condition since most aeroplanes possess aerodynamic symmetry by design.

The lateral-directional equations of motion describing small perturbations about an equilibrium trim condition, referred to wind axes, are given by the state equation (4.70) as follows:

$$\begin{bmatrix} \dot{v} \\ \dot{p} \\ \dot{r} \\ \dot{\phi} \end{bmatrix} = \begin{bmatrix} y_v & y_p & y_r & y_\phi \\ l_v & l_p & l_r & l_\phi \\ n_v & n_p & n_r & n_\phi \\ 0 & 1 & 0 & 0 \end{bmatrix} \begin{bmatrix} v \\ p \\ r \\ \phi \end{bmatrix} + \begin{bmatrix} y_\xi & y_\zeta \\ l_\xi & l_\zeta \\ n_\xi & n_\zeta \\ 0 & 0 \end{bmatrix} \begin{bmatrix} \xi \\ \zeta \end{bmatrix} \quad (7.1)$$

The solution of equation (7.1) produces two sets of four response transfer functions, one set describing motion in response to aileron input and a second set describing response to rudder input. As for the longitudinal response transfer functions, it is convenient to adopt a shorthand style of writing them. The transfer functions describing response to aileron are conveniently written as

$$\frac{v(s)}{\xi(s)} \equiv \frac{N_\xi^v(s)}{\Delta(s)} = \frac{k_v(s + 1/T_{\beta_1})(s + 1/T_{\beta_2})}{(s + 1/T_s)(s + 1/T_r)(s^2 + 2\zeta_d\omega_d s + \omega_d^2)} \quad (7.2)$$

$$\frac{p(s)}{\xi(s)} \equiv \frac{N_\xi^p(s)}{\Delta(s)} = \frac{k_p s(s^2 + 2\zeta_\phi\omega_\phi s + \omega_\phi^2)}{(s + 1/T_s)(s + 1/T_r)(s^2 + 2\zeta_d\omega_d s + \omega_d^2)} \quad (7.3)$$

$$\frac{r(s)}{\xi(s)} \equiv \frac{N_\xi^r(s)}{\Delta(s)} = \frac{k_r(s + 1/T_\psi)(s^2 + 2\zeta_\psi\omega_\psi s + \omega_\psi^2)}{(s + 1/T_s)(s + 1/T_r)(s^2 + 2\zeta_d\omega_d s + \omega_d^2)} \quad (7.4)$$

$$\frac{\phi(s)}{\xi(s)} \equiv \frac{N_\xi^\phi(s)}{\Delta(s)} = \frac{k_\phi(s^2 + 2\zeta_\phi\omega_\phi s + \omega_\phi^2)}{(s + 1/T_s)(s + 1/T_r)(s^2 + 2\zeta_d\omega_d s + \omega_d^2)} \quad (7.5)$$

and the transfer functions describing response to rudder are conveniently written as

$$\frac{v(s)}{\zeta(s)} \equiv \frac{N_\zeta^v(s)}{\Delta(s)} = \frac{k_v(s + 1/T_{\beta_1})(s + 1/T_{\beta_2})(s + 1/T_{\beta_3})}{(s + 1/T_s)(s + 1/T_r)(s^2 + 2\zeta_d\omega_d s + \omega_d^2)} \quad (7.6)$$

$$\frac{p(s)}{\zeta(s)} \equiv \frac{N_\zeta^p(s)}{\Delta(s)} = \frac{k_p s(s + 1/T_{\phi_1})(s + 1/T_{\phi_2})}{(s + 1/T_s)(s + 1/T_r)(s^2 + 2\zeta_d\omega_d s + \omega_d^2)} \quad (7.7)$$

$$\frac{r(s)}{\zeta(s)} \equiv \frac{N_\zeta^r(s)}{\Delta(s)} = \frac{k_r(s + 1/T_\psi)(s^2 + 2\zeta_\psi\omega_\psi s + \omega_\psi^2)}{(s + 1/T_s)(s + 1/T_r)(s^2 + 2\zeta_d\omega_d s + \omega_d^2)} \quad (7.8)$$

$$\frac{\phi(s)}{\zeta(s)} \equiv \frac{N_\zeta^\phi(s)}{\Delta(s)} = \frac{k_\phi(s + 1/T_{\phi_1})(s + 1/T_{\phi_2})}{(s + 1/T_s)(s + 1/T_r)(s^2 + 2\zeta_d\omega_d s + \omega_d^2)} \quad (7.9)$$

The solution of the equations of motion results in polynomial descriptions of the transfer function numerators and common denominator as set out in Appendix 3. The polynomials factorise into real and complex pairs of roots that are most explicitly quoted in the style of equations (7.2)–(7.9). Since the roots are interpreted as time constants, damping ratios, and natural frequencies, this style makes the essential information instantly available. It should also be noted that the numerator and denominator factors are typical for a conventional aeroplane. Sometimes pairs of complex roots may be replaced with two real roots and vice versa. However, this does not usually mean that the dynamic response characteristics of the aeroplane become dramatically different. Differences in the interpretation of response may be evident but are not necessarily large.

Transfer functions (7.2) through (7.9) each describe uniquely different, but related, variables in the motion of the aeroplane in response to a control input. However, it will be observed that the

notation adopted indicates similar values for some numerator terms in both aileron and rudder response transfer functions. For example, k_r , T_ψ , ζ_ψ , and ω_ψ appear in both $N'_\xi(s)$ and $N'_\zeta(s)$. **It must be understood that the numerator parameters are context-dependent and usually have a numerical value which is unique to the transfer function in question.** To repeat the comment made previously, the notation is a convenience for allocating particular numerator terms, and it serves only to identify the role of each term as a gain, time constant, damping ratio, or frequency.

As before, the denominator of the transfer functions describes the characteristic polynomial, which in turn describes the lateral-directional stability characteristics of the aeroplane. The transfer function denominator is therefore common to all response transfer functions. Thus the response of all variables to an aileron or a rudder input is dominated by the denominator parameters—namely, time constant, damping ratio, and natural frequency. The differences between the individual responses are entirely determined by their respective numerators, and the *response shapes* of the individual variables are determined by the common denominator and “coloured” by their respective numerators.

EXAMPLE 7.1

The equations of motion and aerodynamic data for the Douglas DC-8 aircraft were obtained from [Teper \(1969\)](#). At the flight condition of interest, the aircraft has a total weight of 190,000 Lb and is flying at Mach 0.44 at an altitude of 15,000 ft. The source data are referenced to aircraft body axes and, for the purposes of this illustration, have been converted to a wind axes reference using the transformations given in Appendices 7 and 8. The equations of motion, referred to wind axes and quoted in terms of concise derivatives, are, in state space format

$$\begin{bmatrix} \dot{v} \\ \dot{p} \\ \dot{r} \\ \dot{\phi} \end{bmatrix} = \begin{bmatrix} -0.1008 & 0 & -468.2 & 32.2 \\ -0.00579 & -1.232 & 0.397 & 0 \\ 0.00278 & -0.0346 & -0.257 & 0 \\ 0 & 1 & 0 & 0 \end{bmatrix} \begin{bmatrix} v \\ p \\ r \\ \phi \end{bmatrix} + \begin{bmatrix} 0 & 13.48416 \\ -1.62 & 0.392 \\ -0.01875 & -0.864 \\ 0 & 0 \end{bmatrix} \begin{bmatrix} \xi \\ \zeta \end{bmatrix} \quad (7.10)$$

Since it is useful to have the transfer function describing sideslip angle β as well as sideslip velocity v , the output equation is augmented as described in Section 5.7. Thus the output equation is

$$\begin{bmatrix} v \\ p \\ r \\ \phi \\ \beta \end{bmatrix} = \begin{bmatrix} 1 & 0 & 0 & 0 \\ 0 & 1 & 0 & 0 \\ 0 & 0 & 1 & 0 \\ 0 & 0 & 0 & 1 \\ 0.00214 & 0 & 0 & 0 \end{bmatrix} \begin{bmatrix} v \\ p \\ r \\ \phi \end{bmatrix} \quad (7.11)$$

Again, the numerical values of the matrix elements in [equations \(7.10\) and \(7.11\)](#) have been rounded to five decimal places in order to keep the equations to a reasonable written size. This should not be done with the equations used in the actual computation.

Solution of the equations of motion using Program CC produced the following two sets of transfer functions. First, the transfer functions describing response to aileron are as follows:

$$\begin{aligned}\frac{v(s)}{\xi(s)} &= \frac{8.779(s + 0.197)(s - 7.896)}{(s + 0.0065)(s + 1.329)(s^2 + 0.254s + 1.433)} \text{ ft/s/rad} \\ \frac{p(s)}{\xi(s)} &= \frac{-1.62s(s^2 + 0.362s + 1.359)}{(s + 0.0065)(s + 1.329)(s^2 + 0.254s + 1.433)} \text{ rad/s/rad (deg/s/deg)} \\ \frac{r(s)}{\xi(s)} &= \frac{-0.0188(s + 1.59)(s^2 - 3.246s + 4.982)}{(s + 0.0065)(s + 1.329)(s^2 + 0.254s + 1.433)} \text{ rad/s/rad (deg/s/deg)} \quad (7.12) \\ \frac{\phi(s)}{\xi(s)} &= \frac{-1.62(s^2 + 0.362s + 1.359)}{(s + 0.0065)(s + 1.329)(s^2 + 0.254s + 1.433)} \text{ rad/rad (deg/deg)} \\ \frac{\beta(s)}{\xi(s)} &= \frac{0.0188(s + 0.197)(s - 7.896)}{(s + 0.0065)(s + 1.329)(s^2 + 0.254s + 1.433)} \text{ rad/rad (deg/deg)}\end{aligned}$$

Second, the transfer functions describing response to rudder are as follows:

$$\begin{aligned}\frac{v(s)}{\zeta(s)} &= \frac{13.484(s - 0.0148)(s + 1.297)(s + 30.207)}{(s + 0.0065)(s + 1.329)(s^2 + 0.254s + 1.433)} \text{ ft/s/rad} \\ \frac{p(s)}{\zeta(s)} &= \frac{0.392s(s + 1.85)(s - 2.566)}{(s + 0.0065)(s + 1.329)(s^2 + 0.254s + 1.433)} \text{ rad/s/rad (deg/s/deg)} \\ \frac{r(s)}{\zeta(s)} &= \frac{-0.864(s + 1.335)(s^2 - 0.03s + 0.109)}{(s + 0.0065)(s + 1.329)(s^2 + 0.254s + 1.433)} \text{ rad/s/rad (deg/s/deg)} \quad (7.13) \\ \frac{\phi(s)}{\zeta(s)} &= \frac{0.392(s + 1.85)(s - 2.566)}{(s + 0.0065)(s + 1.329)(s^2 + 0.254s + 1.433)} \text{ rad/rad (deg/deg)} \\ \frac{\beta(s)}{\zeta(s)} &= \frac{0.029(s - 0.0148)(s + 1.297)(s + 30.207)}{(s + 0.0065)(s + 1.329)(s^2 + 0.254s + 1.433)} \text{ rad/rad (deg/deg)}\end{aligned}$$

The characteristic equation is given by equating the denominator to zero:

$$\Delta(s) = (s + 0.0065)(s + 1.329)(s^2 + 0.254s + 1.433) = 0 \quad (7.14)$$

The first real root describes the spiral mode with time constant

$$T_s = \frac{1}{0.0065} \cong 154 \text{ s}$$

The second real root describes the roll subsidence mode with time constant

$$T_r = \frac{1}{1.329} = 0.75 \text{ s}$$

The pair of complex roots describe the oscillatory dutch roll mode with the following characteristics:

Damping ratio $\zeta_d = 0.11$

Undamped natural frequency $\omega_d = 1.2 \text{ rad/s}$

Since both real roots are negative and the pair of complex roots have negative real parts, the mode characteristics indicate the airframe to be aerodynamically stable.

The response of the aeroplane to a unit (1 deg) aileron pulse, held for two seconds and then returned to zero, is shown in Fig. 7.1. All of the variables obtained in the solution of the equations of motion are shown, the individual responses being characterised by the transfer functions, equations (7.12).

The dynamics associated with the three stability modes are visible in the responses, although at first glance they appear to be dominated by the oscillatory dutch roll mode since its damping is relatively low. Because the non-oscillatory spiral and roll modes are not so distinct, and because the dynamic coupling between modes is significant, it is rather more difficult to expose the modes analytically unless some care is taken in their graphical presentation. This subject is discussed in greater detail in Section 7.6. Both the roll and spiral modes appear as exponentially convergent characteristics since they are both stable in this example. The roll mode converges relatively quickly with a time constant of 0.75 s, whereas the spiral mode converges very slowly indeed with a time constant of 154 s. The roll mode is most clearly seen in the roll rate response p , where it determines the exponential rise at 0 s and the exponential recovery when the pulse is removed at 2 s. The spiral mode characteristic is rather more subtle and is most easily seen in the roll attitude response ϕ , where it determines the longer term convergence to zero and is fully established at 30 s.

Once again, all of the response shapes are determined by the common stability mode dynamics, and the obvious differences between them are due to the unique numerators in each transfer function. All of the response variables shown in Fig. 7.1 eventually decay to zero in the time scale of the spiral mode (about 200 seconds) since the aircraft is stable.

The response of the aeroplane to a unit (1°) rudder step input is shown in Fig. 7.2. All of the variables obtained in the solution of the equations of motion are shown, the individual responses being characterised by the transfer functions, equations (7.13). Again, it is very clear that the response is dominated by the oscillatory dutch roll mode. However, unlike the previous illustration, the roll and spiral modes are not discernible in the response. This is due to the fact that a step was chosen as the input that simply causes the aircraft to diverge from its initial equilibrium. This motion, together with the dutch roll oscillation, effectively masks the two non-oscillatory modes.

Now, it is possible to observe another interesting phenomenon in the response. Inspection of the transfer functions, equations (7.12) and (7.13), reveals that a number possess non-minimum phase numerator terms. The effect of these non-minimum phase terms would seem to be insignificantly small since they are not detectable in the responses shown in Figs 7.1 and 7.2, with one exception. The roll rate response p to rudder, shown in Fig. 7.2, exhibits a sign reversal for the first second or so of its response; this is the manifestation of the non-minimum phase effect. In aeronautical parlance it is referred to as *adverse roll* in response to rudder.

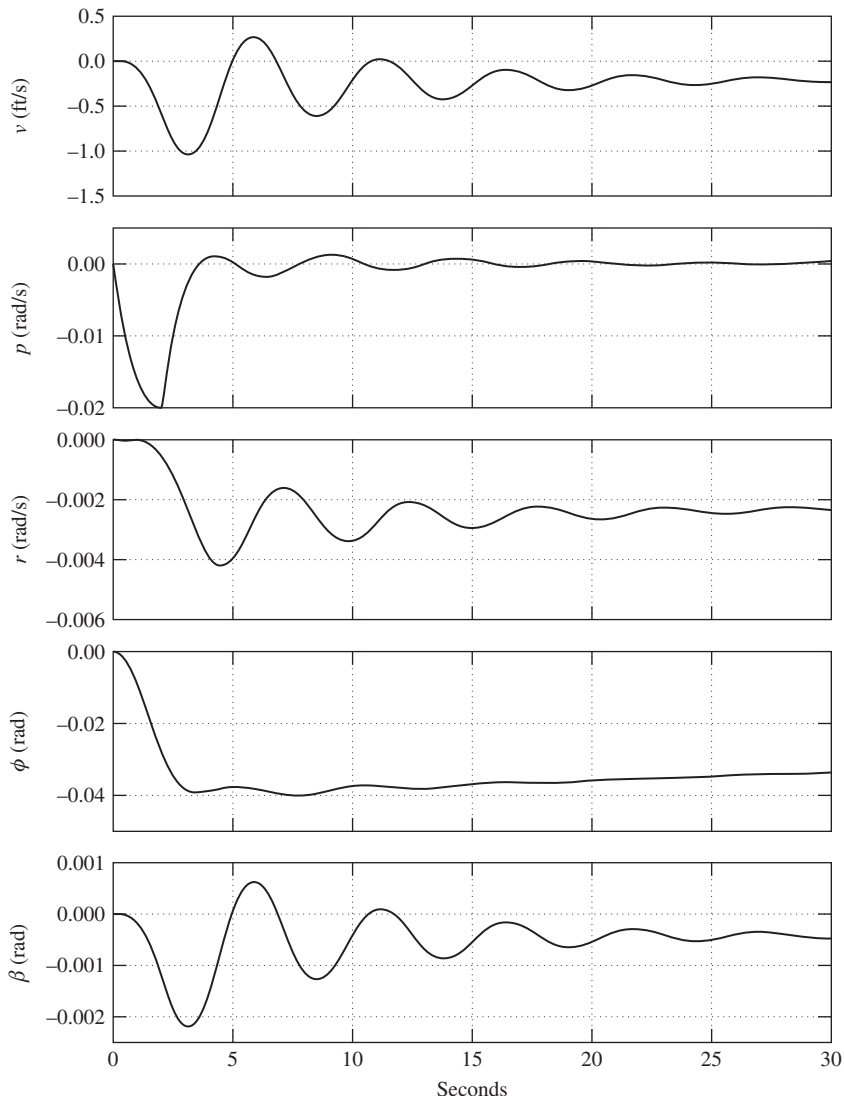


FIGURE 7.1 Aircraft response to a 1 deg, 2 s aileron pulse input.

A positive rudder step input is assumed that causes the aircraft to turn to the left, which is a negative response in accordance with the notation. Once the turn is established this results in negative yaw and yaw rate together with negative roll and roll rate induced by yaw-roll coupling. These general effects are correctly portrayed in the responses shown in Fig. 7.2. However,

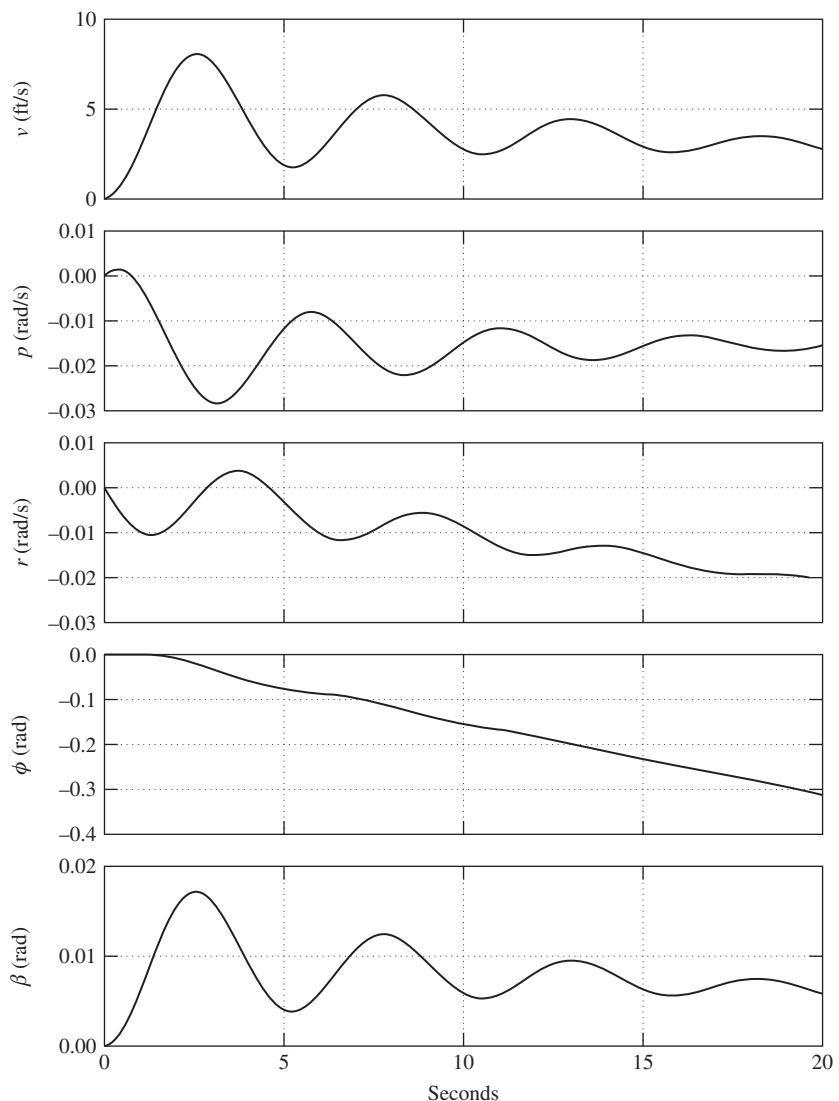


FIGURE 7.2 Aircraft response to a 1 deg rudder step input.

when the rudder is deflected, initially a substantial side force is generated at the centre of pressure of the fin, which in turn generates the yawing moment causing the aircraft to turn. However, the side force acts at some distance above the roll axis and also generates a rolling moment, which causes the aircraft to roll in the opposite sense to that induced by the yawing

motion. Since inertia in roll is somewhat lower than inertia in yaw, the aircraft responds quicker in roll and starts to roll in the “wrong” direction, but as the yawing motion becomes established the aerodynamically induced rolling moment eventually overcomes the adverse rolling moment and the aircraft then rolls in the “correct” sense.

This behaviour is clearly visible in Fig. 7.2 and is a characteristic found in most aircraft. The magnitude of the effect is aircraft dependent and, if not carefully controlled by design, can lead to unpleasant handling characteristics. A similar characteristic, *adverse yaw* in response to aileron, is caused by the differential drag effects associated with aileron deflection, giving rise to an adverse yawing moment. This characteristic is also commonly observed in many aircraft; reference to equations (7.12) indicates that it is present in the DC-8 but is insignificantly small at the chosen flight condition.

The mode content in each of the motion variables is given most precisely by the eigenvectors. The relevance of eigenvectors is discussed in Section 5.6, and the analytical procedure for obtaining them is illustrated in Example 5.7. With the aid of MATLAB, the eigenvector matrix \mathbf{V} was obtained from the state matrix in equation (7.10):

$$\mathbf{V} = \left[\begin{array}{cc|cc} \text{dutch roll mode} & & \text{roll mode} & \text{spiral mode} \\ -0.845 + 0.5291j & -0.845 - 0.5291j & -0.9970 & 0.9864 \\ 0.0012 - 0.0033j & 0.0012 + 0.0033j & -0.0619 & -0.0011 \\ 0.0011 + 0.0021j & 0.0011 - 0.0021j & 0.0006 & 0.0111 \\ -0.0029 - 0.0007j & -0.0029 + 0.0007j & 0.0466 & 0.1641 \end{array} \right] : \begin{matrix} v \\ p \\ r \\ \phi \end{matrix} \quad (7.15)$$

To facilitate interpretation of the eigenvector matrix, the magnitude of each component eigenvector is calculated as follows:

$$|\mathbf{V}| = \left[\begin{array}{cc|cc} 0.9970 & 0.9970 & 0.9970 & 0.9864 \\ 0.0035 & 0.0035 & 0.0619 & 0.0011 \\ 0.0024 & 0.0024 & 0.0006 & 0.0111 \\ 0.0030 & 0.0030 & 0.0466 & 0.1641 \end{array} \right] : \begin{matrix} v \\ p \\ r \\ \phi \end{matrix}$$

Clearly, the content of all three modes in sideslip velocity v , and hence in β , is of similar order: The roll mode is dominant in roll rate p and the spiral mode is dominant in roll attitude response ϕ . These observations correlate well with the responses shown in Fig. 7.1 and Fig. 7.2, but the low dutch roll damping obscures the observation in some response variables. Although not the case in this example, eigenvector analysis can be particularly useful for interpreting lateral-directional response in aircraft where mode coupling is rather more pronounced and the modes are not so distinct.

The steady-state values of the motion variables following a unit step (1 deg) aileron or rudder input may be determined by the application of the final value theorem, equation (5.33), to the transfer functions, equations (7.12) and (7.13). (The calculation procedure is illustrated in

Example 6.1 and is not repeated here.) Thus the steady state response of all the motion variables to an aileron unit step input is

$$\begin{bmatrix} v \\ p \\ r \\ \phi \\ \beta \end{bmatrix}_{\text{steady state}} = \begin{bmatrix} -19.24 \text{ ft/s} \\ 0 \\ -11.99 \text{ deg/s} \\ -177.84 \text{ deg} \\ -2.35 \text{ deg} \end{bmatrix}_{\text{aileron}} \quad (7.16)$$

and the steady-state response to a rudder unit step input is

$$\begin{bmatrix} v \\ p \\ r \\ \phi \\ \beta \end{bmatrix}_{\text{steady state}} = \begin{bmatrix} -11.00 \text{ ft/s} \\ 0 \\ -10.18 \text{ deg/s} \\ -150.36 \text{ deg} \\ -1.35 \text{ deg} \end{bmatrix}_{\text{rudder}} \quad (7.17)$$

It must be realised that the steady-state values given in [equations \(7.16\) and \(7.17\)](#) serve only to give an indication of the control sensitivity of the aeroplane. At such large roll attitudes the small perturbation model ceases to apply and in practice significant changes in aerodynamic operating conditions would accompany the response. The actual steady state values are undoubtedly somewhat different and can be ascertained only with a full nonlinear simulation model. This illustration indicates the limiting nature of a small-perturbation model for the analysis of lateral-directional dynamics and the need to exercise care in its interpretation.

7.1.1 The characteristic equation

The lateral-directional characteristic polynomial for a classical aeroplane is fourth order; it determines the common denominator of the lateral and directional response transfer functions and, when equated to zero, defines the characteristic equation, which may be written as

$$As^4 + Bs^3 + Cs^2 + Ds + E = 0 \quad (7.18)$$

The characteristic [equation \(7.18\)](#) most commonly factorises into two real roots and a pair of complex roots, which are most conveniently written as

$$(s + 1/T_s)(s + 1/T_r)(s^2 + 2\zeta_d\omega_d s + \omega_d^2) = 0 \quad (7.19)$$

As indicated previously, the first real root in [equation \(7.19\)](#) describes the non-oscillatory spiral mode, the second real root describes the nonoscillatory roll subsidence mode, and the pair of complex roots describe the oscillatory dutch roll mode. Now, since the equations of motion from which the characteristic equation is derived are referred to wind axes, the stability modes comprising [equation \(7.19\)](#) provide a complete description of the lateral-directional stability properties of the aeroplane with respect to the total steady velocity vector and subject to the constraints of small-perturbation motion.

When the equations of motion are referred to a body axes system, the state equation (4.69) is fifth order, as is the characteristic equation. The solution of the characteristic equation then has the following factors:

$$s(s + 1/T_s)(s + 1/T_r)(s^2 + 2\zeta_d\omega_d s + \omega_d^2) = 0 \quad (7.20)$$

The modes are unchanged except for the addition of a zero root, which indicates neutral stability. The zero root results from the addition of yaw angle to the state equation and indicates neutral stability in yaw or heading. Interpretation of lateral-directional dynamics is unchanged, and the additional information indicates that the aeroplane has an indeterminate yaw or heading angle. In other words, lateral-directional dynamics are evaluated about the steady total velocity vector, which assumes an arbitrary direction in azimuth, yaw, or heading. Interpretation of the non-zero roots of the characteristic equation is most easily accomplished if reference is first made to the properties of the classical mass-spring-damper system, which are summarised in Appendix 6.

Unlike the longitudinal dynamics, interpretation of lateral-directional dynamics is not quite so straightforward because the stability modes are not as distinct; there usually exists a significantly greater degree of mode coupling, or interaction. This tends to make the necessary simplifying assumptions less appropriate, with a consequent reduction of confidence in the observations. However, an assortment of well tried procedures for interpreting the dynamic characteristics of the well behaved aeroplane exist, and these are discussed below.

The principal objective, of course, is to identify the aerodynamic drivers for each of the stability modes. The connection between the observed dynamics of the aeroplane and its aerodynamic characteristics is made by comparing [equation \(7.18\)](#) with either [equation \(7.19\)](#) or [equation \(7.20\)](#) and then referring to Appendix 3 for the definitions of the coefficients in [equation \(7.18\)](#) in terms of aerodynamic stability derivatives. It will be appreciated immediately that further analytical progress is impossibly difficult unless some gross simplifying assumptions are made. Dealing with this difficulty requires the derivation of reduced order models, as described in [Section 7.3](#).

7.2 The dynamic stability modes

As for the longitudinal stability modes, whenever the aeroplane is disturbed from its equilibrium trim state the lateral-directional stability modes are also excited. Again, the disturbance may be initiated by pilot control action, a change in power setting, airframe configuration changes such as flap deployment, and external influences such as gusts and turbulence.

7.2.1 The roll subsidence mode

The *roll subsidence mode*, or simply *roll mode*, is a nonoscillatory lateral characteristic which is usually substantially decoupled from the spiral and dutch roll modes. Since it is nonoscillatory, it is described by a single real root of the characteristic polynomial, and manifests itself as an exponential lag characteristic in rolling motion. The aeromechanical principles governing the behaviour of the mode are illustrated in [Fig. 7.3](#).

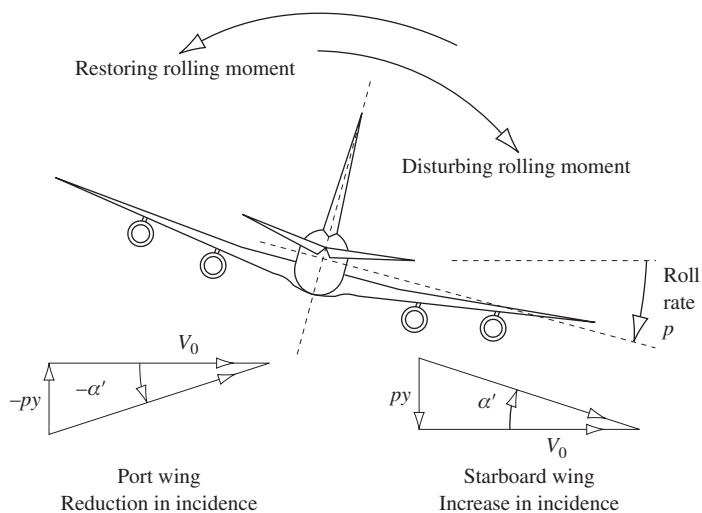


FIGURE 7.3 Roll subsidence mode.

With reference to Fig. 7.3, the aircraft is viewed from the rear, so the indicated motion is shown in the same sense as experienced by the pilot. Assume that the aircraft is constrained to single degree of freedom motion in roll about the ox axis only, and that it is initially in trimmed wings level flight. If the aeroplane experiences a positive disturbing rolling moment, it commences to roll with an angular acceleration in accordance with Newton's second law of motion. In rolling motion the wing experiences a component of velocity normal to the wing py , where y is the spanwise coordinate measured from the roll axis ox . As indicated in Fig. 7.3, this results in a small increase in incidence on the down-going starboard wing and a small decrease in incidence on the up-going port wing. The resulting differential lift gives rise to a restoring rolling moment as indicated. The corresponding resulting differential induced drag also gives rise to a yawing moment, but this is usually small enough to be ignored. Thus, following a disturbance the roll rate builds up exponentially until the restoring moment balances the disturbing moment and a steady roll rate is established.

In practice, of course, this kind of behaviour would be transient rather than continuous as implied in this illustration. The physical behaviour explained is simple “paddle” damping and is stabilising in effect in all aeroplanes operating in normal, aerodynamically linear flight regimes. For this reason, the stability mode is sometimes referred to as *damping in roll*.

In some modern combat aeroplanes designed to operate in seriously nonlinear aerodynamic conditions—for example, at angles of attack approaching 90 deg, it is possible for the physical conditions governing the roll mode to break down completely. The consequent loss of roll stability can result in rapid roll departure followed by complex lateral-directional motion of a hazardous nature. However, in the conventional aeroplane the roll mode appears to the pilot as a lag in roll response to controls. The lag time constant is largely dependent on the moment of inertia in roll and the aerodynamic properties of the wing, and is typically around 1 s or less.

7.2.2 The spiral mode

The *spiral mode* is also nonoscillatory and is determined by the other real root in the characteristic polynomial. When excited, the mode dynamics are usually slow to develop and involve complex coupled motion in roll, yaw, and sideslip. The dominant aeromechanical principles governing the mode dynamics are illustrated in Fig. 7.4. The mode characteristics are very dependent on the lateral static stability and the directional static stability of the aeroplane. These topics are discussed in Sections 3.4.1 and 3.4.2.

The spiral mode is usually excited by a disturbance in sideslip, which typically follows a disturbance in roll and causes a wing to drop. Assume that the aircraft is initially in trimmed wings level flight and that a disturbance causes a small positive roll angle ϕ to develop. Left unchecked, this results in a small positive sideslip velocity v as indicated at (a) in Fig. 7.4. The sideslip puts the fin at incidence β , which produces lift and, in turn, generates a yawing moment to turn the aircraft into the direction of the sideslip. The yawing motion produces differential lift across the wing span, which in turn results in a rolling moment, causing the starboard wing to drop further thereby exacerbating the situation. This developing divergence is indicated at (b) and (c) in Fig. 7.4. Simultaneously, the dihedral effect of the wing generates a negative restoring rolling moment due to sideslip which acts to return the wing to a level attitude. Some additional restoring rolling moment is also generated by the fin lift force when it acts at a point above the roll axis ox , which is usual.

The situation is thus one in which the fin effect, or directional static stability, and the dihedral effect, or lateral static stability, act in opposition to create this interesting dynamic condition.

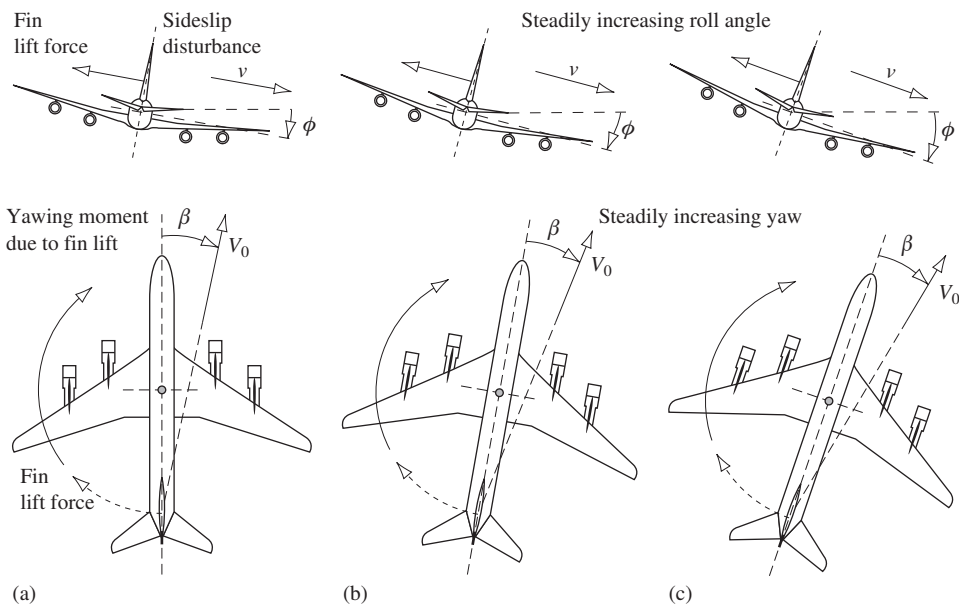


FIGURE 7.4 Spiral mode development.

Typically, the requirements for lateral and directional static stability are such that the opposing effects are very nearly equal. When the dihedral effect is greater, the spiral mode is stable and hence convergent; when the fin effect is greater, the spiral mode is unstable and hence divergent. Since these effects are nearly equal, the spiral mode is nearly neutrally stable, and sometimes it may even be neutrally stable—that is, it is neither convergent nor divergent. Since the mode is non-oscillatory, it manifests itself as a classical exponential convergence or divergence and, since it is nearly neutral, the time constant is very large, typically 100 s or more. This means that when the mode is stable the wing is slow to recover a level attitude following a disturbance, and when it is unstable the rate at which it diverges is also very slow. When it is neutral the aircraft simply flies a turn at constant roll attitude.

It is the unstable condition which attracts the most attention, for obvious reasons. Once the mode is excited the aircraft flies a slowly diverging path in both roll and yaw, and since the vertical forces are no longer in equilibrium the aircraft also loses height. Thus the unstable flight path is a spiral descent which, if left unchecked, ends when the aircraft hits the ground! However, since the rate at which the mode diverges is usually very slow, most pilots can cope with it. For this reason, an unstable spiral mode is permitted provided its time constant is sufficiently large. Because the mode is very slow to develop, the accelerations in the resulting motion are insignificantly small and the motion cues available to the pilot are almost imperceptible. In a spiral departure the visual cues become the most important cues to the pilot. It is also important to appreciate that a spiral departure is not the same as a spin. Spinning motion is a fully stalled flight condition, whereas in a spiral descent the wing continues to fly in the usual sense.

7.2.3 The dutch roll mode

The *dutch roll* mode is a classical damped oscillation in yaw, about the oz axis of the aircraft, which couples into roll and, to a lesser extent, into sideslip. The motion it describes is therefore a complex interaction between all three lateral-directional degrees of freedom. The characteristics of the dutch roll mode are described by the pair of complex roots in the characteristic polynomial. Fundamentally, the dutch roll mode is the lateral-directional equivalent of the longitudinal short-period mode. Since the moments of inertia in pitch and yaw are of similar magnitude, the frequency of the dutch roll mode and the longitudinal short-period mode are of similar order. However, the fin is generally less effective than the tailplane as a damper and the damping of the dutch roll mode is often inadequate. The dutch roll mode is so called because the motion of the aeroplane following its excitation is said to resemble the rhythmical flowing motion of a Dutch skater on a frozen canal. One cycle of typical dutch rolling motion is shown in Fig. 7.5.

The physical situation applying in a dutch roll disturbance can be appreciated by imagining that the aircraft is restrained in yaw by a torsional spring acting about the yaw axis oz , the spring stiffness being aerodynamic and determined largely by the fin. Thus, when in straight, level trimmed equilibrium flight, a disturbance in yaw causes the “aerodynamic spring” to produce a restoring yawing moment which results in classical oscillatory motion. However, once the yaw oscillation is established the relative velocity of the air over the port and starboard wings also varies in an oscillatory manner, giving rise to oscillatory differential lift and drag perturbations. This aerodynamic coupling in turn creates an oscillation in roll which lags the oscillation in yaw by approximately 90 deg. This phase difference between yawing and rolling motion means that the forward going wing

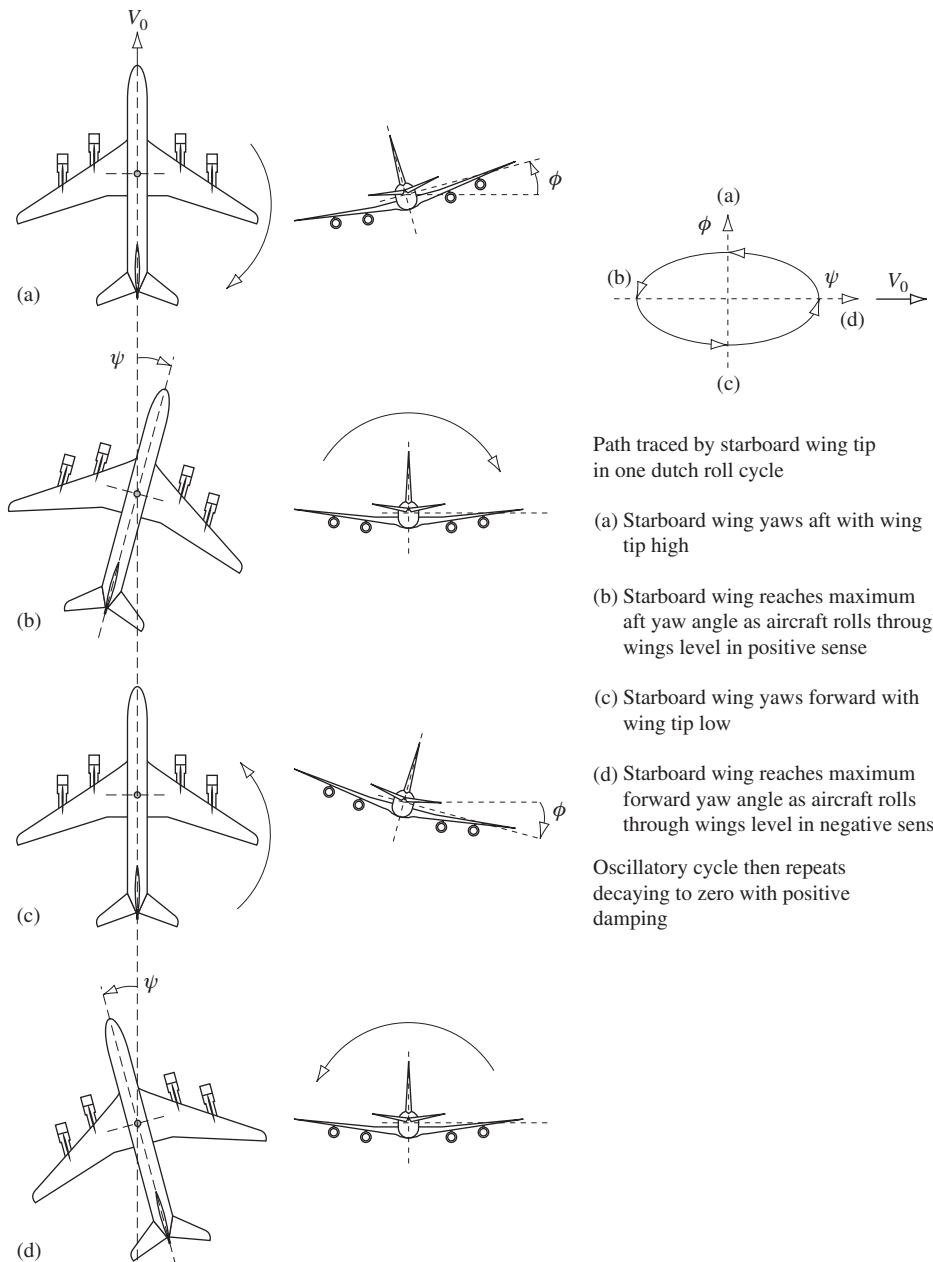


FIGURE 7.5 Oscillatory dutch roll mode.

panel is low and the aft going wing panel is high, as indicated in Fig. 7.5. Consequently, the classical manifestation of the dutch roll mode is given by the path described by the wing tips relative to the horizon and is usually elliptical, also as shown in Fig. 7.5. The ratio of peak roll to peak yaw is usually less than 1, as indicated, and is usually associated with a stable dutch roll mode. However, when the ratio is greater than 1 an unstable dutch roll mode is more likely.

Whenever the wing is disturbed from level trim, the aeroplane, left to its own devices, starts to slip sideways in the direction of the low wing. Thus the oscillatory rolling motion leads to some oscillatory sideslipping motion in dutch rolling motion, although the sideslip velocity is generally small. For this reason, it is fairly easy to build a visual picture of the complex interactions involved in the dutch roll mode. In fact, the motion experienced in a dutch rolling aircraft seems analogous to that of a ball bearing dropped into an inclined channel having a semicircular cross section. The ball bearing rolls down the inclined channel whilst oscillating from side to side on the circular surface.

Both the damping and stiffness in yaw, which determine the characteristics of the mode, are largely determined by the aerodynamic properties of the fin, a large fin being desirable for a well behaved stable dutch roll mode. Unfortunately, this contradicts the requirement for a stable spiral mode. The resulting aerodynamic design compromise usually results in aeroplanes with a mildly unstable spiral mode and a poorly damped dutch roll mode. Of course, the complexity of the dynamics associated with this mode suggests that there must be other aerodynamic contributions to the mode characteristics in addition to the fin. This is generally the case, and it is quite possible for the additional aerodynamic effects to be as significant as the aerodynamic properties of the fin, if not more so. However, one thing is quite certain: It is very difficult to quantify all aerodynamic contributions to the dutch roll mode with any degree of confidence.

7.3 Reduced order models

Unlike the longitudinal equations of motion, it is more difficult to solve the lateral-directional equations of motion approximately. Because of the motion coupling present, to a greater or lesser extent, in all three modes dynamics, the modes are not so distinct and simplifying approximations are thus less relevant, with a consequent loss of accuracy. Response transfer functions derived from reduced order models based on simplified approximate equations of motion are generally insufficiently accurate to be of any real use other than to enhance understanding of the aeromechanics of lateral-directional motion.

The simplest, and most approximate, solution of the characteristic equation provides an initial estimate for the two real roots only. This approximate solution of the lateral-directional characteristic equation (7.18) is based on the observation that conventional aeroplanes give rise to coefficients A , B , C , D , and E that have relative values which do not change very much with flight condition. Typically, A and B are relatively large whilst D and E are relatively small; in fact, E is often close to zero. Further, it is observed that $B >> A$ and $E \ll D$ suggesting the following real roots as approximate solutions of the characteristic equation:

$$\begin{aligned}(s + 1/T_r) &\cong (s + B/A) \\ (s + 1/T_s) &\cong (s + E/D)\end{aligned}\tag{7.21}$$

No such simple approximation for the pair of complex roots describing the dutch roll mode may be determined. Further insight into the aerodynamic drivers governing the characteristics of the roll and spiral modes may be made, with some difficulty, by applying assumptions based on the observed behaviour of the modes to the polynomial expressions for A , B , D , and E given in Appendix 3. Fortunately, the same information may be deduced by a rather more orderly process involving a reduction in order of the equations of motion. The approximate solutions for the nonoscillatory modes as given by [equations \(7.21\)](#) are only useful for preliminary mode evaluations, or for checking computer solutions, when the numerical values of the coefficients in the characteristic equation are known.

7.3.1 The roll mode approximation

Provided that the perturbation is small, the roll subsidence mode is observed to involve almost pure rolling motion with little coupling into sideslip or yaw. Thus a reduced order model of the lateral-directional dynamics retaining only the roll mode follows by removing the side force and yawing moment equations from the lateral-directional state [equation \(7.1\)](#):

$$\begin{bmatrix} \dot{p} \\ \dot{\phi} \end{bmatrix} = \begin{bmatrix} l_p & l_\phi \\ 1 & 0 \end{bmatrix} \begin{bmatrix} p \\ \phi \end{bmatrix} + \begin{bmatrix} l_\xi & l_\zeta \\ 0 & 0 \end{bmatrix} \begin{bmatrix} \xi \\ \zeta \end{bmatrix} \quad (7.22)$$

Further, if aircraft wind axes are assumed, then $l_\phi = 0$ and [equation \(7.22\)](#) reduces to the single degree of freedom rolling moment equation,

$$\dot{p} = l_p p + l_\xi \xi + l_\zeta \zeta \quad (7.23)$$

The roll response to aileron transfer function is easily derived from [equation \(7.23\)](#). Taking the Laplace transform of that equation, assuming zero initial conditions, and assuming that the rudder is held fixed, $\zeta = 0$, then

$$sp(s) = l_p p(s) + l_\xi \xi(s) \quad (7.24)$$

which, on rearranging, may be written as

$$\frac{p(s)}{\xi(s)} = \frac{l_\xi}{(s - l_p)} \equiv \frac{k_p}{(s + 1/T_r)} \quad (7.25)$$

The transfer function given by [equation \(7.25\)](#) is the approximate reduced order equivalent of the transfer function given by [equation \(7.3\)](#) and is the transfer function of a simple first order lag with time constant T_r . For small perturbation motion, [equation \(7.25\)](#) describes the first one or two seconds of roll response to aileron with a reasonable degree of accuracy; it is especially valuable as a means for identifying the dominant physical properties of the airframe which determine the roll mode time constant. With reference to definitions of the concise aerodynamic stability derivatives in Appendix 2, the roll mode time constant is determined approximately by

$$T_r \cong -\frac{1}{l_p} = -\frac{(I_x I_z - I_{xz}^2)}{\left(I_z \dot{L}_p + I_{xz} \dot{N}_p\right)} \quad (7.26)$$

Since $I_x \gg I_{xz}$ and $I_z \gg I_{xz}$, equation (7.26) may be further simplified to give the classical approximate expression for the roll mode time constant:

$$T_r \cong -\frac{I_x}{\dot{L}_p} \quad (7.27)$$

where I_x is the moment of inertia in roll and \dot{L}_p is the dimensional derivative describing the aerodynamic damping in roll.

7.3.2 The spiral mode approximation

Since the spiral mode is very slow to develop following a disturbance, it is usual to assume that the motion variables v , p , and r are quasi-steady relative to the time scale of the mode. Whence $\dot{v} = \dot{p} = \dot{r} = 0$, and the lateral-directional state equation (7.1) may be written as

$$\begin{bmatrix} 0 \\ 0 \\ 0 \\ \dot{\phi} \end{bmatrix} = \begin{bmatrix} y_v & y_p & y_r & y_\phi \\ l_v & l_p & l_r & l_\phi \\ n_v & n_p & n_r & n_\phi \\ 0 & 1 & 0 & 0 \end{bmatrix} \begin{bmatrix} v \\ p \\ r \\ \phi \end{bmatrix} + \begin{bmatrix} y_\xi & y_\zeta \\ l_\xi & l_\zeta \\ n_\xi & n_\zeta \\ 0 & 0 \end{bmatrix} \begin{bmatrix} \xi \\ \zeta \end{bmatrix} \quad (7.28)$$

Further, if aircraft wind axes are assumed $l_\phi = n_\phi = 0$, and if the controls are assumed fixed such that unforced motion only is considered, $\xi = \zeta = 0$, equation (7.28) simplifies to

$$\begin{bmatrix} 0 \\ 0 \\ 0 \\ \dot{\phi} \end{bmatrix} = \begin{bmatrix} y_v & y_p & y_r & y_\phi \\ l_v & l_p & l_r & 0 \\ n_v & n_p & n_r & 0 \\ 0 & 1 & 0 & 0 \end{bmatrix} \begin{bmatrix} v \\ p \\ r \\ \phi \end{bmatrix} \quad (7.29)$$

The first three rows in this equation may be rearranged to eliminate the variables v and r to give a reduced-order equation in which the variables are roll rate p and roll angle ϕ only:

$$\begin{bmatrix} 0 \\ \dot{\phi} \end{bmatrix} = \begin{bmatrix} y_v \frac{(l_p n_r - l_r n_p)}{(l_r n_v - l_v n_r)} + y_p + y_r \frac{(l_v n_p - l_p n_v)}{(l_r n_v - l_v n_r)} & y_\phi \\ 1 & 0 \end{bmatrix} \begin{bmatrix} p \\ \phi \end{bmatrix} \quad (7.30)$$

The first element of the first row of this reduced-order state matrix may be simplified since the terms involving y_v and y_p are assumed to be insignificantly small compared with the term involving y_r . Thus the equation may be rewritten as

$$\begin{bmatrix} 0 \\ \dot{\phi} \end{bmatrix} = \begin{bmatrix} y_r \frac{(l_v n_p - l_p n_v)}{(l_r n_v - l_v n_r)} & y_\phi \\ 1 & 0 \end{bmatrix} \begin{bmatrix} p \\ \phi \end{bmatrix} \quad (7.31)$$

Since $\dot{\phi} = p$, equation (7.31) may be reduced to the single degree of freedom equation describing, approximately, the unforced rolling motion involved in the spiral mode:

$$\dot{p} + \left(\frac{y_\phi (l_r n_v - l_v n_r)}{y_r (l_v n_p - l_p n_v)} \right) p = 0 \quad (7.32)$$

The Laplace transform of equation (7.32), assuming zero initial conditions, is

$$\phi(s) \left(s + \frac{y_\phi(l_r n_v - l_v n_r)}{y_r(l_v n_p - l_p n_v)} \right) \equiv \phi(s)(s + 1/T_s) = 0 \quad (7.33)$$

It should be noted that equation (7.33) is the reduced order lateral-directional characteristic equation retaining a very approximate description of the spiral mode characteristics only. Whence an approximate expression for the time constant of the spiral mode is defined:

$$T_s \cong \frac{y_r(l_v n_p - l_p n_v)}{y_\phi(l_r n_v - l_v n_r)} \quad (7.34)$$

The spiral mode time constant (7.34) may be expressed conveniently in terms of the dimensional or dimensionless aerodynamic stability derivatives to provide a more direct link with the aerodynamic mode drivers. With reference to Appendix 2 and noting that $Y_r < mU_e$ and so $y_r \cong -U_e \equiv -V_0$, and that $y_\phi = g$ since aircraft wind axes are assumed, equation (7.34) may be restated as

$$T_s \cong -\frac{U_e(\dot{L}_v \dot{N}_p - \dot{L}_p \dot{N}_v)}{g(\dot{L}_r \dot{N}_v - \dot{L}_v \dot{N}_r)} \equiv -\frac{V_0(L_v N_p - L_p N_v)}{g(L_r N_v - L_v N_r)} \quad (7.35)$$

A stable spiral mode requires that the time constant T_s is positive. Typically for most aeroplanes, especially in subsonic flight,

$$(L_v N_p - L_p N_v) > 0$$

and the condition for the mode to be stable simplifies to the approximate classical requirement that

$$L_v N_r > L_r N_v \quad (7.36)$$

Further analysis of this requirement is only possible if the derivatives in equation (7.36) are expressed in terms of the aerodynamic properties of the airframe. This means that L_v , dihedral effect, and N_r , damping in yaw, should be large whilst N_v , yaw stiffness, should be small. Rolling moment due to yaw rate, L_r , is usually significant in magnitude and positive. In very simple terms, aeroplanes with small fins and reasonable dihedral are more likely to have a stable spiral mode.

7.3.3 The dutch roll mode approximation

For the purpose of creating a reduced-order model to describe the dutch roll mode, it is usual to make the rather gross assumption that dutch rolling motion involves no rolling motion at all. This is clearly contradictory, but is based on the fact that the mode is first a yawing oscillation and aerodynamic coupling causes rolling motion as a secondary effect. It is probably true that for most aeroplanes the roll to yaw ratio in dutch rolling motion is less than 1 and in some cases may be much less than 1, which gives the assumption some small credibility. Thus the lateral-directional state equation (7.1) may be simplified by writing

$$\dot{p} = p = \dot{\phi} = \phi = 0$$

As before, if aircraft wind axes are assumed, $l_\phi = n_\phi = 0$, and if the controls are assumed fixed such that unforced motion only is considered, $\xi = \zeta = 0$, then equation (7.1) simplifies to

$$\begin{bmatrix} \dot{v} \\ \dot{r} \end{bmatrix} = \begin{bmatrix} y_v & y_r \\ n_v & n_r \end{bmatrix} \begin{bmatrix} v \\ r \end{bmatrix} \quad (7.37)$$

If equation (7.37) is written as

$$\dot{\mathbf{x}}_d = \mathbf{A}_d \mathbf{x}_d$$

then the reduced-order characteristic equation describing the approximate dynamic characteristics of the dutch roll mode is given by

$$\Delta_d(s) = \det[s\mathbf{I} - \mathbf{A}_d] = \begin{vmatrix} s - y_v & -y_r \\ -n_v & s - n_r \end{vmatrix} = 0$$

or

$$\Delta_d(s) = s^2 - (n_r + y_v)s + (n_r y_v - n_v y_r) = 0 \quad (7.38)$$

Therefore, the damping and frequency properties of the mode are given approximately by

$$\begin{aligned} 2\zeta_d \omega_d &\cong -(n_r + y_v) \\ \omega_d^2 &\cong (n_r y_v - n_v y_r) \end{aligned} \quad (7.39)$$

With reference to Appendix 2, the expressions given by equations (7.39) can be restated in terms of dimensional aerodynamic stability derivatives. Further approximating simplifications are made by assuming that $Y_r \ll mU_e$, so that $y_r \cong -U_e \equiv -V_0$, and by assuming, quite correctly, that both I_x and I_z are usually much greater than I_{xz} . It then follows that

$$\begin{aligned} 2\zeta_d \omega_d &\cong -\left(\frac{\dot{N}_r}{I_z} + \frac{\dot{Y}_v}{m}\right) \\ \omega_d^2 &\cong \left(\frac{\dot{N}_r \dot{Y}_v}{I_z m} + V_0 \frac{\dot{N}_v}{I_z}\right) \cong V_0 \frac{\dot{N}_v}{I_z} \end{aligned} \quad (7.40)$$

Comparing the damping and frequency terms in the expressions in equations (7.40) with those of the mass-spring-damper in Appendix 6, it is easy to identify the roles of those aerodynamic stability derivatives which are dominant in determining the characteristics of the dutch roll mode. For example, N_r is referred to as the yaw damping derivative and N_v is referred to as the yaw stiffness derivative; both are very dependent on the aerodynamic design of the fin and the fin volume ratio.

Although the dutch roll mode approximation gives a rather poor impression of the real thing, it is useful as a means for gaining insight into the physical behaviour of the mode and its governing aerodynamics.

EXAMPLE 7.2

It has been stated that the principle use of the lateral-directional reduced-order models is to provide insight into the aerodynamic mode drivers. With the exception of the transfer function describing roll rate response to aileron, transfer functions derived from the reduced-order models are not commonly used in analytical work because their accuracy is generally poor. However, it is instructive to compare the values of the mode characteristics obtained from the reduced-order models with those obtained in the solution of the full order equations of motion.

Consider the Douglas DC-8 aircraft of Example 7.1. The equations of motion referred to wind axes are given by [equation \(7.10\)](#), and the solution gives the characteristic [equation \(7.14\)](#). The unfactorised characteristic equation is

$$\Delta(s) = s^4 + 1.5898s^3 + 1.7820s^2 + 1.9200s + 0.0125 = 0 \quad (7.41)$$

In accordance with the expression given in [equations \(7.21\)](#), approximate values for the roll mode and spiral mode time constants are given by

$$\begin{aligned} T_r &\cong \frac{A}{B} = \frac{1}{1.5898} = 0.629 \text{ s} \\ T_s &\cong \frac{D}{E} = \frac{1.9200}{0.0125} = 153.6 \text{ s} \end{aligned} \quad (7.42)$$

The approximate roll mode time constant does not compare particularly well with the exact value of 0.75 seconds, whereas the spiral mode time constant compares extremely well with the exact value of 154 s.

The approximate roll rate response to aileron transfer function, given by [equation \(7.25\)](#), may be evaluated by obtaining the values for the concise derivatives l_p and l_ξ from [equation \(7.10\)](#). Whence

$$\frac{p(s)}{\xi(s)} = \frac{-1.62}{(s + 1.232)} \text{ deg/s/deg} \quad (7.43)$$

With reference to [equation \(7.25\)](#), an approximate value for the roll mode time constant is given by

$$T_r \cong \frac{1}{1.232} = 0.812 \text{ s} \quad (7.44)$$

which compares rather more favourably with the exact value. The short term roll rate response of the DC-8 to a 1 deg aileron step input, as given by [equation \(7.43\)](#), is shown in [Fig. 7.6](#), where it is compared with the exact response of the full order model, as given by [equations \(7.12\)](#).

Clearly, for the first two seconds, or so, the match is extremely good, which confirms the assumptions made about the mode to be valid provided the period of observation of roll behaviour is limited to the time scale of the roll mode. The approximate roll mode time constant calculated by substituting into the expression given by [equation \(7.27\)](#) the appropriate derivative

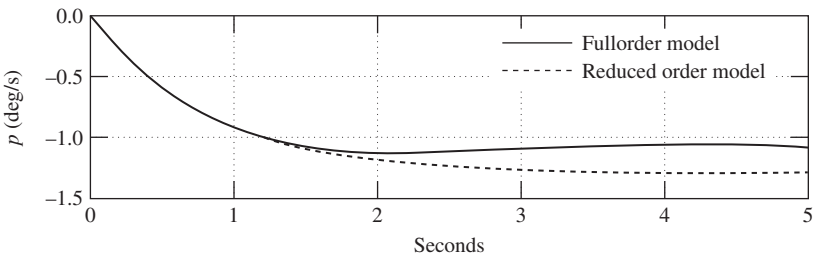


FIGURE 7.6 Roll rate response to a 1 deg aileron step input.

and roll inertia values, given in the aircraft data, results in a value almost the same as that given by equation (7.44). This simply serves to confirm the validity of the assumptions made about the roll mode.

With reference to equations (7.34) and (7.35), the approximate spiral mode time constant may be written in terms of concise derivatives as

$$T_s \cong -\frac{U_e(l_v n_p - l_p n_v)}{g(l_r n_v - l_v n_r)} \quad (7.45)$$

Substituting values for the concise derivatives obtained from equation (7.10), the velocity U_e and g , then

$$T_s \cong -\frac{468.2(0.0002 + 0.00343)}{32.2(0.0011 - 0.00149)} = 135.34 \text{ s} \quad (7.46)$$

Clearly, this approximate value of the spiral mode time constant does not compare so well with the exact value of 154 s. However, this is not so important since the mode is very *slow* in the context of normal piloted manoeuvring activity. The classical requirement for spiral mode stability given by the inequality condition of equation (7.36) is satisfied since $0.00149 > 0.0011$.

Notice how close the values of the two numbers are, suggesting that the mode is close to neutrally stable in the time scale of normal transient response. This observation is quite typical of a conventional aeroplane like the DC-8.

Approximate values for the dutch roll mode damping ratio and undamped natural frequency are obtained by substituting the relevant values for the concise derivatives, obtained from equation (7.10), into the expressions given by equations (7.39). Thus, approximately,

$$\begin{aligned}\omega_d &\cong 1.152 \text{ rad/s} \\ \zeta_d &\cong 0.135\end{aligned}$$

These approximate values compare reasonably well with the exact values, which are a natural frequency of 1.2 rad/s and a damping ratio of 0.11. Such a good comparison is not always

achieved and merely emphasises once more the validity of the assumptions about the dutch roll mode in this particular application. The implication is that at the flight condition of interest the roll-to-yaw ratio of the dutch roll mode in the DC-8 is significantly less than 1 and, indeed, this may be inferred from either Fig. 7.1 or Fig. 7.2.

7.4 Frequency response

It is useful, and sometimes necessary, to investigate the lateral-directional response properties of an aeroplane in the frequency domain. The reasons that such an investigation might be made are much the same as those given for the longitudinal case in Section 6.4. Again, the Bode diagram is the most commonly used graphical tool for lateral-directional frequency response analysis. The method of constructing the diagram and its interpretation follow the general principles described in Section 6.4 and are not repeated here. Since it is difficult to generalise, a typical illustration of lateral-directional frequency response analysis is given in the following example.

EXAMPLE 7.3

The lateral-directional frequency response of the Douglas DC-8 aircraft is evaluated for the same flight condition as in Examples 7.1 and 7.2. The total number of transfer functions which could be evaluated in a Bode diagram is 10, given by equations (7.12) and (7.13), but to create 10 Bode diagrams would be prohibitively lengthy in the present context. Since the essential frequency response information can be obtained from a much smaller number of transfer functions, the present example is limited to 4. The chosen transfer functions were selected from equations (7.12) and (7.13); all are referred to aircraft wind axes and are repeated here for convenience.

$$\begin{aligned}\frac{\phi(s)}{\xi(s)} &= \frac{-1.62(s^2 + 0.362s + 1.359)}{(s + 0.0065)(s + 1.329)(s^2 + 0.254s + 1.433)} \text{ rad/rad (deg/deg)} \\ \frac{\beta(s)}{\xi(s)} &= \frac{0.0188(s + 0.197)(s - 7.896)}{(s + 0.0065)(s + 1.329)(s^2 + 0.254s + 1.433)} \text{ rad/rad (deg/deg)} \\ \frac{r(s)}{\zeta(s)} &= \frac{-0.864(s + 1.335)(s^2 - 0.03s + 0.109)}{(s + 0.0065)(s + 1.329)(s^2 + 0.254s + 1.433)} \text{ rad/s/rad (deg/s/deg)} \\ \frac{p(s)}{\zeta(s)} &= \frac{0.392s(s + 1.85)(s - 2.566)}{(s + 0.0065)(s + 1.329)(s^2 + 0.254s + 1.433)} \text{ rad/s/rad (deg/s/deg)}\end{aligned}\tag{7.47}$$

The first two transfer functions in equations (7.47) describe lateral response to the lateral command (aileron) variable; the third describes directional response to the directional command (rudder) variable; the fourth was chosen to illustrate cross-coupling and describes lateral response to the directional command variable. Now consider the frequency response of each transfer function in turn.

The frequency response of roll attitude ϕ to aileron input ξ is shown in Fig. 7.7. The most obvious features of the Bode diagram are the very high steady-state gain, 45 dB, and the very

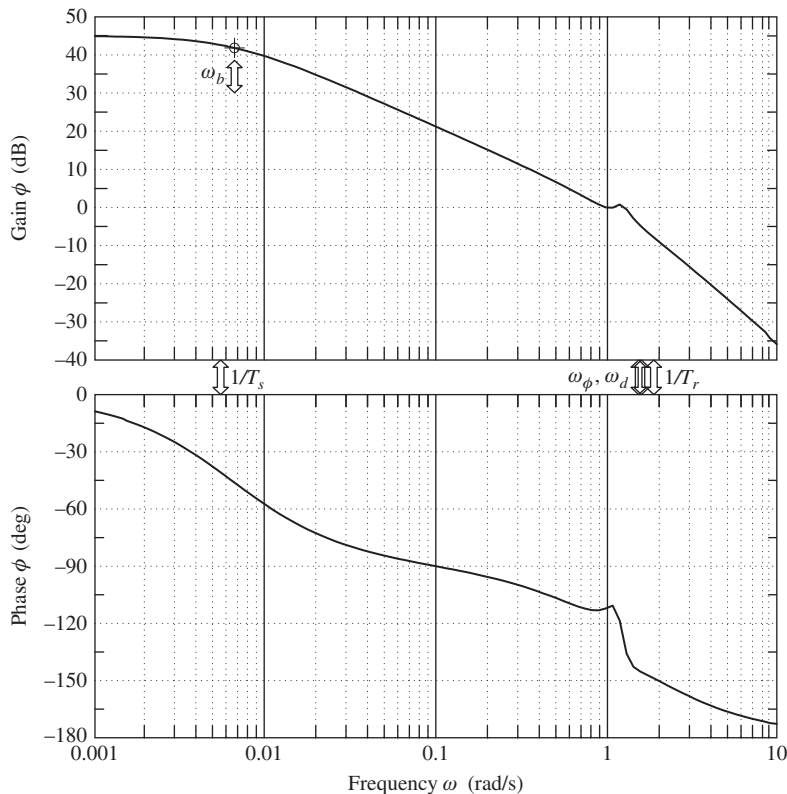


FIGURE 7.7 DC-8 roll attitude frequency response to aileron.

small peak at the dutch roll frequency. The *roll-off* in phase behaves quite conventionally in accordance with the transfer function properties. The high zero frequency gain corresponds with a gain ratio of approximately 180. This means that following a 1 deg aileron step input the aeroplane settles at a roll attitude of -180 degrees—in other words, inverted! Clearly, this is most inappropriate for a large civil transport aeroplane and serves as yet another illustration of the limitations of linear system modelling. Such a large amplitude excursion is definitely not a small perturbation and should not be regarded as such.

Nevertheless, the high zero frequency, or steady-state, gain provides a good indication of roll control sensitivity. As the control input frequency is increased, the attitude response attenuates steadily with increasing phase lag, the useful bandwidth being a little above the spiral mode break frequency $1/T_s$. However, at all frequencies up to that corresponding with the roll subsidence mode break frequency, $1/T_r$, the aeroplane responds to aileron because the gain is always

greater than 0 dB; it is the steady reduction in control sensitivity that will be noticed by the pilot.

Since the dutch roll damping ratio is relatively low at 0.11, an obvious peak might be expected in the gain plot at the dutch roll frequency, but clearly this is not the case. Inspection of the relevant transfer function in [equations \(7.47\)](#) shows that the second order numerator factor very nearly cancels the dutch roll roots in the denominator. This means that the dutch roll dynamics are not very obvious in the roll attitude response to aileron in accordance with the observation. This conclusion is also confirmed by the time history response shown in [Fig. 7.1](#). In fact, the dutch roll cancellation is sufficiently close that it is permissible to write the transfer function in approximate form with little loss of meaning:

$$\frac{\phi(s)}{\xi(s)} = \frac{-1.62}{(s + 0.0065)(s + 1.329)} \text{ rad/rad (deg/deg)} \quad (7.48)$$

The time response plot and the Bode diagram derived from this approximate transfer function correspond closely with those derived from the full transfer function and may be interpreted to achieve the same conclusions for all practical purposes.

The frequency response of sideslip angle β to aileron input ξ is shown in [Fig. 7.8](#) and corresponds with the second transfer function given in [equations \(7.47\)](#). Again, there are no real surprises here. The transfer function is non-minimum phase since the numerator term $1/T_{\beta_2}$ is negative, which introduces 90 deg of phase lag at the corresponding break frequency. In this response variable the dutch roll gain peak is clearly visible. However, at the dutch roll frequency the gain is attenuated by about -20 dB, which means that the pilot sees no significant oscillatory sideslip behaviour. Again, it is established that the usable bandwidth is a little higher than the spiral mode break frequency $1/T_s$.

The frequency response of yaw rate r to rudder input ζ is shown in [Fig. 7.9](#). This transfer function describes the typical classical directional response to control, and the frequency response, shown in the figure, has some interesting features. The gain plot indicates a steady but significant attenuation with increasing frequency to reach a minimum of about -30 dB at ω_ψ , the resonant frequency of the second-order numerator factor. The gain rises rapidly with a further increase in frequency to reach a maximum of 10 dB at the dutch roll frequency, only to decrease rapidly thereafter.

At very low input frequencies the phase lag increases gently in accordance with the spiral mode dynamics until the effect of the second-order numerator term becomes apparent. The rate of change in phase is then very dramatic since the effective damping ratio of the second-order numerator term is very small and negative. At the dutch roll frequency, approximately, the phase reaches -360 degrees and the response appears to be in phase again, only to roll off smartly at higher frequency. Again, the effective bandwidth is a little higher than the spiral mode break frequency $1/T_s$. These unusual frequency response characteristics are easily appreciated in a flight demonstration.

If the pilot approximates a sinusoidal rudder input by pedalling gently on the rudder pedals, then, at very low frequencies approaching the steady state, the yaw rate response follows the input easily and obviously, since the gain is approximately 20 dB, with very little phase lag. As

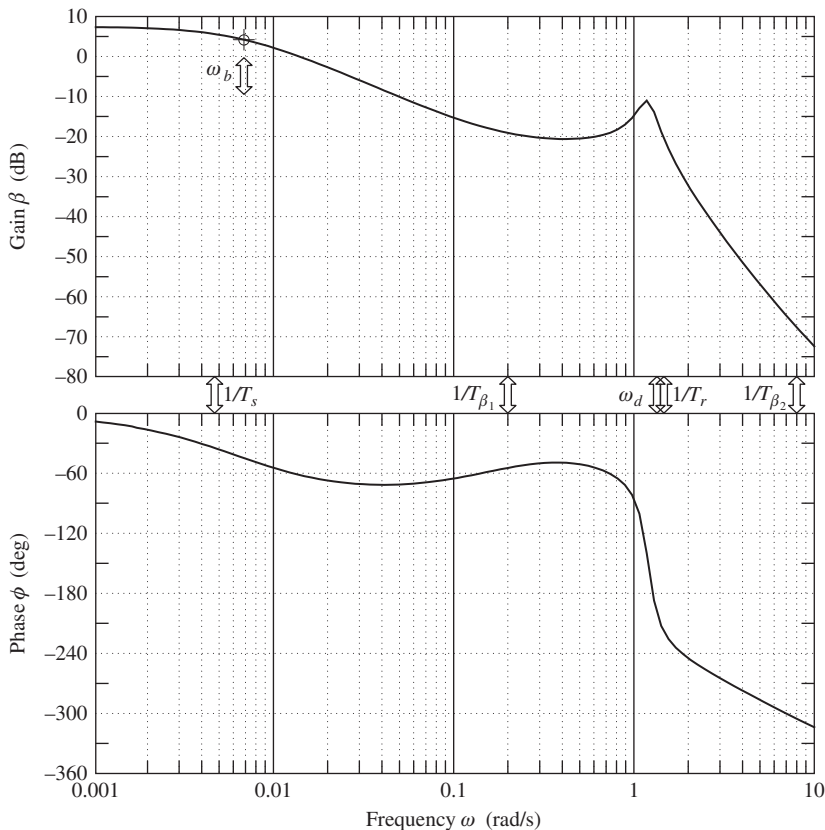


FIGURE 7.8 DC-8 sideslip angle frequency response to aileron.

the pilot increases the frequency of pedalling, the response lags the input and the magnitude of the response reduces very quickly until there is no significant observable response. If the pilot increases the frequency of his forcing yet further, the aircraft springs to life again as the dutch roll frequency (resonance) is reached, at which point the yaw rate response is approximately in phase with the input. At still higher frequencies the response rapidly attenuates for good. The substantial dip in both gain and phase response with frequency, caused by the second-order numerator factor, effectively isolates the dutch roll mode to a small window in the frequency band. This makes it very easy for the pilot to identify and excite the dutch roll mode by rudder pedaling—which is very good for flight demonstration but may not be so good for handling if the dutch roll damping is low and the second-order numerator factor is not too close in frequency to that of the dutch roll mode.

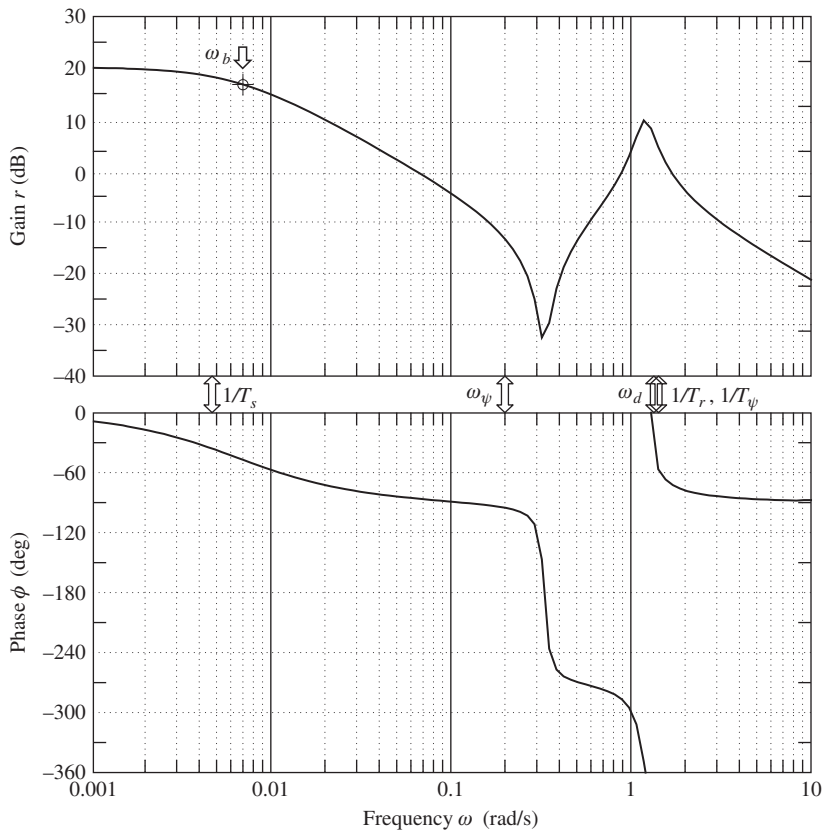


FIGURE 7.9 DC-8 yaw rate frequency response to rudder.

The frequency response of roll rate p to rudder input ζ is shown in Fig. 7.10. This frequency response example is interesting since it represents a cross-coupling case. In the steady state or, equivalently, at zero frequency, roll rate in response to rudder input would not be expected. This is clearly evident in the gain plot, where the gain is $-\infty$ dB at zero frequency. This observation is driven by the zero in the numerator, which also introduces 90 degrees of phase lead at the very lowest frequencies. This zero also very nearly cancels with the spiral mode denominator root such that, at input frequencies above the spiral mode break frequency $1/T_s$, the response in both gain and phase is essentially flat until the effects of the remaining numerator and denominator roots come into play, all at frequencies around the dutch roll frequency. The dutch roll resonant peak in gain and the subsequent roll-off in both gain and phase are absolutely classical and easily interpreted. These frequency response observations correspond well with the response time history shown in Fig. 7.2, where the effects of the roll subsidence mode and the dutch roll

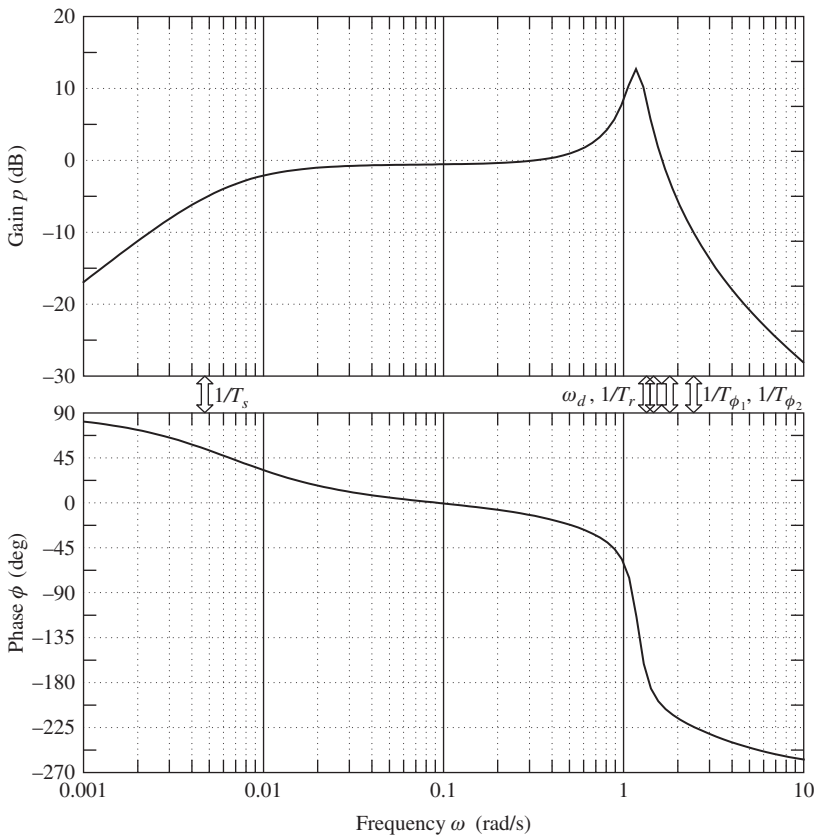


FIGURE 7.10 DC-8 roll rate frequency response to rudder.

mode are clearly visible whilst the longer term convergence associated with the spiral mode is not visible at all. In this example, bandwidth tends to lose its meaning. However, it is not unrealistic to suggest that the usable bandwidth is a little higher than the dutch roll mode frequency, provided the effects at very low frequency are ignored. This then assumes that the zero numerator factor cancels with the spiral mode denominator factor to give the approximate transfer function:

$$\frac{p(s)}{\zeta(s)} = \frac{0.392(s + 1.85)(s - 2.566)}{(s + 1.329)(s^2 + 0.254s + 1.433)} \text{ rad/s/rad (deg/s/deg)} \quad (7.49)$$

As before, this may be interpreted in both the time domain and the frequency domain with little loss of meaning over the usable frequency band.

7.5 Flying and handling qualities

As with longitudinal stability, the lateral-directional stability characteristics of the aeroplane are critically important in the determination of flying and handling qualities, and there is no doubt that they must be correct. Traditionally, the emphasis on lateral-directional flying and handling qualities has been much less than the emphasis on longitudinal flying and handling qualities. Unlike longitudinal flying and handling qualities, lateral-directional flying and handling qualities do not usually change significantly with flight condition, especially in the context of small-perturbation modelling. Thus, once they have been fixed by the aerodynamic design of the airframe, they tend to remain more or less constant irrespective of flight condition. Any major lateral-directional departures from nominally small perturbations about trim are likely to be transient, under full pilot control, and consequently are unlikely to give rise to serious handling problems. However, this is not necessarily a safe assumption when considering highly augmented aircraft, a topic which is beyond the scope of the present discussion.

It is a recurrent theme in handling qualities work that short-term dynamics are properly controlled by design. The typical frequencies involved in short-term dynamics are similar to human pilot frequencies, and their inadvertent mismatch is a sure recipe for potential handling problems. So, for reasons similar to those discussed in greater detail in Section 6.5 referring to longitudinal dynamics, it is therefore equally important that the lateral-directional short-period stability modes be properly controlled. This may be interpreted to mean that the damping of both the roll subsidence mode and the dutch roll mode should be adequate.

The roll subsidence mode appears to the pilot as a lag in the response to control and, clearly, if the time constant becomes too large, roll response to control becomes too sluggish. A large roll mode time constant is the direct result of low roll stability, although the mode is usually stable as discussed in [Section 7.2.1](#). Generally, acceptable levels of roll mode stability result in a time constant or roll response lag which is almost imperceptible to the pilot. However, it is quite common to find aircraft in which roll mode damping is inadequate, but it is unusual to find overdamped aircraft.

The spiral mode, being a long-period mode, does not usually significantly influence short-term handling. When it is stable and its time constant is sufficiently long, it has little or no impact on flying and handling qualities, but when it is unstable it manifests itself as a trimming problem because the aeroplane continually attempts to diverge laterally. When its time constant is short, the mode is more unstable and the rate of divergence becomes faster with a corresponding increase in pilot workload. Since the mode is generally so slow to develop, the motion cues associated with it may well be imperceptible to the pilot. Thus a hazardous situation may easily arise if the external visual cues available to the pilot are poor or absent altogether, such as in Instrument Meteorological Conditions (IMC) flight conditions. It is not unknown for inexperienced pilots to become disorientated in such circumstances, with the inevitable outcome! Therefore, the general requirement is that the spiral mode should be stable; however, since this is difficult to achieve in many aeroplanes, when unstable the time constant should be greater than a defined minimum.

Since the dutch roll mode is a short-period mode and is the directional equivalent of the longitudinal short-period mode, its importance to handling is similarly critical. Generally, it is essential that the dutch roll mode is stable and that its damping is greater than a defined minimum. Similarly

tight constraints are placed on the permitted range of combinations of frequency and damping. However, a level of damping lower than that of the longitudinal short-period mode is permitted. This is perhaps convenient but is more likely to result from the design conflict with the spiral mode, which must not have more than a limited degree of instability.

7.6 Mode excitation

Unlike the longitudinal stability modes, the lateral-directional stability modes usually exhibit significant dynamic coupling; as a result, it is more difficult to excite the modes independently for the purposes of demonstration or measurement. However, the lateral-directional stability modes may be excited selectively by the careful application of a sympathetic aileron or rudder input to the trimmed aircraft. Again, the methods developed for in-flight mode excitation reflect an intimate understanding of the dynamics involved and are generally easily adapted to the analytical environment. Because the lateral-directional stability modes usually exhibit dynamic coupling, the choice and shape of the disturbing input are critical to the mode under investigation. As always, standard experimental procedures have been developed to achieve consistency in the flight test or analytical process so that meaningful comparative studies may be carried out.

The roll subsidence mode may be excited by applying a short duration square pulse to the aileron with the other controls remaining fixed at their trim settings. The magnitude and duration of the pulse must be carefully chosen if the aeroplane is not to roll too rapidly through a large attitude change and thereby exceed the limit of small-perturbation motion. Since the mode involves almost pure rolling motion only, no significant motion coupling is seen in its relatively short time scale. Therefore, to see the classical characteristics of the roll subsidence mode it is only necessary to observe roll response for a few seconds.

An example of roll response showing the roll subsidence mode recorded during a flight test exercise in a Handley Page Jetstream aircraft is shown in Fig. 7.11. The input aileron pulse is clearly seen and has a magnitude of about 4 deg and duration of about 4 s. The shape of this input will have been established by the pilot by trial and error since the ideal input is very much aircraft dependent. The effect of the roll mode time constant, is clearly visible since it governs the exponential rise in roll rate p as the response attempts to follow the leading edge of the input ξ . The same effect is seen again in reverse when the input is returned to its datum at the end of the pulse. The barely perceptible oscillation in roll rate during the “steady part” of the response is, in fact, due to a small degree of coupling with the dutch roll mode.

To conduct the flight experiment without large excursions in roll attitude ϕ , it is usual to first establish the aircraft in a steady turn with, in this illustration, -30 degrees of roll attitude. On application of the input pulse, the aircraft rolls steadily through to +30 degrees of roll attitude when the motion is terminated by returning the aileron to datum. This can be seen in Fig. 7.11. The effect of the roll mode time constant on the roll attitude response is to smooth the entry to, and exit from, the steady part of the response. Since the roll mode time constant is small, around 0.4 s for the Jetstream, its effect is only just visible in the roll attitude response. It is interesting to observe that the steady part of the roll response is achieved when the moment due to damping in roll becomes established at a value equal and opposite to the disturbing moment in roll caused by

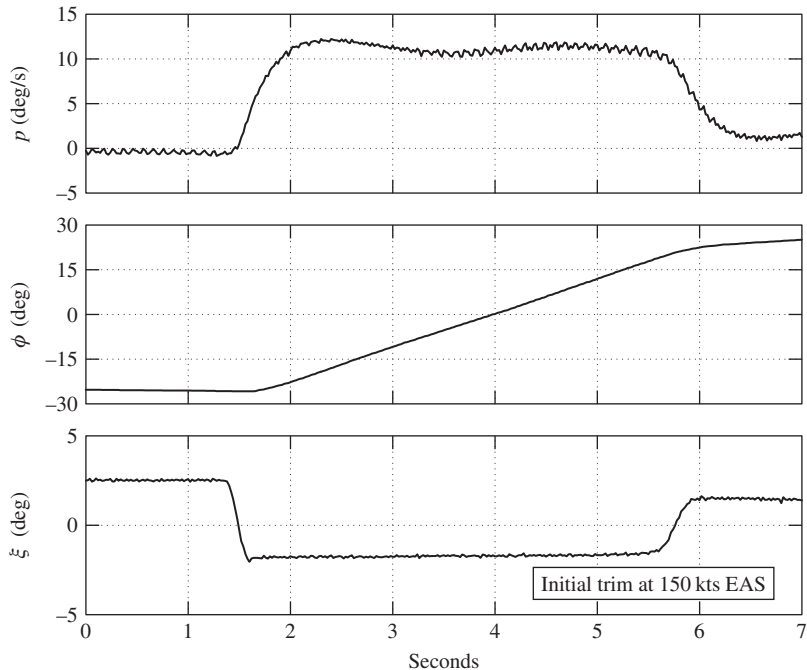


FIGURE 7.11 Flight recording of the roll subsidence mode.

aileron deflection. Clearly, therefore, the roll subsidence mode governs the transient entry to, and exit from, all rolling motion.

The spiral mode may be excited by applying a small step input to rudder ζ , with the remaining controls being held at their trim settings. The aeroplane responds by starting to turn, the wing on the inside of the turn starts to drop, and sideslip develops in the direction of the turn. When the roll attitude reaches about 20 degrees the rudder is gently returned to datum and the aeroplane is left to its own devices. When the spiral mode is stable the aeroplane slowly recovers wings level flight, the recovery being exponential with spiral mode time constant. When the mode is unstable the coupled roll-yaw-sideslip departure continues to develop exponentially with spiral mode time constant.

An example of an unstable spiral mode, captured from the time the disturbing rudder input is returned gently to datum and recorded during a flight test exercise in a Handley Page Jetstream, is shown in Fig. 7.12. The slow exponential divergence is clearly visible in all recorded variables, with the possible exception of sideslip angle β , which is rather noisy. In any event, the magnitude of sideslip is normally limited to a small value by the weathercock effect of the fin. Although speed and altitude play no part in determining the characteristic of the mode, the exponential departure in these variables is a classical, and very visible, consequence of an unstable spiral mode. Once excited, since the aircraft is no longer in wings-level flight, lift is insufficient to maintain altitude and so an accelerating descent follows and the spiral flight path is determined by the mode's

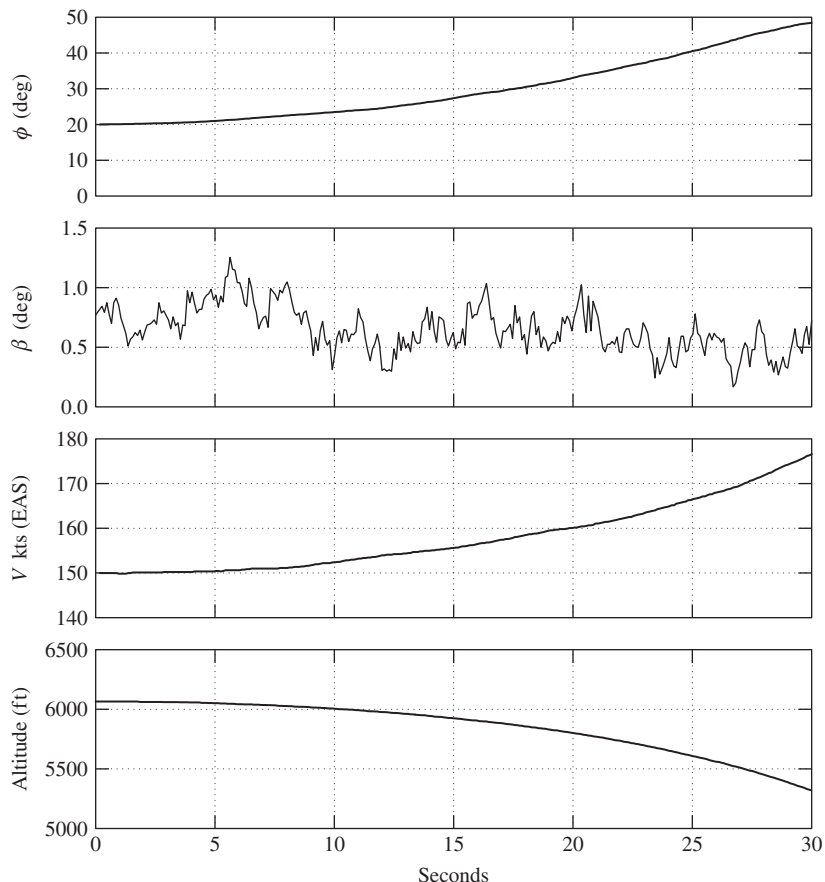


FIGURE 7.12 Flight recording of the spiral mode departure.

aeromechanics of the mode. The first 30 s of the descent is shown in Fig. 7.12. Obviously, the departure must be terminated after a short time if the safety of the aeroplane and its occupants are not to be jeopardised.

Ideally, the dutch roll mode may be excited by applying a doublet to the rudder pedals with a period matched to that of the mode, with all other controls remaining at their trim settings. In practice the pilot pedals continuously and cyclically on the rudder pedal, and by adjusting the frequency it is easy to find the resonant condition. (See the related comments in Example 7.3 and note that the dutch roll frequency is comfortably within the human bandwidth.) In this manner a forced oscillation may easily be sustained. On ceasing the forcing input, the free transient characteristics of the dutch roll mode may be seen. This free response is shown in the flight recording in Fig. 7.13, which was made in a Handley Page Jetstream. The rudder input ζ shows the final doublet before ceasing the forcing at about 5 s; the obvious oscillatory rudder motion after 5 s is due to the cyclic

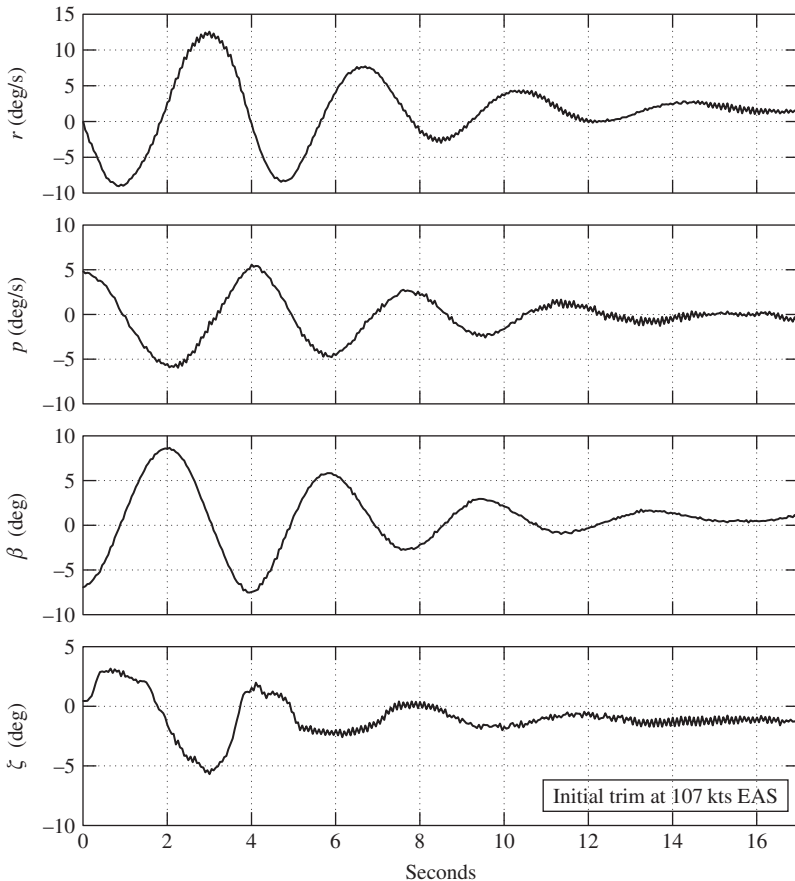


FIGURE 7.13 Flight recording of the dutch roll mode.

aerodynamic load on the free rudder. The classical damped oscillatory motion is clearly visible in the variables shown: yaw rate r , roll rate p , and sideslip angle β . The motion would also be clearly evident in both roll and yaw attitude variables, which are not shown. Note the relative magnitudes of, and the phase shift between, yaw rate r and roll rate p , observations which are consistent with the classical physical explanation of the mode dynamics.

As for the longitudinal modes discussed in Section 6.6, the above flight recordings of the lateral-directional stability modes illustrate the *controls-free* dynamic stability characteristics. The same exercise could be repeated with the controls held fixed following the disturbing input. Obviously, in this event the *controls-fixed* dynamic stability characteristics would be observed and, in general, the differences between the responses would be small. To reiterate the important comments made in Section 6.6, controls-free dynamic response is only possible in aeroplanes with reversible controls, which includes most small classical aeroplanes.

Virtually all larger modern aircraft have powered controls, driven by electronic flight control systems, which are effectively irreversible. This means that they are only capable of exhibiting controls-fixed dynamic response. For this reason, most theoretical modelling and analysis today is concerned only with controls-fixed dynamics, as is the case throughout this book. However, a discussion of the differences between controls-fixed and controls-free aeroplane dynamics may be found in [Hancock \(1995\)](#).

When it is required to investigate analytically the dynamics of a single mode in isolation, the best approach is to emulate flight test practice as much as possible. It is necessary to choose the most appropriate transfer functions to show the dominant response variables in the mode of interest. For example, the roll subsidence mode may only be observed sensibly in the dominant response variable p and, to a lesser extent, in ϕ . Similarly for the spiral and dutch roll modes, it is important to observe the motion in the dominant variables, and hence the most visible in the mode dynamics. It is also essential to apply a control input disturbance sympathetic to the mode dynamics, and it is necessary to observe the response for an appropriate period of time. Otherwise, the dynamics of interest are inevitably obscured by motion coupling effects. For example, [Fig. 7.11](#) shows both the roll subsidence mode and the dutch roll mode, but the excitation, the choice of output variables, and the time scale were chosen to optimise the recording of the roll subsidence mode. The form of control input is not usually difficult to arrange in analytical work since most software packages have built-in impulse, step, and pulse functions, whilst more esoteric functions can usually be programmed by the user. For the analysis of lateral-directional mode dynamics especially, this kind of informed approach is critical if the best possible visualisation of the modes and their associated dynamics are to be obtained.

References

- Hancock, G. J. (1995). *An introduction to the flight dynamics of rigid aeroplanes*. Ellis Horwood.
 Teper, G. L. (1969). *Aircraft stability and control data*. STI Technical Report 176-1. Hawthorne, CA: Systems Technology, Inc, Nasa Contractor Report, National Aeronautics and Space Administration, Washington D.C. 20546.

PROBLEMS

- 7.1** Describe the possible modes of lateral-directional motion of an aircraft when disturbed slightly from steady flight.

An aircraft in steady horizontal flight is disturbed slightly in the lateral plane. If the inertia forces associated with the angular accelerations in the resulting motion are neglected, as well as the components of the acceleration and aerodynamic forces along the oy axis, show that the resulting motion is either a divergence or a subsidence depending in general on the sign of $(L_vN_r - L_rN_v)$. Describe how the stability of an aircraft in this mode changes with an increase in fin size.

(CU 1979)

- 7.2** A transport aircraft whose wing span is 35.8 m is flying at 262 kts at an altitude where the lateral relative density parameter $\mu_2 = 24.4$. The dimensionless controls-fixed lateral-directional characteristic equation is

$$\lambda^4 + 5.8\lambda^3 + 20.3\lambda^2 + 79.0\lambda + 0.37 = 0$$

- (a) What can be deduced about the lateral-directional stability of the aircraft from inspection of the characteristic equation?
- (b) Solve the characteristic equation approximately; determine estimates for the time constants of the nonoscillatory modes and the frequency and damping ratio of the oscillatory mode.
- (c) Comment on the acceptability of this aircraft.

(CU 1980)

- 7.3** Answer the following questions:

- (a) What is the lateral-directional weathercock stability of an aircraft?
- (b) State the main aerodynamic contributions to weathercock stability.

(CU 1982)

- 7.4** The Navion is a small light aeroplane of conventional layout and in a low speed level flight condition, the coefficients of the dimensionless lateral-directional stability quartic are given by

$$\lambda^4 + B_2\lambda^3 + C_2\lambda^2 + D_2\lambda + E_2 = 0$$

where

$$B_2 = 20.889$$

$$C_2 = 46.714 - k_v$$

$$D_2 = 115.120 - 18.636k_v$$

$$E_2 = 55.570 + 1.994k_v$$

and

$$k_v = -\frac{\mu_2 N_v}{i_z}$$

The lateral relative density parameter $\mu_2 = 11.937$, and the dimensionless moment of inertia in yaw $i_z = 0.037$. The quartic factorises to

$$(\lambda + B_2) \left(\lambda + \frac{E_2}{D_2} \right) (\lambda^2 + k_1\lambda + k_2) = 0$$

Show that if the fin were made too large, the aircraft would become dynamically unstable. What would happen to the aircraft if a critical value were exceeded?

(CU 1983)

- 7.5** Describe and explain the physical characteristics of the roll subsidence stability mode. Assuming that the motion associated with the mode comprises pure rolling only, write the equation of motion assuming the rudder to be fixed ($\zeta = 0$). By taking the Laplace transform of this equation, show that the roll control transfer function is given by

$$\frac{p(s)}{\xi(s)} = \frac{-k}{(1 + sT_r)}$$

where $k = \dot{L}_\xi / \dot{L}_p$ and $T_r = -I_x / \dot{L}_p$. State any assumptions made in obtaining the transfer function.

- (a) Obtain the inverse Laplace transform of the transfer function to show that the roll rate response to a unit step of aileron is given by

$$p(t) = -k \left(1 - e^{-\frac{t}{T_r}} \right)$$

- (b) The Republic F-105 Thunderchief aircraft has a wing span of 10.4 m and a moment of inertia in roll of 13965 kg/m². In a cruise flight condition at Mach 0.9 at an altitude of 35,000 ft, the dimensionless derivatives have the following values: $L_p = -0.191$ and $L_\xi = -0.029$. Sketch the roll rate response to a 1° step of aileron deflection and comment on the roll handling of the aircraft.

(CU 1986)

- 7.6** The aircraft described below is flying at a true airspeed of 150 m/s at sea level. At this flight condition it is required to have a steady roll rate of 60 deg/s, when each aileron is deflected through 10 degrees. Assuming that the outboard edges of the ailerons are at the wing tip, calculate the required aileron span. If the ailerons produce 17,500 Nm of adverse yawing moment, calculate the rudder deflection required for trim.

Aircraft data:

Rectangular unswept wing	Fin	
Span = 15 m	Area = 3 m ²	
Area = 27 m ²	Moment arm from cg = 6 m	
$L_p = -0.2$	Rudder	Area = 1.2 m ²
Aileron	$dC_L/d\xi = 2$ 1/rad	$dC_L/d\zeta = 2.3$ 1/rad

(LU 2001)

- 7.7** Using a simple model, show that the time to half-amplitude of the roll subsidence mode may be approximated by

$$t_{\frac{1}{2}} = -\frac{I_x}{\dot{L}_p} \ln(2)$$

Given that the rolling moment due to roll rate derivative may be written as

$$\dot{L}_p = -\rho V_0 \int_0^s \left(C_D + \frac{dC_L}{d\alpha} \right)_y c_y y^2 dy$$

determine the time to half amplitude of the roll subsidence mode for an aircraft with the following characteristics when it is flying at sea level at 100 m/s.

Wing span = 10 m $dC_L/d\alpha$ at root = 5.7 1/rad

Wing root chord = 1.5 m $dC_L/d\alpha$ at tip = 5.7 1/rad

Wing tip chord = 0.75 m $C_D = 0.005$ (constant)

Inertia in roll = 8000 kg/m²

Assume that $dC_L/d\alpha$ varies linearly along the span.

(LU 2002)

- 7.8** For the aircraft described below, determine the value of wing dihedral required to make the spiral mode neutrally stable. The rolling moment due to sideslip derivative is given by

$$L_v = -\frac{1}{Ss} \int_0^s c_y a_y \Gamma y dy$$

and the time to half (double) amplitude for the spiral mode is given by

$$t_{\frac{1}{2}} = \frac{V_0}{g} \left(\frac{L_v N_p - L_p N_v}{L_v N_r - L_r N_v} \right) \ln(2)$$

Aircraft data:

Wing area	$S = 52 \text{ m}^2$
Wing span	$B = 14.8 \text{ m}$
Wing root chord	5.0 m
Wing tip chord	2.0 m
Fin area	$S_F = 8.4 \text{ m}^2$
Fin roll arm	$h_F = 1.8 \text{ m}$
Wing lift curve slope	$a_y = 3.84 \text{ 1/rad}$
Fin lift curve slope	$a_{IF} = 2.2 \text{ 1/rad}$
L_r	-0.120
N_r	-0.120
N_v	0.158

Discuss how the geometry of the wing and fin influence the stability of the spiral mode.

(LU 2003)

Manoeuvrability

8

8.1 Introduction

8.1.1 Manoeuvring flight

What is a manoeuvre? An aeroplane executing aerobatics in a vast blue sky or aeroplanes engaged in aerial combat are the images associated with manoeuvring flight. By their very nature, such manoeuvres are difficult to quantify, especially when it is required to describe manoeuvrability in an analytical framework. In reality, most manoeuvres are comparatively mundane and simply involve changing from one trimmed flight condition to another. When a pilot wishes to manoeuvre away from the current flight condition, he applies control inputs which upset the equilibrium trim state by producing forces and moments to manoeuvre the aeroplane toward the desired flight condition. The temporary out-of-trim forces and moments cause the aeroplane to *accelerate* in a sense determined by the combined action of the control inputs. Thus manoeuvring flight is sometimes called *accelerated flight* and is defined as the condition in which the airframe is subject to temporary, or transient, out-of-trim linear and angular accelerations resulting from the displacement of the controls relative to their trim settings. In analytical terms, the manoeuvre is regarded as an *increment* in steady motion, over and above the initial trim state, in response to an increment in control angle.

The main aerodynamic force producing device in an aeroplane is the wing, and wing lift acts normal to the direction of flight in the plane of symmetry. Normal manoeuvring involves rotating the airframe in roll, pitch, and yaw to point the lift vector in the desired direction, and the simultaneous adjustment of both angle of attack and speed enables the lift force to generate the acceleration to manoeuvre. For example, in turning flight the aeroplane is rolled to the desired bank angle when the horizontal component of lift causes it to turn in the desired direction. Simultaneous aft displacement of the pitch stick is required to generate pitch rate, which in turn generates an increase in angle of attack to produce more lift such that the vertical component is sufficient to balance the weight of the aeroplane and hence to maintain level flight in the turn. (The requirements for simple turning flight are illustrated in Example 2.3.) Thus manoeuvrability is mainly concerned with the ability to rotate about aircraft axes, the modulation of the normal or lift force, and the modulation of the axial or thrust force. The use of lateral sideforce to manoeuvre is not common in conventional aeroplanes since it is aerodynamically inefficient and is both unnatural and uncomfortable for the pilot. The principal aerodynamic manoeuvring force is therefore lift, which acts in the plane of symmetry of the aeroplane; this is controlled by operating the control column in the pitch sense. When the pilot pulls back on the pitch stick the aeroplane pitches up to generate an increased lift force; since this results in out-of-trim normal acceleration, the pilot senses, and is

very sensitive to, the change in acceleration. He senses what appears to be an increase in the earth's gravitational acceleration g and so is said to be *pulling g*.

8.1.2 Stability

Aircraft stability is generally concerned with the requirement that trimmed equilibrium flight can be achieved and that small transient upsets from equilibrium decay to zero. However, in manoeuvring flight the *transient upset* is the deliberate result following a control input; it may not be small and it may well be prolonged. In the manoeuvre the aerodynamic forces and moments may be significantly different from the steady trim values, and it is essential that the changes do not impair the stability of the aeroplane. In other words, there must be no tendency for the aeroplane to diverge in manoeuvring flight.

The classical theory of manoeuvrability is generally attributed to [Gates and Lyon \(1944\)](#), and various interpretations of that original work may be found in most books on aircraft stability and control. Perhaps one of the most comprehensive and accessible summaries of the theory is included in [Babister \(1961\)](#). In this chapter the subject is introduced at the most basic level in order to provide an understanding of the concepts involved, since they are critically important in the broader considerations of flying and handling qualities. The original work makes provision for the effects of compressibility. In the following analysis subsonic flight only is considered in the interest of simplicity and hence understanding.

The traditional analysis of *manoeuvre stability* is based on the concept of the steady manoeuvre in which the aeroplane is subject to a steady normal acceleration in response to a pitch control input. Although rather contrived, this approach does enable the manoeuvre stability of an aeroplane to be explained analytically. The only realistic manoeuvres which can be flown at constant normal acceleration are the inside or outside loop and the steady banked turn. For the purpose of analysis, the loop is simplified to a pull-up, or push-over, which is just a small segment of the circular flight path. Whichever manoeuvre is analysed, the resulting conditions for stability are the same.

Since the steady acceleration is constrained to the plane of symmetry, the problem simplifies to the analysis of *longitudinal manoeuvre stability* and, since the motion is steady, this analysis is a simple extension of that applied to *longitudinal static stability* as described in Chapter 3. Consequently, it leads to the concept of the *longitudinal manoeuvre margin*, the stability margin in manoeuvring flight, which in turn gives rise to the corresponding control parameters *stick displacement per g* and *stick force per g*.

8.1.3 Aircraft handling

It is not difficult to appreciate that the manoeuvrability of an airframe is a critical factor in its overall flying and handling qualities. Too much manoeuvre stability means that large control displacements and forces are needed to encourage the development of the normal acceleration vital to effective manoeuvring. On the other hand, too little manoeuvre stability implies that an enthusiastic pilot could overstress the airframe by applying excessive levels of normal acceleration. Clearly, the difficult balance between control power, manoeuvre stability, static stability, and dynamic stability must be correctly controlled over the entire flight envelope of the aeroplane.

Today, considerations of manoeuvrability in the context of aircraft handling have moved on from the simple analysis of normal acceleration response to controls alone. Important additional considerations concern accompanying roll, pitch, and yaw rates and accelerations that may be achieved from control inputs, since these determine how quickly a manoeuvre can become established. Manoeuvre entry is also *coloured* by transients associated with the short-term dynamic stability modes. The aggressiveness with which a pilot may fly a manoeuvre and the motion cues available to him also contribute to his perception of the over-all handling characteristics of the aeroplane. The “picture” therefore becomes very complex, and it is further complicated by the introduction of flight control systems to the aeroplane. The subject of *aircraft agility* is a relatively new and exciting topic of research which embraces the ideas just mentioned and which is, unfortunately, beyond the scope of the present book.

8.1.4 The steady symmetric manoeuvre

The analysis of longitudinal manoeuvre stability is based on steady motion which results in constant additional, or incremental, normal acceleration; as mentioned previously, the simplest such manoeuvre to analyse is the pull-up.

In symmetric flight, inertial normal acceleration, referred to the *cg*, is given by equation (5.39):

$$a_z = \dot{w} - qU_e \quad (8.1)$$

Since the manoeuvre is steady, $\dot{w} = 0$ and the aeroplane must fly a steady pitch rate in order to generate the normal acceleration required to manoeuvre. A steady turn enables this condition to be maintained ad infinitum in flight but is less straightforward to analyse. In symmetric flight, a short-duration pull-up can be used to represent the lower segment of a continuous circular flight path in the vertical plane because a continuous loop is not practical for many aeroplanes.

It is worth noting that many modern combat aeroplanes and some advanced civil transport aeroplanes have flight control systems which feature *direct lift control* (DLC). In such aeroplanes pitch rate is not an essential prerequisite for the generation of normal acceleration because the wing is fitted with a system of flaps for producing lift directly. However, in some applications it is common to mix DLC flap control with conventional elevator control to improve manoeuvrability—manoeuvre entry in particular. The manoeuvrability of aeroplanes fitted with DLC systems may be significantly enhanced, although the analysis may become rather more complex.

8.2 The steady pull-up manoeuvre

An aeroplane flying initially in steady level flight at speed V_0 is subject to a small elevator input $\delta\eta$ which causes it to pull up with steady pitch rate q . Consider the situation when the aircraft is at the lowest point of the vertical circle flight path as shown in Fig. 8.1.

To sustain flight in the vertical circle it is necessary that the lift L balances not only the weight mg but also the centrifugal force; thus the lift is greater than the weight and

$$L = nmg \quad (8.2)$$

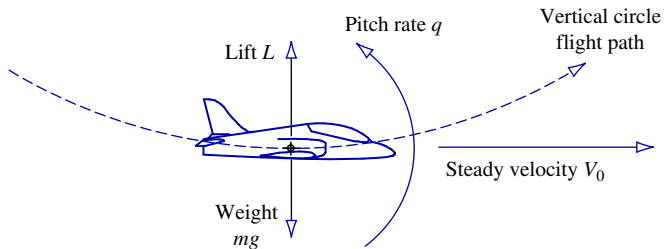


FIGURE 8.1 Symmetric pull-up manoeuvre.

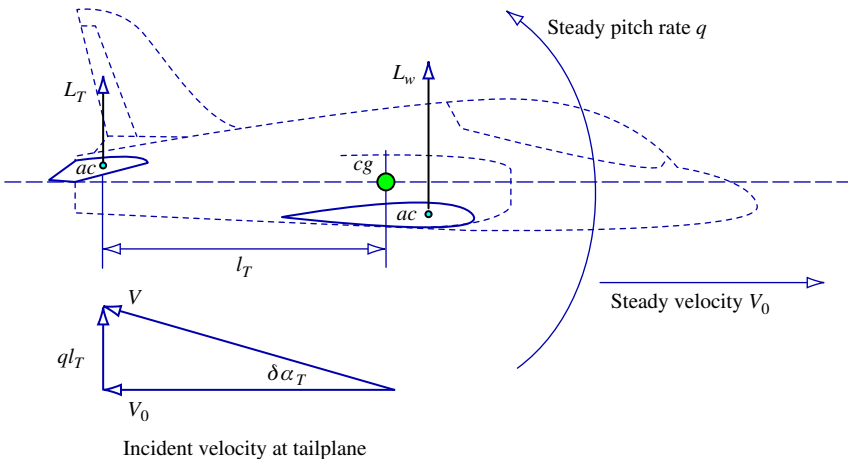


FIGURE 8.2 Incremental tailplane incidence in pull-up manoeuvre.

where n is the italic for emphasis. The normal load factor therefore quantifies the total lift necessary to maintain the manoeuvre and in steady level flight $n = 1$. The centrifugal force balance is therefore given by

$$L - mg = mV_0q \quad (8.3)$$

and the incremental normal load factor may be derived directly:

$$\delta n = (n - 1) = \frac{V_0 q}{g} \quad (8.4)$$

Now, as the aircraft is pitching up steadily, the tailplane experiences an increase in incidence $\delta\alpha_T$ from the pitch manoeuvre as indicated in Fig. 8.2.

Since small-perturbation motion is assumed, the increase in tailplane incidence is given by

$$\delta\alpha_T \cong \tan\delta\alpha_T = \frac{ql_T}{V_0} \quad (8.5)$$

where l_T is the moment arm of the aerodynamic centre of the tailplane with respect to the centre of rotation in pitch, the *cg*. Eliminating pitch rate q from [equations \(8.4\) and \(8.5\)](#),

$$\delta\alpha_T = \frac{(n - 1)gl_T}{V_0^2} \quad (8.6)$$

In the steady level flight condition about which the manoeuvre is executed, the lift and weight are now equal; whence

$$V_0^2 = \frac{2mg}{\rho SC_{L_w}} \quad (8.7)$$

where C_{L_w} is the steady level flight value of the wing-body lift coefficient. Thus, from [equations \(8.6\) and \(8.7\)](#),

$$\delta\alpha_T = \frac{(n - 1)\rho SC_{L_w} l_T}{2m} = \frac{(n - 1)C_{L_w} l_T}{\mu_1 \bar{c}} \equiv \frac{\delta C_{L_w} l_T}{\mu_1 \bar{c}} \quad (8.8)$$

where μ_1 is the *longitudinal relative density parameter* and is defined

$$\mu_1 = \frac{m}{\frac{1}{2}\rho S \bar{c}} \quad (8.9)$$

and the increment in lift coefficient, alternatively referred to as incremental g , necessary to sustain the steady manoeuvre is given by

$$\delta C_{L_w} = (n - 1)C_{L_w} = \delta n C_{L_w} \quad (8.10)$$

Care should be exercised when using the longitudinal relative density parameter since various definitions are in common use.

8.3 The pitching moment equation

Subject to the same assumptions about thrust, drag, speed effects, and so on, in the steady symmetric manoeuvre the pitching moment equation in coefficient form given by [equation \(3.7\)](#) applies and may be written as

$$C'_m = C_{m_0} + C'_{L_w}(h - h_0) - C'_{L_T} \bar{V}_T \quad (8.11)$$

where a dash indicates the manoeuvring value of the coefficient and

$$\begin{aligned} C'_m &= C_m + \delta C_m \\ C'_{L_w} &= C_{L_w} + \delta C_{L_w} \equiv n C_{L_w} \\ C'_{L_T} &= C_{L_T} + \delta C_{L_T} \end{aligned}$$

where C_m , C_{L_w} , and C_{L_T} denote the steady trim values of the coefficients and δC_m , δC_{L_w} , and δC_{L_T} denote the increments in the coefficients required to manoeuvre.

The corresponding expression for the tailplane lift coefficient is given by equation (3.8), which for manoeuvring flight may be written as

$$C'_{L_T} = a_1 \alpha'_T + a_2 \eta' + a_3 \beta_\eta \quad (8.12)$$

It is assumed that the tailplane has a symmetric aerofoil section, $a_0 = 0$, and that the tab angle β_η is held at the constant steady trim value throughout the manoeuvre. In other words, the manoeuvre is the result of elevator input only. Thus, using the above notation,

$$\begin{aligned}\alpha'_T &= \alpha_T + \delta\alpha_T \\ \eta' &= \eta + \delta\eta\end{aligned}$$

Tailplane incidence is given by equation (3.11); in the manoeuvre this may be written as

$$\alpha_T = \frac{C'_{L_w}}{a} \left(1 - \frac{d\varepsilon}{d\alpha} \right) + \eta_T \quad (8.13)$$

Total tailplane incidence in the manoeuvre is therefore given by the sum of [equations \(8.8\)](#) and [\(8.13\)](#):

$$\alpha'_T = \frac{C'_{L_w}}{a} \left(1 - \frac{d\varepsilon}{d\alpha} \right) + \eta_T + \frac{\delta C_{L_w} l_T}{\mu_1 \bar{c}} \quad (8.14)$$

Substituting for α'_T in [equation \(8.12\)](#), the expression for tailplane lift coefficient in the manoeuvre may be written as

$$C'_{L_T} = \frac{C'_{L_w} a_1}{a} \left(1 - \frac{d\varepsilon}{d\alpha} \right) + a_1 \eta_T + \frac{\delta C_{L_w} a_1 l_T}{\mu_1 \bar{c}} + a_2 \eta' + a_3 \beta_\eta \quad (8.15)$$

Substitute the expression for tailplane lift coefficient, [equation \(8.15\)](#), into [equation \(8.11\)](#) and, after some rearrangement, the pitching moment equation may be written as

$$C'_m = C_{m_0} + C'_{L_w} (h - h_0) - \bar{V}_T \left(\frac{C'_{L_w} a_1}{a} \left(1 - \frac{d\varepsilon}{d\alpha} \right) + a_1 \eta_T + \frac{\delta C_{L_w} a_1 l_T}{\mu_1 \bar{c}} + a_2 \eta' + a_3 \beta_\eta \right) \quad (8.16)$$

[Equation \(8.16\)](#) describes the total pitching moment in the manoeuvre. To obtain the incremental pitching moment equation which describes the manoeuvre effects only, it is first necessary to replace the “dashed” variables and coefficients in [equation \(8.16\)](#) with their equivalent expressions. Then, after some rearrangement, [equation \(8.16\)](#) may be written as

$$\begin{aligned}C_m + \delta C_m &= \left\{ C_{m_0} + C'_{L_w} (h - h_0) - \bar{V}_T \left(\frac{C'_{L_w} a_1}{a} \left(1 - \frac{d\varepsilon}{d\alpha} \right) + a_1 \eta_T + a_2 \eta' + a_3 \beta_\eta \right) \right\} \\ &\quad + \left\{ \delta C_{L_w} (h - h_0) - \bar{V}_T \left(\frac{\delta C_{L_w} a_1}{a} \left(1 - \frac{d\varepsilon}{d\alpha} \right) + \frac{\delta C_{L_w} a_1 l_T}{\mu_1 \bar{c}} + a_2 \delta \eta \right) \right\}\end{aligned} \quad (8.17)$$

Now, in the steady equilibrium flight condition about which the manoeuvre is executed, the pitching moment is zero; therefore,

$$C_m = C_{m_0} + C_{L_w}(h - h_0) - \bar{V}_T \left(\frac{C_{L_w} a_1}{a} \left(1 - \frac{d\varepsilon}{d\alpha} \right) + a_1 \eta_T + a_2 \eta + a_3 \beta_\eta \right) = 0 \quad (8.18)$$

and equation (8.17) simplifies to that describing the incremental pitching moment coefficient,

$$\delta C_m = \delta C_{L_w}(h - h_0) - \bar{V}_T \left(\frac{\delta C_{L_w} a_1}{a} \left(1 - \frac{d\varepsilon}{d\alpha} \right) + \frac{\delta C_{L_w} a_1 l_T}{\mu_1 \bar{c}} + a_2 \delta \eta \right) \quad (8.19)$$

8.4 Longitudinal manoeuvre stability

As for longitudinal static stability, discussed in Chapter 3, to achieve a stable manoeuvre the following condition must be satisfied:

$$\frac{dC'_m}{dC'_{L_w}} < 0 \quad (8.20)$$

and for the manoeuvre to remain steady,

$$C'_m = 0 \quad (8.21)$$

Analysis and interpretation of these conditions leads to the definition of *controls-fixed manoeuvre stability* and *controls-free manoeuvre stability*, which correspond with the parallel concepts derived in the analysis of longitudinal static stability.

8.4.1 Controls-fixed stability

The total pitching moment equation (8.16) may be written as

$$C'_m = C'_{m_0} + C'_{L_w}(h - h_0) - \bar{V}_T \left(\frac{C'_{L_w} a_1}{a} \left(1 - \frac{d\varepsilon}{d\alpha} \right) + a_1 \eta_T + \frac{(C'_{L_w} - C_{L_w}) a_1 l_T}{\mu_1 \bar{c}} + a_2 \eta' + a_3 \beta_\eta \right) \quad (8.22)$$

and since, by definition, the controls are held fixed in the manoeuvre,

$$\frac{d\eta'}{dC'_{L_w}} = 0$$

Applying the condition for stability, equation (8.20), to equation (8.22) and noting that C_{L_w} and β_η are constant at their steady level flight values and that η_T is also a constant of the aircraft configuration, then

$$\frac{dC'_m}{dC'_{L_w}} = (h - h_0) - \bar{V}_T \left(\frac{a_1}{a} \left(1 - \frac{d\varepsilon}{d\alpha} \right) + \frac{a_1 l_T}{\mu_1 \bar{c}} \right) \quad (8.23)$$

or

$$H_m = -\frac{dC'_m}{dC'_{L_w}} = h_m - h \quad (8.24)$$

where H_m is the *controls-fixed manoeuvre margin*; the location of the *controls-fixed manoeuvre point* h_m on the mean aerodynamic chord $\bar{\bar{c}}$ is given by

$$h_m = h_0 + \bar{V}_T \left(\frac{a_1}{a} \left(1 - \frac{d\varepsilon}{d\alpha} \right) + \frac{a_1 l_T}{\mu_1 \bar{\bar{c}}} \right) = h_n + \frac{\bar{V}_T a_1 l_T}{\mu_1 \bar{\bar{c}}} \quad (8.25)$$

Clearly, for controls-fixed manoeuvre stability, the manoeuvre margin H_m must be positive, which, with reference to [equation \(8.24\)](#), implies that the *cg* must be ahead of the manoeuvre point. [Equation \(8.25\)](#) indicates that the controls-fixed manoeuvre point is aft of the corresponding neutral point by an amount depending on the aerodynamic properties of the tailplane. It therefore follows that

$$H_m = K_n + \frac{\bar{V}_T a_1 l_T}{\mu_1 \bar{\bar{c}}} \quad (8.26)$$

which indicates that the controls-fixed manoeuvre stability is greater than the controls-fixed static stability. With reference to Appendix 8, [equation \(8.26\)](#) may be restated in terms of aerodynamic stability derivatives:

$$H_m = -\frac{M_w}{a} - \frac{M_q}{\mu_1} \quad (8.27)$$

A most important conclusion is, then, that additional stability in manoeuvring flight is provided by the aerodynamic pitch damping properties of the tailplane. However, caution is advised because this conclusion may not apply to all aeroplanes in large-amplitude manoeuvring or to manoeuvring in conditions where the assumptions do not apply.

As for controls-fixed static stability, the meaning of controls-fixed manoeuvre stability is easily interpreted by considering the pilot action required to establish a steady symmetric manoeuvre from an initial trimmed level flight condition. Since the steady (fixed) incremental elevator angle needed to induce the manoeuvre is of interest, the incremental pitching moment [equation \(8.19\)](#) is applicable. In a stable steady—and hence by definition—non-divergent manoeuvre, the incremental pitching moment δC_m is zero. [Equation \(8.19\)](#) may therefore be rearranged to give

$$\frac{\delta\eta}{\delta C_{L_w}} = \frac{1}{\bar{V}_T a_2} \left\{ (h - h_0) - \bar{V}_T \left(\frac{a_1}{a} \left(1 - \frac{d\varepsilon}{d\alpha} \right) + \frac{a_1 l_T}{\mu_1 \bar{\bar{c}}} \right) \right\} = \frac{-H_m}{\bar{V}_T a_2} \quad (8.28)$$

Or, in terms of aerodynamic stability derivatives,

$$\frac{\delta\eta}{\delta C_{L_w}} = \frac{-H_m}{M_\eta} = \frac{1}{M_\eta} \left(\frac{M_w}{a} + \frac{M_q}{\mu_1} \right) \quad (8.29)$$

Referring to [equation \(8.10\)](#),

$$\delta C_{L_w} = (n - 1) C_{L_w}$$

which describes the incremental aerodynamic load acting on the aeroplane causing it to execute the manoeuvre, expressed in coefficient form and measured in units of “g.” Thus, both [equation \(8.28\)](#) and [equation \(8.29\)](#) express the *elevator displacement per g* capability of the aeroplane, which is proportional to the controls-fixed manoeuvre margin and inversely proportional to the elevator control power, quantified by the aerodynamic control derivative M_η .

8.4.2 Normal acceleration response to elevator

Since elevator angle and pitch control stick angle are directly related by the control gearing, the very important *stick displacement per g* control characteristic follows directly and is also proportional to the controls-fixed manoeuvre margin. This latter control characteristic is critically important in the determination of longitudinal handling qualities. Measurements of elevator angle and normal acceleration in steady manoeuvres for a range of values of normal load factor provide an effective means for determining controls-fixed manoeuvre stability from flight experiments. However, in such experiments it is not always possible to ensure that all of the underlying assumptions can be adhered to.

Alternatively, and in the context of *small-perturbation* normal acceleration response to controls, it is instructive to use transfer function descriptions in the analysis. Because short-term steady-state response to controls is the principal interest, it is convenient to utilise the longitudinal reduced-order transfer functions for the mathematical analysis. In longitudinal motion the normal acceleration a_z referred to the centre of gravity is given by [equation \(8.1\)](#) and for symmetric manoeuvring is

$$a_z = \dot{w} - qU_e \quad (8.30)$$

where U_e is the steady axial component of velocity. The Laplace transform of [equation \(8.30\)](#), assuming zero initial conditions, may be written as

$$a_z(s) = sw(s) - q(s)U_e \quad (8.31)$$

Or, expressing [equation \(8.31\)](#) in terms of elevator response transfer functions,

$$a_z(s) = s \frac{N_\eta^w(s)}{\Delta(s)} \eta(s) - U_e \frac{N_\eta^q(s)}{\Delta(s)} \eta(s) = \frac{(sN_\eta^w(s) - U_e N_\eta^q(s))\eta(s)}{\Delta(s)} \quad (8.32)$$

where

$$\frac{N_\eta^w(s)}{\Delta(s)} = \frac{k_w(s + 1/T_\alpha)}{(s^2 + 2\zeta_s \omega_s s + \omega_s^2)} \quad \frac{N_\eta^q(s)}{\Delta(s)} = \frac{k_q(s + 1/T_{\theta_2})}{(s^2 + 2\zeta_s \omega_s s + \omega_s^2)} \quad (8.33)$$

Defining, the incremental normal load factor δn due to manoeuvring as

$$\delta n = -\frac{a_z}{g} \quad (8.34)$$

and since normal acceleration response to elevator is largely determined by the dynamic characteristics of the short-period pitching oscillation, the reduced-order longitudinal transfer functions $w(s)/\eta(s)$ and $q(s)/\eta(s)$ given in [equations \(8.33\)](#) may be substituted in [equation \(8.32\)](#) to give the

transfer function for normal load factor response to an increment of elevator displacement as follows:

$$\frac{\delta n(s)}{\delta \eta(s)} = -\frac{(k_w(s + 1/T_\alpha)s - k_q(s + 1/T_{\theta_2})U_e)}{g\Delta(s)} \quad (8.35)$$

Application of the final value theorem to [equation \(8.35\)](#), assuming a unit elevator input, leads to an expression for the steady-state gain:

$$\left. \frac{\delta n}{\delta \eta} \right|_{state}^{steady} \equiv \frac{k_q U_e}{g \omega_s^2 T_{\theta_2}} \quad (8.36)$$

where $k_q = m_\eta$, the concise elevator control derivative. Note the dependence of normal acceleration response to elevator on the dynamic stability parameters ω_s and T_{θ_2} . This is entirely consistent with the understanding that longitudinal dynamic handling is significantly related to the aircraft acceleration motion cue in response to control. Alternatively, [equation \(8.36\)](#) may be expressed entirely in terms of concise aerodynamic stability derivatives:

$$\left. \frac{\delta n}{\delta \eta} \right|_{state}^{steady} = -\frac{m_\eta z_w U_e}{g(m_q z_w - m_w U_e)} \quad (8.37)$$

With reference to Appendices 2 and 8, the concise derivatives in [equation \(8.37\)](#) may be written in terms of the dimensionless derivatives, which in turn may be substituted with their basic aerodynamic definitions to give, after a substantial algebraic manipulation,

$$\left. \frac{\delta n}{\delta \eta} \right|_{state}^{steady} = -\frac{\bar{V}_T a_2 U_e^2 \left(1 - \frac{\bar{V}_T a_1 \frac{d\varepsilon}{d\alpha}}{\mu_1} \right)}{g \mu_1 \bar{c} \left(H_m - \left(\frac{\bar{V}_T a_1}{\mu_1} \right)^2 \frac{l_T}{\bar{c}} \frac{d\varepsilon}{d\alpha} \right)} \quad (8.38)$$

Alternatively, and omitting insignificantly small terms in [equation \(8.38\)](#),

$$\left. \frac{\delta n}{\delta \eta} \right|_{state}^{steady} \approx -\frac{g \mu_1 \bar{c} H_m}{\bar{V}_T a_2 U_e^2} \quad (8.39)$$

[Equation \(8.39\)](#) is the equivalent to [equation \(8.28\)](#) and confirms that elevator angle η per g to manoeuvre is proportional to the controls-fixed manoeuvre margin H_m .

8.4.3 Controls-free stability

The controls-free manoeuvre is not a practical way of controlling an aeroplane. It does, of course, imply that the elevator angle required to achieve the manoeuvre is obtained by adjustment of the tab angle. As in the case of controls-free static stability, this equates to the control force required to

achieve the manoeuvre, a most important control characteristic. Control force derives from elevator hinge moment in a conventional aeroplane; the elevator hinge moment coefficient in manoeuvring flight is given by equation (3.21) and may be restated as

$$C'_H = C_H + \delta C_H = b_1 \alpha'_T + b_2 \eta' + b_3 \beta_\eta \quad (8.40)$$

Since the elevator angle in a controls-free manoeuvre is indeterminate, it is convenient to express η' in terms of hinge moment coefficient by rearranging equation (8.40):

$$\eta' = \frac{1}{b_2} C'_H - \frac{b_1}{b_2} \alpha'_T - \frac{b_3}{b_2} \beta_\eta \quad (8.41)$$

Substitute the expression for α'_T , equation (8.14), into equation (8.41) to obtain

$$\eta' = \frac{1}{b_2} C'_H - \frac{b_1}{ab_2} \left(1 - \frac{d\varepsilon}{d\alpha} \right) C'_{L_w} - \frac{b_1}{b_2} \eta_T - \frac{b_1 l_T}{b_2 \mu_1 \bar{c}} \delta C_{L_w} - \frac{b_3}{b_2} \beta_\eta \quad (8.42)$$

Equation (8.42) may be substituted into the manoeuvring pitching moment equation (8.16) to replace the indeterminate elevator angle by hinge moment coefficient. After some algebraic rearrangement, the manoeuvring pitching moment may be expressed in the same format as equation (8.22):

$$C'_m = C_{m_0} + C'_{L_w} (h - h_0) - \bar{V}_T \left(\begin{array}{l} C'_{L_w} \frac{a_1}{a} \left(1 - \frac{d\varepsilon}{d\alpha} \right) \left(1 - \frac{a_2 b_1}{a_1 b_2} \right) + a_1 \eta_T + C'_H \frac{a_2}{b_2} \\ + (C'_{L_w} - C_{L_w}) \frac{a_1 l_T}{\mu_1 \bar{c}} \left(1 - \frac{a_2 b_1}{a_1 b_2} \right) + \beta_\eta \left(1 - \frac{a_2 b_3}{a_3 b_2} \right) \end{array} \right) \quad (8.43)$$

and since, by definition, the controls are free in the manoeuvre,

$$C'_H = 0$$

Applying the condition for stability, equation (8.20), to equation (8.43) and noting that, as before, C_{L_w} and β_η are constant at their steady level flight values and that η_T is also a constant of the aircraft configuration, then

$$\frac{dC'_m}{dC'_{L_w}} = (h - h_0) - \bar{V}_T \left(\frac{a_1}{a} \left(1 - \frac{d\varepsilon}{d\alpha} \right) + \frac{a_1 l_T}{\mu_1 \bar{c}} \right) \left(1 - \frac{a_2 b_1}{a_1 b_2} \right) \quad (8.44)$$

or

$$H'_m = - \frac{dC'_m}{dC'_{L_w}} = h'_m - h \quad (8.45)$$

where H'_m is the *controls-free manoeuvre margin* and the location of the *controls-free manoeuvre point* h'_m on the mean aerodynamic chord \bar{c} is given by

$$\begin{aligned} h'_m &= h_0 + \bar{V}_T \left(\frac{a_1}{a} \left(1 - \frac{d\varepsilon}{d\alpha} \right) + \frac{a_1 l_T}{\mu_1 \bar{c}} \right) \left(1 - \frac{a_2 b_1}{a_1 b_2} \right) \\ &= h'_n + \bar{V}_T \frac{a_1 l_T}{\mu_1 \bar{c}} \left(1 - \frac{a_2 b_1}{a_1 b_2} \right) \end{aligned} \quad (8.46)$$

Clearly, for controls-free manoeuvre stability, the manoeuvre margin H'_m must be positive. With reference to equation (8.45), this implies that the *cg* must be ahead of the manoeuvre point. Equation (8.46) indicates that the controls-free manoeuvre point is aft of the corresponding neutral point by an amount again dependent on the aerodynamic damping properties of the tailplane. It therefore follows that

$$H'_m = K'_n + \bar{V}_T \frac{a_1 l_T}{\mu_1 \bar{c}} \left(1 - \frac{a_2 b_1}{a_1 b_2} \right) \equiv K'_n + \frac{M_q}{\mu_1} \left(1 - \frac{a_2 b_1}{a_1 b_2} \right) \quad (8.47)$$

which indicates that the controls-free manoeuvre stability is greater than the controls-free static stability when

$$\left(1 - \frac{a_2 b_1}{a_1 b_2} \right) > 0 \quad (8.48)$$

Since a_1 and a_2 are both positive, the degree of controls-free manoeuvre stability, over and above controls-free static stability, is controlled by the signs of the hinge moment parameters b_1 and b_2 . This, in turn, depends on the aerodynamic design of the elevator control surface.

As for controls-free static stability, the meaning of controls-free manoeuvre stability is easily interpreted by considering the pilot action required to establish a steady symmetric manoeuvre from an initial trimmed level flight condition. Since the controls are “free,” this equates to a steady tab angle increment or, more appropriately, a steady control force increment that causes the aeroplane to manoeuvre. Equation (8.43) may be rewritten in terms of the steady and incremental contributions to the total controls-free manoeuvring pitching moment in the same way as equation (8.17):

$$\begin{aligned} C_m + \delta C_m &= \left\{ C_{m_0} + C_{L_w}(h - h_0) - \bar{V}_T \left(C_{L_w} \frac{a_1}{a} \left(1 - \frac{d\varepsilon}{d\alpha} \right) \left(1 - \frac{a_2 b_1}{a_1 b_2} \right) \right. \right. \\ &\quad \left. \left. + a_1 \eta_T + C_H \frac{a_2}{b_2} + \beta_\eta \left(1 - \frac{a_2 b_3}{a_3 b_2} \right) \right) \right\} \\ &+ \left\{ \delta C_{L_w}(h - h_0) - \bar{V}_T \left(\delta C_{L_w} \frac{a_1}{a} \left(1 - \frac{d\varepsilon}{d\alpha} \right) \left(1 - \frac{a_2 b_1}{a_1 b_2} \right) \right. \right. \\ &\quad \left. \left. + \delta C_H \frac{a_2}{b_2} + \delta C_{L_w} \frac{a_1 l_T}{\mu_1 \bar{c}} \left(1 - \frac{a_2 b_1}{a_1 b_2} \right) \right) \right\} \end{aligned} \quad (8.49)$$

Now, in the steady equilibrium flight condition about which the manoeuvre is executed, the pitching moment is zero; thus

$$C_m = C_{m_0} + C_{L_w}(h - h_0) - \bar{V}_T \begin{pmatrix} C_{L_w} \frac{a_1}{a} \left(1 - \frac{d\varepsilon}{d\alpha} \right) \left(1 - \frac{a_2 b_1}{a_1 b_2} \right) \\ + a_1 \eta_T + C_H \frac{a_2}{b_2} + \beta_\eta \left(1 - \frac{a_2 b_3}{a_3 b_2} \right) \end{pmatrix} = 0 \quad (8.50)$$

and [equation \(8.49\)](#) simplifies to that describing the incremental controls-free pitching moment coefficient:

$$\delta C_m = \delta C_{L_w}(h - h_0) - \bar{V}_T \begin{pmatrix} \delta C_{L_w} \frac{a_1}{a} \left(1 - \frac{d\varepsilon}{d\alpha} \right) \left(1 - \frac{a_2 b_1}{a_1 b_2} \right) \\ + \delta C_H \frac{a_2}{b_2} + \delta C_{L_w} \frac{a_1 l_T}{\mu_1 \bar{c}} \left(1 - \frac{a_2 b_1}{a_1 b_2} \right) \end{pmatrix} \quad (8.51)$$

In the steady manoeuvre the incremental pitching moment δC_m is zero and [equation \(8.51\)](#) may be rearranged to give

$$\frac{\delta C_H}{\delta C_{L_w}} = \frac{b_2}{a_2 \bar{V}_T} \left\{ (h - h_0) - \bar{V}_T \left(\frac{a_1}{a} \left(1 - \frac{d\varepsilon}{d\alpha} \right) + \frac{a_1 l_T}{\mu_1 \bar{c}} \right) \left(1 - \frac{a_2 b_1}{a_1 b_2} \right) \right\} = - \frac{b_2 H'_m}{a_2 \bar{V}_T} \quad (8.52)$$

In a conventional aeroplane the hinge moment coefficient relates directly to the control stick force, as shown in [equation \(3.32\)](#). [Equation \(8.52\)](#) therefore indicates the very important result that the *stick force per g* control characteristic is proportional to the controls-free manoeuvre margin. This control characteristic is critically important in the determination of longitudinal handling qualities, and it must have the correct value. In other words, the controls-free manoeuvre margin must lie between precisely defined upper and lower bounds. As stated above, in an aerodynamically controlled aeroplane this control characteristic can be adjusted independently of the other stability characteristics by selective design of the values of the hinge moment parameters b_1 and b_2 . The controls-free manoeuvre stability is critically dependent on the ratio b_1/b_2 , which controls the magnitude and sign of the expression [\(8.48\)](#).

For conventional aeroplanes fitted with a plain flap-type elevator control, both b_1 and b_2 are usually negative and, as shown in [equation \(8.47\)](#), the controls-free manoeuvre stability is greater than the controls-free static stability. Adjustment of b_1 and b_2 is normally achieved by aeromechanical means which are designed to modify the elevator hinge moment characteristics. Typically, this involves carefully tailoring the aerodynamic balance of the elevator by means such as set back hinge line, horn balances, spring tabs, servo tabs, and so on. Excellent descriptions of these devices may be found in [Dickinson \(1968\)](#) and [Babister \(1961\)](#).

8.4.4 Elevator deflection and stick force

The elevator hinge moment is denoted H , where

$$H = \frac{1}{2} \rho U_e^2 S_\eta \bar{c}_\eta C_H \quad (8.53)$$

Whence, stick force F_η is given by

$$F_\eta = g_\eta H = \frac{1}{2} \rho U_e^2 S_\eta \bar{c}_\eta g_\eta C_H \quad (8.54)$$

where g_η is the stick-to-elevator gearing constant, which has a negative value to be consistent with the controls notation. Now, in order to utilise [equation \(8.54\)](#) to relate normal acceleration to stick force, it is first necessary to express stick force F_η in terms of elevator angle η .

The *controls-fixed* manoeuvre margin H_m defines the relationship between the elevator angle and the increment in lift to manoeuvre about trim, as given by [equation \(8.29\)](#):

$$\frac{\delta\eta}{\delta C_{Lw}} = -\frac{H_m}{\bar{V}_T a_2} \quad (8.55)$$

Similarly, the controls-free manoeuvre margin H'_m defines the relationship between the control hinge moment and the increment in lift to manoeuvre about trim as given by [equation \(8.52\)](#):

$$\frac{\delta C_H}{\delta C_{Lw}} = -\frac{b_2 H'_m}{\bar{V}_T a_2} \quad (8.56)$$

Thus from [equations \(8.55\) and \(8.56\)](#),

$$\frac{\delta C_H}{\delta\eta} = \frac{b_2 H'_m}{H_m} \quad (8.57)$$

From [equations \(8.54\) and \(8.57\)](#), the stick force per unit of elevator required to manoeuvre about trim is easily derived:

$$\frac{\delta F_\eta}{\delta\eta} = \frac{g_\eta \delta H}{\delta\eta} = \frac{1}{2} \rho U_e^2 S_\eta \bar{c}_\eta g_\eta \frac{\delta C_H}{\delta\eta} = \frac{\frac{1}{2} \rho U_e^2 S_\eta \bar{c}_\eta g_\eta b_2 H'_m}{H_m} \quad (8.58)$$

The *incremental stick force per g* then follows by multiplying [equation \(8.58\)](#) by [equation \(8.39\)](#):

$$\frac{\delta F_\eta}{\delta n} = \frac{\delta F_\eta}{\delta\eta} \frac{\delta\eta}{\delta n} = -\frac{b_2 S_\eta c_\eta}{a_2 \bar{V}_T S} g_\eta mg H'_m \quad (8.59)$$

Referring to [equation \(8.59\)](#), it is clear that adjustment to stick force per g , without otherwise disturbing the aerodynamic design, can only be effected by modifying the control heaviness parameter b_2 or the mechanical gearing g_η . However, the mechanical gearing g_η is chosen to give the correct control sensitivity, rather than optimising the control force. Thus the only effective means for adjusting control force in a mechanical flying control system remains the surface hinge moment parameters b_1 and b_2 . In the event that this solution is inadequate, some form of artificial spring feel system is required. Additionally a servo, geared or spring tab, may be used such that the tab angle β_η becomes

a function of elevator angle η . In many instances it is also necessary to employ non-linear gearing in place of linear gearing g_η to ensure adequate handling qualities at all flight conditions.

The measurement of stick force per g is easily undertaken in flight. The aeroplane is flown in steady manoeuvring flight, the turn probably being the simplest way of achieving a steady incremental normal acceleration for a period long enough to enable good-quality measurements to be made. Measurements of stick force and normal acceleration permit estimates of the controls-free manoeuvre margin and the location of the controls-free manoeuvre point. With greater experimental difficulty, stick force per g can also be measured in steady pull-ups and steady push-overs. However the experiment is done, it must be remembered that it is not always possible to ensure that all of the assumptions can be adhered to.

8.5 Aircraft dynamics and manoeuvrability

The preceding analysis shows how the stability of an aeroplane in manoeuvring flight is dependent on the manoeuvre margins and, further, that the magnitude of the manoeuvre margins determines the critical handling characteristics, stick displacement per g , and stick force per g . However, the manoeuvre margins are also instrumental in determining some of the dynamic response characteristics of the aeroplane. This fact further reinforces the statement made elsewhere that static, manoeuvre, and dynamic stability and control characteristics are very much inter-related and should not be treated entirely as isolated topics.

In Chapter 6, reduced-order models of an aircraft are discussed. Also, from the longitudinal model representing short-term dynamic stability and response, an approximate expression for the short-period-mode undamped natural frequency is derived, equation (6.21), in terms of dimensional aerodynamic stability derivatives. With reference to Appendix 2, this expression may be restated in terms of dimensionless derivatives:

$$\omega_s^2 = \frac{\frac{1}{2}\rho V_0^2 S \bar{C}}{I_y} \left(\frac{\frac{1}{2}\rho S \bar{C}}{m} M_q Z_w + M_w \right) = \frac{\frac{1}{2}\rho V_0^2 S \bar{C}}{I_y} \left(\frac{M_q Z_w}{\mu_1} + M_w \right) \quad (8.60)$$

where μ_1 is the longitudinal relative density factor defined in [equation \(8.9\)](#).

Now, with reference to Appendix 8, an approximate expression for Z_w is given as

$$Z_w \cong -C_D - \frac{\partial C_L}{\partial \alpha} = -C_D - a \quad (8.61)$$

for small-perturbation motion in subsonic flight. Since $a > C_D$, [equation \(8.61\)](#) may be approximated further, and substituting for Z_w in [equation \(8.60\)](#) to obtain

$$\omega_s^2 = \frac{\frac{1}{2}\rho V_0^2 S \bar{C} a}{I_y} \left(-\frac{M_q}{\mu_1} - \frac{M_w}{a} \right) = k H_m \equiv k \left(K_n - \frac{M_q}{\mu_1} \right) \quad (8.62)$$

where k is a constant at the given flight condition. [Equation \(8.62\)](#) therefore shows that the undamped natural frequency of the longitudinal short-period mode is directly dependent on the

controls-fixed manoeuvre margin. Alternatively, this may be interpreted as a dependency on the controls-fixed static margin and pitch damping. Clearly, since the controls-fixed manoeuvre margin must lie between carefully defined boundaries if satisfactory handling is to be ensured, this implies that the longitudinal short-period mode must also be constrained to a corresponding frequency band. Requirements for flying qualities have been developed from this kind of understanding and are discussed in Chapter 10.

In many modern aeroplanes the link between the aerodynamic properties of the control surface and the stick force is broken by a servo-actuator and other components of the flight control system. In this case, the control forces are provided artificially and may not inter-relate with other stability and control characteristics in the classical way. However, it is obviously important that the pilot's perception of the handling qualities of his aeroplane look like those of an aeroplane with acceptable aerodynamic manoeuvre margins. Since many of the subtle aerodynamic inter-relationships do not exist in aeroplanes employing sophisticated flight control systems, it is critically important to be fully aware of the handling qualities implications at all stages of a flight control system design.

8.6 Aircraft with stability augmentation

All aircraft with a flight control system for enhancing flying qualities require a power actuator to drive the control surfaces, and this breaks, or modifies, the mechanical force feedback path between the surface and the control stick. Consequently, some form of artificial feel system is usually required to restore the control force gradient to an acceptable value. In this illustration it is assumed that all of the stick force is provided by an artificial feel unit whereas in practice some of the feel force might be provided by a feel unit and some may be derived from the surface hinge moment via the mechanical feedback linkage around the surface actuator and/or via the addition of a bob-weight to the mechanical stick installation. The feel unit can take many different forms—for example, a simple linear or non-linear spring or an electric or hydraulic device with characteristics scheduled with appropriate flight parameters. A functional block diagram of a typical simple control system is shown in Fig. 8.3.

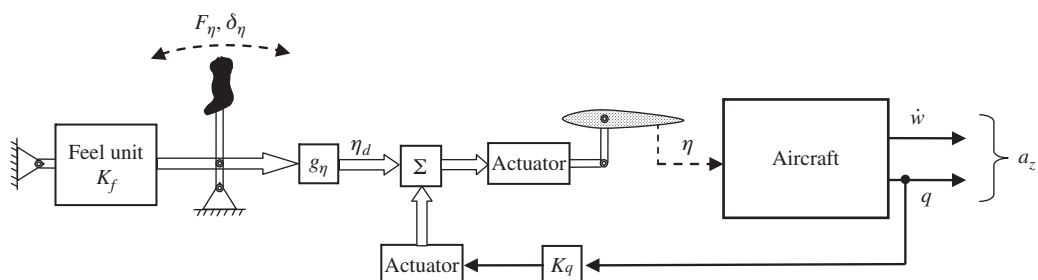


FIGURE 8.3 Simple augmented aircraft control system.

8.6.1 Stick force

The stick force F_η is provided entirely by a “spring” feel unit such that

$$F_\eta = K_f \delta_\eta \quad (8.63)$$

where K_f , the spring constant, may be non-linear and scheduled with flight condition.

8.6.2 Stick force per g

With reference to Fig. 8.3, the closed-loop reduced-order transfer functions relating the response variables w and q to the elevator demand variable η_d are given by equations (8.64):

$$\frac{w(s)}{\eta_d(s)} = \frac{k_w(s + 1/T_\alpha)}{(\Delta(s) + K_q k_q(s + 1/T_{\theta_2}))} \quad \frac{q(s)}{\eta_d(s)} = \frac{k_q(s + 1/T_{\theta_2})}{(\Delta(s) + K_q k_q(s + 1/T_{\theta_2}))} \quad (8.64)$$

Note that K_q is the feedback gain and that the actuator transfer functions are not included in this simple model. Similar to the derivation of equation (8.35), the closed-loop normal load factor response to η_d may be derived using transfer functions (8.64):

$$\frac{\delta n(s)}{\eta_d(s)} = - \frac{(k_w(s + 1/T_\alpha)s - k_q(s + 1/T_{\theta_2})U_e)}{g(\Delta(s) + K_q k_q(s + 1/T_{\theta_2}))} \quad (8.65)$$

Application of the final value theorem to equation (8.65) leads to an expression for the steady-state gain characteristic,

$$\left. \frac{\delta n}{\eta_d} \right|_{state}^{steady} = \frac{k_q U_e}{g(\omega_s^2 T_{\theta_2} + K_q k_q)} \quad (8.66)$$

From equation (8.63) it is easily shown that

$$F_\eta = \frac{K_f}{g_\eta} \eta_d \quad (8.67)$$

Substituting for η_d from equation (8.67) into equation (8.66), the stick force per g characteristic for the augmented aircraft is revealed:

$$\frac{F_\eta}{\delta n} = \frac{K_f g}{g_\eta U_e} \left(\frac{\omega_s^2 T_{\theta_2}}{k_q} + K_q \right) \quad (8.68)$$

Note that the computation of acceleration response to control command, as given by equation (8.66), can normally be obtained as a response transfer function in the solution of the reduced-order equations of motion. Further, acceleration response referred to the *cg*, the pilot’s seat, or both can be obtained by this means as required for analysis. Application of equation (8.68) then enables assessment of the stick force per g control characteristic and the design of the feel unit spring constant K_f to achieve the desired manoeuvre handling qualities.

EXAMPLE 8.1

To illustrate the use of transfer functions to evaluate stick force per g , consider the Lockheed F-104A Starfighter aircraft data, which were obtained from [Heffley and Jewell \(1972\)](#). The equations of motion and the data for limited basic handling qualities are given for 10 flight conditions covering the aircraft flight envelope.

For the present example the longitudinal equations of motion for the unaugmented aircraft corresponding to Mach 0.9 at an altitude of 15,000 ft are given by

$$\begin{bmatrix} \dot{u} \\ \dot{w} \\ \dot{q} \\ \dot{\theta} \end{bmatrix} = \begin{bmatrix} -0.0167 & 0.089 & -79.66 & -32.1 \\ -0.0199 & -1.22 & 948.66 & -1.546 \\ 6.1095e-3 & -0.01942 & -1.4095 & 7.3899e-4 \\ 0 & 0 & 1 & 0 \end{bmatrix} \begin{bmatrix} u \\ w \\ q \\ \theta \end{bmatrix} + \begin{bmatrix} 17.6 \\ -209 \\ -33.5 \\ 0 \end{bmatrix} \eta \quad (8.69)$$

Note that American imperial units are retained to be consistent with the source data. Since only short-term response to control is of interest, it is appropriate to use the reduced-order model, extracted from the state [equation \(8.69\)](#), as follows:

$$\begin{bmatrix} \dot{w} \\ \dot{q} \end{bmatrix} = \begin{bmatrix} -1.22 & 948.66 \\ -0.01942 & -1.4095 \end{bmatrix} \begin{bmatrix} w \\ q \end{bmatrix} + \begin{bmatrix} -209 \\ -33.5 \end{bmatrix} \eta \quad (8.70)$$

The normal acceleration response of interest is measured at the pilot's seat and is given by

$$a_{z_p} = a_z - l_x \dot{q} = \dot{w} - U_e q - l_x \dot{q} \quad (8.71)$$

where a_z is the normal acceleration at the aircraft cg and l_x is the distance of the pilot's seat forward of the cg . At the flight condition in question, $l_x = 18.1$ ft and $U_e = 948.66$ ft/s, and expressions for \dot{w} and \dot{q} may be obtained from [equation \(8.70\)](#). Thus, from [equation \(8.71\)](#), expressions for the normal acceleration at the cg and the normal acceleration at the cockpit may be written as

$$\begin{aligned} a_z &= -1.22w - 209\eta \\ a_{z_p} &= -0.8686w + 25.5112q + 397.35\eta \end{aligned} \quad (8.72)$$

[Equations \(8.72\)](#) may be included in the system output equation to provide the acceleration response transfer functions in the solution of the equations of motion. The system state description may then be written as

$$\begin{aligned} \dot{\mathbf{x}} &= \mathbf{Ax} + \mathbf{Bu} \\ \mathbf{y} &= \mathbf{Cx} + \mathbf{Du} \end{aligned}$$

where

$$\mathbf{x}^T = [w \quad q]$$

$$\mathbf{u} = \eta$$

$$\mathbf{y}^T = [w \quad q \quad a_z \quad a_{z_p}]$$

and

$$\dot{\mathbf{x}} = \begin{bmatrix} -1.22 & 948.66 \\ -0.01942 & -1.4095 \end{bmatrix} \mathbf{x} + \begin{bmatrix} -209 \\ -33.5 \end{bmatrix} \mathbf{u}$$

$$\mathbf{y} = \begin{bmatrix} 1 & 0 \\ 0 & 1 \\ -1.22 & 0 \\ -0.8686 & 25.511 \end{bmatrix} \mathbf{x} + \begin{bmatrix} 0 \\ 0 \\ -209 \\ 397.35 \end{bmatrix} \mathbf{u} \quad (8.73)$$

Solution of equations (8.73) gives the reduced-order response transfer functions:

$$\frac{w(s)}{\eta(s)} = \frac{-209(s + 153.5)}{(s^2 + 2.629s + 20.14)} \frac{\text{ft/s}}{\text{rad}}$$

$$\frac{q(s)}{\eta(s)} = \frac{-33.5(s + 1.099)}{(s^2 + 2.629s + 20.14)} \frac{\text{rad/s}}{\text{rad}}$$

$$\frac{a_z(s)}{\eta(s)} = \frac{-209(s - 12.24)(s + 13.65)}{(s^2 + 2.629s + 20.14)} \frac{\text{ft/s}^2}{\text{rad}} \quad (8.74)$$

$$\frac{a_{z_p}(s)}{\eta(s)} = \frac{397.4(s^2 + 0.9353s + 87.871)}{(s^2 + 2.629s + 20.14)} \frac{\text{ft/s}^2}{\text{rad}}$$

Applying the final value theorem to the acceleration response transfer functions, assuming a unit input, values for the steady-state incremental normal acceleration at the *cg* and at the cockpit are easily determined:

$$\left. \frac{a_z(s)}{\eta(s)} \right|_{\substack{\text{steady} \\ \text{state}}} \equiv \left. \frac{a_{z_p}(s)}{\eta(s)} \right|_{\substack{\text{steady} \\ \text{state}}} = 1733.863 \frac{\text{ft/s}^2}{\text{rad}} \equiv -0.9397 \frac{\text{g}}{\text{deg}} \quad (8.75)$$

It is important to recognise that the quasi-steady manoeuvre value given in equation (8.75) is the same when measured at both the *cg* and the cockpit at the flight condition of interest. However, the dynamic transient response shapes are not the same since the numerators of the acceleration transfer functions in equation (8.74) are clearly different. The difference is shown in Fig. 8.4, where the acceleration response to a unit step input is plotted for the reduced-order transfer functions given in equation (8.74).

It is clear from the figure that the peak transient values of normal acceleration experienced by the pilot at the cockpit are approximately 0.1 g less than at the *cg*. The dynamic response “shapes” are otherwise very similar. It is also clear that, by placing the pilot a distance ahead of the *cg*, the instantaneous response to control at $t = 0$ is in the same sense as the command input, whereas at the *cg* the characteristic non-minimum phase effect causes the adverse value of the instantaneous acceleration response. These characteristic differences in normal acceleration contribute positively to the handling qualities of the aircraft, which are based on motion cues measured at the cockpit. To relate the normal acceleration response properties of the airframe to the

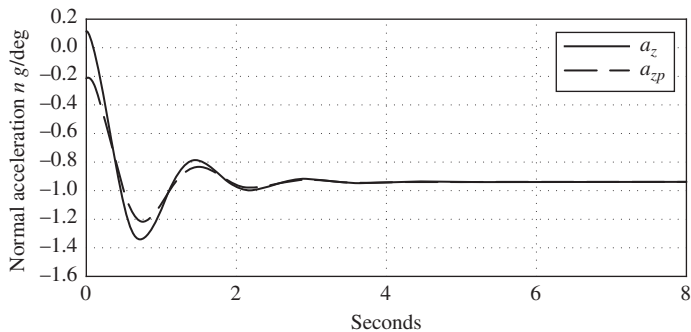


FIGURE 8.4 Normal acceleration response to a unit step input.

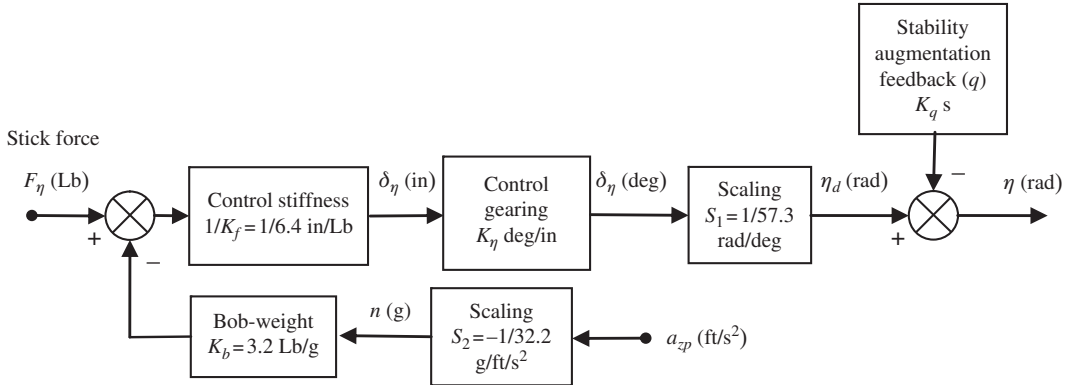


FIGURE 8.5 F-104A longitudinal flying controls.

longitudinal control characteristics requires additional knowledge of the longitudinal flying control system. To facilitate interpretation of the acceleration response characteristics in terms of flying qualities requirements, as discussed in Chapter 10, it is useful to calculate the derivative n_α at this stage:

$$n_\alpha = \frac{U_e}{gT_{\theta_2}} = \frac{948.66}{32.2} 1.099 = 32.378 \frac{\text{g}}{\text{rad}} \quad (8.76)$$

The longitudinal flying control arrangement of the F-104A, as given by Heffley and Jewell (1972), is shown in Fig. 8.5 using a consistent notational style. In common with many aeroplanes of the late 1950s, the airframe is stable, the controls are mechanical and incorporate artificial feel, and simple rate feedback is used to augment the stability to a more uniform level over the

flight envelope. No information about the stability augmentation system is given, but it is safe to assume that pitch rate feedback is used to augment pitch damping and that the feedback gain values typically lie in the range $-0.1 \leq K_q \leq -0.5$ rad/rad/s. A description of the mechanical layout of the system is not given, so it is not known how the artificial feel is implemented.

The stick force reacts against what appears to be mechanical spring stiffness, 6.4 Lb force being required to move the stick control grip 1 in. The stick displacement is then converted to an angular elevator demand η_d through the gearing K_η . The gearing schedule varies non-linearly with trim elevator angle over the range $-2 \leq K_\eta \leq -1.5$ deg/in. approximately. Its purpose is to harmonise control sensitivity over the flight envelope with available elevator travel. To avoid over space control in manoeuvring flight, the stick force required to manoeuvre is increased with the total normal load factor by means of a mechanical bob-weight. The bob-weight is designed to apply a force of 3.2 Lb/g to oppose the pilot force input F_η . Thus the pilot has to pull/push harder to achieve a given manoeuvre as the normal load factor increases. This arrangement represents a fairly rudimentary implementation of mechanical stick force scheduling with flight condition and is typical of combat aircraft of the period.

With reference to Fig. 8.5, the *control law* may be written as

$$\eta_d = \frac{K_\eta S_1}{K_f} F_\eta - \frac{K_b K_\eta S_1 S_2}{K_f} a_{z_p} \quad (8.77)$$

and

$$\eta = \eta_d - K_q q \quad (8.78)$$

Eliminating η_d between equations (8.77) and (8.78), and after some rearrangement,

$$F_\eta = \frac{K_f}{K_\eta S_1} \eta + \frac{K_f K_q}{K_\eta S_1} q + K_b S_2 a_{z_p} \quad (8.79)$$

Whence stick force per g referred to the cockpit may be written as

$$\begin{aligned} \frac{F_\eta}{\delta n_p} &= \frac{-g F_\eta}{a_{z_p}} = \frac{-g K_f}{K_\eta S_1} \frac{\eta}{a_{z_p}} - \frac{g K_f K_q}{K_\eta S_1} \frac{q}{a_{z_p}} - g K_b S_2 \\ &= \frac{K_f}{K_\eta S_1} \frac{\eta}{\delta n_p} \left(1 + K_q \frac{q}{\eta} \right) + K_b \end{aligned} \quad (8.80)$$

In order to determine the steady stick force per g , it is convenient to write equation (8.80) in terms of steady-state transfer functions:

$$\frac{F_\eta}{\delta n} \equiv \frac{F_\eta(s)}{\delta n(s)} \Big|_{state}^{steady} = \frac{K_f}{K_\eta S_1} \frac{\eta(s)}{\delta n(s)} \Big|_{state}^{steady} \left(1 + K_q \frac{q(s)}{\eta(s)} \Big|_{state}^{steady} \right) + K_b \quad (8.81)$$

From equations (8.33) and (8.36) it is easily established that

$$\frac{\eta(s)}{\delta n(s)} \Big|_{\text{state}}^{\text{steady}} = \frac{g\omega_s^2 T_{\theta_2}}{k_q U_e} \quad \frac{q(s)}{\eta(s)} \Big|_{\text{state}}^{\text{steady}} = \frac{k_q}{\omega_s^2 T_{\theta_2}} \quad (8.82)$$

Whence equation (8.81) may be written as

$$\frac{F_\eta}{\delta n} = \frac{gK_f}{g_\eta U_e} \left(\frac{\omega_s^2 T_{\theta_2}}{k_q} + K_q \right) + K_b \quad (8.83)$$

Note that $g_\eta = K_\eta S_1$. Comparison of equation (8.83) with equation (8.68) shows that the effect of the bob-weight is additive and simply increases the apparent stick force per g control characteristic.

Since the pitch rate feedback gain K_q is not given, it is a simple matter to design a suitable value with the aid of the root locus plot using the procedure described in Example 11.4. Since pitch rate feedback to elevator is required to augment longitudinal stability, the root locus is constructed using the second transfer function in equations (8.74). To raise the short-period mode damping to $\zeta_s = 0.7$ requires a feedback gain of $K_q = -0.13 \text{ rad/rad/s}$, the gain value used in the following analysis.

The values of the additional parameters in equation (8.83) required to evaluate the stick force per g at the flight condition of interest were obtained from Heffley and Jewell (1972) and from the solution of the equations of motion (8.74). They are given in Table 8.1.

Table 8.1 Stick Force per g Parameter Values

Parameter	Value	Units
g	32.2	ft/s^2
K_f	6.4	Lb/in
K_η	-1.49	deg/in.
U_e	948.66	ft/s
ω_s^2	20.14	$1/\text{s}^2$
T_{θ_2}	0.9099	s
k_q	-33.5	1/s
K_q	-0.13	s
K_b	3.2	Lb/g
S_1	1/57.3	rad/deg
S_2	-1/32.2	g/ft/s^2
$g_\eta = K_\eta S_1$	-0.026	rad/in.

Whence

$$\frac{F_\eta}{\delta n} = 8.856 \text{ Lb/g}$$

or

$$\frac{F_\eta}{\delta n} = 7.77 \text{ Lb/g}$$

when $K_q = 0$.

The value of $F_\eta/\delta n$ given by Heffley and Jewell (1972) is 7.76 Lb/g. A value close to this is obtained from equation (8.83) when the pitch rate feedback gain K_q is assumed zero, presumably on the basis that its magnitude is small. Since a value for K_q is not given with the aircraft data, it is assumed that its contribution to the transfer function information given by Heffley and Jewell (1972) is ignored on the basis that its significance is small in the present context.

Equivalently, it may be more convenient to calculate stick force per g using the steady values of transfer functions as given by equation (8.81). From equations (8.74), applying the final value theorem for a unit input, the steady-state value of the pitch rate response transfer function is easily evaluated:

$$\left. \frac{q(s)}{\eta(s)} \right|_{\substack{\text{steady} \\ \text{state}}} = -1.828 \text{ 1 rad/s/rad}$$

From equation (8.75),

$$\left. \frac{\eta(s)}{\delta n(s)} \right|_{\substack{\text{steady} \\ \text{state}}} = -\frac{1}{53.847} = -0.01857 \text{ rad/g}$$

Thus, evaluating equation (8.81) directly, it is confirmed that stick force per g for the augmented aircraft at the example flight condition is

$$\frac{F_\eta}{\delta n} = 8.856 \text{ Lb/g}$$

References

- Babister, A. W. (1961). *Aircraft stability and control*. London: Pergamon Press.
- Dickinson, B. (1968). *Aircraft stability and control for pilots and engineers*. London: Pitman.
- Gates, S. B., & Lyon, H. M. (1944). *A continuation of longitudinal stability and control analysis; part 1, general theory*. Reports and Memoranda No. 2027. Aeronautical Research Council Her Majesty's Stationery Office, London.
- Heffley, R. K., & Jewell, W. F. (1972). *Aircraft handling qualities data*. NASA Contractor Report, NASA CR-2144. Washington, DC: National Aeronautics and Space Administration.

Stability

9

9.1 Introduction

Stability is referred to frequently in the foregoing chapters without a formal definition, so it is perhaps useful to revisit the subject in a little more detail in this chapter. Having established the implications of both static and dynamic stability in the context of aircraft response to controls, it is convenient to develop some simple analytical and graphical tools to help in the interpretation of aircraft stability.

9.1.1 A definition of stability

There are many different definitions of stability which are dependent on the kind of system to which they are applied. Fortunately, in the present context the aircraft model is linearised by limiting its motion to small perturbations. The definition of the stability of a linear system is the simplest and most commonly encountered, and it is adopted here for application to the aeroplane. The definition of stability of a linear system may be found in many texts in applied mathematics, in system analysis, and in control theory. A typical definition of the stability of a linear system with particular reference to the aeroplane may be stated as follows.

A system which is initially in a state of static equilibrium is said to be stable if, after a disturbance of finite amplitude and duration, the response ultimately becomes vanishingly small.

Stability is therefore concerned with the nature of the free motion of the system following a disturbance. When the system is linear the nature of the response, and hence its stability, is independent of the nature of the disturbing input. The small-perturbation equations of motion of an aircraft are linear since, by definition, the perturbations are small. Consequently, it is implied that the disturbing input must also be small to preserve that linearity. When, as is often the case, input disturbances which are not really small are applied to the linear small-perturbation equations of motion, some degradation in the interpretation of stability from the observed response must be anticipated. However, for most applications this does not give rise to major difficulties because the linearity of the aircraft model usually degrades relatively slowly with increasing perturbation amplitude. Thus it is considered reasonable to use linear system stability theory for general aircraft applications.

9.1.2 Non-linear systems

Many modern aircraft, especially combat aircraft, which depend on flight control systems for their normal flying qualities, can, under certain conditions, demonstrate substantial non-linearity in their

behaviour. This may be due, for example, to large amplitude manoeuvring at the extremes of the flight envelope, where the aerodynamic properties of the airframe are decidedly non-linear. A rather more common source of non-linearity, often found in an otherwise nominally linear aeroplane and often overlooked, arises from the characteristics of common flight control system components. For example, control surface actuators all demonstrate static friction, hysteresis, amplitude and rate limiting to a greater or lesser extent. The non-linear response associated with these characteristics is not normally intrusive unless the demands on the actuator are limiting, such as might be the case in the fly-by-wire control system of a high-performance aircraft.

The mathematical models describing non-linear behaviour are much more difficult to create and the applicable stability criteria are rather more sophisticated; in any event, they are beyond the scope of the present discussion. Non-linear system theory, more popularly known as *chaotic system theory* today, is developing rapidly to provide the mathematical tools, understanding, and stability criteria for dealing with the problems posed by modern highly augmented aircraft.

9.1.3 Static and dynamic stability

Any discussion of stability must consider the total stability of the aeroplane at the flight condition of interest. However, it is usual and convenient to discuss static stability and dynamic stability separately since the related dependent characteristics can be identified explicitly in aircraft behaviour. In reality, static and dynamic stability are inseparable and must be considered as an entity. An introductory discussion of static and dynamic stability is presented in Chapter 3 (Section 3.1), and simple definitions of the two are re-iterated here. Static stability is commonly interpreted to describe the tendency of the aircraft to converge on the initial equilibrium condition following a small disturbance from trim. Dynamic stability describes the transient motion involved in recovery of equilibrium following the disturbance. It is very important that an aeroplane possesses both static and dynamic stability in order for it to be safe. However, the degree of stability is also very important since this determines the effectiveness of the controls of the aeroplane.

9.1.4 Control

By definition, a stable aeroplane is resistant to disturbance; in other words, it attempts to remain at its trimmed equilibrium flight condition. The “strength” of the resistance to disturbance is determined by the *degree* of stability possessed by the aeroplane. It follows, then, that a stable aeroplane is reluctant to respond when a disturbance is deliberately introduced as the result of pilot control action. Thus the degree of stability is critically important to aircraft handling. An aircraft which is very stable requires a greater pilot control action in order to manoeuvre about the trim state, and clearly, too much stability may limit its controllability and hence its manoeuvrability. On the other hand, too little stability in an otherwise stable aeroplane may give rise to an over responsive aeroplane with the resultant pilot tendency to over control. Therefore, too much stability can be as hazardous as too little, and it is essential to place upper and lower bounds on the acceptable degree of stability in order that the aeroplane shall remain completely controllable at all flight conditions.

As described in Chapter 3, the degree of static stability is governed by *cg* position, and this has a significant effect on controllability and the pilot workload. Interpretation of control characteristics as a function of degree of stability and, consequently *cg* position is summarised in Fig. 9.1.

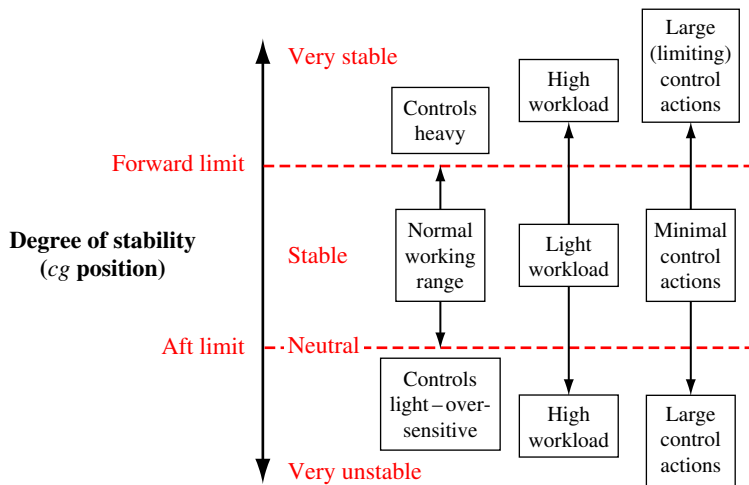


FIGURE 9.1 Stability and control.

In particular, the control action, interpreted as stick displacement and force, becomes larger at the extremes of stability, which has implications for pilot workload. It is also quite possible for very large pilot action to reach the limit of stick displacement or the limit of the pilot's ability to move the control against the force. For this reason, constraints are placed on the permitted *cg* operating range in the aircraft, as discussed in Chapter 3.

The control characteristics are also influenced by the dynamic stability properties, which are governed by *cg* position and also by certain aerodynamic properties of the airframe. This has implications for pilot workload if the dynamic characteristics of the aircraft are not within acceptable limits. However, the dynamic aspects of control are rather more concerned with the time dependency of the response, but in general the observations shown in Fig. 9.1 remain applicable. By reducing the total stability to static and dynamic components, which are further reduced to the individual dynamic modes, it becomes relatively easy to assign the appropriate degree of stability to each mode in order to achieve a safe controllable aeroplane in total. However, this may require the assistance of a command and stability augmentation system, and it may also require control force shaping by means of an artificial feel system.

9.2 The characteristic equation

It was shown in previous chapters that the denominator of every aircraft response transfer function defines the characteristic polynomial, the roots of which determine the stability modes of the aeroplane. Equating the characteristic polynomial to zero defines the classical characteristic equation, and thus far two such equations have been identified. Since only decoupled motion is considered,

solution of the equations of motion of the aeroplane results in two fourth-order characteristic equations, one relating to longitudinal symmetric motion and one relating to lateral-directional asymmetric motion. In the event that the decoupled equations of motion provide an inadequate aircraft model, as is often the case for the helicopter, then a single characteristic equation, typically of eighth order, describes the stability characteristics of the aircraft in total.

For aircraft with significant stability augmentation, the flight control system introduces additional dynamics, resulting in a higher order characteristic equation. For advanced combat aircraft the longitudinal characteristic equation, for example, can be of order 30 or more! Interpretation of high order characteristic equations can be something of a challenge for the flight dynamicist.

The characteristic equation of a general system of order n may be expressed in the familiar format as a function of the Laplace operator s :

$$\Delta(s) = a_n s^n + a_{n-1} s^{n-1} + a_{n-2} s^{n-2} + a_{n-3} s^{n-3} + \dots + a_1 s + a_0 = 0 \quad (9.1)$$

and the stability of the system may be determined by the n roots of this equation. Provided that the constant coefficients in [equation \(9.1\)](#) are real, the roots may be real, complex pairs, or a combination of the two. Thus the roots may be written in the general form as follows:

Single real roots—for example, $s = -\sigma_1$ with time solution $k_1 e^{-\sigma_1 t}$

Complex pairs of roots—for example, $s = -\sigma_2 \pm j\gamma_2$ with time solution $k_2 e^{-\sigma_2 t} \sin(\gamma_2 t + \phi_2)$ or, more familiarly, $s^2 + 2\sigma_2 s + (\sigma_2^2 + \gamma_2^2) = 0$

where σ is the real part, γ is the imaginary part, ϕ is the phase angle, and k is a gain constant. When all the roots have negative real parts, the transient component of the response to a disturbance decays to zero as $t \rightarrow \infty$ and the system is said to be stable. The system is unstable when any root has a positive real part, and neutrally stable when any root has a zero real part. Thus the stability and dynamic behaviour of any linear system is governed by the sum of the dynamics associated with each root of its characteristic equation. The interpretation of the stability and dynamics of a linear system is summarised in Appendix 6.

9.3 The Routh-Hurwitz stability criterion

The development of a criterion for testing the stability of linear systems is generally attributed to Routh. Application of the criterion involves an analysis of the characteristic equation, and methods for interpreting and applying the criterion are very widely known and used, especially in control systems analysis. A similar analytical procedure for testing the stability of a system by analysis of the characteristic equation was developed simultaneously, and quite independently, by Hurwitz. As a result, both authors share the credit and the procedure is commonly known to control engineers as the Routh-Hurwitz criterion. The criterion provides an analytical means for testing the stability of a linear system of any order without having to obtain the roots of the characteristic equation.

With reference to the typical characteristic [equation \(9.1\)](#), if any coefficient is zero or if any coefficient is negative, then at least one root has a zero or positive real part, indicating the system to be unstable or, at best, neutrally stable. However, it is a necessary but not sufficient condition

for stability that all coefficients in [equation \(9.1\)](#) be non-zero and of the same sign. When this condition exists the stability of the system described by the characteristic equation may be tested as follows.

An array, commonly known as the Routh array, is constructed from the coefficients of the characteristic equation arranged in descending powers of s as follows:

$$\begin{array}{c|ccccc} s^n & a_n & a_{n-2} & a_{n-4} & a_{n-6} & \dots \dots \\ s^{n-1} & a_{n-1} & a_{n-3} & a_{n-5} & a_{n-7} & \dots \dots \\ s^{n-2} & u_1 & u_2 & u_3 & u_4 & \cdot \\ s^{n-3} & v_1 & v_2 & v_3 & \cdot & \\ \cdot & \cdot & \cdot & \cdot & & \\ \cdot & \cdot & \cdot & \cdot & & \\ \cdot & \cdot & \cdot & \cdot & & \\ s^1 & y & & & & \\ s^0 & z & & & & \end{array} \quad (9.2)$$

The first row is written to include alternate coefficients starting with the highest power term; the second row includes the remaining alternate coefficients starting with the second highest-power term as indicated. The third row is constructed as follows:

$$u_1 = \frac{a_{n-1}a_{n-2} - a_n a_{n-3}}{a_{n-1}} \quad u_2 = \frac{a_{n-1}a_{n-4} - a_n a_{n-5}}{a_{n-1}} \quad u_3 = \frac{a_{n-1}a_{n-6} - a_n a_{n-7}}{a_{n-1}}$$

and so on, until all remaining u are zero. The fourth row is constructed similarly from coefficients in the two rows immediately above as follows:

$$v_1 = \frac{u_1 a_{n-3} - u_2 a_{n-1}}{u_1} \quad v_2 = \frac{u_1 a_{n-5} - u_3 a_{n-1}}{u_1} \quad v_3 = \frac{u_1 a_{n-7} - u_4 a_{n-1}}{u_1}$$

and so on, until all remaining v are zero. This process is repeated until all remaining rows of the array are completed. The array is triangular as indicated, and the last two rows comprise only one term each, y and z , respectively.

The Routh-Hurwitz criterion states,

The number of roots of the characteristic equation with positive real parts (unstable) is equal to the number of changes of sign of the coefficients in the first column of the array.

Thus, for the system to be stable, all the coefficients in the first column of the array must have the same sign.

EXAMPLE 9.1

The lateral-directional characteristic equation for the Douglas DC-8 aircraft in a low-altitude cruise flight condition, obtained from [Teper \(1969\)](#), is

$$\Delta(s) = s^4 + 1.326s^3 + 1.219s^2 + 1.096s - 0.015 = 0 \quad (9.3)$$

Inspection of this equation indicates an unstable aeroplane since the last coefficient has a negative sign. The number of unstable roots may be determined by constructing the array as described earlier:

$$\begin{array}{c|ccc} s^4 & 1 & 1.219 & -0.015 \\ s^3 & 1.326 & 1.096 & 0 \\ s^2 & 0.393 & -0.015 & 0 \\ s^1 & 1.045 & 0 & 0 \\ s^0 & -0.015 & 0 & 0 \end{array} \quad (9.4)$$

Working down the first column, there is one sign change, from 1.045 to -0.015 , which indicates the characteristic equation has one unstable root. This is verified by obtaining the exact roots of the characteristic equation (9.2):

$$\begin{aligned} s &= -0.109 \pm 0.99j \\ s &= -1.21 \\ s &= +0.013 \end{aligned} \quad (9.5)$$

The complex pair of roots with negative real parts describes the stable dutch roll mode; the real root with negative real part describes the stable roll subsidence mode; and the real root with positive real part describes the unstable spiral mode. This is a typical solution for a classical aeroplane.

9.3.1 Special cases

Two special cases which may arise in the application of the Routh-Hurwitz criterion need to be considered, although they are unlikely to occur in aircraft applications. The first case occurs when, in the routine calculation of the array, a coefficient in the first column is zero. The second case occurs when, also in the routine calculation of the array, all coefficients in a row are zero. In either case no further progress is possible and an alternative procedure is required. The methods for dealing with these cases are best illustrated by example.

EXAMPLE 9.2

Consider the arbitrary characteristic equation

$$\Delta(s) = s^4 + s^3 + 6s^2 + 6s + 7 = 0 \quad (9.6)$$

the array for which is constructed in the usual way:

$$\begin{array}{c|ccc} s^4 & 1 & 6 & 7 \\ s^3 & 1 & 6 & 0 \\ s^2 & \varepsilon & 7 & 0 \\ s^1 & \left(\frac{6\varepsilon - 7}{\varepsilon} \right) & 0 & 0 \\ s^0 & 7 & 0 & 0 \end{array} \quad (9.7)$$

Normal progress cannot be made beyond the third row since the first coefficient is zero. To proceed, the zero is replaced with a small positive number, denoted ε . The array can be completed as at (9.7) and as $\varepsilon \rightarrow 0$, so the first coefficient in the fourth row tends to a large negative value. The signs of the coefficients in the first column are then easily determined:

$$\begin{array}{c|c} s^4 & + \\ s^3 & + \\ s^2 & + \\ s^1 & - \\ s^0 & + \end{array} \quad (9.8)$$

There are two changes of sign, from row 3 to row 4 and from row 4 to row 5. Therefore, the characteristic equation (9.6) has two roots with positive real parts, which is verified by the exact solution,

$$\begin{aligned} s &= -0.6454 \pm 0.9965j \\ s &= +0.1454 \pm 2.224j \end{aligned} \quad (9.9)$$

EXAMPLE 9.3

To illustrate the required procedure when all coefficients in a row of the array are zero, consider the arbitrary characteristic equation

$$\Delta(s) = s^5 + 2s^4 + 4s^3 + 8s^2 + 3s + 6 = 0 \quad (9.10)$$

If the array is constructed in the usual way,

$$\begin{array}{c|ccc} s^5 & 1 & 4 & 3 \\ s^4 & 2 & 8 & 6 \\ s^3 & 0 & 0 & 0 \end{array} \quad (9.11)$$

no further progress is possible because the third row comprises all zeros. To proceed, the zero row, the third row in this example, is replaced by an auxiliary function derived from the preceding non-zero row. Thus the function is created from the row commencing with the coefficient of s to the power of four as follows:

$$2s^4 + 8s^2 + 6 = 0 \text{ or, equivalently, } s^4 + 4s^2 + 3 = 0 \quad (9.12)$$

Only terms in alternate powers of s are included in the auxiliary function (9.12), commencing with the highest power term determined from the row of the array from which it is derived. The auxiliary function is differentiated with respect to s , and the resulting polynomial is used to replace the zero row. Equation (9.12) is differentiated to obtain

$$4s^3 + 8s = 0 \text{ or, equivalently, } s^3 + 2s = 0 \quad (9.13)$$

Substituting [equation \(9.13\)](#) into the third row of array (9.11), the array may then be completed in the usual way:

$$\begin{array}{c|ccc} s^5 & 1 & 4 & 3 \\ s^4 & 2 & 8 & 6 \\ s^3 & 1 & 2 & 0 \\ s^2 & 4 & 6 & 0 \\ s^1 & 0.5 & 0 & 0 \\ s^0 & 6 & 0 & 0 \end{array} \quad (9.14)$$

Inspection of the first column of (9.14) indicates that all roots of the characteristic equation [\(9.10\)](#) have negative real parts. However, the fact that, in the derivation of the array, one row comprises zero coefficients suggests that something is different. The exact solution of [equation \(9.10\)](#) confirms this suspicion:

$$\begin{aligned} s &= 0 \pm 1.732j \\ s &= 0 \pm 1.0j \\ s &= -2.0 \end{aligned} \quad (9.15)$$

Clearly the system is neutrally stable since the two pairs of complex roots both have zero real parts.

9.4 The stability quartic

Since both the longitudinal and lateral-directional characteristic equations derived from the aircraft small perturbation equations of motion are fourth order, considerable emphasis has always been placed on the solution of a fourth order polynomial, sometimes referred to as the *stability quartic*. A general quartic equation applicable to either longitudinal or lateral-directional motion may be written as

$$As^4 + Bs^3 + Cs^2 + Ds + E = 0 \quad (9.16)$$

When all of the coefficients in [equation \(9.16\)](#) are positive, as is often the case, no conclusions may be drawn concerning stability unless the roots are found or the Routh-Hurwitz array is constructed. Constructing the Routh-Hurwitz array as described in [Section 9.3](#), we obtain

$$\begin{array}{c|ccc} s^4 & A & C & E \\ s^3 & B & D & \\ s^2 & \left(\frac{BC - AD}{B} \right) & E & \\ s^1 & \left(\frac{D(BC - AD) - B^2E}{BC - AD} \right) & & \\ s^0 & E & & \end{array} \quad (9.17)$$

Assuming that all of the coefficients in the characteristic [equation \(9.16\)](#) are positive and that B and C are large compared with D and E , as is usually the case, then the coefficients in the first column of (9.17) are also positive with the possible exception of the coefficient in the fourth row. Writing

$$R = D(BC - AD) - B^2E \quad (9.18)$$

R is called *Routh's discriminant* and, since $(BC - AD)$ is positive, the outstanding condition for stability is

$$R > 0$$

For most classical aircraft operating within the constraints of small perturbation motion, the only coefficient in the characteristic [equation \(9.16\)](#) likely to be negative is E . Thus, typically, the necessary and sufficient conditions for an aeroplane to be stable are

$$R > 0 \quad \text{and} \quad E > 0$$

When an aeroplane is unstable some conclusions about the nature of the instability can be made simply by observing the values of R and E .

9.4.1 Interpretation of conditional instability

Case 1: When $R < 0$ and $E > 0$.

Observation of the signs of the coefficients in the first column of array (9.17) indicates that two roots of the characteristic [equation \(9.16\)](#) have positive real parts. For longitudinal motion this implies a pair of complex roots; in most cases this means an unstable phugoid mode since its stability margin is usually the smallest. For lateral-directional motion the implication is that either the two real roots or the pair of complex roots have positive real parts. This means either that the spiral and roll subsidence modes are unstable or that the dutch roll mode is unstable. Within the limitations of small-perturbation modeling, an unstable roll subsidence mode is not possible. Therefore, the instability must be determined by the pair of complex roots describing the dutch roll mode.

Case 2: When $R < 0$ and $E < 0$.

For this case, the signs of the coefficients in the first column of array (9.17) indicate that only one root of the characteristic [equation \(9.16\)](#) has a positive real part. Clearly, the “unstable” root can only be a real root. For longitudinal motion this may be interpreted to mean that the phugoid mode has changed such that it is no longer oscillatory and is therefore described by a pair of real roots, one of which has a positive real part. The “stable” real root typically describes an exponential heave characteristic, whereas the “unstable” root describes an exponentially divergent speed mode. For lateral-directional motion the interpretation is similar, and in this case the only “unstable” real root must be that describing the spiral mode. This, of course, is a commonly encountered condition in lateral-directional dynamics.

Case 3: When $R > 0$ and $E < 0$.

As with the previous case, the signs of the coefficients in the first column of array (9.17) indicate that only one root of the characteristic [equation \(9.16\)](#) has a positive real part. Again, the “unstable” root can only be a real root. Interpretation of the stability characteristics corresponding with this particular condition is exactly the same as described in *Case 2*.

When all coefficients in the characteristic equation (9.16) are positive and R is negative, the instability can only be described by a pair of complex roots, the interpretation of which is described in *Case 1*. Since the unstable motion is oscillatory, the condition $R > 0$ is sometimes referred to as the criterion for dynamic stability. Alternatively, the most common unstable condition arises when the coefficients in the characteristic equation (9.16) are positive with the exception of E . In this case the instability can only be described by a single real root, the interpretation of which is described in *Case 3*. Now, the instability is clearly identified as a longitudinal speed divergence or as the divergent lateral-directional spiral mode, both of which are dynamic characteristics. However, the aerodynamic contribution to E is substantially dependent on static stability effects, and when $E < 0$ the cause is usually static instability. Consequently, the condition $E > 0$ is sometimes referred to as the criterion for static stability. This simple analysis emphasises the role of the characteristic equation in describing the *total stability* of the aeroplane and reinforces the reason that, in reality, static and dynamic stability are inseparable and should not be considered without referencing one to the other.

9.4.2 Interpretation of the coefficient E

Assuming the longitudinal equations of motion to be referred to a system of aircraft wind axes, the coefficient E in the longitudinal characteristic equation may be obtained directly from Appendix 3 as

$$E = mg \left(\dot{M}_w \dot{Z}_u - \dot{M}_u \dot{Z}_w \right) \quad (9.19)$$

and the longitudinal static stability criterion may be expressed in terms of dimensionless derivatives as

$$M_w Z_u > M_u Z_w \quad (9.20)$$

For most aeroplanes the derivatives in equation (9.20) have negative values so that the terms on either side of the inequality are usually both positive. M_w is a measure of the controls-fixed longitudinal static stability margin; Z_u is largely dependent on lift coefficient; Z_w is dominated by lift curve slope; and M_u only assumes significant values at a high Mach number. Thus, provided the aeroplane possesses a sufficient margin of controls-fixed longitudinal static stability, M_w is sufficiently large to ensure that inequality (9.20) is satisfied. At higher Mach numbers, when M_u becomes larger, the inequality is generally maintained because the associated aerodynamic changes also cause M_w to increase.

The coefficient E in the lateral-directional characteristic equation may similarly be obtained directly from Appendix 3 as

$$E = mg \left(\dot{L}_v \dot{N}_r - \dot{L}_r \dot{N}_v \right) \quad (9.21)$$

and the lateral-directional static stability criterion may be expressed in terms of dimensionless derivatives as

$$L_v N_r > L_r N_v \quad (9.22)$$

For most aeroplanes the derivatives L_v and N_r are both negative, the derivative L_r is usually positive, and the derivative N_v is always positive. Thus the terms on either side of inequality (9.22) are usually both positive. Satisfaction of the inequality is usually determined by the relative

magnitudes of the derivatives L_v and N_v . Now, L_v and N_v are the derivatives describing the lateral and directional controls-fixed static stability of the aeroplane, respectively, as discussed in Sections 3.4.1 and 3.4.2. The magnitude of the derivative L_v is determined by the *lateral dihedral effect*, and the magnitude of the derivative N_v is determined by the *directional weathercock effect*. Inequality (9.22) also determines the condition for a stable spiral mode as described in Section 7.3.2 and, once again, the inseparability of static and dynamic stability is illustrated.

9.5 Graphical interpretation of stability

Today, the foregoing analysis of stability is of limited practical value since all of the critical information is normally obtained in the process of solving the equations of motion exactly and directly using suitable computer software tools, as described elsewhere. However, its greatest value is in the understanding and interpretation of stability it provides. Of much greater practical value are the graphical tools much favoured by the control engineer for the interpretation of stability on the *s-plane*.

9.5.1 Root mapping on the s-plane

The roots of the characteristic equation are either real or complex pairs, as stated in Section 9.2. The possible forms of the roots may be mapped onto the *s-plane* as shown in Fig. 9.2. Since the roots describe various dynamic and stability characteristics possessed by the system to which they relate, the location of the roots on the *s-plane* conveys the same information in a highly accessible

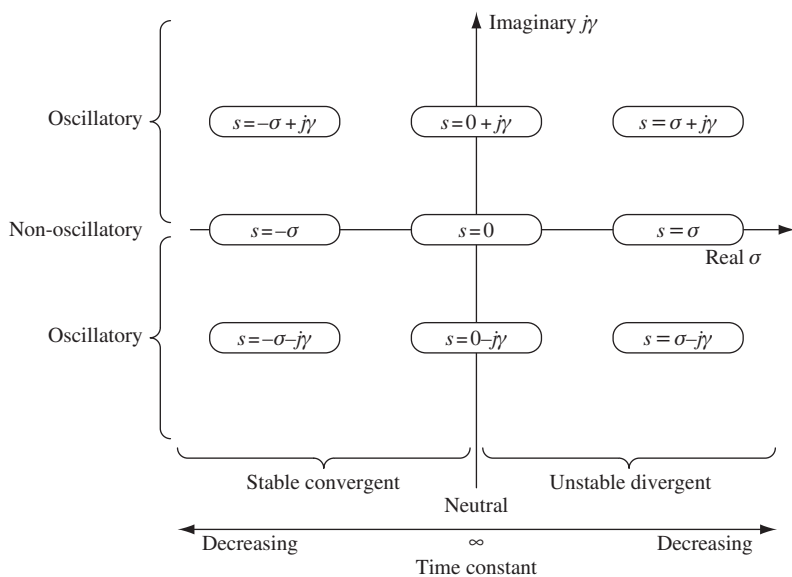


FIGURE 9.2 Roots on the s-plane.

form. “Stable” roots have negative real parts and lie on the left half of the s -plane; “unstable” roots have positive real parts and lie on the right half of the s -plane; roots describing neutral stability have zero real parts and lie on the imaginary axis. Complex roots lie in the upper half of the s -plane; their conjugates lie in the lower half, and, since their locations are mirrored in the real axis, it is usual to show the upper half of the plane only. Complex roots describe oscillatory motion, so all roots lying in the plane and not on the real axis describe such characteristics. Roots lying on the real axis describe non-oscillatory motions, the time constants of which are given by $T = 1/\sigma$. A root lying at the origin is therefore neutrally stable and has an infinite time constant. As real roots move away from the origin, their time constants decrease—in the stable sense on the left half of the plane and in the unstable sense on the right half of the plane.

Consider the interpretation of a complex pair of roots on the s -plane in rather greater detail. As stated in [Section 9.2](#), the typical pair of complex roots may be written as

$$(s + \sigma + j\gamma)(s + \sigma - j\gamma) = s^2 + 2\sigma s + (\sigma^2 + \gamma^2) = 0 \quad (9.23)$$

which is equivalent to the familiar expression

$$s^2 + 2\zeta\omega s + \omega^2 = 0 \quad (9.24)$$

Whence

$$\begin{aligned} \zeta\omega &= \sigma \\ \omega^2 &= \sigma^2 + \gamma^2 \\ \zeta &= \cos\phi = \frac{\sigma}{\sqrt{\sigma^2 + \gamma^2}} \end{aligned} \quad (9.25)$$

where ϕ is referred to as the *damping angle*. This information is readily interpreted on the s -plane as shown in [Fig. 9.3](#). The complex roots of [equation \(9.23\)](#) are plotted at p , with only the upper half of

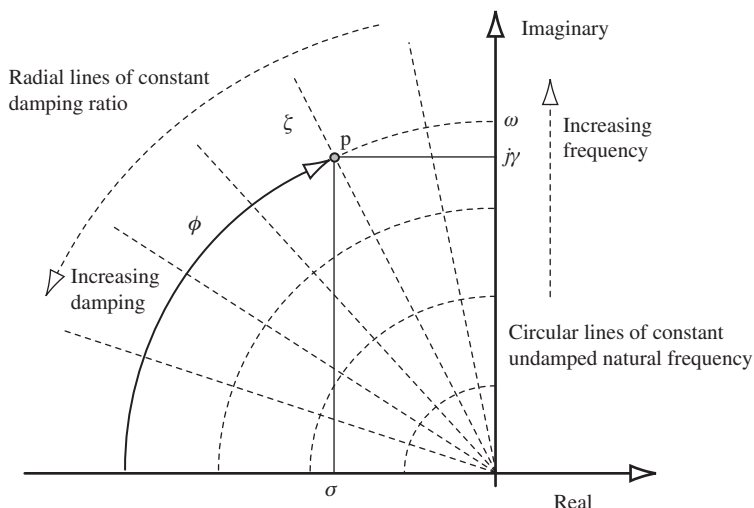


FIGURE 9.3 Typical complex roots on the s -plane.

the s -plane being shown since the lower half containing the complex conjugate root is a *mirror image* in the real axis. With reference to [equations \(9.24\) and \(9.25\)](#), it is evident that undamped natural frequency is given by the magnitude of the line joining the origin and the point p . Thus lines of constant frequency are circles concentric with the origin provided that both axes have the same scales. Care should be exercised when the scales are dissimilar, which is often the case, as the lines of constant frequency then become ellipses. Thus, clearly, roots indicating low frequency dynamics are near the origin and vice versa.

Whenever possible, it is good practice to draw s -plane plots and *root locus plots* on axes having the same scales to facilitate the easy interpretation of frequency. With reference to [equations \(9.25\)](#), it is evident that radial lines drawn through the origin are lines of constant damping. The imaginary axis then becomes a line of zero damping and the real axis becomes a line of *critical damping* where the damping ratio is unity and the roots become real. The upper left quadrant of the s -plane shown in [Fig. 9.3](#) contains the stable region of positive damping ratio in the range $0 \leq \zeta \leq 1$ and is therefore the region of critical interest in most practical applications. Thus roots indicating stable well damped dynamics are seen towards the left of the region and *vice versa*. Thus, information about the dynamic behaviour of a system is instantly available on inspection of the roots of its characteristic equation on the *s-plane*. The interpretation of the stability of an aeroplane on the s -plane becomes especially useful for the assessment of stability augmentation systems on the *root locus plot* described in Chapter 11.

EXAMPLE 9.4

The Boeing B-747 is typical of a large classical transport aircraft, and the following characteristics were obtained from [Heffley and Jewell \(1972\)](#). The flight case chosen is representative of typical cruising flight at Mach 0.65 at an altitude of 20,000 ft. The longitudinal characteristic equation is

$$\Delta(s) = s^4 + 1.1955s^3 + 1.5960s^2 + 0.0106s + 0.00676 \quad (9.26)$$

with roots

$$\begin{aligned} s &= -0.001725 \pm 0.0653j \\ s &= -0.596 \pm 1.1101j \end{aligned} \quad (9.27)$$

describing stability mode characteristics

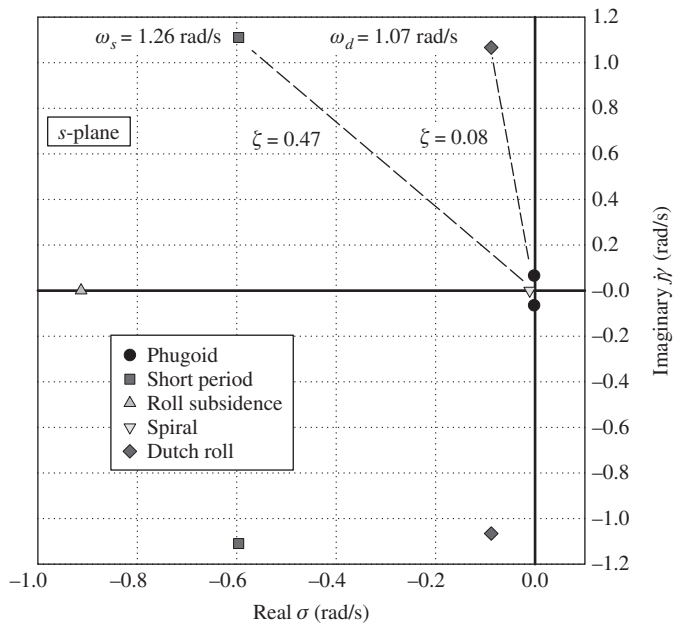
$$\begin{aligned} \omega_p &= 0.065 \text{ rad/s} & \zeta_p &= 0.0264 \\ \omega_s &= 1.260 \text{ rad/s} & \zeta_s &= 0.4730 \end{aligned} \quad (9.28)$$

The corresponding lateral-directional characteristic equation is

$$\Delta(s) = s^4 + 1.0999s^3 + 1.3175s^2 + 1.0594s + 0.01129 \quad (9.29)$$

with roots

$$\begin{aligned} s &= -0.0108 \\ s &= -0.9130 \\ s &= -0.0881 \pm 1.0664j \end{aligned} \quad (9.30)$$

FIGURE 9.4 Boeing B-747 stability modes on the *s*-plane.

describing stability mode characteristics

$$\begin{aligned} T_s &= 92.6 \text{ s} \\ T_r &= 1.10 \text{ s} \\ \omega_d &= 1.070 \text{ rad/s} \quad \zeta_d = 0.082 \end{aligned} \tag{9.31}$$

The longitudinal roots given by equation (9.27) and the lateral-directional roots given by equation (9.30) are mapped on to the *s*-plane as shown in Fig. 9.4. The plot is absolutely typical for a large number of aeroplanes and shows the *stability modes*, represented by their corresponding roots, on regions of the *s*-plane normally associated with the modes. For example, the *slow modes*, the phugoid and the spiral, are clustered around the origin, whereas the *faster modes* are further out in the plane. Since the vast majority of aeroplanes have longitudinal and lateral-directional control bandwidths of less than 10 rad/s, the scales of the *s*-plane plot normally lie in the range $-10 \text{ rad/s} < \text{real} < 0 \text{ rad/s}$ and $-10 \text{ rad/s} < \text{imaginary} < 10 \text{ rad/s}$. Clearly, the control bandwidth of the B-747 at the chosen flight condition is a little over 1 rad/s, as might be expected for such a large aeroplane. The important observation to be made from this illustration is the relative locations of the stability mode roots on the *s*-plane since they are quite typical of many aeroplanes.

References

- Heffley, R. K., & Jewell, W. F. (1972). *Aircraft handling qualities data*. NASA Contractor Report, NASA CR-2144. Washington, DC: National Aeronautics and Space Administration.
- Teper, G. L. (1969). *Aircraft stability and control data*. Systems Technology, STI Technical Report 176-1. Hawthorne, CA: Systems Technology, Inc.
-

PROBLEMS

- 9.1** By applying the Routh-Hurwitz stability criterion to the longitudinal characteristic equation, show that the minimum condition for stability, assuming a conventional aircraft, is $E > 0$ and $R > 0$, where the Routh discriminant R is given by

$$R = (BC - AD)D - B^2E$$

Using these conditions, test the longitudinal stability of the aircraft whose dimensional characteristics equation is

$$s^4 + 5.08s^3 + 13.2s^2 + 0.72s + 0.52 = 0$$

Verify your findings by obtaining the approximate solution of the equation. Describe in detail the characteristic longitudinal modes of the aircraft.

(CU 1982)

- 9.2** The Republic F-105B Thunderchief aircraft, data for which are given in [Teper \(1969\)](#), has a wing span of 10.6 m and is flying at a speed of 518 kts at an altitude where the lateral relative density parameter is $\mu_2 = 221.46$. The dimensionless controls-fixed lateral-directional stability quartic is

$$\lambda^4 + 29.3\lambda^3 + 1052.7\lambda^2 + 14913.5\lambda - 1154.6 = 0$$

- (a) Using the Routh-Hurwitz stability criterion, test the lateral-directional stability of the aircraft.
 (b) Given that the time constant of the spiral mode is $T_s = 115$ s and the time constant of the roll subsidence mode is $T_r = 0.5$ s, calculate the characteristics of the remaining mode. Determine the time to half or double amplitude of the non-oscillatory modes and hence describe the physical characteristics of the lateral-directional modes of motion of the aircraft.

(CU 1982)

- 9.3** The longitudinal characteristic equation for an aircraft may be written

$$As^4 + Bs^3 + Cs^2 + Ds + E = 0$$

It may be assumed that it describes the usual short-period pitching oscillation and phugoid. State the Routh-Hurwitz stability criterion and thus show that for a conventional

aircraft the conditions for stability are, $B > 0$, $D > 0$, $E > 0$, and $R > 0$, where Routh's discriminant R is given by

$$R = BCD - AD^2 - B^2E$$

Describe the significance of the coefficient E on the stability of the aircraft by considering the form of the roots of the quartic when E is positive, negative, or zero.

(CU 1985)

- 9.4** Explain the Routh-Hurwitz stability criterion as it might apply to the following typical aircraft stability quartic:

$$As^4 + Bs^3 + Cs^2 + Ds + E = 0$$

What is Routh's discriminant R ? Explain the special significance of R and of the coefficient E in the context of the lateral-directional stability characteristics of an aircraft.

- (a) The coefficients of the lateral-directional stability quartic of an aircraft are

$$\begin{aligned} A &= 1 & B &= 9.42 & C &= 9.48 + N_v & D &= 10.29 + 8.4N_v \\ E &= 2.24 - 0.39N_v \end{aligned}$$

Find the range of values of N_v for which the aircraft will be both statically and dynamically stable. What do the limits on N_v mean in terms of the dynamic stability characteristics of the aircraft, and on what do they depend?

(CU 1987)

- 9.5** An unstable fly-by-wire combat aircraft has the longitudinal characteristic equation

$$s^4 + 36.87s^3 - 4.73s^2 + 1.09s - 0.13 = 0$$

- (a) Test its stability using the Routh-Hurwitz criterion.
 (b) The roots of the characteristic equation are $s = 0.0035 \pm 0.1697j$, $s = 0.122$, and $s = -37.0$. Describe the longitudinal stability modes of the aircraft.

(CU 1989)

Flying and Handling Qualities

10

10.1 Introduction

Some general concepts describing the meaning of *flying and handling qualities* were introduced in Chapter 1 and so are not repeated in full here. However, it is useful to recall that flying and handling qualities are those properties which govern the ease and precision with which the aeroplane responds to pilot commands in the execution of the flight task. Although these rather intangible properties are described qualitatively and are formulated in terms of *pilot opinion*, it becomes necessary to find alternative quantitative descriptions for more formal analyses. As described previously, flying and handling qualities of an aeroplane are, in part, intimately dependent on its stability and control characteristics, including the effects of a flight control system if one is installed. It was shown in previous chapters how the stability and control properties of an aeroplane may be quantified, and these are commonly used as indicators and measures of flying and handling qualities. The object here, then, is to introduce, at an introductory level, the way in which stability and control parameters are used to quantify those qualities.

10.1.1 Stability

A stable aeroplane is an aeroplane which can be established in an equilibrium flight condition where it will remain, showing no tendency to diverge. Therefore, a stable aeroplane is in general a safe aeroplane. However, it has already been established that too much stability can be as hazardous as too little stability. The degree of stability determines the magnitude of the control action, measured in terms of control displacement and force, required to manoeuvre about a given flight path. Thus *controllability* is concerned with the correct *harmonisation* of control power with the degrees of static, manoeuvre, and dynamic stability of the airframe. Because of the interdependence of the various aspects of stability and control, the provision of well-harmonised control characteristics by entirely aerodynamic means over the entire flight envelope may well be difficult, if not impossible, to achieve. This is especially so in many modern aeroplanes which are required to operate over extended flight envelopes and in aerodynamically difficult flight regimes. The solution to this problem is found in the installation of a *control and stability augmentation system* (CSAS), where the object is to restore good flying qualities by *artificial* non-aerodynamic means.

Aircraft handling is generally concerned with two relatively distinct aspects of response to controls, the short term, or transient, response and the rather longer-term response. Short term handling is very much concerned with the short-period dynamic modes and their critical influence on manoeuvrability. The ability of a pilot to handle the short term dynamics satisfactorily is critically dependent on the speed and stability of response. In other words, the bandwidth of the human pilot

and the control bandwidth of the aeroplane must be compatible, and the stability margins of the dynamic modes must be adequate. An aeroplane with poor, or inadequate, short term dynamic stability and control characteristics is simply not acceptable. Thus, the provision of good short term handling tends to be the main consideration in flying and handling qualities studies.

Longer term handling is concerned with the establishment and maintenance of a steady flight condition, or trimmed equilibrium, which is determined by static stability in particular and is influenced by the long-period dynamic modes. The dynamic modes associated with long term handling tend to be slow, and the frequencies involved are relatively low. Thus their control is well within the bandwidth and capabilities of the average pilot, even when the modes are marginally unstable. As a result, the requirements for the stability of low frequency dynamics are more relaxed. However, those aspects of control which are dependent on static and manoeuvre stability parameters are very important and result in well defined boundaries for the static and manoeuvre margins.

10.2 Short term dynamic models

As explained previously, the critical aspects of aircraft handling qualities are concerned mainly with the dynamics of the initial, or transient, response to controls. Thus since the short term dynamics are of greatest interest, it is common practice to conduct handling qualities studies using reduced order dynamic models derived from the full order equations of motion. The advantage of this approach is that it gives maximum *functional visibility* to the motion drivers of greatest significance. It is therefore easier to interpret and understand the role of the fundamental aerodynamic and dynamic properties of the aeroplane in the determination of its handling qualities. It also goes without saying that the reduced order models are much easier to work with because they are algebraically simpler.

10.2.1 Controlled motion and motion cues

Reduced to the simplest interpretation, when a pilot applies a control input to the aeroplane, he is simply commanding a change in flight path. The change might be temporary, such as manoeuvring about the flight path to return to the original flight path on completion of the manoeuvre. Alternatively, the change might be permanent, such as manoeuvring to effect a change in trim state involving a change in flight path direction. Whatever the ultimate objective, the method of control is much the same. Normal manoeuvring involves rotating the airframe in roll, pitch, and yaw to point the lift vector in the desired direction; by operating the pitch control, the pilot adjusts the angle of attack to produce the lift force required to generate the acceleration to manoeuvre. Thus the pilot's perception of the handling qualities of the aeroplane is concerned with the precise way in which it responds to commands, sensed predominantly as the change in normal acceleration. Indeed, the pilot is extremely sensitive to even the smallest changes in acceleration in all three axes. Clearly, then, short term normal acceleration dynamics provide a vitally important cue in considerations of aircraft handling qualities and are most easily modelled with the reduced order equations of motion. Obviously, other motion cues are equally important to the pilot, such as attitude, angular rate, and angular acceleration, although these variables were not, in the past, regarded with the same level of importance as normal acceleration. Thus, in the analysis of aircraft handling qualities, by far the greatest emphasis is on the longitudinal short term dynamic response to controls.

10.2.2 The longitudinal reduced order model

The reduced order longitudinal state equation describing short term dynamics only is given by equation (6.1) in terms of concise derivatives and may be written as

$$\begin{bmatrix} \dot{\alpha} \\ \dot{q} \end{bmatrix} = \begin{bmatrix} z_w & 1 \\ m_w & m_q \end{bmatrix} \begin{bmatrix} \alpha \\ q \end{bmatrix} + \begin{bmatrix} z_\eta \\ U_e \\ m_\eta \end{bmatrix} \eta \quad (10.1)$$

since $z_q \approx U_e$ and w is replaced by α . Solution of equation (10.1) gives the two short term response transfer functions

$$\frac{\alpha(s)}{\eta(s)} = \frac{\frac{z_\eta}{U_e} \left(s + U_e \frac{m_\eta}{z_\eta} \right)}{(s^2 - (m_q + z_w)s + (m_q z_w - m_w U_e))} \equiv \frac{k_\alpha(s + 1/T_\alpha)}{(s^2 + 2\zeta_s \omega_s s + \omega_s^2)} \quad (10.2)$$

$$\frac{q(s)}{\eta(s)} = \frac{m_\eta(s - z_w)}{(s^2 - (m_q + z_w)s + (m_q z_w - m_w U_e))} \equiv \frac{k_q(s + 1/T_{\theta_2})}{(s^2 + 2\zeta_s \omega_s s + \omega_s^2)} \quad (10.3)$$

Equations (10.2) and (10.3) compare directly with equations (6.17) and (6.18), respectively. The short term response transfer function describing pitch attitude response to elevator follows directly from equation (10.3):

$$\frac{\theta(s)}{\eta(s)} = \frac{k_q(s + 1/T_{\theta_2})}{s(s^2 + 2\zeta_s \omega_s s + \omega_s^2)} \quad (10.4)$$

With reference to Section 5.5, the short term response transfer function describing, approximately, the normal acceleration response to elevator may be derived from equations (10.2) and (10.3):

$$\frac{a_z(s)}{\eta(s)} = \frac{m_\eta z_w U_e}{(s^2 - (m_q + z_w)s + (m_q z_w - m_w U_e))} \equiv \frac{k_{a_z}}{(s^2 + 2\zeta_s \omega_s s + \omega_s^2)} \quad (10.5)$$

In the derivation it is assumed that z_η/U_e is insignificantly small. With reference to Section 5.7.3, the short-term response transfer function describing flight path angle response to elevator is also readily derived from equations (10.2) and (10.4):

$$\frac{\gamma(s)}{\eta(s)} = \frac{-m_\eta z_w}{s(s^2 - (m_q + z_w)s + (m_q z_w - m_w U_e))} \equiv \frac{k_\gamma}{s(s^2 + 2\zeta_s \omega_s s + \omega_s^2)} \quad (10.6)$$

and, again, it is assumed that z_η/U_e is insignificantly small. By dividing equation (10.6) by equation (10.4), it may be shown that

$$\frac{\gamma(s)}{\theta(s)} = \frac{1}{(1 + sT_{\theta_2})} \quad (10.7)$$

which gives the important result that, in the short term, flight path angle response lags pitch attitude response by T_{θ_2} , sometimes referred to as *incidence lag*.

For the purpose of longitudinal short term handling analysis, the responsiveness or manoeuvrability of the aeroplane is quantified by the derivative parameter *normal load factor per unit angle of attack*, denoted n_α . Since this parameter relates to the aerodynamic lift generated per unit angle of attack at a given flight condition, it is proportional to the lift curve slope and the square of the velocity. An expression for n_α is easily derived from the previous short term transfer functions. Assuming a unit step input to elevator such that $\eta(s) = 1/s$, the Laplace transform of the incidence response follows from [equation \(10.2\)](#):

$$\alpha(s) = \frac{\frac{z_\eta}{U_e} \left(s + U_e \frac{m_\eta}{z_\eta} \right)}{(s^2 - (m_q + z_w)s + (m_q z_w - m_w U_e))} \frac{1}{s} \quad (10.8)$$

Applying the final value theorem, [equation \(5.33\)](#), to [equation \(10.8\)](#), the resultant steady value of incidence may be obtained:

$$\alpha(t) \Big|_{ss} = \frac{m_\eta}{(m_q z_w - m_w U_e)} \quad (10.9)$$

In a similar way the corresponding resultant steady value of normal acceleration may be derived from [equation \(10.5\)](#):

$$a_z(t) \Big|_{ss} = \frac{m_\eta z_w U_e}{(m_q z_w - m_w U_e)} \quad (10.10)$$

Now the normal load factor per unit angle of attack is given by

$$n_\alpha = \frac{n_z(t)}{\alpha(t)} \Big|_{ss} \equiv -\frac{1}{g} \frac{a_z(t)}{\alpha(t)} \Big|_{ss} \quad (10.11)$$

Thus, substituting [equations \(10.9\)](#) and [\(10.10\)](#) into [equation \(10.11\)](#), the important result is obtained:

$$n_\alpha = -\frac{z_w U_e}{g} \equiv \frac{U_e}{g T_{\theta_2}} \quad (10.12)$$

since, approximately, $T_{\theta_2} = -1/z_w$.

The transfer functions given by [equations \(10.2\) through \(10.7\)](#) describe the classical longitudinal short term response to elevator and represent the foundation on which most modern ideas of handling qualities are based; see, for example, [Gibson \(1995\)](#). For the classical aeroplane the response characteristics are determined by the aerodynamic properties of the airframe, which are usually linear, bounded, and predictable. It is also clear that the short term dynamics are those of a linear second order system, and aeroplanes which possess similar dynamic behaviour are said to have *second order like* response characteristics. The response properties of all real aeroplanes diverge to some extent from these very simple and rather idealised models. Actual response is coloured by longer term dynamics, non-linear aerodynamic airframe characteristics, and, of course, the influence of a stability augmentation system when fitted. However, whatever the degree of complexity of the aeroplane and its operating conditions, a sound design objective is to achieve second order like dynamic response properties.

EXAMPLE 10.1

The classical second order like response characteristics are most easily seen in simple light aircraft having a limited subsonic flight envelope and flying qualities which are determined entirely by aerodynamic design. Such an aeroplane is the Navion Aircraft Corporation, Navion/H, for which the equations of motion were obtained from Teper (1969). The flight condition corresponds with a cruising speed of 176 ft/s at sea level. The longitudinal reduced order state equation is

$$\begin{bmatrix} \dot{\alpha} \\ \dot{q} \end{bmatrix} = \begin{bmatrix} -0.0115 & 1 \\ -0.0395 & -2.9857 \end{bmatrix} \begin{bmatrix} \alpha \\ q \end{bmatrix} + \begin{bmatrix} -0.1601 \\ -11.0437 \end{bmatrix} \eta \quad (10.13)$$

and the reduced order longitudinal response transfer functions are

$$\frac{\alpha(s)}{\eta(s)} = \frac{-0.1601(s + 71.9844)}{(s^2 + 5.0101s + 12.9988)} \quad (10.14)$$

$$\frac{q(s)}{\eta(s)} = \frac{-11.0437(s + 1.9236)}{(s^2 + 5.0101s + 12.9988)} \text{ 1/s} \quad (10.15)$$

$$\frac{\theta(s)}{\eta(s)} = \frac{-11.0437(s + 1.9236)}{s(s^2 + 5.0101s + 12.9988)} \quad (10.16)$$

$$\frac{a_z(s)}{\eta(s)} = \frac{-28.1700(s - 10.1241)(s + 13.1099)}{(s^2 + 5.0101s + 12.9988)} \text{ ft/s}^2/\text{rad} \quad (10.17)$$

$$\frac{\gamma(s)}{\eta(s)} = \frac{0.1601(s - 10.1241)(s + 13.1099)}{s(s^2 + 5.0101s + 12.9988)} \quad (10.18)$$

The first 5 s of the longitudinal response of the Navion to a 1 degree elevator step input, as defined by equations (10.14) through (10.18), is shown in Fig. 10.1. The response plots in the figure are absolutely typical of the second order like characteristics of a classical aeroplane.

The key parameters defining the general response shapes are

Short-period undamped natural frequency $\omega_s = 3.61 \text{ rad/s}$

Short-period damping ratio $\zeta_s = 0.7$

Incidence lag $T_{\theta_2} = \frac{1}{1.9236} = 0.52 \text{ s}$

These parameters may be obtained directly from inspection of the appropriate transfer functions given above.

It will be observed that the normal acceleration response transfer functions given by equations (10.5) and (10.17) have different numerators; the same is true for the flight path angle response transfer functions given by equations (10.6) and (10.18). This is due to the fact that the algebraic forms are based on a number of simplifying approximations, whereas the numerical forms were obtained from an exact solution of the state equation (10.8) without approximation. However, with reference to Fig. 10.1, both equation (10.17) and equation (10.18) may be approximated by

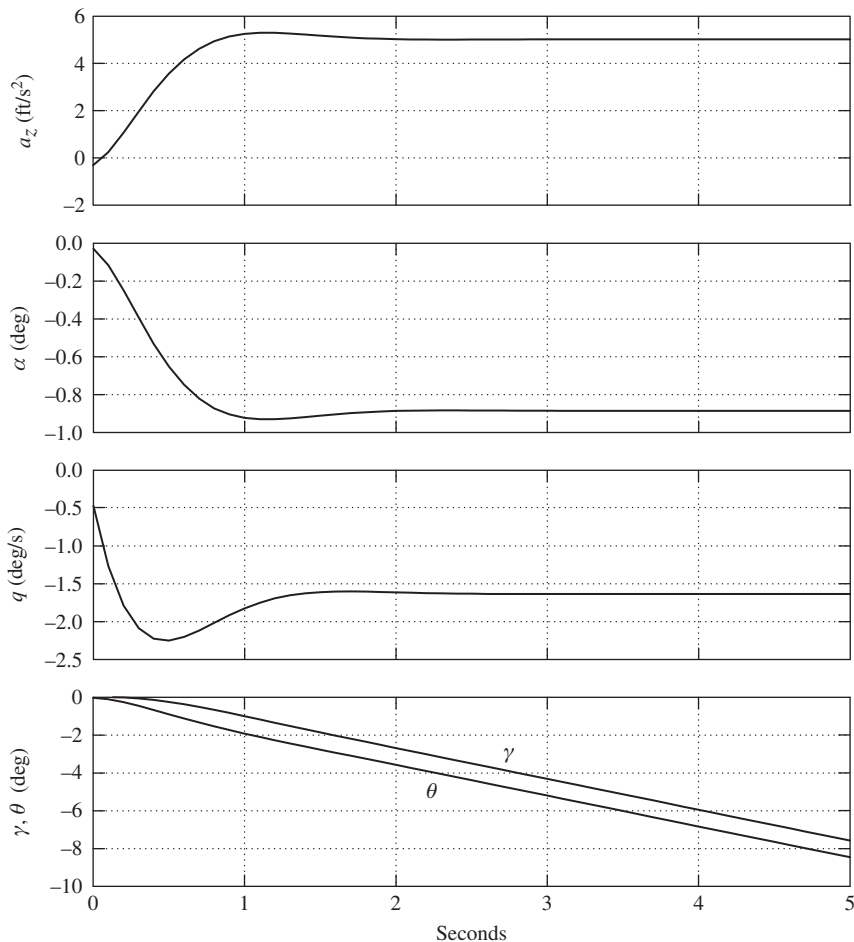


FIGURE 10.1 Longitudinal short term response to elevator step input.

transfer functions having constant numerators in the style of equations (10.5) and (10.6), respectively, and in both cases the response shapes are essentially identical. Equations (10.17) and (10.18) may be approximated by

$$\frac{a_z(s)}{\eta(s)} = \frac{3738.89}{(s^2 + 5.0101s + 12.9988)} \text{ ft/s}^2/\text{rad} \quad (10.19)$$

$$\frac{\gamma(s)}{\eta(s)} = \frac{-1.6347}{s(s^2 + 5.0101s + 12.9988)} \quad (10.20)$$

With reference to Fig. 10.1, it is clear that following a steady elevator step input the short term response, after the short-period transient has damped out, results in steady normal acceleration a_z , steady incidence α , and steady pitch rate q . The corresponding pitch attitude θ and flight path angle γ responses increase linearly with time, the aeroplane behaving like a simple integrator in this respect. It is evident from the latter response plots that flight path angle γ lags pitch attitude θ by about 0.5 s (see equation (10.7)), which corresponds very well with the exact value of T_{θ_2} . These response characteristics are quite typical and do not change significantly with flight condition since the Navion has a very limited flight envelope.

Operation of the elevator causes tailplane camber change, which results in instantaneous change in tailplane lift. This in turn generates a pitching moment causing the aeroplane to respond in pitch. Thus, as a result of his control action, the pilot sees a change in pitch attitude as the primary response. Or, for a steady step input, the response is a steady pitch rate, at least for the first few seconds. For this reason, the nature of control is referred to as a *rate command* characteristic, which is typical of all three control axes because the aerodynamic mechanism of control is similar. With reference to Fig. 10.1, the pitch rate response couples with forward speed to produce the incidence response, which in turn results in the normal acceleration response. This explains why a steady pitch rate is accompanied by steady incidence and normal acceleration responses.

In an actual aeroplane these simple relationships are modified by the influence of the longer term phugoid dynamics. In particular, the pitch rate and normal acceleration response tend to decay with the damped phugoid motion. However, incidence tends to remain more nearly constant at its trim value throughout. Thus, viewed more broadly, the nature of longitudinal control is sometimes referred to alternatively as an *incidence command* characteristic. These ideas may be more easily appreciated by referring to Examples 6.1 and 6.2.

Since the traditional longitudinal motion cue has always focused on normal acceleration, and since in the short term approximation this is represented by a transfer function with a constant numerator, equation (10.19), the only parameters defining the response shape are the short-period mode damping ratio and undamped natural frequency. Similarly, it is evident that incidence dynamics are governed by the same parameters. Pitch rate response is similar in shape to both normal acceleration and incidence responses with the exception of the peak overshoot, which is governed by the value of the numerator term $1/T_{\theta_2}$. However, T_{θ_2} is determined largely by the value of the wing lift curve slope which, for a simple aeroplane like the Navion, is essentially constant throughout the flight envelope. So for a classical aeroplane with second order like response characteristics it is concluded that the short term dynamics are predictable and that the transient is governed predominantly by short-period mode dynamics. Thus it is not surprising that the main emphasis in the specification of aeroplane flying qualities has been on the correct design of the damping and frequency of the short term stability modes, in particular the longitudinal short-period mode.

10.2.3 The “thumb print” criterion

For the reasons outlined, the traditional indicators of the short term longitudinal handling qualities of an aeroplane were securely linked to the damping ratio and undamped natural frequency of the short-period mode. As experience grew over the years of evolutionary development of aeroplanes, the short-period dynamics which resulted in good handling characteristics became established fact. A tradition of experimental flight tests using variable stability aeroplanes was established in the early years after the Second World War specifically for investigating flying and handling qualities. In particular, much of this early experimental work was concerned with longitudinal short term handling qualities. This research has enabled the definition of many *handling qualities criteria* and the production of *flying qualities specification* documents. The tradition of experimental flight tests for handling qualities research is still continued today, mainly in the United States.

One of the earliest flying qualities criteria, the so-called longitudinal short-period *thumb print* criterion, became an established tool in the 1950s; see, for example, Chalk (1958). The thumb print criterion provides guidance for aeroplane designers and evaluators concerning the best combinations of longitudinal short-period mode damping and frequency to give good handling qualities. However, it must be remembered that the information provided is empirical and based entirely on pilot opinion. The common form of presentation of the criterion is shown in Fig. 10.2, and the example shown relates to typical classical aeroplanes in which the undamped short-period mode frequency is around 3 rad/s.

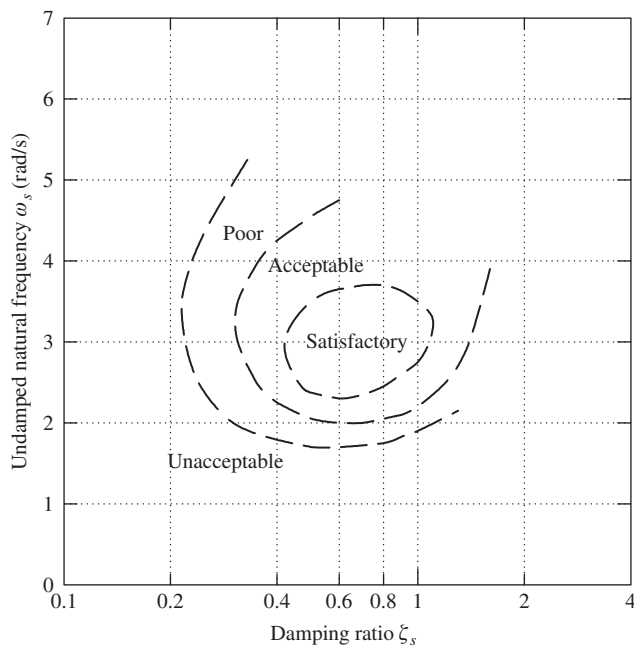


FIGURE 10.2 Longitudinal short-period pilot opinion contours: The thumb print criterion.

Although the criterion is still most applicable to the modern aeroplane, as has been suggested, the achievement of excellent short-period mode dynamics does not necessarily guarantee excellent longitudinal handling qualities. Indeed, many other factors play an important part, and some of these are discussed in the following paragraphs.

10.2.4 Incidence lag

The incidence lag T_{θ_2} is critically important in the determination of the longitudinal handling characteristics of an aeroplane. For classical subsonic aeroplanes, T_{θ_2} remains near constant over the flight envelope and, consequently, the short term pitch dynamics also remain near constant for a given short-period mode damping and frequency. Therefore, the overall longitudinal handling qualities tend to remain nicely consistent over the flight envelope. For this reason incidence lag was not accorded a great deal of attention in the past. However, as aeroplanes have become larger and their operating altitude and Mach number envelopes have been greatly extended, the variation in lift curve slope has become significant. The result of this is that the variation in T_{θ_2} over the flight envelope of typical modern high performance aeroplanes can no longer be ignored. Incidence lag has therefore become as important as short-period mode damping and frequency in the determination of longitudinal short term handling.

Gibson (1995) suggests that, typically, T_{θ_2} may vary from less than 0.5 s at high speed at sea level to greater than 4.0 s at low speed at high altitude. Other significant changes might be introduced by camber control or by direct lift control, as frequently found in advanced modern aircraft of all types. To illustrate the effect of incidence lag on short term pitch response, consider the following transfer functions, which are based nominally on those of Example 10.1:

$$\begin{aligned}\frac{q(s)}{\eta(s)} &= \frac{-13(1 + 0.5s)}{(s^2 + 5s + 13)} \quad 1/\text{s} \\ \frac{\theta(s)}{\eta(s)} &= \frac{-13(1 + 0.5s)}{s(s^2 + 5s + 13)}\end{aligned}\tag{10.21}$$

and, clearly, $\omega_s = 3.6 \text{ rad/s}$, $\zeta_s = 0.69$, and $T_{\theta_2} = 0.5 \text{ s}$.

The response to a stick pull, equivalent to a 1 degree elevator step input, is shown in Fig. 10.3. Also shown are the responses for an incidence lag of 1, 2, and 4 seconds, the short-period mode parameters being held constant throughout. In accordance with the models given by equations (10.2), (10.5), and (10.6), the corresponding incidence, normal acceleration, and flight path angle responses remain unchanged. However, the pitch motion cue to the pilot may well suggest a reduction in damping in view of the significant increase in pitch rate overshoot at larger values of T_{θ_2} . This is of course not the case since the short-period mode damping ratio is 0.69 throughout. The pilot also becomes aware of the increase in lag between the pitch attitude response and acquisition of the desired flight path.

10.3 Flying qualities requirements

Most countries involved in aviation have national agencies to oversee aeronautical activity in their territories. In the United Kingdom the Civil Aviation Authority (CAA) regulates all non-military

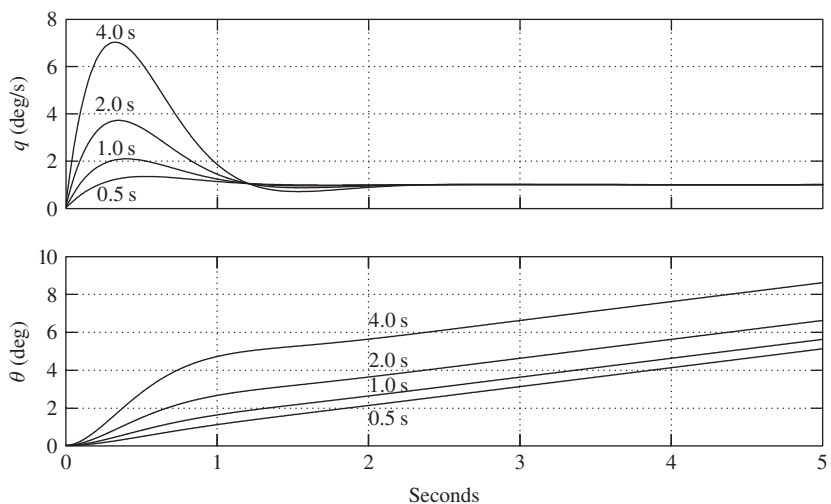


FIGURE 10.3 Effect of variation in incidence lag on pitch response.

aviation and the Ministry of Defence (MoD) oversees all military aeronautical activity. Additionally, a group of European countries have agreed to cooperate in the development of Joint Aviation Requirements (JARs) and, where relevant, these requirements supersede the British Civil Airworthiness Requirements (BCARs). The Joint Aviation Authority which administers this activity comprises the aviation authorities from the participating countries. Thus, for example, in the United Kingdom the JAR documents are issued by the CAA. In the United States the corresponding agencies are the [Federal Aviation Administration](#) (FAA) and the Department of Defense (DoD), respectively. All of these agencies issue extensive documentation specifying the minimum acceptable standards for construction, performance, operation, and safety of all air vehicles operated under their jurisdiction. In more recent years the emphasis has been on the adoption of common standards, for obvious reasons. In the absence of their own standards, many countries adopt those of the American, British, or joint European agencies, which is obviously constructive in achieving very high standards of aviation safety worldwide.

All of the above mentioned agencies issue documents which specify the minimum acceptable standard of flying qualities in some detail, more commonly known as *flying qualities requirements*. Some of the relevant documents are listed in the references at the end of this chapter. In very general terms, the flying qualities requirements for civil aircraft issued by the CAA and FAA are primarily concerned with safety; specific requirements relating to stability, control, and handling are relatively relaxed. On the other hand, the flying qualities requirements issued by the MoD and DoD are specified in much greater detail in every respect. It is the responsibility of the aircraft manufacturer, or supplier, to demonstrate that its aircraft *complies* with the appropriate specification prior to acceptance by the operator. Thus *demonstration of compliance* with the specification is the principal interest of the regulating agencies.

Since the military flying qualities requirements in particular are relatively complex, their correct interpretation may not always be obvious. To alleviate this difficulty the documents also include advisory information on *acceptable means of compliance* to help the manufacturer or supplier apply the requirements to his particular aeroplane. The extensive programme of flight tests which most new aeroplanes undergo prior to service are, in part, used to demonstrate compliance with the flying qualities requirements. However, it is unlikely that an aeroplane will satisfy the requirements completely unless it has been designed to do so from the outset. Therefore, the flying qualities requirements documents are also vitally important to the aircraft designer and to the flight control system designer. In this context, the specifications define the *rules* by which stability, control and handling must be designed and evaluated.

The formal specification of flying and handling qualities is intended to assure flying qualities that provide adequate mission performance and flight safety. Since the most comprehensive, and hence demanding, requirements are included in the military documents, it is these on which the material in the following paragraphs is based. As the military use all kinds of aeroplanes, including small light trainers, large transports, and high performance combat aircraft, flying qualities requirements applicable to all types are quantified in the specification documents. Further, an aeroplane designed to meet military flying and handling qualities requirements undoubtedly also meets civil requirements. Since most of the requirements are quantified in terms of stability and control parameters, they are most readily applied in the current analytical context.

The object here is to provide an overview of the flying qualities requirements as set out in the military specification documents. Liberal reference has been made to the British Defence Standard DEF-STAN 00-970 and to the American Military Specification MIL-F-8785C, which are very similar in style and convey much the same information. This is not surprising since the former was deliberately modelled on the latter in the interests of uniformity. Using an amalgam of material from both sources, no attempt is made to reproduce the requirements with great accuracy or in great detail (for a complete appreciation the reader should consult the references). Rather, the emphasis is on a limited review of the material relevant to the fundamental stability and control properties of the aeroplane as described in earlier chapters.

It is important to appreciate that the requirements in both DEF-STAN 00-970 and MIL-F-8785C are based on the dynamics of classical aeroplanes whose short term response is essentially second order like. This is simply due to the fact that the requirements are empirical and have evolved to capitalise on many years of accumulated experience and pilot opinion. Although attempts have been made to revise the requirements to allow for aeroplanes with stability augmentation, this has had only limited success. Aeroplanes with simple stability augmentation which behave essentially like classical unaugmented aeroplanes are generally adequately dealt with. However, in recent years it has become increasingly obvious that the requirements in both DEF-STAN 00-970 and MIL-F-8785C are unable to cope with aeroplanes whose flying qualities are substantially dependent on a flight control system. For example, there is evidence that some advanced technology aeroplanes have been designed to meet the flying qualities requirements very well, only to attract adverse pilot opinion concerning their handling qualities. With the advent of the fly-by-wire (FBW) aeroplane, it became necessary to seek additional or alternative methods for quantifying and specifying flying qualities requirements.

The obvious deficiencies of the earlier flying qualities requirements for dealing with highly augmented aeroplanes spawned considerable research activity from the late 1960s onward. As a result,

all kinds of criteria have emerged, a few of which have enjoyed enduring, but limited, success. Nevertheless, understanding has improved considerably, and the first serious attempt at producing a flying qualities requirements document suitable for application to highly augmented aeroplanes resulted in the proposal reported by Hoh et al. (1982). This report eventually evolved into the formal American Military Standard MIL-STD-1797A. However, the report by Hoh et al. (1982) is a useful alternative to the Military Standard since it contains some supporting explanatory material. These newer flying qualities requirements still include much of the classical material derived from the earlier specifications, but with the addition of material relating to the influence of command and stability augmentation systems on aircraft handling qualities. Although Hoh et al. (1982) and MIL-STD-1797A provide a very useful progression from DEF-STAN 00-970 and MIL-F-8785C, the material relating to highly augmented aeroplanes takes the subject well beyond the scope of the present book. The interested reader will find an excellent overview of the ideas relating to the handling qualities of advanced technology aeroplanes in Gibson (1995).

10.4 Aircraft role

It is essential that the characteristics of any dynamic system which is subject to direct human control are bounded. Outside these bounds the system would not be capable of human control. However, the human is particularly adaptable such that the variation in acceptable dynamic characteristics within the performance boundary of the system is considerable. In terms of aeroplane dynamics, this means that wide variation in stability and control characteristics can be tolerated within the bounds of acceptable flying qualities. However, it is important that the flying qualities be appropriate to the type of aeroplane in question and to the task the aeroplane is carrying out. For example, the dynamic handling qualities appropriate to a fighter aircraft in an air combat situation are quite inappropriate to a large civil transport aircraft on final approach. Thus it is easy to appreciate that the stability and control characteristics which comprise flying qualities requirements are bounded by the limitations of the human pilot; within those bounds, however, the characteristics are defined in a way which is most appropriate to the prevailing flight condition.

Thus flying qualities requirements are formulated to allow for the type, or *class*, of aeroplane and for the flight task, or *flight phase*, in question. Further, the degree of excellence of flying qualities is described as the *level of flying qualities*. Thus prior to referring to the appropriate flying qualities requirements the aeroplane must be classified and its flight phase defined. A designer would then design to achieve the highest level of flying qualities whereas, an evaluator would seek to establish that the aeroplane achieved the highest level of flying qualities in all normal operating states.

10.4.1 Aircraft classification

Aeroplane types are classified broadly according to size and weight as follows:

Class I: small, light

Class II: medium weight, low to medium manoeuvrability

Class III: large, heavy, low to medium manoeuvrability

Class IV: high manoeuvrability

10.4.2 Flight phase

A sortie or mission may be completely defined as a sequence of piloting tasks. Alternatively, a mission may be described as a succession of flight phases. Flight phases are grouped into three *categories*, and each category comprises a variety of tasks requiring similar flying qualities for successful execution. The tasks are separately defined in terms of *flight envelopes*. The flight phase categories are defined as follows:

- Category A:** non-terminal flight phases that require rapid manoeuvring, precision tracking, or precise flight path control
- Category B:** non-terminal flight phases that require gradual manoeuvring, less precise tracking, and accurate flight path control
- Category C:** terminal flight phases that require gradual manoeuvring and precision flight path control

10.4.3 Levels of flying qualities

The levels of flying qualities quantify the degree of acceptability of an aeroplane in terms of its ability to complete the mission for which it is designed. The three levels of flying qualities seek to indicate the severity of the *pilot workload* in the execution of a mission flight phase and are defined as follows:

- Level 1:** flying qualities clearly adequate for the mission flight phase
- Level 2:** flying qualities adequate to accomplish the mission flight phase but with an increase in pilot workload and/or degradation in mission effectiveness
- Level 3:** degraded flying qualities but such that the aeroplane can be controlled, inadequate mission effectiveness, and high, or limiting, pilot workload

Level 1 flying qualities imply a fully functional aeroplane which is 100% capable of achieving its mission with acceptable pilot workload at all times. It follows, then, that any fault or failure occurring in airframe, engines, or systems may well degrade the level of flying qualities. Consequently, the *probability* of such a situation arising during a mission becomes an important issue. This means that the levels of flying qualities are very much dependent on the *aircraft failure state*, which in turn is dependent on the reliability of the critical functional components of the aeroplane. The development of this aspect of flying qualities assessment is a subject in its own right and is beyond the scope of the present book.

10.4.4 Flight envelopes

The operating boundaries of altitude, Mach number, and normal load factor define the *flight envelope* for an aeroplane. Flight envelopes describe the absolute “never exceed” limits of the airframe and define the operating limits required for a particular mission or flight phase.

Permissible flight envelope

The permissible flight envelope describes the limiting flight condition boundaries within which an aeroplane may be flown and safely recovered without exceptional pilot skill.

Table 10.1 Operational Flight Envelopes

Flight Phase Category	Flight Phase
A	Air-to-air combat
	Ground attack
	Weapon delivery/launch
	Reconnaissance
	In-flight refuel (receiver)
	Terrain following
	Maritime search
	Aerobatics
	Close formation flying
B	Climb
	Cruise
	Loiter
	In-flight refuel (tanker)
	Descent
	Aerial delivery
C	Take-off
	Approach
	Overshoot
	Landing

Service flight envelope

The service flight envelope defines the boundaries of altitude, Mach number, and normal load factor pertaining to all operational mission requirements. It denotes the limits to which an aeroplane may normally be flown without risk of exceeding those limits.

Operational flight envelope

The operational flight envelope lies within the service flight envelope and defines the boundaries of altitude, Mach number, and normal load factor for each flight phase. It is a requirement that the aeroplane be capable of operation up to those boundaries. The operational flight envelopes defined in DEF-STAN 00-970 are listed in **Table 10.1**.

When assessing the flying qualities of an aeroplane, **Table 10.1** may be used to determine which flight phase category is appropriate for the flight condition in question.

EXAMPLE 10.2

To illustrate the altitude–Mach number flight envelope, consider the McDonnell-Douglas A4-D Skyhawk and its possible deployment in a *ground attack* role. The service flight envelope for the

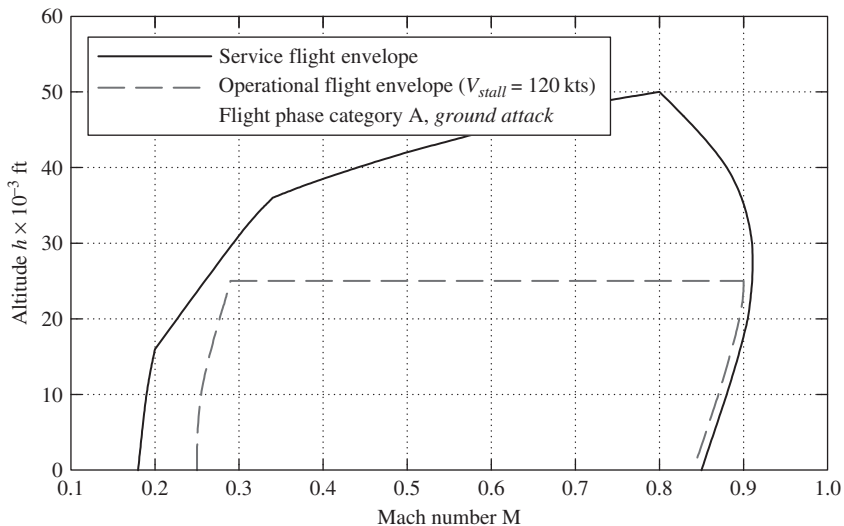


FIGURE 10.4 Flight envelopes for the McDonnell-Douglas A4-D Skyhawk.

aircraft was obtained from Teper (1969) and is shown in Fig. 10.4. Assuming that this aircraft is to be procured by the Royal Air Force, it must meet the operational flight envelope requirement for the ground attack role as defined in DEF-STAN 00-970. The altitude-speed requirements for this role are given as follows:

Minimum operational speed: $V_{0\min} = 1.4V_{stall}$

Maximum operational speed: $V_{0\max} = V_{MAT}$

Minimum operational altitude: $h_{0\min} = \text{Mean sea level (MSL)}$

Maximum operational altitude: $h_{0\max} = 25000\text{ft}$

where V_{MAT} is the maximum speed at *maximum augmented thrust* in level flight. The operational flight envelope for the ground attack role is superimposed on the service flight envelope for the aircraft as shown in Fig. 10.4; the implications of these limits are self-evident for the role in question.

EXAMPLE 10.3

To illustrate the normal load factor–speed flight envelope, consider the Morane Saulnier MS-760 Paris aircraft as registered by the CAA for operation in the United Kingdom. The Paris is a small four seat twin jet fast liaison aircraft which first flew in the late 1950s. It is a classical “aerodynamic” aircraft, with an unswept wing and a T-tail, and is typical of the small jet

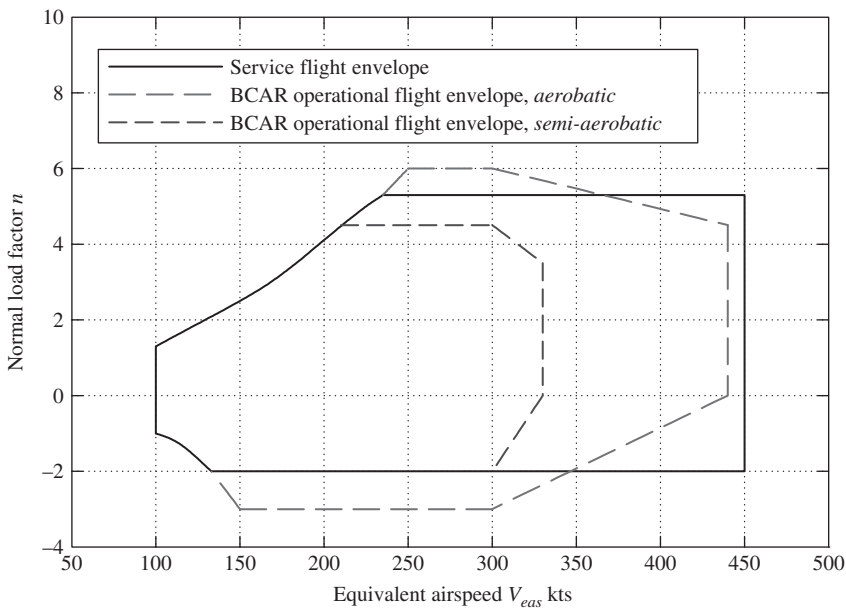


FIGURE 10.5 Flight envelopes for the Morane-Saulnier MS-760 Paris.

trainers of the period. The manoeuvring flight envelopes for this aircraft were obtained from “Notes for Technical Observers” (College of Aeronautics, 1965) and are reproduced in Fig. 10.5. Clearly the service flight envelope fully embraces the BCAR operational flight envelope for *semi-aerobatic* aircraft, whereas some parts of the BCAR operational flight envelope for *fully aerobatic* aircraft are excluded. Consequently, the aircraft is registered in the semi-aerobatic category and certain aerobatic manoeuvres are prohibited. It is clear from Fig. 10.5 that the Paris was designed with structural normal load factor limits of +5.2g, -2g which are inadequate for fully aerobatic manoeuvring.

10.5 Pilot opinion rating

Pilot opinion rating scales have been in use for a considerable time and provide a formal procedure for the qualitative assessment of aircraft flying qualities by experimental means. Since qualitative assessment is very subjective, the development of a formal method for the interpretation of pilot opinion has turned a rather “imprecise art” into a useful tool which is routinely used in flight test programmes. The current pilot opinion rating scale was developed by Cooper and Harper (1969) and is universally known as the *Cooper-Harper rating scale*.

Table 10.2 The Cooper-Harper Handling Qualities Rating Scale

Adequacy for Selected Task	Aircraft Characteristic	Demands on Pilot (workload)	Pilot Rating
Satisfactory	Excellent	Very low	1
Satisfactory	Good	Low	2
Satisfactory	Fair	Minimal pilot compensation required	3
Unsatisfactory—warrants improvements	Minor deficiencies	Moderate pilot compensation required	4
Unsatisfactory—warrants improvements	Moderate deficiencies	Considerable pilot compensation required	5
Unsatisfactory—warrants improvements	Tolerable deficiencies	Extensive pilot compensation required	6
Unacceptable—requires improvements	Major deficiencies	Adequate performance not attainable	7
Unacceptable—requires improvements	Major deficiencies	Considerable pilot compensation required for control	8
Unacceptable—requires improvements	Major deficiencies	Intense pilot compensation required for control	9
Catastrophic—improvement mandatory	Major deficiencies	Loss of control likely	10

Table 10.3 Equivalence of Cooper-Harper Rating Scale with Levels of Flying Qualities

Level of Flying Qualities	Level 1		Level 2		Level 3		Below Level 3			
Cooper-Harper rating scale	1	2	3	4	5	6	7	8	9	10

The Cooper-Harper rating scale is used to assess the flying qualities or, more specifically, the handling qualities of an aeroplane in a given flight phase. The procedure for conducting the flight test evaluation and the method for post-flight reduction and interpretation of pilot comments are defined. The result of the assessment is a *pilot rating* between 1 and 10. A rating of 1 suggests excellent handling qualities and low pilot workload, whereas a rating of 10 suggests an aircraft with many handling deficiencies. The adoption of a common procedure for rating handling qualities enables pilots to clearly state their assessment without ambiguity or the use of misleading terminology. A summary of the Cooper-Harper handling qualities rating scale is shown in [Table 10.2](#).

It is usual and convenient to define an equivalence between the qualitative Cooper-Harper rating scale and quantitative Level of flying qualities. This permits easy and meaningful interpretation of flying qualities between the piloting and analytical domains. The equivalence is summarised in [Table 10.3](#).

10.6 Longitudinal flying qualities requirements

10.6.1 Longitudinal static stability

It was shown in Chapter 3 that longitudinal static stability determines pitch control displacement and force to trim. Clearly this must be of the correct magnitude if effective control of the aeroplane is to be maintained at all flight conditions. For this to be so, the controls-fixed and controls-free static margins must not be too large or too small.

In piloting terms, a change of trim is seen as a change in airspeed, or Mach number, and involves a forward stick push to increase speed and an aft stick pull to decrease speed when the aeroplane possesses a normal level of static stability. The requirement states that variation in pitch control position and force with speed is to be smooth and the gradients at the nominal trim speed are to be stable or, at worst, neutrally stable. In other words, the static margins are to be greater than or equal to zero. The maximum acceptable degree of static stability is not specified, but it is limited by the available control power and the need to be able to lift the nose wheel at rotation for take-off at a reasonable airspeed. Abrupt changes in gradient with airspeed are not acceptable. Typical stable gradients are shown in Fig. 10.6, where it is indicated that the control characteristics do not have to be linear but changes in gradient must be smooth. The minimum acceptable control characteristics obviously correspond with neutral static stability.

In the transonic flight regime in particular, the static stability margins can change significantly such that the aeroplane may become unstable for some part of its speed envelope. The requirements recognise such conditions and permit mildly unstable pitch control force gradients in transonic flight provided that the flight condition is transitory. Maximum allowable unstable gradients are quantified, and a typical boundary is indicated in Fig. 10.6. Aeroplanes which may be required to

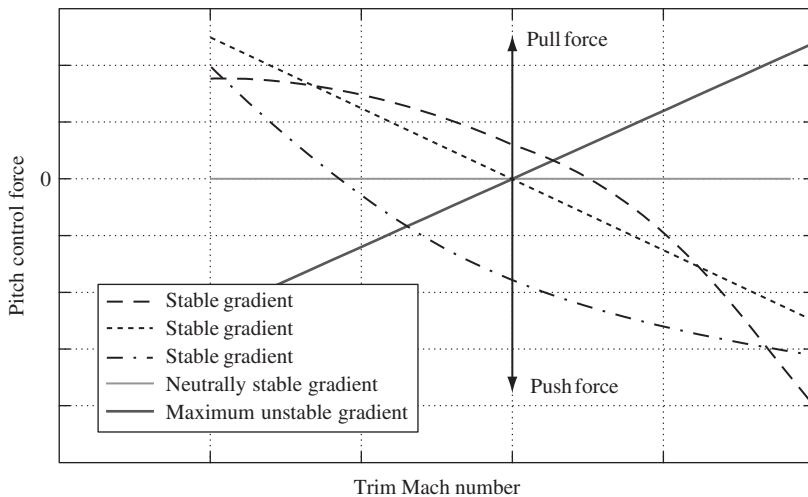


FIGURE 10.6 Typical pitch control force gradients.

operate for prolonged periods in transonic flight conditions are not permitted to have unstable control force gradients.

10.6.2 Longitudinal dynamic stability

Short-period pitching oscillation

For the reasons explained in [Section 10.2](#), the very important normal acceleration motion cue and the short-period dynamics are totally interdependent. The controls-fixed manoeuvre margin H_m and the short-period frequency ω_s are also interdependent, as explained in Chapter 8 (Section 8.5). The requirements for short-period mode frequency reflect these relationships and are relatively complex. A typical illustration is shown in [Fig. 10.7](#).

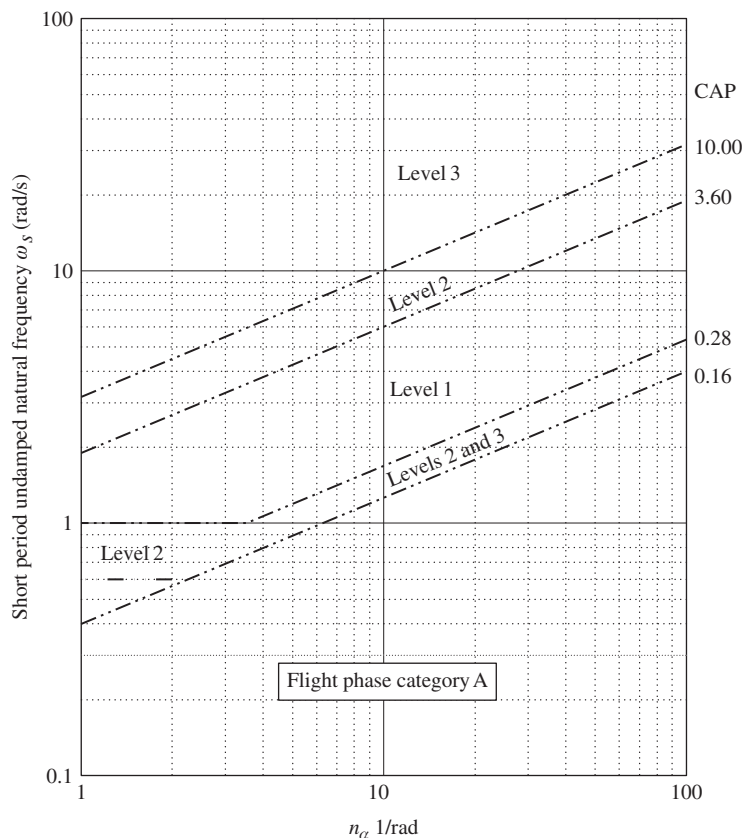


FIGURE 10.7 Typical short-period mode frequency requirements.

Three similar charts are given, one for each flight phase category. That for category A is presented in Fig. 10.7. The boundaries shown are equivalent to lines of constant *control anticipation parameter* (CAP), which is proportional to the controls-fixed manoeuvre margin. The boundaries therefore implicitly specify the constraint on manoeuvrability, quantified in terms of short-period mode undamped natural frequency. The meaning of CAP is explained in Section 10.7.

Now, the derivative parameter n_α quantifies the normal load factor per unit angle of attack, or incidence, as defined by equation (10.11). As its value increases with speed, the lower values of n_α correlate with the lower speed characteristics of the aeroplane and vice versa. As speed increases the aerodynamic pitch stiffness of the aeroplane also increases, which in turn results in an increase in short-period mode frequency. This natural phenomenon is reflected in the requirements, as the boundaries allow for increasing frequency with increasing n_α .

Acceptable limits on the stability of the short-period mode are quantified in terms of maximum and minimum values of the damping ratio as a function of flight phase category and Level of flying qualities, as set out in Table 10.4.

The maximum values of short-period mode damping ratio obviously imply that a stable nonoscillatory mode is acceptable.

Table 10.4 Short-Period Mode Damping

Flight Phase	Level 1		Level 2		Level 3
	$\zeta_s \text{ min}$	$\zeta_s \text{ max}$	$\zeta_s \text{ min}$	$\zeta_s \text{ max}$	$\zeta_s \text{ min}$
CAT A	0.35	1.30	0.25	2.00	0.10
CAT B	0.30	2.00	0.20	2.00	0.10
CAT C	0.50	1.30	0.35	2.00	0.25

Phugoid

Upper and lower values for phugoid frequency are not quantified. However, it is recommended that the phugoid and short-period mode frequencies be well separated. Also, it is suggested that handling difficulties may become obtrusive if the frequency ratio of the modes $\omega_p/\omega_s \leq 0.1$. Generally the phugoid dynamics are acceptable provided the mode is stable and damping ratio limits are quantified as shown in Table 10.5.

Table 10.5 Phugoid Damping Ratio

Level of Flying Qualities	Minimum ζ_p
1	0.04
2	0
3	Unstable, period $T_p > 55$ s

10.6.3 Longitudinal manoeuvrability

The requirements for longitudinal manoeuvrability are largely concerned with manoeuvring control force, or *stick force per g*. It is important that the value of this control characteristic is not too large or too small. In other words, the controls-free manoeuvre margin must be constrained to an acceptable and appropriate range. If the control force is too *light*, there is a danger that the pilot may inadvertently apply too much normal acceleration to the aircraft with the consequent possibility of structural failure. On the other hand, if the control force is too *heavy*, the pilot may not be strong enough to fully utilise the manoeuvring flight envelope of the aircraft.

Thus the requirements define the permitted upper and lower limits for controls-free manoeuvre margin expressed in terms of the pitch control manoeuvring force gradient because this is the quantifiable parameter seen by the pilot. Further, the limits are functions of the type of control inceptor, a single stick or wheel type, and the limiting normal load factor appropriate to the airframe in question. The rather complex requirements are tabulated, and their interpretation for an aircraft with a single stick controller and a limiting normal load factor of $n_L = 7.0$ is shown in Fig. 10.8. Again, the limits on stick force per g are expressed as a function of the flight condition parameter n_α .

10.7 Control anticipation parameter

It has been reported by Bihrl (1966) that, *in order to make precise adjustments to the flight path, the pilot must be able to anticipate the ultimate response of the airplane, and that angular pitching acceleration is used for this purpose*. Aeroplanes which have good second order like short term longitudinal response properties generally provide the pilot with good anticipatory handling cues. Clearly, this depends on the damping and frequency of the short-period pitching mode in particular. However, Bihrl (1966) reports pilot observation that, *for airplanes having high inertia or low static stability, the angular pitching acceleration accompanying small adjustments to flight path may fall below the threshold of perception*. In other words, the anticipatory nature of the response cues may become insignificant, thereby giving rise to poor handling qualities. To deal with such cases Bihrl defines a quantifiable measure of the anticipatory nature of the response which he calls *control anticipation parameter (CAP)*. The formal definition of CAP is, *the amount of instantaneous angular pitching acceleration per unit of steady-state normal acceleration*.

The steady normal acceleration response to a pitch control input is determined by the aerodynamic properties of the aeroplane, the wing and tailplane in particular. However, the transient peak magnitude of angular pitching acceleration immediately following the control input is largely determined by the short-period dynamics, which in turn are dependent on the longitudinal static stability and moment of inertia in pitch. Thus CAP effectively quantifies acceptable short-period mode characteristics appropriate to the aerodynamic properties and operating condition of the aeroplane.

A simple expression for CAP is easily derived from the longitudinal short-term transfer functions described in Section 10.2.2.

The angular pitch acceleration transfer function is obtained from equation (10.3):

$$\frac{\dot{q}(s)}{\eta(s)} = \frac{m_\eta s(s - z_w)}{(s^2 - (m_q + z_w)s + (m_q z_w - m_w U_e))} \quad (10.22)$$

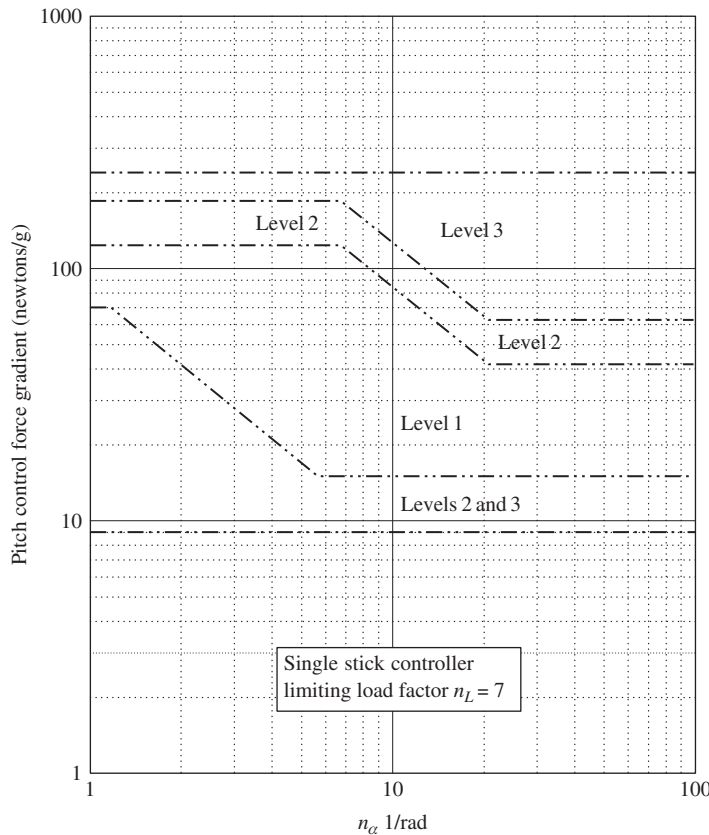


FIGURE 10.8 Typical pitch control manoeuvring force gradients.

The initial pitch acceleration may be derived by assuming a unit elevator step input and applying the initial value theorem, equation (5.34), to [equation \(10.22\)](#). Whence

$$\dot{q}(0) = \lim_{s \rightarrow \infty} \left(s \frac{m_\eta s(s - z_w)}{(s^2 - (m_q + z_w)s + (m_q z_w - m_w U_e))} \frac{1}{s} \right) = m_\eta \quad (10.23)$$

Similarly, the steady-state normal acceleration may be derived by assuming a unit elevator input and applying the final value theorem, equation (5.33), to [equation \(10.5\)](#). Whence

$$a_z(\infty) = \lim_{s \rightarrow 0} \left(s \frac{m_\eta z_w U_e}{(s^2 - 2\zeta_s \omega_s s + \omega_s^2)} \frac{1}{s} \right) = \frac{m_\eta z_w U_e}{\omega_s^2} \quad (10.24)$$

The dimensionless normal acceleration, or load factor, is given by

$$n_z(\infty) = -\frac{a_z(\infty)}{g} = -\frac{m_\eta z_w U_e}{g \omega_s^2} \quad (10.25)$$

and CAP is given by

$$\text{CAP} = \frac{\dot{q}(0)}{n_z(\infty)} = -\frac{g\omega_s^2}{z_w U_e} = \frac{g\omega_s^2 T_{\theta_2}}{U_e} \quad (10.26)$$

since, approximately, $T_{\theta_2} = -1/z_w$.

With reference to [equation \(10.12\)](#), an alternative and more commonly used expression for CAP follows:

$$\text{CAP} = \frac{\omega_s^2}{n_\alpha} \quad (10.27)$$

This is the boundary parameter shown in [Fig. 10.7](#).

Now, [equation \(8.62\)](#) states that

$$\omega_s^2 = \frac{1/2\rho V_0^2 S \bar{c} a}{I_y} H_m \quad (10.28)$$

With reference to Appendix 2, it may be shown that

$$z_w \cong \frac{\dot{Z}_w}{m} = \frac{1/2\rho V_0 S Z_w}{m} \quad (10.29)$$

assuming, as is usually the case, that $\dot{Z}_w < m$. With reference to Appendix 8, it may be determined that

$$Z_w \cong -\frac{\partial C_L}{\partial \alpha} \equiv -a \quad (10.30)$$

which is the lift curve slope.

Thus, substituting [equations \(10.28\), \(10.29\), and \(10.30\)](#) into [equation \(10.26\)](#), the expression for CAP reduces to the important result,

$$\text{CAP} = \frac{mg\bar{c}}{I_y} H_m = \frac{g\bar{c}}{k^2} H_m \quad (10.31)$$

where k denotes the *longitudinal radius of gyration*. Since aircraft axes are assumed to be wind axes throughout, $U_e \equiv V_0$. Thus it is shown that CAP is directly proportional to the controls-fixed manoeuvre margin H_m and that the constant of proportionality is dependent on aircraft geometry and mass distribution.

10.8 Lateral-directional flying qualities requirements

10.8.1 Steady lateral-directional control

Unlike the longitudinal flying qualities requirements the lateral–directional requirements do not address static stability in quite the same way. In general, lateral-directional static stability is independent of *cg* position and flight condition and, once set by the aerodynamic design of the

aeroplane, does not change significantly. The main concerns centre on adequate control power for maintaining control in steady asymmetric flight conditions or in otherwise potentially limiting conditions in symmetric flight. Further, it is essential that the control forces required to cope with such conditions not exceed the physical capabilities of the average pilot.

General normal lateral-directional control requirements specify limits for the roll stick and rudder pedal forces, and require that the force gradients have the correct sense and do not exceed prescribed limits. The control requirement for trim is addressed, as is the requirement for roll-yaw control coupling, which must be correctly harmonised. In particular, it is important that the pilot can fly properly coordinated turns with similar and acceptable degrees of effort in control of both roll and yaw.

The lateral-directional requirements relating to asymmetric, or otherwise potentially difficult control conditions, are concerned with steady sideslip, flight in crosswind, steep dives, and engine out conditions resulting in asymmetric thrust. For each condition the requirements specify the maximum permissible roll and yaw control forces necessary to maintain controlled flight up to relatively severe adverse levels. Since the specified conditions interrelate and have to take into account aircraft class, flight phase, and level of flying qualities, many tables of quantitative limits are needed to embrace all eventualities. Thus, the flying qualities requirements relating to steady lateral-directional flight are comprehensive and of necessity substantial.

10.8.2 Lateral-directional dynamic stability

Roll subsidence mode

Since the roll subsidence mode describes short term lateral dynamics, it is critical in the determination of lateral handling qualities. For this reason the limiting acceptable values of its time constant are specified precisely as listed in [Table 10.6](#).

There seems to be no common agreement as to a suitable maximum value of the time constant for Level 3 flying qualities. It is suggested in DEF-STAN 00-970 that a suitable value is in the range $6 \text{ s} < T_r < 8 \text{ s}$, whereas MIL-F-8785C quotes a value of 10 s.

Table 10.6 Roll Subsidence Mode Time Constant

Aircraft Class	Flight Phase Category	Maximum Value of T_r (s)		
		Level 1	Level 2	Level 3
I, IV	A, C	1.0	1.4	-
II, III	A, C	1.4	3.0	-
I, II, III, IV	B	1.4	3.0	-

Spiral mode

A stable spiral mode is acceptable irrespective of its time constant. However, since its time constant is dependent on lateral static stability (dihedral effect), the maximum level of stability is determined by the maximum acceptable roll control force. Because the mode gives rise to very slow dynamic behavior, it is not too critical to handling unless it is very unstable. For this reason,

minimum acceptable degrees of instability are quantified in terms of time to double bank angle T_2 in an uncontrolled departure from straight and level flight. The limiting values are shown in [Table 10.7](#).

For analytical work it is sometimes more convenient to express the spiral mode requirement in terms of time constant T_s rather than time to double bank angle. If it is assumed that the unstable mode characteristic gives rise to a purely exponential divergence in roll, it is easily shown that the time constant and the time to double bank angle are related by the following expression:

$$T_s = \frac{T_2}{\log_e 2} \quad (10.32)$$

Thus, the requirement may be alternatively quantified as listed in [Table 10.8](#).

Table 10.7 Spiral Mode Time to Double Bank Angle

Flight Phase Category	Minimum Value of T_2 (s)		
	Level 1	Level 2	Level 3
A, C	12	8	5
B	20	8	5

Table 10.8 Spiral Mode Time Constant

Flight Phase Category	Minimum Value of T_s (s)		
	Level 1	Level 2	Level 3
A, C	17.3	11.5	7.2
B	28.9	11.5	7.2

Dutch roll mode

Since the dutch roll is a short-period mode, it has an important influence on lateral-directional handling and, as a consequence, its damping and frequency requirements are specified in some detail. This mode is approximately the lateral-directional equivalent of the longitudinal short-period mode and has frequency of the same order because pitch and yaw inertias are usually similar in magnitude. However, yaw damping is frequently low as a result of the design conflict with the need to constrain spiral mode instability with dihedral. Although the longitudinal short-period mode and the dutch roll mode are similar in bandwidth, the latter is not as critical to handling. In fact, a poorly damped dutch roll is seen more as a handling irritation than a serious problem.

The acceptable minima for damping ratio, undamped natural frequency, and damping ratio-frequency product are specified for various combinations of aircraft class and flight phase category in [Table 10.9](#).

Table 10.9 Dutch Roll Frequency and Damping

Aircraft Class	Flight Phase	Minimum Values							
		Level 1			Level 2			Level 3	
		ζ_d	$\zeta_d\omega_d$	ω_d	ζ_d	$\zeta_d\omega_d$	ω_d	ζ_d	ω_d
I, IV	Cat. A	0.19	0.35	1.0	0.02	0.05	0.5	0	0.4
II, III	Cat. A	0.19	0.35	0.5	0.02	0.05	0.5	0	0.4
All	Cat. B	0.08	0.15	0.5	0.02	0.05	0.5	0	0.4
I, IV	Cat. C	0.08	0.15	1.0	0.02	0.05	0.5	0	0.4
II, III	Cat. C	0.08	0.10	0.5	0.02	0.05	0.5	0	0.4

10.8.3 Lateral-directional manoeuvrability and response

The lateral-directional manoeuvrability requirements are largely concerned with limiting roll oscillations, sideslip excursions, and roll and yaw control forces to acceptable levels during rolling and turning manoeuvres.

Oscillation in roll response to controls occurs whenever the dutch roll is intrusive and poorly damped. For this reason, limiting the magnitude and characteristics of oscillation in roll effectively imposes additional constraints on the dutch roll mode when it is intrusive. Oscillation is also possible in cases when the roll and spiral modes couple to form a second pair of complex roots in the lateral-directional characteristic equation. However, the influence of this characteristic on handling is not well understood, and it is recommended that the condition be avoided.

Sideslip excursions during lateral-directional manoeuvring are normal and expected, especially in entry and exit to turning manoeuvres. It is required that the rudder control displacement and force increase approximately linearly with an increase in sideslip response for sideslip of modest magnitude. It is also required that the effect of dihedral is not too great; otherwise, excessive roll control displacement and force may be needed to manoeuvre. Remember that too much stability can be as hazardous as too little! It seems that the main emphasis is on acceptable levels of roll and yaw control displacement, with particular concern for entry and exit to turning manoeuvres, which after all represent lateral-directional manoeuvring flight.

10.9 Flying qualities requirements on the *s*-plane

In Chapter 9, the mapping of the roots of the characteristic equation onto the *s*-plane was illustrated to facilitate graphical interpretation of aircraft stability. By superimposing boundaries defined by the appropriate flying qualities requirements onto the same *s*-plane plots, the stability characteristics of an aeroplane may be assessed directly with respect to those requirements. This graphical approach is particularly useful for analysis and design and is employed extensively in flight control system design.

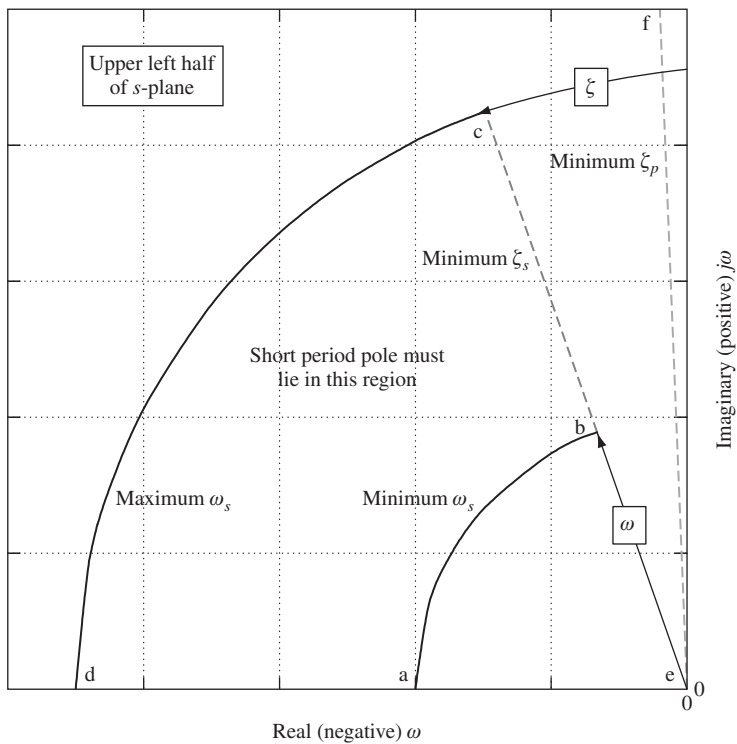


FIGURE 10.9 Longitudinal flying qualities requirements on the *s*-plane.

10.9.1 Longitudinal modes

Typical boundaries describing the limits on longitudinal mode frequency and damping on the *s*-plane are shown in Fig. 10.9. It is not usually necessary to show more than the upper left half of the *s*-plane since stable characteristics are of primary interest and the lower half is simply the mirror image of the upper half reflected in the real axis.

The upper and lower short-period mode frequency boundaries are described by arcs cd and ab , respectively. The frequency limits are determined from charts like Fig. 10.7 and depend on the operating flight condition, which is determined by n_a . Alternatively, the boundaries may be determined from a consideration of the limiting CAP values, also given in charts like Fig. 10.7, at the flight condition of interest. Note that when the *s*-plane is drawn to the same scale on both the x and y axes, the frequency boundaries become circular arcs about the origin. When the scales are not the same, the arcs become ellipses, which can be more difficult to interpret. The minimum short-period mode damping ratio is obtained from Table 10.4 and maps into the line bc radiating from the origin. The maximum permitted damping ratio is greater than 1, which obviously means that the corresponding roots lie on the real axis. Thus when the short-period mode roots, or poles, are mapped onto the *s*-plane, they must lie within the region bounded by $abcd$ and its mirror image in the real

axis. If the damping ratio is greater than 1, the pair of roots must lie on the real axis in locations bounded by the permitted maximum value of the damping ratio.

The minimum phugoid damping ratio is given in Table 10.5 and, for Level 1 flying qualities, maps onto the s -plane as the boundary ef . Thus, when the phugoid roots, or poles, are mapped onto the s -plane, they must lie to the left of the line ef to meet Level 1 flying qualities requirements. The Level 3 requirement on phugoid damping obviously allows for the case when the poles become real, one of which may be unstable and thereby give rise to divergent motion. In this case, the limit implicitly defines a minimum acceptable value for the corresponding time constant. This is mapped on to the s -plane in exactly the same way that the lateral-directional spiral mode boundary is mapped, as described next.

10.9.2 Lateral-directional modes

Typical boundaries describing the limits on lateral-directional mode frequency and damping on the s -plane are shown in Fig. 10.10. Again, the upper left half of the s -plane is shown but now with a small extension into the upper right half to include the region appropriate to the unstable spiral

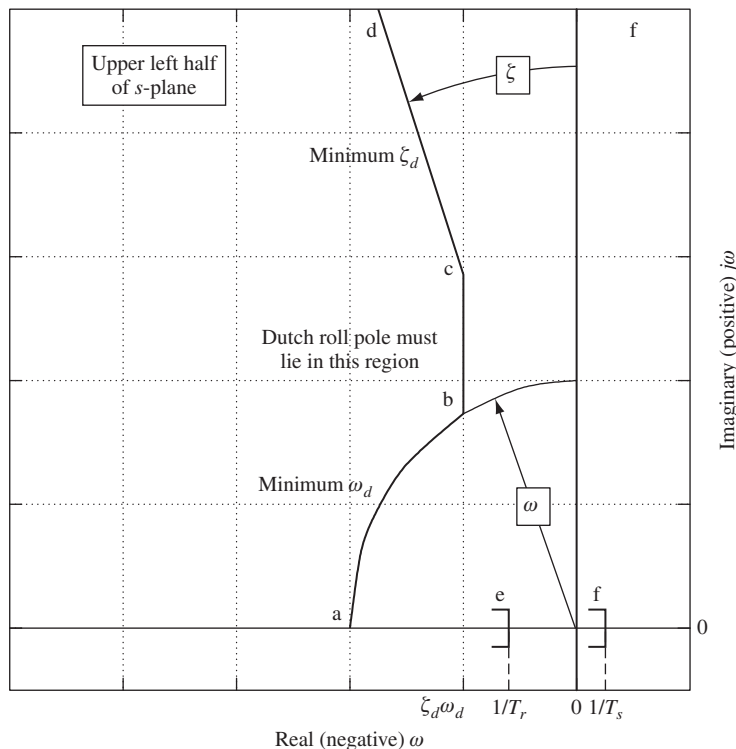


FIGURE 10.10 Lateral-directional flying qualities requirements on the s -plane.

mode. As for the longitudinal case, interpretation implicitly includes the lower half of the *s*-plane, which is the mirror image of the upper half of the *s*-plane in the real axis.

The maximum permitted value of the roll subsidence mode time constant is given in [Table 10.6](#) and maps into the boundary *e* since the corresponding real root is given by the inverse of the time constant T_r . Further, since the mode must always be stable, it always lies on the negative real axis. The precise location of the boundary *e* is determined by aircraft class, flight phase category, and required flying qualities. However, at the appropriate operating flight condition, the pole describing the roll subsidence mode must lie on the real axis to the left of the boundary *e*.

The location of the spiral mode boundary *f* is established in the same way. Since the required limits apply to the mode only when it is unstable, the corresponding boundary lies on the right half of the *s*-plane. The precise location of the boundary may be determined from the minimum acceptable value of the time constant T_s , given in [Table 10.8](#) and, again, this depends on aircraft class and required flying qualities. Thus, the spiral mode pole must always lie on the real axis to the left of the boundary *f*.

The limiting frequency and damping requirements for the dutch roll mode are given in [Table 10.9](#) and are interpreted in much the same way as the requirements for the longitudinal short-period mode. The minimum permitted frequency boundary is described by the arc *ab* and the minimum permitted damping ratio boundary, by the line *cd*. The minimum permitted value of $\zeta_d \omega_d$ maps into the line *bc* to complete the dutch roll mode boundary and, as before, the boundary has its mirror image in the lower half of the *s*-plane. The dutch roll mode roots, or poles, must therefore always lie to the left of the boundary *abcd* at the flight condition of interest. Clearly, the precise location of the boundary is determined by the appropriate combination of aircraft class, flight phase category, and required level of flying qualities.

EXAMPLE 10.4

To illustrate the application of the flying qualities requirements, consider the McDonnell F-4 Phantom, the following data for which were obtained from [Heffley and Jewell \(1972\)](#). Since the available data are limited to the equations of motion and some supporting material, this assessment is limited to basic stability and control characteristics only.

For the case selected, the general flight condition parameters given are:

Altitude	h	35000 ft
Mach number	M_0	1.2
Weight	mg	38925 Lb
Trim airspeed	V_0	1167 ft/s
Trim body incidence	α_e	1.6 deg
Flight path angle	γ_e	0
Normal load factor derivative	n_α	22.4 g/rad
Control anticipation parameter	CAP	1.31 1/s ²
“Elevator” angle per <i>g</i>	η/g	3.64 deg/g

The Phantom is a high-performance combat aircraft; thus, for the purposes of assessment, it is described as a *class IV* aircraft. The flight task to which the data relate is not stated. Therefore, it may be assumed that the aircraft is either in steady cruising flight, flight phase category B, or is manoeuvring about the given condition, in which case flight phase category A applies. For this illustration, *flight phase category A* is assumed since it determines the most demanding flying qualities requirements. It is interesting to see that the parameter “*elevator*” angle per g is given, which is of course a measure of the controls-fixed manoeuvre margin.

Consider the longitudinal stability and control characteristics first. Sufficient information about the stability characteristics of the basic airframe is given by the pitch attitude response to “elevator” transfer function, which for the chosen flight condition is

$$\frac{\theta(s)}{\eta(s)} \equiv \frac{N_\eta^\theta(s)}{\Delta(s)} = \frac{-20.6(s + 0.0131)(s + 0.618)}{(s^2 + 0.0171s + 0.00203)(s^2 + 1.759s + 29.49)} \quad (10.33)$$

The essential longitudinal stability and control parameters may be obtained on inspection of transfer function (10.33) as follows:

Phugoid damping ratio	$\zeta_p = 0.19$
Phugoid undamped natural frequency	$\omega_p = 0.045 \text{ rad/s}$
Short-period damping ratio	$\zeta_s = 0.162$
Short-period undamped natural frequency	$\omega_s = 5.43 \text{ rad/s}$
Numerator time constant	$T_{\theta_1} = 1/0.0131 = 76.34 \text{ s}$
Numerator time constant (incidence lag)	$T_{\theta_2} = 1/0.618 = 1.62 \text{ s}$

Since the Phantom is an American aeroplane, it would seem appropriate to assess its basic stability characteristics against the requirements of MIL-F-8785C. However, in practice it would be assessed against the requirements document specified by the procuring agency.

With reference to [Table 10.5](#), which is directly applicable, the phugoid damping ratio is greater than 0.04 and, since $\omega_p/\omega_s < 0.1$, the phugoid achieves Level 1 flying qualities and is unlikely to give rise to handling difficulties at this flight condition.

With reference to the short-period mode frequency chart for flight phase category A, which is the same as in [Fig. 10.7](#), at $n_\alpha = 22.4 \text{ g/rad}$ and for Level 1 flying qualities, it is required that

$$2.6 \text{ rad/s} \leq \omega_s \leq 9.0 \text{ rad/s}$$

or, equivalently,

$$0.28 \text{ } 1/\text{s}^2 \leq \omega_s^2/n_\alpha (\text{CAP}) \leq 3.6 \text{ } 1/\text{s}^2$$

Clearly, the short-period undamped natural frequency achieves Level 1 flying qualities. Unfortunately, the short-period mode damping ratio is less than desirable. A table similar to [Table 10.4](#) indicates that the damping achieves Level 3 flying qualities only; to achieve Level 1 it would need to be in the range $0.35 \leq \zeta_s \leq 1.3$.

Considering now the lateral-directional stability and control characteristics, sufficient information about the stability characteristics of the basic airframe is given, for example, by the roll rate response to aileron transfer function, which for the chosen flight condition is

$$\frac{p(s)}{\xi(s)} \equiv \frac{N_\xi^p(s)}{\Delta(s)} = \frac{-10.9s(s^2 + 0.572s + 13.177)}{(s + 0.00187)(s + 1.4)(s^2 + 0.519s + 12.745)} \quad (10.34)$$

The essential lateral-directional stability and control parameters may be obtained on inspection of transfer function (10.34) as follows:

Roll mode time constant	$T_r = 1/1.4 = 0.714 \text{ s}$
Spiral mode time constant	$T_s = 1/0.00187 = 535 \text{ s}$
Dutch roll damping ratio	$\zeta_d = 0.0727$
Dutch roll undamped natural frequency	$\omega_d = 3.57 \text{ rad/s}$
Dutch roll damping ratio-frequency product	$\zeta_d \omega_d = 0.26 \text{ rad/s}$

At this flight condition the spiral mode is clearly stable with a very long time constant. In fact, it approaches neutral stability for all practical considerations. Since the mode is stable, it achieves Level 1 flying qualities and is most unlikely to give rise to handling difficulties.

A table similar to [Table 10.6](#) indicates that the roll subsidence mode damping achieves Level 1 flying qualities since $T_r < 1.0 \text{ s}$.

The dutch roll mode characteristics are less than desirable since its damping is very low. A table similar to [Table 10.9](#) indicates that the damping ratio achieves only Level 2 flying qualities. To achieve the desirable Level 1 flying qualities the mode characteristics would need to meet the following:

Dutch roll damping ratio	$\zeta_d \geq 0.19$
Dutch roll undamped natural frequency	$\omega_d \geq 1.0 \text{ rad/s}$
Dutch roll damping ratio-frequency product	$\zeta_d \omega_d \geq 0.35 \text{ rad/s}$

It is therefore concluded that both the longitudinal short-period mode and the lateral-directional dutch roll mode damping ratios are too low at the flight condition evaluated. In all other respects, the aeroplane achieves Level 1 flying qualities. The deficient aerodynamic damping of the Phantom, in common with many other aeroplanes, is augmented artificially by a feedback control system.

It must be emphasised that this illustration is limited to an assessment of the basic stability properties of the airframe only. This determines the need, or otherwise, for stability augmentation. Once the stability has been satisfactorily augmented by an appropriate control system then, further and more far reaching assessments of the control and handling characteristics of the augmented aeroplane would be made. The scope of this kind of evaluation may be appreciated by reference to the specification documents discussed earlier. In any event, analytical assessment requires the addition of a simulation model developed from the linearised equations of motion in order to properly investigate some of the dynamic control and response properties.

References

- Bihrl, W. (1966). *A Handling Qualities Theory for Precise Flight Path Control*. Technical Report AFFDL-R-198, Air Force Flight Dynamics Laboratory, Ohio: Wright-Patterson Air Force Base.
- Chalk, C. R. (1958). *Additional Flight Evaluations of Various Longitudinal Handling Qualities in a Variable-Stability Jet Fighter*. Wright Air Development Center Technical Report, WADC TR 57-719, Ohio: Wright-Patterson Air Force Base.
- Civil Aviation Authority. British civil airworthiness requirements-section K-Light aeroplanes. Civil Aviation Authority, London.
- College of Aeronautics (1965). *Morane Saulnier M.S.760: Notes for technical observers*. Cranfield, UK: College of Aeronautics, Cranfield University.
- Cooper, G. E., & Harper, R. P. (1969). The use of pilot rating in the evaluation of aircraft handling qualities. AGARD Report 567.
- Department of Defense (1980). *Military specification: Flying qualities of piloted airplanes*. MIL-F-8785C. Washington, DC: Department of Defense.
- Department of Defense. (1987). *Military standard: Flying qualities of piloted airplanes*. MIL-STD-1797A (USAF). Washington, DC: Department of Defense.
- Federal Aviation Administration. Federal aviation regulations—Part 25, subpart B—Flight. Federal Aviation Administration, US Department of Transportation.
- Gibson, J. C. (1995). *The definition, understanding and design of aircraft handling qualities*. Report LR-756. The Netherlands: Delft University of Technology, Faculty of Aerospace Engineering, Delft.
- Heffley, R. K., & Jewell, W. F. (1972). *Aircraft handling qualities data*. Washington, DC: National Aeronautics and Space Administration, NASA Contractor Report CR-2144.
- Hoh, R. H., Mitchell, D. G., Ashkenas, I. L., Klein, R. H., Heffley, R. K., & Hodgkinson, J. (1982). *Proposed MIL standard and handbook: Flying qualities of air vehicles, Vol. 2: Proposed MIL handbook*. Technical Report AFWAL-TR-82-3081. Wright-Patterson AFB, OH: Air Force Wright Aeronautical Laboratory.
- Joint Aviation Authority. (1994). *Joint aviation requirements—JAR 25-large aeroplanes, section 1-requirements, subpart B-Flight*. The Netherlands: Joint Aviation Authority, Hoofddorp.
- Ministry of Defence. (1983). Design and airworthiness requirements for service aircraft. Defence Standard 00-970/Issue 1, Volume 1, Book 2, Part 6: *Aerodynamics, flying qualities and performance*. London: Ministry of Defence.
- Teper, G. L. (1969). *Aircraft stability and control data*. STI Technical Report 176-1. Hawthorne, CA.: Systems Technology, Inc.

PROBLEMS

- 10.1** What are flying and handling qualities requirements? In the context of flying and handling qualities requirements, explain the following:
- Flight envelope
 - Aircraft class
 - Flight phase category
 - Level of flying quality
 - Cooper-Harper rating scale

- (a) The pitch rate response to elevator control transfer function for the Northrop F-5 Tiger aircraft in level flight cruise at an altitude of 30,000 ft is given by

$$\frac{q(s)}{\eta(s)} = \frac{-14.6s(s + 0.0159)(s + 0.474)}{(s^2 + 1.027s + 7.95)(s^2 + 0.0169s + 0.0031)} \text{ 1/s}$$

Evaluate the flying qualities of the aircraft at this flight condition. Note that $n_\alpha = 12.9$ 1/rad for this flight condition.

- (b) With the aid of MATLAB or Program CC, draw a root locus plot to show the effect of pitch rate feedback to elevator and show both modes clearly. Draw the flying qualities boundaries on the plot and hence determine a suitable value for the feedback gain k_q to ensure that the aircraft meets the requirements. Compare the characteristics of the stability modes at this gain with those of the unaugmented aircraft.

(CU 1985)

- 10.2** Describe the service and operational flight envelopes for an aircraft and explain how they are related. In the context of flying and handling qualities, what is meant by flight phase category? Why are the stability requirements associated with each flight phase category different?

(CU 1986)

- 10.3** The Lockheed Jetstar is a small four-engined utility transport aircraft. When cruising at Mach 0.5 at an altitude of 40,000 ft, the roll and yaw transfer functions are given by

$$N_\xi^p(s) = 0.929(s - 0.0133)(s^2 + 0.133s + 0.79) \text{ 1/s}$$

$$N_\zeta^r(s) = -0.511(s + 0.36)(s^2 + 0.114s + 0.335) \text{ 1/s}$$

$$\Delta(s) = (s - 0.0008)(s + 0.5)(s^2 + 0.009s + 1.59)$$

- (a) Evaluate the stability mode characteristics at this flight condition against the flying qualities requirements.
 (b) What negative feedback is required to improve the stability characteristics of this aircraft? Illustrate your answer with a italic of the appropriate root locus plot(s), and state the most significant effects of the feedback with reference to the requirements.

(CU 1990)

- 10.4** Explain why the characteristics of the short term stability modes are critical to good flying qualities.

(CU 2001)

Command and Stability Augmentation

11

11.1 Introduction

In the previous chapter it was shown how the stability and control characteristics of an aeroplane may be assessed in the context of flying and handling qualities requirements. In the event that the aeroplane fails to meet the requirements in some way, it is necessary to consider remedial action. For all except perhaps the most trivial of problems, it is not usually practical to modify the aerodynamic design of the aeroplane once it has been finalised. Quite often the deficiencies occur simply as a result of the requirement for the aeroplane to operate over an extended flight envelope and not necessarily as a result of an aerodynamic design oversight. Alternatively, this might be explained as the effects of aerodynamic non-linearity. The preferred solution is, therefore, to artificially modify, or *augment*, the apparent stability characteristics of the airframe. This is most conveniently achieved by the introduction of *negative feedback* in which the output signals from motion sensors are processed in some way and used to drive the appropriate control surfaces via actuators.

The resultant *closed-loop control system* is similar in many respects to the classical servo-mechanism familiar to the control engineer. A significant advantage of this approach is that the analysis of the augmented, or closed-loop, aircraft makes full use of the control engineer's well-established tools. The *systems* approach to flight dynamics analysis was introduced in earlier chapters, where, for example, control engineering tools were utilised for solving the equations of motion.

A functional block diagram of a typical *flight control system* (FCS) is shown in Fig. 11.1. It is assumed that the primary flying controls are mechanical such that pilot commands drive the control surfaces via control actuators, which augment the available power to levels sufficient to overcome the aerodynamic loads on the surfaces. The *electronic flight control system* (EFCS) comprises two feedback loops, both of which derive their control signals from motion sensors appropriate to the requirements of the *control laws*. The outputs from the inner- and outer-loop controllers are summed electronically, and the resultant signal controls the aircraft via a small servo-actuator. Typically, the servo-actuator is an electro-hydraulic device which converts low-power electrical signals to mechanical signals at a power level compatible with those originating at the pilot, to which it is summed mechanically. Although only a single control axis is indicated in Fig. 11.1, it is important to appreciate that the FCS, in general, includes closed-loop controllers operating simultaneously on the roll, pitch, and yaw control axes of the aircraft and may even extend to include closed-loop engine control as well. Thus multivariable feedback involving many separate control loops is implied, which is typical of many modern FCS.

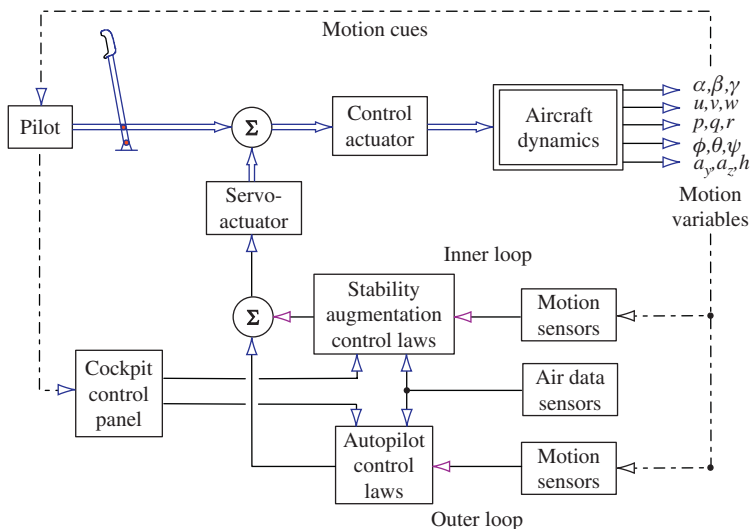


FIGURE 11.1 Typical flight control system.

The *inner loop* provides stability augmentation and is usually regarded as essential for continuous proper operation of the aircraft. The inner-loop control system alone makes up the *stability augmentation system* (SAS); it is usually the first part of the FCS to be designed and, together with the airframe, comprises the *augmented aircraft*.

The *outer loop* provides the *autopilot*, which, as its name suggests, enables the pilot to fly various manoeuvres under automatic control. Although necessary for operational reasons, an autopilot is not essential to a safe well-behaved aircraft. The *autopilot control modes* are designed to function with the augmented aircraft and may be selectively engaged as required to automate the piloting task. Their use is intended to release the pilot from the monotony of flying steady conditions manually and to fly precision manoeuvres in adverse conditions which may be at, or beyond, the limits of human capability. Autopilot control modes vary from the very simple—for example, *height hold*—to the very complex—for example, *automatic landing*.

Since, typically, for most aircraft the *control law gains* required to effect good stability, control, and handling vary with operating condition, it is necessary to make provision for their continuous adjustment. These variations often arise as a result of variations in the aerodynamic properties of the airframe over the flight envelope. For example, at low speed the aerodynamic effectiveness of the control surfaces is generally less than at high speed. This means that higher *control gains* are required at low speeds and vice versa. It is therefore common practice to vary, or *schedule*, gains as a function of flight condition. Commonly used flight condition variables are dynamic pressure, Mach number, altitude, and so on—information which is grouped under the description of *air data*. Generally, air data information is available to all control laws in a FCS, as indicated in Fig. 11.1.

A control panel is provided in the cockpit to enable the pilot to control and monitor the operation of the FCS. SAS controls are usually minimal and enable the pilot to monitor the system for

correct, and thus safe, operation. In some cases the pilot may also be provided with means for selectively isolating parts of the SAS. On the other hand, the autopilot control panel is rather more substantial. Controls are provided to enable the pilot to set up, engage, and disengage the various autopilot mode functions. The control panel also enables him to monitor progress during the automated manoeuvre selected.

In piloted phases of flight the autopilot is normally disengaged and, as indicated in Fig. 11.1, the pilot derives his perception of flying and handling qualities from the motion cues provided by the augmented aircraft. Thus the inner-loop control system provides the means by which all aspects of stability, control, and handling may be tailored to improve the characteristics of the basic aircraft.

11.1.1 The control law

The control law is a mathematical expression which describes the function implemented by an augmentation or autopilot controller. For example, a very simple and very commonly used control law describing an inner-loop control system for augmenting yaw damping is

$$\zeta(s) = K_\zeta \delta_\zeta(s) - K_r \left(\frac{s}{1 + sT} \right) r(s) \quad (11.1)$$

Equation 11.1 simply states that the control signal applied to the rudder $\zeta(s)$ comprises the sum of the pilot command $\delta_\zeta(s)$ and the yaw rate feedback $r(s)$. The gain K_ζ is the mechanical gearing between rudder pedals and rudder, and the gain K_r is the all-important feedback gain chosen by design to optimise damping in yaw. The second term in equation (11.1) is negative since negative feedback is required to increase stability in yaw. The second term also, typically, includes a *wash-out*, or *high-pass*, filter with a time constant of around 1 or 2 seconds. The filter is included to block yaw rate feedback in steady turning flight to prevent the feedback loop opposing the pilot command once the rudder pedals are returned to centre after manoeuvre initiation. However, the filter is effectively *transparent* during transient motion, thereby enabling the full effect of the feedback loop to quickly damp out the yaw oscillation.

11.1.2 Safety

In any aeroplane fitted with a flight control system, safety is the most critical issue. Since the FCS has direct “access” to the control surfaces, considerable care must be exercised in the design of the system to ensure that under no circumstances can a maximum instantaneous uncontrolled command be applied to any control surface. For example, a sensor failure might cause its output to *saturate* at its maximum possible value. This signal, in turn, is *conditioned* by the control law to apply what could well be a demand of sufficient magnitude to cause a maximum control surface displacement. The resulting *failure transient* might be some kind of hazardous divergent response. Clearly, steps must be taken in the design of the flight control system architecture to incorporate mechanisms to protect the aircraft from partial or total system malfunction.

The design of *safety-critical* flight control system architectures, as opposed to the simpler problem of control law design, is a substantial subject in its own right. However, at an introductory level, it is sufficient to appreciate that the requirements for safety can sometimes override the

requirements for control, especially when relatively large control system gains are necessary. For simple stability augmentation systems of the kind exemplified by the control law, [equation \(11.1\)](#), the problem may be overcome by limiting the maximum values of the control signals, giving rise to what is referred to as a *limited-authority* control system. In more complex FCS where authority limiting is not acceptable for control reasons, it may be necessary to employ control system *redundancy*. Redundant FCS comprise two or more systems which are functionally similar and which normally operate in parallel. In the event of a system malfunction, the faulty equipment is isolated, leaving the remaining *healthy* system components to continue the augmentation task. In such systems, automatic fault containment can reduce the failure transient to an imperceptible level. It is then necessary to provide the pilot with information enabling him to continuously *monitor* the health of the FCS on an appropriate cockpit display.

11.1.3 Stability augmentation system architecture

The architecture of an inner-loop stability augmentation system is shown in Fig. 11.2. This classical system description assumes an aeroplane with mechanical flying controls to which the EFCS connects via the servo-actuator. The system is typical of those applied to many aeroplanes of the 1950s and 1960s. For the purpose of discussion, only one control axis is shown in the figure, but it applies equally well to the remaining axes.

As previously stated, the essential element of the SAS is the control law; the remaining components are the necessary by-products of its implementation. Noise filtering is often required to remove unwanted information from sensor outputs. At best, noise can cause unnecessary actuator activity and, at worst, may even give rise to unwanted aircraft motion. Sometimes, when the sensor is located in a region of significant structural flexibility, the "noise" may be due to normal structure distortion. The control demand may then exacerbate structure bending to result in structural divergence. Thus an unwanted unstable structural feedback loop can be created inadvertently. The cure

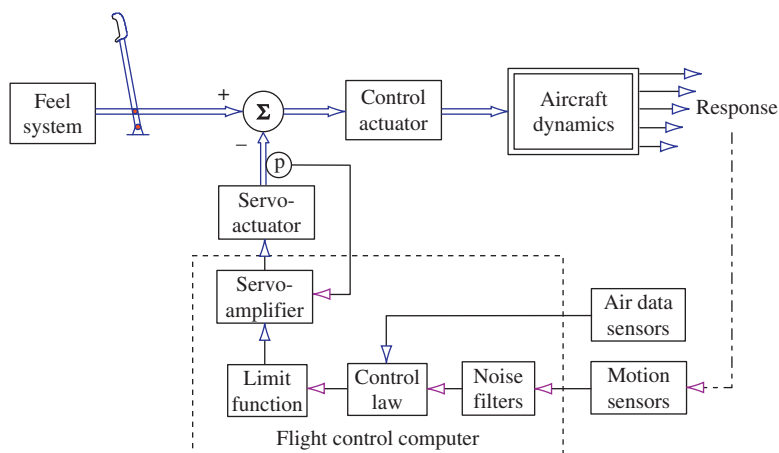


FIGURE 11.2 Typical stability augmentation system.

usually involves narrow-band filtering to remove information from the sensor output signal at sensitive structural bending mode frequencies.

The fundamental role of the SAS is to minimise response transients following an upset from equilibrium. Therefore, when the system is working correctly in non-maneuvring flight, the response variables have values at or near zero since the action of the negative feedback loop is to drive the *error* to zero. Thus a SAS does not normally require large authority control, and the limit function typically limits the amplitude of the control demand to, say, $\pm 10\%$ of the total surface deflection. The limiter may also incorporate a rate limit function to further contain transient response by imposing a maximum actuator slew rate demand. It is important to realise that whenever the control demand exceeds the limit, the system saturates, becoming temporarily open loop, and the dynamics of the aircraft revert to those of the unaugmented airframe. This is not usually considered a problem because saturation is most likely to occur during manoeuvring flight when the pilot has very “tight” manual control of the aeroplane and effectively replaces the SAS control function.

The servo-amplifier, together with the servo-actuator, provides the interface between the flight control system and the mechanical flying controls. These two elements make up a classical position servo-mechanism as indicated by the electrical feedback from a position sensor on the output of the servo-actuator. Mechanical amplitude limiting may well be applied to the servo-actuator as well as, or instead of the electronic limits programmed into the flight control computer.

Since the main power control actuator, also a classical mechanical servo-mechanism, breaks the direct mechanical link between the pilot’s controller and the control surface, the control feel may bear little resemblance to the aerodynamic surface loads. The feedback loop around the control actuator is normally mechanical because it may well need to function with the SAS inoperative. It is therefore necessary to augment the controller feel characteristics as well. The feel system may be a simple non-linear spring, but is more commonly an electro-hydraulic device, often referred to as a *Q-feel system* since its characteristics are scheduled with dynamic pressure *Q*. Careful design of the feel system enables the apparent controls-free manoeuvre margin of the aircraft to be adjusted independently of the other interrelated stability parameters.

When the mechanical flying controls are dispensed with altogether and replaced by an electrical or electronic link, the resultant stability augmentation system is described as a *fly-by-wire* (FBW) system. When the FCS shown in Fig. 11.2 is implemented as a FBW system, its functional structure is changed to that shown in Fig. 11.3. The SAS inner control loop remains unchanged; the only changes relate to the primary control path and the actuation systems.

Since the only mechanical elements in the FCS are the links between the control actuator and the surfaces, it is usual for the servo-actuator and the control actuator to be combined into one unit. Its input is then the electrical control demand from the flight control computer and its output is the control surface deflection. An advantage of an integrated actuation system is the facility for mechanical simplification, since the feedback loops may be closed electrically rather than by a combination of electrical and mechanical feedbacks. Mechanical feedback is an unnecessary complication because, in the event of a flight control computer failure, the aeroplane becomes uncontrollable. Clearly, this puts a rather more demanding emphasis on the safety of the flight control system.

Primary control originates at the pilot’s control inceptors which, since they are not constrained by mechanical control linkages, may now take alternative forms—for example, a *side-stick*

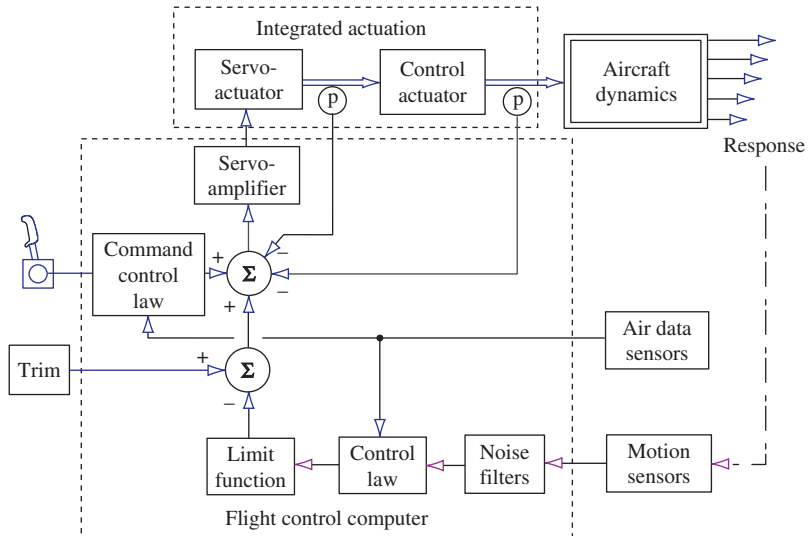


FIGURE 11.3 Typical fly-by-wire command and stability augmentation system.

controller. The control command signal is conditioned by a command control law which determines the control and response characteristics of the augmented aircraft. Since the command control law is effectively *shaping* the command signal in order to achieve acceptable response characteristics, its design is a means for augmenting handling qualities independently of stability augmentation. For this reason, a FCS with the addition of command path augmentation is known as a *command and stability augmentation system* (CSAS).

Provision is shown in Fig. 11.3 for an electrical trim function since not all aircraft with advanced technology FCS employ mechanical trimmers. The role of the trim function is to set the datum control signal value, and thus the control surface angle, to that required to maintain the chosen equilibrium flight condition. The precise trim function utilised is application-dependent, and in some cases an entirely automatic trim system may be implemented. In this latter case no pilot trimming facility is required.

The pilot must have full-authority control over the aircraft at all times, so it is implied that the actuation system must also have full-authority control. Obviously, the implications for safety following a failure in any component in the primary control path are critical. As for the simple SAS, the feedback control signal may be authority-limited prior to summing with the primary control commands; this protects the system against failures within the stability augmentation function. However, this solution cannot be used in the primary control path. Consequently, FBW systems must have reliability of a very high order, which usually means significant levels of redundancy in the control system architecture together with sophisticated mechanisms for identifying and containing the worst effects of system malfunction.

In this brief description of a FBW system, it is assumed that all control signals are electrical and transmitted by normal electrical cables. However, since most modern flight control computers

are digital, the transmission of control signals also involves digital technology. Digital signals can be transmitted optically with some advantage, especially in the demanding environment within aircraft. Today it is common for optical signal transmission to be used in FCSs if for no other reason than to maintain electrical isolation between redundant components within the system. There is no reason why optical signalling should not be used for primary flight control, and there is a number of optically signalled systems currently flying. Such a control system is referred to as a *fly-by-light* (FBL) system, and the control function is essentially the same as that of the FBW system or the simple stability augmentation system it replaces. In fact, it is most important to recognise that for a given aeroplane the stability augmentation function required of the flight control system is the same irrespective of the architecture adopted for its implementation. In the context of stability augmentation, there is nothing special or different in a FBW or in a FBL system solution.

11.1.4 Scope

In the preceding sections an attempt has been made to introduce and review some of the important issues concerning flight control system design in general. In particular, the emphasis has been on the role of the SAS or CSAS and the possible limitation of the control function imposed by the broader concerns of system structure. The temptation now is to embark on a discussion of FCS design, but such a vast subject is, unfortunately, beyond the scope of the present book.

Rather, the remainder of this chapter is concerned with the very fundamental, and sometimes subtle, way in which feedback may be used to augment the dynamics of the basic aircraft. It is very important that the flight dynamicist understands the way in which his chosen control system design augments the stability and control properties of the airframe. It is not good enough to treat the aircraft like an arbitrary *plant* and to design a *controller* to meet a predefined set of performance requirements, an approach much favoured by control system designers. It is vital that the FCS designer retains a complete understanding of the implications of his design decisions throughout the design process. In the interests of *functional visibility*, and hence of safety, it is important that FCS are made as simple as possible. This is often achievable only when the designer has a complete and intimate understanding of the design process.

11.2 Augmentation system design

The most critical aspect of flight control system design is concerned with the design of the inner-loop control law, the design objective being to endow the aircraft with good stability, control, and handling characteristics throughout its flight envelope. Today, a FBW system gives the designer the greatest freedom of choice in allocating the control law functions for “optimum” performance. The main CSAS control functions are indicated in the rather oversimplified representation shown in Fig. 11.4. The problem confronting the FCS designer is to design suitable functions for the command, feed-forward, and feedback paths of the CSAS, and it is obviously necessary to appreciate the role of each path in the overall context of aircraft stability augmentation.

The *feedback path* comprises the classical inner-loop stability augmentation system, the primary role of which is to augment static and dynamic stability. It generally improves flying and handling

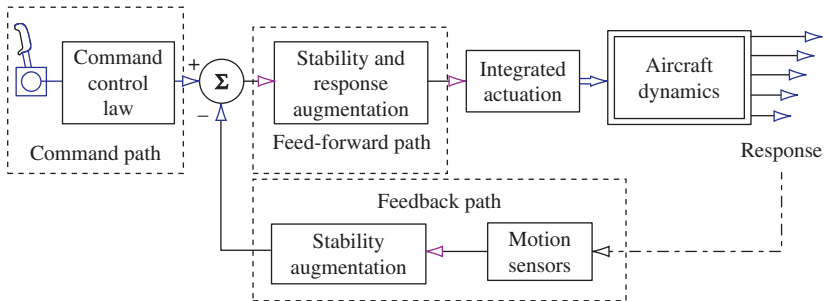


FIGURE 11.4 Inner-loop control functions.

qualities, but may not necessarily lead to ideal handling qualities since it has insufficient direct control over *response shaping*.

The *feed-forward path* is also within the closed loop, and its function augments stability in exactly the same way as the feedback path. However, it has a direct influence on command signals as well, and by careful design its function may also be used to exercise some degree of response shaping. Its use in this role is limited because the stability augmentation function must take priority.

The *command path* control function, sometimes described as *command augmentation*, provides the principal means for response shaping; it has no influence on stability since it is outside the closed loop. This assumes, of course, that the augmented aircraft may be represented as a *linear* system. The command path indicated in Fig. 11.4 assumes entirely electronic signalling as appropriate to a FBW system. However, there is no reason why the command and feed-forward paths should not comprise a combination of parallel electrical and mechanical paths - an architecture commonly employed in aircraft of the 1960s and 1970s. In such systems it is only really practical to incorporate all, except very simple, signal shaping into the electrical signal paths.

Further analysis of the simple CSAS structure may be made if it is represented by its transfer function equivalent, as shown in Fig. 11.5, with reference to which the *control error* signal $\varepsilon(s)$ is given by

$$\varepsilon(s) = C(s)\delta(s) - H(s)r(s) \quad (11.2)$$

where $\delta(s)$ and $r(s)$ are the command and response signals, respectively, and $C(s)$ and $H(s)$ are, the command path and feedback path transfer functions respectively. The output response $r(s)$ is given by

$$r(s) = F(s)G(s)\varepsilon(s) \quad (11.3)$$

where $F(s)$ is the feed-forward path transfer function and $G(s)$ is the all-important transfer function representing the basic airframe. Combining equations (11.2) and (11.3) to eliminate the error signal, the closed-loop transfer function is obtained:

$$\frac{r(s)}{\delta(s)} = C(s) \left(\frac{F(s)G(s)}{1 + F(s)G(s)H(s)} \right) \quad (11.4)$$

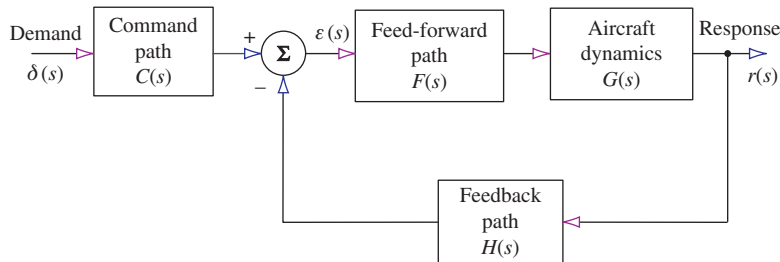


FIGURE 11.5 Inner-loop transfer function.

Thus the transfer function given by equation (11.4) is that of the augmented aircraft and replaces that of the unaugmented aircraft $G(s)$. Clearly, by appropriate choice of $C(s)$, $F(s)$, and $H(s)$, the flight control system designer has considerable scope for tailoring the handling characteristics of the augmented aircraft. The characteristic equation of the augmented aircraft is given by

$$\Delta(s)_{\text{aug}} = 1 + F(s)G(s)H(s) = 0 \quad (11.5)$$

Note that the command path transfer function $C(s)$ does not appear in the characteristic equation; therefore, as noted previously, it cannot influence stability in any way.

Let the aircraft transfer function be denoted by its numerator and denominator in the usual way:

$$G(s) = \frac{N(s)}{\Delta(s)} \quad (11.6)$$

Let the feed-forward transfer function be a simple proportional gain,

$$F(s) = K \quad (11.7)$$

and let the feedback transfer function be represented by a typical lead-lag function:

$$H(s) = \left(\frac{1 + sT_1}{1 + sT_2} \right) \quad (11.8)$$

Then the transfer function of the augmented aircraft, equation (11.4), may be written as

$$\frac{r(s)}{\delta(s)} = C(s) \left(\frac{KN(s)(1 + sT_2)}{\Delta(s)(1 + sT_2) + KN(s)(1 + sT_1)} \right) \quad (11.9)$$

Now let the roles of $F(s)$ and $H(s)$ be reversed; whence

$$F(s) = \left(\frac{1 + sT_1}{1 + sT_2} \right) H(s) = K \quad (11.10)$$

In this case, the transfer function of the augmented aircraft, equation (11.4), may be written as

$$\frac{r(s)}{\delta(s)} = C(s) \left(\frac{KN(s)(1 + sT_1)}{\Delta(s)(1 + sT_2) + KN(s)(1 + sT_1)} \right) \quad (11.11)$$

Comparing the closed-loop transfer functions, [equations \(11.9\) and \(11.11\)](#), it is clear that the stability of the augmented aircraft is unchanged since the denominators are the same. However, the numerators are different, implying a difference in the response to control which can be exploited to some advantage in some FCS applications.

Now, if the gains in the control system transfer functions $F(s)$ and $H(s)$ are deliberately made large such that at all frequencies over the bandwidth of the aeroplane

$$F(s)G(s)H(s) \gg 1 \quad (11.12)$$

then the closed-loop transfer function, [equation \(11.4\)](#), is given approximately by

$$\frac{r(s)}{\delta(s)} \cong \frac{C(s)}{H(s)} \quad (11.13)$$

[Equation \(11.13\)](#) demonstrates the important result that in highly augmented aircraft the stability and control characteristics may be substantially independent of the dynamics of the basic airframe. In other words, the stability, control, and handling characteristics are largely determined by the design of the CSAS—in particular, the design of the transfer functions $C(s)$ and $H(s)$. In practice, this situation is likely to be encountered only when the basic airframe is significantly unstable. This illustration implies that augmentation would be provided by a FBW system but ignores the often intrusive effects of the dynamics of the FCS components.

11.3 Closed-loop system analysis

For the purpose of illustrating how motion feedback augments basic airframe stability, consider the very simple example in which pitch attitude is fed back to elevator. The most basic essential features of the control system are shown in [Fig. 11.6](#). In this example the controller comprises a simple gain constant K_θ in the feedback path.

The control law is given by

$$\eta(t) = \delta_\eta(t) - K_\theta\theta(t) \quad (11.14)$$

and the appropriate aircraft transfer function is

$$\frac{\theta(s)}{\eta(s)} = G(s) = \frac{N_\eta^\theta(s)}{\Delta(s)} \quad (11.15)$$

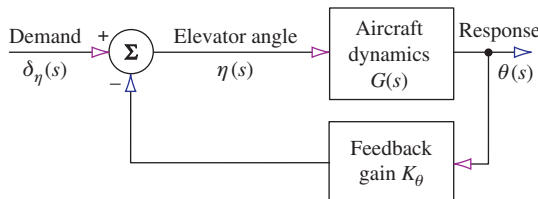


FIGURE 11.6 Simple pitch attitude feedback system.

Therefore, the closed-loop transfer function of the augmented aircraft is

$$\frac{\theta(s)}{\delta_\eta(s)} = \frac{N_\eta^\theta(s)}{\Delta(s) + K_\theta N_\eta^\theta(s)} \quad (11.16)$$

and the augmented characteristic equation is

$$\Delta(s)_{aug} = \Delta(s) + K_\theta N_\eta^\theta(s) = 0 \quad (11.17)$$

Thus, for a given aircraft transfer function, stability may be augmented by selecting a suitable value of feedback gain K_θ . Clearly, when K_θ is zero there is no feedback, the aircraft is said to be *open-loop*, and its stability characteristics are unmodified. As the value of K_θ is increased, the degree of augmentation is increased and the stability modes increasingly diverge from those of the open-loop aircraft. Note that the open- and closed-loop transfer function numerators, [equations \(11.15\) and \(11.16\)](#), are the same in accordance with the findings of [Section 11.2](#).

Alternatively, the closed-loop equations of motion may be obtained by incorporating the control law into the open-loop equations of motion. The open-loop equations of motion in state-space form, referred to a body axis system, are given by equation (4.67):

$$\begin{bmatrix} \dot{u} \\ \dot{w} \\ \dot{q} \\ \dot{\theta} \end{bmatrix} = \begin{bmatrix} x_u & x_w & x_q & x_\theta \\ z_u & z_w & z_q & z_\theta \\ m_u & m_w & m_q & m_\theta \\ 0 & 0 & 1 & 0 \end{bmatrix} \begin{bmatrix} u \\ w \\ q \\ \theta \end{bmatrix} + \begin{bmatrix} x_\eta & x_\tau \\ z_\eta & z_\tau \\ m_\eta & m_\tau \\ 0 & 0 \end{bmatrix} \begin{bmatrix} \eta \\ \tau \end{bmatrix} \quad (11.18)$$

Substitute the control law expression for η , [equation \(11.14\)](#), into [equation \(11.18\)](#) and rearrange to obtain the closed-loop state equation:

$$\begin{bmatrix} \dot{u} \\ \dot{w} \\ \dot{q} \\ \dot{\theta} \end{bmatrix} = \begin{bmatrix} x_u & x_w & x_q & x_\theta - K_\theta x_\eta \\ z_u & z_w & z_q & z_\theta - K_\theta z_\eta \\ m_u & m_w & m_q & m_\theta - K_\theta m_\eta \\ 0 & 0 & 1 & 0 \end{bmatrix} \begin{bmatrix} u \\ w \\ q \\ \theta \end{bmatrix} + \begin{bmatrix} x_\eta & x_\tau \\ z_\eta & z_\tau \\ m_\eta & m_\tau \\ 0 & 0 \end{bmatrix} \begin{bmatrix} \delta_\eta \\ \tau \end{bmatrix} \quad (11.19)$$

The effect of θ feedback is obviously to modify, or augment, the derivatives x_θ , z_θ , and m_θ . For a given value of the feedback gain K_θ , [equation \(11.19\)](#) may be solved in the usual way to obtain all of the closed-loop longitudinal response transfer functions:

$$\frac{u(s)}{\delta_\eta(s)} = \frac{N_\eta^u(s)}{\Delta(s)_{aug}} \quad \frac{w(s)}{\delta_\eta(s)} = \frac{N_\eta^w(s)}{\Delta(s)_{aug}} \quad \frac{q(s)}{\delta_\eta(s)} = \frac{N_\eta^q(s)}{\Delta(s)_{aug}} \quad \frac{\theta(s)}{\delta_\eta(s)} = \frac{N_\eta^\theta(s)}{\Delta(s)_{aug}}$$

and

$$\frac{u(s)}{\tau(s)} = \frac{N_\tau^u(s)}{\Delta(s)_{aug}} \quad \frac{w(s)}{\tau(s)} = \frac{N_\tau^w(s)}{\Delta(s)_{aug}} \quad \frac{q(s)}{\tau(s)} = \frac{N_\tau^q(s)}{\Delta(s)_{aug}} \quad \frac{\theta(s)}{\tau(s)} = \frac{N_\tau^\theta(s)}{\Delta(s)_{aug}}$$

where $\Delta(s)_{aug}$ is given by [equation \(11.17\)](#).

An obvious problem with this analytical approach is the need to solve [equation \(11.19\)](#) repetitively for a range of values of K_θ in order to determine the value which gives the desired stability characteristics. Fortunately, the *root locus plot* is an extremely effective graphical tool for determining feedback gain without the need for repetitive computation.

EXAMPLE 11.1

The pitch attitude response to elevator transfer function for the Lockheed F-104 Starfighter in a take-off configuration was obtained from [Teper \(1969\)](#) and may be written in factorised form as

$$\frac{\theta(s)}{\eta(s)} = \frac{-4.66(s + 0.133)(s + 0.269)}{(s^2 + 0.015s + 0.021)(s^2 + 0.911s + 4.884)} \quad (11.20)$$

Inspection of the denominator of [equation \(11.20\)](#) enables the stability mode characteristics to be written as

$$\begin{aligned} \text{Phugoid damping ratio } \zeta_p &= 0.0532 \\ \text{Phugoid undamped natural frequency } \omega_p &= 0.145 \text{ rad/s} \\ \text{Short-period damping ratio } \zeta_s &= 0.206 \\ \text{Short-period undamped natural frequency } \omega_s &= 2.21 \text{ rad/s} \end{aligned}$$

The values of these characteristics suggests that the short-period mode damping ratio is unacceptably low, the remainder being acceptable. Therefore, stability augmentation is required to increase the short period damping ratio.

In the first instance, assume a stability augmentation system in which pitch attitude is fed back to elevator through a gain constant K_θ in the feedback path. The SAS is then exactly the same as that shown in [Fig. 11.6](#) and, as before, the control law is given by [equation \(11.14\)](#). However, since the aircraft transfer function, [equation \(11.20\)](#), is negative, a negative feedback loop effectively results in overall positive feedback, which of course is destabilising. This situation arises frequently in aircraft control and, whenever a negative open-loop transfer function is encountered, it is necessary to assume a positive feedback loop or, equivalently, a negative value of the feedback gain constant, in order to obtain a stabilising control system. *Care must always be exercised in this context*. For this reason, in this particular example, when the negative sign of the open-loop transfer function is taken into account, the closed-loop transfer function of the augmented aircraft, [equation \(11.16\)](#), may be written as

$$\frac{\theta(s)}{\delta_\eta(s)} = \frac{N_\eta^\theta(s)}{\Delta(s) - K_\theta N_\eta^\theta(s)} \quad (11.21)$$

Substitute the open-loop numerator and denominator polynomials from [equation \(11.20\)](#) into [equation \(11.21\)](#) and rearrange to obtain the closed-loop transfer function:

$$\frac{\theta(s)}{\delta_\eta(s)} = \frac{-4.66(s + 0.133)(s + 0.269)}{s^4 + 0.926s^3 + (4.919 + 4.66K_\theta)s^2 + (0.095 + 1.873K_\theta)s + (0.103 + 0.167K_\theta)} \quad (11.22)$$

Thus the augmented characteristic equation is

$$\begin{aligned} \Delta(s)_{\text{aug}} &= s^4 + 0.927s^3 + (4.919 + 4.66K_\theta)s^2 + (0.095 + 1.873K_\theta)s \\ &\quad + (0.103 + 0.167K_\theta) = 0 \end{aligned} \quad (11.23)$$

The effect of the feedback gain K_θ on the longitudinal stability modes of the F-104 can only be established by repeatedly solving [equation \(11.23\)](#) for a range of suitable gain values.

However, a reasonable appreciation of the effect of K_θ on the stability modes can be obtained from the approximate solution of equation (11.23). Writing equation (11.23) as

$$As^4 + Bs^3 + Cs^2 + Ds + E = 0 \quad (11.24)$$

an approximate solution can be obtained from equation (6.13).

Thus the characteristics of the short-period mode are given approximately by

$$s^2 + \frac{B}{A}s + \frac{C}{A} = s^2 + 0.927s + (4.919 + 4.66K_\theta) = 0 \quad (11.25)$$

Whence

$$\begin{aligned}\omega_s &= \sqrt{(4.919 + 4.66K_\theta)} \\ 2\zeta_s\omega_s &= 0.927 \text{ rad/sec}\end{aligned} \quad (11.26)$$

In this way, it is easy to see how the mode characteristics change as the feedback gain is increased from zero to a large value—or, more generally, as $K_\theta \rightarrow \infty$. Thus

$$\begin{aligned}\omega_s &\rightarrow \infty \\ \zeta_s &\rightarrow 0\end{aligned} \quad (11.27)$$

Similarly, with reference to equation (6.13), the characteristics of the phugoid mode are given approximately by

$$\begin{aligned}s^2 + \frac{(CD - BE)}{C^2}s + \frac{E}{C} &= s^2 + \left(\frac{8.728K_\theta^2 + 9.499K_\theta + 0.369}{21.716K_\theta^2 + 45.845K_\theta + 24.197} \right)s \\ &+ \left(\frac{0.103 + 0.167K_\theta}{4.919 + 4.66K_\theta} \right) = 0\end{aligned} \quad (11.28)$$

Again, as $K_\theta \rightarrow \infty$,

$$\begin{aligned}\omega_p &\rightarrow \sqrt{\frac{0.167}{4.66}} = 0.184 \text{ rad/s} \\ 2\zeta_p\omega_p &\rightarrow \frac{8.728}{21.716} = 0.402 \text{ rad/s}\end{aligned} \quad (11.29)$$

and allowing for rounding errors,

$$\zeta_p \rightarrow 1.0 \quad (11.30)$$

The conclusion is then, that negative pitch attitude feedback to elevator tends to destabilise the short period mode and increase its frequency whereas its effect on the phugoid mode is more beneficial. Phugoid stability is increased whilst its frequency, which also tends to increase a little, is bounded by an acceptable maximum value. For all practical purposes, the frequency is assumed to be approximately constant. This result is perhaps not too surprising since pitch attitude is a dominant motion variable in phugoid dynamics and is less significant in short-period

pitching motion. It is quite clear that pitch attitude feedback to elevator is not the correct way to augment the longitudinal stability of the F-104.

What this approximate analysis does not show is the relative sensitivity of each mode to the feedback gain. This can only be evaluated by solving the characteristic equation repeatedly for a range of values of K_θ from zero to a suitably large value. A typical practical range of values might be $0 \leq K_\theta \leq 2$ rad/rad. This kind of analysis is most conveniently achieved with the aid of a *root locus plot*.

11.4 The root locus plot

The *root locus plot* is a relatively simple tool for obtaining, by graphical means, detailed information about the stability of a closed-loop system knowing only the open-loop transfer function. The plot shows the roots, or *poles*, of the closed-loop system characteristic equation for every value of a single-loop variable, typically the feedback gain. It is therefore not necessary to calculate the roots of the closed-loop characteristic equation for every value of the chosen loop variable. As its name implies, the root locus plot shows loci on the *s*-plane of all roots of the closed-loop transfer function denominator as a function of the single-loop gain variable.

The root locus plot was proposed by [Evans \(1954\)](#), and from its first appearance it rapidly gained importance as an essential control systems design tool. Consequently, it is described in most books concerned with linear control systems theory. [Friedland \(1987\)](#) is one example. Because of the relative mathematical complexity of the underlying theory, [Evans's \(1954\)](#) main contribution was the development of an approximate asymptotic procedure for manually “sketching” closed-loop root loci on the *s*-plane without recourse to extensive calculation. This was achieved with the aid of a set of “rules” which resulted in a plot of sufficient accuracy for most design purposes. It was therefore essential for control system designers to be familiar with the rules. Today, the root locus plot is universally produced by computational means. It is no longer necessary for the designer to know the rules, although he must know how to interpret the plot correctly and, of course, know its limitations.

In aeronautical applications it is vital to understand the correct interpretation of the root locus plot. This is especially so when it is being used to evaluate augmentation schemes for the precise control of the stability characteristics of an aircraft over the flight envelope. In the author’s opinion, this understanding can only be achieved from the position of strength which comes with a secure knowledge of the rules for plotting a root locus by hand. For this reason, the rules are set out in Appendix 11. It is not advocated that root locus plots should be drawn by hand; this is unnecessary when computational tools such as CODAS, MATLAB, and Program CC are readily available. The processes involved in the construction of a root locus plot are best illustrated by example as follows.

EXAMPLE 11.2

Consider the use of the root locus plot to evaluate the effect of pitch attitude feedback to elevator on the F-104 aircraft at the same flight condition as discussed in Example 11.1.

The applicable block diagram for the closed-loop system is shown in Fig. 11.6. The open-loop system transfer function, from equation (11.20), is

$$\frac{\theta(s)}{\eta(s)} = \frac{-4.66K_\theta(s + 0.133)(s + 0.269)}{(s^2 + 0.015s + 0.021)(s^2 + 0.911s + 4.884)} \text{ rad/rad} \quad (11.31)$$

with poles and zeros

$$p_1 = -0.0077 + 0.1448j$$

$$p_2 = -0.0077 - 0.1448j$$

$$p_3 = -0.4553 + 2.1626j \quad \text{whence number of poles } n_p$$

$$p_4 = -0.4553 - 2.1626j \quad \text{number of zeros } n_z = 2$$

$$z_1 = -0.133$$

$$z_2 = -0.269$$

The open-loop poles and zeros are mapped on to the s -plane as shown in Fig. 11.7. The loci of the closed-loop poles are then plotted as the feedback gain K_θ is allowed to increase from zero to a large value. In this example the loci were obtained computationally and are discussed in the context of the rules set out in Appendix 11.

Rule 1 locates the poles and zeros on the s -plane and determines that, since there are two more poles than zeros, four loci commence at the poles, two of which terminate at the zeros and two of which go off to infinity as $K_\theta \rightarrow \infty$.

Rule 2 determines that the real axis between the two zeros is part of a locus.

Rule 3 determines that the two loci which go off to infinity do so asymptotically to lines at 90 degrees and 270 degrees to the real axis.

Rule 4 determines that the asymptotes radiate from the *cg* of the plot located at -0.262 on the real axis.

Rule 5 determines the point on the real axis at which two loci break into the locus between the two zeros. Method 1, the approximate method, determines the break-in point at -0.2 . Method 2, the exact method, determines the break-in point at -0.186 . Either value is satisfactory for all practical purposes.

Rule 6 simply states that the two loci branching into the real axis do so at ± 90 degrees to the real axis.

Rule 7 determines the angle of departure of the loci from the poles and the angles of arrival at the zeros. This is rather more difficult to calculate by hand; to do so, the entire s -plane plot is required. The angles given by the computer program used to plot the loci are as follows:

Angle of departure from p_1 , 194 deg

Angle of departure from p_2 , -194 deg

Angle of departure from p_3 , 280 deg

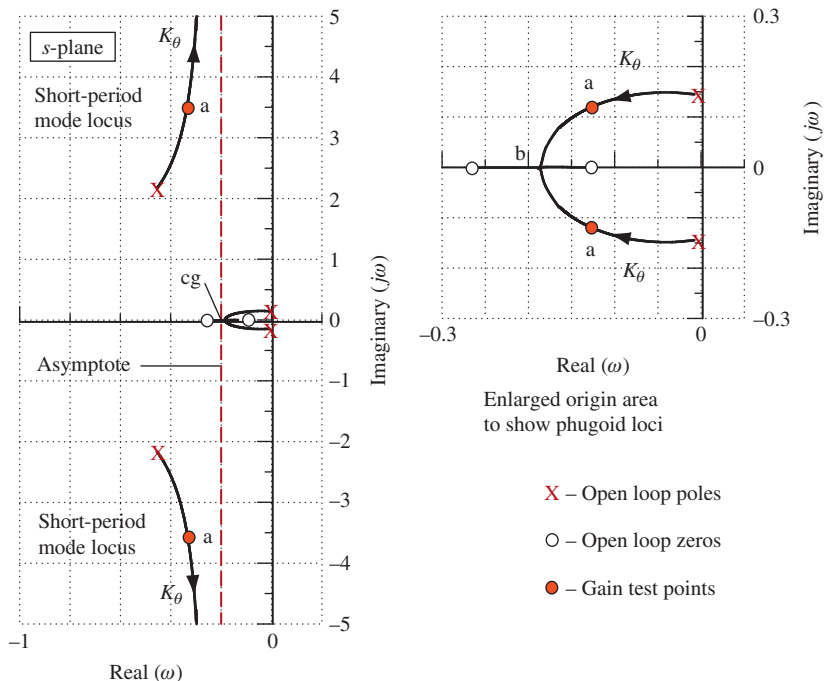


FIGURE 11.7 Example of root locus plot construction.

Angle of departure from p_4 , -280 deg

Angle of arrival at z_1 , 180 deg

Angle of arrival at z_2 , 0 deg

Note that these values compare well with those calculated by hand from protractor measurements made on the s -plane.

Rule 8 enables the total loop gain to be evaluated at any point on the loci.

Rule 8 is particularly tedious to do by hand; it requires a plot showing the entire s -plane and it is not always accurate, especially if the plot is drawn to a small scale. However, since this is the primary reason for plotting root loci in the first instance, all computer programs designed to produce root locus plots provide a means for obtaining the feedback gain values at test points on the loci. Not all such programs provide the information given by rules 4, 5, and 7. In this example the feedback gain at test point a is $K_\theta = -1.6$; at test point b , the break-in point, $K_\theta = -12.2$. Note that in this example the feedback gain has units deg/deg or, equivalently, rad/rad. When all test points of interest have been investigated, the root locus plot is complete.

One of the more powerful features of the root locus plot is that it gives explicit information about the relative sensitivity of the stability modes to the feedback in question. In this example, the open-loop aircraft stability characteristics are

$$\begin{aligned}\text{Phugoid damping ratio } \zeta_p &= 0.0532 \\ \text{Phugoid undamped natural frequency } \omega_p &= 0.145 \text{ rad/s} \\ \text{Short-period damping ratio } \zeta_s &= 0.206 \\ \text{Short-period undamped natural frequency } \omega_s &= 2.21 \text{ rad/s}\end{aligned}$$

and at test point a, where $K_\theta = -1.6$, the closed-loop stability characteristics are

$$\begin{aligned}\text{Phugoid damping ratio } \zeta_p &= 0.72 \\ \text{Phugoid undamped natural frequency } \omega_p &= 0.17 \text{ rad/s} \\ \text{Short-period damping ratio } \zeta_s &= 0.10 \\ \text{Short-period undamped natural frequency } \omega_s &= 3.49 \text{ rad/s}\end{aligned}$$

Thus the phugoid damping is increased by about 14 times and its frequency remains nearly constant. In fact, the oscillatory phugoid frequency can never exceed 0.186 rad/s. Moreover, the short-period mode damping is approximately halved whilst its frequency is increased by about 50%. Obviously, the phugoid damping is the parameter which is most sensitive to the feedback gain by a substantial margin. A modest feedback gain of, say, $K_\theta = -0.1$ rad/rad results in a very useful increase in phugoid damping whilst causing only very small changes in the other stability parameters. However, the fact remains that pitch attitude feedback to elevator destabilises the short-period mode by reducing the damping ratio from its open-loop value. This, then, is not the cure for the poor short-period mode stability exhibited by the open-loop F-104 aircraft at this flight condition. All of these conclusions support the findings of Example 11.1 but, it is clear that much greater analytical detail is directly available from inspection of the root locus plot.

Additional important points relating to the application of the root locus plot to aircraft stability augmentation include the following:

- Since the plot is symmetric about the real axis, it is not necessary to show the lower half of the s -plane unless the plot is constructed by hand. All of the relevant information provided by the plot is available in the upper half of the s -plane.
- At typical scales it is frequently necessary to obtain a plot of the origin area at enlarged scale in order to resolve the essential detail. This is usually very easy to achieve with most computational tools.
- As mentioned previously, it is essential to be aware of the sign of the open-loop aircraft transfer function. Most root locus plotting computer programs assume the standard positive transfer function with negative feedback. A negative transfer function results in an incorrect locus. The easy solution to this problem is to enter the transfer function with a positive sign and to change the sign of the feedback gains given by the program. However, it is important to remember the changes made when assessing the result of the investigation.

EXAMPLE 11.3

In Examples 11.1 and 11.2 it is shown that pitch attitude feedback to elevator is not the most appropriate means for augmenting the deficient short-period mode damping of the F-104. The correct solution is to augment pitch damping by implementing pitch rate feedback to elevator—velocity feedback in servo-mechanism terms. The control system functional block diagram is shown in Fig. 11.8.

For the same flight condition, a take-off configuration as in the previous examples, the pitch rate response to elevator transfer function for the Lockheed F-104 Starfighter was obtained from Teper (1969) and may be written in factorised form:

$$\frac{q(s)}{\eta(s)} = \frac{-4.66s(s + 0.133)(s + 0.269)}{(s^2 + 0.015s + 0.021)(s^2 + 0.911s + 4.884)} \text{ rad/s/rad} \quad (11.32)$$

As before, the stability modes of the open-loop aircraft are

$$\begin{aligned} \text{Phugoid damping ratio } \zeta_p &= 0.0532 \\ \text{Phugoid undamped natural frequency } \omega_p &= 0.145 \text{ rad/s} \\ \text{Short-period damping ratio } \zeta_s &= 0.206 \\ \text{Short-period undamped natural frequency } \omega_s &= 2.21 \text{ rad/s} \end{aligned}$$

With reference to MIL-F-8785C (1980), defining the F-104 as a class IV aircraft operating in flight phase category C and assuming that Level 1 flying qualities are desired, the following constraints on the stability modes may be determined:

$$\begin{aligned} \text{Phugoid damping ratio } \zeta_p &\geq 0.04 \\ \text{Short-period damping ratio } \zeta_s &\geq 0.5 \\ \text{Short-period undamped natural frequency } 0.8 \leq \omega_s &\leq 3.0 \text{ rad/s} \end{aligned}$$

The upper limit on the short-period mode damping ratio is ignored since it is greater than 1. Additionally, the closed-loop phugoid frequency should ideally conform to $\omega_p \leq 0.1\omega_s$, where here ω_s is the closed-loop short-period mode frequency. The unaugmented aircraft clearly meets these flying qualities requirements with the exception of the short-period mode damping ratio, which is much too low.

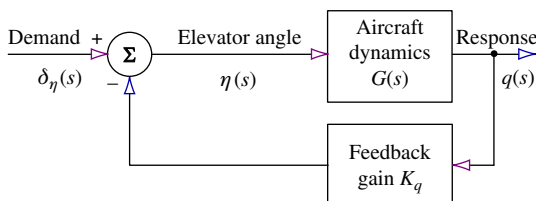


FIGURE 11.8 Simple pitch rate feedback system.

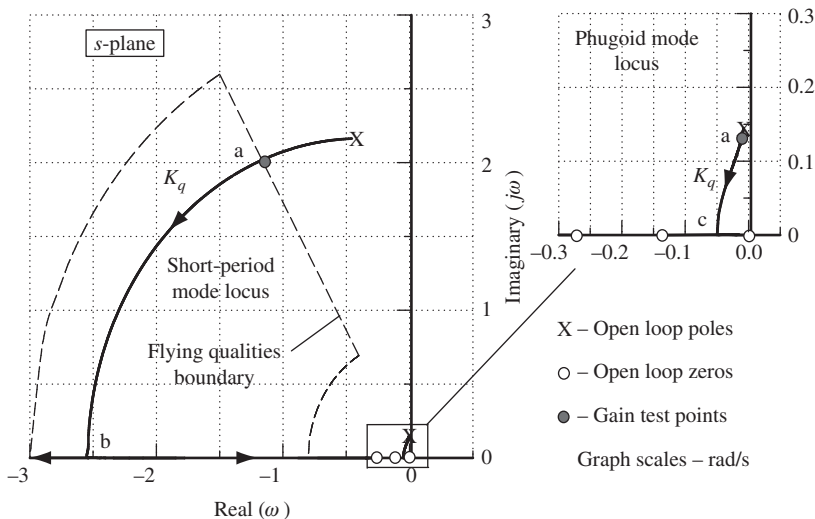


FIGURE 11.9 Root locus plot: pitch rate feedback to elevator.

The root locus plot constructed from the transfer function, equation (11.32), is shown in Fig. 11.9. Also shown on the same *s*-plane plot are the flying qualities short-period mode boundaries according to the limits determined from MIL-F-8785C and quoted previously.

The figure shows that pitch rate feedback to elevator is ideal since it causes the damping of both the phugoid and short-period modes to increase, although the short-period mode is most sensitive to feedback gain. Further, the frequency of the short-period mode remains more or less constant through the usable range of values of feedback gain K_q . For the same range of feedback gains, the frequency of the phugoid mode is reduced, thereby increasing the separation between the frequencies of the two modes. At test point a $K_q = -0.3$ rad/rad/s, which is the smallest feedback gain required to bring the closed-loop short-period mode into agreement with the flying qualities boundaries. Allowing for a reasonable margin of error and uncertainty, a practical choice of feedback gain might be $K_q = -0.5$ rad/rad/s. The stability augmentation control law is then

$$\eta = \delta_\eta + 0.5q \quad (11.33)$$

This augmentation system is the classical *pitch damper* used on many aeroplanes from the same period as the Lockheed F-104, and typical feedback gains are in the range $-0.1 \leq K_q \leq -1.0$ rad/rad/s. It is not known what value of feedback gain is used in the F-104 at this flight condition, but the published description of the longitudinal augmentation system structure is the same as that shown in Fig. 11.8.

Substituting the control law, equation (11.33), into the open-loop longitudinal equations of motion as described in Section 11.3 enables the closed-loop equations of motion to be derived.

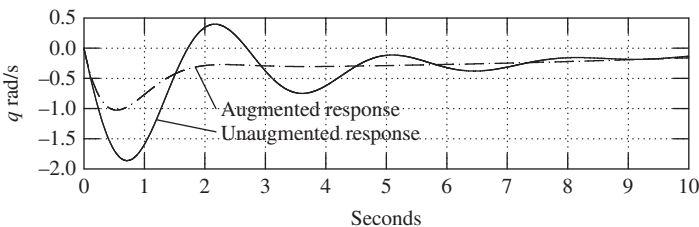


FIGURE 11.10 Pitch rate response to a unit elevator step input.

Solution of the equations in the usual way gives the response transfer functions for the augmented aircraft. Solution of the closed-loop characteristic equation determines that at $K_q = -0.5$ rad/rad/s the longitudinal modes have the following characteristics:

$$\begin{aligned} \text{Phugoid damping ratio } \zeta_p &= 0.079 \\ \text{Phugoid undamped natural frequency } \omega_p &= 0.133 \text{ rad/s} \\ \text{Short-period damping ratio } \zeta_s &= 0.68 \\ \text{Short-period undamped natural frequency } \omega_s &= 2.41 \text{ rad/s} \end{aligned}$$

At this value of feedback gain the flying qualities requirements are clearly completely met, with margins sufficient to allow for uncertainty. The closed-loop system thus defined provides the basis for further analytical studies concerning implementation architecture and safety issues.

The pitch rate response of the aircraft before and after the addition of the augmentation loop is illustrated in Fig. 11.10. The first 10 seconds of the response to a unit elevator step input is shown to emphasise the considerable improvement in short-period mode stability. The longer-term response is not shown because it is not changed significantly by the augmentation and in any event the phugoid dynamics are acceptable.

11.5 Longitudinal stability augmentation

In Examples 11.2 and 11.3 it was shown how negative feedback with a single variable can be used to selectively augment the stability characteristics of an aeroplane. It was also shown how the effect of single-variable feedback may be readily evaluated with the aid of a root locus plot.

Now, clearly, the choice of feedback variable is important in determining the nature of the change in the stability characteristics of the aeroplane, since each variable results in a unique combination of changes. Provided that the aircraft is equipped with the appropriate motion sensors, various feedback control schemes are possible; it then becomes necessary to choose the feedback variable(s) best suited to augment the deficiencies of the basic airframe. It is also useful to appreciate what effect each feedback variable has on the stability modes when assessing a flight control system design. However complex the functional structure of the system, the basic augmentation

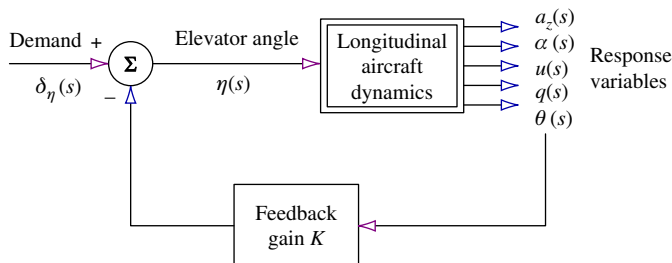


FIGURE 11.11 Longitudinal feedback options.

effect of each feedback variable does not change. Feedback is also used for reasons other than stability augmentation—for example, in autopilot functions. In such cases, augmentation also occurs and may not be desirable. If so, a thorough understanding of the effects of the most commonly used feedback variables is invaluable.

To evaluate the effect of feedback utilising a particular response variable, it is instructive to conduct a survey of all single-loop feedback options. In every case, the feedback loop is reduced to a simple gain component only. By this means the possible intrusive effects of other loop components, such as noise filters, phase compensation filters, and sensor and actuator dynamics, are prevented from masking the true augmentation effects. The longitudinal stability augmentation options are summarised in Fig. 11.11, in which it is implied that a negative feedback loop may be closed between any of the motion variables and the elevator. Other loops may, of course, be closed between the motion variables and alternative longitudinal control motivators, or engine thrust control, for example, but these are not considered here.

The survey is conducted by taking each motion variable in turn and evaluating its influence on the closed-loop stability characteristics as a function of the loop gain K . The root locus plot is especially useful for this purpose since it enables simultaneous assessment of the relative influence on, and relative sensitivity of, each stability mode. As the detailed effect of feedback depends on the aircraft and flight condition of interest, it is not easy to generalise and is best illustrated by example. Consequently, the following survey, Example 11.4, is based on a typical aircraft operating at a typical flight condition, and the observations may be applied loosely to the longitudinal stability augmentation of most aircraft.

EXAMPLE 11.4

Transfer function data for the McDonnell Douglas A-4D Skyhawk aircraft were obtained from Teper (1969). The flight condition chosen corresponds with an all-up weight of 17,578 Lb at an altitude of 35,000 ft at Mach 0.6. In factorised form the longitudinal characteristic equation is

$$\Delta(s) = (s^2 + 0.014s + 0.0068)(s^2 + 1.009s + 5.56) = 0 \quad (11.34)$$

and the longitudinal stability mode characteristics are

$$\begin{aligned} \text{Phugoid damping ratio } \zeta_p &= 0.086 \\ \text{Phugoid undamped natural frequency } \omega_p &= 0.082 \text{ rad/s} \\ \text{Short-period damping ratio } \zeta_s &= 0.214 \\ \text{Short-period undamped natural frequency } \omega_s &= 2.358 \text{ rad/s} \end{aligned}$$

These stability mode characteristics would normally be considered acceptable with the exception of the short-period mode damping ratio, which is too low. The Skyhawk is typical of combat aeroplanes of the 1960s in which only modest degrees of augmentation are required to rectify the stability deficiencies of the basic airframe. This, in turn, implies that only modest feedback gains are required in the typical range of, say, $0 \leq K \leq 2.0$. In modern FBW aircraft having unstable airframes, rather larger gain values are required to achieve the same levels of augmentation. Generally, the greater the required change in the stability characteristics, the greater the feedback gains needed to effect the change. In the following catalogue of root locus plots, each plot illustrates the effect of a single feedback loop closure as a function of increasing feedback gain K .

Pitch Attitude Feedback to Elevator

The open-loop aircraft transfer function is

$$\frac{\theta(s)}{\eta(s)} \equiv \frac{N_\eta^\theta(s)}{\Delta(s)} = \frac{-8.096(s - 0.0006)(s + 0.3591)}{(s^2 + 0.014s + 0.0068)(s^2 + 1.009s + 5.56)} \text{ rad/rad} \quad (11.35)$$

and the corresponding root locus plot is shown in Fig. 11.12.

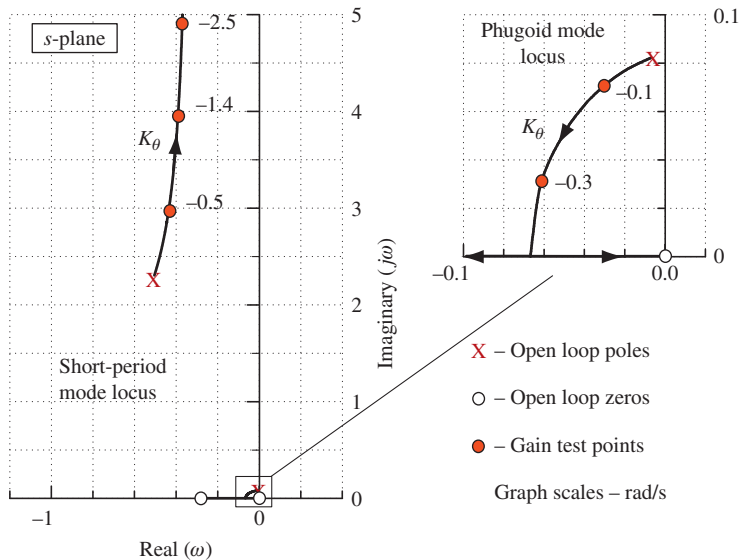


FIGURE 11.12 Root locus plot: pitch attitude feedback to elevator.

As K_θ is increased the phugoid damping increases rapidly whilst the frequency remains nearly constant; however, the short-period mode frequency increases whilst the damping decreases, both characteristics changing relatively slowly. Thus, as might be expected, since pitch attitude is a dominant variable in the phugoid mode, this mode is considerably more sensitive to the loop gain than the short-period mode. Since this feedback option further destabilises the short-period mode, its usefulness in a SAS is very limited indeed. However, it does improve phugoid stability, the mode becoming critically damped at a gain of $K_\theta = -0.37$ rad/rad. A practical gain value might be $K_\theta = -0.1$ rad/rad, which would result in a good level of closed-loop phugoid stability without reducing short-period mode stability too much. These observations are, of course, in good agreement with the findings of Example 11.2.

Pitch Rate Feedback to Elevator

The open-loop aircraft transfer function is

$$\frac{q(s)}{\eta(s)} \equiv \frac{N_\eta^q(s)}{\Delta(s)} = \frac{-8.096s(s - 0.0006)(s + 0.3591)}{(s^2 + 0.014s + 0.0068)(s^2 + 1.009s + 5.56)} \text{ rad/s/rad} \quad (11.36)$$

and the corresponding root locus plot is shown in Fig. 11.13.

As K_q is increased the short-period mode damping increases rapidly whilst the frequency remains nearly constant; Whereas, as K_q is increased the phugoid frequency and damping decrease relatively slowly. More typically, a slow increase in phugoid damping is seen. Thus, as might be expected, since pitch rate is a dominant variable in the short-period mode, this mode is considerably more sensitive to the loop gain than the short-period mode. As discussed in Example 11.3,

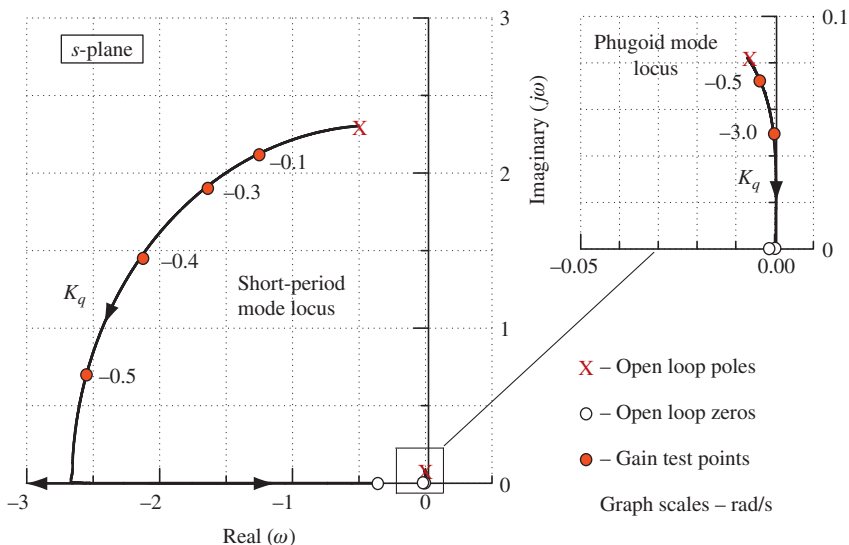


FIGURE 11.13 Root locus plot: pitch rate feedback to elevator.

this feedback option describes the classical pitch damper and is found on many aeroplanes. It also exactly describes the longitudinal stability augmentation solution used on the Skyhawk. Its dominant effect is to artificially increase the magnitude of the derivative m_q ; it also increases the magnitude of the derivatives x_q and z_q but to a lesser degree.

The short-period mode becomes critically damped at a gain of $K_q = -0.53$ rad/rad/s. A practical gain value might be $K_q = -0.3$ rad/rad/s, which would result in an adequate level of closed-loop short-period mode stability whilst simultaneously increasing the frequency separation between the two modes. However, at this value of feedback gain the changes in the phugoid characteristics are almost insignificant. As before, these observations are in good agreement with the findings of Example 11.3.

Velocity Feedback to Elevator

The open-loop aircraft transfer function is

$$\frac{u(s)}{\eta(s)} \equiv \frac{N_\eta^u(s)}{\Delta(s)} = \frac{6.293(s^2 + 0.615s + 0.129)(s + 115.28)}{(s^2 + 0.014s + 0.0068)(s^2 + 1.009s + 5.56)} \text{ ft/s/rad} \quad (11.37)$$

and the corresponding root locus plot is shown in Fig. 11.14.

As K_u is increased the short-period mode frequency increases quite rapidly whilst, initially, the damping decreases. However, at very large gain values the damping begins to increase again, eventually becoming critical. However, as K_u is increased both the frequency and damping of the phugoid mode increase relatively rapidly. Thus, at this flight condition, both modes appear to have similar sensitivity to feedback gain. The stabilising influence on the phugoid mode is

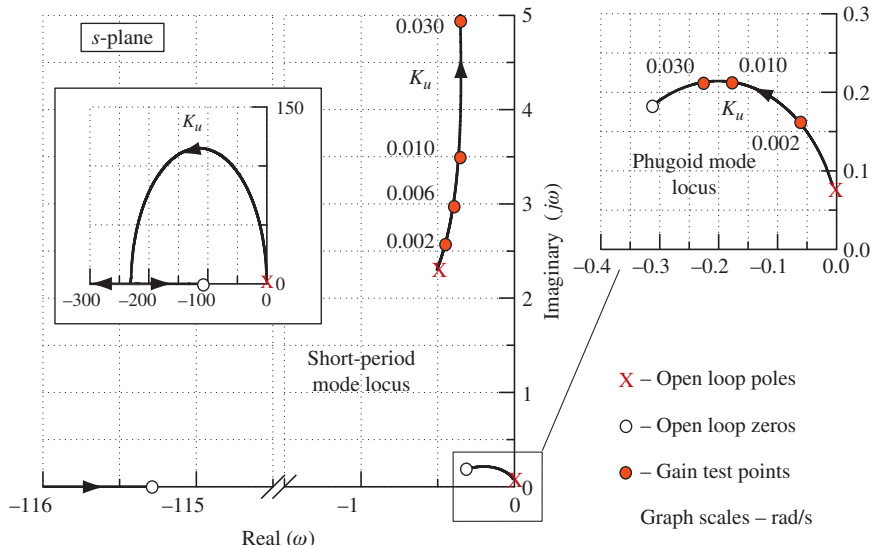


FIGURE 11.14 Root locus plot: velocity feedback to elevator.

much as might be expected since velocity is the dominant variable in the mode dynamics. The dominant effect of the feedback is therefore to artificially increase the magnitude of the derivative m_u , and since m_u is usually small it is not surprising that even modest values of feedback gain have a significant effect on phugoid stability. It also increases the magnitude of the derivatives x_u and z_u but to a lesser degree. A practical gain value might be $K_u = 0.001 \text{ rad/ft/s}$, which would result in a significant improvement in closed-loop phugoid mode stability whilst simultaneously decreasing the stability of the short-period mode by a small amount. However, such feedback gain values are quite impractically small, and in any event this feedback option does not find much useful application in a conventional longitudinal SAS.

Incidence Angle Feedback to Elevator

The open-loop aircraft transfer function is

$$\frac{\alpha(s)}{\eta(s)} \equiv \frac{N_\eta^\alpha(s)}{\Delta(s)} = \frac{-0.04(s^2 - 0.0027s + 0.0031)(s + 203.34)}{(s^2 + 0.014s + 0.0068)(s^2 + 1.009s + 5.56)} \text{ rad/rad} \quad (11.38)$$

and the corresponding root locus plot is shown in Fig. 11.15.

As K_α is increased the short-period mode frequency increases very rapidly whilst, initially, the damping decreases slowly. However, as the gain increases further the damping slowly starts to increase, eventually becoming critical at an impractically large value of feedback gain. At all practical gain values the damping remains more or less constant. As K_α is increased both the frequency and damping of the phugoid are reduced, the mode becoming unstable at a gain of $K_\alpha = -3.5 \text{ rad/rad}$ in this example.

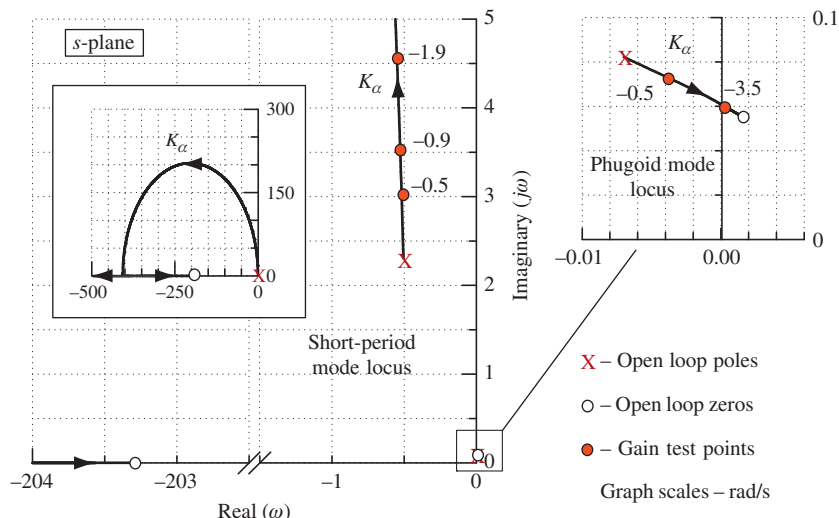


FIGURE 11.15 Root locus plot: incidence feedback to elevator.

Incidence feedback to elevator is a powerful method for augmenting the longitudinal static stability of an aeroplane; it finds extensive application in unstable FBW aircraft. The effect of the feedback is equivalent to increasing aircraft pitch stiffness, which artificially increases the magnitude of the derivative $m_w (\partial C_m / \partial \alpha)$ and, to a lesser degree, increases the magnitude of the derivatives x_w and z_w . Thus the increase in short-period mode frequency, together with the less significant influence on damping, is entirely consistent with the augmentation option. Since phugoid dynamics are typically very nearly incidence constant, the expected effect of the feedback on the mode is negligible. This is not the case in this example, probably because of aerodynamic effects at the relatively high subsonic Mach number. The fact that the phugoid roots do not even approximately cancel with the complex pair of numerator roots, as may normally be expected, confirms this. It is therefore expected that some incidence variation in the phugoid dynamics would be seen.

Normal Acceleration Feedback to Elevator

The open-loop aircraft transfer function is

$$\frac{a_z(s)}{\eta(s)} \equiv \frac{N_{\eta}^{a_z}(s)}{\Delta(s)} = \frac{-23.037(s - 0.018)(s - 0.0003)(s + 8.717)(s - 8.203)}{(s^2 + 0.014s + 0.0068)(s^2 + 1.009s + 5.56)} \text{ ft/s}^2/\text{rad} \quad (11.39)$$

and the corresponding root locus plot is shown in Fig. 11.16. Since the transfer function is *not proper*, care must be exercised in the production of the root locus plot and in its interpretation. However, at typically small values of feedback gain interpretation seems quite straightforward.

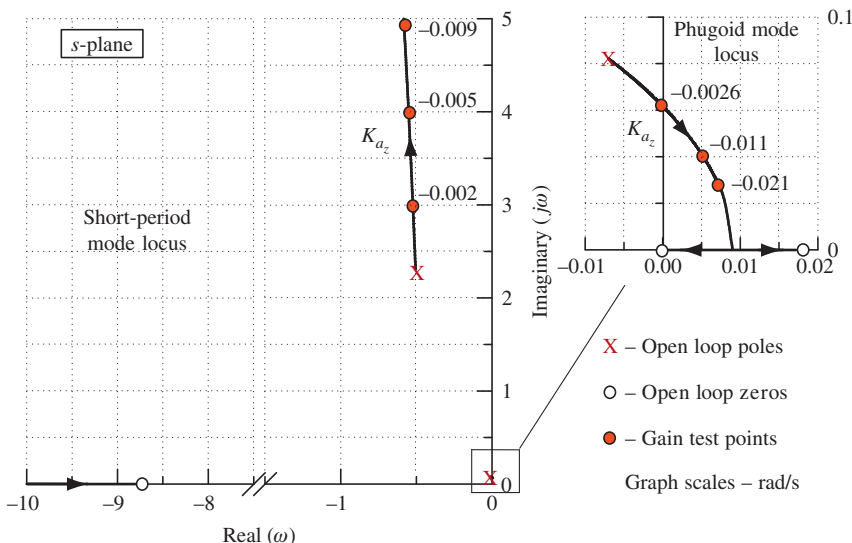


FIGURE 11.16 Root locus plot: normal acceleration feedback to elevator.

Since an accelerometer is rather more robust than an incidence sensor, normal acceleration feedback to elevator is commonly used instead of, or to complement, incidence feedback. Both feedback variables have a similar effect on the phugoid and short-period stability modes at practical values of feedback gain. However, both modes are rather more sensitive to feedback gain because very small values result in significant changes to the mode characteristics. As K_{a_z} is increased the short-period mode frequency increases very rapidly whilst, initially, the damping decreases slowly. However, as the gain increases further the damping slowly starts to increase, eventually becoming critical at an impractically large value of feedback gain. At all practical gain values the damping remains more or less constant. The full short-period mode branch of the locus is not shown in Fig. 11.16 since the gain range required exceeded the capability of the computational software used to produce the plots. As K_{a_z} is increased both the frequency and the damping of the phugoid are reduced, the mode becoming unstable at a gain of $K_{a_z} = 0.0026 \text{ rad/ft/s}^2$ in this example.

Because the normal acceleration variable comprises a mix of incidence, velocity, and pitch rate (see Section 5.5), the augmentation it provides in a feedback control system may be regarded as equivalent to the sum of the effects of feedback of the separate variables. At moderate gains, then, the increase in pitch stiffness is significant and results in a rapid increase in short-period mode frequency. The corresponding increase in short-period mode damping is rather greater than that achieved with incidence feedback alone due to the effect of implicit pitch rate feedback. Since the incidence dependent term dominates the determination of normal acceleration, it is not surprising that normal acceleration feedback behaves like incidence feedback. It is approximately equivalent to artificially increasing the magnitude of the derivative m_w and, to a lesser degree, also increases the magnitude of the derivatives x_w and z_w .

11.6 Lateral-directional stability augmentation

As for the longitudinal stability augmentation options described in Section 11.5, it is instructive to conduct a survey of all lateral-directional single-loop feedback options. The lateral-directional stability augmentation options are summarised in Fig. 11.17, in which it is implied that a negative feedback loop may be closed between any of the motion variables and either the ailerons or the rudder. Other loops can be closed between the motion variables and alternative lateral-directional control motivators, but, again, these are not considered here.

As before, the survey is conducted by taking each motion variable in turn and evaluating its influence on the closed-loop stability characteristics as a function of the loop gain K . The detailed effects of the lateral-directional feedback options are much more dependent on the aircraft and the flight condition than the longitudinal feedback options. Therefore, it is more difficult, and probably less appropriate, to generalise. Thus, as before, the effects are best illustrated by example. The following survey, Example 11.5, is based on a typical aircraft operating at a typical flight condition, and the observations may be interpreted as being applicable to the lateral-directional stability augmentation of most aircraft. However, care must be exercised when applying the observations to other aircraft, and every new application should be evaluated in its own right.

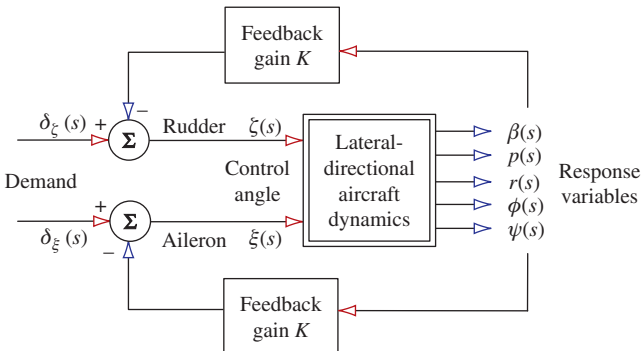


FIGURE 11.17 Lateral-directional feedback options.

EXAMPLE 11.5

Transfer function data for the Northrop T-38 Talon aircraft were obtained from [Teper \(1969\)](#). The flight condition chosen corresponds with an all-up weight of 10,000 Lb at Mach 0.8 at sea level. In factorised form the lateral-directional characteristic equation is

$$\Delta(s) = (s - 0.0014)(s + 4.145)(s^2 + 1.649s + 38.44) = 0 \quad (11.40)$$

and the lateral-directional stability mode characteristics are

$$\text{Spiral mode time constant } T_s = -714 \text{ s}$$

$$\text{Roll mode time constant } T_r = 0.24 \text{ s}$$

$$\text{Dutch roll damping ratio } \zeta_d = 0.133$$

$$\text{Dutch roll undamped natural frequency } \omega_d = 6.2 \text{ rad/s}$$

Clearly, the spiral mode is unstable, which is quite typical, and the time constant is sufficiently large that it is most unlikely to give rise to handling problems. In fact, all of the stability characteristics are better than the minimum acceptable for Level 1 flying qualities. However, the aircraft is fitted with a simple yaw damper to improve the lateral-directional flying and handling qualities at all flight conditions, including some where the minimum standards are not met.

In the following catalogue of root locus plots, each plot illustrates the effect of a single feedback loop closure as a function of increasing feedback gain K . It should be noted that in the original data source the sign convention for aileron angle is opposite to that adopted in this book. In the following illustrations the aileron sign convention is changed to be consistent with British notation.

Sideslip Angle Feedback to Aileron

The open-loop transfer function is

$$\frac{\beta(s)}{\xi(s)} \equiv \frac{N_\xi^\beta(s)}{\Delta(s)} = \frac{1.3235(s - 0.0832)(s + 7.43)}{(s - 0.0014)(s + 4.145)(s^2 + 1.649s + 38.44)} \text{ rad/rad} \quad (11.41)$$

and the corresponding root locus plot is shown in [Fig. 11.18](#).

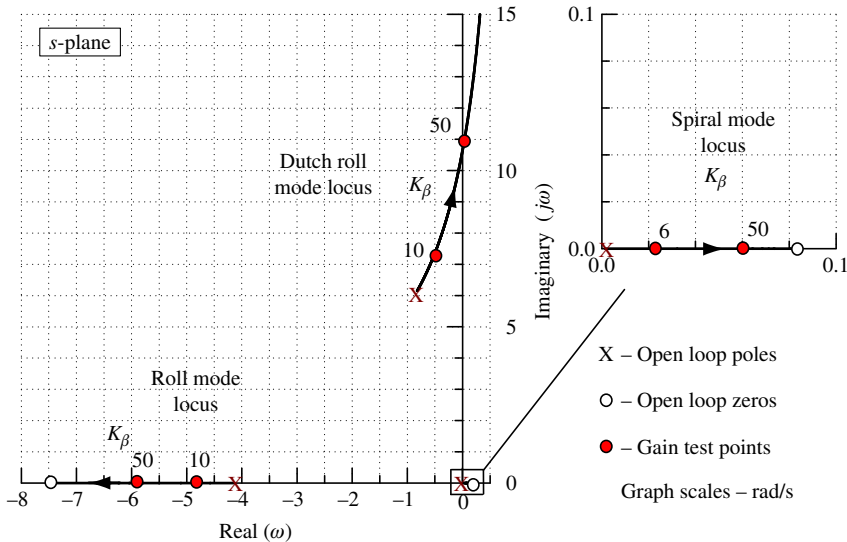


FIGURE 11.18 Root locus plot: sideslip angle feedback to aileron.

As K_β is increased the spiral mode pole moves further to the right on the *s*-plane and its instability worsens as its time constant decreases. The roll mode stability is increased as the gain K_β is increased since its pole moves to the left on the *s*-plane. As K_β is increased the dutch roll frequency is increased whilst its damping is decreased; eventually it becomes unstable at a gain of approximately $K_\beta = 50$ rad/rad. All three modes are relatively insensitive to feedback since large gains are required to achieve modest changes in the mode characteristics; however, the spiral mode is the most sensitive. Negative feedback of sideslip angle to aileron is equivalent to an increase in dihedral effect. In particular, for this example, it augments the magnitude of the stability derivatives l_v and n_v and the degree of augmentation of each derivative depends on the value of K_β and the aileron control derivatives l_ξ and n_ξ respectively. Clearly, the effect is to artificially increase the lateral stiffness of the aeroplane, resulting in an increase in dutch roll frequency and a corresponding increase in roll damping. It is unlikely that sideslip angle feedback to aileron alone would find much use in stability augmentation systems.

Roll Rate Feedback to Aileron

The open-loop transfer function is

$$\frac{p(s)}{\xi(s)} \equiv \frac{N_\xi^p(s)}{\Delta(s)} = \frac{-27.75(s - 0.0005)(s^2 + 1.55s + 41.91)}{(s - 0.0014)(s + 4.145)(s^2 + 1.649s + 38.44)} \text{ rad/s/rad} \quad (11.42)$$

and the corresponding root locus plot is shown in Fig. 11.19. Note that both the spiral mode pole and the dutch roll poles are approximately cancelled by the numerator zeros. This means that both modes are insensitive to this feedback option.

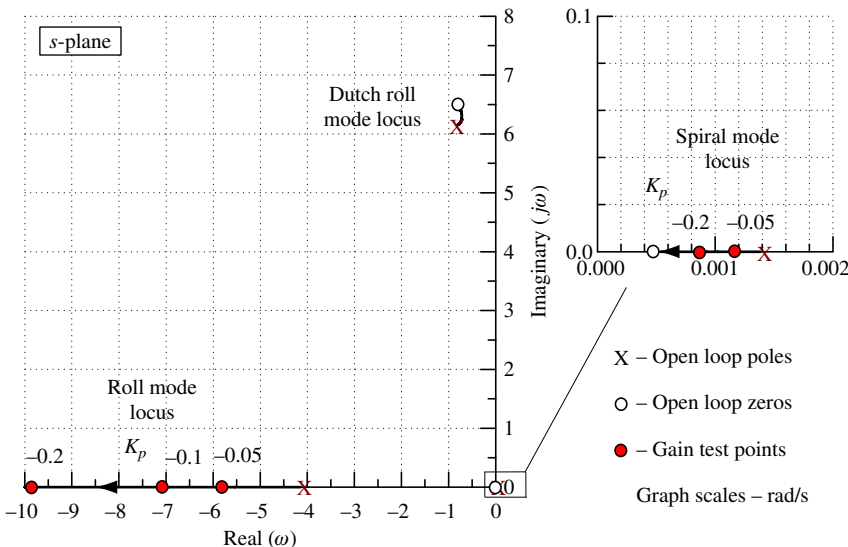


FIGURE 11.19 Root locus plot: roll rate feedback to aileron.

As K_p is increased the spiral mode pole moves to the left on the s -plane and its instability is reduced as its time constant is increased. However, the spiral mode remains unstable at all values of K_p , although roll rate feedback to aileron generally improves the handling qualities associated with the spiral mode. Roll mode stability increases rapidly as the gain K_p is increased since its pole moves to the left on the s -plane. The roll mode is most sensitive to this feedback option. In fact, roll rate feedback to aileron describes the classical roll damper and is used in many aeroplanes.

Whatever the value of K_p , the effect on the stability characteristics of the dutch roll mode is insignificant, as stated previously. At all levels of feedback gain the dutch roll mode poles remain in a very small localised area on the s -plane. Negative roll rate feedback to aileron is equivalent to an increase in the roll-damping properties of the wing. In particular, it augments the magnitude of the stability derivative l_p and, to a lesser extent, n_p . As before, the degree of augmentation of each derivative depends on the value of K_p and the aileron control derivatives l_ξ and n_ξ , respectively.

Yaw Rate Feedback to Aileron

The open-loop transfer function is

$$\frac{r(s)}{\xi(s)} \equiv \frac{N_\xi^r(s)}{\Delta(s)} = \frac{-1.712(s + 5.405)(s^2 + 1.788s + 4.465)}{(s - 0.0014)(s + 4.145)(s^2 + 1.649s + 38.44)} \text{ rad/s/rad} \quad (11.43)$$

and the corresponding root locus plot is shown in Fig. 11.20.

As K_r is increased the spiral mode pole moves to the left on the s -plane becoming stable at a small value of gain. At a gain of approximately $K_r = 6.0$ rad/rad/s, which is somewhat greater

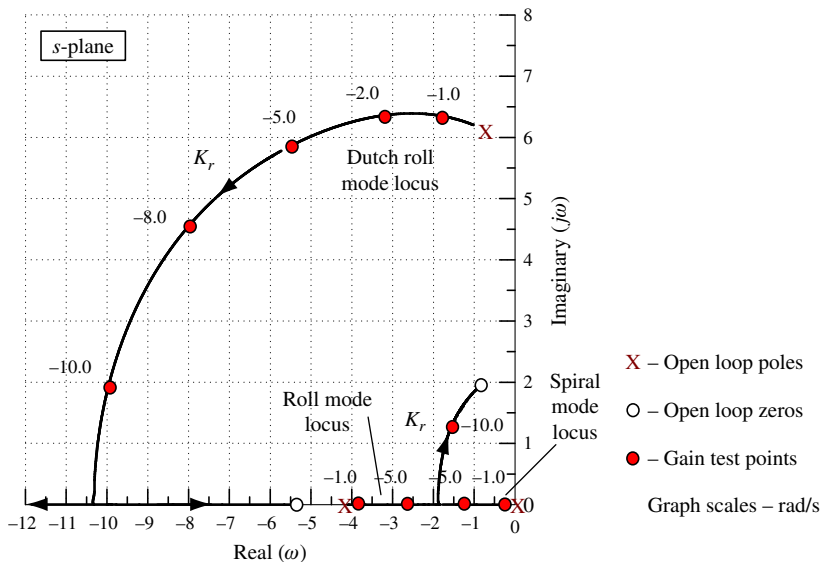


FIGURE 11.20 Root locus plot: yaw rate feedback to aileron.

than a practical value, the spiral and roll modes couple to form a low-frequency oscillatory characteristic. The roll mode stability decreases as the gain K_r is increased since its pole moves to the right on the s -plane before coupling with the spiral mode. The dutch roll mode is the most sensitive mode: As K_r is increased the damping increases rapidly whilst the frequency increases rather more slowly. At practical levels of feedback gain, the most useful improvements are to stabilise the spiral mode and to improve dutch roll damping whilst degrading roll mode stability only slightly. However, yaw rate feedback to aileron cross-couples both the roll and yaw control axes of the aeroplane and, for safety reasons, is not so desirable. The feedback is equivalent to an increase in the yaw-damping properties of the wing. In particular, it augments the magnitude of the stability derivatives l_r and n_r .

Roll Attitude Feedback to Aileron

The open-loop transfer function is

$$\frac{\phi(s)}{\xi(s)} \equiv \frac{N_\xi^\phi(s)}{\Delta(s)} = \frac{-27.75(s^2 + 1.55s + 41.91)}{(s - 0.0014)(s + 4.145)(s^2 + 1.649s + 38.44)} \text{ rad/rad} \quad (11.44)$$

and the corresponding root locus plot is shown in Fig. 11.21. Note that the dutch roll poles are approximately cancelled by the numerator zeros, which implies that the mode is insensitive to this feedback option.

As K_ϕ is increased the spiral mode pole moves to the left on the s -plane and its stability increases very rapidly, a very small value of gain being sufficient to place the pole on the left

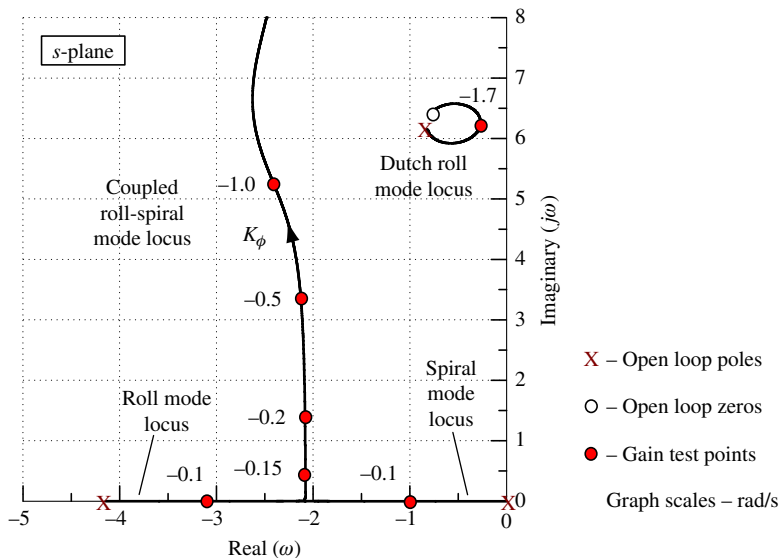


FIGURE 11.21 Root locus plot: roll attitude feedback to aileron.

half of the s -plane. At a slightly larger value of gain, $K_\phi = -0.14$ rad/rad, the spiral and roll modes couple to form a low-frequency oscillatory characteristic as in the previous illustration. Therefore, roll mode stability decreases rapidly as the gain K_ϕ is increased, until its pole couples with that of the spiral mode. Clearly, both the roll and spiral modes are most sensitive to this feedback option.

As expected, for all values of K_ϕ the effect on the stability characteristics of the dutch roll mode is insignificant. At all levels of feedback gain the dutch roll mode poles remain in a very small localised area on the s -plane and the minimum damping corresponds with a feedback gain of $K_\phi = -1.7$ rad/rad. Negative roll attitude feedback to aileron is, very approximately, equivalent to an increase in roll stiffness and at quite small feedback gain values manifests itself as the coupled roll-spiral oscillatory mode, which may be regarded as a kind of lateral pendulum mode.

Yaw Attitude Feedback to Aileron

The open-loop transfer function is

$$\frac{\psi(s)}{\xi(s)} \equiv \frac{N_\xi^\psi(s)}{\Delta(s)} = \frac{-1.712(s + 5.405)(s^2 + 1.788s + 4.465)}{s(s - 0.0014)(s + 4.145)(s^2 + 1.649s + 38.44)} \text{ rad/rad} \quad (11.45)$$

and the corresponding root locus plot is shown in Fig. 11.22.

As K_ψ is increased the spiral mode pole moves to the left on the s -plane toward the pole at the origin, to which it couples at a very small value of gain to form a low-frequency

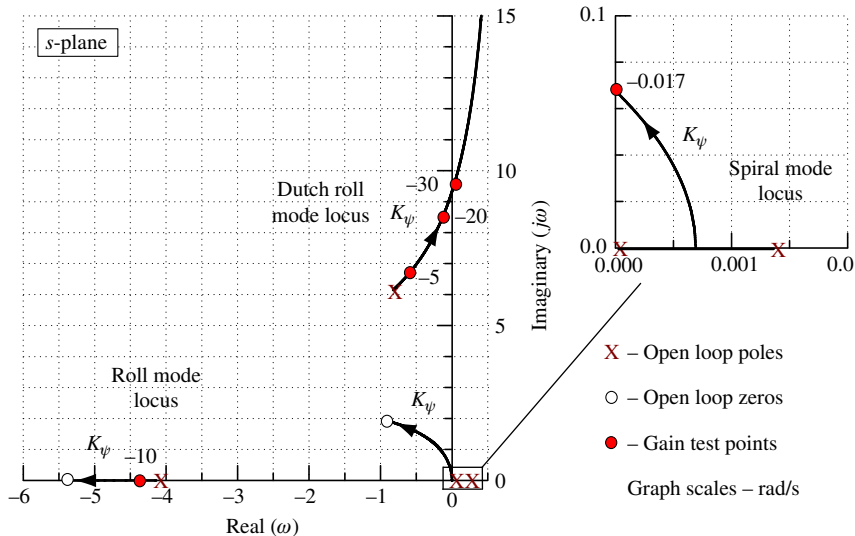


FIGURE 11.22 Root locus plot: yaw attitude feedback to aileron.

unstable oscillatory characteristic. At a gain of approximately $K_\psi = -0.017$ rad/rad, the low-frequency oscillatory characteristic becomes stable. The roll mode stability increases very slowly as the gain K_ψ is increased since its pole moves to the left on the s -plane toward the zero at -5.404 .

As K_ψ is increased the dutch roll mode frequency increases whilst the damping decreases, both characteristics changing rather slowly. The dutch roll mode eventually becomes unstable at a gain of approximately $K_\psi = -30.0$ rad/rad. At practical levels of feedback gain, the effect on the roll and dutch roll modes is almost insignificant. On the other hand, the effect of the feedback on the spiral mode is most significant, even at very low values of gain. As for yaw rate feedback to aileron, yaw attitude feedback to aileron cross couples both the roll and yaw control axes of the aeroplane and is not so desirable for safety reasons. The feedback is equivalent to an increase in the yaw stiffness properties of the wing.

Sideslip Angle Feedback to Rudder

The open-loop transfer function is

$$\frac{\beta(s)}{\zeta(s)} \equiv \frac{N_\zeta^\beta(s)}{\Delta(s)} = \frac{0.10(s - 0.0015)(s + 4.07)(s + 113.4)}{(s - 0.0014)(s + 4.145)(s^2 + 1.649s + 38.44)} \text{ rad/rad} \quad (11.46)$$

and the corresponding root locus plot is shown in Fig. 11.23. Note that both the spiral and roll mode poles are very nearly cancelled by numerator zeros. It may therefore be expected that negative sideslip angle feedback to rudder significantly augments the dutch roll mode only.

As expected, as K_β is increased both the spiral mode pole and the roll mode pole move to the right on the s -plane; however, the reduction in stability is insignificant. As K_β is increased both

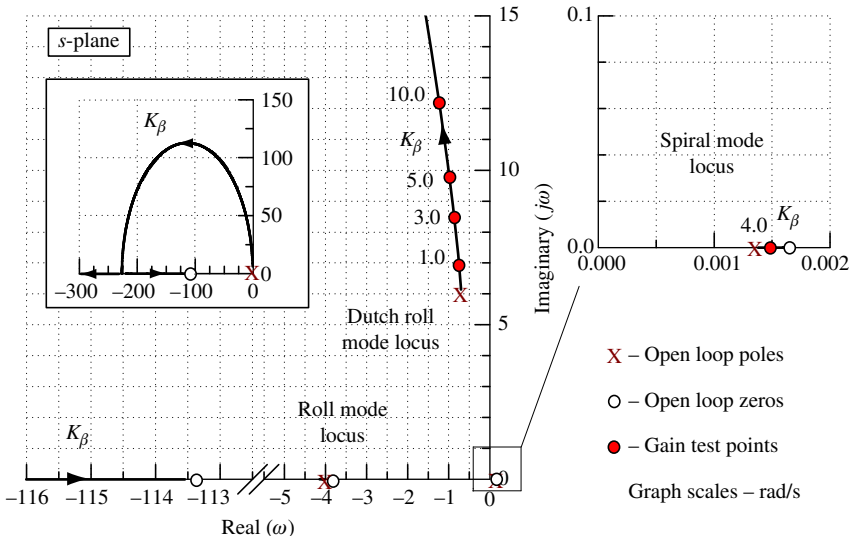


FIGURE 11.23 Root locus plot: sideslip angle feedback to rudder.

the dutch roll frequency and damping are increased, the mode eventually becoming critically damped at the absurdly high frequency of $\omega_d = -226$ rad/s at a gain of approximately $K_\beta = -4500$ rad/rad! Negative feedback of sideslip angle to rudder is equivalent to an increase in the weathercock effect of the fin, or yaw stiffness. For this example in particular, it very effectively augments the magnitude of the stability derivative n_v and to a lesser extent l_v . The degree of augmentation of each derivative depends on the value of K_β and the rudder control derivatives n_ζ and l_ζ , respectively. Clearly, the effect is to artificially increase the directional stiffness of the aeroplane, resulting in an increase in dutch roll frequency and a corresponding, but much slower, increase in roll damping. At all practical values of feedback gain, the dutch roll damping remains more or less constant at its open-loop value.

Roll Rate Feedback to Rudder

The open-loop transfer function is

$$\frac{p(s)}{\zeta(s)} \equiv \frac{N_\zeta^p(s)}{\Delta(s)} = \frac{16.65(s - 0.0006)(s - 0.79)(s + 1.09)}{(s - 0.0014)(s + 4.145)(s^2 + 1.649s + 38.44)} \text{ rad/s/rad} \quad (11.47)$$

and the corresponding root locus plot is shown in Fig. 11.24. Note that the spiral mode pole is very approximately cancelled by a numerator zero.

As expected, the effect on the spiral mode of this feedback option is insignificant. The roll mode stability increases rapidly as the gain K_p is increased since its pole moves to the left on the s -plane. The roll mode is quite sensitive to this feedback option, which is not surprising since roll rate is the dominant motion variable in the aircraft dynamics associated with the mode.

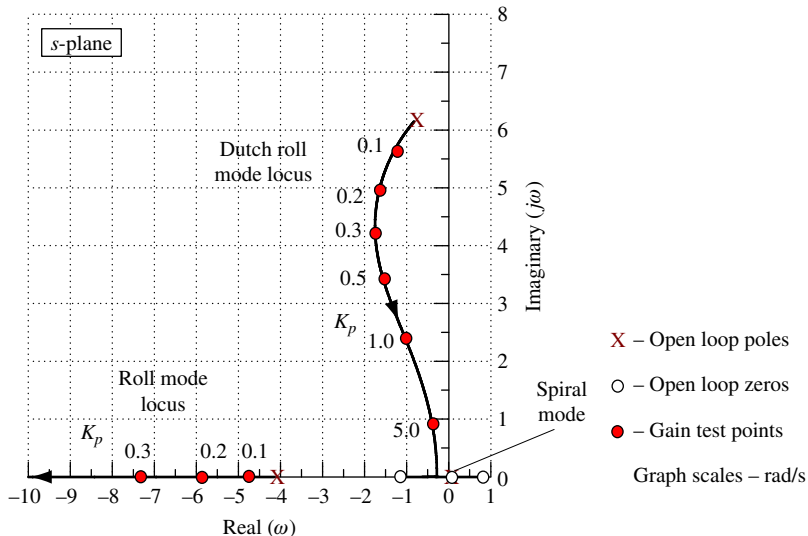


FIGURE 11.24 Root locus plot: roll rate feedback to rudder.

The dutch roll mode is also very sensitive to this feedback option. As K_p is increased the dutch roll damping increases rapidly whilst the frequency is reduced. For values of the feedback gain $K_p \geq 8.9$ rad/rad/s, the dutch roll mode is critically damped and is therefore non-oscillatory. Negative roll rate feedback to rudder is equivalent to an increase in the yaw damping properties of the wing. In particular, it augments the magnitude of the stability derivative n_p and, to a lesser extent, l_p . As before, the degree of augmentation of each derivative depends on the value of K_p and the rudder control derivatives n_ζ and l_ζ , respectively.

Yaw Rate Feedback to Rudder

The open-loop transfer function is

$$\frac{r(s)}{\zeta(s)} \equiv \frac{N_\zeta^r(s)}{\Delta(s)} = \frac{-11.01(s + 0.302)(s + 0.366)(s + 4.11)}{(s - 0.0014)(s + 4.145)(s^2 + 1.649s + 38.44)} \text{ rad/s/rad} \quad (11.48)$$

and the corresponding root locus plot is shown in Fig. 11.25. Note that the roll mode pole is almost exactly cancelled by a numerator zero. It is therefore expected that the roll mode will be insensitive to this feedback option.

The spiral mode stability increases rapidly as the gain K_r is increased since its pole moves to the left on the s -plane. The spiral mode is very sensitive to this feedback option and becomes stable at a gain of $K_r = -0.4$ rad/rad/s. As expected, the effect of this feedback option on the roll mode is insignificant. The branching of the loci around the roll mode simply indicates that the pole-zero cancellation is not exact. The dutch roll mode is also very sensitive to this feedback option. As K_r is increased the dutch roll damping increases rapidly whilst the frequency

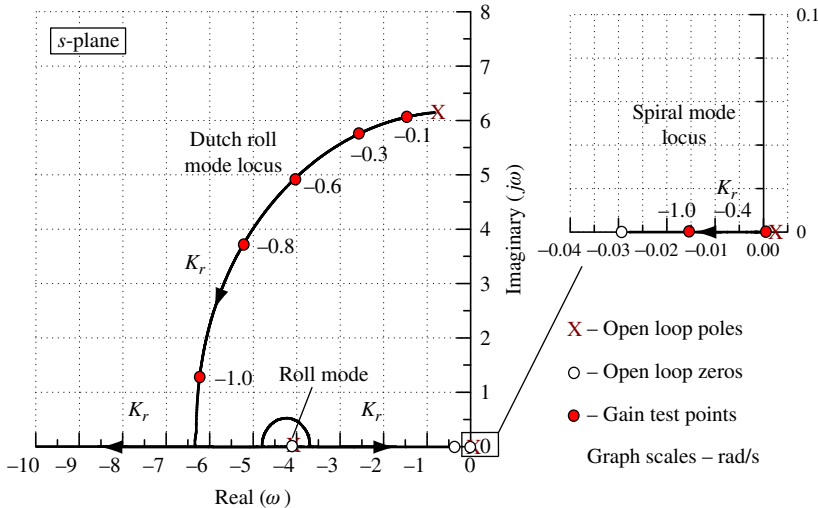


FIGURE 11.25 Root locus plot: yaw rate feedback to rudder.

remains almost constant. For values of the feedback gain $K_r \geq -1.2$ rad/rad/s, the dutch roll mode becomes critically damped. Practical values of feedback gain are, typically, in the range $0 \geq K_r \geq -0.7$ rad/rad/s.

The dutch roll mode damping is most sensitive to this feedback option, and yaw rate feedback to rudder describes the classical yaw damper, which is probably the most common augmentation system. However, its use brings a bonus since it also significantly improves spiral mode stability. Negative yaw rate feedback to rudder is equivalent to an increase in the yaw damping properties of the aeroplane or to an increase in the effectiveness of the fin as a damper. In particular, it augments the magnitude of the stability derivative n_r and, to a lesser extent, l_r .

Roll Attitude Feedback to Rudder

The open-loop transfer function is

$$\frac{\phi(s)}{\zeta(s)} \equiv \frac{N_\zeta^\phi(s)}{\Delta(s)} = \frac{16.5(s - 0.825)(s + 1.08)}{(s - 0.0014)(s + 4.145)(s^2 + 1.649s + 38.44)} \text{ rad/rad} \quad (11.49)$$

and the corresponding root locus plot is shown in Fig. 11.26.

As K_ϕ is increased the spiral mode pole moves to the right on the s -plane and its stability decreases slowly. The roll mode stability also decreases slowly as the gain K_ϕ is increased, a gain of $K_\phi \approx 4.0$ rad/rad being required to double the time constant, for example. As K_ϕ is increased the dutch roll mode frequency increases relatively quickly. The damping ratio also increases a little initially, but as the gain is increased further, the damping decreases steadily to zero at infinite feedback gain. Negative roll attitude feedback to rudder is, very approximately,

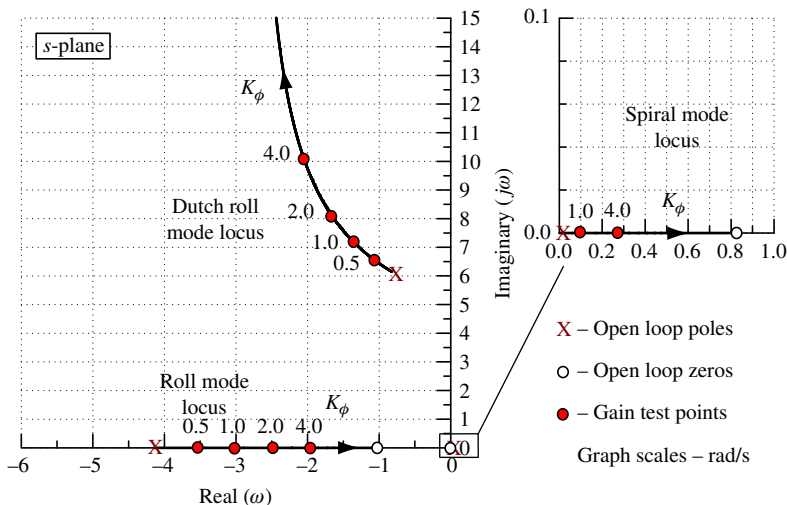


FIGURE 11.26 Root locus plot: roll attitude feedback to rudder.

equivalent to an increase in directional stiffness and is not commonly used in autostabilisation systems because it introduces cross-coupling between the roll and yaw control axes.

Yaw Attitude Feedback to Rudder

The open-loop transfer function is

$$\frac{\psi(s)}{\zeta(s)} \equiv \frac{N_\zeta^\psi(s)}{\Delta(s)} = \frac{-11.01(s + 0.0302)(s + 0.367)(s + 4.11)}{s(s - 0.0014)(s + 4.145)(s^2 + 1.649s + 38.44)} \text{ rad/rad} \quad (11.50)$$

and the corresponding root locus plot is shown in Fig. 11.27. Note that the roll mode pole is almost exactly cancelled by a numerator zero, indicating that the mode is not sensitive to this feedback option.

As K_ψ is increased the spiral mode pole moves to the left on the s -plane toward the pole at the origin, to which it couples at a very small value of gain to form a stable low-frequency oscillatory characteristic at all practical small values of gain. At a gain of approximately $K_\psi = -1.5$ rad/rad, the low-frequency oscillatory characteristic becomes critically damped. Since the frequency of this mode is so low, and when stable is reasonably well damped, it is unlikely to give rise to handling problems. As expected, the roll mode stability remains effectively unchanged by this feedback option. As K_ψ is increased the dutch roll mode frequency increases whilst the damping decreases, both characteristics changing relatively slowly. The dutch roll mode eventually becomes neutrally stable at infinite feedback gain. At practical levels of feedback gain the effect on the dutch roll mode is to increase the frequency, with only a very small reduction in damping. Negative yaw attitude feedback to rudder is equivalent to an increase in directional stiffness and is not commonly used in autostabilisation systems.

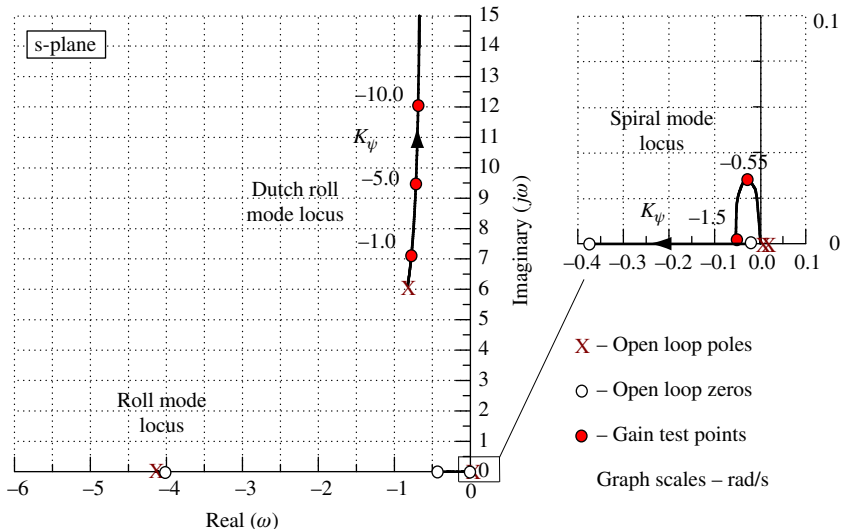


FIGURE 11.27 Root locus plot: yaw attitude feedback to rudder.

11.7 The pole placement method

The *pole placement method* is an alternative and very powerful method for designing feedback gains for autostabilisation systems. It is based on the manipulation of the equations of motion in state-space form and makes full use of the appropriate computational tools in the analytical process. Practical application of the method to aeroplanes is limited since it assumes that all state, or motion, variables are available for use in an augmentation system, which is not usually the case. However, regardless of the limitations of the method, it can be very useful to the FCS designer in the initial stages of assessment of augmentation system structure.

The state and output matrix equations describing the unaugmented, or open-loop, aircraft, equations (5.48), are written as

$$\begin{aligned}\dot{\mathbf{x}}(t) &= \mathbf{A}\mathbf{x}(t) + \mathbf{B}\mathbf{u}(t) \\ \mathbf{y}(t) &= \mathbf{C}\mathbf{x}(t) + \mathbf{D}\mathbf{u}(t)\end{aligned}\quad (11.51)$$

Assuming that augmentation is achieved by negative feedback of the state vector $\mathbf{x}(t)$ to the input vector $\mathbf{u}(t)$, the control law may be written as

$$\mathbf{u}(t) = \mathbf{v}(t) - \mathbf{K}\mathbf{x}(t) \quad (11.52)$$

where $\mathbf{v}(t)$ is a vector of input demand variables and \mathbf{K} is a matrix of feedback gains. Note that equation (11.52) is the general multivariable equivalent of equation (11.14). The closed-loop state

and output equations describing the augmented aircraft are obtained by substituting [equation \(11.52\)](#) into [equations \(11.51\)](#):

$$\begin{aligned}\dot{\mathbf{x}}(t) &= [\mathbf{A} - \mathbf{B}\mathbf{K}]\mathbf{x}(t) + \mathbf{B}\mathbf{v}(t) \\ \mathbf{y}(t) &= [\mathbf{C} - \mathbf{D}\mathbf{K}]\mathbf{x}(t) + \mathbf{D}\mathbf{v}(t)\end{aligned}\quad (11.53)$$

or, more simply,

$$\begin{aligned}\dot{\mathbf{x}}(t) &= \mathbf{A}_{\text{aug}}\mathbf{x}(t) + \mathbf{B}\mathbf{v}(t) \\ \mathbf{y}(t) &= \mathbf{C}_{\text{aug}}\mathbf{x}(t) + \mathbf{D}\mathbf{v}(t)\end{aligned}\quad (11.54)$$

[Equations \(11.54\)](#) are solved exactly as are those of the open-loop aircraft, [equations \(11.51\)](#), to obtain the response transfer functions for the augmented aircraft. Note that, as discussed in Section 5.6, for typical aircraft applications the direct matrix $\mathbf{D} = 0$, the output matrix $\mathbf{C} = \mathbf{I}$, the identity matrix, and [equations \(11.51\) through \(11.54\)](#) simplify accordingly.

Now the characteristic equation of the augmented aircraft is given by

$$\Delta_{\text{aug}}(s) = |s\mathbf{I} - \mathbf{A}_{\text{aug}}| \equiv |s\mathbf{I} - \mathbf{A} + \mathbf{B}\mathbf{K}| = 0 \quad (11.55)$$

and the roots of [equation \(11.55\)](#) or, equivalently, the eigenvalues of \mathbf{A}_{aug} describe the stability characteristics of the augmented aircraft.

Subject to the constraint that the open-loop state [equation \(11.51\)](#) describe a *controllable system*, which an aircraft is, then a feedback matrix \mathbf{K} exists such that the eigenvalues of the closed-loop system may be completely specified. Thus, if the required stability and control characteristics of the augmented aircraft are specified, the roots of [equation \(11.55\)](#) may be calculated; also, knowing the open-loop state and input matrices, \mathbf{A} and \mathbf{B} , respectively, [equation \(11.55\)](#) may be solved to find \mathbf{K} . Thus this method enables the stability characteristics of the augmented aircraft to be designed completely and exactly as required. Equivalently, the poles of the closed-loop aircraft may be *placed* on the s -plane exactly as required. However, full-state feedback is essential if all of the closed-loop poles are to be placed on the s -plane.

When the controlled system is *single-input*, the feedback matrix \mathbf{K} is unique and only one set of feedback gains provides the required stability characteristics. When the controlled system is *multi-input*, an infinite number of gain matrices \mathbf{K} may be found which provide the required stability characteristics. Consequently, most control system design problems involving the use of the pole placement method are solved by arranging the open-loop system to be single-input. This is most easily done when dealing with aircraft stability augmentation because the inputs naturally separate into elevator, ailerons, rudder, and thrust at the most basic level. It is a simple matter to arrange the state equation to include only one input variable and then to apply the pole placement method to design an augmentation system feedback structure.

EXAMPLE 11.6

The longitudinal equations of motion for the McDonnell Douglas F-4C Phantom aircraft were obtained from [Heffley and Jewell \(1972\)](#). At the chosen flight condition the weight is 38,925 Lb

and the aircraft is flying at Mach 1.1 at sea level. The state [equations \(11.51\)](#) were derived for the unaugmented aircraft from the data provided to give

$$\mathbf{A} = \begin{bmatrix} -0.068 & -0.011 & 0 & -9.81 \\ 0.023 & -2.10 & 375 & 0 \\ 0.011 & -0.160 & -2.20 & 0 \\ 0 & 0 & 1 & 0 \end{bmatrix} \quad \mathbf{B} = \begin{bmatrix} -0.41 & 1.00 \\ -77.0 & -0.09 \\ -61.0 & -0.11 \\ 0 & 0 \end{bmatrix}$$

with state vector $\mathbf{x}^T = [u \ w \ q \ \theta]$ and input vector $\mathbf{u}^T = [\eta \ \tau]$. Note that two input variables are given in the model, elevator angle η and thrust τ .

Using Program CC the equations of motion were solved and the open-loop characteristic polynomial was found:

$$\Delta(s) = (s^2 + 4.3s + 64.6)(s^2 + 0.07s + 0.003) \quad (11.56)$$

The corresponding longitudinal stability mode characteristics are

$$\begin{aligned} \text{Phugoid damping ratio } \zeta_p &= 0.646 \\ \text{Phugoid undamped natural frequency } \omega_p &= 0.054 \text{ rad/s} \\ \text{Short-period damping ratio } \zeta_s &= 0.267 \\ \text{Short-period undamped natural frequency } \omega_s &= 8.038 \text{ rad/s} \end{aligned}$$

Referring to the flying qualities requirements in MIL-F-8785C (1980), it was found that for a class IV aeroplane in the most category, category A flight phase, the Phantom comfortably meets Level 1 requirements with the exception of short-period mode damping, which is too low. Clearly, some augmentation is required to improve the pitch damping in particular.

The design decision was made to increase the short-period mode damping ratio to 0.7 whilst retaining the remaining stability characteristics at the nominal values of the basic unaugmented airframe. A short-period mode damping ratio of 0.7 was chosen since this gives a good margin of stability and results in the shortest mode settling time after a disturbance. However, the exact value chosen is not important provided that the margin of stability is adequate to allow for uncertainty in the modelling. Therefore, the pole placement method may be used to give the augmented aircraft the following longitudinal stability characteristics:

$$\begin{aligned} \text{Phugoid damping ratio } \zeta_p &= 0.65 \\ \text{Phugoid undamped natural frequency } \omega_p &= 0.054 \text{ rad/s} \\ \text{Short-period damping ratio } \zeta_s &= 0.7 \\ \text{Short-period undamped natural frequency } \omega_s &= 8.0 \text{ rad/s} \end{aligned}$$

Thus the required closed-loop characteristic polynomial is

$$\Delta_{\text{aug}}(s) = (s^2 + 11.2s + 64.0)(s^2 + 0.07s + 0.003) \quad (11.57)$$

Since a single-input control system is required, the input being elevator angle, the open-loop state equation is modified accordingly simply by removing the thrust terms. The open-loop state equation may then be written as

$$\begin{bmatrix} \dot{u} \\ \dot{w} \\ \dot{q} \\ \dot{\theta} \end{bmatrix} = \begin{bmatrix} -0.068 & -0.011 & 0 & -9.81 \\ 0.023 & -2.10 & 375 & 0 \\ 0.011 & -0.160 & -2.20 & 0 \\ 0 & 0 & 1 & 0 \end{bmatrix} \begin{bmatrix} u \\ w \\ q \\ \theta \end{bmatrix} + \begin{bmatrix} -0.41 \\ -77.0 \\ -61.0 \\ 0 \end{bmatrix} \eta \quad (11.58)$$

With the aid of the pole placement tool in Program CC, the feedback gain matrix required to give the augmented aircraft the characteristic polynomial, [equation \(11.57\)](#), is determined:

$$\mathbf{K} = [K_u \ K_w \ K_q \ K_\theta] = [-7.7 \times 10^{-6} \ 5.99 \times 10^{-4} \ -0.114 \ -1.96 \times 10^{-4}] \quad (11.59)$$

Care is required to maintain the correct units of the elements in the feedback matrix. The stability augmentation system control law is obtained by substituting for \mathbf{K} in [equation \(11.52\)](#); whence

$$\eta = \delta_\eta - K_u u - K_w w - K_q q - K_\theta \theta \quad (11.60)$$

The corresponding closed-loop control system structure follows and is shown in [Fig. 11.28](#).

Clearly, the choice of closed-loop stability characteristics has resulted in a gain matrix in which the gains K_u , K_w , and K_θ are impractically and insignificantly small. This is simply due to the fact that the only significant change between the open- and closed-loop stability characteristics is the increase in short-period mode damping and, as has already been established in Examples 11.3 and 11.4, the pole placement method confirms that this can be achieved with pitch rate feedback to elevator alone. If additional changes in the stability characteristics were required, the gains K_u , K_w , and K_θ would, of course, not necessarily be insignificant. Let the

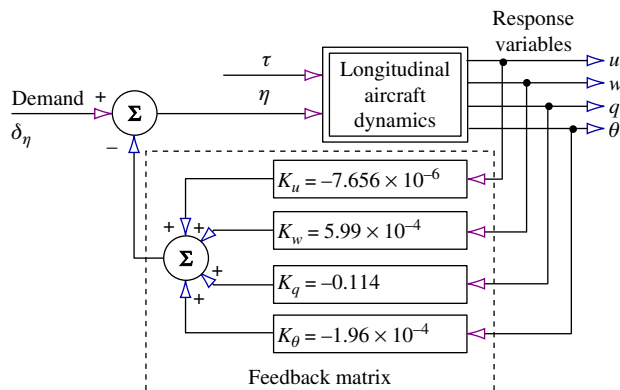


FIGURE 11.28 Stability augmentation system with full state feedback.

feedback gain matrix be simplified to include only practical gain values, and equation (11.59) may be written as

$$\mathbf{K} = [0 \ 0 \ -0.12 \ 0] \quad (11.61)$$

The closed-loop state equation (11.53) may then be calculated by writing

$$\mathbf{K} = \begin{bmatrix} 0 & 0 & -0.12 & 0 \\ 0 & 0 & 0 & 0 \end{bmatrix} \quad (11.62)$$

where the second row describes the feedback to the second, thrust, input, which is not used in this example for the reason given previously. $[\mathbf{A} - \mathbf{B}\mathbf{K}]$ is easily calculated with the aid of Program CC, for example, and the closed-loop state equation, written to include both input variables, is

$$\begin{bmatrix} \dot{u} \\ \dot{w} \\ \dot{q} \\ \dot{\theta} \end{bmatrix} = \begin{bmatrix} -0.068 & -0.011 & -0.049 & -9.81 \\ 0.023 & -2.10 & 366 & 0 \\ 0.011 & -0.160 & -9.52 & 0 \\ 0 & 0 & 1 & 0 \end{bmatrix} \begin{bmatrix} u \\ w \\ q \\ \theta \end{bmatrix} + \begin{bmatrix} -0.41 & 1.00 \\ -77.0 & -0.09 \\ -61.0 & -0.11 \\ 0 & 0 \end{bmatrix} \begin{bmatrix} \eta \\ \tau \end{bmatrix} \quad (11.63)$$

Comparison of the open-loop equation (11.58) and the closed-loop equation (11.63) indicates, as expected, that the only changes occur in the third column of the state matrix, the column associated with the variable q . The augmented state equation (11.63) is readily solved to obtain the closed-loop transfer function matrix:

$$\begin{bmatrix} u(s) \\ w(s) \\ q(s) \\ \theta(s) \end{bmatrix} = \mathbf{G}(s) \begin{bmatrix} \eta(s) \\ \tau(s) \end{bmatrix} = \frac{\mathbf{N}(s)}{\Delta_{aug}(s)} \begin{bmatrix} \eta(s) \\ \tau(s) \end{bmatrix} \quad (11.64)$$

where the numerator matrix is given by

$$\mathbf{N}(s) = \begin{bmatrix} -0.41(s + 1.36)(s - 44.45)(s + 45.31) & 1.0(s + 0.027)(s^2 + 11.60s + 79.75) \\ -77.0(s - 0.003)(s + 0.071)(s + 299.3) & -0.09(s + 0.008)(s - 0.044)(s + 456.4) \\ -61.0s(s + 0.068)(s + 1.90) & -0.11s(s - 0.022)(s + 1.96) \\ -61.0(s + 0.068)(s + 1.90) & -0.11(s - 0.022)(s + 1.96) \end{bmatrix} \quad (11.65)$$

and the closed-loop characteristic polynomial is

$$\Delta_{aug}(s) = (s^2 + 11.62s + 78.49)(s^2 + 0.07s + 0.002) \quad (11.66)$$

The corresponding longitudinal stability mode characteristics are

$$\begin{aligned} \text{Phugoid damping ratio } \zeta_p &= 0.71 \\ \text{Phugoid undamped natural frequency } \omega_p &= 0.049 \text{ rad/s} \\ \text{Short-period damping ratio } \zeta_s &= 0.656 \\ \text{Short-period undamped natural frequency } \omega_s &= 8.86 \text{ rad/s} \end{aligned}$$

Thus by simplifying the feedback gain matrix to an approximate equivalent it is not surprising that the specified stability characteristics, defined by [equation \(11.57\)](#), have also been achieved only approximately. However, the differences are small and are quite acceptable. The main objective, to increase the short-period mode damping to a reasonable level, has been achieved comfortably. The changes in the stability characteristics caused by the feedback are in complete agreement with the observations made in Examples 11.3 and 11.4.

Note that the numerators of the closed-loop transfer functions describing response to elevator, given in the first column of the numerator matrix in [equation \(11.65\)](#), are unchanged by the feedback, which is also in accordance with earlier findings concerning the effect of feedback. However, the numerators of the closed-loop transfer functions describing response to thrust, given in the second column of the numerator matrix in [equation \(11.65\)](#), include some changes. The numerators $N_\tau^u(s)$ and $N_\tau^w(s)$ are both changed a little by the effect of feedback, whereas the numerators $N_\tau^q(s)$ and $N_\tau^\theta(s)$ remain unchanged.

It will be noted that the longitudinal stability augmentation for the F-4A could just as easily have been “designed” with the aid of a single-input–single-output root locus plot as described in Example 11.3. However, the subsequent calculation of the closed-loop response transfer functions would have been rather more laborious. The pole placement method is undoubtedly a very powerful design tool, especially for the preliminary assessment of the feedback gains needed to achieve a specified level of closed-loop stability. Once the gains required to achieve a given set of augmented stability characteristics have been determined, their values are not significantly changed by subsequent increases in flight control system complexity.

The main disadvantage of the pole placement method, especially in aircraft applications, is that it assumes that all motion variables are sensed and are available for use in a control system. This is often not the case. If not, it is necessary to simplify the feedback structure, making use of the understanding provided by Examples 11.4 and 11.5, to achieve a reasonable performance compromise—much as illustrated by this example. It is also good practice to minimise the demands on the augmentation system by limiting the required changes to the stability characteristics. Remember that small changes result in small feedback gains, again much as illustrated by this example.

11.8 Command augmentation

It is commonly found that even in augmented aircraft with well-designed flying qualities, pilots report that the handling qualities are less than ideal. The temptation may then be to redesign the feedback control loops in an attempt to rectify the reported shortcomings. However, although this may result in some alleviation of handling qualities deficiencies, the cost may be degradation of the stability and control properties. The cause of this apparent contradiction may, typically, reside in the numerator characteristics of the closed-loop response transfer functions. The stability and control characteristics of the augmented aircraft may be optimum as a result of good inner-loop design, but the transfer function numerator dynamics may adversely shape the response to controls.

The correct approach to rectifying deficiencies in handling qualities is not to redesign the stability augmentation feedback loops, since these have been designed to meet the flying qualities requirements for stability, but to introduce command path augmentation for input signal shaping. A significant advantage of this approach to CSAS design is that the command path filtering does not change the carefully designed closed-loop stability and control characteristics, as illustrated in Section 11.2.

The implementation of a closed-loop control system invariably introduces unwanted response dynamics from sensors, actuators, computer transport delay, high- and low-pass filters, high-order notch filters, and so on. Although all of these system components are designed to have minimal perceived impact on the control task, it is inevitable that pilots are very aware of intrusive response deficiencies arising from such sources. Closed-loop stability properties associated with these components are taken care of in the design of the feedback loop gains, but this leaves the dynamics of the closed-loop transfer function numerators to contend with, and when they are intrusive to the piloting task they can be alleviated by careful command path filter design.

A simple, but very important, example of pitch response shaping by a transfer function numerator term is given in Section 10.2.4 and is termed *incidence lag* because it quantifies the short time lag between pitch attitude response and flight path angle response to control. This appears as a phase advance property in the pitch response of the aircraft; it is governed by the aerodynamic properties of the wing and shapes the initial pitch rate overshoot ratio in response to a control command. When the characteristic is intrusive, it can lead to handling qualities degradation in an otherwise correctly stabilised aircraft, and to conclude that pitch damping is inadequate is an erroneous interpretation of the situation. Fortunately it is easily corrected with a command path compensation filter.

11.8.1 Command path filter design

A typical longitudinal command and stability augmentation system architecture is shown in Fig. 11.29, where it is seen that the command path compensation filter, or *prefilter*, lies outside the stability augmentation loops.

A typical formulation for the pitch control transfer function of the augmented aircraft, omitting control system hardware contributions, is given by equation (6.4), which may be restated as

$$\frac{q(s)}{q'_d(s)} = \frac{k_q s (s + 1/T_{\theta_1}) (s + 1/T_{\theta_2})}{(s^2 + 2\zeta_p \omega_p s + \omega_p^2)(s^2 + 2\zeta_s \omega_s s + \omega_s^2)} \quad (11.67)$$

The coefficients of the transfer function polynomial factors are of course determined by airframe aerodynamics, controller structure, and feedback gains. If, for example, analysis of the closed-loop system response reveals that the numerator factor $(s + 1/T_{\theta_2})$ gives rise to excessive overshoot, its effect can be controlled by designing the prefilter as

$$\frac{q'_d(s)}{q_d(s)} = \frac{T'_{\theta_2}}{T_{\theta_2}} \frac{(s + 1/T'_{\theta_2})}{(s + 1/T_{\theta_2})} \quad (11.68)$$

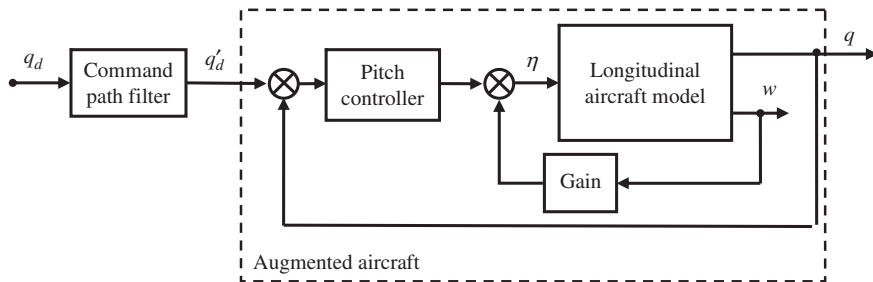


FIGURE 11.29 Augmented aircraft with command path filter.

Thus the command-response transfer function becomes

$$\begin{aligned} \frac{q(s)}{q_d(s)} &= \frac{k_q s (s + 1/T_{\theta_1}) (s + 1/T_{\theta_2})}{(s^2 + 2\zeta_p \omega_p s + \omega_p^2)(s^2 + 2\zeta_s \omega_s s + \omega_s^2)} \frac{T'_{\theta_2}}{T_{\theta_2}} \frac{(s + 1/T'_{\theta_2})}{(s + 1/T_{\theta_2})} \\ &\equiv \frac{k'_q s (s + 1/T_{\theta_1}) (s + 1/T'_{\theta_2})}{(s^2 + 2\zeta_p \omega_p s + \omega_p^2)(s^2 + 2\zeta_s \omega_s s + \omega_s^2)} \end{aligned} \quad (11.69)$$

Equation (11.69) shows that T_{θ_2} has been cancelled out of the transfer function and replaced with a more suitable value denoted T'_{θ_2} ; the transfer function gain k_q becomes

$$k'_q = k_q \frac{T'_{\theta_2}}{T_{\theta_2}} \quad (11.70)$$

which maintains the overall steady-state gain of unity. The prefilter is thus the common lag-lead or lead-lag transfer function, and numerous methods for its design may be used depending on the requirement. However, it is important that its frequency response properties are fully appreciated since the phase shift it introduces can contribute to other handling problems. The following points are especially important.

- When pole-zero cancellation is the objective, as in this illustration, it is quite possible that the cancellation will not be exact because of modelling uncertainty. In this case, it is important to check that the residual visible phase shift does not intrude significantly on the aircraft handling qualities.
- Since the prefilter is in the command path, all closed-loop transfer functions are multiplied by its transfer function, but pole-zero cancellation only occurs in the chosen motion variable response, q and θ . Thus all other response transfer functions are modified by the frequency response properties of the prefilter; again, it is essential to ensure that these effects are not intrusive.

- The design of the replacement transfer function zero $1/T'_{\theta_2}$, the numerator of the prefilter, is simply determined by the *pitch attitude dropback* handling qualities criterion, which leads to the requirement that

$$T'_{\theta_2} = \frac{2\zeta_s}{\omega_s} \quad (11.71)$$

where ζ_s and ω_s are the damping ratio and undamped natural frequency of the short-period mode of the augmented aircraft. A discussion of the underlying flight physics is beyond the scope of this book, but the interested reader will find an explanation in [Gibson \(1999\)](#).

- Alternative approaches to the design of a prefilter are equally valid with or without pole-zero cancellation. In the most general case, the prefilter is treated as a frequency-dependent phase compensation filter and its time constants are designed to introduce the required phase shift at a target frequency. Filter design is reasonably straightforward provided that there is adequate prior analysis of the augmented aircraft response, that the required command compensation is properly determined, and that the frequency response properties of the filter are comprehensively understood. The Bode plot provides a most useful means for filter design and assessment of its likely impact on the overall system.

11.8.2 The frequency response of a phase compensation filter

Let the transfer function for a generic *lead-lag* or *lag-lead* phase compensation filter be written as

$$F(s) = \left(\frac{1 + sT_1}{1 + sT_2} \right) \quad (11.72)$$

The frequency response of $F(s)$ may be derived by writing $s = j\omega$:

$$F(j\omega) = \left(\frac{1 + j\omega T_1}{1 + j\omega T_2} \right)$$

The *gain* G_F is readily calculated in the usual way:

$$G_F = \sqrt{\frac{1 + \omega^2 T_1^2}{1 + \omega^2 T_2^2}} \quad (11.73)$$

The *phase* ϕ_F may also be calculated as follows. Let the numerator phase lead contribution be

$$\tan(\phi_{lead}) = \omega T_1$$

and the denominator phase lag contribution be

$$\tan(\phi_{lag}) = \omega T_2$$

Then total phase shift ϕ_F is given by

$$\begin{aligned}\tan \phi_F &= \tan(\phi_{lead} - \phi_{lag}) = \frac{\tan \phi_{lead} - \tan \phi_{lag}}{1 + \tan \phi_{lead} \tan \phi_{lag}} \\ \tan \phi_F &= \frac{\omega(T_1 - T_2)}{(1 + \omega^2 T_1 T_2)}\end{aligned}\quad (11.74)$$

The maximum phase shift occurs at a frequency between the break frequencies ω_1 and ω_2 , where

$$\omega_1 = \frac{1}{T_1} \quad \text{and} \quad \omega_2 = \frac{1}{T_2}$$

The frequency at which this occurs is given by

$$\frac{d(\tan \phi_F)}{d\omega} = \frac{(T_1 - T_2)(1 - \omega^2 T_1 T_2)}{(1 + \omega^2 T_1 T_2)^2} = 0$$

Thus the frequency at which the maximum, or peak value of, phase shift occurs is readily calculated:

$$(T_1 - T_2)(1 - \omega_{pk}^2 T_1 T_2) = 0 \quad \text{hence} \quad \omega_{pk} = \sqrt{\frac{1}{T_1 T_2}} \quad (11.75)$$

The peak phase shift ϕ_{Fpk} may be determined by substituting the value of ω_{pk} given by equation (11.75) into the expression for phase shift given by equation (11.47); whence

$$\tan \phi_{Fpk} = \frac{(T_1 - T_2)}{2\sqrt{T_1 T_2}} \quad (11.76)$$

The design of a command path compensation filter requires a choice of the peak phase shift and the frequency at which the peak occurs. Gain compensation can usually be adjusted subsequently by means of a series gain function. A useful plot to assist with making the design choice is shown in Fig. 11.30. It shows the phase response of a generic lead-lag transfer function for a range of values T_1/T_2 centred on a frequency of $\omega_{pk} = 1$ rad/s.

Note that when $T_1 > T_2$, the peak phase is positive and a *lead-lag* filter is determined. When $T_2 > T_1$, the peak phase is negative and a *lag-lead* filter is determined; the plots shown in Fig. 11.30 become negative with the same peak magnitude determined by the ratio T_2/T_1 . In this way, the design of the compensation filter is concerned with the selection of suitable values of T_1 and T_2 to satisfy the requirements of equations (11.75) and (11.76).

11.8.3 Introduction of a command path filter to the system state model

To facilitate further mathematical analysis with the command path compensation filter in place, it is convenient to incorporate the filter transfer function into the closed-loop aircraft system state equation. The mathematical process for incorporating a first-order command path filter into an aircraft state model is summarised as follows.

With reference to Fig. 11.29, the command path filter transfer function may be written as

$$\frac{q'_d(s)}{q_d(s)} = \frac{(1 + sT_1)}{(1 + sT_2)} = k \frac{(s + a)}{(s + b)} \quad (11.77)$$

where $k = T_1/T_2$, $a = 1/T_1$, and $b = 1/T_2$, and the closed-loop state equation of the augmented aircraft may be written as

$$\dot{\mathbf{x}} = \mathbf{Ax} + \mathbf{B}q'_d \quad (11.78)$$

From [equation \(11.77\)](#),

$$s(q'_d(s) - kq_d(s)) = kaq_d(s) - bq'_d(s) \quad (11.79)$$

Define an additional “dummy” state variable,

$$v(s) = (q'_d(s) - kq_d(s)) \quad (11.80)$$

whence [equation \(11.79\)](#) may be written as

$$sv(s) = kaq_d(s) - bq'_d(s) \quad (11.81)$$

Assuming zero initial conditions, the time domain equivalent of [equation \(11.81\)](#) may be written as

$$v(t) = kaq_d(t) - bq'_d(t) \quad (11.82)$$

and similarly, from [equation \(11.80\)](#),

$$v(t) = q'_d(t) - q_d(t) \quad (11.83)$$

Eliminate $q'_d(t)$ from [equations \(11.82\) and \(11.83\)](#) to obtain the filter state equation,

$$\dot{v}(t) = -bv(t) + k(a - b)q_d(t) \quad (11.84)$$

Finally, eliminate $q'_d(t)$ from [equation \(11.78\)](#) by substitution from [equation \(11.83\)](#) and augment the resulting equation with [equation \(11.84\)](#) to obtain the full system state equation:

$$\begin{bmatrix} \dot{\mathbf{x}} \\ \dot{v} \end{bmatrix} = \begin{bmatrix} \mathbf{A} & \mathbf{B} \\ \mathbf{0} & -b \end{bmatrix} \begin{bmatrix} \mathbf{x} \\ v \end{bmatrix} + k \begin{bmatrix} \mathbf{B} \\ (a - b) \end{bmatrix} q_d \quad (11.85)$$

or, equivalently, in terms of the filter time constants,

$$\begin{bmatrix} \dot{\mathbf{x}} \\ \dot{v} \end{bmatrix} = \begin{bmatrix} \mathbf{A} & \mathbf{B} \\ \mathbf{0} & -1/T_2 \end{bmatrix} \begin{bmatrix} \mathbf{x} \\ v \end{bmatrix} + \frac{T_1}{T_2} \begin{bmatrix} \mathbf{B} \\ (1/T_1 - 1/T_2) \end{bmatrix} q_d \quad (11.86)$$

Note that the zero coefficient in the second row of the state matrix is a row matrix with the same number of zero coefficients as order \mathbf{A} .

The solution of [equation \(11.85\)](#) or [equation \(11.86\)](#) simply gives the closed-loop aircraft transfer functions obtained in the solution of [equation \(11.78\)](#) multiplied by the command path filter transfer function, which should be clearly visible. The previous mathematical procedure can of course be used with a command path prefilter of any order.

EXAMPLE 11.7

With reference to the augmented aircraft control system structure shown in [Fig. 11.29](#), the longitudinal state equation for an augmented civil transport aircraft in a cruise flight condition is given by

$$\begin{bmatrix} \dot{u} \\ \dot{\alpha} \\ \dot{q} \\ \dot{\theta} \\ \dot{\eta} \end{bmatrix} = \begin{bmatrix} -0.0141 & 1.0877 & 0 & -9.81 & 0 \\ -2.94e-4 & -0.811 & 1 & 0 & -0.0422 \\ 8.12e-4 & 0.3575 & -1.171 & 0 & -3.75 \\ 0 & 0 & 1 & 0 & 0 \\ 0 & 22.6 & 9 & 0 & -10 \end{bmatrix} \begin{bmatrix} u \\ \alpha \\ q \\ \theta \\ \eta \end{bmatrix} + (-3.9417) \begin{bmatrix} 0 \\ 0 \\ 0 \\ 0 \\ 10 \end{bmatrix} q'_d \quad (11.87)$$

The model includes the elevator actuator, which has a 0.1 s time constant. Note that the input matrix is multiplied by the gain -3.9417 to adjust the short-term steady-state gain ratio q/q'_d to approximately unity, simply to facilitate response comparison in this example. The solution of equation (11.87) gives the closed-loop transfer functions:

$$\begin{aligned} \frac{u(s)}{q'_d(s)} &= \frac{1.835(s + 0.917)(s - 711.8)}{(s^2 + 0.0137s + 0.00257)(s^2 + 0.579s + 19.263)(s + 6.192)} \text{ m/s/rad/s} \\ \frac{\alpha(s)}{q'_d(s)} &= \frac{1.687(s^2 + 0.141s + 0.00294)(s + 89.97)}{(s^2 + 0.0137s + 0.00257)(s^2 + 0.579s + 19.263)(s + 6.192)} \text{ rad/rad/s} \\ \frac{q(s)}{q'_d(s)} &= \frac{149.8s(s + 0.0145)(s + 0.8146)}{(s^2 + 0.0137s + 0.00257)(s^2 + 0.579s + 19.263)(s + 6.192)} \\ \frac{\theta(s)}{q'_d(s)} &= \frac{149.8(s + 0.0145)(s + 0.8146)}{(s^2 + 0.0137s + 0.00257)(s^2 + 0.579s + 19.263)(s + 6.192)} \text{ rad/rad/s} \\ \frac{\eta(s)}{q'_d(s)} &= \frac{-39.417(s^2 - 0.00287s + 0.0088)(s + 0.3817)(s + 1.617)}{(s^2 + 0.0137s + 0.00257)(s^2 + 0.579s + 19.263)(s + 6.192)} \text{ rad/rad/s} \end{aligned} \quad (11.88)$$

Inspection of the closed-loop characteristic polynomial in equations (11.88) gives the following stability properties:

Phugoid mode damping and frequency $\zeta_p = 0.135\omega_p = 0.05 \text{ rad/s}$

Short-period mode damping and frequency $\zeta_s = 0.66\omega_s = 4.39 \text{ rad/s}$

Closed-loop actuator mode time constant $T_a = 1/6.192 = 0.16 \text{ s}$

These characteristics are adequate for Level 1 flying qualities. However, it is important to be aware of the effect of loop closure on the actuator mode *lag* time constant, which is increased from the open-loop value of 0.1 s to a value of 0.16 s. Since this change is small it is unlikely to give rise to handling problems although, in general, any increase in closed loop lag is undesirable, but it is the inevitable consequence of closing a feedback loop around the actuator.

As mentioned in Section 11.8.1, the incidence lag time constant is also of significance in determining longitudinal handling qualities. With reference to the pitch response transfer functions in equations (11.88), its value is given by

$$T_{\theta_2} = 1/0.8146 = 1.23 \text{ s}$$

The short term pitch response of the aircraft to a unit pitch rate pulse demand of 5 s duration is shown as the solid line in Fig. 11.30. In terms of flying qualities requirements, the response indicates a well-damped second-order-like characteristic which is entirely satisfactory. However,

from the point of view of pitch-tracking handling qualities, Gibson (1999) states that the initial pitch rate overshoot and the corresponding pitch attitude dropback are excessive. The cause of the problem is the *phase lead* introduced by the numerator zero $(s + 1/T_{\theta_2}) = (s + 0.8146)$ in the pitch response transfer functions, [equations \(11.88\)](#). The problem is easily resolved if, in accordance with [equation \(11.71\)](#),

$$T'_{\theta_2} = \frac{2\zeta_s}{\omega_s} = \frac{1.32}{4.39} = 0.3 \text{ s} \quad (11.89)$$

and a suitable prefilter is determined as defined by [equation \(11.68\)](#):

$$\frac{q'_d(s)}{q_d(s)} = \frac{T'_{\theta_2}}{T_{\theta_2}} \frac{(s + 1/T'_{\theta_2})}{(s + 1/T_{\theta_2})} = 0.2444 \frac{(s + 3.33)}{(s + 0.8146)} \quad (11.90)$$

When it is included in the command path, the modified response characteristics are shown for comparison in [Fig. 11.30](#). According to Gibson (1999), the optimum pitch attitude dropback should be approximately zero, at which condition the short-term pitch attitude response is *k/s-like*, which is another way of saying that the aircraft response is like that of an integrator. This is clearly the case here, as indicated by the dashed line in the pitch attitude response plot in the figure.

The prefilter transfer function, [equation \(11.90\)](#), is a *lag-lead* filter; using [equations \(11.75\)](#) and [\(11.76\)](#) its properties are easily determined:

$$T_1 = 0.3 \text{ s} \quad T_2 = 1.23 \text{ s} \quad \omega_{pk} = 1.646 \text{ rad/s} \quad \phi_{pk} = -37.42 \text{ deg}$$

The filter phase lag cancels, or compensates for, the unwanted phase lead due to the action of the $(s + 1/T_{\theta_2})$ zero in the closed-loop aircraft pitch response transfer functions. Note that its peak

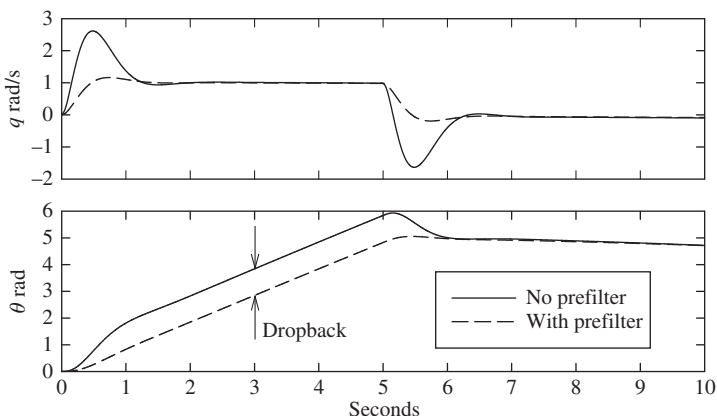


FIGURE 11.30 Pitch response to a 5-sec unit pulse pitch rate demand.

effect occurs at a frequency a little lower than the short-period mode frequency—that part of the frequency response spectrum of greatest significance to the handling dynamics of the aircraft.

The closed-loop system state equation (11.87) may be further augmented to include the command path filter, as illustrated by equation (11.86):

$$\begin{bmatrix} \dot{u} \\ \dot{\alpha} \\ \dot{q} \\ \dot{\theta} \\ \dot{\eta} \\ \dot{v} \end{bmatrix} = \begin{bmatrix} -0.0141 & 1.0877 & 0 & -9.81 & 0 & 0 \\ -2.94e-4 & -0.811 & 1 & 0 & -0.0422 & 0 \\ 8.12e-4 & 0.3575 & -1.171 & 0 & -3.75 & 0 \\ 0 & 0 & 1 & 0 & 0 & 0 \\ 0 & 22.6 & 9 & 0 & -10 & 10 \\ 0 & 0 & 0 & 0 & 0 & -0.8146 \end{bmatrix} \begin{bmatrix} u \\ \alpha \\ q \\ \theta \\ \eta \\ v \end{bmatrix} + (-0.96) \begin{bmatrix} 0 \\ 0 \\ 0 \\ 0 \\ 10 \\ 2.5154 \end{bmatrix} q_d \quad (11.91)$$

Solution of equation (11.91) gives the compensated response transfer functions as follows:

$$\begin{aligned} \frac{u(s)}{q_d(s)} &= \frac{0.441(s + 0.917)(s + 3.33)(s - 711.8)}{(s^2 + 0.0137s + 0.00257)(s + 0.8146)(s^2 + 0.579s + 19.263)(s + 6.192)} \text{ m/s/rad/s} \\ \frac{\alpha(s)}{q_d(s)} &= \frac{0.4055(s^2 + 0.141s + 0.00294)(s + 3.33)(s + 89.97)}{(s^2 + 0.0137s + 0.00257)(s + 0.8146)(s^2 + 0.579s + 19.263)(s + 6.192)} \text{ rad/rad/s} \\ \frac{q(s)}{q_d(s)} &= \frac{36s(s + 0.0145)(s + 0.8146)(s + 3.33)}{(s^2 + 0.0137s + 0.00257)(s + 0.8146)(s^2 + 0.579s + 19.263)(s + 6.192)} \\ \frac{\theta(s)}{q_d(s)} &= \frac{36(s + 0.0145)(s + 0.8146)(s + 3.33)}{(s^2 + 0.0137s + 0.00257)(s + 0.8146)(s^2 + 0.579s + 19.263)(s + 6.192)} \text{ rad/rad/s} \\ \frac{\eta(s)}{q_d(s)} &= \frac{-9.6(s^2 - 0.00287s + 0.0088)(s + 0.3817)(s + 1.617)(s + 3.33)}{(s^2 + 0.0137s + 0.00257)(s + 0.8146)(s^2 + 0.579s + 19.263)(s + 6.192)} \text{ rad/rad/s} \end{aligned} \quad (11.92)$$

Observe that transfer functions (11.92) are the same as transfer functions (11.88) multiplied by the command path filter transfer function. Note that pole-zero cancellation occurs only in the pitch attitude θ and pitch rate q transfer functions, and that these variables demonstrate the desired response dynamics as shown in Fig. 11.30. All other variables demonstrate the additional lag in their responses due to the filter. It is important to be aware of this fact and to ensure that the lag does not compromise the aircraft flying qualities in some other way.

EXAMPLE 11.8

An alternative illustration of command path filtering is given by the design of a simple automatic speed controller, or autothrottle, for a small unmanned aerial vehicle (UAV). The system architecture is shown in Fig. 11.31; note that the throttle actuator is omitted for simplicity. The gas turbine engine is represented by a first-order lag with time constant 0.334 s and the loop gain is $K_u = 0.2 \text{ N/m/s}$.

The closed-loop system state equation is given by

$$\begin{bmatrix} \dot{u} \\ \dot{w} \\ \dot{q} \\ \dot{\theta} \\ \dot{\tau} \end{bmatrix} = \begin{bmatrix} -0.0324 & 0.1375 & -2.2382 & -9.7972 & 2.5267 \\ -0.252 & -3.7906 & 44.4781 & -0.5006 & 0 \\ 0.0291 & -0.7668 & 0.2658 & -0.0132 & -0.1134 \\ 0 & 0 & 1 & 0 & 0 \\ -0.5988 & 0 & 0 & 0 & -2.994 \end{bmatrix} \begin{bmatrix} u \\ w \\ q \\ \theta \\ \tau \end{bmatrix} + \begin{bmatrix} 0 \\ 0 \\ 0 \\ 0 \\ 0.5988 \end{bmatrix} \delta_u \quad (11.93)$$

The solution of this equation gives the closed-loop system transfer functions from which the speed u response to demand δ_u transfer function is selected:

$$\frac{u(s)}{\delta_u(s)} = \frac{1.513(s + 0.03762)(s^2 + 4.12s + 35.52)^*}{(s^2 + 0.675s + 0.132)(s + 2.358)(s^2 + 4.05s + 35.106)^*} \quad (11.94)$$

Inspection of the characteristic polynomial in equation (11.94) shows the closed-loop modes, comprising the phugoid, the engine lag, and the short-period mode, all of which are stable. Note also that the short-period mode dynamics are effectively cancelled by the second-order numerator term because the short-period mode is quasi-steady in the time scale of the speed response of the aircraft. (indicated by *) Therefore, to a good approximation, equation (11.94) may be written as

$$\frac{u(s)}{\delta_u(s)} = \frac{1.513(s + 0.03762)}{(s^2 + 0.675s + 0.132)(s + 2.358)} \quad (11.95)$$

Thus, the essential dynamics governing the speed response properties of the control system are clearly and adequately defined. The corresponding response to a unit step demand is shown in Fig. 11.32.

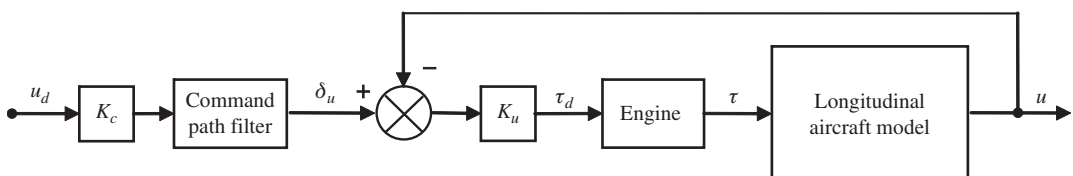


FIGURE 11.31 Automatic speed control system.

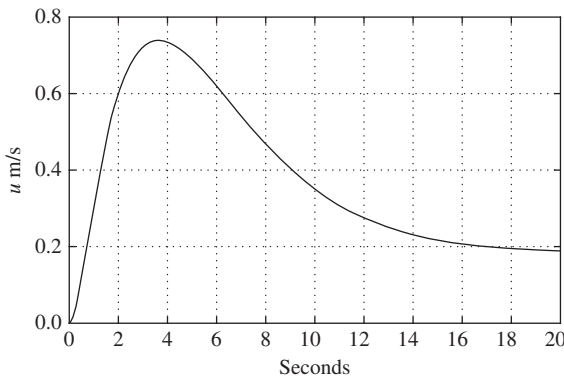


FIGURE 11.32 Speed response to a unit step demand.

Clearly, the response to a unit input is not very satisfactory, as it takes nearly 20 s to settle to a nominally steady state and the initial overshoot appears to be excessive. Also, the steady-state gain of the system is 0.1854 rather than 1.0, but this is easily adjusted with the command path gain K_c . However, the system stability is entirely satisfactory. With reference to equation (11.95), the phugoid mode is nearly critically damped—a consequence of effective velocity damping by means of the feedback loop—so the large overshoot must be caused by the phase lead introduced by the low-frequency zero ($s + 0.03762$). The closed-loop engine mode time constant is sufficiently small not to cause excessive visible lag in the response.

A lag-lead command path filter can be designed to alleviate the unwanted response dynamics without upsetting the closed-loop stability of the system. Let the filter be denoted

$$F(s) = \frac{T_1(s + 1/T_1)}{T_2(s + 1/T_2)} \quad (11.96)$$

The excessive low-frequency phase lead can be “removed” by setting $T_2 = 1/0.03762 \cong 27$ s, which cancels the low-frequency zero in the closed-loop transfer function (11.95). The choice of T_1 then provides a means for tuning the response shape to give improved performance. The design problem is to find a value for the filter peak phase frequency ω_{pk} to minimise the system response overshoot and settling time. A possible solution would, of course, be to set $T_1 = 0$ and write $F(s)$ as a simple lag transfer function. However, the inclusion of $(s + 1/T_1)$ introduces phase lead, which provides considerable flexibility for tailoring the response shape. It is helpful to sketch Bode gain and phase plots to assist with the initial design choice of the value for T_1 .

Once the excessive lead in equation (11.95) introduced by the low-frequency zero ($s + 0.03762$) is “removed” by cancellation, the remaining visible response dynamics are shaped by the dominant and heavily damped phugoid mode. Thus, in order for $F(s)$ to have some useful

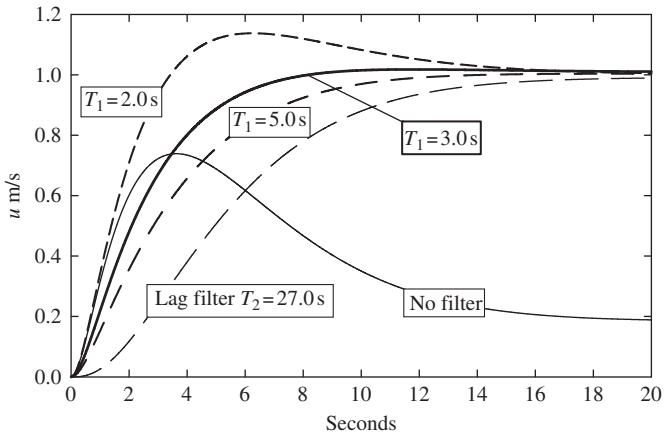


FIGURE 11.33 Effect of a command path filter on speed response.

impact on response, it seems appropriate to choose a break frequency $1/T_1$ in the vicinity of the phugoid frequency. This places the filter peak phase frequency ω_{pk} a little lower than the phugoid natural frequency. Accordingly, the effect of several values of T_1 on the response of the system to a unit input are evaluated as shown in Fig. 11.33.

Selecting the command path gain $K_c = 1/0.1854 = 5.39$, the steady-state response to a unit step input is adjusted to 1.0, as shown in the figure. When the command path filter is limited to a simple lag, the response exhibits significant lag due to the phugoid dynamics as discussed previously. It is clear that if, as an alternative, a lag-lead filter is specified, the effect of phase lead can be used to optimise the response quite readily as shown. A design choice of $T_1 = 3$ s results in an ideal response, with minimal overshoot which settles to the steady state in approximately 8 s.

Thus the command path control law may be written as

$$\delta_u = K_c \left(\frac{1 + T_1 s}{1 + T_2 s} \right) u_d = 5.39 \left(\frac{1 + 3s}{1 + 27s} \right) u_d \equiv 0.6 \left(\frac{s + 0.33}{s + 0.037} \right) u_d \quad (11.97)$$

and the filter properties are determined from equations (11.75) and (11.76):

$$\omega_{pk} = \sqrt{\frac{1}{T_1 T_2}} = 0.11 \text{ rad/s} \quad (11.98)$$

$$\begin{aligned} \tan \phi_{Fpk} &= \frac{(T_1 - T_2)}{2\sqrt{T_1 T_2}} = -1.32 \\ \therefore \phi_{Fpk} &= -52.85 \text{ deg} \end{aligned} \quad (11.99)$$

The closed-loop state [equation \(11.93\)](#) may be augmented to include the control law (11.97), as described in [Section 11.8.3](#), to give

$$\begin{bmatrix} \dot{u} \\ \dot{w} \\ \dot{q} \\ \dot{\theta} \\ \dot{\tau} \\ \dot{v} \end{bmatrix} = \begin{bmatrix} -0.0324 & 0.1375 & -2.2382 & -9.7972 & 2.5267 & 0 \\ -0.252 & -3.7906 & 44.4781 & -0.5006 & 0 & 0 \\ 0.0291 & -0.7668 & 0.2658 & -0.0132 & -0.1134 & 0 \\ 0 & 0 & 1 & 0 & 0 & 0 \\ -0.5988 & 0 & 0 & 0 & -2.994 & 0.5988 \\ 0 & 0 & 0 & 0 & 0 & -0.037 \end{bmatrix} \begin{bmatrix} u \\ w \\ q \\ \theta \\ \tau \\ v \end{bmatrix} + \begin{bmatrix} 0 \\ 0 \\ 0 \\ 0 \\ 0.3653 \\ 0.1787 \end{bmatrix} u_d \quad (11.100)$$

Solution of this equation gives the response transfer functions for the completed control system as follows:

$$\begin{aligned} \frac{u(s)}{u_d(s)} &= \frac{0.9229(s+0.03762)^*(s+0.33)(s^2+4.12s+35.52)^*}{(s+0.037)^*(s^2+0.675s+0.132)(s+2.358)(s^2+4.05s+35.106)^*} \\ \frac{w(s)}{u_d(s)} &= \frac{-2.075(s-0.1599)(s+0.33)(s-0.356)}{(s+0.037)(s^2+0.675s+0.132)(s+2.358)(s^2+4.05s+35.106)} \\ \frac{q(s)}{u_d(s)} &= \frac{-0.04142s(s+0.33)(s-1.434)(s+4.608)}{(s+0.037)(s^2+0.675s+0.132)(s+2.358)(s^2+4.05s+35.106)} \text{ rad/s} \\ \frac{\theta(s)}{u_d(s)} &= \frac{-0.04142(s+0.33)(s-1.434)(s+4.608)}{(s+0.037)(s^2+0.675s+0.132)(s+2.358)(s^2+4.05s+35.106)} \text{ rad} \\ \frac{\tau(s)}{u_d(s)} &= \frac{0.3653(s^2+0.0358s+0.0844)(s+0.33)(s^2+4.053s+35.13)^*}{(s+0.037)(s^2+0.675s+0.132)(s+2.358)(s^2+4.05s+35.106)^*} \text{ N} \end{aligned} \quad (11.101)$$

where (*) indicates pole-zero cancellation. The approximate speed control dynamics are thus described by the following transfer function:

$$\frac{u(s)}{u_d(s)} = \frac{0.9229(s+0.33)}{(s^2+0.675s+0.132)(s+2.358)} \quad (11.102)$$

As in Example 11.7, it is important to be aware that the command path filter premultiplies all response transfer functions, as shown in [equations \(11.101\)](#), but pole-zero cancellation occurs only in the speed response transfer function and in the thrust response transfer function. All of the remaining response variables demonstrate an additional phase lag of -52.85 deg, and the effect of this on other aspects of vehicle control and response should be assessed to ensure overall compatibility. It is also important to assess the thrust response to speed demand transfer function τ/u_d to ensure that the thrust dynamics remain within the capability of the engine.

References

- Department of Defense (1980). *Military specification: Flying qualities of piloted airplanes*. Washington, DC: Department of Defense, MIL-F-8785C.
- Evans, W. R. (1954). *Control system dynamics*. New York: McGraw-Hill.
- Friedland, B. (1987). *Control system design*. New York: McGraw-Hill.
- Gibson, J. C. (1999). *Development of a methodology for excellence in handling qualities for fly by wire aircraft*. Ph.D diss. Delft, The Netherlands: Delft University of Technology.
- Heffley, R. K., & Jewell, W. F. (1972). *Aircraft handling qualities data*. Washington, DC: National Aeronautics and Space Administration, NASA Contractor Report, NASA CR-2144.
- Teper, G. L. (1969). *Aircraft stability and control data*. Hawthorne, CA: Systems Technology, Inc., STI Technical Report 176-1.

PROBLEMS

- 11.1** Discuss and illustrate why, in a simple stability augmentation system, is it sometimes necessary to vary the feedback gain with flight condition.
(CU 1986)
- 11.2** The damping of the longitudinal short-period mode may be augmented with pitch rate feedback to elevator.
- Write the reduced-order longitudinal equations of motion in matrix form to include the feedback term. It may be assumed that the derivative Z_q is negligibly small.
 - From the closed-loop equations of motion, obtain an expression for the characteristic equation and thus show that when the derivative $M_{\dot{w}}$ is assumed to be negligibly small, the value of feedback gain K_q required to double the damping ratio of the short-period mode is given by
- $$K_q = - \left(\frac{I_y}{m} \frac{\ddot{Z}_w}{\dot{M}_{\eta}} + \frac{\ddot{M}_q}{\dot{M}_{\eta}} \right)$$
- (c)** Using the following aerodynamic data for the Republic F-105 Thunderchief aircraft, calculate a value of K_q and comment on the practicality of using such a value.
(CU 1986)

Flight Condition			Dimensionless Derivatives			
Altitude	h	35,000 ft	X_u	-0.0599	M_u	0
Flight path angle	γ	0 deg	X_w	0.0714	M_w	-0.8021
Body incidence	α_e	0 deg	X_q	0	$M_{\dot{w}}$	-0.8718
Airspeed	V_0	270 m/s	X_{η}	0	M_q	-4.1303
Mass	m	18,680 kg	Z_u	-0.1427	M_{η}	-1.365
Pitch inertia	I_y	189,812 kgm ²	Z_w	-4.1188		
Air density	ρ	0.3798 kg/m ³	Z_q	0		
Wing area	S	36.45 m ²	Z_{η}	-0.7672		
mac	\bar{c}	3.54 m				

- 11.3** The open-loop yaw rate response to rudder transfer function for the Republic F-105 Thunderchief flying at Mach 0.9 at an altitude of 35,000 ft is given by

$$\frac{r(s)}{\zeta(s)} = \frac{-4.71(s + 1.848)(s^2 + 0.053s + 0.067)}{(s - 0.0087)(s + 2.13)(s^2 + 1.211s + 10.82)} \text{ 1/s}$$

Draw a root locus plot to show the effect of yaw rate feedback to rudder with feedback gain K_r .

- (a) With the aid of the root locus plot, explain how it may be used to evaluate the effect of feedback on the characteristics modes of motion.
- (b) How does yaw rate feedback to rudder improve lateral-directional flying qualities?
- (c) What value of gain K_r is required to increase the dutch roll mode damping ratio to 0.25? For this value of K_r , obtain values for the roots of the closed-loop characteristic equation and compare the characteristics of the three modes with those of the unaugmented aircraft.

(CU 1986)

- 11.4** Assuming that the lateral response to aileron control comprises pure rolling motion only, derive the reduced-order roll rate response to aileron control transfer function for an aircraft.

- (a) When the lateral stability of the aircraft is augmented by feeding back roll rate to aileron via the gain K_p , show that the augmented roll damping derivative is given by

$$\overset{\circ}{L_{p_{\text{aug}}}} = \overset{\circ}{L_p} - K_p \overset{\circ}{L_\xi}$$

where $\overset{\circ}{L_p}$ is the rolling moment due to roll rate and $\overset{\circ}{L_\xi}$ is the rolling moment due to aileron for the unaugmented aircraft.

- (b) Using the simple lateral model, assess the roll subsidence mode of the Northrop T-38 Talon aircraft. Data for the aircraft are tabulated in the following table. What is the minimum value of K_p for which the aircraft will meet the flying qualities requirements?

Flight Condition		Dimensionless Derivatives				
Altitude	h	25,000 ft	Y_v	-1.260	N_v	0.240
Flight path angle	γ	0 deg	Y_p	0	N_p	0.0430
Body incidence	α_e	0 deg	Y_r	0	N_r	-0.170
Airspeed	V_0	123.7 m/s	Y_ξ	0	N_ξ	0.007
Mass	m	4540 kg	Y_ζ	0.160	N_ζ	-0.103
Roll inertia	I_x	5965 kgm^2				
Yaw inertia	I_z	46097 kgm^2	L_v	-0.097		
Inertia product	I_{xz}	0 kgm^2	L_p	-0.110		
Air density	ρ	0.549 kg/m^3	L_r	0.078		
Wing area	S	15.79 m^2	L_ξ	0.040		
Wing span	b	7.69 m	L_ζ	0.017		

(CU 1987)

- 11.5** Longitudinal flight condition and aerodynamic derivative data are given in the following table for a canard-configured fly-by-wire combat aircraft.

Flight Condition			Dimensionless Derivatives			
Altitude	h	Sea level	X_u	0.050	M_u	0.003
Flight path angle	γ	0 deg	X_w	0.260	M_w	0.280
Body incidence	α_e	0 deg	X_q	0	$M_{\dot{w}}$	0.380
Airspeed	V_0	100 m/s	X_η	0	M_q	-0.500
Mass	m	12,500 kg	Z_u	-1.200	M_η	0.160
Pitch inertia	I_y	105,592 kgm ²	Z_w	-2.800		
Air density	ρ	1.225 kg/m ³	$Z_{\dot{w}}$	-0.700		
Wing area	S	50.0 m ²	Z_q	-1.200		
<i>mac</i>	\bar{c}	5.7 m	Z_η	-0.040		

- (a) Write down the reduced-order longitudinal equations of motion appropriate to the aircraft and thus show that the short-period mode characteristic equation is given approximately in terms of concise derivatives by

$$s^2 - (z_w + m_q + m_{\dot{w}}U_e)s - (m_wU_e - z_wm_q) = 0$$

State all assumptions made.

- (b) Since the aircraft is unstable, it is augmented with a control law of form

$$\eta = \delta_\eta - K_q q - K_\alpha \alpha$$

What values of the feedback gains K_q and K_α are required to produce an augmented short-period mode with natural frequency 5 rad/s and damping ratio 0.5?

(CU 1989)

- 11.6** Explain why the dutch roll mode characteristics are often unacceptable in large civil transport aircraft.

- (a) The yaw control transfer function for a large civil transport aircraft cruising at 33,000 ft is given by

$$\frac{N_\zeta^r(s)}{\Delta(s)} = \frac{-1.17(s + 1.28)(s^2 - 0.04s + 0.10)}{(s + 0.004)(s + 1.25)(s^2 + 0.20s + 2.25)} \text{ 1/s}$$

Evaluate the stability modes characteristics and assess these for Level 1 flying qualities.

- (b) The aircraft is fitted with a yaw damper to improve the dutch roll characteristics. Draw a root locus plot showing the effect of yaw rate feedback to rudder via gain K_r . Draw mode limit boundaries on the root locus plot corresponding with Level 1 flying qualities

and suggest a suitable value for K_r . Evaluate all three modes for the chosen value of feedback gain and comment on the comparison with those of the unaugmented aircraft.
(CU 1989)

- 11.7** Explain why the stability characteristics of the short-term stability modes are critical to good flying qualities. Explain and illustrate how they may be augmented when those of the basic airframe are inadequate.

(CU 2001)

Aerodynamic Modelling

12

12.1 Introduction

Probably the most difficult task confronting the flight dynamicist is the identification and quantification of the aerodynamic description of the aeroplane for use in the equations of motion. *Aerodynamic modelling* is concerned with the development of mathematical models to describe the aerodynamic forces and moments acting on the airframe. As the flow conditions around the airframe are generally complex, any attempt to describe the aerodynamic phenomena mathematically must result in compromise. Obviously, the most desirable objective is the most accurate mathematical description of the airframe aerodynamics as can possibly be devised. Unfortunately, even if accurate mathematical models can be devised, they are often difficult to handle in an analytical context and do not, in general, lend themselves to application to the linearised equations of motion.

The solution to the problem is to seek simpler approximate aerodynamic models which can be used in the equations of motion and which represent the aerodynamic properties of the airframe with acceptable accuracy. A consequence of this is that the aerodynamic models are only valid for a small range of operating conditions; therefore, the solution of the equations of motion is also valid only for the same limited range of conditions. By repeating this procedure at many points in the flight envelope of the aeroplane, an acceptable “picture” of its dynamic properties can be built up, subject of course to the limitations of the modelling techniques used.

In the present context, *aerodynamic stability and control derivatives* are used to model the aerodynamic properties of the aeroplane. The concept of the aerodynamic derivative as a means for describing aerodynamic force and moment characteristics is introduced and described in Chapter 4 (Section 4.2). The use of the aerodynamic derivative as a means for explaining the dependence of the more important dynamic characteristics of the aeroplane on its dominant aerodynamic properties is discussed in Chapters 6 and 7. In the illustrations, only those derivatives associated with the dominant aerodynamic effects are discussed. Clearly, if the most important aerodynamic properties ascribed to every derivative are known, a more subtle and expansive interpretation of aircraft dynamics may be made in the analysis of the response transfer functions. Thus, a good understanding of the origin, meaning, and limitation of the aerodynamic derivatives provides the means by which the flight dynamicist may achieve very considerable insight into the subtleties of aircraft dynamics and into flying and handling qualities. In the author’s opinion, this knowledge is also essential for the designer of stability augmentation systems for the reasons illustrated in Chapter 11.

This chapter is concerned with a preliminary review of, and introduction to, aerodynamic stability and control derivatives at the simplest level consistent with the foregoing material.

However, it must be remembered that alternative methods for aerodynamic modelling are commonly in use when rather greater detail is required in the equations of motion. For example, in continuous simulation models, the equations of motion may well be non-linear and the aerodynamic models are correspondingly rather more complex. Today, it is common practice to investigate analytically the dynamic behaviour of combat aircraft at very high angles of incidence, conditions which may be grossly non-linear and for which the aerodynamic derivative would be incapable of providing an adequate description of the aerodynamics. For such applications experimental or semi-empirical sources of aerodynamic information are more appropriate.

Whatever the source of the aerodynamic models, simple or complex, the best that can be achieved is an *estimate* of the aerodynamic properties. This immediately prompts the question, *how good is the estimate?* This question is not easy to answer and depends ultimately on the confidence in the aerodynamic modelling process and the fidelity of the aircraft dynamics derived from the aerodynamic model.

12.2 Quasi-static derivatives

To appreciate the “meaning” of the aerodynamic derivative, consider, for example, the derivative which quantifies *normal force due to rate of pitch*, denoted

$$\overset{\circ}{Z}_q = \frac{\partial Z}{\partial q} \quad (12.1)$$

The component of normal force experienced by the aircraft resulting from a pitch velocity perturbation is therefore given by

$$Z = \overset{\circ}{Z}_q q \quad (12.2)$$

Now, in general, the disturbance giving rise to the pitch rate perturbation also includes perturbations in the other motion variables, which give rise to additional components of normal force as indicated by the appropriate terms in the aerodynamic normal force model in equations (4.37). However, when considering the derivative $\overset{\circ}{Z}_q$ it is usual to consider its effect in isolation, as if the perturbation comprised only pitch rate. Similarly, the effects of all the other derivatives are considered in isolation by assuming the perturbation to comprise only the motion appropriate to the derivative in question.

By definition, the equations of motion, equations (4.37), in which the derivatives appear describe small perturbation motion about a steady trimmed equilibrium flight condition. Thus, for example, in the undisturbed state the component of normal force Z given by equation (12.2) is zero since the perturbation variable q is zero. Similarly, all aerodynamic force and moment components in all small perturbation equations of motion are zero at the trim condition. The point of this perhaps obvious statement is to emphasise that, in the present context, the aerodynamic derivatives only play a part in determining the motion of the aeroplane when it is in a state of “dynamic upset” with respect to its initial trim condition. As described in earlier chapters, the state of dynamic upset is referred to equivalently as a perturbation about the equilibrium condition, and it is usually transient. Thus, to be strictly applicable to the dynamic conditions they describe, the derivatives

should be expressed in terms of the non-steady aerodynamic conditions they attempt to quantify. Clearly a difficult demand!

Since the motion of interest is limited, by definition, to small perturbations about equilibrium then, in the limit, the perturbations tend to zero and the dynamic condition becomes coincident with the equilibrium flight condition. It is therefore common practice to evaluate the aerodynamic derivatives at the steady equilibrium condition and to assume that they are applicable to the small perturbation motion about that equilibrium. This procedure gives rise to the so-called *quasi-static aerodynamic derivatives*—quantities based on, and derived from, static aerodynamic conditions but used in the description of dynamically varying aerodynamic conditions. Aerodynamic derivatives obtained by this means seem to be quite adequate for studies of small perturbation dynamics but, not surprisingly, become increasingly inappropriate as the magnitude of the perturbation is increased. As suggested previously, studies of large amplitude dynamics require rather more sophisticated methods of aerodynamic modelling.

To illustrate the concept of the quasi-static derivative, consider the contribution of aerodynamic drag D to the axial force X acting on the aircraft in a disturbance. Assuming that the aircraft axes are wind axes, then

$$X = -D \quad (12.3)$$

A typical plot of aerodynamic drag against velocity is shown in Fig. 12.1. Let the steady equilibrium velocity be V_0 at the flight condition of interest which defines the operating point p on the plot. Now let the aeroplane be subjected to a disturbance giving rise to a small velocity perturbation $\pm u$ about the operating point as indicated. The derivative *axial force due to velocity* is defined as

$$\dot{X}_u = \frac{\partial X}{\partial U} \equiv \frac{\partial X}{\partial V} \quad (12.4)$$

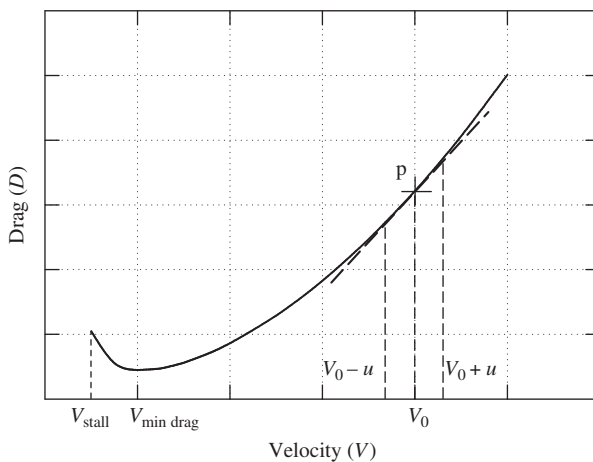


FIGURE 12.1 Typical aerodynamic drag-velocity characteristic.

where the total perturbation velocity component along the x axis is given by

$$U = U_e + u \equiv V_0 + u \equiv V \quad (12.5)$$

Whence

$$\dot{X}_u = -\frac{\partial D}{\partial V} \quad (12.6)$$

and the slope of the drag-velocity plot at p gives the quasi-static value of the derivative \dot{X}_u at the flight condition corresponding with the trimmed velocity V_0 . Some further simple analysis is possible since the drag is given by

$$D = \frac{1}{2}\rho V^2 S C_D \quad (12.7)$$

Assuming the air density ρ remains constant, since the perturbation is small, then

$$\frac{\partial D}{\partial V} = \frac{1}{2}\rho V S \left(2C_D + V \frac{\partial C_D}{\partial V} \right) \quad (12.8)$$

To define the derivative \dot{X}_u at the flight condition of interest, let the perturbation become vanishingly small such that $u \rightarrow 0$ and hence $V \rightarrow V_0$. Then, from [equations \(12.6\) and \(12.8\)](#),

$$\dot{X}_u = -\frac{1}{2}\rho V_0 S \left(2C_D + V_0 \frac{\partial C_D}{\partial V} \right) \quad (12.9)$$

where C_D and $\partial C_D / \partial V$ are evaluated at velocity V_0 . Thus in order to evaluate the derivative the governing aerodynamic properties are *linearised about the operating point* of interest, which is a direct consequence of the assumption that the perturbation is small. A similar procedure enables all of the aerodynamic stability and control derivatives to be evaluated, although the governing aerodynamic properties may not always lend themselves to such simple interpretation.

It is important to note that in the previous illustration the derivative \dot{X}_u varies with velocity. In general, most derivatives vary with velocity, or Mach number, altitude, and incidence. In fact many derivatives demonstrate significant and sometimes abrupt changes over the flight envelope, especially in the transonic region.

12.3 Derivative estimation

A number of methods are used to evaluate the aerodynamic derivatives. However, whichever method is used, the resulting evaluations can, at best, be regarded only as *estimates* of the exact values. The degree of confidence associated with the derivative estimates is dependent on the quality of the aerodynamic source material and the method of evaluation used. It is generally possible to obtain estimates of the longitudinal aerodynamic derivatives with a greater degree of confidence than can usually be ascribed to estimates of the lateral-directional aerodynamic derivatives.

12.3.1 Calculation

The calculation of derivatives from first principles using approximate mathematical models of airframe aerodynamic properties is probably the simplest and least accurate method of estimation. In particular, it can provide estimates of questionable validity, especially for the lateral-directional derivatives. However, since the approximate aerodynamic models are based on an understanding of the physical phenomena involved, simple calculation confers significant advantage as a means for gaining insight into the dominant aerodynamic properties driving the airframe dynamics. Thus an appreciation of the theoretical methods for estimating aerodynamic derivatives provides a sound foundation on which to build most analytical flight dynamics studies.

To improve on the often poor derivative estimates obtained by calculation, *semi-empirical* methods of estimation have evolved in the light of experience gained from the earliest days of aviation to the present day. Semi-empirical methods are based on simple theoretical calculation modified with the addition of generalised aerodynamic data obtained from experimental sources and accumulated over many years. They are generally made available in various reference documents, and today many are also available as interactive computer programs. In the United Kingdom the Engineering Sciences Data Unit ([ESDU](#)) publishes a number of volumes on aerodynamics, some of which are specifically concerned with aerodynamic derivative estimation. Similar source material is also published in the United States (by DATCOM) and elsewhere.

Use of semi-empirical data items requires, at the outset, some limited information about the geometry and aerodynamics of the subject aeroplane. The investigator then works through the estimation process, which involves calculation and frequent reference to graphical data and nomograms, to arrive at an estimate of the value of the derivative at the flight condition of interest. Such is the state of development of these methods that it is now possible to obtain derivative estimates of good accuracy, at least for aeroplanes having conventional configurations.

Because of the recurring need to estimate aircraft stability and control derivatives, a number of authors have written computer programs to calculate derivatives with varying degrees of success. Indeed, a number of the [ESDU](#) data items are now available as computer software. The program by [Mitchell \(1973\)](#) and its subsequent modification by [Ross and Benger \(1975\)](#) has enjoyed some popularity, especially for preliminary estimates of the stability and control characteristics of new aircraft configurations. The text by [Smetana \(1984\)](#) also includes listings for a number of useful computer programs concerned with aircraft performance and stability.

12.3.2 Wind tunnel measurement

The classical wind tunnel test is one in which a reduced scale model of the aircraft is attached to a balance and the six components of force and moment are measured for various combinations of wind velocity, incidence angle, sideslip angle, and control surface angle. The essential feature of such tests is that the conditions are *static* when the measurements are made. Provided they are carefully designed and executed, wind tunnel tests can give good estimates of the force-velocity and moment-velocity derivatives in particular. Scale effects can give rise to accuracy problems, especially when difficult full scale flight conditions are simulated; although some derivatives can be estimated with good accuracy, it may be very difficult to devise experiments to adequately measure others. However, despite the limitations of the experimental methods, measurements are

made for real aerodynamic flow conditions, and in principle it is possible to obtain derivative estimates of greater fidelity than is likely by calculation.

Dynamic, or non-stationary, experiments can be conducted, from which estimates for the force-rotary and moment-rotary derivatives can be made. The simplest of these requires a special rig in which to mount the model which enables the model to undergo a single degree of freedom free or forced oscillation in roll, or in pitch, or in yaw. Analysis of the oscillatory time response obtained in such an experiment enables estimates to be made of the relevant damping and stiffness derivatives. For example, an oscillatory pitch experiment enables estimates to be made of M_q and M_w . More complex multi-degree of freedom test rigs become necessary when the intent is to measure the motion coupling derivatives—for example, yawing moment due to roll rate N_p . As the experimental complexity is increased so the complexity of the analysis required to calculate the derivative estimates from the measurements is also increased and, consequently, it becomes more difficult to guarantee the accuracy of the derivatives thus obtained.

12.3.3 Flight test measurement

The estimation of aerodynamic derivatives from flight test measurements is an established and well developed experimental process. However, derivative estimates are usually obtained indirectly since it is not possible to measure the aerodynamic components of force and moment acting on the airframe directly. Also, since the aircraft has six degrees of freedom, it is not always possible to perturb the single motion variable of interest without perturbing some, or all, of the others as well. However, as in wind tunnel testing, some derivatives are easily estimated from flight test experiments with a good degree of confidence, whereas others can be notoriously difficult to estimate.

Although it is relatively easy to set up approximately steady conditions in flight from which direct estimates of some derivatives can be made—for example, a steady sideslip for the estimation of Y_v , L_v and N_v —the technique often produces results of indifferent accuracy and has limited usefulness. Today *parameter identification* techniques are commonly used in which measurements are made following the deliberate excitation of multi-variable dynamic conditions. Complex multi-variable response analysis then follows, from which it is possible to derive a complete estimate of the mathematical model of the aircraft corresponding with the flight condition at which the measurements were made. Parameter identification is an analytical process in which full use is made of state-space computational tools to estimate the aircraft state description that best matches the input-output response measured in flight. It is essentially a multi-variable curve fitting procedure, and the computational output consists of the coefficients in the aircraft state equation from which estimates of the aerodynamic stability and control derivatives may be obtained. This method is complex, and success depends, to a considerable extent, on the correct choice of computational algorithm appropriate to the experiment.

A simple diagram containing the essential functions of the parameter identification procedure is shown in Fig. 12.2. A flight test exercise is undertaken in the fully instrumented subject aircraft, and the pilot applies control inputs designed to excite the dynamic response of interest. The control inputs and the full complement of dynamic response variables are recorded in situ or may be telemetered directly to a ground station for online analysis. The parameter identification process is entirely computational and is based on a mathematical model of the aeroplane which is deliberately

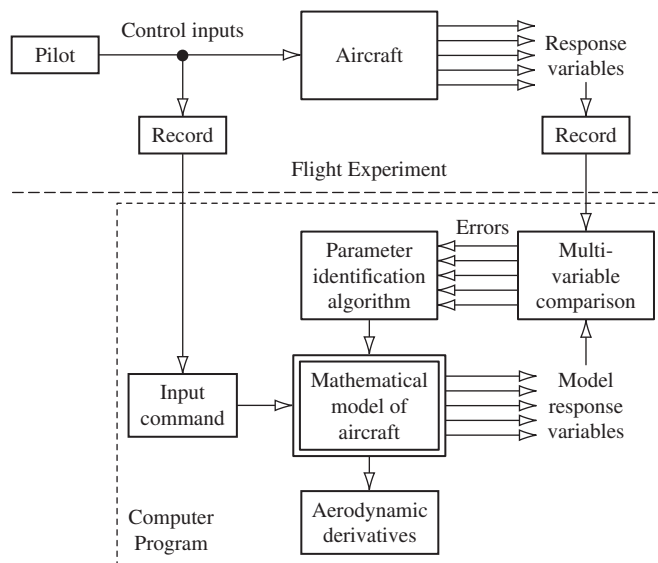


FIGURE 12.2 Parameter identification.

structured to include the terms appropriate to the flight experiment. The object is then to identify the coefficients in the aircraft model which give the best match with the dynamics of the experimental response. The recorded control inputs are applied to the model of the aircraft, and its multi-variable response is compared with the recorded response made in the flight experiment. Response matching errors are then used to adjust the coefficients in the aircraft model according to the parameter identification algorithm, and the process is repeated iteratively until the response matching errors are minimised.

All of the recorded signals contain noise, measurement errors, and uncertainties of various kinds to a greater or lesser extent. The complexity of the identification process is therefore magnified considerably since statistical analysis methods play an essential part in all modern algorithms. For example, Kalman filtering techniques are frequently used to first obtain consistent, and essentially error free, estimates of the state variables for subsequent use in the identification process. Typical commonly encountered parameter identification algorithms include the *equation error* method, the *maximum likelihood* method, and various methods based on *statistical regression*. The development of parameter identification methods for application to aeronautical problems has been the subject of considerable research over the last 25 years or so, and a vast wealth of published material is available. A more detailed discussion of the subject is well beyond the scope of this book.

Until recently few books have been published which are concerned with aircraft parameter identification, see Klein and Morelli (2006), for example. Most of the available material appears to be contained in research papers, but the interested reader will find a useful collection of aircraft related papers in AGARD (1979). It is rare to find published listings of parameter identification computer programs; thus the work by Ross and Foster (1976) is especially useful, if somewhat dated. Probably two

of the more useful sources of information on current developments in aircraft parameter identification are the proceedings of the AIAA annual Flight Mechanics and biannual Flight Test conferences.

The main disadvantages of parameter identification methods include the requirement for substantial computational “power” and the essential need for recorded flight data of the very highest quality. Despite these constraints, the process is now used routinely by many leading flight test organisations. Given adequate resources, the advantages of parameter identification are significant. All of the aerodynamic stability and control derivatives can be estimated in one pass, and the dynamic conditions to which they relate do not necessarily have to be linear. For example, it is now routinely possible to identify aircraft models in extreme manoeuvring conditions such as stall, spin, and at very high angles of attack when the aerodynamics are substantially non-linear. It is interesting that this method can also be used for estimating aerodynamic derivatives from “dynamic” wind tunnel experiments.

12.4 The effects of compressibility

The onset of compressible flow conditions gives rise to changes in the aerodynamic properties of the aeroplane which in general lead to corresponding changes in the stability and control characteristics. Clearly, this means a change in the flying and handling qualities of the aeroplane as the Mach number envelope is traversed. Typically, compressibility effects begin to become apparent at a Mach number of approximately 0.3, although changes in the stability and control characteristics may not become significant until the Mach number reaches 0.6 or higher. As Mach number increases the changes due to compressibility are continuous and gradual. However, in the transonic flow regime changes can be dramatic and abrupt. When appropriate, it is therefore important that the aerodynamic changes arising from the effects of compressibility are allowed for in even the simplest and most approximate aerodynamic derivative estimation.

An interesting chapter on the effects of compressibility on aircraft stability, control, and handling may be found in [Hilton \(1952\)](#). However, it must be remembered that, although at the time the book was written the problems were very clearly recognised, the mathematical models used to describe the phenomena were in most cases at an early stage of development. Today, sophisticated computational tools are commonly used to deal with the problems of modelling compressible aerodynamics. Nevertheless, the simpler models described by [Hilton \(1952\)](#) are still applicable, as is shown in the following sections, provided their limitations are appreciated.

12.4.1 Some useful definitions

Mach number M is defined as the ratio of the local flow velocity V to the local speed of sound a . Whence

$$M = \frac{V}{a} \quad (12.10)$$

The *critical Mach number* M_{crit} is the free stream Mach number at which the local flow Mach number just reaches unity at some point on the airframe. In general, $M_{crit} \leq 1.0$ and is typically in the order of 0.9.

Subsonic flight commonly refers to local aerodynamic flow conditions where $M < 1.0$. Practically, this means that the free stream Mach number is less than approximately 0.8. *Transonic flight* usually refers to generally subsonic flight but where the local flow Mach number $M \geq 1.0$. Transonic flight conditions are assumed when the free stream Mach number lies in the range $0.8 < M_0 < 1.2$. The greatest degree of aerodynamic unpredictability is associated with this Mach number range. *Supersonic flight* commonly refers to aerodynamic flow conditions when $M > 1.0$ everywhere in the local flow field. As with transonic conditions, supersonic flow conditions are assumed when the free stream Mach number is greater than approximately 1.2.

A *shock wave* is a compression wave front which occurs in the supersonic flow field around an airframe. A shock wave originating at a point on the airframe, such as the nose, is initially a plane wave front normal to the direction of the flow. As the flow Mach number is increased, the shock wave becomes a conical wave front, or *Mach cone*, the apex angle of which decreases with increasing Mach number. As the air flow traverses the shock wave, it experiences an abrupt increase in pressure, density, and temperature, and the energy associated with these changes is extracted from the total flow energy to result in reduced velocity behind the wave front. Collectively, these changes are seen as an abrupt increase in drag in particular and may be accompanied by significant changes in trim and in the stability and control characteristics of the aeroplane.

The *shock stall* is sometimes used to describe the abrupt aerodynamic changes experienced when an aeroplane accelerating through the transonic flight regime first reaches the critical Mach number. At the critical Mach number, shock waves begin to form at various places on the airframe and are accompanied by abrupt reduction in local lift, abrupt increase in local drag, and some associated change in pitching moment. Since the effect of these aerodynamic changes is not unlike that of the classical low speed stall, it is referred to as the shock stall. However, unlike the classical low speed stall, the aeroplane continues to fly through the condition.

12.4.2 Aerodynamic models

Because of the aerodynamic complexity of the conditions applying to an aeroplane in a compressible flow field, it is difficult to derive other than the very simplest mathematical models to describe those conditions. Thus for analytical application, as required in aerodynamic derivative estimation, mathematical modelling is usually limited to an approximate description of the effects of compressibility on the lifting surfaces of the aeroplane only. In particular, the ease with which the aerodynamic properties of a wing in compressible flow can be estimated is dependent, to a large extent, on the leading edge flow conditions.

As flow Mach number is increased to unity, a shock wave forms a small distance ahead of the leading edge of a typical wing and the shock wave is said to be *detached*. As the Mach number is increased further, the shock wave moves nearer to the leading edge of the wing and eventually moves onto the wing when it is said to be *attached*. Since the flow velocity behind the shock wave is lower than the free stream value, when the shock wave is detached the leading edge of the wing is typically in subsonic flow. In this condition the pressure distribution on the wing, in particular, the leading edge suction peak, is subsonic and the aerodynamic characteristics of the wing are quite straightforward to estimate. However, when the shock wave is attached, the leading edge of the wing is typically in supersonic flow and estimation of the aerodynamic properties, in particular, the drag rise, is much less straightforward. Since the incident flow velocity direction is always

considered perpendicular to the leading edge of the wing, it is always lower on a swept wing because it is equivalent to the free stream velocity resolved through the leading edge sweep angle. Further, since wing sweep brings more, or more likely, all of the wing within the Mach cone, the high drag associated with a supersonic leading edge is reduced or avoided altogether for a larger range of supersonic Mach numbers.

12.4.3 Subsonic lift, drag, and pitching moment

The theoretical maximum value of lift curve slope for a rectangular flat plate wing of infinite span in incompressible flow is given by

$$a_{\infty} = 2\pi \cos A_{le} \text{ rad}^{-1} \quad (12.11)$$

where A_{le} is the leading edge sweep angle. For a wing of finite thickness this value of lift curve slope is reduced, and [Houghton and Carpenter \(1993\)](#) give an approximate empirical expression which is a function of geometric thickness to chord ratio t/c such that [equation \(12.11\)](#) becomes

$$a_{\infty} = 1.8\pi \left(1 + 0.8 \frac{t}{c}\right) \cos A_{le} \text{ rad}^{-1} \quad (12.12)$$

For a wing of finite span the lift curve slope is reduced further as a function of aspect ratio A and is given by the expression

$$a = \frac{a_{\infty}}{\left(1 + \frac{a_{\infty}}{\pi A}\right)} \quad (12.13)$$

For Mach numbers below M_{crit} , but when the effects of compressibility are evident, the *Prandtl-Glauert rule* provides a means for estimating the lifting properties of a wing. For an infinite span wing with leading edge sweep angle A_{le} , the lift curve slope a_{∞_c} in the presence of compressibility effects is given by

$$a_{\infty_c} = \frac{a_{\infty_i}}{\sqrt{1 - M^2 \cos^2 A_{le}}} \quad (12.14)$$

where, a_{∞_i} is the corresponding incompressible lift curve slope given, for example, by [equation \(12.12\)](#). An equivalent expression for a wing of finite span with aspect ratio A is quoted in [Babister \(1961\)](#) and is given by

$$a_c = \frac{(A + 2\cos A_{le})a_{\infty_i}}{2\cos A_{le} + A\sqrt{1 - M^2 \cos^2 A_{le}}} \quad (12.15)$$

For Mach numbers below M_{crit} , the zero lift drag coefficient C_{D_0} remains at its nominal incompressible value and the changes in drag due to the effects of compressibility result mainly from the induced drag contribution. Thus the classical expression for the drag coefficient applies:

$$C_{D_c} = C_{D_0} + kC_{L_c}^2 = C_{D_0} + ka_c^2 \alpha^2 \quad (12.16)$$

In general, the effect of compressibility on pitching moment coefficient in subsonic flight is small and is often disregarded. However, in common with lift and drag coefficient, such changes in pitching moment coefficient as may be evident increase as the Mach number approaches unity. Further, these changes are more pronounced in aircraft with a large wing sweep angle and result from a progressive aft shift in aerodynamic centre. Since the effect is dependent on the inverse of $\sqrt{1 - M^2 \cos^2 A_{le}}$, or its equivalent for a wing of finite span, it does not become significant until, approximately, $M \geq 0.6$.

It is important to appreciate that the Prandtl-Glauert rule applies to subsonic flight only in the presence of the effects of compressibility. The models given previously become increasingly inaccurate at Mach numbers approaching and exceeding unity. In other words, the Prandtl-Glauert rule is not applicable to transonic flight conditions.

12.4.4 Supersonic lift, drag, and pitching moment

The derivation of simple approximate aerodynamic models to describe lift, drag, and pitching moment characteristics in supersonic flow conditions is much more difficult. Such models as are available depend on the location of the shocks on the principal lifting surfaces and, in particular, on whether the leading edge of the wing is subsonic or supersonic. In every case the aerodynamic models require a reasonable knowledge of the geometry of the wing, including the aerofoil section. The three commonly used theoretical tools are, in order of increasing complexity, the linearised Ackeret theory, the second order Busemann theory, and the shock expansion method. A full discussion of these is not appropriate here, and only the simplest linear models are summarised. The material is included in most aerodynamics texts, such as [Bertin and Smith \(1989\)](#) and [Houghton and Carpenter \(1993\)](#).

The lift curve slope of an infinite span swept wing in supersonic flow, which implies a supersonic leading edge condition, is given by

$$a_{\infty_c} = \frac{4 \cos A_{le}}{\sqrt{M^2 \cos^2 A_{le} - 1}} \quad (12.17)$$

Clearly, equation (12.17) is valid only for Mach number $M > \sec A_{le}$; at lower Mach number the leading edge is subsonic since it is within the Mach cone. For a wing of finite span the expression given by equation (12.17) is “corrected” for aspect ratio. Thus

$$a_c = a_{\infty_c} \left(1 - \frac{1}{2A \sqrt{M^2 \cos^2 A_{le} - 1}} \right) \quad (12.18)$$

and the parameter $A \sqrt{M^2 \cos^2 A_{le} - 1}$ is termed the *effective aspect ratio* by [Liepmann and Roshko \(1957\)](#).

The drag of an aeroplane in supersonic flight is probably one of the most difficult aerodynamic parameters to estimate with any accuracy. The drag of a wing with a supersonic leading edge comprises three components: the *drag due to lift*, the *wave drag*, and the *skin friction drag*. The drag due to lift, sometimes known as *wave drag due to lift*, is equivalent to the induced drag in subsonic flight. Wave drag, also known as *form drag* or *pressure drag*, occurs only in compressible flow

conditions and is a function of aerofoil section geometry. Skin friction drag is the same as the familiar zero lift drag in subsonic flight, which is a function of wetted surface area.

A simple approximate expression for the drag coefficient of an infinite span swept wing in supersonic flight is given by

$$C_{D_\infty} = \frac{4\alpha^2 \cos \Lambda_{le}}{\sqrt{M^2 \cos^2 \Lambda_{le} - 1}} + \frac{k \left(\frac{t}{c}\right)^2 \cos^3 \Lambda_{le}}{\sqrt{M^2 \cos^2 \Lambda_{le} - 1}} + C_{D_0} \quad (12.19)$$

where the first term is the drag coefficient due to lift, the second term is the wave drag coefficient, and the third term is the zero lift drag coefficient. Here, in the interest of simplicity, the wave drag is shown to be dependent only on the ratio of aerofoil section thickness to chord ratio, t/c , which implies that the section is symmetrical. When the section has camber, the wave drag includes a second term which is dependent on the square of the local angle of attack with respect to the mean camber line. The camber term is not included in [equation \(12.19\)](#) because many practical supersonic aerofoils are symmetric or near symmetric. The constant k is also a function of the aerofoil section geometry and is 2/3 for bi-convex or typical modified double wedge sections, both of which are symmetric.

For a finite span wing with aspect ratio A the drag coefficient is given very approximately by

$$C_{D_\infty} = \left(\frac{4\alpha^2 \cos \Lambda_{le}}{\sqrt{M^2 \cos^2 \Lambda_{le} - 1}} + \frac{k \left(\frac{t}{c}\right)^2 \cos^3 \Lambda_{le}}{\sqrt{M^2 \cos^2 \Lambda_{le} - 1}} \right) \left(1 - \frac{1}{2A\sqrt{M^2 \cos^2 \Lambda_{le} - 1}} \right) + C_{D_0} \quad (12.20)$$

It is assumed that the wing to which [equation \(12.20\)](#) relates is of constant thickness with span and that it has a rectangular planform, which is most unlikely for a real, practical wing. Alternative and rather more complex expressions can be derived which are specifically dependent on wing geometry to a much greater extent. However, there is no guarantee that the estimated drag coefficient is more accurate since it remains necessary to make significant assumptions about the aerodynamic operating conditions of the wing.

It is also difficult to obtain a simple and meaningful expression for pitching moment coefficient in supersonic flight conditions. However, it is relatively straightforward to show that, for an infinite span flat plate wing, the aerodynamic centre moves aft to the half chord point in supersonic flow. This results in an increase in nose down pitching moment together with an increase in the longitudinal static stability margins, with corresponding changes in the longitudinal trim, stability, and control characteristics of the aeroplane. An increase in thickness and a reduction in aspect ratio of the wing causes the aerodynamic centre to move forward from the half chord point with a corresponding reduction in stability margins. Theoretical prediction of these changes for anything other than a simple rectangular wing is not generally practical.

12.4.5 Summary

It is most important to realise that the aerodynamic models outlined in [Sections 12.4.3 and 12.4.4](#) describe, approximately, the properties of the main lifting wing of the aeroplane only. Since the wing provides most of the lift, with perhaps smaller contributions from the fuselage and tailplane, or foreplane, it is expected that [equations \(12.15\) and \(12.18\)](#) would give a reasonable indication of

the lift curve slope of a complete aeroplane. However, this is not necessarily expected of the drag estimates given by [equations \(12.16\) and \(12.20\)](#). The drag contributions from the fuselage and tailplane, or foreplane, may well be a large fraction of the total, so estimates obtained with these equations should be treated accordingly. It is suggested that the main purpose of the material given in [Sections 12.4.3 and 12.4.4](#) is to provide an appreciation of the primary aerodynamic effects of compressibility as they relate to stability and control and to provide a means for checking estimates obtained by other, especially computational, means.

Little mention has been made of the transonic flight regime, for the simple reason that analytical models suitable for the estimation of aerodynamic stability and control properties at the present level of interest are not available. Considerable research has been undertaken in recent years into transonic aerodynamics, but the analysis remains complex and has found greatest use in computational methods for flow prediction. When it is necessary to have estimates of the aerodynamic properties of a complete aeroplane configuration in compressible flow conditions, reference to source material such as the [ESDU](#) data items is preferable.

Today, increasing use is made of computational methods for estimating the aerodynamic properties of complete aeroplane configurations, at all flight conditions. Provided the geometry of the airframe can be described in sufficient detail, computational methods, such as the *vortex lattice method* or the *panel method*, can be used to obtain estimates of aerodynamic characteristics at acceptable levels of accuracy. By such means, aerodynamic information can be obtained for conditions which would otherwise be impossible using analytical methods.

EXAMPLE 12.1

A substantial database of aerodynamic stability and control parameters for the McDonnell-Douglas F-4C Phantom aircraft is provided by [Heffley and Jewell \(1972\)](#). Data are given for altitudes from sea level to 55,000 ft and for Mach numbers from 0.2 to 2.2, and the aircraft shows most of the classical effects of translation from subsonic to supersonic flight. Some limited additional information was obtained from Jane's (1969–1970). The main geometric parameters of the aircraft used in the example are

Wing area (reference area)	$S = 530 \text{ ft}^2$
Wing span	$b = 38.67 \text{ ft}$
Mean geometric chord (reference chord)	$\bar{c} = 16.04 \text{ ft}$
Average thickness–chord ratio	$t/c = 0.051$
Aspect ratio	$A = 2.82$
Leading edge sweep angle	$\Lambda_{le} = 50 \text{ deg}$
Centre of gravity position	$h = 0.289$

The lift, drag, and pitching moment characteristics are summarised in [Fig. 12.3](#) as a function of Mach number for two altitudes, 15,000 ft and 35,000 ft, because the data for these two altitudes extend over the entire Mach number envelope.

Lifting properties are represented by the plot of lift curve slope a as a function of Mach number. The effect of compressibility becomes obvious at Mach 0.8 at the onset of the transonic flow regime. The lift curve slope reaches a maximum at Mach 1.0, and its gentle reduction

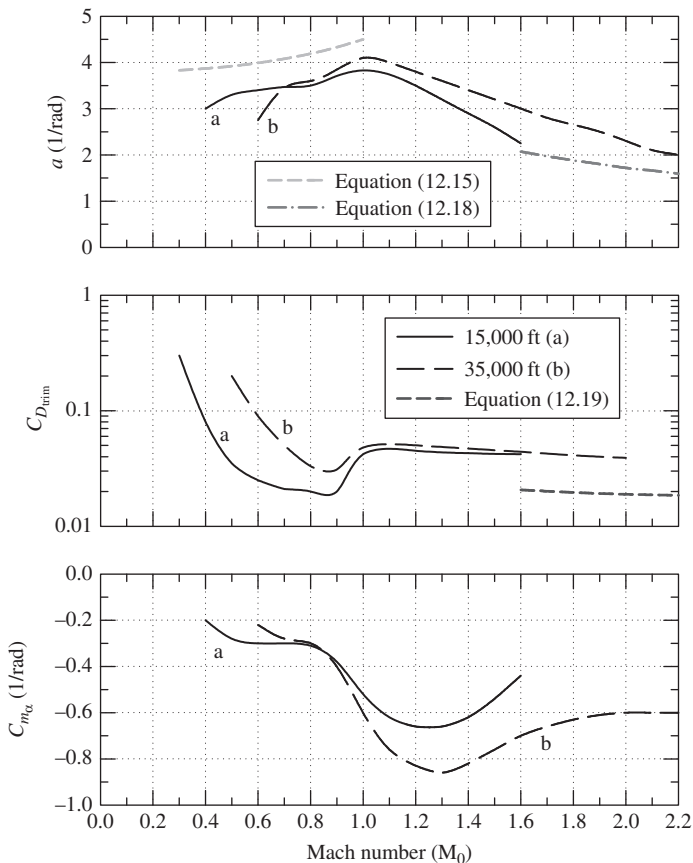


FIGURE 12.3 Lift, drag, and pitching moment variation with Mach number.

thereafter is almost linear with Mach number. The Prandtl-Glauert rule approximation, as given by [equation \(12.15\)](#), is shown for comparison in the subsonic Mach number range. The approximation assumes a 2D lift curve slope calculated according to [equation \(12.12\)](#) and shows the correct trend; however, it gives an overestimate of total lift curve slope. The linear supersonic approximation for lift curve slope, as given by [equation \(12.18\)](#), is also shown for completeness. In this case the 2D lift curve slope was calculated using [equation \(12.17\)](#). Again, the trend matches reasonably well, but the model gives a significant underestimate. It is prudent to recall at this juncture that both models describe the lift curve slope of a finite wing only, whereas the F-4C data describe the entire airframe characteristic.

The drag properties are represented by the trim drag coefficient, plotted on a logarithmic scale, as a function of Mach number. The use of a logarithmic scale helps to emphasise the

abrupt drag rise at Mach 1.0. In the subsonic Mach number range, the drag coefficient reduces with increasing Mach number, the classical characteristic, which implies that the drag coefficient is dominated by the induced drag contribution, as might be expected. However, in supersonic flight the drag coefficient remains almost constant, the contribution due to lift is small as both C_L and α are small, and the main contributions are due to wave drag and skin friction.

Shown on the same plot is the supersonic drag coefficient calculated according to [equation \(12.19\)](#) and clearly the match is poor. The trend is correct, but the magnitude is about half the actual airframe value. Once again, it should be remembered that [equation \(12.19\)](#) relates to a finite wing and not to a complete airframe. It is reasonably easy to appreciate that the fuselage and tail surfaces make a significant contribution to the overall drag of the aeroplane. Careful scrutiny of the aerodynamic data for 35,000 ft enables the expression for the subsonic drag coefficient, [equation \(12.16\)](#), to be estimated as

$$C_D = C_{D_0} + kC_L^2 = 0.017 + 0.216C_L^2 \quad (12.21)$$

This expression gave a good fit to the actual data, and the value of C_{D_0} was used in the evaluation of the supersonic drag coefficient, [equation \(12.19\)](#).

The final plot in [Fig. 12.3](#) represents the effect of Mach number on pitching moment and shows the variation in the slope, denoted C_{m_α} , of the $C_m-\alpha$ curve as a function of Mach number. Since C_{m_α} is proportional to the controls-fixed static margin, it becomes more negative as the aerodynamic centre moves aft. This is clearly seen in the plot, and the increase in stability margin commences at a Mach number of 0.8. Now the relationship between controls-fixed stability margin, neutral point, and centre of gravity locations is given by equation (3.17):

$$K_n = h_n - h \quad (12.22)$$

With reference to Appendix 8, the expression for the derivative M_w is given by

$$M_w = \frac{\partial C_m}{\partial \alpha} = -aK_n \quad (12.23)$$

Thus, from [equations \(12.22\) and \(12.23\)](#), an expression for the location of the controls-fixed neutral point is easily calculated:

$$h_n = h - \frac{1}{a} \frac{\partial C_m}{\partial \alpha} \equiv h - \frac{1}{a} C_{m_\alpha} \quad (12.24)$$

Using [equation \(12.24\)](#) with the F-4C data for an altitude of 15,000 ft, the variation in neutral point position as a function of Mach number was calculated and the result is shown in [Fig. 12.4](#).

Since the neutral point corresponds with the centre of pressure for the whole aeroplane, its aft shift with Mach number agrees well with the predictions given by “simple” aerofoil theory. Over the transonic Mach number range, the neutral point moves back to the midpoint of the mean aerodynamic chord and then moves forward a little at higher Mach numbers. It is interesting that at subsonic Mach numbers the neutral point remains more or less stationary at around $0.37\bar{c}$, which is quite typical for many aeroplanes.

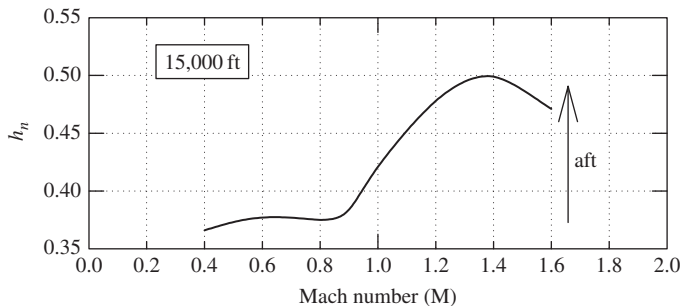


FIGURE 12.4 Variation of controls-fixed neutral point position with Mach number.

12.5 Limitations of aerodynamic modelling

Simple expressions for the aerodynamic stability and control derivatives may be developed from first principles based on analysis of the aerodynamic conditions following an upset from equilibrium. The cause of the upset may be external, the result of a gust for example, or internal, the result of a pilot control action. It is important to appreciate that in either event the disturbance is of short duration and that the controls remain fixed at their initial settings for the duration of the response. As explained in Section 12.2, the derivatives are then evaluated by linearising the aerodynamics about the nominal operating, or trim, condition. The aerodynamic models thus derived are limited in their application to small perturbation motion about the trim condition only. The simplest possible analytical models for the aerodynamic stability and control derivatives are developed, subject to the limitations outlined in this chapter, and described in Chapter 13.

References

- AGARD. (1979). *Parameter Identification*. Lecture Series, AGARD-LS-104. Advisory Group for Aerospace Research & Development, 7 Rue Ancelle 92200, Neuilly-sur-Seine, France.
- Babister, A. W. (1961). *Aircraft Stability and Control*. Oxford: Pergamon Press.
- Bertin, J. J., & Smith, M. L. (1989). *Aerodynamics for Engineers*. (Second Edition). New Jersey: Prentice Hall, Englewood Cliffs.
- ESDU Aerodynamics Series (2006). Engineering Sciences Data, ESDU International Ltd., 27 Corsham Street, London. www.esdu.com.
- Heffley, R. K., & Jewell, W. F. (1972). *Aircraft Handling Qualities Data*. Washington, D.C. 20546: National Aeronautics and Space Administration, NASA Contractor Report, NASA CR-2144.
- Hilton, W. F. (1952). *High Speed Aerodynamics*. London: Longmans, Green and Co.
- Houghton, E. L., & Carpenter, P. W. (1993). *Aerodynamics for Engineering Students*. (Fourth Edition). London: Edward Arnold.
- Liepmann, H. W., & Roshko, A. (1957). *Elements of Gas Dynamics*. New York: John Wiley and Sons, Inc.
- McDonnell-Douglas Corp. (1960). *USAF stability and control handbook (DATCOM)*. St Louis, MO: McDonnell-Douglas Corp.

- Mitchell, C. G. B. (1973). *A Computer Programme to Predict the Stability and Control Characteristics of Subsonic Aircraft*. Royal Aircraft Establishment Technical Report, RAE TR-73079. Farnborough: Royal Aircraft Establishment.
- Ross, A. J., & Benger, N. J. (1975). *Modifications to a Computer Program for Predicting the Stability and Control Characteristics of Subsonic Aircraft (RAE Technical Report TR-73079)*. Royal Aircraft Establishment Technical Memorandum, RAE Tech Memo FS 40. Farnborough: Royal Aircraft Establishment.
- Ross, A. J., & Foster, G. W. (1976). *FORTRAN Programs for the Determination of Aerodynamic Derivatives from Transient Longitudinal or Lateral Responses of Aircraft*. Aeronautical Research Council, Current Papers, ARC-P 1344. London: Her Majesty's Stationery Office.
- Smetana, F. O. (1984). *Computer Assisted Analysis of Aircraft Performance Stability and Control*. New York: McGraw Hill Book Co.
- Taylor, J. W. R. (Ed.), (1969–70). *Jane's All The World's Aircraft*. London: Jane's Yearbooks, Haymarket Publishing.

Aerodynamic Stability and Control Derivatives

13

13.1 Introduction

As is usual in aerodynamic analysis, for the purposes of obtaining simple expressions for the stability and control derivatives a wind axis reference system is assumed throughout. The choice of wind axes is convenient since it reduces the derivatives to their simplest possible description by retaining only the essential contributions and hence, maximises the *visibility* of the physical phenomena involved. It is therefore very important to remember that if the derivatives thus obtained are required for use in equations of motion referred to an alternative axis, then the appropriate axis transformation must be applied to the derivatives. Some useful transformations are given in Appendices 7 and 8. In all cases analytical expressions are obtained for the derivatives assuming subsonic flight conditions; it is then relatively straightforward to develop the expressions further to allow for the effects of Mach number as suggested in Section 12.4.

It has already been established that simple analytical expressions for the derivatives rarely give accurate estimates. Their usefulness is significantly more important as a means for explaining their physical origins, thereby providing the essential link between aircraft dynamics and airframe aerodynamics. The analytical procedure for obtaining simple derivative expressions has been well established for very many years, and the approach commonly encountered in the United Kingdom today is comprehensively described by Babister (1961) and, in less detail, by Babister (1980). The following paragraphs owe much to that work since it is unlikely that the treatment can be bettered. For the calculation of more reliable estimates of derivative values, reference to the ESDU data items is advised. The reader requiring a more detailed aerodynamic analysis of stability and control derivatives will find much useful material in Hancock (1995).

13.2 Longitudinal aerodynamic stability derivatives

For convenience, a summary of the derivative expressions derived in this paragraph is included in Table A8.1, Appendix 8.

13.2.1 Preliminary considerations

A number of expressions are required repeatedly in the derivative analysis, so it is convenient to assemble these expressions prior to embarking on the analysis. A longitudinal small perturbation is

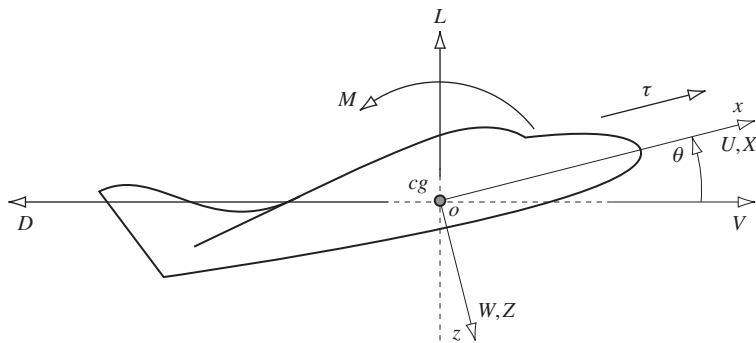


FIGURE 13.1 Perturbed wind axes.

shown in Fig. 13.1 in which the aircraft axes are wind axes and the initial condition assumes steady symmetric level flight at velocity V_0 . Although not strictly an aerodynamic force, the thrust τ is shown since it may behave like an aerodynamic variable in a perturbation. As indicated, the thrust force is tied to the aircraft x axis and moves with it.

In the perturbation the total velocity becomes V with components U and W along the ox and oz axes respectively. Whence

$$V^2 = U^2 + W^2 \quad (13.1)$$

and

$$\begin{aligned} U &= U_e + u = V\cos\theta \\ W &= W_e + w = V\sin\theta \end{aligned} \quad (13.2)$$

Since wind axes are assumed, the pitch attitude perturbation θ and the incidence perturbation α are the same and are given by

$$\tan\theta \equiv \tan\alpha = \frac{W}{U} \quad (13.3)$$

Differentiate equation (13.1) with respect to U and W in turn to obtain the following partial derivatives:

$$\frac{\partial V}{\partial U} = \frac{U}{V} \quad \text{and} \quad \frac{\partial V}{\partial W} = \frac{W}{V} \quad (13.4)$$

Substitute for U and W from equation (13.2) to obtain

$$\frac{\partial V}{\partial U} = \cos\theta \cong 1 \quad \text{and} \quad \frac{\partial V}{\partial W} = \sin\theta \cong 0 \quad (13.5)$$

since, by definition, θ is a small angle.

In a similar way, differentiate equation (13.3) with respect to U and W in turn and substitute for U and W from equation (13.2) to obtain

$$\begin{aligned}\frac{\partial \theta}{\partial U} &\equiv \frac{\partial \alpha}{\partial U} = \frac{-\sin\theta}{V} \approx 0 \\ \frac{\partial \theta}{\partial W} &\equiv \frac{\partial \alpha}{\partial W} = \frac{\cos\theta}{V} \approx \frac{1}{V}\end{aligned}\quad (13.6)$$

since again, by definition, θ is a small angle.

From equation (12.10),

$$\frac{\partial}{\partial V} = \frac{1}{a} \frac{\partial}{\partial M} \quad (13.7)$$

which is useful for transforming from a velocity dependency to a Mach number dependency and where, here, a is the local speed of sound.

13.2.2 Aerodynamic force and moment components

With reference to Fig. 13.1 the lift and drag forces may be resolved into the disturbed aircraft axes to give the following components of aerodynamic force. The perturbed axial force is

$$X = L\sin\theta - D\cos\theta + \tau = \frac{1}{2} \rho V^2 S (C_L \sin\theta - C_D \cos\theta) + \tau \quad (13.8)$$

and the perturbed normal force is

$$Z = -L\cos\theta - D\sin\theta = -\frac{1}{2} \rho V^2 S (C_L \cos\theta + C_D \sin\theta) \quad (13.9)$$

In the initial steady trim condition, by definition the pitching moment M is zero. However, in the perturbation the transient pitching moment is nonzero and is given by

$$M = \frac{1}{2} \rho V^2 S \bar{C}_m \quad (13.10)$$

Note that considerable care is needed in order not to confuse pitching moment M and Mach number M .

13.2.3 Force derivatives due to velocity perturbations

$$\dot{X}_u = \frac{\partial X}{\partial U} \quad \textbf{Axial force due to axial velocity}$$

Differentiate equation (13.8) to obtain

$$\begin{aligned}\frac{\partial X}{\partial U} &= \frac{1}{2} \rho V^2 S \left(\frac{\partial C_L}{\partial U} \sin\theta + C_L \cos\theta \frac{\partial \theta}{\partial U} - \frac{\partial C_D}{\partial U} \cos\theta + C_D \sin\theta \frac{\partial \theta}{\partial U} \right) \\ &\quad + \rho V S \frac{\partial V}{\partial U} (C_L \sin\theta - C_D \cos\theta) + \frac{\partial \tau}{\partial U}\end{aligned}\quad (13.11)$$

Substitute for $\partial V/\partial U$ from [equation \(13.5\)](#) and for $\partial\theta/\partial U$ from [equation \(13.6\)](#). As θ is a small angle, in the limit, $\cos\theta \cong 1$ and $\sin\theta \cong 0$ and [equation \(13.11\)](#) simplifies to

$$\frac{\partial X}{\partial U} = -\frac{1}{2}\rho V^2 S \frac{\partial C_D}{\partial U} - \rho V S C_D + \frac{\partial \tau}{\partial U} \quad (13.12)$$

Now,

$$\frac{\partial C_D}{\partial U} = \frac{\partial C_D}{\partial V} \frac{\partial V}{\partial U} = \frac{\partial C_D}{\partial V} \quad (13.13)$$

and, similarly,

$$\frac{\partial \tau}{\partial U} = \frac{\partial \tau}{\partial V} \quad (13.14)$$

In the limit the total perturbation velocity tends to the equilibrium value and $V \cong V_0$. Whence [equation \(13.12\)](#) may be written as

$$\dot{X}_u = \frac{\partial X}{\partial U} = -\rho V_0 S C_D - \frac{1}{2}\rho V_0^2 S \frac{\partial C_D}{\partial V} + \frac{\partial \tau}{\partial V} \quad (13.15)$$

With reference to Appendix 2, the dimensionless form of the derivative is given by

$$X_u = \frac{\dot{X}_u}{\frac{1}{2}\rho V_0 S} = -2C_D - V_0 \frac{\partial C_D}{\partial V} + \frac{1}{\frac{1}{2}\rho V_0 S} \frac{\partial \tau}{\partial V} \quad (13.16)$$

Alternatively, using [equation \(13.7\)](#), the dimensionless derivative may be expressed in terms of Mach number rather than velocity:

$$X_u = -2C_D - \frac{1}{M_0} \frac{\partial C_D}{\partial M} + \frac{1}{\frac{1}{2}\rho M_0 S a^2} \frac{\partial \tau}{\partial M} \quad (13.17)$$

Expressions for the remaining force velocity derivatives are obtained in a similar way as follows.

$$\dot{Z}_u = \frac{\partial Z}{\partial U} \quad \textbf{Normal force due to axial velocity}$$

By differentiating [equation \(13.9\)](#) with respect to U , it is easily shown that

$$\dot{Z}_u = \frac{\partial Z}{\partial U} = -\rho V S C_L - \frac{1}{2}\rho V^2 S \frac{\partial C_L}{\partial U} \quad (13.18)$$

Now, in the manner of [equation \(13.13\)](#),

$$\frac{\partial C_L}{\partial U} = \frac{\partial C_L}{\partial V} \frac{\partial V}{\partial U} = \frac{\partial C_L}{\partial V} \quad (13.19)$$

Thus in the limit $V \cong V_0$ and [equation \(13.18\)](#) may be written as

$$\dot{Z}_u = -\rho V_0 S C_L - \frac{1}{2}\rho V_0^2 S \frac{\partial C_L}{\partial V} \quad (13.20)$$

With reference to Appendix 2, the dimensionless form of the derivative is given by

$$\dot{Z}_u = \frac{\dot{Z}_u}{\frac{1}{2}\rho V_0 S} = -2C_L - V_0 \frac{\partial C_L}{\partial V} \quad (13.21)$$

or, alternatively, expressed in terms of Mach number rather than velocity,

$$Z_u = -2C_L - M_0 \frac{\partial C_L}{\partial M} \quad (13.22)$$

$$\dot{X}_w = \frac{\partial X}{\partial W} \quad \textbf{Axial force due to normal velocity}$$

As before, it may be shown that by differentiating equation (13.8) with respect to W ,

$$\dot{X}_w = \frac{\partial X}{\partial W} = \frac{1}{2} \rho V^2 S \left(\frac{1}{V} C_L - \frac{\partial C_D}{\partial W} \right) + \frac{\partial \tau}{\partial W} \quad (13.23)$$

Now, with reference to equation (13.6) and noting that $\alpha = \theta$,

$$\frac{\partial C_D}{\partial W} = \frac{\partial C_D}{\partial \theta} \frac{\partial \theta}{\partial W} \equiv \frac{1}{V} \frac{\partial C_D}{\partial \alpha} \quad (13.24)$$

Similarly, it may be shown that

$$\frac{\partial \tau}{\partial W} \equiv \frac{1}{V} \frac{\partial \tau}{\partial \alpha} = 0 \quad (13.25)$$

since it is assumed that thrust variation resulting from small incidence perturbations is negligible. Thus, in the limit equation (13.23) may be written as

$$\dot{X}_w = \frac{1}{2} \rho V_0 S \left(C_L - \frac{\partial C_D}{\partial \alpha} \right) \quad (13.26)$$

With reference to Appendix 2, the dimensionless form of the derivative is given by

$$X_w = \frac{\dot{X}_w}{\frac{1}{2}\rho V_0 S} = \left(C_L - \frac{\partial C_D}{\partial \alpha} \right) \quad (13.27)$$

$$\dot{Z}_w = \frac{\partial Z}{\partial W} \quad \textbf{Normal force due to normal velocity}$$

As before, by differentiating equation (13.9) with respect to W and with reference to equation (13.24) it may be shown that

$$\dot{Z}_w = \frac{\partial Z}{\partial W} = -\frac{1}{2} \rho V^2 S \left(\frac{\partial C_L}{\partial W} + \frac{1}{V} C_D \right) = -\frac{1}{2} \rho V S \left(\frac{\partial C_L}{\partial \alpha} + C_D \right) \quad (13.28)$$

In the limit equation (13.28) may be rewritten as

$$\dot{Z}_w = -\frac{1}{2} \rho V_0 S \left(\frac{\partial C_L}{\partial \alpha} + C_D \right) \quad (13.29)$$

With reference to Appendix 2, the dimensionless form of the derivative is given by

$$Z_w = \frac{\dot{Z}_w}{\frac{1}{2} \rho V_0 S} = - \left(\frac{\partial C_L}{\partial \alpha} + C_D \right) \quad (13.30)$$

13.2.4 Moment derivatives due to velocity perturbations

$$\dot{M}_u = \frac{\partial M}{\partial U} \quad \textbf{Pitching moment due to axial velocity}$$

In a perturbation the pitching moment becomes nonzero and is given by equation (13.10). Differentiating equation (13.10) with respect to U ,

$$\frac{\partial M}{\partial U} = \frac{1}{2} \rho V^2 S \bar{c} \frac{\partial C_m}{\partial U} + \rho V S \bar{c} C_m \quad (13.31)$$

and with reference to equation (13.5),

$$\frac{\partial C_m}{\partial U} = \frac{\partial C_m}{\partial V} \frac{\partial V}{\partial U} = \frac{\partial C_m}{\partial V} \quad (13.32)$$

Now, in the limit, as the perturbation tends to zero, the pitching moment coefficient C_m in the second term in equation (13.31) tends to the steady equilibrium value, which is, of course, zero. Therefore, in the limit equation (13.31) simplifies to

$$\dot{M}_u = \frac{\partial M}{\partial U} = \frac{1}{2} \rho V_0^2 S \bar{c} \frac{\partial C_m}{\partial V} \quad (13.33)$$

With reference to Appendix 2, the dimensionless form of the derivative is given by

$$M_u = \frac{\dot{M}_u}{\frac{1}{2} \rho V_0 S \bar{c}} = V_0 \frac{\partial C_m}{\partial V} \quad (13.34)$$

Alternatively, using equation (13.7), the dimensionless derivative may be expressed in terms of Mach number rather than velocity:

$$M_u = M_0 \frac{\partial C_m}{\partial M} \quad (13.35)$$

In subsonic flight the pitching moment coefficient C_m is very nearly independent of velocity, or Mach number; thus the derivative M_u is often assumed to be negligibly small for those flight conditions.

$$\dot{M}_w = \frac{\partial M}{\partial W} \quad \textbf{Pitching moment due to normal velocity}$$

As previously, differentiating equation (13.10) with respect to W and with reference to equation (13.24), it may be shown that

$$\dot{M}_w = \frac{\partial M}{\partial W} = \frac{1}{2} \rho V^2 S \bar{c} \frac{\partial C_m}{\partial W} = \frac{1}{2} \rho V S \bar{c} \frac{\partial C_m}{\partial \alpha} \quad (13.36)$$

In the limit $V \cong V_0$ and equation (13.36) may be written as

$$\dot{M}_w = \frac{1}{2} \rho V_0 S \bar{c} \frac{\partial C_m}{\partial \alpha} \quad (13.37)$$

and with reference to Appendix 2, the dimensionless form of the derivative is given by

$$M_w = \frac{\dot{M}_w}{\frac{1}{2} \rho V_0 S \bar{c}} = \frac{\partial C_m}{\partial \alpha} \quad (13.38)$$

Further, assuming that linear aerodynamic conditions apply, such as are typical of subsonic flight, then with reference to equation (3.17),

$$M_w = \frac{dC_m}{d\alpha} = \frac{dC_L}{d\alpha} \frac{dC_m}{dC_L} = -a K_n \quad (13.39)$$

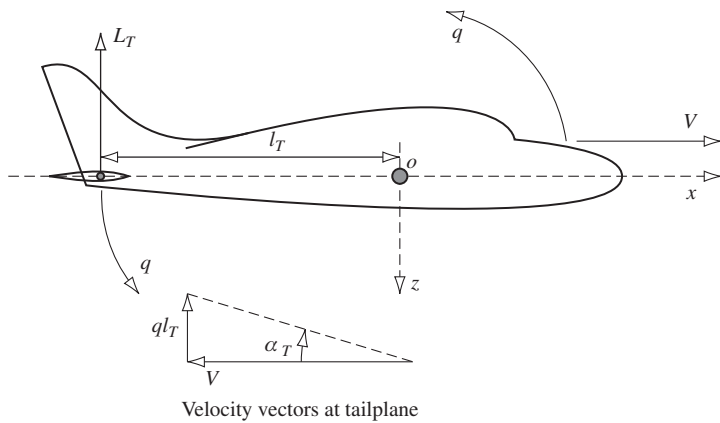
where, here, a denotes the lift curve slope and K_n is the controls-fixed static margin. As shown in Chapter 6 the derivative M_w is a measure of the *pitch stiffness* of the aeroplane and plays an important part in the determination of the longitudinal short-term dynamics.

13.2.5 Derivatives due to a pitch velocity perturbation

It is usually assumed that the longitudinal aerodynamic properties of an aeroplane are dominated by those of the wing and tailplane. However, when the disturbance is a small perturbation in pitch rate q it is assumed that the dominating aerodynamic properties are those of the tailplane. Thus, in the first instance the resulting aerodynamic changes contributing to the stability derivatives are assumed to arise entirely from tailplane effects. By so doing it is acknowledged that the wing contribution may not necessarily be small and that its omission will reduce the accuracy of the derivative estimates. However, experience has shown that the error incurred by adopting this assumption is usually acceptably small.

An aeroplane pitching through its equilibrium attitude with pitch rate perturbation q is shown in Fig. 13.2. Since the effect of the pitch rate is to cause the tailplane to experience a normal velocity component due to rotation about the cg , the resultant effect is a change in the local incidence α_T of the tailplane. The total perturbation velocity is V and the tailplane incidence perturbation is given by

$$\alpha_T \cong \tan \alpha_T = \frac{q l_T}{V} \quad (13.40)$$

**FIGURE 13.2 Tailplane incidence due to pitch rate.**

since, by definition, α_T is a small angle. It is important to appreciate that α_T is the change, or increment, in tailplane incidence relative to its equilibrium value and, like the pitch rate perturbation, is transient in nature. From [equation \(13.40\)](#) it follows that

$$\frac{\partial \alpha_T}{\partial q} = \frac{l_T}{V} \quad (13.41)$$

$$\dot{X}_q = \frac{\partial X}{\partial q} \quad \textbf{Axial force due to pitch rate}$$

In this instance, for the reasons given above, it is assumed that the axial force perturbation arises from the tailplane drag perturbation only; thus

$$X = -D_T = -\frac{1}{2} \rho V^2 S_T C_{D_T} \quad (13.42)$$

Assuming V to be independent of pitch rate q , differentiate [equation \(13.42\)](#) with respect to the perturbation variable q :

$$\frac{\partial X}{\partial q} = -\frac{1}{2} \rho V^2 S_T \frac{\partial C_{D_T}}{\partial q} \quad (13.43)$$

Now, with reference to [equation \(13.41\)](#) write

$$\frac{\partial C_{D_T}}{\partial q} = \frac{\partial C_{D_T}}{\partial \alpha_T} \frac{\partial \alpha_T}{\partial q} = \frac{l_T}{V} \frac{\partial C_{D_T}}{\partial \alpha_T} \quad (13.44)$$

Substitute [equation \(13.44\)](#) into [equation \(13.43\)](#); then, in the limit $V \cong V_0$ and [equation \(13.43\)](#) may be written as

$$\dot{X}_q = \frac{\partial X}{\partial q} = -\frac{1}{2} \rho V_0 S_T l_T \frac{\partial C_{D_T}}{\partial \alpha_T} \quad (13.45)$$

and with reference to Appendix 2, the dimensionless form of the derivative is given by

$$X_q = \frac{\dot{X}_q}{\frac{1}{2}\rho V_0 S \bar{c}} = -\bar{V}_T \frac{\partial C_{D_T}}{\partial \alpha_T} \quad (13.46)$$

where the *tail volume ratio* is given by

$$\bar{V}_T = \frac{S_T l_T}{S \bar{c}} \quad (13.47)$$

Since the rate of change of tailplane drag with incidence is usually small, it is customary to assume that the derivative X_q is insignificantly small and it is frequently ignored in aircraft stability and control analysis.

$$\dot{Z}_q = \frac{\partial Z}{\partial q} \quad \textbf{Normal force due to pitch rate}$$

Similarly, it is assumed that in a pitch rate perturbation the change in normal force arises from tailplane lift only; thus

$$Z = -L_T = -\frac{1}{2} \rho V^2 S_T C_{L_T} \quad (13.48)$$

Differentiate equation (13.48) with respect to q and with reference to equation (13.44); then

$$\frac{\partial Z}{\partial q} = -\frac{1}{2} \rho V S_T l_T \frac{\partial C_{L_T}}{\partial \alpha_T} = -\frac{1}{2} \rho V S_T l_T a_1 \quad (13.49)$$

where, again, it is assumed that V is independent of pitch rate q and that, additionally, the tailplane lift coefficient is a function of incidence only with lift curve slope denoted a_1 . Whence in the limit $V \cong V_0$ and equation (13.49) may be written as

$$\dot{Z}_q = \frac{\partial Z}{\partial q} = -\frac{1}{2} \rho V_0 S_T l_T a_1 \quad (13.50)$$

and with reference to Appendix 2, the dimensionless form of the derivative is given by

$$Z_q = \frac{\dot{Z}_q}{\frac{1}{2}\rho V_0 S \bar{c}} = -\bar{V}_T a_1 \quad (13.51)$$

$$\dot{M}_q = \frac{\partial M}{\partial q} \quad \textbf{Pitching moment due to pitch rate}$$

Again, in a pitch rate perturbation q , the pitching moment is assumed to arise entirely from the moment of the tailplane normal force perturbation, given by equation (13.48), about the *cg*. Thus, in the perturbation,

$$M = Z l_T = -\frac{1}{2} \rho V^2 S_T l_T C_{L_T} \quad (13.52)$$

Differentiate equation (13.52) with respect to q to obtain the relationship

$$\dot{M}_q = \frac{\partial M}{\partial q} = l_T \frac{\partial Z}{\partial q} = l_T \dot{Z}_q \quad (13.53)$$

It therefore follows that

$$\dot{M}_q = -\frac{1}{2} \rho V_0 S_T l_T^2 a_1 \quad (13.54)$$

and with reference to Appendix 2, the dimensionless form of the derivative is given by

$$M_q = \frac{\dot{M}_q}{\frac{1}{2} \rho V_0 S \bar{c}^2} = -\bar{V}_T \frac{l_T}{\bar{c}} a_1 \equiv \frac{l_T}{\bar{c}} Z_q \quad (13.55)$$

It is shown in Chapter 6 that M_q is the all important pitch damping derivative. Although this simple model illustrates the importance of the tailplane in determining the pitch damping characteristics of the aeroplane, wing and body contributions may also be significant. Equation (13.55) should therefore be regarded as the first estimate rather than the definitive estimate of the derivative. However, it is often good enough for preliminary analysis of stability and control.

13.2.6 Derivatives due to acceleration perturbations

The derivatives due to the acceleration perturbations \dot{u} , \dot{w} , and \dot{q} are not commonly encountered in the longitudinal equations of motion since their numerical values are usually insignificantly small. Their meaning is perhaps easier to appreciate when the longitudinal equations of motion are written in matrix form, equation (4.65), to include all of the acceleration derivatives. To recap, the state equation is given by

$$\mathbf{M}\dot{\mathbf{x}} = \mathbf{A}'\mathbf{x} + \mathbf{B}'\mathbf{u} \quad (13.56)$$

with state vector, $\mathbf{x}^T = [u \ w \ q \ \theta]$ and input vector $\mathbf{u}^T = [\eta \ \tau]$. The state matrix \mathbf{A}' and input matrix \mathbf{B}' remain unchanged whereas the mass matrix \mathbf{M} is modified to include all the additional acceleration derivatives:

$$\mathbf{M} = \begin{bmatrix} \left(m - X_{\dot{u}}\right) & -X_{\dot{w}} & -X_{\dot{q}} & 0 \\ -Z_{\dot{u}} & \left(m - Z_{\dot{w}}\right) & -Z_{\dot{q}} & 0 \\ -M_{\dot{u}} & -M_{\dot{w}} & \left(I_y - M_{\dot{q}}\right) & 0 \\ 0 & 0 & 0 & 1 \end{bmatrix} \quad (13.57)$$

Since all of the acceleration derivatives appear in the mass matrix alongside the normal mass and inertia terms, their effect is to change (increase) the apparent mass and inertia properties of the aircraft. For this reason they are sometimes referred to as *apparent* or *virtual* mass and inertia terms. Whenever the aeroplane moves, some of the surrounding displaced air mass is entrained and moves with the aircraft, and it is the mass and inertia of this air which modifies the apparent mass and inertia of the aeroplane. The acceleration derivatives quantify this effect. For most aircraft,

since the mass of the displaced air is a small fraction of the mass of the aircraft, the acceleration derivatives are insignificantly small. An exception to this is the airship, for which the apparent mass and inertia can be as much as 50% larger than the actual physical value. Other vehicles in which these effects may be nonnegligible include balloons, parachutes, and underwater vehicles which operate in a much denser fluid medium.

For many modern high-performance aeroplanes the derivatives due to a rate of change of normal velocity perturbation \dot{w} ($\dot{\alpha}$) may not be negligible. A rate of change of normal velocity perturbation causes a transient disturbance in the downwash field behind the wing which passes over the tailplane a short time later. The disturbance to the moving air mass in the vicinity of the wing is, in itself, insignificant for the reason given above. However, since the tailplane sees this as a transient in incidence, a short time later it responds accordingly and the effect on the airframe is not necessarily insignificant. This particular characteristic is known as the *downwash lag* effect.

An expression for the total incidence of the tailplane is given by equation (3.9), which, for the present application, may be written as

$$\alpha_T(t) = \alpha_e + \eta_T - \varepsilon(t) \quad (13.58)$$

where α_e is the steady equilibrium incidence of the wing, η_T is the tailplane setting angle, and $\varepsilon(t)$ is the downwash flow angle at the tailplane. Thus any change in downwash angle at the tailplane in otherwise steady conditions gives rise to a change in tailplane incidence of equal magnitude and opposite sign. It is important to appreciate that the perturbation at the tailplane is observed at time t and is due to an event on the wing which took place some time earlier. For this reason the flow conditions on the wing at time t are assumed to have recovered their steady equilibrium state.

With reference to Fig. 13.3, the point a in the flow field around the wing arrives at point b in the flow field around the tailplane at a time l_T/V_e later, referred to as the *downwash lag* and where, for convenience, the mean distance travelled is assumed to be equal to the tail moment arm l_T . Thus a perturbation in \dot{w} ($\dot{\alpha}$) causes a perturbation in the wing downwash field which arrives at the tailplane after the downwash lag time interval. Therefore, there is a short delay between cause and effect.

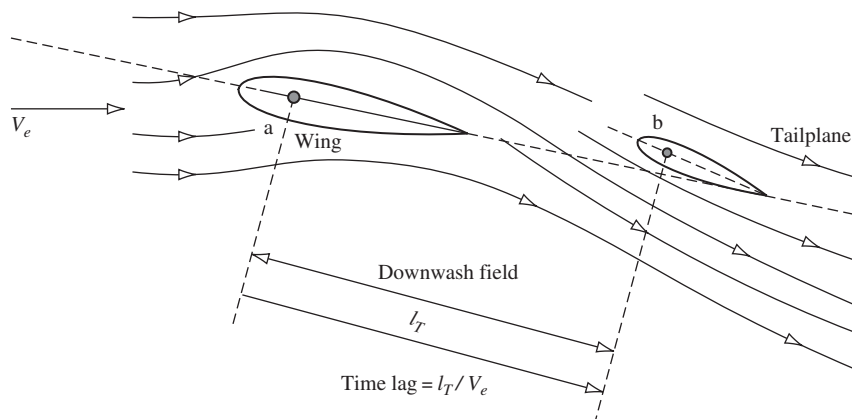


FIGURE 13.3 Typical downwash field.

The downwash angle $\varepsilon(t)$ at the tailplane at time t is therefore a function of the incidence of the wing at time $t' = t - l_T/V_0$ and may be expressed as

$$\begin{aligned}\varepsilon(t) &= \frac{d\varepsilon}{d\alpha} \alpha(t') = \frac{d\varepsilon}{d\alpha} \frac{d\alpha}{dt} \left(t - \frac{l_T}{V_0} \right) \\ &= \frac{d\varepsilon}{d\alpha} \alpha_e - \frac{d\varepsilon}{d\alpha} \frac{\dot{w}l_T}{V_0^2} = \varepsilon_e - \frac{d\varepsilon}{d\alpha} \frac{\dot{w}l_T}{V_0^2}\end{aligned}\quad (13.59)$$

since

$$\frac{d\alpha}{dt} t = \alpha(t) \equiv \alpha_e \quad (13.60)$$

and

$$\alpha \cong \tan \alpha = \frac{w}{V_0} \quad (13.61)$$

whence

$$\frac{d\alpha}{dt} = \frac{\dot{w}}{V_0} \quad (13.62)$$

Thus, with reference to equations (13.58) and (13.59) the total tailplane incidence during a downwash perturbation may be written as

$$\alpha_{T_e} + \alpha_T(t) = \alpha_e + \eta_T - \varepsilon_e + \frac{d\varepsilon}{d\alpha} \frac{\dot{w}l_T}{V_0^2} \quad (13.63)$$

The perturbation in tailplane incidence due to the downwash lag effect is therefore given by

$$\alpha_T(t) = \frac{d\varepsilon}{d\alpha} \frac{\dot{w}l_T}{V_0^2} \quad (13.64)$$

$$\overset{\circ}{X}_{\dot{w}} = \frac{\partial X}{\partial \dot{w}} \quad \textbf{Axial force due to rate of change of normal velocity}$$

In this instance, it is assumed that the axial force perturbation arises from the perturbation in tailplane drag due solely to the perturbation in incidence; whence

$$X = -D_T = -\frac{1}{2} \rho V^2 S_T C_{D_T} = -\frac{1}{2} \rho V^2 S_T \frac{\partial C_{D_T}}{\partial \alpha_T} \alpha_T \quad (13.65)$$

Now, by definition,

$$X = \overset{\circ}{X}_{\dot{w}} \dot{w} \quad (13.66)$$

and in the limit $V \cong V_0$. Thus substitute equation (13.64) into (13.65) and apply equation (13.66) to obtain

$$\overset{\circ}{X}_{\dot{w}} = -\frac{1}{2} \rho S_T l_T \frac{\partial C_{D_T}}{\partial \alpha_T} \frac{d\varepsilon}{d\alpha} \quad (13.67)$$

and with reference to Appendix 2, the dimensionless form of the derivative is given by

$$\dot{X}_{\dot{w}} = \frac{\dot{X}_{\dot{w}}}{\frac{1}{2}\rho S \bar{c}} = -\bar{V}_T \frac{\partial C_{D_T}}{\partial \alpha_T} \frac{d\varepsilon}{d\alpha} \equiv X_q \frac{d\varepsilon}{d\alpha} \quad (13.68)$$

Since $X_q X_q$ is usually very small and $d\varepsilon/d\alpha < 1$, the derivative $\dot{X}_{\dot{w}}$ is insignificantly small and is usually omitted from the equations of motion.

$$\dot{Z}_{\dot{w}} = \frac{\partial Z}{\partial \dot{w}} \quad \textbf{Normal force due to rate of change of normal velocity}$$

Again, it is assumed that the normal force perturbation arises from the perturbation in tailplane lift due solely to the perturbation in incidence; whence

$$Z = -L_T = -\frac{1}{2} \rho V^2 S_T C_{L_T} = -\frac{1}{2} \rho V^2 S_T \frac{\partial C_{L_T}}{\partial \alpha_T} \alpha_T \quad (13.69)$$

Again, by definition,

$$\dot{Z} = \dot{Z}_{\dot{w}} \dot{w} \quad (13.70)$$

and in the limit $V \cong V_0$. Thus substitute [equation \(13.64\)](#) into (13.69) and apply [equation \(13.70\)](#) to obtain

$$\dot{Z}_{\dot{w}} = -\frac{1}{2} \rho S_T l_T a_1 \frac{d\varepsilon}{d\alpha} \quad (13.71)$$

As in [Section 13.2.4](#), it is assumed that the tailplane lift coefficient is a function of incidence only with lift curve slope denoted a_1 . With reference to Appendix 2, the dimensionless form of the derivative is given by

$$\dot{Z}_{\dot{w}} = \frac{\dot{Z}_{\dot{w}}}{\frac{1}{2}\rho S \bar{c}} = -\bar{V}_T a_1 \frac{d\varepsilon}{d\alpha} \equiv Z_q \frac{d\varepsilon}{d\alpha} \quad (13.72)$$

Care should be exercised since $Z_{\dot{w}}$ is not always insignificant.

$$\dot{M}_{\dot{w}} = \frac{\partial M}{\partial \dot{w}} \quad \textbf{Pitching moment due to rate of change of normal velocity}$$

In this instance the pitching moment is assumed to arise entirely from the moment of the tailplane normal force perturbation about the *cg* resulting from the perturbation in incidence, given by [equation \(13.64\)](#). Thus, in the perturbation,

$$M = Z l_T = -\frac{1}{2} \rho V^2 S_T l_T \frac{\partial C_{L_T}}{\partial \alpha_T} \alpha_T \quad (13.73)$$

Again, by definition,

$$M = \dot{M}_{\dot{w}} \dot{w} \quad (13.74)$$

and in the limit $V \cong V_0$. Thus substitute [equation \(13.64\)](#) into (13.73) and apply [equation \(13.74\)](#) to obtain

$$\dot{M}_{\dot{w}} = -\frac{1}{2} \rho S_T l_T^2 a_1 \frac{d\varepsilon}{d\alpha} \quad (13.75)$$

and with reference to Appendix 2, the dimensionless form of the derivative is given by

$$M_{\dot{w}} = \frac{\dot{M}_{\dot{w}}}{\frac{1}{2} \rho S \bar{c}^2} = -\bar{V}_T \frac{l_T}{\bar{c}} a_1 \frac{d\varepsilon}{d\alpha} \equiv M_q \frac{d\varepsilon}{d\alpha} \quad (13.76)$$

The derivative $M_{\dot{w}}$ is nearly always significant and makes an important contribution to the damping of the short-period pitching oscillation (see [equation \(6.21\)](#)).

13.3 Lateral-directional aerodynamic stability derivatives

For convenience, a summary of the derivative expressions derived in this paragraph is also included in [Table A8.2](#), Appendix 8.

13.3.1 Preliminary considerations

Unlike the longitudinal aerodynamic stability derivatives, the lateral-directional derivatives are much more difficult to estimate with any degree of confidence. The problem arises from the mutual aerodynamic interference between the lifting surfaces, fuselage, power plant, undercarriage, and so forth in asymmetric flow conditions, which makes it difficult to identify the most significant contributions to a particular derivative with any degree of certainty. When a derivative cannot be estimated by the simplest analysis of the often complex aerodynamics, then, the use of *strip theory* is resorted to, which is a method of analysis which also tends to oversimplify the aerodynamic conditions in order that progress can be made. Either way, analytical estimates of the lateral-directional derivatives are often of poor accuracy and, for more reliable estimates, use of the ESDU data items is preferable. However, the simple theories used for the purpose do give a useful insight into the physical phenomena involved and, consequently, are a considerable asset to the proper understanding of aeroplane dynamics.

13.3.2 Derivatives due to sideslip

As seen by the pilot (and consistent with the notation), a positive sideslip is to the right (starboard) and is defined by the small-perturbation lateral velocity transient denoted v . The nature of a free positive sideslip disturbance is such that the right wing tends to drop and the nose tends to swing to the left of the incident *wind vector* as the aeroplane slips to the right. The reaction to the disturbance is stabilising if the aerodynamic forces and moments produced in response to the sideslip velocity tend to restore the aeroplane to a wings-level equilibrium state. The motions involved are discussed in greater detail in the context of lateral static stability in [Section 3.4](#), in the context of directional static stability in [Section 3.5](#), and in the context of dynamic stability in [Section 7.2](#).

$$\dot{Y}_v = \frac{\partial Y}{\partial V} \textbf{Sideforce due to sideslip}$$

Sideforce due to sideslip arises mainly from the fuselage, the fin, the wing (especially a wing with dihedral), and engine nacelles in aircraft with external engines. The derivative is notoriously difficult to estimate with any degree of confidence and simple analysis assumes that the dominant contributions arise from the fuselage and fin only.

With reference to Fig. 13.4, the fuselage creates a sideforce Y_B in a sideslip, which may be regarded as *lateral drag* and is given by

$$Y_B = \frac{1}{2} \rho V_0^2 S_B \beta y_B \quad (13.77)$$

where S_B is the projected fuselage side area and y_B is a dimensionless coefficient. Note that the product βy_B is equivalent to a *lateral drag coefficient* for the fuselage. Further, since the disturbance is small the sideslip angle β is given by

$$\beta \cong \tan \beta = \frac{v}{V_0} \quad (13.78)$$

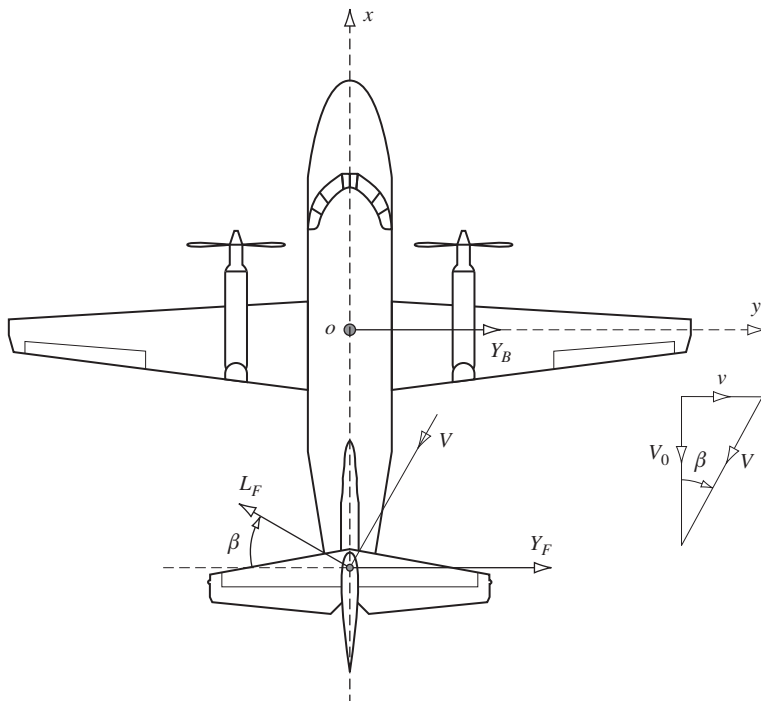


FIGURE 13.4 Sideforce generation in sideslip.

In a sideslip the fin is at incidence β and produces lift as indicated in Fig. 13.4. The fin lift resolves into a sideforce Y_F given by

$$Y_F = -\frac{1}{2} \rho V_0^2 S_F a_{1F} \beta \cos \beta \cong -\frac{1}{2} \rho V_0^2 S_F a_{1F} \beta \quad (13.79)$$

and since the sideslip angle β is small, $\cos \beta \cong 1$.

Let the total sideforce due to sideslip be denoted Y ; then, by definition,

$$v \dot{Y}_v = Y = Y_B + Y_F = \frac{1}{2} \rho V_0^2 (S_B y_B - S_F a_{1F}) \beta \quad (13.80)$$

Substitute the expression for β given by equation (13.78) into equation (13.80) to obtain an expression for the dimensional derivative,

$$\dot{Y}_v = \frac{1}{2} \rho V_0 (S_B y_B - S_F a_{1F}) \quad (13.81)$$

and with reference to Appendix 2, the dimensionless form of the derivative is given by

$$Y_v = \frac{\dot{Y}_v}{\frac{1}{2} \rho V_0 S} = \left(\frac{S_B}{S} y_B - \frac{S_F}{S} a_{1F} \right) \quad (13.82)$$

$$\dot{L}_v = \frac{\partial L}{\partial V} \textbf{Rolling moment due to sideslip}$$

Rolling moment due to sideslip is one of the most important lateral stability derivatives since it quantifies the *lateral static stability* of the aeroplane, discussed in Section 3.4. It is one of the most difficult derivatives to estimate with any degree of confidence since it is numerically small and has many identifiable contributions. Preliminary estimates are based on the most significant contributions, which are usually assumed to arise from wing dihedral, wing sweep, wing-fuselage geometry, and the fin.

In many classical aeroplanes the wing dihedral makes the most significant contribution to the overall value of the derivative. Indeed, dihedral is one of the most important variables available to the aircraft designer with which to tailor the lateral static stability of the aeroplane. The derivative is therefore frequently referred to as *dihedral effect* irrespective of the magnitude of the other contributions. Since the tendency is for the right wing to drop in a positive sideslip disturbance, the associated disturbing rolling moment is also positive. A stabilising aerodynamic reaction is one in which the rolling moment due to sideslip is negative since this will tend to oppose the disturbing rolling moment. Dihedral effect is particularly beneficial in this respect.

In a positive sideslip disturbance to the right, the effect of dihedral is to increase the incidence of the right wing panel indicated in Fig. 13.5. The left wing panel “sees” a corresponding reduction in incidence. Thus the rolling moment is generated by the differential lift across the wing span.

Referring to Fig. 13.5, the component of sideslip velocity perpendicular to the plane of the wing panel is given by

$$v' = v \sin \Gamma \cong v \Gamma \quad (13.83)$$

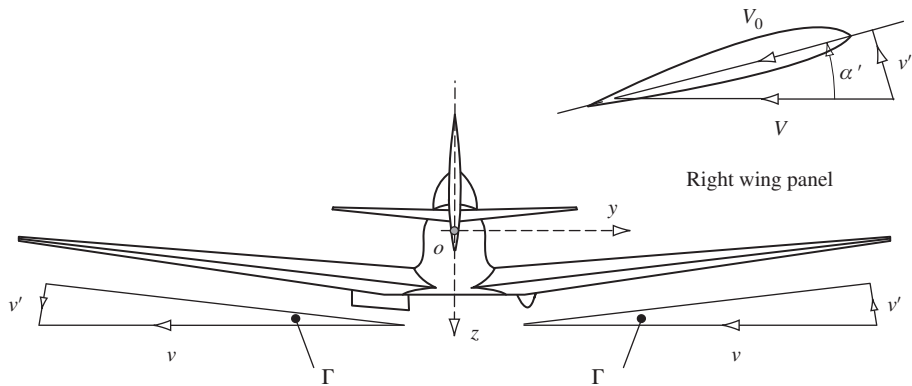


FIGURE 13.5 Incidence due to sideslip on a wing with dihedral.

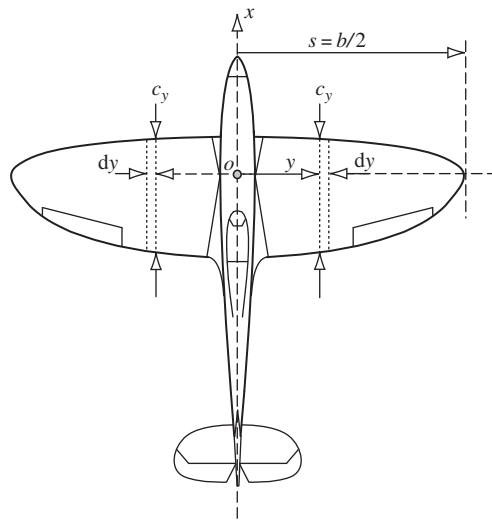


FIGURE 13.6 Chordwise strip element on the right wing panel.

since the dihedral angle Γ is usually small. The velocity component v' gives rise to a small increment in incidence α' as shown, where

$$\alpha' \cong \tan \alpha' = \frac{v'}{V_0} = \frac{v\Gamma}{V_0} \quad (13.84)$$

Consider the lift due to the increment in incidence on the chordwise strip element on the right wing panel as shown in Fig. 13.6. The strip is at spanwise coordinate y measured from the ox axis,

and has elemental width dy and local chord c_y . The lift increment on the strip resolves into a normal force increment δZ given by

$$\delta Z_{right} = -\frac{1}{2} \rho V_0^2 c_y dy a_y \alpha' \cos \Gamma \cong -\frac{1}{2} \rho V_0 c_y a_y v \Gamma dy \quad (13.85)$$

where a_y is the local lift curve slope. The corresponding increment in rolling moment δL is given by

$$\delta L_{right} = \delta Z_{right} y = -\frac{1}{2} \rho V_0 c_y a_y v \Gamma y dy \quad (13.86)$$

The total rolling moment due to the right wing panel may be obtained by integrating equation (13.86) from the root to the tip, whence

$$L_{right} = -\frac{1}{2} \rho V_0 v \int_0^s c_y a_y \Gamma y dy \quad (13.87)$$

Similarly for the left hand wing panel,

$$\delta L_{left} = -\delta Z_{left} y = -y \left(\frac{1}{2} \rho V_0 c_y a_y v \Gamma dy \right) \quad (13.88)$$

Note that the sign of the normal force increment is reversed on the left wing panel since the incidence is in fact a decrement and that the sign of the moment arm is also reversed. Thus

$$L_{left} = -\frac{1}{2} \rho V_0 v \int_0^s c_y a_y \Gamma y dy \quad (13.89)$$

By definition the total rolling moment in the sideslip disturbance is given by

$$v \overset{\circ}{L}_v = L_{right} + L_{left} = L_{total} = -\rho V_0 v \int_0^s c_y a_y \Gamma y dy \quad (13.90)$$

Whence the contribution to the dimensional derivative due to dihedral is

$$\overset{\circ}{L}_{v(dihedral)} = -\rho V_0 \int_0^s c_y a_y \Gamma y dy \quad (13.91)$$

and with reference to Appendix 2, the dimensionless form of the contribution is given by

$$\overset{\circ}{L}_{v(dihedral)} = \frac{\overset{\circ}{L}_{v(dihedral)}}{\frac{1}{2} \rho V_0 S b} = -\frac{1}{S s} \int_0^s c_y a_y \Gamma y dy \quad (13.92)$$

where $b = 2s$ is the wing span. It is clear that for a wing with dihedral the expression given by equation (13.92) will always be negative and hence stabilising. On the other hand, a wing with anhedral will be destabilising.

Wing sweep also makes a significant contribution to L_v . The lift on a yawed wing is determined by the component of velocity normal to the quarter-chord line in subsonic flight and normal to the leading edge in supersonic flight. A swept wing is therefore treated as a yawed wing. With reference to Fig. 13.7, consider an elemental chordwise strip on the right wing panel which is

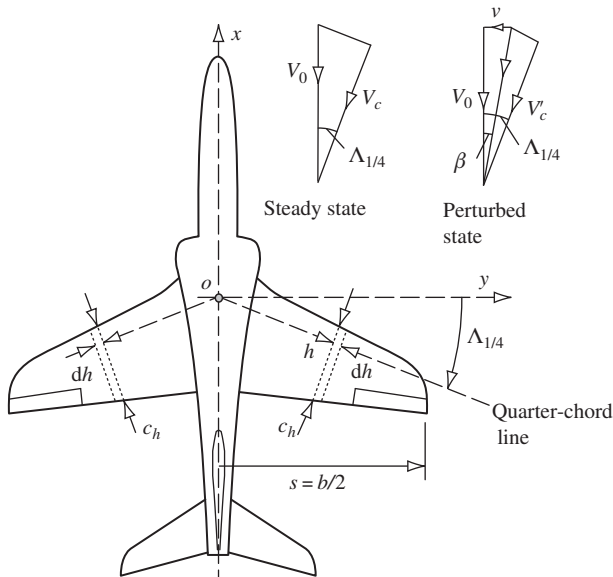


FIGURE 13.7 Swept wing in sideslip.

perpendicular to the quarter-chord line. Subsonic flow conditions are therefore assumed and the flow direction is parallel to the chord line. The strip element is at spanwise distance h from the ox axis, measured along the quarter-chord line, the local chord is c_h , and the width of the strip is dh . In the steady equilibrium flight condition the chordwise component of velocity is given by

$$V_c = V_0 \cos \Lambda_{1/4} \quad (13.93)$$

and in the presence of a positive sideslip disturbance this becomes

$$V'_c = \frac{V_0}{\cos \beta} \cos(\Lambda_{1/4} - \beta) \cong V_0 \cos(\Lambda_{1/4} - \beta) \quad (13.94)$$

where β is the sideslip angle, which is small by definition. The increment in normal force δZ on the chordwise strip due to the sideslip disturbance arises from the difference in lift between the steady flight condition and the perturbed condition and is given by

$$\delta Z_{right} = -\left(\frac{1}{2} \rho V'_c^2 2c_h dha_h \alpha - \frac{1}{2} \rho V_c^2 c_h dha_h \alpha \right) = -\frac{1}{2} \rho (V'_c^2 - V_c^2) c_h dha_h \alpha \quad (13.95)$$

Substitute the velocity expressions, [equations \(13.93\) and \(13.94\)](#), into [equation \(13.95\)](#), rearrange, and make small angle approximations where appropriate to obtain

$$\delta Z_{right} = -\frac{1}{2} \rho V_0^2 (\beta^2 \sin^2 \Lambda_{1/4} + 2\beta \sin \Lambda_{1/4} \cos \Lambda_{1/4}) a_h \alpha c_h dh \quad (13.96)$$

Thus the resulting increment in rolling moment is

$$\begin{aligned}\delta L_{right} &= h \cos \Lambda_{\frac{1}{4}} \delta Z_{right} \\ &= -\frac{1}{2} \rho V_0^2 \cos \Lambda_{\frac{1}{4}} (\beta^2 \sin^2 \Lambda_{\frac{1}{4}} + 2\beta \sin \Lambda_{\frac{1}{4}} \cos \Lambda_{\frac{1}{4}}) a_h \alpha c_h h dh\end{aligned}\quad (13.97)$$

On the corresponding strip element on the left-hand wing panel the chordwise velocity in the sideslip disturbance is given by

$$V_c' = \frac{V_0}{\cos \beta} \cos(\Lambda_{\frac{1}{4}} + \beta) \cong V_0 \cos(\Lambda_{\frac{1}{4}} + \beta) \quad (13.98)$$

It therefore follows that the resulting increment in rolling moment arising from the left wing panel is

$$\begin{aligned}\delta L_{left} &= -h \cos \Lambda_{\frac{1}{4}} \delta Z_{left} \\ &= \frac{1}{2} \rho V_0^2 \cos \Lambda_{\frac{1}{4}} (\beta^2 \sin^2 \Lambda_{\frac{1}{4}} - 2\beta \sin \Lambda_{\frac{1}{4}} \cos \Lambda_{\frac{1}{4}}) a_h \alpha c_h h dh\end{aligned}\quad (13.99)$$

The total increment in rolling moment is given by the sum of the right and left wing panel contributions, (13.97) and (13.99); substituting for β from [equation \(13.78\)](#), then

$$L_{total} = \delta L_{right} + \delta L_{left} = -2\rho V_0 v \sin \Lambda_{\frac{1}{4}} \cos^2 \Lambda_{\frac{1}{4}} a_h \alpha c_h h dh \quad (13.100)$$

Thus the total rolling moment due to the sideslip disturbance is given by integrating [equation \(13.100\)](#) along the quarter-chord line from the root to the wing tip. By definition the total rolling moment due to sweep is given by

$$v \dot{\bar{L}}_{v(sweep)} = \int \delta L_{total} = -2\rho V_0 v \sin \Lambda_{\frac{1}{4}} \cos^2 \Lambda_{\frac{1}{4}} \int_0^{s \sec \Lambda_{\frac{1}{4}}} a_h \alpha c_h h dh \quad (13.101)$$

or

$$\dot{\bar{L}}_{v(sweep)} = -2\rho V_0 \sin \Lambda_{\frac{1}{4}} \cos^2 \Lambda_{\frac{1}{4}} \int_0^{s \sec \Lambda_{\frac{1}{4}}} a_h \alpha c_h h dh \quad (13.102)$$

Now it is more convenient to express the geometric variables in [equation \(13.102\)](#) in terms of spanwise and chordwise parameters measured parallel to the oy and ox axes, respectively. The geometry of the wing determines that $c_y = c_h \cos \Lambda_{\frac{1}{4}}$, $dy = dh \cos \Lambda_{\frac{1}{4}}$, $y = h \cos \Lambda_{\frac{1}{4}}$, and the integral limit $s \sec \Lambda_{\frac{1}{4}}$ becomes s . [Equation \(13.102\)](#) may then be written as

$$\dot{\bar{L}}_{v(sweep)} = -2\rho V_0 \tan \Lambda_{\frac{1}{4}} \int_0^s C_{L_y} c_y y dy \quad (13.103)$$

where $C_{L_y} = a_h \alpha$ is the local lift coefficient. However, in the interests of practicality the constant mean lift coefficient for the wing is often assumed and [equation \(13.103\)](#) then simplifies to

$$\dot{\bar{L}}_{v(sweep)} = -2\rho V_0 C_L \tan \Lambda_{\frac{1}{4}} \int_0^s c_y y dy \quad (13.104)$$

and with reference to Appendix 2, the dimensionless form of the contribution is given by

$$L_{v(sweep)} = \frac{\dot{L}_{v(sweep)}}{\frac{1}{2}\rho V_0 S b} = -\frac{2C_L \tan A_{l4}}{Ss} \int_0^s c_y y dy \quad (13.105)$$

where $b = 2s$ is the wing span. Again, it is clear that for a wing with aft sweep the expression given by equation (13.105) will always be negative and hence stabilising. Thus wing sweep is equivalent to dihedral as a mechanism for improving lateral stability. On the other hand, a wing with forward sweep will be laterally destabilising.

The geometry of the wing and fuselage in combination may also make a significant contribution to dihedral effect since in a sideslip condition the lateral cross-flow in the vicinity of the wing root gives rise to differential lift, which, in turn, gives rise to rolling moment.

As shown in Fig. 13.8 in a positive sideslip perturbation the aeroplane “sees” the lateral sideslip velocity component approaching from the right, it being implied that the right wing starts to drop at the onset of the disturbance. The lateral flow around the fuselage is approximately as indicated, thereby giving rise to small perturbations in upwash and downwash in the vicinity of the wing root. As a consequence of the flow condition the high wing configuration experiences a transient increase in incidence at the right wing root and a corresponding decrease in incidence at the left wing root.

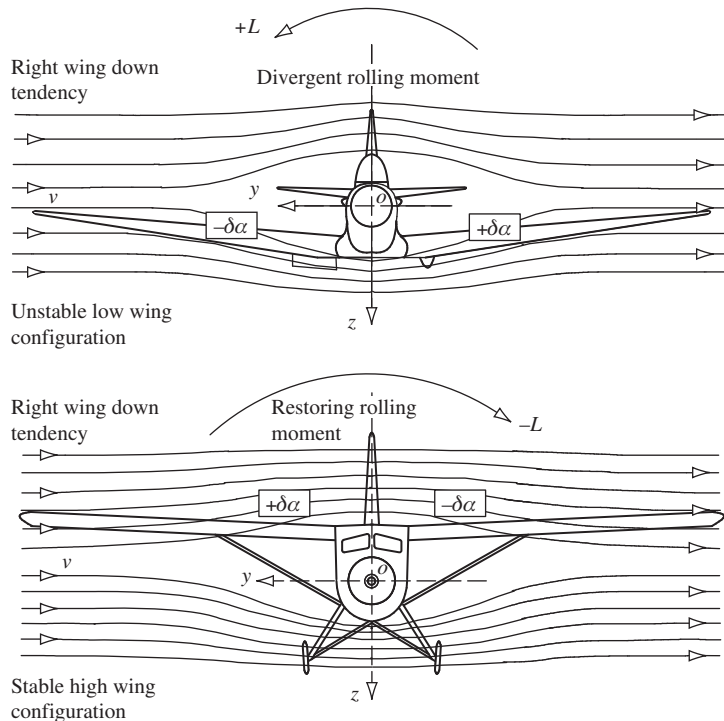


FIGURE 13.8 Lateral cross-flow in sideslip.

The differential lift thus created causes a negative rolling moment, and since this will tend to “pick up” the right wing the effect is stabilising. Clearly, as indicated, a low wing configuration behaves in the opposite manner and the rolling moment due to sideslip is definitely destabilising. Thus a high wing configuration enjoys an additional stabilising contribution to dihedral effect whereas a low wing configuration makes a destabilising contribution.

It is not generally possible to develop simple aerodynamic expressions to quantify the wing-fuselage geometry contribution to rolling moment due to sideslip. The aerodynamic phenomena involved are rather too complex to be modelled simply. It is known, for example, that the magnitude of the contribution is increased with an increase in fuselage width or depth and with an increase in aspect ratio. Reliable values for the contribution are best obtained by measurement or by reference to source documents such as ESDU data items.

The fin contribution to rolling moment due to sideslip arises from the way in which the lift developed on the fin in a sideslip perturbation acts on the airframe. The lift acts at the aerodynamic centre of the fin, which may be above or below the roll axis, thereby giving rise to a rolling moment. A typical situation is shown in Fig. 13.9.

The sideforce Y_F resulting from the lift developed by the fin in a sideslip perturbation is given by equation (13.79), and if the moment arm of the aerodynamic centre about the roll axis (ox axis) is denoted h_F , then in the perturbation by definition

$$\dot{v}_{v(\text{fin})} = L = Y_F h_F = -\frac{1}{2} \rho V_0^2 S_F a_{1F} \beta h_F \quad (13.106)$$

Substitute for β from equation (13.78) to obtain the following expression for the dimensional contribution to the derivative:

$$\dot{L}_{v(\text{fin})} = -\frac{1}{2} \rho V_0 S_F a_{1F} h_F \quad (13.107)$$

With reference to Appendix 2, the dimensionless form of the contribution is given by

$$\dot{L}_{v(\text{fin})} = \frac{\dot{L}_{v(\text{fin})}}{\frac{1}{2} \rho V_0 S b} = -\frac{S_F h_F}{S b} a_{1F} = -\bar{V}_F \frac{h_F}{l_F} a_{1F} \quad (13.108)$$

where the *fin volume ratio* is given by

$$\bar{V}_F = \frac{S_F l_F}{S b} \quad (13.109)$$

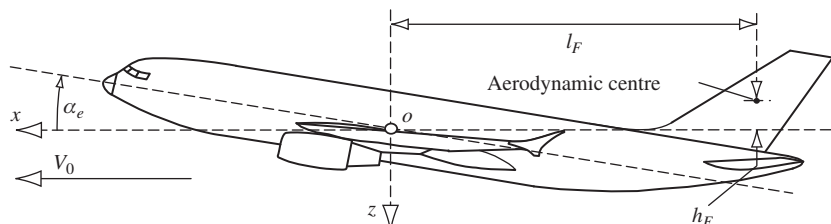


FIGURE 13.9 Rolling moment due to fin lift in sideslip.

When the aerodynamic centre of the fin is above the roll axis, h_F is positive and the expression given by [equation \(13.108\)](#) will be negative and hence stabilising. However, it is evident that, depending on aircraft geometry, h_F may be small and may even change sign at extreme aircraft attitude. Thus at certain flight conditions the contribution to rolling moment due to sideslip arising from the fin may become positive and hence laterally destabilising.

An estimate of the total value of the derivative L_v is obtained by summing the estimates of all the contributions for which a value can be obtained. Since the value of the derivative is usually small and negative, and hence stabilising, even small inaccuracies in the estimated values of the contributions can lead to a very misleading conclusion. Since the derivative is so important in the determination of the lateral stability and control characteristics of an aeroplane, the ESDU data items include a comprehensive procedure for estimating meaningful values of the significant contributions. Although, collectively, all the contributions probably embrace the most complex aerodynamics of all the derivatives, it is, fortunately, relatively easy to measure in both a wind tunnel test and in a flight test.

$$\overset{\circ}{N}_v = \frac{\partial N}{\partial V} \quad \text{Yawing moment due to sideslip}$$

The *weathercock*, or directional static stability, of an aircraft is determined by the yawing moment due to sideslip derivative. It quantifies the tendency of the aeroplane to turn *into wind* in the presence of a sideslip disturbance. Directional static stability is also discussed in greater detail in Section 3.5. In a sideslip disturbance the resulting lift increments arising from wing dihedral, wing sweep, wing-fuselage geometry, and so forth, as described previously, also give rise to associated increments in induced drag. The differential drag effects across the wing span give rise in turn to contributions to yawing moment due to sideslip. However, these contributions are often regarded as insignificant compared with that due to the fin, at least for preliminary estimates. Note that in practice the additional contributions may well be significant and that by ignoring them a degree of inaccuracy is implied in the derivative estimate.

With reference to [Fig. 13.4](#) and [Fig. 13.9](#), consider only the fin contribution which arises from the turning moment in yaw caused by the fin sideforce resulting from the sideslip. By definition this may be quantified as follows:

$$v \overset{\circ}{N}_{v(fin)} = -l_F Y_F = \frac{1}{2} \rho V_0^2 S_F a_{1F} \beta l_F \quad (13.110)$$

where the fin sideforce due to sideslip is given by [equation \(13.79\)](#). Substitute for β from [equation \(13.78\)](#) to obtain the expression for the dimensional derivative:

$$\overset{\circ}{N}_{v(fin)} = \frac{1}{2} \rho V_0 S_F a_{1F} l_F \quad (13.111)$$

With reference to Appendix 2, the dimensionless form of the derivative is given by

$$N_{v(fin)} = \frac{\overset{\circ}{N}_{v(fin)}}{\frac{1}{2} \rho V_0 S b} = \bar{V}_F a_{1F} \quad (13.112)$$

Note that the sign of N_v is positive, which indicates that it is stabilising in effect. In a positive sideslip the incident wind vector is offset to the right of the nose (see [Fig. 13.4](#)), and the stabilising

yawing moment due to sideslip results in a positive yaw response to turn the aircraft to the right until the aircraft aligns directionally with the wind vector. The yawing effect of the sideslip is thus nullified. The contribution from the wing due to differential drag effects is also usually stabilising and may well become the most significant contribution at high angles of attack since a large part of the fin may become immersed in the forebody wake, with the consequent reduction in its aerodynamic effectiveness. The contribution from the *lateral drag* effects on the gross side area ahead of and behind the *cg* may also be significant. However, it is commonly found that the yawing moment due to sideslip arising from the side area is often negative and hence destabilising. For certain classes of aircraft, such as large transport aeroplanes, this destabilising contribution can be very significant and requires a very large fin to ensure a reasonable degree of aerodynamic directional stability.

13.3.3 Derivatives due to rate of roll

As seen by the pilot, positive roll is to the right, consistent with a down-going right wing, and the small-perturbation roll rate transient is denoted p . The nature of a free positive roll rate disturbance is such that as the right wing tends to drop it is accompanied by a tendency for the nose to turn to the right and for the aeroplane to sideslip to the right. The reaction to the roll rate disturbance is stabilising if the aerodynamic forces and moments produced in response tend to restore the aeroplane to a wings-level zero sideslip equilibrium state.

$$\overset{\circ}{Y_p} = \frac{\partial Y}{\partial p} \text{ **Sideforce due to roll rate**}$$

The sideforce due to roll rate is usually considered to be negligible except for aircraft with a large high-aspect-ratio fin. Even then, the effect may well be small. Thus the fin contribution is assumed to be the only significant contribution to the derivative and may be estimated as follows.

With reference to Fig. 13.10, consider the chordwise strip element on the fin of width dh and at coordinate h measured upwards from the ox axis. When the aeroplane experiences a positive roll rate disturbance p , the strip element on the fin experiences a lateral velocity component ph . The resultant total velocity transient V is at incidence α' to the fin and, since the incidence transient is small by definition,

$$\alpha' \cong \tan \alpha' = \frac{ph}{V_0} \quad (13.113)$$

The incidence transient causes a fin lift transient, which resolves into a lateral force increment δY on the chordwise strip element and is given by

$$\delta Y = -\frac{1}{2} \rho V_0^2 c_h dha_h \alpha' = -\frac{1}{2} \rho V_0 p a_h c_h h dh \quad (13.114)$$

where a_h is the local lift curve slope and c_h is the local chord. The total sideforce transient acting on the fin in the roll rate disturbance is given by integrating equation (13.114) from the root to the tip of the fin and, by definition,

$$p \overset{\circ}{Y}_{P(\text{fin})} = Y_F = -\frac{1}{2} \rho V_0 p \int_0^{H_F} a_h c_h h dh \quad (13.115)$$

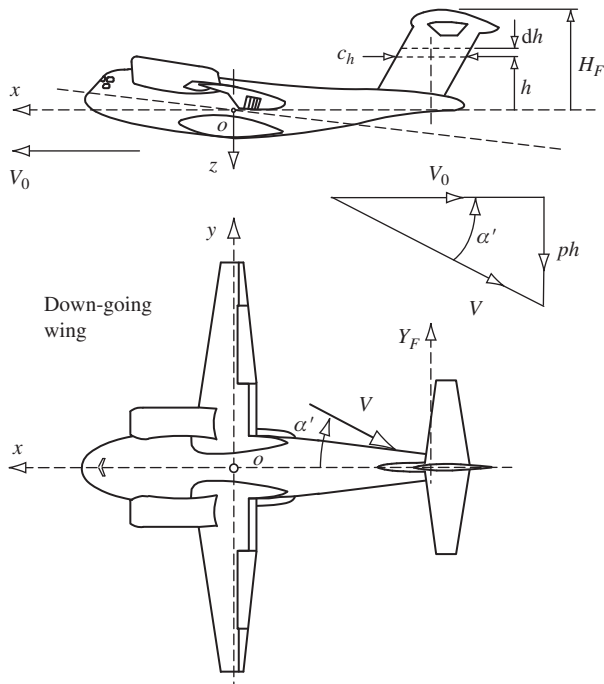


FIGURE 13.10 Fin sideforce generation in rolling flight.

where H_F is the fin span measured from the ox axis. The expression for the fin contribution to the dimensional derivative is therefore given by

$$\dot{Y}_{p(\text{fin})} = -\frac{1}{2} \rho V_0 \int_0^{H_F} a_h c_h h dh \quad (13.116)$$

and with reference to Appendix 2, the dimensionless form of the derivative is given by

$$\dot{Y}_{p(\text{fin})} = \frac{\dot{Y}_{p(\text{fin})}}{\frac{1}{2} \rho V_0 S b} = -\frac{1}{S b} \int_0^{H_F} a_h c_h h dh \quad (13.117)$$

$$\dot{L}_p = \frac{\partial L}{\partial p} \quad \textbf{Rolling moment due to roll rate}$$

Rolling moment due to roll rate arises largely from the wing with smaller contributions from the fuselage, tailplane, and fin. This derivative is most important since it quantifies the damping in roll and is therefore significant in determining the dynamic characteristics of the roll subsidence mode, discussed in some detail in Section 7.2. The following analysis considers the wing contribution only.

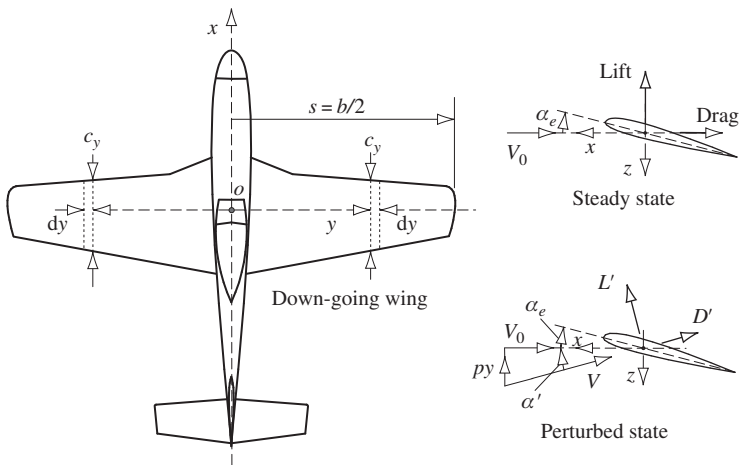


FIGURE 13.11 Wing incidence in rolling flight.

With reference to Fig. 13.11, when the right wing panel experiences a positive perturbation in roll rate p , assuming the aircraft rolls about the ox axis, then the small increase in incidence α' at the chordwise strip element is given by

$$\alpha' \cong \tan \alpha' = \frac{py}{V_0} \quad (13.118)$$

There is, of course, a reduction in incidence on the corresponding chordwise strip element on the left wing panel. Denoting the total lift and drag increments in the disturbance on the chordwise strip element on the right wing panel L' and D' , respectively, then

$$L' = \frac{1}{2} \rho V_0^2 c_y dy a_y (\alpha_e + \alpha') \quad (13.119)$$

and

$$D' = \frac{1}{2} \rho V_0^2 c_y dy C_{D_y} \quad (13.120)$$

The normal force increment $\delta Z_{(right)}$ acting at the chordwise strip element in the roll rate perturbation is given by

$$\delta Z_{(right)} = -L' \cos \alpha' - D' \sin \alpha' \cong -L' - D' \alpha' \quad (13.121)$$

since α' is a small angle. Substitute for L' , D' , and α' from equations (13.119), (13.120), and (13.118), respectively, to obtain

$$\delta Z_{(right)} = -\frac{1}{2} \rho V_0^2 \left(a_y \alpha_e + (a_y + C_{D_y}) \frac{py}{V_0} \right) c_y dy \quad (13.122)$$

The resulting increment in rolling moment is then given by

$$\delta L_{(right)} = y\delta Z_{(right)} = -\frac{1}{2}\rho V_0^2 \left(a_y \alpha_e + (a_y + C_{D_y}) \frac{py}{V_0} \right) c_y y dy \quad (13.123)$$

and the corresponding increment in rolling moment arising from the left wing panel, where the incidence is reduced by α' since the panel is rising with respect to the incident air flow, is given by

$$\delta L_{(left)} = -y\delta Z_{(left)} = \frac{1}{2}\rho V_0^2 \left(a_y \alpha_e - (a_y + C_{D_y}) \frac{py}{V_0} \right) c_y y dy \quad (13.124)$$

The total rolling moment due to roll rate is obtained by summing the increments from the right and left chordwise strips, given by [equations \(13.123\) and \(13.124\)](#), respectively, and integrating from the root to the tip of the wing,

$$L_{total} = \int_{span} (\delta L_{(left)} + \delta L_{(right)}) = -\rho V_0 p \int_0^s (a_y + C_{D_y}) c_y y^2 dy \quad (13.125)$$

and, by definition,

$$p \overset{\circ}{L_p} = L_{total} = -\rho V_0 p \int_0^s (a_y + C_{D_y}) c_y y^2 dy \quad (13.126)$$

Whence the dimensional derivative expression is given by

$$\overset{\circ}{L_p} = -\rho V_0 \int_0^s (a_y + C_{D_y}) c_y y^2 dy \quad (13.127)$$

and with reference to Appendix 2, the dimensionless form of the derivative is given by

$$\overset{\circ}{L_p} = \frac{\overset{\circ}{L_p}}{\frac{1}{2}\rho V_0 S b^2} = -\frac{1}{2Ss^2} \int_0^s (a_y + C_{D_y}) c_y y^2 dy \quad (13.128)$$

where $b = 2s$ is the wing span.

$$\overset{\circ}{N_p} = \frac{\partial \overset{\circ}{N}}{\partial p} \textbf{Yawing moment due to roll rate}$$

Yawing moment due to roll rate is almost entirely determined by the wing contribution, although in some aircraft a large fin may give rise to a significant additional contribution. Only the wing contribution is considered here.

It is shown in [Fig. 13.11](#) that in a roll rate perturbation the chordwise strip element on the right (down-going) wing experiences an incremental increase in lift and induced drag, given by [equations \(13.119\) and \(13.120\)](#), whilst there is an equal decrease in lift and induced drag on the corresponding strip on the left (up-going) wing. The differential drag thereby produced gives rise to the yawing moment perturbation.

With reference to [Fig. 13.11](#), the longitudinal axial force increment acting on the chordwise strip element on the right wing panel is given by

$$\delta X_{(right)} = L' \sin \alpha' - D' \cos \alpha' \cong L' \alpha' - D' \quad (13.129)$$

Substitute for L' and D' from [equations \(13.119\)](#) and [\(13.120\)](#), respectively, and write

$$C_{D_y} = \frac{dC_D}{d\alpha_y}(\alpha_e + \alpha') \quad (13.130)$$

to obtain

$$\delta X_{(right)} = \frac{1}{2} \rho V_0^2 \left(a_y \alpha' - \frac{dC_D}{d\alpha_y} \right) (\alpha_e + \alpha') c_y dy \quad (13.131)$$

The incremental axial force gives rise to a negative increment in yawing moment given by

$$\delta N_{(right)} = -y \delta X_{(right)} = -\frac{1}{2} \rho V_0^2 \left(a_y \alpha' - \frac{dC_D}{d\alpha_y} \right) (\alpha_e + \alpha') c_y y dy \quad (13.132)$$

The reduction in incidence due to roll rate on the corresponding chordwise strip element on the left wing panel gives rise to a positive increment in yawing moment and, in a similar way, it may be shown that

$$\delta N_{(left)} = y \delta X_{(left)} = -\frac{1}{2} \rho V_0^2 \left(a_y \alpha' + \frac{dC_D}{d\alpha_y} \right) (\alpha_e - \alpha') c_y y dy \quad (13.133)$$

The total yawing moment increment due to roll rate is given by summing [equations \(13.132\)](#) and [\(13.133\)](#) and substituting for α' from [equation \(13.118\)](#):

$$\delta N_{total} = \delta N_{(left)} + \delta N_{(right)} = -\rho V_0 p \left(a_y \alpha_e - \frac{dC_D}{d\alpha_y} \right) c_y y^2 dy \quad (13.134)$$

By definition, the total yawing moment due to roll rate is given by

$$\overset{\circ}{p N_p} = N_{total} = \int_{\substack{semi \\ span}} \delta N_{total} = -\rho V_0 p \int_0^s \left(a_y \alpha_e - \frac{dC_D}{d\alpha_y} \right) c_y y^2 dy \quad (13.135)$$

Whence the expression for the dimensional derivative is given by

$$\overset{\circ}{N_p} = -\rho V_0 \int_0^s \left(C_{L_y} - \frac{dC_D}{d\alpha_y} \right) c_y y^2 dy \quad (13.136)$$

where $C_{L_y} = a_y \alpha_e$ is the equilibrium local lift coefficient. With reference to Appendix 2, the dimensionless form of the derivative is given by

$$N_p = \frac{\overset{\circ}{N_p}}{\frac{1}{2} \rho V_0 S b^2} = -\frac{1}{2 S s^2} \int_0^s \left(C_{L_y} - \frac{dC_D}{d\alpha_y} \right) c_y y^2 dy \quad (13.137)$$

13.3.4 Derivatives due to rate of yaw

As seen by the pilot, a positive yaw rate is such that the nose of the aeroplane swings to the right and the small-perturbation yaw rate transient is denoted r . The nature of a free positive yaw rate disturbance is such that as the nose swings to the right the right wing tends to drop and the aeroplane sideslips to the right. The reaction to the yaw rate disturbance is stabilising if the

aerodynamic forces and moments produced in response tend to restore the aeroplane to a symmetric wings-level equilibrium flight condition.

$$\dot{Y}_r = \frac{\partial Y}{\partial r} \quad \textbf{Sideforce due to yaw rate}$$

For most conventional aeroplanes the sideforce due to yaw rate is insignificant unless the fin is relatively large. In such cases the fin lift generated by the yawing motion gives rise to a sideforce of significant magnitude.

Referring to Fig. 13.12, in a yaw rate perturbation the transient incidence of the fin may be written as

$$\alpha' \cong \tan \alpha' = \frac{rl_F}{V_0} \quad (13.138)$$

where l_F is the moment arm of the fin aerodynamic centre about the centre of rotation in yaw, the cg , and, by definition, the incidence transient is a small angle. The resultant transient fin lift L'_F gives rise to a sideforce Y_F ,

$$Y_F = L'_F \cos \alpha' \cong \frac{1}{2} \rho V_0^2 S_F a_{1_F} \alpha' = \frac{1}{2} \rho V_0 S_F l_F a_{1_F} r \quad (13.139)$$

By definition, the sideforce arising in a yaw rate disturbance is given by

$$r \dot{Y}_r = Y_F = \frac{1}{2} \rho V_0 S_F l_F a_{1_F} r \quad (13.140)$$

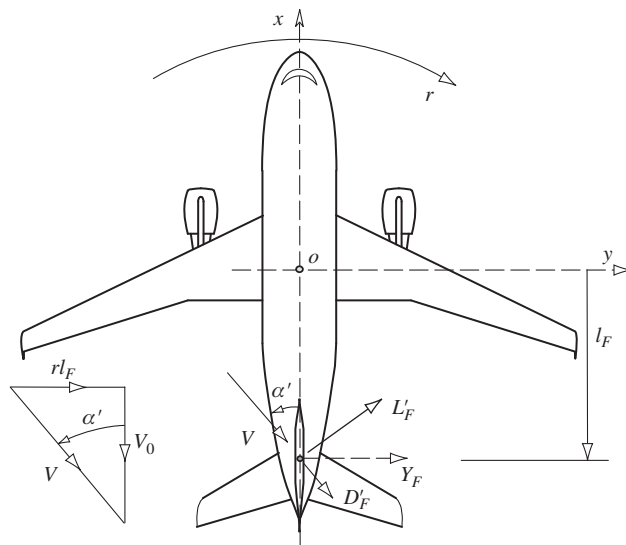


FIGURE 13.12 Fin incidence due to yaw rate.

Whence the expression for the dimensional sideforce due to yaw rate derivative is given by

$$\dot{Y}_r = \frac{1}{2} \rho V_0 S_F l_F a_{1F} \quad (13.141)$$

and with reference to Appendix 2, the dimensionless form of the derivative is given by

$$Y_r = \frac{\dot{Y}_r}{\frac{1}{2} \rho V_0 S b} = \bar{V}_F a_{1F} \quad (13.142)$$

where the *fin volume ratio* \bar{V}_F is given by [equation \(13.109\)](#). Clearly, the resolved component of the induced drag transient on the fin D'_F will also make a contribution to the total sideforce transient. However, this is usually considered to be insignificantly small compared with the lift contribution.

$$\dot{L}_r = \frac{\partial L}{\partial r} \textbf{ Rolling moment due to yaw rate}$$

In positive yawing motion the relative velocity of the air flowing over the right wing panel is decreased whilst the velocity over the left wing panel is increased. This gives rise to an increase in lift and induced drag on the port wing with a corresponding decrease in lift and drag on the starboard wing. The force increments thus produced result in a rolling moment and a yawing moment about the *cg*. A contribution to rolling moment also arises due to the sideforce generated by the fin in yawing motion, although it is generally smaller than the wing contribution.

With reference to [Fig. 13.13](#), the velocity at the chordwise strip element on the right wing during a yaw rate perturbation is given by

$$V = V_0 - ry \quad (13.143)$$

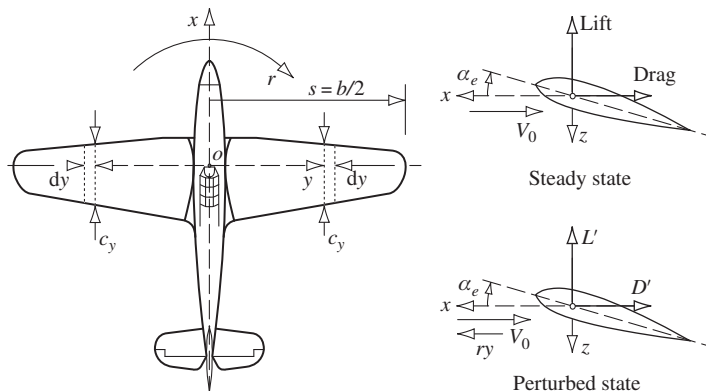


FIGURE 13.13 Wing forces due to yaw rate.

and the total lift on the chordwise strip element during the perturbation is given by

$$\begin{aligned}\delta L'_{(right)} &= \frac{1}{2} \rho V^2 c_y dy C_{L_y} = \frac{1}{2} \rho (V_0 - ry)^2 c_y dy C_{L_y} \\ &= \frac{1}{2} \rho (V_0^2 - 2ryV_0) c_y dy C_{L_y}\end{aligned}\quad (13.144)$$

when products of small quantities are neglected. The rolling moment due to the lift on the chordwise strip element on the right wing is therefore given by

$$\delta L_{(right)} = -\delta L'_{(right)} y = -\frac{1}{2} \rho (V_0^2 - 2ryV_0) c_y y dy C_{L_y} \quad (13.145)$$

Similarly, the rolling moment due to the lift on the chordwise strip element on the left wing is given by

$$\delta L_{(left)} = \delta L'_{(left)} y = \frac{1}{2} \rho (V_0^2 + 2ryV_0) c_y y dy C_{L_y} \quad (13.146)$$

Thus the total rolling moment due to yaw rate arising from the wing is given by integrating the sum of the components due to the chordwise strip elements, [equations \(13.145\) and \(13.146\)](#), over the semi-span:

$$L_{wing} = \int_{\substack{\text{semi} \\ \text{span}}} (\delta L_{(left)} + \delta L_{(right)}) = 2\rho V_0 r \int_0^s C_{L_y} c_y y^2 dy \quad (13.147)$$

By definition, the rolling moment due to wing lift in a yaw rate disturbance is given by

$$r \overset{\circ}{L}_{r(wing)} = L_{wing} = 2\rho V_0 r \int_0^s C_{L_y} c_y y^2 dy \quad (13.148)$$

Whence the expression for the wing contribution to the dimensional rolling moment due to yaw rate derivative is

$$\overset{\circ}{L}_{r(wing)} = 2\rho V_0 \int_0^s C_{L_y} c_y y^2 dy \quad (13.149)$$

and with reference to Appendix 2, the dimensionless form of the derivative is given by

$$L_{r(wing)} = \frac{\overset{\circ}{L}_{r(wing)}}{\frac{1}{2} \rho V_0 S b^2} = \frac{1}{S s^2} \int_0^s C_{L_y} c_y y^2 dy \quad (13.150)$$

where $b = 2s$ is the wing span.

Note that for a large-aspect-ratio rectangular wing it may be assumed that $C_{L_y} = C_L$, the lift coefficient for the whole wing, and that $c_y = c$, the constant geometric chord of the wing. For this special case it is easily shown, from [equation \(13.150\)](#), that

$$L_r = \frac{1}{6} C_L \quad (13.151)$$

However, it should be appreciated that the assumption relating to constant lift coefficient across the span is rather crude, and consequently the result given by equation (13.151) is very approximate, although it can be useful as a guide for checking estimated values of the derivative.

The fin contribution to the rolling moment due to yaw rate derivative arises from the moment about the roll axis of the sideforce generated by the fin in yaw. The sideforce is generated by the mechanism illustrated in Fig. 13.12 and acts at the aerodynamic centre of the fin, which is usually above the roll axis, and hence gives rise to a positive rolling moment. The situation prevailing is illustrated in Fig. 13.14.

With reference to Fig. 13.14, a rolling moment is developed by the fin sideforce due to yaw rate Y_F , which is given by equation (13.139), acting at the aerodynamic centre, which is located h_F above the roll axis. Whence the rolling moment is given by

$$L_{fin} = Y_F h_F = \frac{1}{2} \rho V_0 S_F l_F a_{1F} r h_F \quad (13.152)$$

By definition, the rolling moment due to fin sideforce in a yaw rate disturbance is given by

$$\overset{\circ}{r L_{r(fin)}} = L_{fin} = \frac{1}{2} \rho V_0 S_F l_F a_{1F} r h_F \quad (13.153)$$

Whence the fin contribution to the dimensional derivative is given by

$$\overset{\circ}{L_{r(fin)}} = \frac{1}{2} \rho V_0 S_F l_F a_{1F} h_F \quad (13.154)$$

As before, and with reference to Appendix 2, the dimensionless form of the derivative is given by

$$L_{r(fin)} = \frac{\overset{\circ}{L_{r(fin)}}}{\frac{1}{2} \rho V_0 S b^2} = a_{1F} \bar{V}_F \frac{h_F}{b} \equiv -L_{v(fin)} \frac{l_F}{b} \quad (13.155)$$

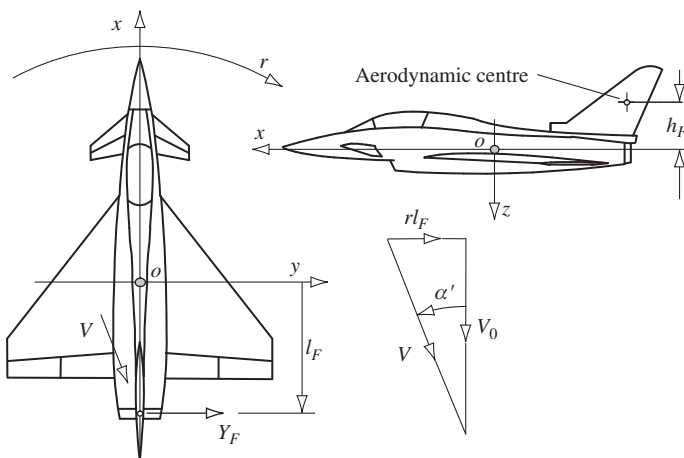


FIGURE 13.14 Rolling moment due to yaw rate arising from fin.

The total value of the rolling moment due to yaw rate derivative is then given by the sum of all the significant contributions.

$$\dot{N}_r = \frac{\partial N}{\partial r} \quad \textbf{Yawing moment due to yaw rate}$$

The yawing moment due to yaw rate derivative is an important parameter in the determination of aircraft directional stability. In particular it is a measure of the damping in yaw and is therefore dominant in determining the stability of the oscillatory dutch roll mode. This significance of this derivative to lateral-directional dynamics is discussed in detail in Section 7.2. The most easily identified contributions to yaw damping arise from the fin and from the wing. However, it is generally accepted that the most significant contribution arises from the fin, although in some aircraft the fin contribution may become significantly reduced at high angles of attack, in which case the wing contribution becomes more important.

Consider the wing contribution first. This arises as a result of the differential drag effect in yawing motion as illustrated in Fig. 13.13. Referring to Fig. 13.13, the total drag on the chordwise strip element on the right wing subject to a steady yaw rate r is reduced for the same reason as the lift, given by equation (13.144), and may be written as

$$\delta D'_{(right)} = \frac{1}{2} \rho (V_0^2 - 2ryV_0) c_y dy C_{D_y} \quad (13.156)$$

The yawing moment about the *cg* generated by the drag on the chordwise strip element is

$$\delta N_{(right)} = \delta D'_{(right)} y = \frac{1}{2} \rho (V_0^2 - 2ryV_0) c_y y dy C_{D_y} \quad (13.157)$$

and similarly for the yawing moment arising at the corresponding chordwise strip on the left wing:

$$\delta N_{(left)} = -\delta D'_{(left)} y = -\frac{1}{2} \rho (V_0^2 + 2ryV_0) c_y y dy C_{D_y} \quad (13.158)$$

Thus the total yawing moment due to yaw rate arising from the wing is given by integrating the sum of the components due to the chordwise strip elements, equations (13.157) and (13.158), over the semi-span:

$$N_{wing} = \int_{\text{semi span}} (\delta N_{(right)} - \delta N_{(left)}) = -2\rho V_0 r \int_0^s C_{D_y} c_y y^2 dy \quad (13.159)$$

By definition, the yawing moment due to differential wing drag in a yaw rate perturbation is given by

$$r \dot{N}_{r(wing)} = N_{wing} = -2\rho V_0 r \int_0^s C_{D_y} c_y y^2 dy \quad (13.160)$$

Whence the expression for the wing contribution to the dimensional yawing moment due to yaw rate derivative is

$$\dot{N}_{r(wing)} = -2\rho V_0 \int_0^s C_{D_y} c_y y^2 dy \quad (13.161)$$

and with reference to Appendix 2, the dimensionless form of the derivative is given by

$$N_{r(wing)} = \frac{\overset{\circ}{N}_{r(wing)}}{\frac{1}{2}\rho V_0 S b^2} = -\frac{1}{S s^2} \int_0^s C_{D_y} c_y y^2 dy \quad (13.162)$$

where $b = 2s$ is the wing span.

As for the derivative L_r , for a large-aspect-ratio rectangular wing it may be assumed that $C_{D_y} = C_D$, the drag coefficient for the whole wing, and that $c_y = c$, the constant geometric chord of the wing. For this special case it is easily shown, from [equation \(13.162\)](#), that

$$N_{r(wing)} = \frac{1}{6} C_D \quad (13.163)$$

Although the result given by [equation \(13.163\)](#) is rather approximate and subject to the assumptions made, it is useful as a guide for checking the value of an estimated contribution to the derivative.

The fin contribution to yawing moment due to yaw rate is generated by the yawing moment of the fin sideforce due to yaw rate. The mechanism for the generation of fin sideforce is illustrated in [Fig. 13.12](#) and, with reference to that figure and to [equation \(13.139\)](#), the yawing moment thereby generated is given by

$$N_{fin} = -Y_F l_F = -\frac{1}{2} \rho V_0 S_F l_F^2 a_{1_F} r \quad (13.164)$$

By definition, the yawing moment due to the fin in a yaw rate perturbation is given by

$$r \overset{\circ}{N}_{r(fin)} = N_{fin} = -\frac{1}{2} \rho V_0 S_F l_F^2 a_{1_F} r \quad (13.165)$$

Whence the expression for the fin contribution to the dimensional yawing moment due to yaw rate derivative is

$$\overset{\circ}{N}_{r(fin)} = -\frac{1}{2} \rho V_0 S_F l_F^2 a_{1_F} \quad (13.166)$$

As before, and with reference to Appendix 2, the dimensionless form of the derivative is given by

$$N_{r(fin)} = \frac{\overset{\circ}{N}_{r(fin)}}{\frac{1}{2}\rho V_0 S b^2} = -a_{1_F} \bar{V}_F \frac{l_F}{b} = -\frac{l_F}{b} N_{v(fin)} \quad (13.167)$$

The fin volume ratio \bar{V}_F is given by [equation \(13.109\)](#). The total value of the yawing moment due to yaw rate derivative is therefore given by the sum of all the significant contributions.

13.4 Aerodynamic control derivatives

Estimates may be made for the aerodynamic control derivatives provided that the controller in question is a simple flap-like device and provided that its aerodynamic properties can be modelled

with a reasonable degree of confidence. However, estimates of the aileron and rudder control derivatives obtained from simple models are unlikely to be accurate since it is very difficult to describe the aerodynamic conditions applying in sufficient detail. Estimates for the lateral-directional aerodynamic control derivatives are best obtained from the appropriate ESDU data items or, preferably, by experimental measurement. However, simple models for the aileron and rudder control derivatives are given here for completeness and in order to illustrate the principles of lateral-directional control.

For convenience, a summary of the derivative expressions derived in the following paragraphs is included in Table A8.3 and Table A8.4, Appendix 8.

13.4.1 Derivatives due to elevator

Typically, the lift coefficient for a tailplane with elevator control is given by

$$C_{L_T} = a_0 + a_1 \alpha_T + a_2 \eta \quad (13.168)$$

where a_1 is the lift curve slope of the tailplane and a_2 is the lift curve slope with respect to elevator angle η . The corresponding drag coefficient may be expressed as

$$C_{D_T} = C_{D_{0_T}} + k_T C_{L_T}^2 \quad (13.169)$$

where all of the parameters in equation (13.169) are tailplane-dependent.

$$\dot{X}_\eta = \frac{\partial X}{\partial \eta} \quad \textbf{Axial force due to elevator}$$

It is assumed that for a small elevator deflection, consistent with a small perturbation, the resulting axial force perturbation arises from the drag change associated with the tailplane only. Whence

$$X \equiv X_T = -D_T = -\frac{1}{2} \rho V^2 S_T C_{D_T} \quad (13.170)$$

Thus

$$\dot{X}_\eta = \frac{\partial X_T}{\partial \eta} = -\frac{1}{2} \rho V^2 S_T k_T C_{L_T} \frac{\partial C_{D_T}}{\partial \eta} \quad (13.171)$$

Substitute for C_{D_T} , from equation (13.169), in equation (13.171) to obtain

$$\dot{X}_\eta = \frac{\partial X_T}{\partial \eta} = -\rho V^2 S_T k_T C_{L_T} \frac{\partial C_{L_T}}{\partial \eta} \quad (13.172)$$

For a small perturbation, in the limit $V \cong V_0$, from equation (13.168) $\partial C_{L_T}/\partial \eta \cong a_2$ and equation (13.172) may be written as

$$\dot{X}_\eta = -\rho V_0^2 S_T k_T C_{L_T} a_2 \quad (13.173)$$

With reference to Appendix 2 the dimensionless form of the derivative is given by

$$X_\eta = \frac{\dot{X}_\eta}{\frac{1}{2} \rho V_0^2 S} = -2 \frac{S_T}{S} k_T C_{L_T} a_2 \quad (13.174)$$

$$\dot{Z}_\eta = \frac{\partial Z}{\partial \eta} \quad \textbf{Normal force due to elevator}$$

As before, it is assumed that for a small elevator deflection the resulting normal force perturbation arises from the lift change associated with the tailplane only. Whence

$$Z \equiv Z_T = -L_T = -\frac{1}{2} \rho V^2 S_T C_{L_T} \quad (13.175)$$

Thus

$$\dot{Z}_\eta = \frac{\partial Z_T}{\partial \eta} = -\frac{1}{2} \rho V^2 S_T \frac{\partial C_{L_T}}{\partial \eta} \quad (13.176)$$

Substitute for C_{L_T} , from equation (13.168), to obtain

$$\dot{Z}_\eta = \frac{\partial Z_T}{\partial \eta} = -\frac{1}{2} \rho V^2 S_T a_2 \quad (13.177)$$

For a small perturbation, in the limit $V \cong V_0$ and with reference to Appendix 2, the dimensionless form of the derivative is given by

$$Z_\eta = \frac{\dot{Z}_\eta}{\frac{1}{2} \rho V_0^2 S} = -\frac{S_T}{S} a_2 \quad (13.178)$$

$$\dot{M}_\eta = \frac{\partial M}{\partial \eta} \quad \textbf{Pitching moment due to elevator}$$

It is assumed that the pitching moment resulting from elevator deflection is due entirely to the moment of the tailplane lift about the *cg*. Whence

$$M \equiv M_T = -L_T l_T = -\frac{1}{2} \rho V^2 S_T l_T C_{L_T} \quad (13.179)$$

Thus it follows that

$$\dot{M}_\eta = \frac{\partial M_T}{\partial \eta} = -\frac{1}{2} \rho V^2 S_T l_T \frac{\partial C_{L_T}}{\partial \eta} = \dot{Z}_\eta l_T \quad (13.180)$$

With reference to Appendix 2 the dimensionless form of the derivative is given by

$$M_\eta = \frac{\dot{M}_\eta}{\frac{1}{2} \rho V_0^2 S \bar{c}} = -\frac{S_T l_T}{S \bar{c}} a_2 = -\bar{V}_T a_2 \quad (13.181)$$

where \bar{V}_T is the tail volume ratio.

13.4.2 Derivatives due to aileron

Typical aileron geometry is shown in Fig. 13.15 and comprises a part span flap in the outboard sections of both port and starboard wings. Differential deflection of the flaps creates the desired

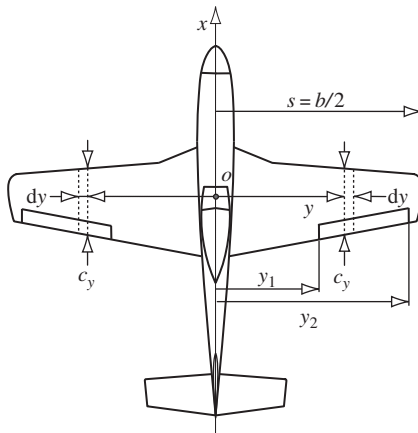


FIGURE 13.15 Aileron control geometry.

control in roll. As described in Section 2.6, a positive aileron deflection results in the starboard (right) surface deflecting trailing edge down and the port (left) surface trailing edge up, and aileron angle ξ is taken to be the mean of the two surface angles. Thus, referring to equation (13.168), the local lift coefficient at spanwise coordinate y is given by

$$\begin{aligned} C_{L_y}|_{right} &= a_0 + a_y \alpha + a_{2A} \xi \\ C_{L_y}|_{left} &= a_0 + a_y \alpha - a_{2A} \xi \end{aligned} \quad (13.182)$$

Since it is not practical to define a simple model for the increment in local drag coefficient due to aileron deflection, let it be defined more generally as

$$\begin{aligned} C_{D_y}|_{right} &= \frac{\partial C_{D_y}}{\partial \xi} \xi \\ C_{D_y}|_{left} &= -\frac{\partial C_{D_y}}{\partial \xi} \xi \end{aligned} \quad (13.183)$$

where it is assumed that, for small aileron angles, the change in drag $\partial C_{D_y}/\partial \xi$ is dominated by induced drag effects and may vary over the aileron span.

$$\dot{Y}_\xi = \frac{\partial Y}{\partial \xi} \quad \textbf{Sideforce due to aileron}$$

For aeroplanes of conventional layout the sideforce due to aileron is zero or insignificantly small. However, for aeroplanes of unconventional layout, with highly swept wings or that utilise differential canard surfaces for roll control, this may not be the case. In such cases, simple analytical models would not be the most appropriate means for obtaining an estimate of the derivative value.

$$\dot{L}_\xi = \frac{\partial L}{\partial \xi} \quad \textbf{Rolling moment due to aileron}$$

This derivative describes the roll control property of the aeroplane, and an accurate estimate of its value is important to flight dynamics analysis. With reference to [equations \(13.182\)](#) and Fig. 3.15, the application of simple strip theory enables the rolling moment due to starboard aileron deflection to be written as

$$L_{right} = -\frac{1}{2} \rho V^2 \int_{y_1}^{y_2} C_{L_y} \Big|_{right} c_y y dy = -\frac{1}{2} \rho V^2 \int_{y_1}^{y_2} (a_0 + a_y \alpha + a_{2A} \xi) c_y y dy \quad (13.184)$$

where a_{2A} is the aileron lift curve slope, which is assumed to be constant over the span of the aileron. Similarly, the rolling moment due to port aileron deflection may be written as

$$L_{left} = \frac{1}{2} \rho V^2 \int_{y_1}^{y_2} C_{L_y} \Big|_{left} c_y y dy = \frac{1}{2} \rho V^2 \int_{y_1}^{y_2} (a_0 + a_y \alpha - a_{2A} \xi) c_y y dy \quad (13.185)$$

It follows that the total rolling moment may be written as

$$\dot{L}_\xi = L_{right} + L_{left} = -\rho V^2 (a_{2A} \xi) \int_{y_1}^{y_2} c_y y dy \quad (13.186)$$

Whence the simple expression for the dimensional derivative is given by

$$\dot{L}_\xi = -\rho V^2 a_{2A} \int_{y_1}^{y_2} c_y y dy \quad (13.187)$$

Alternatively, with reference to Appendix 2, the dimensionless derivative may be written as

$$L_\xi = \frac{\dot{L}_\xi}{\frac{1}{2} \rho V_0^2 S b} = -\frac{1}{Ss} a_{2A} \int_{y_1}^{y_2} c_y y dy \quad (13.188)$$

where $b = 2s$ is the wing span.

$$\dot{N}_\xi = \frac{\partial N}{\partial \xi} \quad \textbf{Yawing moment due to aileron}$$

This derivative describes the adverse yaw property of the aeroplane in response to aileron roll commands. With reference to [equations \(13.183\)](#) and Fig. 3.15, the application of simple strip theory enables the yawing moment due to starboard aileron deflection to be written as

$$N_{right} = \frac{1}{2} \rho V^2 \int_{y_1}^{y_2} C_{D_y} \Big|_{right} c_y y dy = \frac{1}{2} \rho V^2 \int_{y_1}^{y_2} \left(\frac{\partial C_{D_y}}{\partial \xi} \xi \right) c_y y dy \quad (13.189)$$

and, similarly, the yawing moment due to port aileron deflection may be written as

$$N_{left} = -\frac{1}{2} \rho V^2 \int_{y_1}^{y_2} C_{D_y} \Big|_{left} c_y y dy = -\frac{1}{2} \rho V^2 \int_{y_1}^{y_2} \left(-\frac{\partial C_{D_y}}{\partial \xi} \xi \right) c_y y dy \quad (13.190)$$

It follows that the total yawing moment may be written as

$$\overset{\circ}{N}_\xi = N_{right} + N_{left} = \rho V^2 \int_{y_1}^{y_2} \left(\frac{\partial C_{D_y}}{\partial \xi} \xi \right) c_y y dy \quad (13.191)$$

Whence a simple expression for the dimensional derivative is given by

$$\overset{\circ}{N}_\xi = \rho V^2 \int_{y_1}^{y_2} \left(\frac{\partial C_{D_y}}{\partial \xi} \right) c_y y dy \quad (13.192)$$

Alternatively, with reference to Appendix 2, the dimensionless derivative may be written as

$$N_\xi = \frac{\overset{\circ}{N}_\xi}{\frac{1}{2} \rho V_0^2 S b} = \frac{1}{S s} \int_{y_1}^{y_2} \left(\frac{\partial C_{D_y}}{\partial \xi} \right) c_y y dy \quad (13.193)$$

13.4.3 Derivatives due to rudder

In normal trimmed flight the fin and rudder generate zero sideforce. Deflection of the rudder ζ (in the notation a positive rudder angle is trailing edge to the left) generates a positive sideforce, which gives rise to both rolling and yawing moments. With reference to Fig. 13.14, for example, it is assumed that the sideforce acts at the aerodynamic centre of the fin, which is located a distance l_F aft of the cg and a distance h_F above the cg . Since the aerodynamics of the fin and rudder will inevitably be significantly influenced by the presence of the aft fuselage and the horizontal tail-plane, the accuracy of the following models is likely to be poor.

$$\overset{\circ}{Y}_\zeta = \frac{\partial Y}{\partial \zeta} \quad \text{Sideforce due to rudder}$$

The sideforce generated by the fin when the rudder angle is ζ is given approximately by

$$Y = \frac{1}{2} \rho V^2 S_F a_{2R} \zeta \quad (13.194)$$

and, by definition,

$$\overset{\circ}{Y}_\zeta \zeta = Y = \frac{1}{2} \rho V^2 S_F a_{2R} \zeta \quad (13.195)$$

where a_{2R} is the rudder lift curve slope, which is assumed to be constant over the span of the fin and rudder. Whence the very simple expression for the dimensional derivative is

$$\overset{\circ}{Y}_\zeta = \frac{1}{2} \rho V^2 S_F a_{2R} \quad (13.196)$$

Alternatively, with reference to Appendix 2, the dimensionless derivative may be written as

$$Y_\zeta = \frac{\overset{\circ}{Y}_\zeta}{\frac{1}{2} \rho V_0^2 S} = \frac{S_F}{S} a_{2R} \quad (13.197)$$

$$\dot{L}_\zeta = \frac{\partial L}{\partial \zeta} \textbf{ Rolling moment due to rudder}$$

This derivative describes the adverse roll property of the aeroplane in response to rudder yaw commands. Since the sideforce due to rudder acts above the roll axis, the rolling moment due to rudder follows directly:

$$\dot{L}_\zeta \zeta = Y h_F = \frac{1}{2} \rho V^2 S_F h_F a_{2R} \zeta \quad (13.198)$$

Thus a simple expression for the dimensional derivative is

$$\dot{L}_\zeta = \frac{1}{2} \rho V^2 S_F h_F a_{2R} \quad (13.199)$$

and, with reference to Appendix 2, an expression for the dimensionless derivative may be written as

$$L_\zeta = \frac{\dot{L}_\zeta}{\frac{1}{2} \rho V_0^2 Sb} = \frac{S_F h_F}{Sb} a_{2R} \equiv \bar{V}_F \frac{h_F}{l_F} a_{2R} \quad (13.200)$$

where \bar{V}_F is the fin volume ratio.

$$\dot{N}_\zeta = \frac{\partial N}{\partial \zeta} \textbf{ Yawing moment due to rudder}$$

This derivative describes the yaw control property of the aeroplane and, again, an accurate estimate of its value is important to flight dynamics analysis. Since the sideforce due to rudder acts well behind the *cg*, it generates a yawing moment described as follows:

$$\dot{N}_\zeta \zeta = -Y l_F = -\frac{1}{2} \rho V^2 S_F l_F a_{2R} \zeta \quad (13.201)$$

Thus the simple expression for the dimensional derivative is

$$\dot{N}_\zeta = \frac{1}{2} \rho V^2 S_F l_F a_{2R} \quad (13.202)$$

and, with reference to Appendix 2, an expression for the dimensionless derivative may be written as

$$N_\zeta = \frac{\dot{N}_\zeta}{\frac{1}{2} \rho V_0^2 Sb} = -\frac{S_F l_F}{Sb} a_{2R} \equiv -\bar{V}_F a_{2R} \quad (13.203)$$

13.5 North American derivative coefficient notation

An alternative notation for the dimensionless aerodynamic stability and control derivatives, based on the derivatives of aerodynamic force and moment coefficients, is the standard notation used in

North America and commonly used in Europe and elsewhere. Interpretation of the derivatives as quasi-static representations of continuously varying aerodynamic properties of the aircraft remains the same as described in Section 12.2.

To illustrate the mathematical derivation of the coefficient notation, it is useful to remember that in a nonsteady flight condition, with perturbed velocity V , the lift and drag force are described in terms of the dimensionless lift and drag coefficients respectively, namely

$$L = \frac{1}{2} \rho V^2 S C_L$$

$$D = \frac{1}{2} \rho V^2 S C_D$$

In a similar way, the aerodynamic forces and moments in the American normalised dimensional equations of motion (4.72) and (4.73) may be written in terms of dimensionless coefficients. With reference to expressions (4.75), the normalised longitudinal equations of motion (4.72) may thus be written as

$$\begin{aligned}\dot{u} + qW_e &= \frac{X}{m} = \frac{1}{m} \left(\frac{1}{2} \rho V^2 S C_x \right) - g\theta \cos\theta_e \\ \dot{w} - qU_e &= \frac{Z}{m} = \frac{1}{m} \left(\frac{1}{2} \rho V^2 S C_z \right) - g\theta \sin\theta_e \\ \dot{q} &= \frac{M}{I_y} = \frac{1}{I_y} \left(\frac{1}{2} \rho V^2 S \bar{C}_m \right)\end{aligned}\tag{13.204}$$

and, with reference to expressions (4.78), the normalised lateral-directional equations of motion (4.73) may be written as

$$\begin{aligned}\dot{v} - pW_e + rU_e &= \frac{Y}{m} = \frac{1}{m} \left(\frac{1}{2} \rho V^2 S C_y \right) + g\phi \cos\theta_e + g\psi \sin\theta_e \\ \dot{p} - \frac{I_{xz}}{I_x} \dot{r} &= \frac{L}{I_x} = \frac{1}{I_x} \left(\frac{1}{2} \rho V^2 S b C_l \right) \\ \dot{r} - \frac{I_{xz}}{I_z} \dot{p} &= \frac{N}{I_z} = \frac{1}{I_z} \left(\frac{1}{2} \rho V^2 S b C_n \right)\end{aligned}\tag{13.205}$$

Note that, as written, [equations \(13.204\) and \(13.205\)](#) are referenced to a general aircraft body axis system. However, as in the British notation, it is usual (and preferable) to refer the dimensionless aerodynamic derivative coefficients to aircraft wind axes.

13.5.1 The longitudinal aerodynamic derivative coefficients

Consider the longitudinal equations of motion, and by comparing equations (4.77) with (13.204), in a perturbation the aerodynamic, thrust, and control forces and moments may be written as

$$\begin{aligned} \frac{1}{m} \left(\frac{1}{2} \rho V^2 S C_x \right) &= X_u u + X_{\dot{w}} \dot{w} + X_w w + X_q q + X_{\delta_e} \delta_e + X_{\delta_{th}} \delta_{th} \\ \frac{1}{m} \left(\frac{1}{2} \rho V^2 S C_z \right) &= Z_u u + Z_{\dot{w}} \dot{w} + Z_w w + Z_q q + Z_{\delta_e} \delta_e + Z_{\delta_{th}} \delta_{th} \\ \frac{1}{I_y} \left(\frac{1}{2} \rho V^2 S \bar{C}_m \right) &= M_u u + M_{\dot{w}} \dot{w} + M_w w + M_q q + M_{\delta_e} \delta_e + M_{\delta_{th}} \delta_{th} \end{aligned} \quad (13.206)$$

In order to identify the dimensionless derivative coefficients the left-hand sides of [equations \(13.206\)](#) may be expanded in terms of partial derivative functions of the perturbation variables. This mathematical procedure and its application to aerodynamic modelling of aircraft is described in Section 4.2.2. Thus, for example, the axial force equation in (13.204) may be written as

$$\begin{aligned} \frac{1}{m} \left(\frac{1}{2} \rho V^2 S C_x \right) &= \frac{\rho S}{2m} \left(\frac{\partial(V^2 C_x)}{\partial U} u + \frac{\partial(V^2 C_x)}{\partial \dot{W}} \dot{w} + \frac{\partial(V^2 C_x)}{\partial W} w \right. \\ &\quad \left. + \frac{\partial(V^2 C_x)}{\partial q} q + \frac{\partial(V^2 C_x)}{\partial \delta_e} \delta_e + \frac{\partial(V^2 C_x)}{\partial \delta_{th}} \delta_{th} \right) \\ &= X_u u + X_{\dot{w}} \dot{w} + X_w w + X_q q + X_{\delta_e} \delta_e + X_{\delta_{th}} \delta_{th} \end{aligned} \quad (13.207)$$

Equating equivalent terms in [equation \(13.207\)](#), expressions for the normalised derivatives, referred to aircraft wind axes, may thus be derived. Recall the following derivative relationships for small perturbations from [equations \(13.5\) and \(13.6\)](#):

$$\frac{\partial V}{\partial U} = 1 \quad \frac{\partial V}{\partial W} = 0 \quad \frac{\partial \theta}{\partial U} = 0 \quad \frac{\partial \theta}{\partial W} = \frac{1}{V} \quad (13.208)$$

Expressions for the force coefficients follow directly from [equations \(13.8\) and \(13.9\)](#), retaining the aerodynamic terms only:

$$C_x = C_L \sin \theta - C_D \cos \theta \quad (13.209)$$

$$C_z = -C_L \cos \theta - C_D \sin \theta \quad (13.210)$$

Referring to expressions (13.208) and [equation \(13.209\)](#), it follows that

$$\begin{aligned} X_u &= \frac{\rho S}{2m} \frac{\partial(V^2 C_x)}{\partial U} = \frac{\rho VS}{2m} \left(V \frac{\partial C_x}{\partial U} + 2C_x \right) \\ &= \frac{\rho VS}{2m} \left(V \frac{\partial C_L}{\partial U} \sin\theta - V \frac{\partial C_D}{\partial U} \cos\theta + 2C_L \sin\theta - 2C_D \cos\theta \right) \end{aligned} \quad (13.211)$$

In the limit, let the perturbation become vanishingly small such that $\theta \rightarrow 0$, $V \rightarrow V_0$, and Mach number $M_0 = V_0/a$; then

$$X_u = -\frac{\rho VS}{2m} \left(V \frac{\partial C_D}{\partial V} + 2C_D \right) = -\frac{\rho VS}{2m} \left(M \frac{\partial C_D}{\partial M} + 2C_D \right) = -\frac{\rho V_0 S}{2m} (M_0 C_{D_M} + 2C_D) \quad (13.212)$$

It should be noted that $\partial C_D / \partial V$ is not dimensionless and in order to render the derivative dimensionless, velocity dependency is replaced by Mach number dependency. This also has the advantage that the model is then not limited to subsonic flight applications only. Note that [equation \(13.212\)](#) is the direct equivalent of that given in the British notation as equation (12.9) and by [equation \(13.17\)](#).

Similarly, referring to the expressions (13.208) and [equation \(13.209\)](#), it follows that

$$\begin{aligned} X_w &= \frac{\rho S}{2m} \frac{\partial(V^2 C_x)}{\partial W} = \frac{\rho VS}{2m} \left(V \frac{\partial C_x}{\partial W} \right) \\ &= \frac{\rho VS}{2m} \left(V \frac{\partial C_L}{\partial W} \sin\theta - V \frac{\partial C_D}{\partial W} \cos\theta + C_L \cos\theta - C_D \sin\theta \right) \\ &= \frac{\rho VS}{2m} \left(\frac{\partial C_L}{\partial \alpha} \sin\theta - \frac{\partial C_D}{\partial \alpha} \cos\theta + C_L \cos\theta - C_D \sin\theta \right) \end{aligned} \quad (13.213)$$

Since a wind axes reference is assumed, $W = W_e + w = w$ and $w/V = \tan\alpha \cong \alpha$ for small perturbations. As before, let the perturbation become vanishingly small such that $\theta \rightarrow 0$ and $V \rightarrow V_0$; then

$$X_w = \frac{\rho V_0 S}{2m} \left(C_L - \frac{\partial C_D}{\partial \alpha} \right) = \frac{\rho V_0 S}{2m} (C_L - C_{D_\alpha}) \quad (13.214)$$

Although the derivative X_w is usually negligibly small, its derivation in terms of the dimensionless derivative coefficient is illustrated for completeness:

$$X_w = \frac{\rho S}{2m} \frac{\partial(V^2 C_x)}{\partial \dot{W}} = \frac{\rho VS}{2m} \left(V \frac{\partial C_x}{\partial \dot{w}} \right) \equiv \frac{\rho VS}{2m} \left(\frac{\partial C_x}{\partial \dot{\alpha}} \right) = \frac{\rho VS}{2m} \left(\frac{\bar{c} P}{2V} \right) \left(\frac{\partial C_x}{\partial (\dot{\alpha} \bar{c}/2V)} \right) \quad (13.215)$$

$$X_{\dot{w}} = \frac{\rho S \bar{c}}{4m} C_{x_{\dot{\alpha}}}$$

Since a wind axes reference is assumed, $W = W_e + w = w$ and $\dot{W} = \dot{w}$. Also, $w/V = \tan\alpha \cong \alpha$ for small perturbations, and it follows that $\dot{w}/V \cong \dot{\alpha}$. Now the derivative $\partial C_x / \partial \dot{\alpha}$ is not dimensionless as $\dot{\alpha}$ has units rad/s, and in order to render $\partial C_x / \partial \dot{\alpha}$ dimensionless it is necessary to multiply $\dot{\alpha}$ by a *longitudinal reference time* value. The value used for this purpose is $\bar{c}/2V$, the time taken for the aircraft to traverse one half-chord length. It is not possible to take this reduction further without significant additional analysis to define the dependency of C_x on $\dot{\alpha}$. In the context of the derivation of the equivalent British notation, the analysis is set out in [Section 13.2.6](#), where it is seen to describe tailplane aerodynamic response to downwash lag following a perturbation in normal acceleration \dot{w} .

The derivative and X_q are derived in a similar manner, and since C_{x_q} is negligibly small for small perturbations it is usual to omit X_q from the linear longitudinal aircraft model:

$$\begin{aligned} X_q &= \frac{\rho S}{2m} \frac{\partial(V^2 C_x)}{\partial q} = \frac{\rho V^2 S}{2m} \frac{\partial C_x}{\partial q} = \frac{\rho V^2 S}{2m} \left(\frac{\bar{c}}{2V} \right) \left(\frac{\partial C_x}{\partial(q\bar{c}/2V)} \right) \\ X_q &= \frac{\rho V_0 S \bar{c}}{4m} C_{x_q} \end{aligned} \quad (13.216)$$

Again, it is not practical to take this reduction further without significant additional analysis to define the dependency of C_x on pitch rate q . However, the analysis relating to the equivalent British notation is set out in [Section 13.2.5](#) where it is seen to describe tailplane aerodynamic response to a perturbation in pitch rate q .

The control derivatives may be dealt with generically as the independent variable is control angle δ , with a subscript denoting the surface to which it relates, and since it is measured in radians it is treated as dimensionless. When δ is used to denote thrust control, it is also treated as dimensionless and may be considered as a fraction of maximum thrust or, equivalently, as a perturbation in throttle lever angle. Otherwise, the derivation of X_{δ_e} and $X_{\delta_{th}}$ follows the same procedure:

$$\begin{aligned} X_\delta &= \frac{\rho S}{2m} \frac{\partial(V^2 C_x)}{\partial \delta} = \frac{\rho V^2 S}{2m} \frac{\partial C_x}{\partial \delta} \\ X_\delta &= \frac{\rho V_0^2 S}{2m} C_{x_\delta} \end{aligned} \quad (13.217)$$

Again, it is not practical to take the derivation any further since it depends explicitly on the aerodynamic and thrust control layout of a given aeroplane.

The normalised axial force derivative expressions given by [equations \(13.212\) through \(13.217\)](#) are summarised in Appendix 7.

In a similar way, expressions for the normalised normal force derivatives in [equations \(13.206\)](#) may be derived in terms of dimensionless derivative coefficients, and noting that the normal force

coefficient C_z is given by [equation \(13.210\)](#). The results of the derivations follow and are also summarised in Appendix 7:

$$\begin{aligned} Z_u &= -\frac{\rho V_0 S}{2m} (M_0 C_{L_M} + 2C_L) \\ Z_{\dot{w}} &= \frac{\rho S \bar{c}}{4m} C_{z_{\dot{a}}} \\ Z_w &= -\frac{\rho V_0 S}{2m} (C_D + C_{L_a}) \\ Z_q &= \frac{\rho V_0 S \bar{c}}{m} C_{z_q} \\ Z_{\delta} &= \frac{\rho V_0^2 S}{2m} C_{z_{\delta}} \end{aligned} \tag{13.218}$$

Since there are some small differences in the derivation of the moment derivatives, it is useful to review the normalised pitching moment derivative definitions. As before, the left-hand side of the pitching moment equation from [equations \(13.206\)](#) may be expanded in terms of partial derivative functions of the perturbation variables to give

$$\begin{aligned} \frac{1}{I_y} \left(\frac{1}{2} \rho V^2 S \bar{c} C_m \right) &= \frac{\rho S \bar{c}}{2I_y} \left(\begin{array}{l} \frac{\partial(V^2 C_m)}{\partial U} u + \frac{\partial(V^2 C_m)}{\partial \dot{W}} \dot{w} + \frac{\partial(V^2 C_m)}{\partial W} w \\ + \frac{\partial(V^2 C_m)}{\partial q} q + \frac{\partial(V^2 C_m)}{\partial \delta_e} \delta_e + \frac{\partial(V^2 C_m)}{\partial \delta_{th}} \delta_{th} \end{array} \right) \\ &= M_u u + M_{\dot{w}} \dot{w} + M_w w + M_q q + M_{\delta_e} \delta_e + M_{\delta_{th}} \delta_{th} \end{aligned} \tag{13.219}$$

Equating equivalent terms in [equation \(13.219\)](#), expressions for the normalised pitching moment derivatives, referred to aircraft wind axes, may be derived as follows:

$$\begin{aligned} M_u &= \frac{\rho S \bar{c}}{2I_y} \frac{\partial(V^2 C_m)}{\partial U} = \frac{\rho V S \bar{c}}{2I_y} \left(V \frac{\partial C_m}{\partial V} + 2C_m \right) \\ &\equiv \frac{\rho V S \bar{c}}{2I_y} \left(M \frac{\partial C_m}{\partial M} + 2C_m \right) = \frac{\rho V S \bar{c}}{2I_y} (M C_{m_M} + 2C_m) \end{aligned} \tag{13.220}$$

Again, remember that for a wind axes reference $U = U_e + u \equiv V$ and Mach number $M = V/a$. To define the derivative M_u at the flight condition of interest, let the perturbation become vanishingly

small such that $u \rightarrow 0$, hence $V \rightarrow V_0$ and $M \rightarrow M_0$. Further, since the perturbation is a disturbance about trim, and when the aircraft is in trim the pitching moment is zero, as the perturbation becomes vanishingly small $C_m \rightarrow 0$. Whence

$$M_u = \frac{\rho V_0 S \bar{c}}{2I_y} (M_0 C_{m_M}) \quad (13.221)$$

The remaining normalised pitching moment derivative expressions may be derived in a similar manner; for example,

$$\begin{aligned} M_{\dot{w}} &= \frac{\rho S \bar{c}}{2I_y} \frac{\partial(V^2 C_m)}{\partial \dot{W}} = \frac{\rho V^2 S \bar{c}}{2I_y} \frac{\partial C_m}{\partial \dot{w}} = \frac{\rho V S \bar{c}}{2I_y} \frac{\partial C_m}{\partial \dot{\alpha}} = \frac{\rho V S \bar{c}}{2I_y} \left(\frac{\bar{c}}{2V} \right) \frac{\partial C_m}{\partial (\dot{\alpha} \bar{c}/2V)} \\ M_{\dot{w}} &= \frac{\rho S \bar{c}^2}{4I_y} C_{m_{\dot{\alpha}}} \end{aligned} \quad (13.222)$$

and so on. Whence

$$\begin{aligned} M_w &= \frac{\rho V_0 S \bar{c}}{2I_y} C_{m_{\alpha}} \\ M_q &= \frac{\rho V_0 S \bar{c}^2}{4I_y} C_{m_q} \\ M_{\delta} &= \frac{\rho V_0^2 S \bar{c}}{2I_y} C_{m_{\delta}} \end{aligned} \quad (13.223)$$

13.5.2 The lateral-directional aerodynamic derivative coefficients

Similarly, now consider the lateral-directional equations of motion; by comparing equations (4.78), (4.79), and (4.80) with (13.183), in a perturbation the aerodynamic and control forces and moments may be written as

$$\begin{aligned} \frac{1}{m} \left(\frac{1}{2} \rho V^2 S C_y \right) &= Y_v v + Y_p p + Y_r r + Y_{\delta_{\xi}} \delta_{\xi} + Y_{\delta_{\zeta}} \delta_{\zeta} \\ \frac{1}{I_x} \left(\frac{1}{2} \rho V^2 S b C_l \right) &= L_v v + L_p p + L_r r + L_{\delta_{\xi}} \delta_{\xi} + L_{\delta_{\zeta}} \delta_{\zeta} \\ \frac{1}{I_z} \left(\frac{1}{2} \rho V^2 S b C_n \right) &= N_v v + N_p p + N_r r + N_{\delta_{\xi}} \delta_{\xi} + N_{\delta_{\zeta}} \delta_{\zeta} \end{aligned} \quad (13.224)$$

As before, the left-hand sides of equations (13.224) may be expanded in terms of partial derivative functions of the perturbation variables. Thus, for example, the lateral sideforce equation in (13.224) may be written as

$$\frac{1}{m} \left(\frac{1}{2} \rho V^2 S C_y \right) = \frac{\rho V^2 S}{2m} \left(\frac{\partial C_y}{\partial v} v + \frac{\partial C_y}{\partial p} p + \frac{\partial C_y}{\partial r} r + \frac{\partial C_y}{\partial \delta_\xi} \delta_\xi + \frac{\partial C_y}{\partial \delta_\zeta} \delta_\zeta \right)$$

$$= Y_v v + Y_p p + Y_r r + Y_{\delta_\xi} \delta_\xi + Y_{\delta_\zeta} \delta_\zeta \quad (13.225)$$

and it is assumed that in a small lateral-directional perturbation, the motion is decoupled from longitudinal motion such that velocity V is independent of the perturbation variables. As before, equating terms in equation (13.225), expressions for the normalised derivatives referred to aircraft wind axes may be derived. For a wind axes reference $v/V = \tan \beta \cong \beta$, the small perturbation in sideslip angle. Whence

$$Y_v = \frac{\rho V^2 S}{2m} \frac{\partial C_y}{\partial v} \equiv \frac{\rho V S}{2m} \frac{\partial C_y}{\partial \beta}$$

$$Y_v = \frac{\rho V_0 S}{2m} C_{y_\beta} \quad (13.226)$$

or, equivalently,

$$Y_\beta = \frac{\rho V_0^2 S}{2m} C_{y_\beta} \quad (13.227)$$

Although the derivatives Y_p and Y_r are usually insignificantly small, it is instructive to review their derivation in terms of dimensionless coefficients:

$$Y_p = \frac{\rho V^2 S}{2m} \frac{\partial C_y}{\partial p} = \frac{\rho V^2 S}{2m} \left(\frac{b}{2V} \right) \frac{\partial C_y}{\partial (pb/2V)} = \frac{\rho VS b}{4m} C_{y_p}$$

$$Y_r = \frac{\rho V^2 S}{2m} \frac{\partial C_y}{\partial r} = \frac{\rho V^2 S}{2m} \left(\frac{b}{2V} \right) \frac{\partial C_y}{\partial (rb/2V)} = \frac{\rho VS b}{4m} C_{y_r}$$

Since the derivatives $\partial C_y / \partial p$ and $\partial C_y / \partial r$ are not dimensionless, it is necessary to introduce the *lateral reference time* value $b/2V$ as shown. Again, let the perturbation become vanishingly small such that $V \rightarrow V_0$; then

$$Y_p = \frac{\rho V_0 S b}{4m} C_{y_p} \quad (13.228)$$

$$Y_r = \frac{\rho V_0 S b}{4m} C_{y_r} \quad (13.229)$$

Similarly, the control derivatives may be derived:

$$Y_\delta = \frac{\rho V_0^2 S}{2m} C_{y_\delta} \quad (13.230)$$

By repeating this process, the roll and yawing moment normalised derivative expressions may also be derived. For the rolling moment equation in [equations \(13.224\)](#),

$$L_v = \frac{\rho V_0 S b}{2I_x} C_{l_\beta}$$

or equivalently

$$\begin{aligned} L_\beta &= \frac{\rho V_0^2 S b}{2I_x} C_{l_\beta} \\ L_p &= \frac{\rho V_0 S b^2}{4I_x} C_{l_p} \\ L_r &= \frac{\rho V_0 S b^2}{4I_x} C_{l_r} \\ L_\delta &= \frac{\rho V_0^2 S b}{2I_x} C_{l_\delta} \end{aligned} \quad (13.231)$$

and for the yawing moment equation in [equations \(13.224\)](#),

$$N_v = \frac{\rho V_0 S b}{2I_z} C_{n_\beta}$$

or equivalently

$$\begin{aligned} N_\beta &= \frac{\rho V_0^2 S b}{2I_z} C_{n_\beta} \\ N_p &= \frac{\rho V_0 S b^2}{4I_z} C_{n_p} \\ N_r &= \frac{\rho V_0 S b^2}{4I_z} C_{n_r} \\ N_\delta &= \frac{\rho V_0^2 S b}{2I_z} C_{n_\delta} \end{aligned} \quad (13.232)$$

The lateral-directional derivative expressions given by [equations \(13.226\) through \(13.232\)](#) are also summarised in Appendix 7.

13.5.3 Comments

Today it is common for the equations of motion to be presented either in British notation or in American notation, and, further, the units in either notational style can be Imperial or SI. In general, the notational style will depend on the source of the aerodynamic model of the aircraft. It is therefore important that the modern flight dynamicist become sufficiently dexterous to deal with the equations of motion and aerodynamic model in whatever form they are presented. It is evident from the foregoing that the differences between, for example, British dimensionless aerodynamic derivatives and American aerodynamic derivative coefficients can be subtle, and care must be exercised in their interpretation. It can be tempting to convert from one notational style to another for various reasons; however, it cannot be emphasised enough that this process can be fraught with pitfalls unless extreme care is exercised. Experience shows that it is very easy to confuse the

differences between the various dimensionless derivative forms and even to make errors in the translation from one style of units to another. It is therefore most advisable to conduct any flight dynamics analysis of an aeroplane using the equations of motion and aerodynamic model in the notational style presented by the source of that information. After all, irrespective of notational style, all equations of motion appear in a similar format once reduced to the state-space form, and their solution differs only by the applicable units.

EXAMPLE 13.1

The estimation of the stability and control derivatives for an aircraft by analytical means is generally a complex and substantial task, the procedure is laborious, and the results are often of poor accuracy and hence of limited usefulness. In general, the best results are obtained for simple aircraft with moderate flight envelopes and whose properties can be reasonably well defined by classical aerodynamics. The estimation of the stability and control derivatives for advanced-technology aircraft having large flight envelopes, multiple engines, and extensive configuration variables for aerodynamic optimisation is best dealt with by wind tunnel testing, modern computational methods, and/or flight test—as discussed in Chapter 12. However, when it is possible and appropriate to do so, estimation by analytical means can give considerable insight into the way in which the aerodynamic properties of the aircraft determine the stability and control characteristics seen by the pilot. Such background information is also especially valuable for the flight control system designer when it is intended that the aircraft is to incorporate advanced flight control systems.

The Slingsby T51 Dart sailplane is chosen to illustrate the analytical estimation of the aerodynamic stability and control derivatives of an aircraft. A configuration drawing, after [Coates \(1978\)](#), is shown in [Fig. 13.16](#). The reasons for this choice are that the aircraft is aerodynamically simple, it has a limited subsonic flight envelope, and, most important, geometric, mass, aerodynamic, and performance data are readily available in the public domain. It is also clear that the stability and control characteristics of the aircraft are entirely dependent on the aerodynamic configuration. The Dart is a mid-1960s design, manufactured by Slingsby in the United

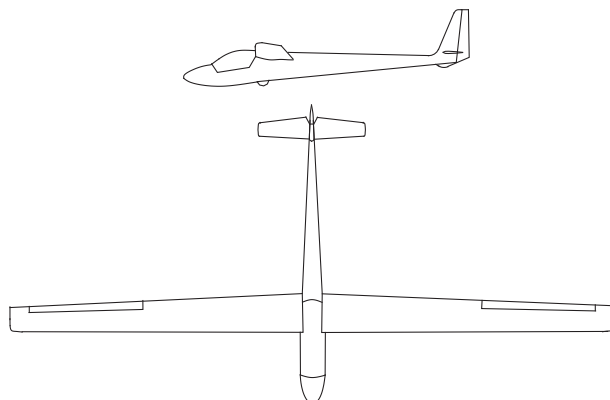


FIGURE 13.16 Slingsby Dart T51 configuration.

Kingdom, and is one of the last competition sailplanes to be built using traditional wood construction. The configuration was designed to meet the requirements of the standard 15 m span, single-seat class of high-performance sailplanes.

Basic aircraft data

Basic configuration, performance, and aerodynamic data were obtained from [Taylor \(1965–66\)](#), [Coates \(1978\)](#), and [Ellison \(1971\)](#). Of particular relevance to the aerodynamic modelling, the wing section is given—NACA 64₃618/615—and its properties are available in [Abbott and von Doenhoff \(1959\)](#). Moment of inertia data are not given in any of the above references. However, the thesis by [Millman \(1971\)](#) reports on the design of a single-seat sailplane to meet the requirements of the 15 m-span standard class. Since the sailplane design has the same all-up weight (AUW) as the Dart and a configuration sufficiently similar, the same mass distribution was assumed. The inertia values computed by [Millman \(1971\)](#) were therefore considered to be sufficiently representative of the Dart and were adopted for this example.

The essential basic data were assembled and set out in [Tables 13.1 through 13.3](#). Additional geometric and dimensional information not given in the references was estimated from the scaled three-view drawing of the aircraft given in [Coates \(1978\)](#). It is important to note that the inertia data obtained from [Millman \(1971\)](#) assumes an aircraft body axes reference. The aspect ratios of the wing and tailplane are sufficiently large that the calculation of their aerodynamic properties based on the simple theory is adequate. However, this is not the case for the fin, since it is subject to the end plate effect of the tailplane above which it is mounted. Calculation of the effective fin aspect ratio was made using information given in the relevant ESDU (2006) data item as noted with the data.

Table 13.1 T51 Dart 15 Performance at AUW of 318 kg

Maximum wing loading	24.8 kg/m ²
Best glide ratio	33.5:1 at 45.8 kt
Minimum sink speed	0.67 m/s at 41.5 kt
Maximum speed in smooth air	116 kt
Maximum speed in rough air	80 kt
Stall speed at maximum AUW (332 kg)	35 kt

Table 13.2 Mass and Inertias

Mass	m	318 kg
Roll inertia	I_{x_b}	1368 kgm ²
Pitch inertia	I_{y_b}	432 kgm ²
Yaw inertia	I_{z_b}	1778 kgm ²
Product of inertia	I_{xz_b}	-4.1 kgm ²
cg position (assumed)	h	0.3

Basic aerodynamic data for the wing, tailplane, and fin are given in [Table 13.4](#) and have been calculated from two-dimensional section data given in [Abbott and von Doenhoff \(1959\)](#). The aerodynamic characteristics of the wing tail and fin were calculated using the methods given in Chapter 1 of [Abbott and von Doenhoff \(1959\)](#). The aerofoil sections used on the tailplane and fin are not given in any of the references, and representative symmetrical NACA sections have been assumed as indicated. The tailplane was assumed to have 6% thickness-to-chord ratio and the fin to have 15% thickness-to-chord ratio. It is also important to note that the Dart has an all-moving tailplane for control instead of a conventional elevator.

Table 13.3 Geometric Data

Wing Geometry					
Span	b	15 m	Root chord	c_{rw}	1.04 m
Area	S	12.7 m^2	Tip chord	c_{tw}	0.63 m
Mean chord	\bar{c}	0.835 m	Taper ratio	λ_w	0.606
Dihedral	Γ	2°	Aspect ratio	A	17.8
Rigging angle	α_{wr}	9°	Sweep c_γ	A	-0.8°
Tailplane Geometry					
Span	b_T	2.61 m	Root chord	c_{rT}	0.574 m
Area	S_T	1.14 m^2	Tip chord	c_{tT}	0.304 m
Tail arm	l_t	4.63 m	Taper ratio	λ_T	0.53
Rigging angle	η_T	0°	Aspect ratio	A_T	5.98
Fin Geometry					
Height	h_F	1.25 m	Root chord	c_{rF}	0.878 m
Net area	S_f	0.54 m^2	Tip chord	c_{tF}	0.405 m
Total area	S_F	0.96 m^2	Taper ratio	λ_F	0.47
Rudder area	S_{FR}	0.42 m^2	Sweep c_γ	A_F	16°
Effective aspect ratio (ESDU 82010)					A_F
					3.26

Table 13.4 Basic Aerodynamic Data

		Wing-Body	Tailplane	Fin
Aerofoil section		NACA 64,618	NACA 65 006	NACA 63,015
Lift curve slope	a	5.55 rad^{-1}	a_1	4.303 rad^{-1}
Maximum lift coefficient	C_{Lmax}	1.29	0.8	1.5
Aerodynamic centre	h_0	0.25	0.25	0.25
Zero-lift pitch moment	C_{m0}	-0.11	0	0
Zero-lift angle of attack	α_0	-4°	0	0

Aerodynamic operating condition

Since the aerodynamic stability and control derivatives are calculated at each trimmed flight condition, the procedure is illustrated here for a range of trimmed operating conditions extending over the flight envelope of the Dart. The Mathcad program AeroTrim, described in Section 3.6.4, with some minor adjustments to suit this application, was used for the purpose.

Key to the representational accuracy of the aerodynamic modelling is the measured drag polar and associated performance data reported by [Torode \(1973\)](#). The drag coefficient was then calculated using the following expression:

$$C_D = 0.013 + 1.13 \frac{C_L^2}{\pi A} \quad (13.233)$$

Similarly, simple performance calculations were made using the standard expressions fitted to measured flight data by [Torode \(1973\)](#). Sink rate, and hence flight path angle, was calculated using

$$v_s = 0.0123 \left(\frac{\frac{1}{2} \rho V^3 S}{mg} \right) + 1.21 \left(\frac{\frac{1}{2} mg \pi}{\rho VSA} \right) \quad (13.234)$$

and minimum drag speed was calculated using

$$V_{md} = \sqrt{\frac{mg}{\frac{1}{2} \rho S}} \left(\frac{1.13}{0.013 \pi A} \right)^{0.25} \quad (13.235)$$

The operating conditions assumed for the example cover a large part of the flight envelope from 35 knots to 85 knots at 5-knot intervals at a constant altitude of 1000 ft. AeroTrim was used to solve the trim equations as set out in Sections 3.6.1, 3.6.2, and 3.6.3 using the drag, sink rate, and minimum drag speed models given in [equations \(13.233\), \(13.234\), and \(13.235\)](#), setting the thrust-dependent terms to zero and simplifying the elevator longitudinal control terms to represent an all-moving tailplane. The calculated trim data required for derivative estimation are summarised in [Table 13.5](#).

Note that the derivative $dC_D/d\alpha$ was estimated from the gradient of the $C_D-\alpha_e$ plot and the computation was incorporated into AeroTrim for this example. This shows the flexibility offered by the use of AeroTrim, which is easily modified or adapted to deal with a wide variety of routine trim computations.

Note also that in this instance α_e represents the trimmed value of the wing incidence—the lift-producing incidence. However, since the wing rigging angle $\alpha_{wr} = 9^\circ$, the aircraft attitude appears significantly nose down, and this is confirmed by reference to [Fig. 13.16](#). Since a glider always descends with flight path angle γ_e in normal trimmed flight and pitch attitude is given by equation (5.127),

$$\gamma = \theta - \alpha$$

where, in this instance, α is the aircraft *body axes incidence*, and when *wind axes* are specified, as for this example, $\alpha = 0$, and it follows that $\theta_e = \gamma_e$.

Table 13.5 Calculated Longitudinal Trim Data

V_0 kt	V_0 m/s	α_e deg	η_e deg	C_L	C_D	γ_e deg	$dC_D/d\alpha$ rad ⁻¹
35	18.025	9.209	-8.403	1.271	0.0457	-2.057	0.254
40	20.6	6.161	-6.432	0.973	0.0321	-1.892	0.226
45	23.175	4.072	-5.08	0.769	0.0249	-1.858	0.177
50	25.75	2.577	-4.113	0.623	0.0208	-1.916	0.143
55	28.325	1.471	-3.398	0.515	0.0184	-2.042	0.118
60	30.9	0.63	-2.854	0.433	0.0168	-2.222	0.099
65	33.475	-0.025	-2.431	0.369	0.0157	-2.446	0.084
70	36.05	-0.544	-2.095	0.318	0.0150	-2.71	0.073
75	38.625	-0.963	-1.824	0.277	0.0146	-3.009	0.063
80	41.2	-1.306	-1.602	0.243	0.0142	-3.34	0.055
85	43.775	-1.59	-1.418	0.216	0.0139	-3.701	0.052

Other useful aerodynamic data output by AeroTrim includes static margin K_n , minimum drag speed V_{md} , and rate of change of downwash with incidence at the tail $d\varepsilon/d\alpha$ with the following values:

$$K_n = 0.247$$

$$V_{md} = 44.06 \text{ knots}$$

$$d\varepsilon/d\alpha = 0.223$$

Note that the minimum drag speed correlates well with the published performance data for the aircraft, and this confers a degree of confidence on the aerodynamic modelling thus far.

Since the moments of inertia assumed for the model are referred to body axes aligned to the *horizontal fuselage datum* axes (HFD), the remaining preparatory work requires that they be converted to a wind, or a stability, axes reference. The conversion formulae are given in Appendix 10, Table A10.1, and the correct value for α_e here is the angle between the aircraft body and wind axes, that is, the value of α_e given in [Table 13.5](#) minus the wing rigging angle $\alpha_{wr} = 9^\circ$ for each trim condition. The results are given in [Table 13.6](#).

It will be seen that the variations in the moments of inertia over the speed envelope are negligibly small and that for all practical purposes a single value for each would be adequate. For example,

$$I_{x_w} = 1370 \text{ kg m}^2$$

$$I_{y_w} = 432 \text{ kg m}^2$$

$$I_{z_w} = 1770 \text{ kg m}^2$$

The value of the product of inertia is relatively small, but it does vary significantly over the speed envelope and it is preferable to use the values shown in [Table 13.6](#).

Table 13.6 Inertias Referred to Wind Axes

$V_0 \text{ kt}$	$I_{x_w} \text{ kgm}^2$	$I_{y_w} \text{ kgm}^2$	$I_{z_w} \text{ kgm}^2$	$I_{x_w z_w} \text{ kgm}^2$
35	1.368×10^3	432	1.778×10^3	-5.599
40	1.369×10^3	432	1.777×10^3	16.199
45	1.370×10^3	432	1.776×10^3	31.052
50	1.372×10^3	432	1.774×10^3	41.58
55	1.374×10^3	432	1.772×10^3	49.298
60	1.375×10^3	432	1.771×10^3	55.12
65	1.377×10^3	432	1.769×10^3	59.618
70	1.378×10^3	432	1.768×10^3	63.165
75	1.379×10^3	432	1.767×10^3	66.011
80	1.380×10^3	432	1.766×10^3	68.33
85	1.380×10^3	432	1.766×10^3	70.245

Estimation of the longitudinal stability and control derivatives

The dimensionless longitudinal stability and control derivatives are estimated using the expressions developed in [Section 13.2](#) subject to a number of simplifying assumptions. In particular, since the speed envelope is very small, 35 knots to 85 knots, and since compressibility effects are negligible, lift, drag, and pitching moment coefficient dependency on speed is assumed insignificant, and the relevant terms are omitted from the derivative expressions. Accordingly, the derivative expressions used are listed below and their evaluation at 50 knots is also illustrated.

$$X_u = -2C_D = -0.042$$

$$X_w = C_L - \frac{dC_D}{d\alpha} = 0.623 - 0.143 = 0.48$$

$$X_q = 0$$

$$X_{\dot{w}} = 0$$

$$X_\eta = 0$$

$$Z_u = -2C_L = -1.246$$

$$Z_w = -(a + C_D) = -(5.55 + 0.02084) = -5.571$$

$$Z_q = -\bar{V}_T a_1 = -0.493 \times 4.303 = -2.122$$

$$Z_{\dot{w}} = Z_q \frac{d\varepsilon}{d\alpha} = -2.121 \times 0.223 = -0.472$$

$$Z_\eta = -\frac{S_T}{S} a_2 = -\frac{1.14}{12.7} \times 4.303 = -0.386$$

$$\begin{aligned}
 M_u &= 0 \\
 M_w &= -aK_n = -5.55 \times 0.247 = -1.373 \\
 M_q &= Z_q \frac{l_T}{\bar{c}} = -2.121 \frac{4.59}{0.835} = -11.663 \\
 M_{\dot{w}} &= M_q \frac{d\varepsilon}{d\alpha} = -11.66 \times 0.223 = -2.595 \\
 M_\eta &= -\bar{V}_T a_2 = -0.493 \times 4.303 = -2.122
 \end{aligned}$$

In addition to the data assembled, in order to complete the derivative calculations shown, it is necessary to calculate a value for the tail volume ratio \bar{V}_T . The expression for this is given by equation (2.32) and the definition requires that the tail moment arm be calculated from the *cg* to the quarter-chord point on the tailplane *mac* (see Fig. 2.9). Accordingly,

$$l_T = l_t - (h - h_0)\bar{c} = 4.63 - (0.3 - 0.25)0.835 = 4.588 \text{ m} \quad (13.236)$$

Thus the tail volume ratio follows:

$$\bar{V}_T = \frac{S_T l_T}{S \bar{c}} = \frac{1.14 \times 4.59}{12.7 \times 0.835} = 0.493 \quad (13.237)$$

For the assumptions made, all derivatives for this model are constant with flight condition with the exception of X_u , X_w , Z_u , and Z_w , which vary with trim speed. The values for these derivatives are given in Table 13.7.

Note again that the value of the derivative Z_w varies little over the speed envelope and that for all practical purposes its value may be taken as $Z_w = -5.6$. This observation should not be surprising as the value of lift curve slope a dominates and for the Dart it remains essentially constant over the flight envelope.

Table 13.7 Longitudinal Velocity-Dependent Derivatives

$V_0 \text{ kt}$	X_u	X_w	Z_u	Z_w
35	-0.091	1.017	-2.542	-5.596
40	-0.064	0.748	-1.946	-5.582
45	-0.050	0.592	-1.538	-5.575
50	-0.042	0.480	-1.246	-5.571
55	-0.037	0.397	-1.029	-5.568
60	-0.034	0.334	-0.865	-5.567
65	-0.031	0.284	-0.737	-5.566
70	-0.030	0.245	-0.636	-5.565
75	-0.029	0.214	-0.554	-5.565
80	-0.028	0.188	-0.487	-5.564
85	-0.028	0.164	-0.431	-5.564

This concludes the estimation of the dimensionless longitudinal stability and control derivatives for the Slingsby Dart T51. However, at this stage it is easy to write the derivatives in alternative formats as required. For example, the dimensionless derivatives, evaluated at 50 knots, may be written in American coefficient format as defined in Appendix 7, Table A7.2, to give

$$\begin{aligned}
 C_{x_u} \equiv X_u &= -0.042 & C_{z_u} \equiv Z_u &= -1.246 & C_{m_u} \equiv M_u &= 0 \\
 C_{x_\alpha} \equiv X_w &= 0.48 & C_{z_\alpha} \equiv Z_w &= -5.571 & C_{m_\alpha} \equiv M_w &= -1.373 \\
 C_{x_q} \equiv 2X_q &= 0 & C_{z_q} \equiv 2Z_q &= -4.244 & C_{m_q} \equiv 2M_q &= -23.326 \\
 C_{x_{\dot{\alpha}}} \equiv 2X_w &= 0 & C_{z_{\dot{\alpha}}} \equiv 2Z_w &= -0.944 & C_{m_{\dot{\alpha}}} \equiv 2M_w &= -5.19 \\
 C_{x_{\delta_e}} \equiv X_\eta &= 0 & C_{z_{\delta_e}} \equiv Z_\eta &= -0.386 & C_{m_{\delta_e}} \equiv M_\eta &= -2.122
 \end{aligned}$$

Estimation of the lateral-directional stability and control derivatives

The dimensionless lateral-directional stability and control derivatives are estimated using the expressions developed in [Section 13.3](#) subject to the same simplifying assumptions referred to previously. However, estimation of the lateral-directional stability and control derivatives by any means usually poses a challenge and the analytical models described in [Section 13.3](#) produce estimates of uncertain accuracy. For this reason recourse is also made to ESDU data items since these can produce significantly better estimates, especially for a conventional aircraft configuration like the Slingsby Dart. Since the Dart is a very-high-aspect-ratio aircraft and its flight envelope is very subsonic, the simple lateral-directional derivative expressions can be applied with a higher degree of confidence than is usually the case. The procedure used for estimating the derivatives requires that the various contributions to each derivative are separately evaluated, as far as that is possible with the information available, and the sum of the contributions for each derivative is then taken to be the best estimate. To illustrate the procedure the derivatives are, once again, evaluated at 50 knots.

Wing contributions

Since the aspect ratio of the wing exceeds the range covered by the ESDU data items, the following derivatives can only be estimated analytically by application of the simple expressions given in [Section 13.3](#). In the following computations it is assumed that lift curve slope a , lift coefficient C_L , drag coefficient C_D , and the derivative of drag coefficient with respect to incidence $dC_D/d\alpha$ are constant over the span of the wing.

$L_{v(wing)}$ —Rolling moment due to sideslip This comprises two components, one due to dihedral and a very much smaller component due to wing sweep. The dihedral component is given by [equation \(13.92\)](#), which may be interpreted in terms of the aerodynamic and geometric properties of the Dart:

$$L_{v(dihedral)} = -\frac{a\Gamma}{Ss} \int_0^s \left(\frac{(c_{tw} - c_{rw})}{s} y + c_{rw} \right) y dy = -\frac{a\Gamma s}{S} \left(\frac{c_{tw}}{3} + \frac{c_{rw}}{6} \right) \quad (13.238)$$

Substituting geometric and aerodynamic data for 50 knots flight speed into [equation \(13.238\)](#), taking care that dihedral angle has radian units, gives

$$L_{v(dihedral)} = -0.0439$$

The wing sweep component is given by [equation \(13.105\)](#), which may similarly be interpreted as

$$L_{v(sweep)} = -\frac{2C_L \tan A}{Ss} \int_0^s \left(\frac{(c_{tw} - c_{rw})}{s} y + c_{rw} \right) y dy = -\frac{2C_L s \tan A}{S} \left(\frac{c_{tw}}{3} + \frac{c_{rw}}{6} \right) \quad (13.239)$$

and, evaluated at 50 knots,

$$L_{v(sweep)} = 0.00394$$

This contribution is very small since the wing sweep angle is small and it is positive (destabilising) since the wing has forward, rather than aft sweep.

Thus the total wing contribution is given by

$$L_{v(wing)} = L_{v(dihedral)} + L_{v(sweep)} = -0.03996$$

L_{p(wing)}—Rolling moment due to roll rate The wing contribution is given by [equation \(13.128\)](#), which may be interpreted as follows:

$$L_{p(wing)} = -\frac{(a + C_D)}{2Ss^2} \int_0^s \left(\frac{(c_{tw} - c_{rw})}{s} y + c_{rw} \right) y^2 dy = -\frac{(a + C_D)s}{2S} \left(\frac{c_{tw}}{4} + \frac{c_{rw}}{12} \right) \quad (13.240)$$

and, evaluated at 50 knots,

$$L_{p(wing)} = -0.4017$$

N_{p(wing)}—Yawing moment due to roll rate The wing contribution is given by [equation \(13.137\)](#), which may be interpreted as follows:

$$N_{p(wing)} = -\frac{\left(C_L - \frac{dC_D}{d\alpha}\right)}{2Ss^2} \int_0^s \left(\frac{(c_{tw} - c_{rw})}{s} y + c_{rw} \right) y^2 dy = -\frac{\left(C_L - \frac{dC_D}{d\alpha}\right)s}{2S} \left(\frac{c_{tw}}{4} + \frac{c_{rw}}{12} \right) \quad (13.241)$$

and, evaluated at 50 knots,

$$N_{p(wing)} = -0.0346$$

L_{r(wing)}—Rolling moment due to yaw rate The wing contribution is given by [equation \(13.150\)](#), which may be interpreted as follows:

$$L_{r(wing)} = \frac{C_L}{Ss^2} \int_0^s \left(\frac{(c_{tw} - c_{rw})}{s} y + c_{rw} \right) y^2 dy = \frac{C_L s}{S} \left(\frac{c_{tw}}{4} + \frac{c_{rw}}{12} \right) \quad (13.242)$$

and, evaluated at 50 knots,

$$L_{r(wing)} = 0.08985$$

Note that this contribution is positive, and hence destabilising in roll, in accordance with the flight physical understanding. (Most stability derivatives are negative for a stable aircraft.)

$N_{r(wing)}$ —Yawing moment due to yaw rate The wing contribution is given by [equation \(13.162\)](#), which may be interpreted as follows:

$$N_{r(wing)} = -\frac{C_D}{Ss^2} \int_0^s \left(\frac{(c_{tw} - c_{rw})}{s} y + c_{rw} \right) y^2 dy = -\frac{C_D s}{S} \left(\frac{c_{tw}}{4} + \frac{c_{rw}}{12} \right) \quad (13.243)$$

and, evaluated at 50 knots,

$$N_{r(wing)} = -0.00301$$

Fin contributions

In the interests of achieving the best possible accuracy, all fin derivatives are evaluated using the relevant ESDU data items. Since the notation used in the calculation process is not always compatible with that adopted throughout this book, where necessary the ESDU notation takes precedence in this example. Application of the calculation methods described in the ESDU data items requires detailed dimensional information relating to the relative geometric location of the centre of gravity, the wing, the tailplane, and the fin. Some of the dimensional data is a part of the general aircraft description as listed at the start of the example. Additional geometric information is required, and for this example these dimensions were estimated from an enlarged copy of the scale three-view drawing of the aircraft given in [Coates \(1978\)](#). It must be emphasized that the accuracy of these dimensions is not likely to be particularly good. In a more formal aircraft design situation, this kind of dimensional information would be available at high accuracy.

In the notation of ESDU 82010, additional fin geometry parameters, assuming a fin-mounted tailplane, were estimated as follows:

Fin moment arm measured from the *cg* to the $c_{vF}m_F = 4.595$ m

$$h_{BF} = 0.13 \text{ m} \quad h_{BW} = 0.777 \text{ m} \quad z_{crF} = 0.118 \text{ m} \quad z_W = -0.237 \text{ m} \quad z_T = 0.135 \text{ m}$$

In accordance with the data item, the following expressions are evaluated:

$$\begin{aligned} \frac{h_{BF}}{h_{BF} + h_F} &= 0.094 \quad \frac{b_T}{h_F} = 2.088 \quad \frac{z_W}{h_{BW}} = -0.305 \\ \frac{z_T}{h_F} &= 0.108 \quad \left(\frac{z_T}{h_F} \right)^2 = 0.012 \end{aligned}$$

It is important to note that the geometric datum axis is the *horizontal fuselage datum* (HFD), or longitudinal body axis, and that the incidence angle α used in the following calculations is the incidence of the HFD to the airflow—that is, as before, the angle between the aircraft body and wind axes.

With this numerical information the nomograms given in the data item are used to determine the following parameters:

$$J_B = 0.8 \quad J_T = 1.0 \quad J_W = 0.81 \quad \bar{z}_F = 0.4 \quad h_F = 0.5 \text{ m}$$

An expression for a modified fin volume ratio is given which allows empirically for the aerodynamic adjustment due to fin sweep.

$$\overline{V}_F = \frac{S_F(m_F + 0.7\bar{z}_F \tan A_{l4F})}{Sb} = 0.024 \quad (13.244)$$

Using the dimensional parameters defined for the aircraft, they are substituted into various expressions in order to arrive at estimated values for the fin derivatives due to sideslip.

$Y_{v(fin)}$ —Sideforce due to sideslip The fin contribution is given by

$$Y_{v(fin)} = -J_B J_T J_W a_{1F} \frac{S_F}{S} \quad (13.245)$$

and this has a constant value at all speeds:

$$Y_{v(fin)} = -0.18$$

$L_{v(fin)}$ —Rolling moment due to sideslip The fin contribution is given in the data item:

$$L_{v(fin)} = Y_{v(fin)} \frac{(z_{crF} + 0.85\bar{z}_F) \cos \alpha - (m_F + 0.7\bar{z}_F \tan A_{l4F}) \sin \alpha}{b} \quad (13.246)$$

The value of this derivative varies with incidence α over the flight envelope and, evaluated at 50 knots, is

$$L_{v(fin)} = -0.0128$$

$N_{v(fin)}$ —Yawing moment due to sideslip The fin contribution is given in the data item:

$$N_{v(fin)} = -Y_{v(fin)} \frac{(z_{crF} + 0.85\bar{z}_F) \sin \alpha + (m_F + 0.7\bar{z}_F \tan A_{l4F}) \cos \alpha}{b} \quad (13.247)$$

The value of this derivative also varies with incidence α over the flight envelope and, evaluated at 50 knots, is

$$N_{v(fin)} = 0.0553$$

Fin contributions arising from yaw rate are set out in ESDU 82017, and the expressions given make use of the same fin geometry parameters as set out above.

$Y_{r(fin)}$ —Sideforce due to yaw rate

$$Y_{r(fin)} = -\frac{Y_{v(fin)}(z_{crF} + 0.85\bar{z}_F) \sin \alpha + (m_F + 0.7\bar{z}_F \tan A_{l4F}) \cos \alpha}{J_W b} \quad (13.248)$$

and, evaluated at 50 knots,

$$Y_{rF} = 0.068$$

$L_{r(fin)}$ —Rolling moment due to yaw rate

$$L_{r(fin)} = Y_{r(fin)} \frac{(z_{crF} + 0.85\bar{z}_F) \cos \alpha - (m_F + 0.7\bar{z}_F \tan A_{l4F}) \sin \alpha}{b} \quad (13.249)$$

and, evaluated at 50 knots,

$$L_{rF} = 0.00485$$

N_{r(fin)}—Yawing moment due to yaw rate

$$N_{r(\text{fin})} = -Y_{r(\text{fin})} \frac{(z_{crF} + 0.85\bar{z}_F)\sin\alpha + (m_F + 0.7\bar{z}_F\tan A_F)\cos\alpha}{b} \quad (13.250)$$

and, evaluated at 50 knots,

$$N_{rF} = -0.021$$

Body (fuselage) contributions

Body contributions to the lateral-directional stability derivatives are notoriously difficult to estimate with any degree of confidence. Contributions due to roll rate and yaw rate are generally considered to be sufficiently small that they can be ignored. However, sideforce and yawing moment due to sideslip are significant. Undoubtedly, the most important contribution is sideforce due to sideslip, and this was estimated for the Dart using ESDU 79006; even this is considered to be of limited accuracy in some applications.

Following ESDU 79006, and in the notation of the data item, the following geometric parameters were estimated:

$$h = 0.88 \text{ m} \quad S_B = 3.88 \text{ m}^2 \quad z = 0.24 \text{ m} \quad d = 0.676 \text{ m}$$

Again, a scaled side view of the aircraft was used from which to estimate the dimensions, and the side view was drawn on squared paper to facilitate the estimation of body side area S_B .

With this numerical information the nomograms given in the data item were used to determine the following parameters:

$$F = 0 \quad F_W = 0.6 \quad \frac{b}{d} = 22.189$$

Substituting these dimensional parameters into the following expression, an estimate of the sideforce due to sideslip for the body was made:

$$Y_{v(\text{body})} = -\left(0.00714 + 0.674 \frac{h^2}{S_B} + \frac{hbFF_W}{S_B} \left(4.95 \frac{|z|}{h} - 0.12\right)\right) \frac{S_B}{S} - 0.006|\Gamma| \quad (13.251)$$

The value is constant for all flight conditions:

$$Y_{v(\text{body})} = -0.055$$

Aileron control derivatives

Estimation of the aileron control derivatives depends on the availability of a representative estimate for the aileron lift curve slope a_{2A} . For a part span aileron, as is the case here, the problem concerns the aileron end losses, which are difficult, if not impossible, to quantify analytically. Thus recourse is made to the empirical estimation of a_{2A} using the appropriate ESDU data item.

Y_s—Sideforce due to aileron For conventional aircraft this derivative is usually assumed to be negligibly small; accordingly its value is taken as zero.

L_s—Rolling moment due to aileron For conventional aircraft of reasonable aspect ratio, the simple analytical model given by equation (13.188) provides an acceptable estimate provided the aileron lift curve slope a_{2A} can be estimated with sufficient accuracy. Since the Slingsby Dart

has a very-high-aspect-ratio wing with part span ailerons, this approach is considered more than adequate. With reference to Fig. 13.15, equation (13.188) may be interpreted as follows:

$$\begin{aligned} L_\xi &= -\frac{1}{Ss} a_{2A} \int_{y_1}^{y_2} c_y y dy = -\frac{1}{Ss} a_{2A} \int_{y_1}^{y_2} \left(\frac{(c_{tw} - c_{rw})}{s} y + c_{rw} \right) y dy \\ &= -\frac{1}{Ss} a_{2A} \left(\frac{(c_{tw} - c_{rw})}{s} \left(\frac{y_2^3 - y_1^3}{3} \right) - c_{rw} \left(\frac{y_2^2 - y_1^2}{2} \right) \right) \end{aligned} \quad (13.252)$$

Referring to ESDU controls 01.01.03, in the notation of the data item the following geometric parameters were calculated from available data:

Wing section thickness to chord ratio $t/c = 0.18$

Mean aileron chord to mean wing chord ratio $c_f/c_w = 0.275$

Referring to Abbott and von Doenhoff (1959), the ratio of the two-dimensional wing section lift curve slope to the three-dimensional lift curve slope for the wing was determined as follows, again in the notation of the ESDU data item:

$$\frac{a_0}{a_{0T}} = \frac{6.19}{6.45} = 0.96$$

With this numerical information the nomograms given in the data item were used to determine the following parameters:

$$a_{20T} = 4.4 \text{ rad}^{-1} \quad a_{2A} = 0.94 a_{20T} = 4.136 \text{ rad}^{-1}$$

The aileron span variables y_1 and y_2 are self-evident in Fig. 13.15. Their values were estimated from the scaled drawing of the Dart given in Coates (1978) as fractions of the span, giving

$$y_1 = 0.56s \quad y_2 = 0.94s$$

Having estimated values for the required numerical data, substitution of the appropriate values into equation (13.252) gives the constant value for the derivative:

$$L_\xi = -0.505$$

N_e—Yawing moment due to aileron This derivative was estimated using the data item ESDU controls 88029. The assumptions made were that the wing has zero spanwise twist, and aileron deflection is symmetric, that is, nondifferential. It was also found necessary to extrapolate the data since the aspect ratio of the Dart exceeds the range given in the data item. Using the previously calculated geometric and aerodynamic parameters, the nomograms given in the data item gave the following parameters:

$$G_1 = 0.066 \quad G_2 = 0.048$$

The yawing moment due to aileron derivative is given by the expression

$$N_\xi = (G_1 - G_2) C_L L_\xi \quad (13.253)$$

and, evaluated at 50 knots,

$$N_\xi = 0.00057$$

Rudder control derivatives

As for the aileron control derivatives, it is first necessary to estimate a representative value for the rudder lift curve slope a_{2R} . The fin section, NACA 63₂015, lift curve slope data was also obtained from [Abbott and von Doenhoff \(1959\)](#), the ratio of the two-dimensional fin section lift curve slope to the three-dimensional lift curve slope was determined as follows, again in the notation of the ESDU data item:

$$\frac{a_0}{a_{0T}} = \frac{5.75}{6.27} = 0.917$$

Again, referring to ESDU controls 01.01.03, in the notation of the data item the following geometric parameters were calculated from available data:

Fin section thickness to chord ratio $t/c = 0.15$

Mean rudder chord to mean fin chord ratio $c_f/c_w = 0.5$

With this numerical information, the nomograms given in the data item were used to determine the rudder lift curve slope as follows:

$$a_{20T} = 5.94 \text{ rad}^{-1} \quad a_{2R} = 0.91 a_{20T} = 5.405 \text{ rad}^{-1}$$

Since the fin has a small aspect ratio, its effect on rudder control power is significant and must be corrected. The method described in [Abbot and von Doenhoff \(1959\)](#) was used for this purpose:

$$a_{2R}(\text{corrected}) = f \frac{a_{2R}}{(1 + a_{2R}/\pi A_F)} \quad (13.254)$$

where $f = 1.0$ is an empirical correction factor determined from the reference. Thus the best estimate for rudder lift curves slope is

$$a_{2R} = 3.538 \text{ rad}^{-1}$$

The simple expressions given in [Section 13.4.3](#) were then evaluated for the rudder control derivatives as follows.

Y_ζ —Sideforce due to rudder From [equations \(13.197\) and \(13.82\)](#), it follows that

$$Y_\zeta = -\frac{a_{2R}}{a_{1F}} Y_{v(\text{fin})} \quad (13.255)$$

Substitution of the appropriate values into [equation \(13.255\)](#) gives the constant value for the derivative:

$$Y_z = 0.173$$

L_ζ—Rolling moment due to rudder From equations (13.200) and (13.108) it follows that

$$L_{\zeta} = -\frac{a_{2R}}{a_{1F}} L_{v(fin)} \quad (13.256)$$

and evaluating at 50 knots gives

$$L_{\zeta} = 0.0125$$

N_ζ—Yawing moment due to rudder From equations (13.203) and (13.112) it follows that

$$N_{\zeta} = -\frac{a_{2R}}{a_{1F}} N_{v(fin)} \quad (13.257)$$

and evaluating at 50 knots gives

$$N_{\zeta} = -0.0529$$

Thus the total value of each of the stability and control derivatives comprises the sum of all the identifiable components, and each is very much an estimate as it is not possible to evaluate some of the more intangible contributions. For the assumptions made, most of the lateral-directional derivatives vary with trim speed as set out in Table 13.8. However, the derivatives Y_v , Y_p , Y_{ζ} , and L_{ξ} remain constant over the flight envelope and take the values calculated above.

Inspection of Table 13.8 indicates that most of the derivatives are near constant over the flight envelope; this is consistent with the view that for subsonic aircraft the lateral-directional stability characteristics remain fixed, approximately, by the symmetric design properties of the aircraft.

Table 13.8 Lateral-Directional Velocity-Dependent Derivatives

V ₀ kt	L _v	L _p	L _r	L _ζ	N _v	N _p	N _r	N _ξ	N _ζ	Y _r
35	-0.042	-0.403	0.187	0.006	0.056	-0.074	-0.028	0.0120	-0.054	0.070
40	-0.047	-0.402	0.145	0.009	0.056	-0.055	-0.026	0.0089	-0.054	0.069
45	-0.05	-0.402	0.117	0.011	0.056	-0.044	-0.025	0.0070	-0.054	0.069
50	-0.053	-0.402	0.097	0.012	0.055	-0.036	-0.024	0.0057	-0.053	0.068
55	-0.054	-0.401	0.082	0.013	0.055	-0.030	-0.023	0.0047	-0.053	0.068
60	-0.056	-0.401	0.070	0.014	0.055	-0.025	-0.023	0.0039	-0.053	0.068
65	-0.057	-0.401	0.061	0.015	0.055	-0.022	-0.023	0.0035	-0.053	0.068
70	-0.058	-0.401	0.054	0.015	0.055	-0.019	-0.023	0.0029	-0.052	0.067
75	-0.058	-0.401	0.048	0.016	0.054	-0.017	-0.022	0.0025	-0.052	0.067
80	-0.059	-0.401	0.044	0.016	0.054	-0.015	-0.022	0.0022	-0.052	0.067
85	-0.059	-0.401	0.040	0.016	0.054	-0.013	-0.022	0.0020	-0.052	0.067

This concludes the estimation of the dimensionless lateral-directional stability and control derivatives for the Slingsby Dart T51. As before, writing the derivatives in American coefficient format as defined in Appendix 7, Table A7.4 and evaluating at 50 knots gives

$$\begin{aligned}
 C_{y_v} &\equiv Y_v = -0.236 & C_{l_v} &\equiv L_v = -0.053 & C_{n_v} &\equiv N_v = 0.055 \\
 C_{y_p} &\equiv 2Y_p = 0 & C_{l_p} &\equiv 2L_p = -0.804 & C_{n_p} &\equiv 2N_p = -0.072 \\
 C_{y_r} &\equiv 2Y_r = 0.136 & C_{l_r} &\equiv 2L_r = 0.194 & C_{n_r} &\equiv 2N_r = -0.048 \\
 C_{y_{\delta A}} &\equiv Y_\xi = 0 & C_{l_{\delta A}} &\equiv L_\xi = -0.505 & C_{n_{\delta A}} &\equiv N_\xi = 0.0057 \\
 C_{y_{\delta R}} &\equiv Y_\zeta = 0.173 & C_{l_{\delta R}} &\equiv L_\zeta = 0.012 & C_{n_{\delta R}} &\equiv N_\zeta = -0.053
 \end{aligned}$$

The concise derivatives

Having achieved a complete set of the estimated dimensionless stability and control derivatives it is usual to go on and study the flight dynamics of the aircraft. The starting point for this process is the assembly of the concise equations of motion, equations (4.67) and (4.69), which requires the derivatives to be in concise format. The concise derivatives may be derived using Appendix 2, Tables A2.5 to A2.8, which, evaluated for the Dart at 50 knots, gives the data shown in [Tables 13.9 and 13.10](#).

Alternatively, the longitudinal and lateral-directional state equations may be assembled using matrix manipulation, and that procedure is illustrated in Examples 4.3 and 4.4.

Table 13.9 Longitudinal Concise Derivatives

x_u	-0.0257	z_u	-0.7550	m_u	0.0239
x_w	0.2936	z_w	-3.3764	m_w	-0.4093
x_q	0	z_q	24.442	m_q	-4.4344
x_θ	-9.8045	z_θ	0.325	m_θ	-0.0103
x_η	0	z_η	-6.0239	m_η	-20.351

Table 13.10 Lateral-Directional Concise Derivatives

y_v	-0.0144	l_v	-0.1101	n_v	0.0879
y_p	0	l_p	-12.864	n_p	-1.1899
y_r	-25.126	l_r	3.079	n_r	-0.52
y_ϕ	9.8045				
y_ψ	-0.3280				
y_ξ	0	l_ξ	-27.676	n_ξ	-0.4089
y_ζ	2.7246	l_ζ	0.5897	n_ζ	-2.2313

References

- Abbott, I. H., & von Doenhoff, A. E. (1959). *Theory of wing sections*. New York: Dover Publications.
- Babister, A. W. (1961). *Aircraft stability and control*. London: Pergamon Press.
- Babister, A. W. (1980). *Aircraft dynamic stability and response*. London: Pergamon Press.
- Coates, A. (1978). *Jane's world sailplanes and motor gliders*. London: Macdonald and Jane's.
- Ellison, N. (1971). *British gliders and aeroplanes 1922–1970*. London: A&C Black.
- ESDU Aerodynamics. London: ESDU International Ltd. (See especially Volume 9: *Stability of Aircraft*.)
- Hancock, G. J. (1995). *An introduction to the flight dynamics of rigid aeroplanes*. Ellis Horwood Ltd.
- Millman, A. F. (1971). *The design of a standard class sailplane*. Cranfield, Bedfordshire: MSc thesis, Department of Aircraft Design, Cranfield Institute of Technology.
- Taylor, J. W. R. (Ed.), (1965). *Jane's all the world's aircraft*. Great Missenden, Buckinghamshire: Sampson Low, Marston & Co.
- Torode, H. A. (1973). *A performance test survey of the aerodynamic development of the Slingsby T51 Dart sailplane*. Cranfield, Bedfordshire: Cranfield Institute of Technology, Cranfield Report Aero. No.16.

PROBLEMS

- 13.1** The centre of gravity of an aircraft is moved aft through a distance δh . Derive expressions relating the dimensionless longitudinal aerodynamic stability derivatives before and after the *cg* shift.
- For an aircraft in steady level flight, using the relevant reduced-order solution of the equations of motion, calculate the aft *cg* limit at which the phugoid mode becomes unstable.
 - The aircraft aerodynamic data, referred to wind axes, are as follows:
 $\text{Air density } \rho = 1.225 \text{ kg/m}^3$ Wing area $S = 24.15 \text{ m}^2$
 $\text{Velocity } V_0 = 560 \text{ kts}$ Mean chord $\bar{c} = 3.35 \text{ m}$
 $\text{Aircraft mass } m = 7930 \text{ kg}$ Tail moment arm $l_T = 4.57 \text{ m}$
 $\text{cg location } h = 0.25$ Pitch inertia $I_y = 35251 \text{ kg.m}^2$
 - The dimensionless stability derivatives are
 $X_u = -0.03 \quad Z_q = 0$
 $X_w = -0.02 \quad M_u = 0.01$
 $X_q = 0 \quad M_w = -0.15$
 $Z_u = -0.09 \quad M_{\dot{w}} = 0$
 $Z_w = -2.07 \quad M_q = -0.58$
 - Assume that the moment of inertia in pitch remains constant. (CU 1979)
- 13.2** Show that, to a good approximation, the following expressions hold for the dimensionless derivatives of a rigid aircraft in a glide with the engine off, $X_u \cong -2C_D$ and $Z_u \cong -2C_L$.
- With power on in level flight, the lift coefficient at the minimum power speed is given by

$$C_{L_{mp}} = \sqrt{3\pi Ae C_{D_0}}$$

and the minimum power speed is given by

$$V_{mp} = \sqrt{\frac{mg}{\rho S C_{L_{mp}}}}$$

- (b) Show that at the minimum power speed the thrust τ_{mp} and velocity V_{mp} satisfy the relation

$$\tau_{mp} V_{mp}^n = k$$

and find corresponding values for the constants k and n . Hence show that

$$X_u = -(n + 2)C_D$$

(CU 1982)

- 13.3** Do the following:

- (a) Explain the physical significance of the aerodynamic stability derivative.
- (b) Discuss the dependence of L_v and N_v on the general layout of an aircraft.
- (c) Show that for an unswept wing with dihedral angle Γ , the effect of sideslip angle β is to increase the incidence of the starboard wing by $\beta\Gamma$, where both β and Γ are small angles.
- (d) Show that fin contribution to N_v is given by

$$N_v = a_{1F} \bar{V}_F$$

(CU 1982)

- 13.4** The Navion light aircraft is a cantilevered low-wing monoplane. The unswept wing has a span of 10.59 m, a planform area of 17.12 m^2 , and dihedral angle 7.5° . The fin has a planform area of 0.64 m^2 and an aspect ratio of 3.0; its aerodynamic centre is 5.5 m aft of the cg .

- (a) Derive an expression for the dimensionless derivative N_v . Find its value for the Navion aircraft given that the lift curve slope a_1 of a lifting panel may be approximated by $a_0A/(A + 2)$, where a_0 is its two dimensional lift curve slope and A its aspect ratio.

(CU 1983)

- 13.5** Do the following:

- (a) Explain roll damping and what its main sources are on an aeroplane.
- (b) Assuming roll damping to be produced entirely by the wing of an aeroplane, show that the dimensionless roll damping stability derivative L_p is given by

$$L_p = -\frac{1}{2Ss^2} \int_0^s (a_y + C_{Dy}) c_y y^2 dy$$

- (c) The Navion light aeroplane has a straight tapered wing of span 33.4 ft, area 184 ft^2 , and root chord length 8 ft. At the given flight condition the wing drag coefficient is 0.02 and the lift curve slope is 4.44 per radian. Estimate a value for the dimensionless roll damping stability derivative L_p . Show all work and state any assumptions made.

(CU 1984)

- 13.6** Explain the physical significance of the aerodynamic stability derivatives M_u and M_w .
(a) The pitching moment coefficient for a wing is given by

$$C_m = \frac{k}{\gamma} \sin \alpha$$

and

$$\gamma = \sqrt{\left(1 - \frac{V^2}{a^2}\right)}$$

where k and a are constants. Obtain expressions for the wing contributions to M_u and M_w .
(CU 1985)

- 13.7** What is roll damping? Explain why the aerodynamic stability derivative L_p must always be negative.

- (a)** An aircraft of mass 5100 kg, aspect ratio 10, and wing span 16 m is in level flight at an equivalent airspeed of 150 kts when an aileron deflection of 5° results in a steady roll rate of $15^\circ/\text{s}$. The aileron aerodynamic characteristics are such that a 10° deflection produces a lift increment of 0.8, the aileron centres of pressure being at 6.5 m from the aircraft longitudinal axis. What is the value of L_p for this aircraft? Take $\rho = 1.225 \text{ kg/m}^3$ and $1 \text{ kt} = 0.515 \text{ m/s}$.

(CU 1985)

- 13.8** What is dihedral effect? Explain the effect of the dihedral angle of a wing on the dimensionless rolling moment due to sideslip derivative L_v .

- (a)** Show that, for a straight tapered wing of semi-span s , dihedral angle Γ , root chord c_r , and tip chord c_t ,

$$L_v = -\frac{\Gamma}{6} \frac{dC_L}{d\alpha} \left(\frac{c_r + 2c_t}{c_r + c_t} \right)$$

assuming the lift curve slope to be constant with span.

- (b)** Calculate the aileron angle required to maintain a steady forced wings-level sideslip angle of 5° given that the dimensionless rolling moment due to aileron control derivative has the value -0.197 per radian. It may be assumed that the rolling moment due to sideslip is entirely due to dihedral effect. The straight tapered wing of the aircraft has a mean chord of 2.4 m, a taper ratio of 1.8, and a dihedral angle of 4° . The lift curve slope of the wing may be assumed to have the constant value of 5.0 per radian.
(CU 1987)

- 13.9** What is the significance of roll damping to the flying and handling qualities of an aircraft?

- (a)** Derive from first principles an expression for the stability derivative L_p , and hence show that for an aircraft with a high-aspect-ratio rectangular wing the derivative is given approximately by

$$L_p = -\frac{1}{12} \left(C_D + \frac{dC_L}{d\alpha} \right)$$

State clearly the assumptions made in arriving at this result.

- (b) The Lockheed NT-33A aircraft has a straight tapered wing of span 11.5 m and is fitted with wing tip fuel tanks each of which has a capacity of 1045 litres. With one tank empty and the other full it is found that the minimum speed at which wings-level flight can be maintained is 168 kts with the maximum aileron deflection of 15° . When both wing tip tanks contain equal quantities of fuel an aileron deflection of 5° results in a steady rate of roll of $17^\circ/\text{s}$ at a velocity of 150 kts. What is the value of the derivative L_p ?

Assume an air density of 1.225 kg/m^3 , a fuel density of 0.8 kg/litre , a wing area of 22.23 m^2 , and that 1 knot is equivalent to 0.52 m/s .

(CU 1990)

- 13.10** Show that for a wing with sweepback Λ and dihedral Γ ,

$$L_v = -\frac{2}{Sb}(\alpha \sin \Lambda + \Gamma \cos \Lambda) \int_0^{s \sec \Lambda} \left(\frac{dC_L}{d\alpha} \right)_h c_h h dh$$

where h is the spanwise coordinate along the quarter-chord line. Assume the following for a chordwise element of the wing:

Chordwise velocity $V_c = V(\cos \Lambda + \beta \sin \Lambda)$

Velocity normal to wing $V_a = V(\alpha + \beta \Gamma)$

An aircraft has a wing with the following planform:

Sweep angle at quarter-chord = 55°

Dihedral angle = 3°

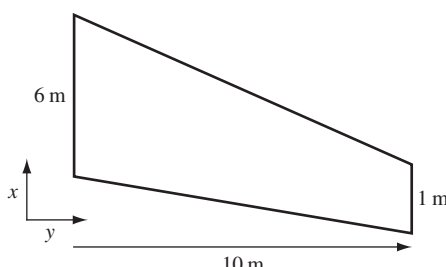
Lift curve slope $5.8/\text{rad}$ at $y = 0$

Lift curve slope $0/\text{rad}$ at $y = 10 \text{ m}$

Calculate the value of L_v when the aircraft is flying at an incidence of 2° .

(LU 2001)

- 13.11** A three-surface aeroplane has the following characteristics:



Foreplane

Span = 4.0 m

Area = 2 m^2

Lift curve slope = $3.2/\text{rad}$

Moment arm about cg = 5 m

Tailplane

Span = 5.0 m

Wing

Span = 12.5 m

Area = 25 m^2

Lift curve slope = $5.4/\text{rad}$

Aerodynamic centre = $0.2\bar{c}$

Complete aircraft

$cg = 0.4\bar{c}$

Area = 6.0 m

Lift curve slope = 3.5/rad

Moment arm about *cg* = 6.0 m

Tailplane efficiency $(1 - d\varepsilon/d\alpha) = 0.95$

When flying at a true airspeed of 100 m/s and an altitude where $\sigma = 0.7$, determine for the complete aircraft (i.e. all three surfaces) values for M_w and M_q . (LU 2002)

- 13.12** A tailless aircraft has the following characteristics:

Aerodynamic mean chord $\bar{c} = 3.0$ m

cg position $h = 0.15 \bar{c}$

Aerodynamic centre $h_0 = 0.30 \bar{c}$

Wing area $S = 24 \text{ m}^2$

Lift curve slope $a = 5.4/\text{rad}$

- (a) When the aircraft is flying at 200 m/s at sea level, calculate $\overset{\circ}{M}_w$ and $\overset{\circ}{M}_q$. Where appropriate, assume $\partial V/\partial U = 0$, $\partial \alpha/\partial U = 0$, $\partial V/\partial W = 0$, and $\partial \alpha/\partial W = 1/V$.
- (b) When the aircraft is in cruising flight with $C_L = 0.3$ and $C_{m_0} = 0.045$, determine a value for M_u . Assume that C_m is invariant with forward speed.

(LU 2004)

Flight in a Non-steady Atmosphere 14

14.1 The influence of atmospheric disturbances on flying qualities

All of the material in the previous chapters is based on the assumption of a quasi-steady atmosphere. However, in reality the atmosphere is anything but steady and it is frequently necessary to assess the likely impact of atmospheric disturbances on aircraft flying qualities. In general, flight in a non-steady atmosphere will make it more difficult for the pilot to carry out his mission task, leading to an increase in workload and consequent degradation in *level* of flying qualities. The perceived nature of this degradation will depend on the stability and control properties of the aircraft, the type of atmospheric disturbance, the disturbance intensity, and the way in which the disturbance excites the flight dynamics.

From a flying qualities perspective, atmospheric disturbances are treated as involuntary inputs to the aircraft that give rise to unwanted response. Clearly, the response dynamics depend totally on the dynamic properties of the airframe and the “shape” and intensity of the atmospheric disturbance. In every situation there exists a limit on the severity of the atmospheric disturbance that can be tolerated, and the degree of tolerance can, to an extent, be designed into an aircraft by tailoring its dynamic properties and by capitalising on the attenuating properties of a stability augmentation system. Today it is also common practice to incorporate explicit gust alleviation features into the flight control systems of advanced technology aeroplanes to alleviate structural loading in particular. Thus all aircraft design, flight control system design, and flight dynamics analysis which address the problems of flight in a non-steady atmosphere must have access to appropriate disturbance models, together with the essential tools and techniques for conducting flight dynamics assessment. The intention here is to set out a summary of the common models, tools, and techniques used in flight dynamics analysis.

Whenever the flying qualities of aircraft in the presence of atmospheric disturbances are under review, the specific flight dynamics concerns are

- Increase in pilot workload
- Degradation in flight path control
- Degradation in ride quality
- Influence on structural integrity
- Erosion of flight control system authority margins

It is therefore a requirement to evaluate aircraft and flight control system behaviour in representative non-steady atmospheric flight conditions. Comprehensive flying qualities requirements and their means of compliance are set out in detail in MIL-F-8785C (1980), MIL-STD-1797A (1987), and Def-Stan 00-970 (2011). Much of the following material is derived from these standards.

Table 14.1 Correlation between Level of Flying Qualities and Atmospheric Disturbance Intensity

Level of Flying Qualities	Atmospheric Disturbance Intensity			
	Light	Moderate	Severe	Extreme
1	Flying qualities adequate for mission	Flying qualities adequate for mission, but with increase in pilot workload and/or degradation in mission effectiveness	Flying qualities adequate for safe control, but with excessive pilot workload and/or inadequate mission effectiveness	Flying qualities sufficient to maintain control to fly out of disturbance
2	Flying qualities adequate for mission, but with increase in pilot workload and/or degradation in mission effectiveness	Flying qualities adequate for safe control, but with excessive pilot workload and/or inadequate mission effectiveness	Flying qualities sufficient to maintain control to fly out of disturbance	Flying qualities sufficient to recover control after upset
3	Flying qualities adequate for safe control, but with excessive pilot workload and/or inadequate mission effectiveness	Flying qualities sufficient to maintain control to fly out of disturbance	Flying qualities sufficient to recover control after upset	No requirement

A rationale for the formal flying qualities requirements is expressed in MIL-STD-1797A: “To provide a rational means for specifying the allowable degradation in flying qualities in the presence of increased intensities of atmospheric disturbances.” This may be interpreted as the means for *quantifying* the effects of flight in the presence of atmospheric disturbances in terms of the apparent degradation in *Level* of flying qualities.

The key parameter in any consideration of flight in the presence of atmospheric disturbances is the disturbance intensity, and four descriptors are universally used: *light*, *moderate*, *severe*, and *extreme*. All of the requirements documents provide a definition of *atmospheric disturbance intensity* and its correlation with *Level* of flying qualities. A useful definition is given by Hoh et al. (1982), which provides the basis for the definitions given in MIL-STD-1797A (see Table 14.1).

14.2 Methods of evaluation

Two methods are used for the evaluation of aircraft response to atmospheric disturbance in the engineering domain. By far the most common method involves the use of continuous simulation models, where the disturbance velocity components are generated synthetically by, for example, filtering white noise and summing the resulting turbulent air velocities with the aircraft velocity components. This modifies the aircraft’s velocity, angle of attack, and angle of sideslip, changing the forces and moments acting on the aircraft and thus producing output response time histories which are then evaluated visually, or by suitable signal processing software or by pilot opinion rating in the piloted flight simulator context. Alternatively, for formal analytical evaluation, frequency

response methods are used to assess, for example, the magnitude and *root mean square* (rms) intensity of the motion variables of interest. Again, the disturbances are modelled in the frequency domain by filtering white noise using transfer functions. In most cases, assessment is concerned with the intensity of acceleration response to atmospheric disturbances, as this has significance for aircraft handling, for structural loading, and for passenger ride comfort.

In all evaluation methods it is important that the atmospheric disturbance models be sufficiently simple to allow meaningful simulation or analysis. To this end it is helpful if the parameters used to describe the atmosphere models have some relationship, or relevance, to the interpretation of aircraft dynamics and flying qualities. In other words, in the formulation of complex atmospheric disturbance models it is necessary to achieve a balance between engineering convenience and physical correctness. Thus, as in many things aeronautical, a compromise is the outcome.

14.3 Atmospheric disturbances

All atmospheric disturbances are defined by their *temporal* characteristics, *spatial* characteristics, and energy content or *intensity*. The apparent magnitude of those characteristics is also dependent on the size and shape of the aircraft, the speed at which it encounters the disturbances, and the altitude. Clearly, an adequate description for mathematical modelling is difficult to quantify, and it becomes necessary to simplify the descriptions to representative but manageable definitions. The four most commonly used models of atmospheric disturbances are *steady wind*, *wind shear*, *discrete gusts*, and *continuous turbulence*, all of which are realistic atmospheric features which tend to occur in combination during flight, depending on local conditions. A summary of each of these, as found in the flying qualities requirements documents, is contained in the following paragraphs.

14.3.1 Steady wind

A steady wind is continuous and assumed to act parallel to the surface of the earth; the principal cases of interest are head wind, tail wind, and crosswind during take-off and landing. Steady wind effects can be balanced out by thrust and the aircraft's flying control surfaces and thus do not normally define a flying qualities problem with the exception of a crosswind. In particular, a crosswind constitutes a potential hazard during take-off and landing when it acts across the runway, and an increasingly strong crosswind requires increasing amounts of rudder and aileron deflection to balance the wind-induced moments. Hence, all aircraft have limits for operation in the presence of crosswind and, for the purposes of flying qualities analysis, typical requirements are given in [Table 14.2](#).

Table 14.2 Crosswind Intensity

Intensity	Reference Value (knots)
Light	0–10
Moderate	11–30
Severe	31–45

14.3.2 Wind shear

Wind shear is defined as a time rate of change in wind speed and direction lasting for 10 seconds or more, the assumption being that shears of less than 10 seconds are unlikely to constitute a flying qualities hazard. See, for example [Hoh et al. \(1982\)](#), which includes a useful discussion of wind shear in the context of flying qualities requirements.

As for steady wind, wind shear presents a problem during take-off and landing and, when encountered, the aircraft will rise or sink according to the relative direction and magnitude of the wind velocity gradient. Since the effect of wind shear on the aircraft is to cause an upset in normal acceleration, the requirements quantify the wind shear limits in terms of acceleration response as given in [Table 14.3](#), where subscript γ_{\max} is the maximum power climb angle and subscript γ_{\min} is the flight idle glide angle.

Table 14.3 Wind Shear Intensity

Wind Shear	Reference Normal Acceleration
Decreasing headwind	$g_{\gamma_{\max}} \leq 1.0 \text{ m/s}^2 (3.4 \text{ ft/s}^2)$
Decreasing tailwind	$g_{\gamma_{\min}} \leq 0.5 \text{ m/s}^2 (1.7 \text{ ft/s}^2)$

14.3.3 Discrete gusts

A discrete gust is a single disturbance event and is usually assumed to be embedded in continuous turbulence. Gusts occur randomly, and their magnitude and duration are usually correlated with the properties of continuous turbulence. Therefore, their definition derives from the definition of continuous turbulence.

14.3.4 Continuous turbulence

Continuous turbulence comprises random disturbances that are observed to occur in *patches* of varying *scale* and *intensity*. Most aeronautical engineers agree on what turbulence is, but agreement on how to describe and quantify turbulence models for use in flying qualities analysis is rather more subjective, and opinions differ.

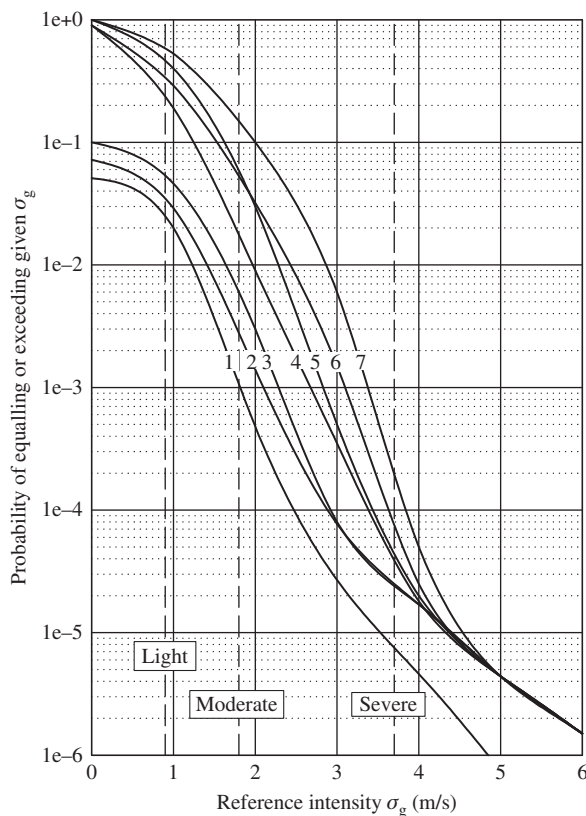
The scale of continuous turbulence is generally determined by the overall magnitude of its effect on aircraft response. Not surprisingly, the scale is defined by the size of the patch of turbulence and by the velocity of the aircraft as it traverses the patch. When the scale is large and the application is concerned with flying and handling qualities analysis, the effects are assumed to act uniformly over the whole airframe. This is interpreted to mean that the disturbance velocities may be taken to act at, or about, the *cg* of the aircraft. This is the simplest interpretation and is certainly the easiest to model. However, when the scale is small it is more appropriate that the disturbances should be variously distributed over the airframe, and this poses an altogether more difficult problem. See, for example, the paper by [Thomasson \(2000\)](#) in which the equations of motion for a vehicle subject to distributed fluid disturbances are developed.

Turbulence intensity quantifies the energy content of the disturbance and is usually defined in terms of the rms value σ_g over the turbulence frequency spectrum. Since turbulence is modelled as

Table 14.4 Gust and Turbulence Intensity

Intensity	Reference rms Velocity σ_g (m/s)
Light	0.9 (3 ft/s)
Moderate	1.8 (6 ft/s)
Severe	3.7 (12 ft/s)
Extreme	7.3 (24 ft/s)

a velocity disturbance, it is reduced to three linear velocity components and three angular velocity components. The velocity components are known to be correlated to an extent, but since the degree of correlation is not fully understood it is usual practice to assume that the velocity components are uncorrelated. The principal component is regarded as the rms horizontal “gust” velocity, and this is used to quantify the turbulence intensity and from which of all velocity components are derived. Typical rms gust and turbulence intensity is defined in **Table 14.4**.

**FIGURE 14.1** Probability of equalling or exceeding a given turbulence reference intensity at specific altitudes.

Broadly, altitude influences the scale of the turbulence and the probability of encountering atmospheric disturbances of a given intensity. At low altitude, where terrain has a significant effect, encounters with disturbances are more frequent; also, the scale of the turbulence is smaller and it includes earth boundary layer effects. At high altitude, encounters with disturbances are less frequent, the scale of turbulence is larger, there is greater homogeneity within patches, and it includes clear air turbulence effects.

The probability of encountering turbulence of a given intensity has been the subject of much research and debate. The American model is similar in general, but differs from the UK model in detail. The reasons for the differences arise because the models are empirical and derived from independent experimental flight research. For example, a substantial programme of flight experiments was undertaken in the United Kingdom in the 1960s and 1970s by the Royal Aircraft Establishment and resulted in the description of what is believed to be a more representative empirical turbulence model. Reference to this work may be found in [Jones \(1973\)](#), and the model provides the basis for the requirements in Def-Stan 00-970. Opinions among experts differ, of course, but most importantly the flying qualities requirements in Def-Stan 00-970 and in MIL-F-8785C share a high degree of numerical conformity. The gust and turbulence intensity model given in Def-Stan 00-970 is reproduced as [Fig. 14.1](#), and the *light*, *moderate*, and *severe* turbulence boundaries are superimposed as indicated. The plots shown in [Fig. 14.1](#) are altitude-dependent, as shown in [Table 14.5](#).

Below an altitude of 75 m, the turbulence reference intensity is taken as constant and may be defined by the values given in [Table 14.4](#). Note in [Fig. 14.1](#) that a step in the high-altitude plots (1–3) occurs at $\sigma_g = 0$; the explanation for this phenomenon is based on the assumption of “*a finite probability of conditions existing with zero turbulence reference intensity*”.

Table 14.5 Gust and Turbulence Altitude Dependency

Plot	Altitude	
1	15,000 m (50,000 ft)	
2	9,000 m (30,000 ft)	
3	3,000 m (10,000 ft)	
4	300 m (1000 ft)	Above flat terrain
5	300 m (1000 ft)	Above hilly terrain
6	$\leq 75 \text{ m } (\leq 250 \text{ ft})$	Above flat terrain
7	$\leq 75 \text{ m } (\leq 250 \text{ ft})$	Above hilly terrain

14.4 Extension of the linear aircraft equations of motion

Atmospheric disturbances are represented by and introduced into the aircraft equations of motion as linear and angular velocity components. Since it is usual to assume that the aircraft is in straight and level flight when it encounters a horizontal patch of turbulence, the disturbance velocity components are referred to the earth axes reference frame. When applying the disturbance velocity components to the equations of motion, it is common practice to refer them directly to aircraft

body axes, without transformation, on the basis that the disturbances are small enough to be regarded as small perturbations and that in level flight the aircraft attitudes are also small angles. However, when evaluating aircraft response to gusts and turbulence at low altitude, below ~ 50 m, it is considered good practice to transform the disturbance velocity components into aircraft axes. The forces and moments due to atmospheric disturbances are introduced to the equations of motion in the manner described in the development of equations (4.20). Since atmospheric disturbances are quantified as velocity disturbances, their effect on the aircraft is determined by the aerodynamic response to linear and angular velocity perturbations and, for linear small-perturbation models, enter the equations of motion via the aerodynamic stability derivatives.

Considering rigid body aircraft response to gusts and turbulence only—that is, when structural modes responses are considered insignificant and omitted from the analysis—the effect on the aircraft is assumed to comprise uniform immersion in the disturbance field and exposure to the linear gradients of the disturbance velocity components as the aircraft traverses the field. Thus the uniform immersion in the gust and turbulence field leads to the assumption that the velocity components u_g , v_g , and w_g act at the aircraft cg and that positive velocity disturbances act along the aircraft reference axes in the positive sense. The total impact of each of the gust velocity components on the aircraft is modelled with a Taylor series expansion comprising the linear term acting at the cg and a series of linear velocity gradient terms. All except the first derivative terms are assumed to be negligible and are omitted from the model. The remaining linear gradients of the disturbance velocity components with distance, as the aircraft traverses the patch of turbulence, give rise to angular velocity response, p_g , q_g , and r_g about the aircraft axes. As before, assume that the aircraft is in steady level flight when it traverses the horizontal patch of turbulence and that the disturbance perturbations are small. Thus, at coordinates $(x, y, 0)$ referred to aircraft body axes, the components of angular velocity due to the linear velocity components acting at the cg are given approximately by

$$p_g = -\frac{\partial w_g}{\partial y} \quad q_g = \frac{\partial w_g}{\partial x} \quad r_g = -\frac{\partial v_g}{\partial x} \quad (14.1)$$

Now,

$$q_g = \frac{\partial w_g}{\partial x} = -\frac{\partial w_g}{\partial t} \frac{\partial t}{\partial x} = -\dot{w}_g \frac{1}{U_e} \quad (14.2)$$

Whence, approximately,

$$\dot{w}_g = -q_g U_e \quad (14.3)$$

14.4.1 Disturbed body incidence and sideslip

Normal gusts and lateral gusts give rise to disturbances in body incidence and sideslip, respectively. These disturbances can be evaluated by means of a simple analysis of the disturbed flow geometry, and knowledge of the estimated values of incidence α_g and sideslip β_g , due to gusts, enables direct estimates of the forces and moments acting on the aircraft in response to atmospheric disturbances. Clearly, this has benefits for estimation of the impact of atmospheric disturbances on the performance, stability, control, and flying qualities of an aircraft without first having to set up and solve the equations of motion.

In steady level flight in an undisturbed atmosphere, the total velocity of the aircraft is given by

$$V_0 = \sqrt{U_e^2 + V_e^2 + W_e^2} \quad (14.4)$$

and in straight flight the steady lateral component of velocity $V_e = 0$. With reference to Section 2.4.1, it is easily shown that steady body incidence and steady sideslip angles are given by

$$\alpha_e = \tan^{-1} \frac{W_e}{U_e} \quad \beta_e = \sin^{-1} \frac{V_e}{V_0} \quad (14.5)$$

In disturbed flight, let the gust velocity components be (u_g, v_g, w_g) ; then equations (14.4) and (14.5) become

$$\begin{aligned} V &= \sqrt{(U_e + u_g)^2 + (V_e + v_g)^2 + (W_e + w_g)^2} \\ \alpha &= \tan^{-1} \left(\frac{W_e + w_g}{U_e + u_g} \right) \\ \beta &= \sin^{-1} \left(\frac{V_e + v_g}{V} \right) \end{aligned} \quad (14.6)$$

Equations (14.6) may be simplified by treating the gust velocity components as small perturbations about steady flight, such that the usual approximations may be applied. Thus

$$U_e \gg u_g \quad U_e \cong V_0 \quad V \cong V_0$$

and

$$\begin{aligned} \alpha &= \alpha_e + \alpha_g \cong \tan^{-1} \left(\frac{W_e + w_g}{V_0} \right) \cong \frac{W_e + w_g}{V_0} = \frac{W_e}{V_0} + \frac{w_g}{V_0} \\ \beta &= \beta_e + \beta_g \cong \sin^{-1} \left(\frac{V_e + v_g}{V_0} \right) \cong \frac{V_e + v_g}{V_0} = \frac{V_e}{V_0} + \frac{v_g}{V_0} \end{aligned} \quad (14.7)$$

It is therefore seen from equations (14.7) that

$$\alpha_g \cong \frac{w_g}{V_0} \quad \text{and} \quad \beta_g \cong \frac{v_g}{V_0} \quad (14.8)$$

14.4.2 The longitudinal equations of motion

The development of the longitudinal equations of motion (4.40), which for the most general case are referred to aircraft body axes, may be written to include the gust and turbulence velocity components. It is important to recognise that the aerodynamic contributions to the equations of motion are determined with respect to the disturbed air mass, and, in accordance with the notation, the dimensional equations (4.40) may be expanded to

$$\begin{aligned}
 m\ddot{u} - \dot{X}_u(u - u_g) - \dot{X}_{\dot{w}}(\dot{w} - \dot{w}_g) - \dot{X}_w(w - w_g) - \dot{X}_q(q - q_g) + mW_e q + mg \cos\theta_e &= \dot{X}_\eta \eta + \dot{X}_\tau \tau \\
 -\dot{Z}_u(u - u_g) + m\dot{w} - \dot{Z}_{\dot{w}}(\dot{w} - \dot{w}_g) - \dot{Z}_w(w - w_g) - \dot{Z}_q(q - q_g) - mU_e q + mg \sin\theta_e &= \dot{Z}_\eta \eta + \dot{Z}_\tau \tau \\
 -\dot{M}_u(u - u_g) - \dot{M}_{\dot{w}}(\dot{w} - \dot{w}_g) - \dot{M}_w(w - w_g) + I_y \dot{q} - \dot{M}_q(q - q_g) &= \dot{M}_\eta \eta + \dot{M}_\tau \tau
 \end{aligned} \tag{14.9}$$

Making the substitution for \dot{w}_g from equation (14.3), equations (14.9) may be rearranged in state-space form:

$$\begin{aligned}
 \begin{bmatrix} m & -\dot{X}_{\dot{w}} & 0 & 0 \\ 0 & m - \dot{Z}_{\dot{w}} & 0 & 0 \\ 0 & -\dot{M}_{\dot{w}} & I_y & 0 \\ 0 & 0 & 0 & 1 \end{bmatrix} \begin{bmatrix} \dot{u} \\ \dot{w} \\ \dot{q} \\ \dot{\theta} \end{bmatrix} &= \begin{bmatrix} \dot{X}_u & \dot{X}_w & \dot{X}_q - mW_e & -mg\cos\theta_e \\ \dot{Z}_u & \dot{Z}_w & \dot{Z}_q + mU_e & -mg\sin\theta_e \\ \dot{M}_u & \dot{M}_w & \dot{M}_q & 0 \\ 0 & 0 & 1 & 0 \end{bmatrix} \begin{bmatrix} u \\ w \\ q \\ \theta \end{bmatrix} \\
 &+ \begin{bmatrix} \dot{X}_\eta & \dot{X}_\tau \\ \dot{Z}_\eta & \dot{Z}_\tau \\ \dot{M}_\eta & \dot{M}_\tau \\ 0 & 0 \end{bmatrix} \begin{bmatrix} \eta \\ \tau \end{bmatrix} + \begin{bmatrix} -\dot{X}_u & -\dot{X}_w & -\dot{X}_q + \dot{X}_{\dot{w}} U_e \\ -\dot{Z}_u & -\dot{Z}_w & -\dot{Z}_q + \dot{Z}_{\dot{w}} U_e \\ -\dot{M}_u & -\dot{M}_w & -\dot{M}_q + \dot{M}_{\dot{w}} U_e \\ 0 & 0 & 0 \end{bmatrix} \begin{bmatrix} u_g \\ w_g \\ q_g \end{bmatrix}
 \end{aligned} \tag{14.10}$$

or

$$\mathbf{M}\dot{\mathbf{x}} = \mathbf{A}'\mathbf{x} + \mathbf{B}'\mathbf{u} + \mathbf{E}'\mathbf{u}_g \tag{14.11}$$

where it is seen that the disturbance terms simply appear as additional inputs to the equations through the gust input matrix \mathbf{E}' and the gust velocity vector \mathbf{u}_g . Alternatively, the equations of motion may be written in concise state-space form by multiplying equations (14.10) by the inverse of the mass matrix \mathbf{M} , with reference to the definitions of the concise derivatives given in Table A2.5 in Appendix 2, to give

$$\begin{aligned}
 \begin{bmatrix} \dot{u} \\ \dot{w} \\ \dot{q} \\ \dot{\theta} \end{bmatrix} &= \begin{bmatrix} x_u & x_w & x_q & x_\theta \\ z_u & z_w & z_q & z_\theta \\ m_u & m_w & m_q & m_\theta \\ 0 & 0 & 1 & 0 \end{bmatrix} \begin{bmatrix} u \\ w \\ q \\ \theta \end{bmatrix} + \begin{bmatrix} x_\eta & x_\tau \\ x_\eta & x_\tau \\ x_\eta & x_\tau \\ 0 & 0 \end{bmatrix} \begin{bmatrix} \eta \\ \tau \end{bmatrix} + \begin{bmatrix} -x_u & -x_w & -x_q - W_e + \frac{2\dot{X}_{\dot{w}} U_e}{(m - \dot{Z}_{\dot{w}})} \\ -z_u & -z_w & -z_q + \frac{U_e(m + \dot{Z}_{\dot{w}})}{(m - \dot{Z}_{\dot{w}})} \\ -m_u & -m_w & -m_q + \frac{2m\dot{M}_{\dot{w}} U_e}{I_y(m - \dot{Z}_{\dot{w}})} \\ 0 & 0 & 0 \end{bmatrix} \begin{bmatrix} u_g \\ w_g \\ q_g \end{bmatrix}
 \end{aligned} \tag{14.12}$$

or

$$\dot{\mathbf{x}} = \mathbf{Ax} + \mathbf{Bu} + \mathbf{Eu}_g \tag{14.13}$$

With controls \mathbf{u} fixed, equation (14.12) simplifies to

$$\begin{bmatrix} \dot{u} \\ \dot{w} \\ \dot{q} \\ \dot{\theta} \end{bmatrix} = \begin{bmatrix} x_u & x_w & x_q & x_\theta \\ z_u & z_w & z_q & z_\theta \\ m_u & m_w & m_q & z_\theta \\ 0 & 0 & 1 & 0 \end{bmatrix} \begin{bmatrix} u \\ w \\ q \\ \theta \end{bmatrix} + \left[\begin{array}{c|c|c} -x_u & -x_w & -x_q - W_e + \frac{2\dot{X}_w U_e}{(m - \dot{Z}_w)} \\ \hline -z_u & -z_w & -z_q + \frac{U_e(m + \dot{Z}_w)}{(m - \dot{Z}_w)} \\ \hline -m_u & -m_w & -m_q + \frac{2m\dot{M}_w U_e}{I_y(m - \dot{Z}_w)} \\ \hline 0 & 0 & 0 \end{array} \right] \begin{bmatrix} u_g \\ w_g \\ q_g \end{bmatrix} \quad (14.14)$$

or, equivalently,

$$\dot{\mathbf{x}} = \mathbf{Ax} + \mathbf{Eu}_g \quad (14.15)$$

and equation (14.15) may be solved in the usual way to obtain the aircraft longitudinal gust response transfer functions.

14.4.3 The lateral-directional equations of motion

In a similar way, the dimensional lateral-directional equations of motion (4.45) for the most general case are also referred to aircraft body axes and may be written to include the gust and turbulence velocity components. Again, it is important to recognise that the aerodynamic contributions to the equations of motion are determined with respect to the disturbed air mass, and, in accordance with the notation, equations (4.45) may be written as

$$\begin{aligned} m\ddot{v} - \ddot{Y}_v(v - v_g) - \ddot{Y}_p(p - p_g) + mW_e p - \ddot{Y}_r(r - r_g) - mU_e r - mg\phi\cos\theta_e - mg\psi\sin\theta_e &= \ddot{Y}_\xi\xi + \ddot{Y}_\zeta\zeta \\ -\ddot{L}_v(v - v_g) + I_x\dot{p} - \ddot{L}_p(p - p_g) - I_{xz}\dot{r} - \ddot{L}_r(r - r_g) &= \ddot{L}_\xi\xi + \ddot{L}_\zeta\zeta \\ -N_v(v - v_g) - I_{xz}\dot{p} - N_p(p - p_g) + I_z\dot{r} - N_r(r - r_g) &= \ddot{N}_\xi\xi + \ddot{N}_\zeta\zeta \end{aligned} \quad (14.16)$$

With reference to Table A2.7 in Appendix 2, and after some rearrangement, equations (14.16) may be written in concise state-space form as follows:

$$\begin{bmatrix} \dot{v} \\ \dot{p} \\ \dot{r} \\ \dot{\phi} \\ \dot{\psi} \end{bmatrix} = \begin{bmatrix} y_v & y_p & y_r & y_\phi & y_\psi \\ l_v & l_p & l_r & l_\phi & l_\psi \\ n_v & n_p & n_r & n_\phi & n_\psi \\ 0 & 1 & 0 & 0 & 0 \\ 0 & 0 & 1 & 0 & 0 \end{bmatrix} \begin{bmatrix} v \\ p \\ r \\ \phi \\ \psi \end{bmatrix} + \begin{bmatrix} y_\xi & y_\zeta \\ l_\xi & l_\zeta \\ n_\xi & n_\zeta \\ 0 & 0 \\ 0 & 0 \end{bmatrix} \begin{bmatrix} \xi \\ \zeta \end{bmatrix} + \begin{bmatrix} -y_v & -y_p + W_e & -y_r - U_e \\ -l_v & -l_p & -l_r \\ -n_v & -n_p & -n_r \\ 0 & 0 & 0 \\ 0 & 0 & 0 \end{bmatrix} \begin{bmatrix} v_g \\ p_g \\ r_g \end{bmatrix} \quad (14.17)$$

With controls \mathbf{u} fixed, [equations \(14.17\)](#) simplify to

$$\begin{bmatrix} \dot{v} \\ \dot{p} \\ \dot{r} \\ \dot{\phi} \\ \dot{\psi} \end{bmatrix} = \begin{bmatrix} y_v & y_p & y_r & y_\phi & y_\psi \\ l_v & l_p & l_r & l_\phi & l_\psi \\ n_v & n_p & n_r & n_\phi & n_\psi \\ 0 & 1 & 0 & 0 & 0 \\ 0 & 0 & 1 & 0 & 0 \end{bmatrix} \begin{bmatrix} v \\ p \\ r \\ \phi \\ \psi \end{bmatrix} + \begin{bmatrix} -y_v & -y_p + W_e & -y_r - U_e \\ -l_v & -l_p & -l_r \\ -n_v & -n_p & -n_r \\ 0 & 0 & 0 \\ 0 & 0 & 0 \end{bmatrix} \begin{bmatrix} v_g \\ p_g \\ r_g \end{bmatrix} \quad (14.18)$$

14.4.4 The equations of motion for aircraft with stability augmentation

The equations of motion given above represent those of the basic unaugmented aircraft, and for both the longitudinal and lateral-directional equations of motion the generic state-space description is given by [equation \(14.13\)](#):

$$\dot{\mathbf{x}} = \mathbf{Ax} + \mathbf{Bu} + \mathbf{Eu}_g$$

All advanced technology aircraft incorporate stability and control augmentation and a typical control law (see for example Section 11.7) would take the form

$$\mathbf{u} = \mathbf{v} - \mathbf{Kx} \quad (14.19)$$

where \mathbf{v} is a vector of input control command variables. Whence, the closed-loop equations of motion are given by substituting [equation \(14.19\)](#) into [equation \(14.13\)](#) to give

$$\dot{\mathbf{x}} = [\mathbf{A} - \mathbf{BK}]\mathbf{x} + \mathbf{Bv} + \mathbf{Eu}_g \quad (14.20)$$

The output equation corresponding with the state [equation \(14.20\)](#) takes the general form

$$\mathbf{y} = \mathbf{Cx} + \mathbf{Dv} + \mathbf{Fu}_g \quad (14.21)$$

where the matrices \mathbf{C} , \mathbf{D} , and \mathbf{F} are specified to give the desired vector of output variables \mathbf{y} .

Clearly, the closed-loop aircraft gust response transfer functions, with controls \mathbf{v} fixed, may be obtained by solving the following state and output equations in the usual way:

$$\begin{aligned} \dot{\mathbf{x}} &= [\mathbf{A} - \mathbf{BK}]\mathbf{x} + \mathbf{Eu}_g \\ \mathbf{y} &= \mathbf{Cx} + \mathbf{Fu}_g \end{aligned} \quad (14.22)$$

In any analysis of aircraft response to atmospheric disturbances, in addition to observing the perturbations in the motion variables it is also of particular relevance to observe the height h response, acceleration responses a_x , a_y , and a_z measured at the cg , and normal load factor n_z response, also measured at the cg . Accordingly, it is good practice to augment [equations \(14.22\)](#) to include those variables using the methods described in Chapter 5.

EXAMPLE 14.1

Stability and control data for the Douglas DC-8 transport aeroplane are given by [Teper \(1969\)](#), and the flight condition describing the aircraft flying a holding pattern at an altitude of 15,000 ft is chosen to illustrate the procedure for obtaining the gust response transfer functions. It is convenient that the equations of motion are referred to wind, or stability, axes, thereby simplifying

the mathematical procedure. Flight condition data are given in [Table 14.6](#), and longitudinal derivative data are given in [Table 14.7](#) in American normalised form, the notation for which is described in Section 4.4.3.

A number of stability derivatives are sufficiently small that they are assumed to be zero—namely, $X_{\dot{w}} = Z_{\dot{w}} = X_q = Z_q \cong 0$. In accordance with the usual American notation, the velocity-dependent stability derivatives, X_u , Z_u , and M_u , represent aerodynamic effects only whereas the derivatives X_u^* , Z_u^* , and M_u^* represent the aerodynamic effects plus the effects of thrust dependency on velocity perturbations. The latter derivatives are used in the equations of motion when the engine and thrust models are not included explicitly. However, if it is known, or assumed, that atmospheric disturbances do not affect thrust, the velocity-dependent derivatives representing aerodynamic effects only, X_u , Z_u , and M_u , should be used when incorporating the gust and turbulence velocity components into the equations of motion.

The longitudinal normalised equations of motion as given, referred to wind axes and omitting zero terms, may be written as

$$\begin{aligned} \dot{u} - X_u u - X_w w + g\theta &= X_{\delta_s} \delta_s \\ -Z_u u + \dot{w} - Z_w w - V_0 q &= Z_{\delta_s} \delta_s \\ -M_u u - M_{\dot{w}} \dot{w} - M_w w + \dot{q} + M_q q &= M_{\delta_s} \delta_s \\ \dot{\theta} &= q \end{aligned} \quad (14.23)$$

Table 14.6 Douglas DC-8 Flight Condition Data

Altitude	h	15,000 ft
Mach number	M_0	0.443
Velocity	V_0	468.2 ft/s
Mass	m	5900 slugs
Moment of inertia in pitch	I_y	2,940,000 slugft ²
Trim pitch attitude	θ_e	0 deg
Gravitational constant	g	32.2 ft/s ²

Table 14.7 Normalised Stability and Control Derivatives

X_u	-0.00707 1/s	Z_{δ_s}	-23.7 ft/s ² /rad
X_u^*	-0.00714 1/s	M_u	-0.000063 1/fts
X_w	0.0321 1/s	M_u^*	-0.000063 1/fts
X_{δ_s}	0 ft/s ² /rad	M_w	-0.0107 1/fts
Z_u	-0.1329 1/s	$M_{\dot{w}}$	-0.00072 1/ft
Z_u^*	-0.1329 1/s	M_q	-0.991 1/s
Z_w	-0.756 1/s	M_{δ_s}	-3.24 1/s ²

The height and normal acceleration auxiliary equations are as follows, where in both equations w is the normal perturbation component of aircraft inertial velocity:

$$\begin{aligned}\dot{h} &= -w + V_0 \theta \\ a_z &= \dot{w} - V_0 q\end{aligned}\quad (14.24)$$

In the manner of equations (14.10), equations (14.23) may be developed to include the gust velocity components, the substitution for \dot{w}_g from equation (14.3) may be made, the height equation (14.24) may be incorporated for completeness, and the whole arranged in state form to give

$$\begin{bmatrix} 1 & 0 & 0 & 0 & 0 \\ 0 & 1 & 0 & 0 & 0 \\ 0 & -M_{\dot{w}} & 1 & 0 & 0 \\ 0 & 0 & 0 & 1 & 0 \\ 0 & 0 & 0 & 0 & 1 \end{bmatrix} \begin{bmatrix} \dot{u} \\ \dot{w} \\ \dot{q} \\ \dot{\theta} \\ \dot{h} \end{bmatrix} = \begin{bmatrix} X_u^* & X_w & 0 & -g & 0 \\ Z_u^* & Z_w & V_0 & 0 & 0 \\ M_u^* & M_w & M_q & 0 & 0 \\ 0 & 0 & 1 & 0 & 0 \\ 0 & -1 & 0 & V_0 & 0 \end{bmatrix} \begin{bmatrix} u \\ w \\ q \\ \theta \\ h \end{bmatrix} + \begin{bmatrix} X_{\delta_s} \\ Z_{\delta_s} \\ M_{\delta_s} \\ 0 \\ 0 \end{bmatrix} \delta_s \quad (14.25)$$

$$+ \begin{bmatrix} -X_u & -X_w & 0 \\ -Z_u & -Z_w & 0 \\ -M_u & -M_w & -M_q + M_{\dot{w}} V_0 \\ 0 & 0 & 0 \\ 0 & 0 & 0 \end{bmatrix} \begin{bmatrix} u_g \\ w_g \\ q_g \end{bmatrix}$$

Substituting numerical values from Tables 14.6 and 14.7 into equations (14.25) and multiplying by the inverse of the mass matrix \mathbf{M} reduces the equations to the standard concise form:

$$\begin{bmatrix} \dot{u} \\ \dot{w} \\ \dot{q} \\ \dot{\theta} \\ \dot{h} \end{bmatrix} = \begin{bmatrix} -7.14e-3 & 0.0321 & 0 & -32.2 & 0 \\ -0.1329 & -0.756 & 468.2 & 0 & 0 \\ 3.2688e-5 & -0.01016 & -1.3281 & 0 & 0 \\ 0 & 0 & 1 & 0 & 0 \\ 0 & -1 & 0 & 468.2 & 0 \end{bmatrix} \begin{bmatrix} u \\ w \\ q \\ \theta \\ h \end{bmatrix} + \begin{bmatrix} 0 \\ -23.7 \\ -3.22294 \\ 0 \\ 0 \end{bmatrix} \delta_s \quad (14.26)$$

$$+ \begin{bmatrix} 7.07e-3 & -0.0321 & 0 \\ 0.1329 & 0.756 & 0 \\ -3.2688e-5 & 0.01016 & 0.65896 \\ 0 & 0 & 0 \\ 0 & 0 & 0 \end{bmatrix} \begin{bmatrix} u_g \\ w_g \\ q_g \end{bmatrix}$$

The aircraft state equation relating response to gust and turbulence input disturbances is given by equation (14.15):

$$\dot{\mathbf{x}} = \mathbf{A}\mathbf{x} + \mathbf{E}\mathbf{u}_g$$

From [equation \(14.26\)](#), assuming controls-fixed, this may be written directly:

$$\begin{bmatrix} \dot{u} \\ \dot{w} \\ \dot{q} \\ \dot{\theta} \\ \dot{h} \end{bmatrix} = \begin{bmatrix} -7.14e-3 & 0.0321 & 0 & -32.2 & 0 \\ -0.1329 & -0.756 & 468.2 & 0 & 0 \\ 3.2688e-5 & -0.01016 & -1.3281 & 0 & 0 \\ 0 & 0 & 1 & 0 & 0 \\ 0 & -1 & 0 & 468.2 & 0 \end{bmatrix} \begin{bmatrix} u \\ w \\ q \\ \theta \\ h \end{bmatrix} + \begin{bmatrix} 7.07e-3 & -0.0321 & 0 \\ 0.1329 & 0.756 & 0 \\ -3.2688e-5 & 0.01016 & 0.65896 \\ 0 & 0 & 0 \\ 0 & 0 & 0 \end{bmatrix} \begin{bmatrix} u_g \\ w_g \\ q_g \end{bmatrix} \quad (14.27)$$

The corresponding output equation is

$$\mathbf{y} = \mathbf{Cx} + \mathbf{Fu}_g \quad (14.28)$$

It is useful to augment the output vector \mathbf{y} to include normal acceleration a_z and normal load factor $n_z = -a_z/g$, as these are response variables of interest in the analysis of aircraft response to gusts and turbulence. The definition of a_z is given in [equations \(14.24\)](#), and the numerical description of \dot{w} may be obtained from the second row of [equations \(14.27\)](#). In this way, the output [equation \(14.28\)](#) may be assembled:

$$\begin{bmatrix} u \\ w \\ q \\ \theta \\ h \\ a_z \\ n_z \end{bmatrix} = \begin{bmatrix} 1 & 0 & 0 & 0 & 0 \\ 0 & 1 & 0 & 0 & 0 \\ 0 & 0 & 1 & 0 & 0 \\ 0 & 0 & 0 & 1 & 0 \\ 0 & 0 & 0 & 0 & 1 \\ -0.1329 & -0.756 & 0 & 0 & 0 \\ 4.12733e-3 & 0.023473 & 0 & 0 & 0 \end{bmatrix} \begin{bmatrix} u \\ w \\ q \\ \theta \\ h \end{bmatrix} + \begin{bmatrix} 0 & 0 & 0 \\ 0 & 0 & 0 \\ 0 & 0 & 0 \\ 0 & 0 & 0 \\ 0.1329 & 0.756 & 0 \\ 4.12733e-3 & -0.023478 & 0 \end{bmatrix} \begin{bmatrix} u_g \\ w_g \\ q_g \end{bmatrix} \quad (14.29)$$

To obtain the aircraft response to a normal gust w_g disturbance, for example, [equations \(14.27\) and \(14.29\)](#) may be solved in the usual way for the single-input variable w_g . Thus, for this particular example, the state-space equations simplify to [equations \(14.30\)](#), which may be

solved using MATLAB, Program CC, or a similar computational tool set to obtain the gust and turbulence response transfer functions. In a similar way, the response transfer functions for u_g and q_g disturbances can be obtained by suitable adjustment of the matrices \mathbf{E} and \mathbf{F} :

$$\dot{\mathbf{x}} = \begin{bmatrix} -7.14e-3 & 0.0321 & 0 & -32.2 & 0 \\ -0.1329 & -0.756 & 468.2 & 0 & 0 \\ 3.2688e-5 & -0.01016 & -1.3281 & 0 & 0 \\ 0 & 0 & 1 & 0 & 0 \\ 0 & -1 & 0 & 468.2 & 0 \end{bmatrix} \mathbf{x} + \begin{bmatrix} -0.0321 \\ 0.756 \\ 0.01016 \\ 0 \\ 0 \end{bmatrix} \mathbf{u}$$

$$\mathbf{y} = \begin{bmatrix} 1 & 0 & 0 & 0 & 0 \\ 0 & 1 & 0 & 0 & 0 \\ 0 & 0 & 1 & 0 & 0 \\ 0 & 0 & 0 & 1 & 0 \\ 0 & 0 & 0 & 0 & 1 \\ -0.1329 & -0.756 & 0 & 0 & 0 \\ 4.12733e-3 & 0.023473 & 0 & 0 & 0 \end{bmatrix} \mathbf{x} + \begin{bmatrix} 0 \\ 0 \\ 0 \\ 0 \\ 0 \\ 0.756 \\ -0.023478 \end{bmatrix} \mathbf{u} \quad (14.30)$$

where

$$\mathbf{x}^T = [u \ w \ q \ \theta \ h]$$

$$\mathbf{u} = w_g$$

$$\mathbf{y}^T = [u \ w \ q \ \theta \ h \ a_z \ n_z]$$

The solution of equations (14.30) gives the following gust response transfer functions:

$$\frac{u(s)}{w_g(s)} = \frac{-0.0321 s^2(s^2 + 1.328s + 10.19)}{s(s^2 + 0.005438s + 0.007685)(s^2 + 2.086s + 5.759)}$$

$$\frac{w(s)}{w_g(s)} = \frac{0.756 s(s + 7.623)(s^2 + 0.0070245s + 0.007679)}{s(s^2 + 0.005438s + 0.007685)(s^2 + 2.086s + 5.759)}$$

$$\frac{q(s)}{w_g(s)} = \frac{0.01016 s^3(s + 0.007037)}{s(s^2 + 0.005438s + 0.007685)(s^2 + 2.086s + 5.759)} \frac{\text{rad/s}}{\text{ft/s}}$$

$$\frac{\theta(s)}{w_g(s)} = \frac{0.01016 s^2(s + 0.007037)}{s(s^2 + 0.005438s + 0.007685)(s^2 + 2.086s + 5.759)} \frac{\text{rad}}{\text{ft/s}} \quad (14.31)$$

$$\frac{h(s)}{w_g(s)} = \frac{-0.756(s^2 - 0.01916s + 0.04304)(s + 1.36)}{s(s^2 + 0.005438s + 0.007685)(s^2 + 2.086s + 5.759)} \frac{\text{ft}}{\text{ft/s}}$$

$$\frac{a_z(s)}{w_g(s)} = \frac{0.756 s^2(s^2 - 0.01916s + 0.04304)(s + 1.36)}{s(s^2 + 0.005438s + 0.007685)(s^2 + 2.086s + 5.759)} \frac{\text{ft/s}^2}{\text{ft/s}}$$

$$\frac{n_z(s)}{w_g(s)} = \frac{-0.2348 s^2(s^2 - 0.01916s + 0.04304)(s + 1.36)}{s(s^2 + 0.005438s + 0.007685)(s^2 + 2.086s + 5.759)} \frac{g}{\text{ft/s}}$$

Observation of the transfer functions (14.31) suggests that aircraft response is consistent with the flight physics associated with a positive small-perturbation disturbance in normal velocity. The stability is governed by the familiar properties of the characteristic polynomial described by the common denominator of the transfer functions. The longitudinal stability characteristics associated with the aircraft at this flight condition are

Phugoid damping ratio	$\zeta_p = 0.031$
Phugoid natural frequency	$\omega_p = 0.088 \text{ rad/s}$
Short-period damping ratio	$\zeta_s = 0.435$
Short-period natural frequency	$\omega_s = 2.4 \text{ rad/s}$

The pole at $s = 0$ corresponds with the height integration characteristic. The information given in [Teper \(1969\)](#) does not include provision for stability augmentation, so it is assumed that the aircraft is not fitted with a longitudinal autostabilisation system. The stability characteristics indicated are entirely consistent with a stable unaugmented aircraft of the late 1950s period.

It should also be noted that the height h , normal acceleration a_z , and normal load factor n_z transfer functions exhibit a significant nonminimum phase property which is entirely consistent with the adverse aerodynamic properties of a large aircraft of this type.

Finally, note that the transfer functions include up to three zeros at $s = 0$. Some of these cancel with the pole at $s = 0$, but they have not been removed from the transfer functions in this example for reasons of clarity of understanding. In the computational solution many of these poles and zeros have a small non-zero value of either sign due to rounding errors in the solution algorithm, and great care must be exercised in their interpretation. For the purpose of comparison, the author used a number of alternative algorithms to solve [equations \(14.30\)](#), and each solution produced small but different values for the poles and zeros which correctly sit at $s = 0$. In this kind of situation it becomes abundantly clear that a good understanding of anticipated aircraft response is essential.

14.5 Turbulence modelling

Random atmospheric disturbances are assumed to comprise continuous turbulence, with embedded discrete gusts, and subject to steady and non-steady wind effects. The disturbances are further assumed to be distributed spatially over a horizontal patch, or field, through which the aircraft flies in steady level flight. For mathematical convenience, the patch, or field of disturbances, is assumed to be stationary in time and space for the period of encounter by the aircraft. This approach to turbulence modelling is sometimes referred to as *frozen field turbulence*. The *spatial frequency* of the turbulence is denoted Ω and has units of radians per unit length, or distance. The time dependency of the response of the aircraft arises from the *frequency of encounter*, which depends on the velocity at which the aircraft traverses the patch of frozen turbulence. Thus the *temporal frequency* ω is given by

$$\omega = \Omega V_0 \text{ with units rad/s} \quad (14.32)$$

Considerable care is required with regard to the units used in turbulence analysis because much is assumed in the flying qualities requirements documents; also, the units most commonly used in atmospheric turbulence modelling are not always consistent with those commonly used in systems analysis using tools like MATLAB and Progam CC. Continuous random disturbances, conveniently referred to as turbulence, are characterised by the *rms intensity*, *power spectral density* (PSD), and *scale*.

14.5.1 The von Kármán model

The von Kármán model defines the power spectra of the linear velocity components of turbulence, where the spectra have a Gaussian, or normal, distribution and the model is generally considered to be the most accurate approximation of real turbulence. The power spectra of the axial u_g , lateral v_g , and normal w_g turbulence velocity components are given by

$$\Phi_{ug}(\Omega) = \sigma_{ug}^2 \frac{2\mathcal{L}_u}{\pi} \frac{1}{(1 + (1.339\mathcal{L}_u\Omega)^2)^{\frac{5}{6}}} \quad (14.33)$$

$$\Phi_{vg}(\Omega) = \sigma_{vg}^2 \frac{\mathcal{L}_v}{\pi} \frac{(1 + \frac{8}{3}(1.339\mathcal{L}_v\Omega)^2)}{(1 + (1.339\mathcal{L}_v\Omega)^2)^{\frac{11}{6}}} \quad (14.34)$$

$$\Phi_{wg}(\Omega) = \sigma_{wg}^2 \frac{\mathcal{L}_w}{\pi} \frac{(1 + \frac{8}{3}(1.339\mathcal{L}_w\Omega)^2)}{(1 + (1.339\mathcal{L}_w\Omega)^2)^{\frac{11}{6}}} \quad (14.35)$$

where \mathcal{L}_u , \mathcal{L}_v , and \mathcal{L}_w are the appropriate scale lengths. The units of the PSD functions given in equations (14.33), (14.34), and (14.35) are $(\text{m/s})^2/(\text{rad/m})$ or $(\text{ft/s})^2/(\text{rad/ft})$. Since the fractional indices in the denominators of the von Kármán model are mathematically difficult to implement in practical applications, the simpler but less accurate Dryden model is commonly used as an alternative.

14.5.2 The Dryden model

The Dryden turbulence model is mathematically simpler and has been developed to model both linear and angular disturbance velocity components. However, it is considered to be a less accurate although acceptable alternative to the von Kármán model for practical flight dynamics investigations. In the past, all aircraft simulation utilised analogue computing techniques and to reproduce the von Kármán turbulence model by this means was difficult in the extreme. Consequently, the Dryden model was adopted as an alternative to alleviate this problem and continues to be used extensively in the simulation environment. Modern computer tools enable both the von Kármán and the Dryden models to be reproduced in a simulation environment with equal facility and, strictly, the von Kármán turbulence model should be the model of choice. However, the Dryden model remains in common usage since it is well understood, it is easier to work with, and it has a long and established acceptability.

The Dryden power spectra of the axial u_g , lateral v_g , and normal w_g turbulence velocity components are given by

$$\Phi_{ug}(\Omega) = \sigma_{ug}^2 \frac{2\mathcal{L}_u}{\pi} \frac{1}{(1 + (\mathcal{L}_u \Omega)^2)} \quad (14.36)$$

$$\Phi_{vg}(\Omega) = \sigma_{vg}^2 \frac{\mathcal{L}_v}{\pi} \frac{(1 + 3(\mathcal{L}_v \Omega)^2)}{(1 + (\mathcal{L}_v \Omega)^2)^2} \quad (14.37)$$

$$\Phi_{wg}(\Omega) = \sigma_{wg}^2 \frac{\mathcal{L}_w}{\pi} \frac{(1 + 3(\mathcal{L}_w \Omega)^2)}{(1 + (\mathcal{L}_w \Omega)^2)^2} \quad (14.38)$$

The units of the Dryden PSD functions are the same as those of the von Kármán functions. Additionally, the power spectra of the roll p_g , pitch q_g , and yaw r_g angular turbulence velocity components are given by

$$\Phi_{pg}(\Omega) = \frac{\sigma_{wg}^2}{\mathcal{L}_w} \frac{0.8 \left(\frac{\pi \mathcal{L}_w}{4b} \right)^{\frac{1}{3}}}{\left(1 + \left(\frac{4b}{\pi} \Omega \right)^2 \right)} \quad (14.39)$$

$$\Phi_{qg}(\Omega) = \frac{\Phi_{wg}(\Omega) \Omega^2}{\left(1 + \left(\frac{4b \Omega}{\pi} \right)^2 \right)} \quad (14.40)$$

$$\Phi_{rg}(\Omega) = \frac{\Phi_{vg}(\Omega) \Omega^2}{\left(1 + \left(\frac{3b \Omega}{\pi} \right)^2 \right)} \quad (14.41)$$

where \mathcal{L}_u , \mathcal{L}_v , \mathcal{L}_w and \mathcal{L}_p are the appropriate scale lengths, and b is the wing span. Note that q_g is dependent on w_g and r_g is dependent on v_g .

The components of angular turbulence velocity are often small and are frequently ignored. A simple test to determine their relative significance is given in [Hoh et al. \(1982\)](#).

When

$$\left(\frac{b}{\mathcal{L}_w} \right)^{\frac{1}{2}} > \frac{L_v}{L_p} \quad \text{then} \quad p_g = 0 \quad (14.42)$$

$$\left(\frac{\pi b}{8\mathcal{L}_w} \right)^{\frac{1}{2}} > \frac{M_w}{M_q} \quad \text{then} \quad q_g = 0 \quad (14.43)$$

$$\left(\frac{\pi b}{6\mathcal{L}_v} \right)^{\frac{1}{2}} > \frac{N_v}{N_r} \quad \text{then} \quad r_g = 0 \quad (14.44)$$

It is interesting to consider the properties of the inequalities (14.42), (14.43), and (14.44). The terms on the left-hand side are functions of wing span b divided by scale length \mathcal{L} , and increase in magnitude as the size of the aircraft increases. The terms on the right-hand side comprise the ratio of the stiffness derivative and damping derivative in roll, pitch, and yaw, respectively. Obviously, the magnitude of the ratio diminishes as damping increases. Thus, in well-damped aeroplanes, the components of angular velocity disturbances may be attenuated to the extent that they can be

omitted from the modelling, and for very large well-damped aeroplanes the angular velocity disturbances are even more likely to be insignificant.

14.5.3 Comparison of the von Kármán and Dryden models

To illustrate the essential differences between the von Kármán and Dryden turbulence models for the axial components of velocity u_g , their power spectra are compared as given by [equations \(14.33\)](#) and [\(14.36\)](#), respectively. By multiplying each equation by the spatial frequency Ω , and with some rearrangement, the normalised power spectral density is plotted against the normalised spatial frequency as shown in [Fig. 14.2](#).

It is evident that the spectral energy distributions for the two models are similar in shape but that the Dryden model tends to overestimate the energy content around the centre frequency and underestimate the energy content at the extreme higher frequencies of the distribution. The high frequency difference is of less concern since the aircraft rigid body dynamics naturally attenuate the effects of disturbances as the frequency increases. However, this may not be the case in the context of structural mode excitation. On the other hand, the low-frequency region of the distributions below the centre frequency is of much greater significance since the natural attenuation of the response to disturbances is generally small. Note in [Fig. 14.2](#) that the lower-frequency distributions of the two models are in very close agreement, thereby endorsing the use of the Dryden model as a good alternative to the von Kármán model for evaluations in which the lower-frequency response to disturbances is of the greatest importance.

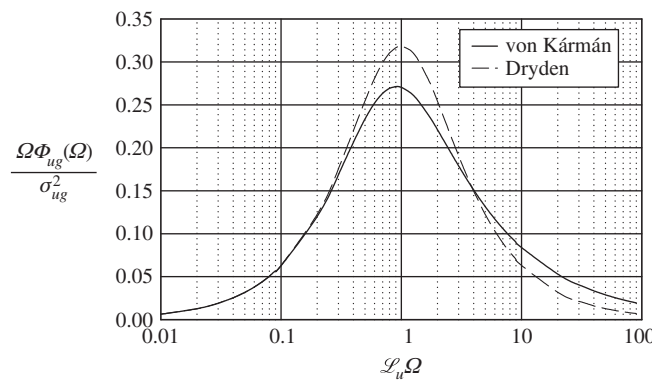


FIGURE 14.2 Comparison of Von Kármán and Dryden power spectra for the axial component of turbulence velocity.

14.5.4 Turbulence scale length

The determination of the appropriate scale, or scale length, of continuous turbulence remains probably one of the most contentious issues in turbulence modelling, and opinions differ among those involved in its application. As aircraft technology has advanced and flight envelopes have expanded, questions have been raised concerning the appropriateness of the scale length requirements set out in

Def-Stan 00-970 and in MIL-F-8587C. Changes have been made from time to time in an attempt to improve their relevance, and it is likely that this process will continue into the future.

Scale length is very much dependent on height above the local terrain, and the definitions for use in the von Kármán power spectra as set out in Def-Stan 00-970 are given in [Table 14.8](#).

The scale length as set out in MIL-F-8785C is similar, but is defined differently as shown in [Table 14.9](#).

It is interesting to compare the turbulence scale length definitions as given in [Tables 14.8](#) and [14.9](#); the comparisons are plotted in [Fig. 14.3](#). Of particular interest is the comparison of the low-altitude scale length models, which are clearly rather different.

The key to the plots is given in [Table 14.10](#).

Table 14.8 Turbulence Scale Length Def-Stan 00-970

Height h	Scale Length \mathcal{L}
Above 750 m (2500 ft)	$\mathcal{L}_u = \mathcal{L}_v = \mathcal{L}_w = 750 \text{ m (}2500 \text{ ft)}$
Below 750 m (2500 ft)	$\mathcal{L}_u = \mathcal{L}_v = 82.5h^{\frac{1}{3}} \text{ m (}184h^{\frac{1}{3}} \text{ ft)}$ $\mathcal{L}_w = h$

Table 14.9 Turbulence Scale Length MIL-F-8785C

Height h	Scale Length \mathcal{L}
Medium to high altitude, above 2000 ft	$\mathcal{L}_u = \mathcal{L}_v = \mathcal{L}_w = 2500 \text{ ft (von Kármán form)}$
Medium to high altitude, above 2000 ft	$\mathcal{L}_u = \mathcal{L}_v = \mathcal{L}_w = 1750 \text{ ft (Dryden form)}$
Low altitude $10 < h < 1000 \text{ ft}$	$\mathcal{L}_u = \mathcal{L}_v = \frac{h}{(0.177 + 0.000823h)^{1.2}} \text{ ft}$ $\mathcal{L}_w = h$

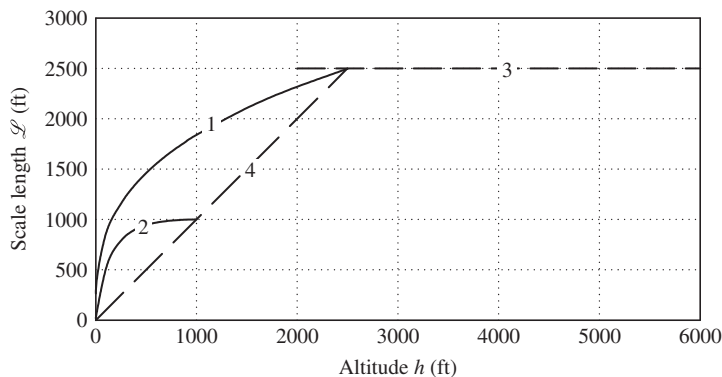


FIGURE 14.3 Comparison of turbulence scale lengths as a function of altitude for Def-Stan 00-970 and MIL-F-8785C.

Table 14.10 Key to Fig. 14.3

Plot	Altitude Range	Def-Stan 00-970	MIL-F-8785C
1	Low altitude to 2500 ft	$\mathcal{L}_u = \mathcal{L}_v$	—
2	Low altitude to 1000 ft	—	$\mathcal{L}_u = \mathcal{L}_v$
3	Medium to high altitude	$\mathcal{L}_u = \mathcal{L}_v = \mathcal{L}_w$ above 2500 ft	$\mathcal{L}_u = \mathcal{L}_v = \mathcal{L}_w$ above 2000 ft
4	Low altitude	\mathcal{L}_w to 2500 ft	\mathcal{L}_w to 1000 ft

It can be seen that the low-altitude scale length defined by MIL-F-8785C applicable to the altitude interval 1000 to 2000 ft is unspecified, although it is not difficult to make a representative estimate from the information available. However, it should be noted that the alternative formulations for defining low altitude scale length are equally acceptable but should be applied in the context of their source document, either Def-Stan 00-970 or MIL-F-8785C.

14.5.5 Turbulence intensity

The reference rms gust and turbulence intensity σ_g in Def-Stan 00-970 is specified as a function of altitude, as shown in Fig. 14.1 and in a similar chart in MIL-F-8785C. The magnitudes of the gust and turbulence velocity component intensities then derive from the reference value.

For the von Kármán model in Def-Stan 00-970, the gust and turbulence component intensities are defined in SI units appropriate to low altitude, below 750 m (2500 ft), as

$$\frac{\sigma_{ug}}{\mathcal{L}_u^{\frac{1}{3}}} = \frac{\sigma_{vg}}{\mathcal{L}_v^{\frac{1}{3}}} = \frac{\sigma_{wg}}{\mathcal{L}_w^{\frac{1}{3}}} = \frac{\sigma_g}{750^{\frac{1}{3}}} \quad (14.45)$$

and at medium to high altitude above 750 m, equation (14.40) simplifies to

$$\sigma_{ug} = \sigma_{vg} = \sigma_{wg} = \sigma_g \quad (14.46)$$

Equation (14.46) is also defined in MIL-F-8785C, in the equivalent American imperial units, for medium to high altitudes above 2000 ft. For low altitude, below 1000 ft, the gust and turbulence component intensities are defined differently:

$$\frac{\sigma_{ug}}{\sigma_{wg}} = \frac{\sigma_{vg}}{\sigma_{wg}} = \frac{1}{(0.177 + 0.000823h)^{0.4}} \quad (14.47)$$

and

$$\sigma_{wg} = 0.1u_{20} \quad (14.48)$$

where u_{20} is the mean wind velocity at 20 ft above the local terrain. Additional information is provided to quantify *light*, *moderate*, and *severe* values for u_{20} , as set out in Table 14.11, and to quantify the probability of exceeding a given reference value.

With reference to the definitions of scale length in Table 14.9, it is easily shown that equation (14.47) may be written alternatively as

$$\frac{\sigma_{ug}}{\mathcal{L}_u^{\frac{1}{3}}} = \frac{\sigma_{vg}}{\mathcal{L}_v^{\frac{1}{3}}} = \frac{\sigma_{wg}}{\mathcal{L}_w^{\frac{1}{3}}} \quad (14.49)$$

Table 14.11 Mean Wind Speed at 20 ft

Intensity	Reference Value u_{20} (knots)
Light	15
Moderate	30
Severe	45

which is identical to [equation \(14.45\)](#). However, it should be remembered that the gust and turbulence scale lengths are defined differently in MIL-F-8785C, as described in [Section 14.5.4](#). This is yet another example which shows that the general approach to mathematical modelling of turbulence is universally accepted but that opinions continue to differ about the way in which scale length should be defined.

Gust and turbulence intensities, expressed in American imperial units, for the Dryden model are, for altitudes below 1750 ft,

$$\frac{\sigma_{ug}^2}{\mathcal{L}_u} = \frac{\sigma_{vg}^2}{\mathcal{L}_v} = \frac{\sigma_{wg}^2}{\mathcal{L}_w} = \frac{\sigma_g^2}{1750} \quad (14.50)$$

and for the intensity of the rotational roll turbulence component it is

$$\sigma_{pg} = \frac{1.9\sigma_{wg}}{(\mathcal{L}_w b)^{\frac{1}{2}}} \quad (14.51)$$

At medium to high altitude above 1750 ft, [equation \(14.46\)](#) applies.

14.6 Discrete gusts

The discrete gust is assumed to be an isolated event which can occur in clear air or can be embedded in a patch of continuous turbulence. When it is embedded in continuous turbulence, the gust shape and its spectral properties are assumed to be related to those of the turbulence. For the purposes of flying qualities evaluations, the gust can take the form of a linear ramp or step function. The essential requirement is that the gust should be defined to excite the aircraft at known resonant frequencies, giving rise to the concept of the *tuned gust*. The preferred gust shapes are based on the “1-cosine” gust, the properties of which can be designed as required to suit the application and which is entirely compatible with the energy distribution of the von Kármán power spectrum.

14.6.1 The “1-cosine” gust

Typical gust shapes are shown in [Fig. 14.4](#). A gust is defined as the ramp-up, or ramp-down, over the gust length distance d . The same shapes and definitions apply to the axial, lateral, and normal gust velocity components u_g , v_g , and w_g , respectively. [Fig. 14.4a](#) shows a symmetric gust, and as the aircraft traverses the gust the velocity V_g ramps up to its maximum value V_{gm} over the distance d and then ramps down again over the same distance. The “1-cosine” function defines the shape of

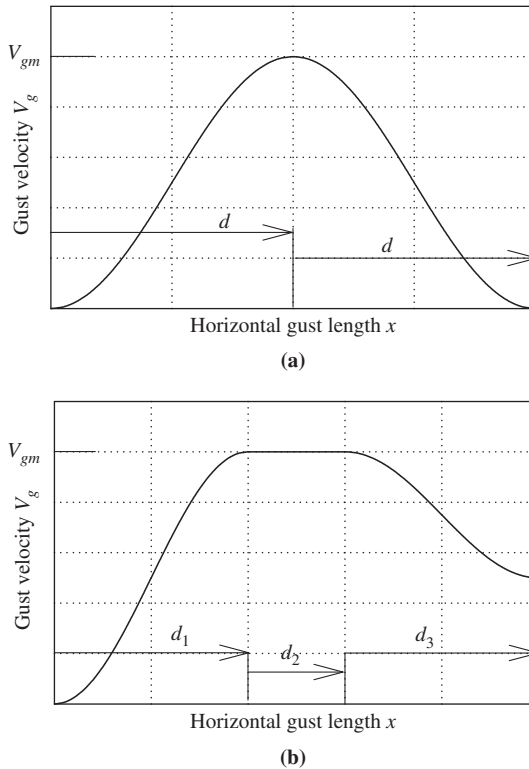


FIGURE 14.4 Typical “1-cosine” gust shapes.

the initial velocity ramp-up to its maximum value and the decay to zero following the peak. The time and frequency properties of the gust are determined by the velocity at which the aircraft traverses it, and d is chosen to excite the aircraft at known resonant frequencies in an attempt to obtain the maximum response for the chosen gust magnitude. The maximum gust velocity V_{gm} , or gust magnitude, is chosen according to the required gust intensity: light, moderate, or severe. The functions describing the gust shape are

$$\text{Ramp-up} \quad V_g = \frac{V_{gm}}{2} \left(1 - \cos\left(\frac{\pi x}{d}\right) \right) \quad (14.52)$$

$$\text{Ramp-down} \quad V_g = \frac{V_{gm}}{2} \left(1 + \cos\left(\frac{\pi x}{d}\right) \right) \quad (14.53)$$

Similarly, alternative shapes can be built up using the “1-cosine” gust function, and a typical example of an asymmetric gust is shown in Fig. 14.4b. In this model, the gust ramps up to a maximum velocity over the distance d_1 , holds the maximum velocity over the distance d_2 , and finally ramps down over the distance d_3 to a non-zero velocity. Clearly, this approach to gust modelling can be used to create any arbitrary tuned gust shape.

14.6.2 Determination of maximum gust velocity and horizontal length

The determination of maximum gust velocity and horizontal length d is treated rather differently in MIL-F-8785C and Def-Stan 00-970. In both cases the determination of gust length is left to the discretion of the investigator and should be chosen to excite the aircraft at a known resonant frequency. For example, in the present context, where only rigid body motion is a consideration, the gust length might be chosen to excite one of the stability modes. The determination of maximum gust velocity is a function of gust length, altitude, and the reference intensity σ_g , as given by Fig. 14.1, or the equivalent in MIL-F-8785C.

The empirical relationship between gust magnitude and gust length is given in MIL-F-8785C in normalised form, as shown in Fig. 14.5, and is applicable for light and moderate intensity gusts only at all altitudes. Severe gust velocity is quantified as a function of aircraft velocity, altitude, and aircraft operating configuration; values are quoted for a number of critical flight conditions, the maximum value quoted being $V_{gm} = 66$ ft/s, which represents a worst case situation for analytical purposes.

A different empirical relationship between gust magnitude and gust length is given in Def-Stan 00-970. The requirements set out in Def-Stan 00-970 have been normalised to facilitate comparison with MIL-F-8785C and are given in Table 14.12 (SI units apply). Notable observations are

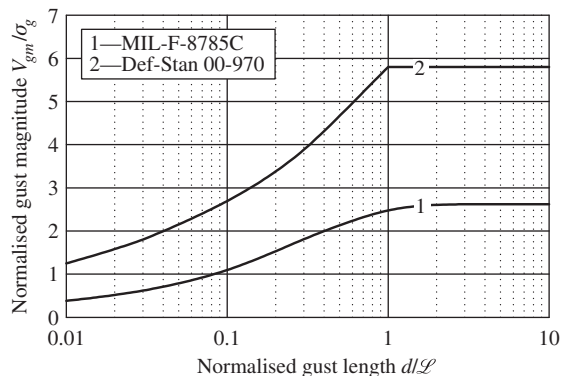


FIGURE 14.5 Normalised gust magnitude and length.

Table 14.12 Normalised Gust Magnitude and Length components as given in Def-Stan 00-970

$d \leq \mathcal{L}$	$d \geq \mathcal{L}$
$\frac{u_{gm}}{\sigma_g} = 1.25J \left(\frac{\mathcal{L}_u}{750} \frac{d_x}{\mathcal{L}_u} \right)^{\frac{1}{3}}$	$\frac{u_{gm}}{\sigma_g} = 1.25J \left(\frac{\mathcal{L}_u}{750} \right)^{\frac{1}{3}}$
$\frac{v_{gm}}{\sigma_g} = 1.45J \left(\frac{\mathcal{L}_v}{750} \frac{d_y}{\mathcal{L}_v} \right)^{\frac{1}{3}}$	$\frac{v_{gm}}{\sigma_g} = 1.45J \left(\frac{\mathcal{L}_v}{750} \right)^{\frac{1}{3}}$
$\frac{w_{gm}}{\sigma_g} = 1.45J \left(\frac{\mathcal{L}_w}{750} \frac{d_z}{\mathcal{L}_w} \right)^{\frac{1}{3}}$	$\frac{w_{gm}}{\sigma_g} = 1.45J \left(\frac{\mathcal{L}_w}{750} \right)^{\frac{1}{3}}$

that when the gust length d is smaller than the turbulence scale length \mathcal{L} the gust magnitude varies with gust length; when d is greater than \mathcal{L} , the gust magnitude is independent of turbulence scale length.

The scale factor J is set at a provisional value of 4.0, but uncertainty is expressed as to exactly what its value should be. Again, this illustrates the difficulty of quantifying atmospheric disturbances in an appropriate way for flying qualities evaluations. The difference between the requirements in MIL-F-8785C and Def-Stan 00-970 become clear when the normalised component magnitude w_{gm}/σ_g from [Table 14.12](#) is plotted on Fig.4.5. It is interesting that the plots are nominally of the same shape but that Def-Stan 00-970 consistently estimates larger gust velocity magnitude than does MIL-F-8785C; this is found to be the case for all gust velocity components over the altitude range.

14.7 Aircraft response to gusts and turbulence

As stated earlier, most applications of aircraft gust and turbulence response relate to the non-linear, continuous-time simulation environment. In this context it is possible to get much closer to reality, especially in the piloted simulation environment. In comparison, the application of gust and turbulence modelling in the linear rigid body dynamics context is of limited scope. However, such limited evaluations as can be made provide a useful preliminary means for assessing aircraft and flight control system performance in non-steady atmospheric conditions. Consequently, the following material is included for completeness, but it is important to realise that its usefulness is limited by the constraints of linearised rigid body modelling.

14.7.1 Variance, power spectral density, and white noise

The application of Parseval's theorem enables the average power, or *variance* σ^2 , of a time-varying random signal $u(t)$ to be determined from either its time domain description or its frequency domain description; thus

$$\sigma_u^2 = \int_{-\infty}^{\infty} u^2(t)dt = \int_{-\infty}^{\infty} |u(f)|^2 df = \int_{-\infty}^{\infty} \Phi_u(f)df \quad (14.54)$$

where f is the *cyclic* frequency (Hz). Since linear systems frequency domain analysis is usually expressed in terms of *angular* frequency ω (rad/s) then, alternatively, it is convenient to write [equation \(14.54\)](#) as

$$\sigma_u^2 = \int_{-\infty}^{\infty} u^2(t)dt = \frac{1}{2\pi} \int_{-\infty}^{\infty} |u(\omega)|^2 d\omega = \frac{1}{2\pi} \int_{-\infty}^{\infty} \Phi_u(\omega)d\omega \quad (14.55)$$

Now, if the function $u(t)$ is symmetric about $t = 0$ such that $u(-t) = u(t)$, then, equivalently, [equation \(14.55\)](#) may be written as

$$\sigma_u^2 = \frac{1}{\pi} \int_0^{\infty} |u(\omega)|^2 d\omega = \frac{1}{\pi} \int_0^{\infty} \Phi_u(\omega)d\omega \quad (14.56)$$

In practical applications to real systems, integration over all positive frequencies is standard practice and the “single-sided” expression given by [equation \(14.56\)](#) is in common use.

Thus the PSD of $u(t)$ is given by

$$\Phi_u(\omega) = |u(\omega)|^2 \text{ with units } (\text{m/s})^2/(\text{rad/s}) \text{ or } (\text{ft/s})^2/(\text{rad/s}) \quad (14.57)$$

$$\Phi_u(f) = |u(f)|^2 \text{ with units } (\text{m/s})^2/\text{Hz} \text{ or } (\text{ft/s})^2/\text{Hz} \quad (14.58)$$

Note that the definitions and units of PSD are emphasized here since it is essential to be precise when dealing with turbulence models if inconsistencies are to be avoided. It is particularly important to note that the definition of variance used in both Def-Stan 00-970 and MIL-F-8785C is derived from [equation \(14.54\)](#) and quoted as

$$\sigma^2 = \int_0^\infty \Phi(\omega) d\omega$$

in which ω is defined as *angular frequency*. However, this formulation of the definition of variance usually assumes a *cyclic frequency* dependency (compare with [equation \(14.54\)](#)), and the inconsistency can be confusing. On the other hand, the computational algorithm used by both MATLAB and Program CC to calculate variance implements [equation \(14.56\)](#) directly. Clearly, this implies an *angular frequency* dependency, which is entirely consistent with the mathematics of linear systems. Since MATLAB and Program CC share the same mathematical origins, many of their computational algorithms are the same; in the present context this applies to *variance*, *covariance*, and *Lyapunov equation* calculations. Consequently, particular care is required when using MATLAB, Program CC, and similar computational tools for atmospheric variance calculations to ensure that the factor $1/\pi$ is correctly allocated. It is considered good practice to check that rms values calculated in the time and frequency domains are consistent.

It is useful now to consider the *rms intensity*, or *standard deviation* σ_u of the random signal $u(t)$ in a practical context, where typically

$$\begin{aligned} u(t) &= 0 \quad \text{for } t < 0 \\ u(t) &\neq 0 \quad \text{for } 0 \leq t \leq T \end{aligned} \quad (14.59)$$

For such a series expression, $u(-t) = u(t)$ can be redefined to allow use of the single-sided integral expression given by [equation \(14.56\)](#).

Assume that n samples of $u(t)$ are recorded in the interval $0 \leq t \leq T$ and that $u(t)$ is a *zero mean value* signal; then

$$\bar{u}(t) = \frac{1}{n} \sum_{i=1}^n u_i(t) = 0 \quad (14.60)$$

and the rms intensity of $u(t)$ is defined by

$$\sigma_u = \sqrt{\frac{1}{n} \sum_{i=1}^n u_i^2(t)} \quad (14.61)$$

Alternatively, rms intensity may be expressed as a function of power spectral density. When the frequency spectrum is expressed in terms of cyclic frequency f , [equation \(14.54\)](#) applies:

$$\sigma_u = \sqrt{\int_0^\infty |u(f)|^2 df} = \sqrt{\int_0^\infty \Phi_u(f) df} \quad (14.62)$$

Or, in terms of angular frequency ω , equation (14.56) applies:

$$\sigma_u = \sqrt{\frac{1}{\pi} \int_0^\infty |u(\omega)|^2 d\omega} = \sqrt{\frac{1}{\pi} \int_0^\infty \Phi_u(\omega) d\omega} \quad (14.63)$$

A *white noise* signal is an artefact of the engineer devised for the convenience of representing naturally occurring random phenomena in engineering applications. In the present context, synthetic turbulence is “manufactured” by filtering a white noise signal such that its output power spectrum matches “real” turbulence as far as that is possible. A white noise signal $N(t)$ is defined as having zero mean value and uniform power distribution over the frequency spectrum $-\infty < f < \infty$ Hz, or $-\infty < \omega < \infty$ rad/s. It follows that “unit” white noise has the following statistical properties which are independent of frequency:

Power spectral density	$\Phi_N(f) = \Phi_N(\omega) = 1.0$
Variance	$\sigma_N^2 = 1.0$
Standard deviation, or rms intensity	$\sigma_N = 1.0$
Mean	$\bar{N}(t) = 0$

(14.64)

The action of filtering white noise produces bandwidth limited white noise, which also has zero mean and a uniform power distribution over the reduced frequency spectrum. Thus, for “unit” white noise input, the output variance and rms intensity also have unit values.

14.7.2 Spatial and temporal equivalence

Gusts and turbulence are characterised by their magnitude and the size of the horizontal area, or patch, over which they occur. Their spectral properties are quantified in terms of spatial frequency Ω , or radians per unit distance. On the other hand, aircraft response to gusts and turbulence is quantified in terms of temporal frequency ω and the temporal characteristics of the disturbance are quantified by the time taken for the aircraft to traverse the gust or patch of turbulence. Assuming frozen turbulence, the time taken for an aircraft travelling at velocity V_0 to traverse a gust or patch of turbulence of size d is given by

$$t = \frac{d}{V_0} \quad (14.65)$$

Consequently, the equivalence between spatial and temporal frequency is given by

$$\omega = V_0 \Omega \quad (14.66)$$

and it follows that the equivalence between temporal and spatial turbulence power spectra is given by

$$\Phi_i(\omega) = \frac{1}{V_0} \Phi_i(\Omega) \quad i = u_g, v_g, w_g \quad (14.67)$$

The rise time t of a discrete gust is given by equation (14.65), and it follows that the period associated with the gust is given by

$$T_g = \frac{2\pi}{\omega} = \frac{2d}{V_0} \quad (14.68)$$

Clearly, the temporal frequency spectrum of turbulence is entirely dependent on the velocity at which the aircraft traverses the patch, and the excitation frequency of a discrete gust is similarly determined by the velocity at which the aircraft traverses the gust ramp. Equation (14.68) provides

the means for determining the suitable gust length d necessary to excite the aircraft at a particular frequency, corresponding, for example, with one of the rigid body stability modes.

14.7.3 Synthetic turbulence

It is usual to synthesize artificial turbulence models by passing white noise through a filter with a transfer function designed to produce an output turbulence velocity component having the correct power spectrum. [Gage \(2003\)](#) discusses at length the difficulties of developing a unified approach for creating MATLAB models and procedures for synthesizing atmospheric turbulence from the various models specified. Given particular attention is the especially difficult problem of modelling the von Kármán power spectra. Thus the problem of generating artificial turbulence reduces to that of designing a family of white noise filters. The process is represented in [Fig. 14.6](#), where $i = u_g, v_g, w_g$.

The relationship between the input and output power spectra is given by

$$\Phi_i(\omega) = |G_i(s)|_{s=j\omega}^2 \Phi_N(\omega) = |G_i(s)|_{s=j\omega}^2 \quad (14.69)$$

since the PSD of white noise is defined as $\Phi_N(\omega) = 1.0$ ($\sigma^2/\text{rad/s}$).

To illustrate the filter design process, consider synthesizing the axial turbulence velocity component u_g using the Dryden spectral form, for which the power spectrum is given by [equation \(14.36\)](#). With reference to [equations \(14.66\)](#) and [\(14.67\)](#), the temporal PSD may be written as

$$\Phi_{ug}(\omega) = \sigma_{ug}^2 \frac{2\mathcal{L}_u}{\pi V_0} \frac{1}{\left(1 + \left(\frac{\mathcal{L}_u}{V_0}\omega\right)^2\right)} \quad (14.70)$$

With reference to [equation \(14.69\)](#) and to the form of [equation \(14.70\)](#), it is evident that a suitable transfer function $G_i(s)$ is given by a simple low-pass filter having the general form

$$G_{ug}(s) = \frac{K_{ug}}{(1 + sT_{ug})} \quad (14.71)$$

Whence [equation \(14.69\)](#) may be written as

$$\begin{aligned} \Phi_{ug}(\omega) &= \sigma_{ug}^2 \frac{2\mathcal{L}_u}{\pi V_0} \frac{1}{\left(1 + \left(\frac{\mathcal{L}_u}{V_0}\omega\right)^2\right)} = |G_{ug}(s)|_{s=j\omega}^2 \\ &= G_{ug}(j\omega)G_{ug}(-j\omega) \\ &= \frac{K_{ug}^2}{(1 + j\omega T_{ug})(1 - j\omega T_{ug})} = \frac{K_{ug}^2}{(1 + \omega^2 T_{ug}^2)} \end{aligned} \quad (14.72)$$

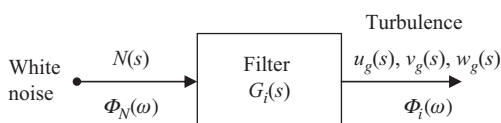


FIGURE 14.6 Turbulence modelling process.

Equating coefficients in equation (14.72), the gain and time constant for the filter are defined:

$$\begin{aligned} K_{ug} &= \sigma_{ug} \sqrt{\frac{2\mathcal{L}_u}{\pi V_0}} = \sigma_{ug} \sqrt{\frac{2T_{ug}}{\pi}} \\ T_{ug} &= \frac{\mathcal{L}_u}{V_0} \end{aligned} \quad (14.73)$$

A more complex illustration is provided by the design of the filter to produce the normal component of turbulence velocity w_g , again using the Dryden form. From equation (14.38) the temporal PSD may be written as

$$\Phi_{wg}(\omega) = \sigma_{wg}^2 \frac{\mathcal{L}_w}{\pi V_0} \frac{\left(1 + 3\left(\frac{\mathcal{L}_w}{V_0}\omega\right)^2\right)}{\left(1 + \left(\frac{\mathcal{L}_w}{V_0}\omega\right)^2\right)^2} \quad (14.74)$$

Equation (14.74) suggests a filter having the following general form:

$$G_{wg}(s) = \frac{K_{wg}(1 + sT_1)}{(1 + sT_2)^2} \quad (14.75)$$

Applying equation (14.69) and substituting equations (14.74) and (14.75), it follows that

$$\Phi_{wg}(\omega) = \sigma_{wg}^2 \frac{\mathcal{L}_w}{\pi V_0} \frac{\left(1 + 3\left(\frac{\mathcal{L}_w}{V_0}\omega\right)^2\right)}{\left(1 + \left(\frac{\mathcal{L}_w}{V_0}\omega\right)^2\right)^2} = \frac{K_{wg}^2(1 + (\omega T_1)^2)}{(1 + (\omega T_2)^2)^2} \quad (14.76)$$

Again, equating coefficients in equation (14.76), the filter gain and time constants are easily identified:

$$\begin{aligned} K_{wg} &= \sigma_{wg} \sqrt{\frac{\mathcal{L}_w}{\pi V_0}} = \sigma_{wg} \sqrt{\frac{T_{wg}}{\pi}} \\ T_1 &= \sqrt{3}T_{wg} = \sqrt{3} \frac{\mathcal{L}_w}{V_0} \\ T_2 &= T_{wg} = \frac{\mathcal{L}_w}{V_0} \end{aligned} \quad (14.77)$$

Whence transfer function (14.75) may be written as

$$G_{wg}(s) = \frac{K_{wg}(1 + \sqrt{3}T_{wg}s)}{(1 + T_{wg}s)^2} \quad (14.78)$$

Similarly, the lateral component of turbulence velocity v_g is derived from the Dryden temporal PSD form of equation (14.37) to give the filter

$$G_{vg}(s) = \frac{K_{vg}(1 + \sqrt{3}T_{vg}s)}{(1 + T_{vg}s)^2} \quad (14.79)$$

where

$$\begin{aligned} K_{vg} &= \sigma_{vg} \sqrt{\frac{\mathcal{L}_v}{\pi V_0}} \\ T_{vg} &= \frac{\mathcal{L}_v}{V_0} \end{aligned} \quad (14.80)$$

14.7.4 Aircraft response to gusts

In the context of linear rigid body modelling, aircraft gust response can be analysed by creating a gust model and using it as the input to the aircraft equations of motion, as described in [Section 14.4](#). Now the spatial description of the tuned gust is given by [equation \(14.52\)](#); since aircraft response is a time-dependent property, it is first necessary to define the gust shape in terms of the desired temporal excitation frequency ω_g , where, for example, ω_g would be chosen (tuned) to excite the aircraft at a known aircraft mode frequency.

With reference to [equation \(14.52\)](#), the distance variable x is related to the time variable t by the aircraft velocity V_0 through

$$x = V_0 t \quad (14.81)$$

and from [equation \(14.68\)](#) the gust length d is defined in terms of temporal frequency ω_g as

$$d = \frac{\pi V_0}{\omega_g} \quad (14.82)$$

Whence it is easily shown that the temporal equivalent of [equation \(14.52\)](#) is

$$V_g(t) = \frac{V_{gm}(t)}{2} (1 - \cos \omega_g t) \quad (14.83)$$

and the equivalent of [equation \(14.53\)](#) may be similarly stated.

Having defined the gust length d , the turbulence scale length \mathcal{L} is determined for the flight condition as described in [Section 14.5.4](#). To complete the gust model the maximum gust velocity V_{gm} may then be determined as described in [Section 14.6.2](#).

To create a disturbance input for the aircraft equations of motion, a gust input vector $\mathbf{u}_g(t)$ is assembled using [equation \(14.83\)](#) to build a time sequence of gust shapes to suit the investigation at hand.

EXAMPLE 14.2

In the interests of simplicity and continuity, this example builds on the model of the Douglas DC-8 developed in Example 14.1, the main task here being to create a suitable gust disturbance model and then to assess the aircraft response to the gust.

The chosen requirement is to create a normal gust w_g of *moderate* intensity such that the ramp-up to maximum velocity is tuned to the longitudinal short-period pitching oscillation. The maximum velocity is then held constant for a few seconds, and the final ramp-down is tuned to the phugoid mode. The flying qualities requirements in MIL-F-8785C are applied, and the Dryden turbulence model is assumed.

The essential data from Example 14.1 are

Altitude $h = 15,000$ ft

Velocity $V_0 = 468.2$ ft/s

Phugoid damping ratio $\zeta_p = 0.031$

Phugoid natural frequency $\omega_p = 0.088$ rad/s

Short-period damping ratio $\zeta_s = 0.435$

Short-period natural frequency $\omega_s = 2.4$ rad/s

From MIL-F-8785C the scale length and gust intensity are determined

Dryden scale length at 15,000 ft (see Table 14.9): $\mathcal{L}_w = 1750$ ft

Moderate rms gust intensity at 15,000 ft: $\sigma_g = 9$ ft/s

For the gust ramp-up tuned to the short-period mode frequency ω_s , the gust length given by equation (14.68) is

$$d_s = \frac{\pi V_0}{\omega_s} = 612.87 \text{ ft} \quad (14.84)$$

and the time taken to traverse this distance is $t = d_s/V_0 = 1.3$ s. Now, since $d_s/\mathcal{L}_w = 0.35$, from the appropriate plot in Fig. 14.5,

$$V_{gm} = 1.9\sigma_g = 17.1 \text{ ft/s}$$

Substituting ω_s and V_{gm} into equation (14.83) gives the initial gust ramp-up tuned to the short-period mode:

$$w_{g1}(t) = \frac{V_{gm}(t)}{2} (1 - \cos \omega_s t) = 8.55(1 - \cos 2.4t) \quad \text{for } t = 0 \text{ to } 1.3 \text{ s} \quad (14.85)$$

For the constant section of the gust following the ramp-up, let the time description be

$$w_{g2} = 1.71 \quad \text{for } t = 1.4 \text{ to } 3.9 \text{ s} \quad (14.86)$$

For the gust ramp-down, following the constant section, tuned to the phugoid mode frequency ω_p , the gust length given by equation (14.68) is

$$d_p = \frac{\pi V_0}{\omega_p} = 16714.7 \text{ ft} \quad (14.87)$$

and the time taken to traverse this distance is $t = d_p/V_0 = 35.7$ s. Again, since $d_p/\mathcal{L}_w = 9.55$, from the appropriate plot on Fig. 14.5,

$$V_{gm} = 2.6\sigma_g = 23.4 \text{ ft/s}$$

Thus, for a gust correctly tuned to the phugoid mode, the maximum gust velocity corresponding to a *moderate* gust intensity is 23.4 ft/s. However, purely for the convenience of this illustration, it is required that the gust sequence conclude at $w_g = 0$; thus the maximum value V_{gm} used for the ramp-down remains at 17.1 ft/s, as for the ramp-up. This implies that, although the gust ramp-down is correctly tuned to the phugoid frequency, its magnitude corresponds with an intensity which is less than moderate. Accordingly, the time description of the ramp-down is

$$w_{g3}(t) = \frac{V_{gm}(t)}{2}(1 + \cos\omega_p t) = 8.55(1 + \cos 2.4t) \quad \text{for } t = 4 \text{ to } 39.7 \text{ s} \quad (14.88)$$

The gust vector comprising the time sequence of gusts was assembled by evaluating equations (14.85), (14.86), and (14.88) over a period of 40 s at 0.1-s time intervals to give

$$w_g = (w_{g1}; w_{g2}; w_{g3}) \quad (14.89)$$

The gust sequence computed according to equation (14.89) is shown in Fig. 14.7, where the indicators 1, 2, and 3 denote the gust contributions w_{g1} , w_{g2} , and w_{g3} , respectively.

To evaluate the DC-8 response to the shaped gust shown in Fig. 14.7, the gust vector w_g given by equation (14.89) is used as the input vector to the aircraft equations of motion (14.30), and then subject to the linear simulation computation in MATLAB or Program CC. When the simulation is run for a total of 50 s, the output response variables obtained are shown in Fig. 14.8. It is quite clear that the gust sequence excites both the short-period and phugoid modes, as intended, and that the settling times are consistent with the mode damping ratios.

The short-term response, associated with the short-period mode dynamics, shows a peak in normal load factor n_z of $-0.2 g$ at about 1 s, and a peak in pitch attitude θ of approximately 1.7 deg at around 2.5 s. Since the longer-term response to the gust sequence is governed by the phugoid dynamics, it is not surprising to see that the peak in normal load factor n_z at around 45 s is very small whereas the peaks in the velocity u and pitch attitude θ perturbations are more evident. The peak in velocity u is approximately 15 ft/s and occurs at about 46 s, and the peak in pitch attitude θ is approximately 2.5 deg and occurs at about 34 s.

14.7.5 Aircraft response to turbulence

For practical reasons, the analytical investigation of aircraft response to atmospheric turbulence is limited when using linear rigid body modelling methods. Typical investigations are confined to the

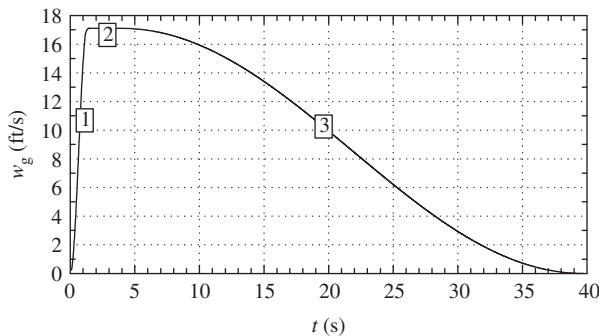


FIGURE 14.7 Tuned w_g gust input.

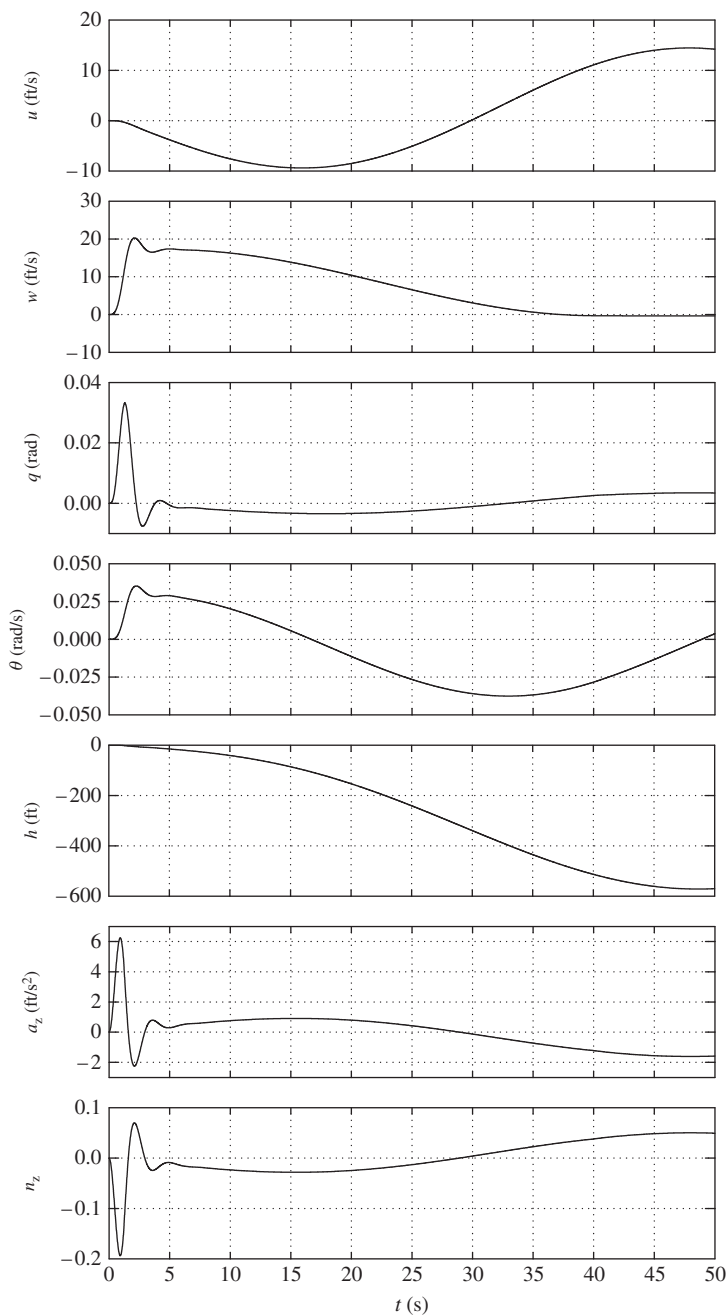


FIGURE 14.8 DC-8 response to a tuned w_g gust of moderate intensity.

evaluation of frequency response properties. More searching investigations would properly be undertaken using non-linear simulation methods as explained previously.

The system model for analytical investigation is shown in Fig. 14.9, where $G_f(t)$ denotes the noise filtering required to generate the turbulence velocity components from a white noise signal input $N(t)$, and $G_A(t)$ denotes the aircraft equations of motion describing the output response $y(t)$ to the turbulence inputs. For analysis, then, the problem simplifies to solution of equation (14.90):

$$y(t) = G_f(t)G_A(t)N(t) \quad (14.90)$$

With reference to equations (14.22), the aircraft state equation may be written as

$$\dot{\mathbf{x}} = \mathbf{Ax} + \mathbf{Eu}_g \quad (14.91)$$

where here the state matrix \mathbf{A} represents the aircraft with or without stability augmentation as appropriate. Similarly, the state equation representing the noise filter may be realised as

$$\dot{\mathbf{x}}_f = \mathbf{Ax}_f + \mathbf{B}_f N \quad (14.92)$$

Thus the state equation for the system shown in Fig. 14.9 may be assembled by augmenting the aircraft state equation (14.91) with the filter state equation (14.92):

$$\begin{bmatrix} \dot{\mathbf{x}} \\ \dot{\mathbf{x}}_f \end{bmatrix} = \left[\begin{array}{c|c} \mathbf{A} & 0 \\ \hline 0 & \mathbf{A}_f \end{array} \right] \begin{bmatrix} \mathbf{x} \\ \mathbf{x}_f \end{bmatrix} + \begin{bmatrix} \mathbf{E} \\ 0 \end{bmatrix} \mathbf{u}_g + \begin{bmatrix} 0 \\ \mathbf{B}_f \end{bmatrix} N \quad (14.93)$$

Consider, for example, the case when the aircraft response to an axial velocity turbulence component is required. From equations (14.14), the longitudinal state equation for the aircraft for the single input u_g , referred to wind axes, may be written in concise form as

$$\begin{bmatrix} \dot{u} \\ \dot{w} \\ \dot{q} \\ \dot{\theta} \end{bmatrix} = \begin{bmatrix} x_u & x_w & x_q & -g \\ z_u & z_w & z_q & 0 \\ m_u & m_w & m_q & 0 \\ 0 & 0 & 1 & 0 \end{bmatrix} \begin{bmatrix} u \\ w \\ q \\ \theta \end{bmatrix} + \begin{bmatrix} -x_u \\ -z_u \\ -m_u \\ 0 \end{bmatrix} u_g \quad (14.94)$$

which is the single-input realisation of equation (14.91). Using the Dryden gust filter transfer function as given by equation (14.71), this may be written as

$$\frac{u_g(s)}{N(s)} = \frac{K_{ug}}{(1 + sT_{ug})} \quad (14.95)$$

Alternatively, equation (14.95) may be written as

$$u_g(s) + s u_g(s) T_{ug} = K_{ug} N(s) \quad (14.96)$$

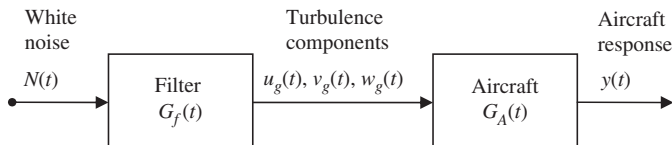


FIGURE 14.9 Analytical system model.

The inverse Laplace transform of [equation \(14.96\)](#) is

$$\dot{u}_g(t)T_{ug} = -u_g(t) + K_{ug}N(t)$$

or

$$\dot{u}_g = -\frac{1}{T_{ug}}u_g + \frac{K_{ug}}{T_{ug}}N \quad (14.97)$$

Note that, in taking the inverse Laplace transform of [equation \(14.96\)](#), zero initial conditions are assumed, which is consistent with the linear systems assumption that aircraft motion is referred to trimmed equilibrium. [Equation \(14.97\)](#) is the state equation for the u_g filter and is the realisation of [equation \(14.92\)](#). Thus [equations \(14.94\)](#) and [\(14.97\)](#) may be substituted into [equation \(14.93\)](#) to give the augmented aircraft state equation describing aircraft response to axial velocity turbulence:

$$\begin{bmatrix} \dot{u} \\ \dot{w} \\ \dot{q} \\ \dot{\theta} \\ \dot{u}_g \end{bmatrix} = \begin{bmatrix} x_u & x_w & x_q & -g & -x_u \\ z_u & z_w & z_q & 0 & -z_u \\ m_u & m_w & m_q & 0 & -m_u \\ 0 & 0 & 1 & 0 & 0 \\ 0 & 0 & 0 & 0 & -\frac{1}{T_{ug}} \end{bmatrix} \begin{bmatrix} u \\ w \\ q \\ \theta \\ u_g \end{bmatrix} + \begin{bmatrix} 0 \\ 0 \\ 0 \\ 0 \\ \frac{K_{ug}}{T_{ug}} \end{bmatrix} N$$

or, substituting for K_{ug} from [equations \(14.73\)](#),

$$\begin{bmatrix} \dot{u} \\ \dot{w} \\ \dot{q} \\ \dot{\theta} \\ \dot{u}_g \end{bmatrix} = \begin{bmatrix} x_u & x_w & x_q & -g & -x_u \\ z_u & z_w & z_q & 0 & -z_u \\ m_u & m_w & m_q & 0 & -m_u \\ 0 & 0 & 1 & 0 & 0 \\ 0 & 0 & 0 & 0 & -\frac{1}{T_{ug}} \end{bmatrix} \begin{bmatrix} u \\ w \\ q \\ \theta \\ u_g \end{bmatrix} + \begin{bmatrix} 0 \\ 0 \\ 0 \\ 0 \\ \sigma_{ug} \sqrt{\frac{2}{\pi T_{ug}}} \end{bmatrix} N \quad (14.98)$$

Realising the state descriptions of the Dryden w_g and v_g turbulence filter transfer functions is a little more difficult because they are both of second order. The process is illustrated for the normal component of turbulence w_g , for which the filter transfer function is given by [equation \(14.78\)](#):

$$\frac{w_g(s)}{N(s)} = \frac{K_{wg}(1 + \sqrt{3}T_{wg}s)}{(1 + T_{wg}s)^2} = \frac{K_{wg}(1 + \sqrt{3}T_{wg}s)}{(1 + 2T_{wg}s + T_{wg}^2s^2)} \quad (14.99)$$

As before, multiplying out [equation \(14.99\)](#) and taking the inverse Laplace transform gives

$$w_g + 2T_{wg}\dot{w}_g + T_{wg}^2\ddot{w}_g = K_{wg}N + K_{wg}\sqrt{3}T_{wg}\dot{N}$$

or

$$\ddot{w}_g + \frac{2}{T_{wg}}\dot{w}_g + \frac{1}{T_{wg}^2}w_g = \frac{K_{wg}}{T_{wg}^2}N + \frac{\sqrt{3}K_{wg}}{T_{wg}}\dot{N} \quad (14.100)$$

Define a dummy variable v such that

$$v = \ddot{w}_g - \frac{\sqrt{3}K_{wg}}{T_{wg}}N \quad \text{or} \quad \dot{w}_g = v + \frac{\sqrt{3}K_{wg}}{T_{wg}}N \quad (14.101)$$

Then

$$\dot{v} = \ddot{w}_g - \frac{\sqrt{3}K_{wg}}{T_{wg}}\dot{N} \quad (14.102)$$

Substituting equations (14.101) and (14.102) into equation (14.100) and rearranging gives

$$\dot{v} + \frac{2}{T_{wg}}v + \frac{1}{T_{wg}^2}w_g = \frac{K_{wg}}{T_{wg}^2}(1 - 2\sqrt{3})N \quad (14.103)$$

Now the second-order filter state equation (14.92) may be assembled from equations (14.101) and (14.103):

$$\begin{bmatrix} \dot{w}_g \\ \dot{v} \end{bmatrix} = \begin{bmatrix} 0 & 1 \\ -\frac{1}{T_{wg}} & -\frac{2}{T_{wg}} \end{bmatrix} \begin{bmatrix} w_g \\ v \end{bmatrix} + \begin{bmatrix} \frac{\sqrt{3}K_{wg}}{T_{wg}} \\ \frac{K_{wg}}{T_{wg}^2}(1 - 2\sqrt{3}) \end{bmatrix} N$$

or, with reference to equations (14.77),

$$\begin{bmatrix} \dot{w}_g \\ \dot{v} \end{bmatrix} = \begin{bmatrix} 0 & 1 \\ -\frac{1}{T_{wg}} & -\frac{2}{T_{wg}} \end{bmatrix} \begin{bmatrix} w_g \\ v \end{bmatrix} + \begin{bmatrix} \sigma_{wg}\sqrt{\frac{3}{\pi T_{wg}}} \\ \sigma_{wg}\sqrt{\frac{1}{\pi T_{wg}^3}(1 - 2\sqrt{3})} \end{bmatrix} N \quad (14.104)$$

Thus, when the aircraft response to the normal velocity turbulence component is required, the concise longitudinal aircraft equations of motion (14.14) may be referred to wind axes, arranged for the single input w_g , and augmented to include the filter state equation (14.104):

$$\begin{bmatrix} \dot{u} \\ \dot{w} \\ \dot{q} \\ \dot{\theta} \\ \dot{w}_g \\ \dot{v} \end{bmatrix} = \begin{bmatrix} x_u & x_w & x_q & -g & -x_w & 0 \\ z_u & z_w & z_q & 0 & -z_w & 0 \\ m_u & m_w & m_q & 0 & -m_w & 0 \\ 0 & 0 & 1 & 0 & 0 & 0 \\ 0 & 0 & 0 & 0 & 0 & 1 \\ 0 & 0 & 0 & 0 & -\frac{1}{T_{wg}^2} & -\frac{2}{T_{wg}} \end{bmatrix} \begin{bmatrix} u \\ w \\ q \\ \theta \\ w_g \\ v \end{bmatrix} + \begin{bmatrix} 0 \\ 0 \\ 0 \\ 0 \\ \sigma_{wg}\sqrt{\frac{3}{\pi T_{wg}}} \\ \sigma_{wg}\sqrt{\frac{1}{\pi T_{wg}^3}(1 - 2\sqrt{3})} \end{bmatrix} N \quad (14.105)$$

It is interesting that, in both equations (14.98) and (14.105), the terms in the input vector are multiplied by the gust intensity σ_{ug} and σ_{wg} , respectively. Since the white noise input has an rms intensity of $\sigma_N = 1.0$, the rms magnitude of the filter output response is simply scaled by σ_{ug} or σ_{wg} , respectively.

The incorporation of gust filters for the lateral velocity component v_g and the rotational gust velocity components, p_g , q_g , and r_g into the aircraft equations of motion follows a similar mathematical procedure.

EXAMPLE 14.3

To illustrate the computation of longitudinal aircraft response to normal turbulence velocity w_g , derivative and other data for the Lockheed F-104A Starfighter corresponding to an approach flight condition were obtained from [Heffley and Jewell \(1972\)](#). Since the derivative data are referred to body axes, they were converted to a wind axes reference using the relationships given in Appendix 9, Tables A9.1 and A9.3. The data as given apply to sea level conditions, but it was decided to evaluate the turbulence response at $h = 500$ ft and at the given approach velocity $V_0 = 287$ ft/s, it being assumed that the error due to altitude difference would be small. The longitudinal equations of motion (14.13), including the turbulence input terms, apply:

$$\dot{\mathbf{x}} = \mathbf{Ax} + \mathbf{Bu} + \mathbf{Eu}_g$$

Thus, in terms of concise derivative data and including only the single turbulence input variable, the longitudinal state equation describing the unaugmented aircraft is given by

$$\begin{bmatrix} \dot{u} \\ \dot{w} \\ \dot{q} \\ \dot{\theta} \end{bmatrix} = \begin{bmatrix} -0.08078 & 0.04174 & 0 & -32.2 \\ -0.22536 & -0.56292 & 287 & 0 \\ 4.2872e-5 & -7.155e-3 & -0.40416 & 0 \\ 0 & 0 & 1 & 0 \end{bmatrix} \begin{bmatrix} u \\ w \\ q \\ \theta \end{bmatrix} + \begin{bmatrix} -0.10663 \\ -29.724 \\ -4.781 \\ 0 \end{bmatrix} \delta_s + \begin{bmatrix} -0.04174 \\ 0.56292 \\ 7.1550e-3 \\ 0 \end{bmatrix} w_g \quad (14.106)$$

It must be remembered that American imperial units apply throughout. To evaluate the stability and control properties of the basic airframe, the turbulence input is set at $w_g = 0$ and the transfer functions describing response to control are obtained by solving [equation \(14.106\)](#) in the usual way to give

$$\begin{aligned} \frac{u(s)}{\delta_s(s)} &= \frac{-0.1066(s + 0.8184)(s - 24.99)(s + 36.6)}{(s^2 + 0.073 s + 0.0232)(s^2 + 0.801 s + 2.274)} \frac{\text{ft/s}}{\text{rad}} \\ \frac{w(s)}{\delta_s(s)} &= \frac{-29.72(s^2 + 0.0802 s + 0.0251)(s + 46.57)}{(s^2 + 0.073 s + 0.0232)(s^2 + 0.801 s + 2.274)} \frac{\text{ft/s}}{\text{rad}} \\ \frac{q(s)}{\delta_s(s)} &= \frac{-4.799 s(s + 0.1036)(s + 0.4937)}{(s^2 + 0.073 s + 0.0232)(s^2 + 0.801 s + 2.274)} \frac{1/\text{s}}{} \\ \frac{\theta(s)}{\delta_s(s)} &= \frac{-4.799(s + 0.1036)(s + 0.4937)}{(s^2 + 0.073 s + 0.0232)(s^2 + 0.801 s + 2.274)} \end{aligned} \quad (14.107)$$

Inspection of the characteristic polynomial, the common denominator of transfer functions (14.107), reveals the basic airframe stability properties:

Phugoid mode: damping ratio $\zeta_p = 0.24$; frequency $\omega_p = 0.15 \text{ rad/s}$

Short-period pitching mode: Damping ratio $\zeta_s = 0.27$; frequency $\omega_s = 1.51 \text{ rad/s}$

The stability and control properties of the basic airframe are quite typical of a combat aircraft of the period and show a stable airframe with an unacceptably low value of pitch damping. The aircraft is fitted with a pitch autostabilisation system, but no information about the system is provided in the reference. Thus, before proceeding with the investigation of turbulence response, it is first necessary to augment the longitudinal stability to an acceptable level by raising the pitch damping. For the purpose of this example, pitch rate feedback to elevator was chosen to raise the pitch damping to approximately $\zeta_s = 0.7$. With the aid of a root locus plot using the transfer function $q(s)/\delta_s(s)$ from transfer functions (14.107), a suitable feedback gain was found to be $K_q = -0.35 \text{ rad/rad/s}$. Thus, with reference to equation (14.19), the feedback gain matrix is

$$\mathbf{K} = [K_u \ K_w \ K_q \ K_\theta] = [0 \ 0 \ -0.35 \ 0] \quad (14.108)$$

With the pitch rate feedback loop closed, the aircraft equations of motion (14.106) become

$$\dot{\mathbf{x}} = [\mathbf{A} - \mathbf{B}\mathbf{K}]\mathbf{x} + \mathbf{B}\mathbf{v} + \mathbf{E}\mathbf{u}_g$$

where now the control input vector \mathbf{v} becomes elevator demand, denoted δ_d . The closed-loop state equation for the aircraft becomes

$$\begin{bmatrix} \dot{u} \\ \dot{w} \\ \dot{q} \\ \dot{\theta} \end{bmatrix} = \begin{bmatrix} -0.08078 & 0.04174 & -0.03732 & -32.2 \\ -0.22536 & -0.56292 & 276.5966 & 0 \\ 4.2872e-5 & -7.155e-3 & -2.0775 & 0 \\ 0 & 0 & 1 & 0 \end{bmatrix} \begin{bmatrix} u \\ w \\ q \\ \theta \end{bmatrix} + \begin{bmatrix} -0.10663 \\ -29.724 \\ -4.781 \\ 0 \end{bmatrix} \delta_d + \begin{bmatrix} -0.04174 \\ 0.56292 \\ 7.1550e-3 \\ 0 \end{bmatrix} w_g \quad (14.109)$$

The closed-loop stability properties of the aircraft may be confirmed on inspection of the characteristic polynomial obtained in the solution of equations (14.109):

$$\Delta(s) = (s^2 + 0.07297 s + .01667)(s^2 + 11.585 s + 3.161) = 0 \quad (14.110)$$

and

Phugoid mode: damping ratio $\zeta_p = 0.28$; frequency $\omega_p = 0.13 \text{ rad/s}$

Short-period pitching mode: damping ratio $\zeta_s = 0.75$; frequency $\omega_s = 1.78 \text{ rad/s}$

For turbulence response assessment, the equations of motion are required in the formulation of equations (14.22), and this may be achieved by assuming controls-fixed, $\delta_d = 0$, by augmenting equation (14.109) to include the additional height variable h and by assembling the output equation to include both normal acceleration a_z and normal load factor n_z referred to the cg .

The mathematical steps required to complete this development are illustrated in Example 14.1. Accordingly, the state model may be written as

$$\begin{bmatrix} \dot{u} \\ \dot{w} \\ \dot{q} \\ \dot{\theta} \\ \dot{h} \end{bmatrix} = \begin{bmatrix} -0.08078 & 0.04174 & -0.03732 & -32.2 & 0 \\ -0.22536 & -0.56292 & 276.5966 & 0 & 0 \\ 4.2872e-5 & -7.155e-3 & -2.0775 & 0 & 0 \\ 0 & 0 & 1 & 0 & 0 \\ 0 & -1 & 0 & 287 & 0 \end{bmatrix} \begin{bmatrix} u \\ w \\ q \\ \theta \\ h \end{bmatrix} + \begin{bmatrix} -0.04174 \\ 0.56292 \\ 7.155e-3 \\ 0 \\ 0 \end{bmatrix} w_g$$

$$\begin{bmatrix} u \\ w \\ q \\ \theta \\ h \\ a_z \\ n_z \end{bmatrix} = \begin{bmatrix} 1 & 0 & 0 & 0 & 0 \\ 0 & 1 & 0 & 0 & 0 \\ 0 & 0 & 1 & 0 & 0 \\ 0 & 0 & 0 & 1 & 0 \\ 0 & 0 & 0 & 0 & 1 \\ -0.22536 & -0.56292 & -10.4034 & 0 & 0 \\ 6.999e-3 & 0.017482 & 0.32309 & 0 & 0 \end{bmatrix} \begin{bmatrix} u \\ w \\ q \\ \theta \\ h \\ a_z \\ n_z \end{bmatrix} + \begin{bmatrix} 0 \\ 0 \\ 0 \\ 0 \\ 0 \\ 0.56292 \\ -0.017482 \end{bmatrix} w_g \quad (14.111)$$

The next task is to define the state description of the appropriate white noise filter to produce normal velocity turbulence w_g as defined by [equations \(14.77\), \(14.78\), and \(14.104\)](#). With reference to [Section 14.5.4](#), the turbulence scale length is given by $\mathcal{L}_w = h = 500$ ft and the aircraft velocity is $V_0 = 287$ ft/s; whence

$$K_{wg} = \sigma_{wg} \sqrt{\frac{\mathcal{L}_w}{\pi V_0}} = 0.7446 \sigma_{wg}$$

$$T_{wg} = \frac{\mathcal{L}_w}{V_0} = 1.7422 \text{ s}$$

Let the rms turbulence intensity be $\sigma_{wg} = 1.0$ ft/s; then the filter transfer function as defined by [equation \(14.69\)](#) is

$$\frac{w_g(s)}{N(s)} = \frac{0.7446(1 + 3.0175 s)}{(1 + 1.74222 s)^2} \quad (14.112)$$

which has the time domain state description, described by [equation \(14.104\)](#),

$$\begin{bmatrix} \dot{w}_g \\ \dot{v} \end{bmatrix} = \begin{bmatrix} 0 & 1 \\ -0.32946 & -1.14797 \end{bmatrix} \begin{bmatrix} w_g \\ v \end{bmatrix} + \begin{bmatrix} 0.74024 \\ -0.6045 \end{bmatrix} N \quad (14.113)$$

where v is the dummy variable defined in [equation \(14.102\)](#). To complete the mathematical model building, it remains to augment the aircraft equations of motion (14.111) to include the

turbulence filter state [equation \(14.113\)](#), which results in the following state and output equations:

$$\begin{bmatrix} \dot{u} \\ \dot{w} \\ \dot{q} \\ \dot{\theta} \\ \dot{h} \\ \dot{w}_g \\ \dot{v} \end{bmatrix} = \begin{bmatrix} -0.08078 & 0.04174 & -0.03732 & -32.2 & 0 & -0.04174 & 0 \\ -0.22536 & -0.56292 & 276.5966 & 0 & 0 & 0.56292 & 0 \\ 4.2872e-5 & -7.155e-3 & -2.0775 & 0 & 0 & 7.155e-3 & 0 \\ 0 & 0 & 1 & 0 & 0 & 0 & 0 \\ 0 & -1 & 0 & 287 & 0 & 0 & 0 \\ 0 & 0 & 0 & 0 & 0 & 0 & 1 \\ 0 & 0 & 0 & 0 & 0 & -0.32946 & -1.14797 \end{bmatrix}$$

$$\times \begin{bmatrix} u \\ w \\ q \\ \theta \\ h \\ w_g \\ v \end{bmatrix} + \begin{bmatrix} 0 \\ 0 \\ 0 \\ 0 \\ 0 \\ 0.74024 \\ -0.6045 \end{bmatrix} N \quad (14.114)$$

$$\begin{bmatrix} u \\ w \\ q \\ \theta \\ h \\ a_z \\ n_z \\ w_g \\ v \end{bmatrix} = \begin{bmatrix} 1 & 0 & 0 & 0 & 0 & 0 & 0 \\ 0 & 1 & 0 & 0 & 0 & 0 & 0 \\ 0 & 0 & 1 & 0 & 0 & 0 & 0 \\ 0 & 0 & 0 & 1 & 0 & 0 & 0 \\ 0 & 0 & 0 & 0 & 1 & 0 & 0 \\ -0.22536 & -0.56292 & -10.4034 & 0 & 0 & 0.56292 & 0 \\ 0.6998e-3 & 0.017482 & 0.323087 & 0 & 0 & -0.017482 & 0 \\ 0 & 0 & 0 & 0 & 0 & 1 & 0 \\ 0 & 0 & 0 & 0 & 0 & 0 & 1 \end{bmatrix}$$

$$\times \begin{bmatrix} u \\ w \\ q \\ \theta \\ h \\ w_g \\ v \end{bmatrix} + \begin{bmatrix} 0 \\ 0 \\ 0 \\ 0 \\ 0 \\ 0 \\ 0 \end{bmatrix} N$$

Solution of [equations \(14.114\)](#) produces the transfer functions describing the aircraft response to filtered white noise when the rms turbulence intensity $\sigma_{wg} = 1.0$ ft/s. Transfer functions of immediate interest are

$$\frac{w(s)}{N(s)} = \frac{0.4167 s(s^2 + 0.08364 s + 0.0167)(s + 0.3313)(s + 5.607)}{s(s^2 + 0.06522 s + 0.01667)(s + 0.574)^2(s^2 + 2.648 s + 3.1613)} \quad (14.115)$$

$$\frac{w_g(s)}{N(s)} = \frac{0.7402(s + 0.3313)}{(s + 0.574)^2} \quad (14.116)$$

$$\frac{n_z(s)}{N(s)} = \frac{-0.01294 s^2(s^2 + 0.0733 s + 0.04752)(s + 0.3313)(s + 1.969)}{s(s^2 + 0.06522 s + 0.01667)(s + 0.574)^2(s^2 + 2.648 s + 3.1613)} \text{ 1/s} \quad (14.117)$$

The statistical properties of the response are quantified by the rms intensity σ for the turbulence input w_g of rms intensity σ_{wg} . Since the noise filter assumes an input rms intensity of $\sigma_{wg} = 1.0 \text{ ft/s}$, the actual magnitude of the input turbulence intensity simply behaves as a scaling factor acting on the response transfer function of interest. The response turbulence intensity may therefore be calculated directly from the response transfer functions by calculating their variance σ^2 , which is easily done using the statistical tools in MATLAB or Program CC.

Since, in accordance with the flying qualities requirements, the PSD of the input is assumed to have *cyclic frequency* dependency, the computed value of output variance must be factored by π as explained in Section 14.7.1. Accordingly, the computed variance of transfer function (14.115) is

$$\sigma_w^2 = 0.70435 \text{ ft}^2/\text{s}^2 \quad (14.118)$$

Whence rms output intensity per unit input intensity σ_{wg} is given by

$$\sigma_w = 0.8393 \text{ ft/s}$$

So, for example, a normal turbulence velocity disturbance of 15 ft/s intensity results in the aircraft normal rms velocity response intensity of 12.59 ft/s. This represents a modest attenuation much as might be expected from the F-104A at low speed on final approach to landing.

Consider now the filter transfer function (14.116) obtained in the general solution of [equations \(14.114\)](#). In the evaluation of the filter gain K_{wg} , output intensity was set at $\sigma_{wg} = 1.0 \text{ ft/s}$; also, since the white noise input N has intensity $\sigma_N = 1.0$, the output variance is also unity. Calculation of the output variance of the filter transfer function (14.116) using either MATLAB or Program CC, when correctly factored by π , gives

$$\begin{aligned} \sigma_{wg}^2 &= 0.318194\pi = 0.999636 \text{ ft}^2/\text{s}^2 \\ \sigma_{wg} &= 0.9998 \text{ ft/s} \end{aligned} \quad (14.119)$$

Note that the variance σ_{wg}^2 , and hence rms intensity σ_{wg} , is not exactly 1.0 since the limit of the numerical integration is not infinite but a suitably large number.

The computational tools available for the evaluation of the statistical properties of entire systems are extremely capable and versatile. In the present context the output variances of the example system defined by the state and output [equations \(14.114\)](#) may be evaluated simultaneously to give the row vector of variances:

$$\boldsymbol{\sigma}^2 = [\sigma_u^2 \quad \sigma_w^2 \quad \sigma_q^2 \quad \sigma_\theta^2 \quad \sigma_h^2 \quad \sigma_{az}^2 \quad \sigma_{nz}^2 \quad \sigma_{wg}^2 \quad \sigma_v^2]$$

Including the factor π , the numerical values of the variances are

$$\sigma^2 = [0.06281 \ 0.704355 \ 2.9634e-6 \ 4.491e-6 \ -6.624303e15 \ 0.156638 \ 1.5107e-4 \ 0.999636 \ 0.747037] \quad (14.120)$$

Thus the output variance of greatest interest in the present context is that for normal load factor response as defined by the transfer function (14.117). From [equation \(14.120\)](#),

$$\begin{aligned} \sigma_{nz}^2 &= 1.510727e-4 \\ \sigma_{nz} &= 0.0123 \frac{g}{ft/s} \end{aligned} \quad (14.121)$$

From MIL-F-8785C, severe rms turbulence intensity at 500 ft is approximately $10 \sim 15$ ft/s, which results in a rms normal load factor response of $0.123 \sim 0.185$ g. Again, this would seem reasonable for the F-104A on a low-speed approach to landing.

EXAMPLE 14.4

It is also instructive to review the magnitude of the aircraft frequency response to turbulence to gain an appreciation of the response spectrum and the degree of attenuation. This is most easily achieved using the reduced-order equations of motion. It is known that output attenuation increases with frequency beyond the natural bandwidth of the aircraft, and reduced-order modeling focuses on the short-period mode frequency region of the response spectrum. Since the degree of attenuation is determined in part by the system damping, the investigation of frequency response provides a means for interpreting the effectiveness of stability augmentation as a mechanism for improving ride quality.

Using the longitudinal model of the F-104A given in Example 14.3, the closed-loop state [equation in \(14.111\)](#) is reduced in order by removing the variables u , θ , and h . The output [equation in \(14.111\)](#) is also reduced in order to match, retaining only normal load factor n_z as an additional output variable. This reduces the system state-space description to a practical minimum format:

$$\begin{aligned} \begin{bmatrix} \dot{w} \\ \dot{q} \\ \dot{w}_g \\ \dot{v} \end{bmatrix} &= \begin{bmatrix} -0.56292 & 276.5966 & 0.56292 & 0 \\ -7.155e-3 & -2.077502 & 7.155e-3 & 0 \\ 0 & 0 & 0 & 1 \\ 0 & 0 & -0.32946 & -1.14797 \end{bmatrix} \begin{bmatrix} w \\ q \\ w_g \\ v \end{bmatrix} + \begin{bmatrix} 0 \\ 0 \\ 0.74024 \\ -0.6045 \end{bmatrix} N \\ \begin{bmatrix} w \\ q \\ w_g \\ v \\ n_z \end{bmatrix} &= \begin{bmatrix} 1 & 0 & 0 & 0 \\ 0 & 1 & 0 & 0 \\ 0 & 0 & 1 & 0 \\ 0 & 0 & 0 & 1 \\ 0.017482 & 0.323087 & -0.017482 & 0 \end{bmatrix} \begin{bmatrix} w \\ q \\ w_g \\ v \end{bmatrix} + \begin{bmatrix} 0 \\ 0 \\ 0 \\ 0 \\ 0 \end{bmatrix} N \end{aligned} \quad (14.122)$$

Equation (14.122) may be solved in the usual way to obtain the reduced order turbulence response transfer functions describing the response to white noise input N as follows:

$$\begin{aligned}\frac{w(s)}{N(s)} &= \frac{0.4167(s + 0.3313)(s + 5.593)}{(s + 0.574)^2(s^2 + 2.64 s + 3.147)} \\ \frac{q(s)}{N(s)} &= \frac{0.005296 s(s + 0.3313)}{(s + 0.574)^2(s^2 + 2.64 s + 3.147)} \frac{\text{rad/s}}{\text{ft/s}} \\ \frac{w_g(s)}{N(s)} &= \frac{0.7402(s + 0.3313)(s^2 + 2.64 s + 3.147)}{(s + 0.574)^2(s^2 + 2.64 s + 3.147)} = \frac{0.7402(s + 0.3313)}{(s + 0.574)^2} \\ \frac{v(s)}{N(s)} &= \frac{-0.6045(s + 0.4034)(s^2 + 2.64 s + 3.147)}{(s + 0.574)^2(s^2 + 2.64 s + 3.147)} = \frac{-0.6045(s + 0.4034)}{(s + 0.574)^2} \\ \frac{n_z(s)}{N(s)} &= \frac{-0.01294 s(s + 0.3313)(s + 1.945)}{(s + 0.574)^2(s^2 + 2.64 s + 3.147)} 1/\text{s}\end{aligned}\quad (14.123)$$

As before, w , q , and n_z describe aircraft response, and w_g and v describe the noise filter variables, where w_g is the effective aerodynamic input to the aircraft. Note also that the filter transfer functions simplify by cancellation to correctly represent the filter as originally defined in Example 14.3.

The frequency response of the reduced order system model (14.122) or of the individual transfer functions (14.123) can be obtained using MATLAB or Program CC; the magnitudes of the responses for the variables w_g , w , and n_z are shown in Fig. 14.10. The responses shown are essentially the Bode gain plots over a limited frequency range, chosen to reveal the high frequency properties of the reduced order model. When interpreting the responses, it is important to recall, from the characteristic polynomial of the transfer functions (14.123), that the short-period mode damping ratio is $\zeta_s = 0.744$, a relatively high value, and the frequency is $\omega_s = 1.774 \text{ rad/s}$. These short-period mode properties clearly influence the shapes of the aircraft response to turbulence, as shown in Fig. 14.10.

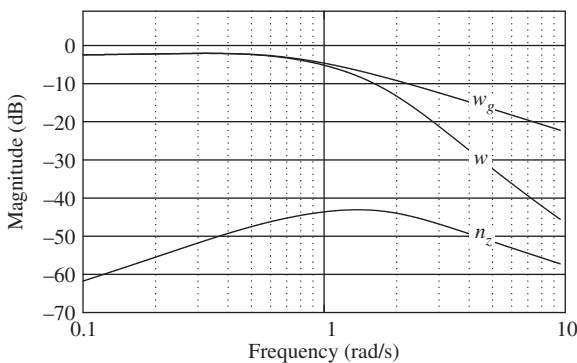


FIGURE 14.10 Longitudinal reduced-order frequency response of the Lockheed F104-A Starfighter for $\sigma_{wg} = 1 \text{ ft/s}$.

The output of the filter w_g , when $\sigma_{wg} = 1$ ft/s, shows that the magnitude starts to “roll off” at a frequency a little below 1.0 rad/s and is otherwise unremarkable. The normal velocity w response of the aircraft follows the turbulence at low frequency with no significant attenuation, much as might be expected. Since the break frequency corresponds with the short-period mode frequency 1.774 rad/s, and since the system damping is very high, $\zeta_s = 0.744$, there is no visible peak in the response and it then “rolls off” very rapidly as frequency increases. The normal load factor n_z response shows a very high level of attenuation with a peak close to the short-period mode frequency. Bearing in mind that the aircraft is flying very slowly on approach, acceleration response to both control and external disturbances is subdued. At low frequency the response to turbulence is sufficiently slow and sufficiently well damped such that normal acceleration is not very perceptible. It is entirely consistent with the flight physics that the peak response in normal acceleration is at a frequency near the short-period mode, but as the mode damping is very high the response remains well attenuated. At higher frequency the magnitude of the normal load factor response “rolls off” much as expected.

The variances of the system variables in equations (14.122) were computed as described in Example 14.3 to give

$$\begin{aligned}\boldsymbol{\sigma}^2 &= [\sigma_w^2 \quad \sigma_q^2 \quad \sigma_{wg}^2 \quad \sigma_v^2 \quad \sigma_{nz}^2] \\ &= [0.6864063 \quad 2.856818e-6 \quad 0.9996355 \quad 0.7470366 \quad 1.541607e-4]\end{aligned}\quad (14.124)$$

These values compare well with those for the full-order system model in equation (14.120) and, correctly, the output variance of the turbulence filter is exactly the same.

The variance of normal load factor response, as defined by the reduced-order transfer function in (14.123), is given by the last term in the vector (14.124):

$$\begin{aligned}\sigma_{nz}^2 &= 1.541607e-4 \\ \sigma_{nz} &= 0.0123 \frac{g}{ft/s}\end{aligned}\quad (14.125)$$

Whence, as in Example 14.3, at height 500 ft, for severe rms turbulence intensity of approximately $10 \sim 15$ ft/s, it is confirmed that this results in a rms normal load factor response intensity of $0.123 \sim 0.185$ g.

References

- Department of Defense (1980). *Military specification: Flying qualities of piloted airplanes*. Washington, DC: Department of Defense, MIL-F-8785C.
- Department of Defense (1987). *Military standard: Flying qualities of piloted airplanes*. Washington, DC: Department of Defense, MIL-STD-1797A (USAF).
- Gage, S. (2003). Creating a unified graphical wind turbulence model from multiple specifications. AIAA paper 2003-5529, *AIAA modeling and simulation technologies conference*, Austin, Texas.
- Heffley, R. K., & Jewell, W. F. (1972). *Aircraft handling qualities data*. Washington, DC: National Aeronautics and Space Administration, NASA Contractor Report, NASA CR-2144.
- Hoh, R. H., Mitchell, D. G., Ashkenas, I. L., Klein, R. H., Heffley, R. K., & Hodgkinson, J. (1982). *Proposed MIL standard and handbook: Flying qualities of air vehicles, Vol. 2: Proposed MIL handbook*. Wright-Patterson AFB, OH: Air Force Wright Aeronautical Laboratory, Technical Report AFWAL-TR-82-3081.

- Jones, J. G. (1973). *Statistical discrete gust theory for aircraft loads: a progress report*. RAE Technical Report 73167, Royal Aircraft Establishment, Farnborough, Hampshire.
- Ministry of Defence (2011). *Design and airworthiness requirements for service aircraft*. London: Ministry of Defence, Defence Standard 00-970/Issue 7, Part 1: *Fixed Wing*, Section 2: *Flight*.
- Teper, G. L. (1969). *Aircraft stability and control data*. Hawthorne, CA: Systems Technology, Inc., STI Technical Report 176-1.
- Thomasson, P. G. (2000). Equations of motion of a vehicle in a moving fluid. *AIAA Journal of Aircraft*, 37(4), 630–639.

Coursework Studies

15

15.1 Introduction

A number of coursework studies, or assignments, have been prepared for assessing the understanding and ability of graduate students to apply the material to protracted exercises. These are intended to reflect real-world practice. The five exercises included in this chapter are typical of the basic evaluations that are undertaken routinely in a professional flight dynamics environment and require the application of much of the material in this book. Further, since the aircraft models are of real aircraft the interested reader may easily expand the scope of the exercises by obtaining additional information and data from the source references. The exercises provide an opportunity for students to develop competence in the essential enabling skills relevant to the areas of flight control, flight dynamics, and flight test.

The notational style, theoretical background, and other information has been edited such that it is generally consistent with the material in this book, as far as that is possible. However, care should be taken with units, as both SI and American imperial units are used—again reflecting a relatively common situation in industry.

15.1.1 Working the assignments

Each assignment requires a mix of hand calculation, computational analysis, and graph plotting. Any convenient computational tools may be used, but they should be identified in the report. The use of MATLAB, Program CC, or similar is essential for these assignments; MS Excel may also be found useful for some data manipulation. Each assignment is structured as a set of tasks which should be undertaken sequentially to achieve satisfactory completion of the exercise. To provide experience in the solution process, the tasks are set out in the order in which they must be completed since, in most cases, each task builds on the output of the previous task. Clearly it is therefore most important that the solution process be undertaken in an orderly way and that the results of each task be assessed for correctness and validity before moving on to the next task.

15.1.2 Reporting

Plan and write a short report to summarise and present the results of each assignment and note that accurate presentation of results is important. For example, strip chart plots provide the most convenient illustration format for time history responses. Care should be exercised to show and explain the steps undertaken in working the assignment since the overall objective is to assess understanding, not the ability to simply process sequential calculations using tools like MATLAB or similar software. Supporting material and calculations may be included in appendices, but undocumented computer printout is generally unacceptable.

15.2 Assignment 1: Stability augmentation of the North American X-15 hypersonic research aeroplane

(CU 2011)

The North American X-15 ([Heffley and Jewell, 1972](#)) was a hypersonic research aeroplane which first flew in 1960. This rocket-powered aeroplane was capable of speeds as high as Mach 6 at up to 300,000 ft altitude. The aeroplane was carried under a B-52 to an altitude of about 45,000 ft, from which it was launched at a speed of about Mach 0.8. Following the powered phase of flight, recovery entailed gliding flight to a normal landing—much in the same way as the space shuttle recovery.

The first objective of the assignment is to review the stability and control properties of the aircraft for one typical flight condition. Since the aircraft was fitted with damping augmentation in each axis, the second objective is to design a simple damping augmentation control law for each control axis and to show the improvement in response thereby achieved.

15.2.1 The aircraft model

The aircraft equations of motion are given in the form of the decoupled state equations as follows. The flight condition assumed corresponds with Mach 2.0 at an altitude of 60,000 ft.

The longitudinal state equation is

$$\begin{bmatrix} \dot{u} \\ \dot{w} \\ \dot{q} \\ \dot{\theta} \end{bmatrix} = \begin{bmatrix} -0.00871 & -0.019 & -135 & -32.12 \\ -0.0117 & -0.311 & 1931 & -2.246 \\ 0.000471 & -0.00673 & -0.182 & 0 \\ 0 & 0 & 1 & 0 \end{bmatrix} \begin{bmatrix} u \\ w \\ q \\ \theta \end{bmatrix} + \begin{bmatrix} 6.24 \\ -89.2 \\ -9.80 \\ 0 \end{bmatrix} \delta_e$$

The lateral-directional state equation is

$$\begin{bmatrix} \dot{\beta} \\ \dot{p} \\ \dot{r} \\ \dot{\phi} \end{bmatrix} = \begin{bmatrix} -0.127 & 0.0698 & -0.998 & 0.01659 \\ -2.36 & -1.02 & 0.103 & 0 \\ 11.1 & -0.00735 & -0.196 & 0 \\ 0 & 1 & 0 & 0 \end{bmatrix} \begin{bmatrix} \beta \\ p \\ r \\ \phi \end{bmatrix} + \begin{bmatrix} -0.00498 & 0.0426 \\ 28.7 & 5.38 \\ 0.993 & -6.90 \\ 0 & 0 \end{bmatrix} \begin{bmatrix} \delta_a \\ \delta_r \end{bmatrix}$$

Velocities are given in ft/s, angular velocities in rad/s, and angles in rad ($g = 32.2 \text{ ft/s}^2$).

15.2.2 The solution tasks

- (1) Set up the longitudinal output equation to include the additional variables angle of attack α and flight path angle γ . Solve the longitudinal equations of motion and obtain a full set of properly annotated transfer functions.
- (2) Review the longitudinal stability properties of the aeroplane and produce response time histories to best illustrate the longitudinal stability modes. Comment on the likely requirement for stability augmentation.
- (3) Set up the lateral-directional output equation, solve the lateral-directional equations of motion, and obtain a full set of properly annotated transfer functions.

- (4) Review the lateral-directional stability properties of the aeroplane and produce response time histories to best illustrate the lateral-directional stability modes. Comment on the likely requirement for stability augmentation.
- (5) With the aid of an appropriate root locus plot for each control axis, design three simple damping augmentation control laws. Clearly state the design decisions and the expected change to the stability modes. The root locus plots should be annotated appropriately for this purpose.
- (6) Augment the open-loop longitudinal state equation to include the control law, thereby creating the closed-loop state equation. Solve the closed-loop equations of motion and obtain a full set of properly annotated transfer functions.
- (7) Augment the open-loop lateral-directional state equation to include the control laws, thereby creating the closed-loop state equation. Solve the closed-loop equations of motion and obtain a full set of properly annotated transfer functions.
- (8) Compare the longitudinal closed-loop stability modes with those of the basic airframe and produce time histories to best illustrate the improvements to the response properties of the aeroplane.
- (9) Compare the lateral-directional closed-loop stability modes with those of the basic airframe and produce time histories to best illustrate the improvements to the response properties of the aeroplane.
- (10) Summarise the flight control system design and state the main changes seen in the augmented aeroplane. Draw simple block diagrams to illustrate the structure of the stability augmentation system.

15.3 Assignment 2: The stability and control characteristics of a civil transport aeroplane with relaxed longitudinal static stability

(CU 2001)(CU 2002)

The increasing use of fly-by-wire flight control systems in advanced civil transport aeroplanes has encouraged designers to consider seriously the advantages of relaxing the longitudinal controls-fixed static stability of the airframe. However, not all of the changes to the flying qualities of the aircraft with relaxed static stability (RSS) are beneficial, and some degree of design compromise is inevitable. The purpose of this assignment is to demonstrate by example typical changes to a conventional civil transport aeroplane following relaxation of its controls-fixed longitudinal stability margin. The implications for flight control system design are not considered.

15.3.1 The aircraft model

The Convair CV-880 was a 130-passenger, four-engined civil transport aeroplane which first flew in 1960. It was very similar in layout to most other jet transport aeroplanes of the time and had very benign stability and control characteristics. Flying controls were entirely mechanical and comprised servo tab deflected ailerons, elevator, and rudder, together with power operated spoilers for additional lateral-directional control. The aircraft does not appear to have been fitted with any kind of automatic stabilisation system. Data for this exercise was obtained, or derived, from

that given by Heffley and Jewell (1972) and is reasonably accurate, as far as can be ascertained. The data should be read in the context of the longitudinal geometry of the CV-880 shown in Fig. 15.1. A typical level flight cruise condition has been selected for this exercise defined by the following parameters:

Free-stream Mach number	M_0	0.8
Free-stream velocity	V_0	779 ft/s
Dynamic pressure	$Q = \frac{1}{2} \rho V_0^2$	224 Lb/ft ²
Altitude	h	35,000 ft
Air density	ρ	0.000738 slug/ft ³
Body trim incidence	α_e	4.7 deg

Aircraft geometric, weight, and *cg* information are given as follows:

Weight	W	155,000	Lb
Mass	m	4814	slug
Moment of inertia in pitch	I_y	251,0000	slugft ²
Mean geometric chord (<i>mgc</i>)	\bar{c}	18.94	ft
Wing area	S_w	2000	ft ²
Wing span	b	120	ft
Tailplane area	S_T	400	ft ²
Tail moment arm	l_T	57	ft
Tailplane trim angle	η_T	-3.0	deg
<i>cg</i> position (referenced to <i>mgc</i>)	h	0.25	
Wing-body aerodynamic centre position (referenced to <i>mgc</i>)	h_0	0.09	
Thrust line inclination wrt HFD	i	3	deg
Thrust moment arm about <i>cg</i>	l_{tr}	2	ft

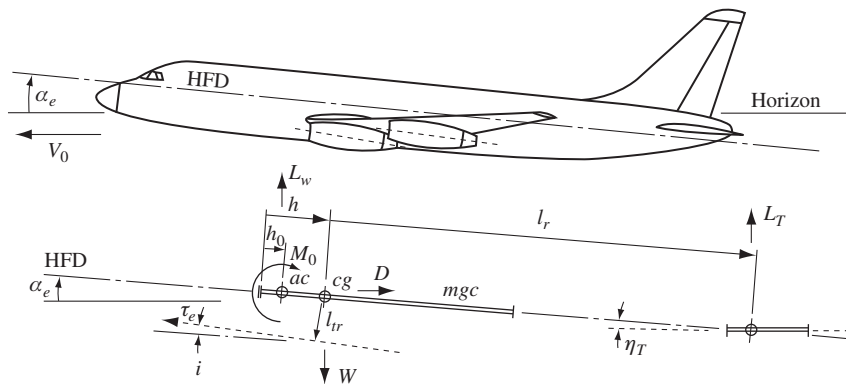


FIGURE 15.1 Longitudinal geometry of the Convair CV-880.

Note that the reference chord given is the mean geometric chord (*mgc*) rather than the more usual mean aerodynamic chord (*mac*), and it may be used in the same way in the calculations. The aircraft is fitted with an all-moving tailplane for trim, and its trim angle is equivalent to the tailplane setting angle of a fixed tailplane. The longitudinal geometric reference is the horizontal fuselage datum (HFD).

Relevant aerodynamic characteristics at the operating flight condition are as follows:

Total drag coefficient	C_D	0.024
Wing-body aerodynamic pitching moment coefficient	C_{m_0}	-0.1
Wing lift curve slope	a	4.8 rad^{-1}
Tailplane lift curve slope	a_1	3.75 rad^{-1}
Elevator lift curve slope	a_2	0.95 rad^{-1}
Wing downwash at tail	$d\varepsilon/d\alpha$	0.37

The dimensionless longitudinal aerodynamic stability and control derivatives referred to aircraft wind axes for the flight condition of interest are given as follows:

X_u	-0.0485	Z_q	-3.7091
Z_u	-0.6978	$M_{\dot{w}}$	-2.2387
M_u	-0.0055	M_q	-5.9983
X_w	0.1920		
Z_w	-4.8210	X_η	-0.0001
M_w	-0.6492	Z_η	-0.1456
$Z_{\dot{w}}$	-1.3543	M_η	-0.4408

15.3.2 The governing trim equations

Lift forces: $L_{total} = L_w + L_T + \tau \sin(i + \alpha_e) = W$

Drag forces: $D = \tau \cos(i + \alpha_e)$

Pitching moment about cg: $M = M_0 + L_w(h - h_0)\bar{c}\cos\alpha_e + D(h - h_0)\bar{c}\sin\alpha_e + \tau l_{tr} - L_T l_T$

Tailplane lift coefficient, assuming a symmetric aerofoil section: $C_{L_T} = a_1(\alpha_T + \eta_T) + a_2\eta$

Tailplane angle of attack: $\alpha_T = \frac{C_{L_w}}{a} \left(1 - \frac{d\varepsilon}{d\alpha}\right)$

15.3.3 Basic aircraft stability and control analysis

Working with the equations in coefficient form, obtain values for the following:

Trim wing-body lift coefficient: C_{L_w}

Trim tailplane lift coefficient: C_{L_T}

Trim elevator angle: η

Controls-fixed neutral point: h_n

Controls-fixed static margin: K_n

What tailplane trim angle η_T would be required to enable the elevator trim angle to be set at zero?

Set up and solve the equations of motion referred to wind axes and obtain values for the stability modes characteristics. By applying the final value theorem to each of the control transfer functions, assuming a unit step input, obtain estimates for the steady-state control sensitivity of the aircraft.

15.3.4 Relaxing the stability of the aircraft

The longitudinal static stability of the aircraft is now relaxed by shifting the cg aft by 12% of the mgc . In practice this would also be accompanied by design changes to the aerodynamic configuration of the aircraft, especially of the tail geometry. However, for the purpose of this exercise, the aerodynamic properties of the aeroplane are assumed to remain unchanged.

Clearly, this change will modify the trim state and it will also modify those aerodynamic stability and control derivatives which have a dependency on tail volume ratio and tail moment arm. Calculate a new value for tail volume ratio and tail moment arm, and calculate new values for those derivatives affected by the aft shift in cg position.

15.3.5 Relaxed stability aircraft stability and control analysis

Repeat the computational stability and control exercise for the relaxed-stability aircraft to obtain new values for all of the variables defining the stability and control characteristics at the same flight condition.

15.3.6 Evaluation of results

Tabulate the results of the analyses to facilitate comparison of the unmodified aircraft stability and control characteristics with those of the relaxed-stability aircraft. Summarise the observations with particular reference to the advantages and disadvantages of relaxing the stability of a civil transport aircraft. Comment also on the obvious limitations of this exercise and the validity of the estimated variable changes.

15.3.7 Postscript

Do not expect to see dramatic changes in the stability and control characteristics of the aircraft following relaxation of stability by shifting the cg aft.

15.4 Assignment 3: Lateral-directional handling qualities design for the Lockheed F-104 Starfighter aircraft

(CU 2011)

The lateral-directional flying qualities of the Lockheed F-104 aircraft are typical of many high-performance aircraft. The airframe is not very stable, and its stability and control characteristics vary considerably with flight condition. Consequently, it is necessary to augment the stability

and control characteristics by means of a flight control system. Since the airframe properties vary with flight condition, it is necessary to vary, or schedule, the control system gains with flight condition in order to achieve reasonably even handling qualities over the flight envelope.

The objective of the assignment is to evaluate the lateral-directional stability and control characteristics of the F-104 at three representative Mach numbers at sea level only. With an understanding of the basic unaugmented airframe, the task is then to design a simple command and stability augmentation system to give the aircraft acceptable roll handling characteristics over the Mach number range. This will require proposing suitably simple schedules for the flight control system gains.

15.4.1 The aircraft model

The Lockheed F-104 Starfighter aircraft is a small single-engined combat aircraft which first flew in the mid-1950s. The aircraft was supplied to many air forces around the world and remained in service well into the 1970s, and during its service life many variants were developed. The aircraft configuration is typical of the time: a long slender fuselage, low-aspect-ratio unswept wing, and a T tail mounted on a relatively small fin. The airframe is nominally stable at all flight conditions, although the degree of stability is generally unacceptably low. The flying controls are entirely mechanical with a simple three-axis stability augmentation system. The aircraft is capable of a little over Mach 1.0 at sea level and as much as Mach 2.0 at high altitude. Data for this exercise were obtained from [Heffley and Jewell \(1972\)](#) and is reasonably accurate, as far as is known.

Note that American imperial units are implied throughout and should be retained in this work. The American sign convention for aileron and rudder control is the reverse of that defined in this book.

The Laplace transform of the lateral-directional equations of motion, referred to a body axis system, is given in the following format:

$$\begin{bmatrix} 1 - y_v & -\frac{W_e s + g \cos \theta_e}{V_e} & \frac{U_e s - g \sin \theta_e}{V_e s} \\ -l_\beta & s(s - l_p) & -l_r \\ -n_\beta & -n_p s & s - n_r \end{bmatrix} \begin{bmatrix} \beta(s) \\ p(s)/s \\ r(s) \end{bmatrix} = \begin{bmatrix} y_\xi & y_\zeta \\ l_\xi & l_\zeta \\ n_\xi & n_\zeta \end{bmatrix} \begin{bmatrix} \xi(s) \\ \zeta(s) \end{bmatrix}$$

with auxiliary equations

$$v(s) = V_e \beta(s)$$

$$\phi(s) = \frac{p(s)}{s} + \frac{r(s)}{s} \tan \theta_e$$

$$\psi(s) = \frac{1}{\cos \theta_e} \frac{r(s)}{s}$$

Note that the derivatives are concise derivatives; they have dimensions and are equivalent to the usual dimensional derivatives divided by mass or inertia terms as appropriate.

Numerical data for the three sea-level flight conditions are given in the following table.

Aerodynamic Data for the Lockheed F-104A Starfighter Aircraft					
Flight Condition	#		1	2	3
Trim Data					
Altitude	h	ft	0	0	0
Air density	ρ_0	slug/ft ³	0.00238	0.00238	0.00238
Speed of sound	a_0	ft/s	1116.44	1116.44	1116.44
Gravitational constant	g	ft/s ²	32.2	32.2	32.2
Trim Mach number	M_e		0.257	0.800	1.100
Trim attitude	θ_e	deg	2.30	2.00	1.00
Concise Derivative Data					
y_v		1/s	-0.178	-0.452	-0.791
l_β		1/s ²	-20.9	-146.0	-363.0
n_β		1/s ²	2.68	13.60	42.70
l_p		1/s	-1.38	-4.64	-7.12
n_p		1/s	-0.0993	-0.188	-0.341
l_r		1/s	1.16	3.67	7.17
n_r		1/s	-0.157	-0.498	-1.060
y_ξ		1/s	0	0	0
l_ξ		1/s ²	4.76	49.6	81.5
n_ξ		1/s ²	0.266	3.510	6.500
y_ζ		1/s	0.0317	0.0719	0.0621
l_ζ		1/s ²	5.35	41.50	57.60
n_ζ		1/s ²	-0.923	-7.070	-8.720

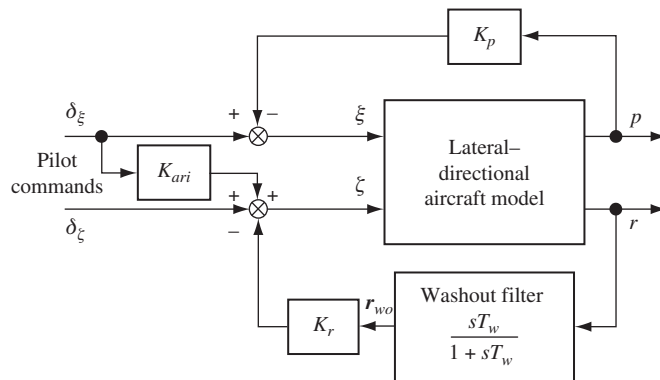
15.4.2 Lateral-directional autostabiliser structure

A typical lateral-directional autostabiliser structure is shown in Fig. 15.2 and is quite representative of the system fitted to the F-104. Note that it is simplified by removing sensor dynamics, artificial feel system dynamics, surface actuator dynamics, and various feedback signal filtering. The feedback gains K_p and K_r are chosen to augment the lateral-directional stability modes to acceptable levels of stability. The washout filter time constant T_w is chosen to give the aircraft acceptable steady turning performance. The *aileron-rudder interlink* gain K_{ari} is chosen to minimise adverse sideslip during the turn entry.

15.4.3 Basic aircraft stability and control analysis

(1) Derive the open-loop aircraft state equation, which should have the following form:

$$\dot{\mathbf{x}}(t) = \mathbf{Ax}(t) + \mathbf{Bu}(t)$$

**FIGURE 15.2 Simplified lateral-directional autostabiliser.**

where the state vector

$$\mathbf{x}(t)^T = [\beta(t) \quad p(t) \quad r(t) \quad \phi(t)]$$

and the input vector

$$\mathbf{u}(t)^T = [\xi(t) \quad \zeta(t)].$$

State clearly any assumptions made.

- (2) Obtain the response transfer functions from the solution of the state equation for the three flight conditions for which data are provided. Show the transfer functions in factorised form.
- (3) Obtain time history plots showing the response to a short pulse of aileron and a short pulse of rudder. The plots should be presented in strip chart form showing all four variables for a period of 10 seconds. The pulse lengths should be chosen to emphasize the dynamics of turn entry.
- (4) Comment on the stability modes characteristics and their variation over the flight envelope of interest, and identify any deficiencies needing improvement. Comment also on the turn performance of the aircraft and suggest how this might be improved. Remember that the pilot commands a turn using the aileron and only uses the rudder to “tidy” the turn entry.

15.4.4 Augmenting the stability of the aircraft

- (5) With the aid of the appropriate root locus plots, investigate the feedback gains, K_p and K_r , required to improve the stability modes characteristics for all three flight conditions. Ignore the washout filter at this stage. Aim to achieve the following closed-loop mode characteristics: roll mode time constant of less than one second, a stable spiral mode, and dutch roll damping $0.5 > \zeta_d > 0.3$. Explain why a roll rate feedback gain $K_p = 0$ is a good solution for the lateral axis at all three flight conditions.

- (6) It is typical to schedule feedback gains with dynamic pressure ($Q = \frac{1}{2}\rho V_0^2$), as shown in Fig. 15.3. Plot out the upper and lower limits of the values of K_r that meet the stability requirements for each flight condition as a function of Q . Hence design a gain schedule like that shown in Fig. 15.3. State the value of K_r for each flight condition according to your schedule and confirm that the values are consistent with your analysis of tasks (3) and (4). These are the values that you should use in your subsequent work.
- (7) With reference to Fig. 15.2, the autostabiliser control law may be written as

$$\mathbf{u}(t) = \mathbf{L}\mathbf{u}_1(t) - \mathbf{K}\mathbf{x}(t)$$

where

$$\mathbf{u}_1(t)^T = [\delta_\xi \quad \delta_\zeta]$$

is the vector of pilot commands,

$$\mathbf{L} = \begin{bmatrix} 1 & 0 \\ K_{ari} & 1 \end{bmatrix}$$

is the input mixing matrix, and \mathbf{K} is the matrix of feedback gains. Omitting the aileron-rudder interlink for the moment, $K_{ari} = 0$, write down the matrices \mathbf{K} and \mathbf{L} and calculate the closed-loop state equation for all three flight conditions,

$$\dot{\mathbf{x}}(t) = \mathbf{A}\mathbf{x}(t) + \mathbf{B}\mathbf{u}_1(t)$$

where now, of course, the matrices \mathbf{A} and \mathbf{B} are the closed-loop versions.

- (8) Obtain the response transfer functions from the solution of the closed-loop state equation developed in (7) for the three flight conditions for which data is provided. Show the transfer functions in factorised form.
- (9) Obtain time history plots showing the response to a short pulse of aileron and a short pulse of rudder. Again, the plots should be presented in strip chart form showing all four variables for a period of 10 seconds. The object here is to show and confirm the improvement in the basic airframe dynamics; the time histories also provide a “baseline” with which to compare the responses developed in the following sections.

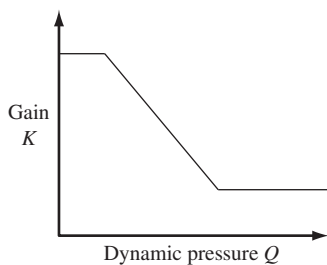


FIGURE 15.3 Typical gain schedule.

15.4.5 Inclusion of the washout filter in the model

- (10) Modify the open-loop aircraft state equation derived in (1) to include the additional state variable r_{wo} introduced by the filter, so that the state vector becomes

$$\mathbf{x}(t)^T = [\beta(t) \quad p(t) \quad r(t) \quad \phi(t) \quad r_{wo}(t)].$$

Set the washout filter time constant to the typical value of one second, $T_w = 1.0$ s. Obtain the open-loop state equation for each of the three flight conditions.

- (11) Modify the control law derived in (7) to include the additional washout filter state variable and calculate the closed-loop state equation for the three flight conditions. Take care to re-define the feedback matrix \mathbf{K} correctly and set the aileron-rudder interlink gain to zero as before.
- (12) Obtain the revised closed-loop response transfer functions for the three flight conditions and show the transfer functions in factorised form. What does the addition of the washout filter do to the closed-loop stability modes of the aircraft?
- (13) Obtain time history plots showing the response to a short pulse of aileron and a short pulse of rudder. Compare the responses with those obtained in (9) by plotting both sets of time histories on the same axes; once again, the plots should be presented in strip chart form showing the four aircraft motion variables only.
- (14) Identify the differences in the plots and hence explain the purpose of the washout filter. Remember that the object is to review turning performance in response to aileron command. Comment also on the initial transient in sideslip angle.

15.4.6 Designing the aileron-rudder interlink gain

- (15) The objective here is to design a suitable value for the interlink gain K_{ari} for each of the three flight conditions. In the present context this may be done only by choosing a test value and including it in the input mixing matrix \mathbf{L} in the closed-loop model developed in (11), obtaining the transfer functions, and observing the response to an aileron command. The correct value of K_{ari} is the minimum value that will cancel the adverse sideslip response seen in the transient immediately following application of the aileron command. Suitable values of gain lie in the range $0 < K_{ari} < 0.5$. Define a simple gain schedule as a function of dynamic pressure Q .
- (16) Write down the fully developed closed-loop state equations for all three flight conditions, including the aileron-rudder interlink gain according to the schedule designed in (15).
- (17) Obtain and show in factorised form the response transfer functions for all three flight conditions. Note any changes due to the inclusion of the aileron-rudder interlink gain.
- (18) Demonstrate the turning performance of the F-104 with the fully developed control law by showing the response to an aileron pulse. As before, the response of all four motion variables should be shown in strip chart format.
- (19) Identify the key attributes of the turning performance as refined by the control law design. In particular explain the response changes due to the aileron-rudder interlink. This will be easier to do if a comparison is made with the responses obtained in (8).

15.5 Assignment 4: Analysis of the effects of Mach number on the longitudinal stability and control characteristics of the LTV A7-A Corsair aircraft

(CU 2003)

The object of the assignment is to analyse, illustrate, and explain the effects of compressibility on the longitudinal aerodynamics, stability, and control of a typical 1960s combat aeroplane.

15.5.1 The aircraft model

The aircraft chosen for this exercise is the Ling-Tempco-Vought (LTV) A7-A Corsair, a carrier-based aircraft which first flew in the mid-1960s. The aircraft is typical for its time: a single pilot, single engine aircraft built to withstand the rigours of operating from a carrier deck. The airframe is nominally stable at all flight conditions, although the degree of stability is generally unacceptably low. Consequently, the aircraft is fitted with a simple three-axis stability augmentation system. The aircraft is capable of speeds up to approximately Mach 1.2, and four data sets covering the full Mach number range at an altitude of 15,000 ft are given in [Teper \(1969\)](#). The data for this exercise were obtained directly, or derived, from the data given in Teper; it is listed in [Table 15.1](#) and has been adjusted to a consistent set of units, with the exception of altitude, which is retained in ft units. Be aware that some variables are given for information only and are not required in the calculations.

The aerodynamic data are referenced to an aircraft wind axis system.

15.5.2 The assignment tasks

All assumptions made should be very clearly stated.

Assembling the derivatives

Using simple mathematical approximations for the longitudinal stability and control derivatives together with the data given in [Table 15.1](#), calculate values for the dimensionless derivatives and the static and manoeuvre stability parameters; hence complete [Table 15.2](#) for all four flight conditions. Note that the usual tailplane approximation for the derivatives M_q , M_η , and Z_η is not assumed. These derivatives should be calculated from first principles, for example, in the same way as M_u and Z_w .

Solving the equations of motion

Writing the longitudinal state equation as $\mathbf{M}\dot{\mathbf{x}} = \mathbf{A}'\mathbf{x} + \mathbf{B}'\mathbf{u}$, write down the matrices \mathbf{M} , \mathbf{A}' , and \mathbf{B}' in algebraic form, stating the elements in terms of dimensionless derivatives. In the interests of simplicity, the equations of motion should be referred to aircraft wind axes. Hence, obtain the aircraft response transfer functions for each of the four flight conditions.

Assessing the dynamic stability characteristics

Tabulate the closed-loop longitudinal stability modes characteristics for each of the four flight conditions. Produce response time histories which best show the stability modes dynamics for the unaugmented aircraft for all flight conditions. Assess the stability modes against the requirements for Level 1 flying qualities.

Table 15.1 LTV A-7A Corsair Aerodynamic, Geometric, and Flight Condition Data

Flight Case #		1	2	3	4
Altitude	h (ft)	15000	15000	15000	15000
Mach number	M_0	0.3	0.6	0.9	1.1
Air density	ρ (kg/m ³)	0.7708	0.7708	0.7708	0.7708
Velocity	V_0 (m/s)	96.6	193.6	290.2	354.8
Trim body incidence	α_e (deg)	13.3	4.0	2.5	2.9
Trim elevator angle	η_e (deg)	-8.80	-3.80	-3.85	-4.95
Trim lift coefficient	C_L	0.420	0.200	0.095	0.030
Trim drag coefficient	C_D	0.036	0.018	0.020	0.054
	$\partial C_L / \partial \alpha$ (1/rad)	3.90	4.35	5.35	4.80
	$\partial C_D / \partial \alpha$ (1/rad)	1.20	0.30	0.23	0.22
	$\partial C_m / \partial \alpha$ (1/rad)	-0.48	-0.44	-0.59	-1.08
	$\partial C_m / \partial q$ (1/rad/s)	-0.0664	-0.0337	-0.0231	-0.0188
	$\partial C_L / \partial M$	0.030	0.012	0.058	0.047
	$\partial C_D / \partial M$	0.054	0	0.090	-0.013
	$\partial C_m / \partial M$	0	0.0010	-0.0360	-0.0055
	$\partial C_L / \partial \eta$ (1/rad)	0.585	0.600	0.550	0.400
	$\partial C_m / \partial \eta$ (1/rad)	-0.89	-0.91	-0.89	-0.63
	$d\varepsilon/d\alpha$	0.179	0.202	0.246	-0.247
Mass	m (kg)	9924	9924	9924	9924
Pitch inertia	I_y (kgm ²)	79946	79946	79946	79946
cg position	h	0.3	0.3	0.3	0.3
Wing area	S (m ²)	34.84	34.84	34.84	34.84
Mean chord	\bar{c} (m)	3.29	3.29	3.29	3.29
Tail moment arm	l_T (m)	5.5	5.5	5.5	5.5

Stability augmentation

Assuming a simple pitch damping stability augmentation system and, with the aid of root locus plots, design values for pitch rate feedback gain K_q in order to achieve a short-period mode damping ratio of about $0.5 \sim 0.7$ for each of the four flight conditions. Calculate the closed-loop state equations and hence obtain the response transfer functions for the augmented aircraft. Tabulate the closed-loop longitudinal stability modes characteristics for each of the four flight conditions. Produce response time histories which best show the stability modes dynamics for the augmented aircraft. It is most helpful if the response time histories for the previous tasks are plotted on the same axes for comparison purposes.

Assessing the effects of Mach number

Plot the following parameters against Mach number: C_L , C_D , α_e , η_e , K_n , H_m , Z_η , M_η , and K_q . Plot also the stability modes change with Mach number for both the unaugmented and augmented aircraft on the s -plane. Discuss and explain briefly the effect of Mach number on the following:

Table 15.2 LTV A-7A Corsair Aerodynamic Stability and Control Summary

Flight Case #		1	2	3	4
Altitude	h (ft)	15000	15000	15000	15000
Mach number	M_0	0.3	0.6	0.9	1.1
Air density	ρ (kg/m ³)	0.7708	0.7708	0.7708	0.7708
Velocity	V_0 (m/s)	96.6	193.6	290.2	354.8
Trim body incidence	α_e (deg)	13.3	4.0	2.5	2.9
Trim elevator angle	η_e (deg)	-8.80	-3.80	-3.85	-4.95
Trim lift coefficient	C_L	0.420	0.200	0.095	0.030
Trim drag coefficient	C_D	0.036	0.018	0.020	0.054
Dimensionless Aerodynamic Stability and Control Derivatives Referred to Wind Axes					
	X_u				
	X_w				
	X_q	0	0	0	0
	$X_{\dot{w}}$	0	0	0	0
	Z_u				
	Z_w				
	Z_q				
	$Z_{\dot{w}}$				
	M_u				
	M_w				
	M_q				
	$M_{\dot{w}}$				
	X_η	0	0	0	0
	Z_η				
	M_η				
Aircraft Geometric, Mass, and Inertia Data					
Mass	m (kg)	9924	9924	9924	9924
Pitch inertia	I_y (kg.m ²)	79946	79946	79946	79946
Wing area	S (m ²)	34.84	34.84	34.84	34.84
Mean chord	\bar{c} (m)	3.29	3.29	3.29	3.29
Tail moment arm	l_T (m)	5.5	5.5	5.5	5.5
Aircraft Stability and Control Parameters					
cg position	h	0.3	0.3	0.3	0.3
Static margin—controls-fixed	K_n				
Neutral point—controls-fixed	h_n				
Longitudinal relative density factor	μ_l				
Manoeuvre margin—controls-fixed	H_m				
Manoeuvre point—controls-fixed	h_m				

- Static stability and trim
- Dynamic stability and response
- Elevator control characteristics
- Feedback gain schedule

15.6 Assignment 5: The design of a longitudinal primary flight control system for an advanced-technology UAV

All assumptions made should be very clearly stated.

The object of the study is to design a representative longitudinal *primary flight control system* (PFCS) for an advanced technology UAV. The purpose of the PFCS is to provide a stable controllable aircraft platform with provision for pitch attitude command and speed command inputs. Typically, control commands originate from an automatic guidance and control system, or from a remote manual control station. Since the aircraft is pilotless, the application of handling qualities design criteria is not appropriate. However, the design of the PFCS should anticipate and reflect performance characteristics compatible with the aircraft role. Conventional aircraft flying qualities requirements may provide appropriate guidance in this context, although strict adherence to performance limits determined for piloted aircraft is not necessary.

15.6.1 The aircraft model

The Demon aircraft, shown in Fig. 15.4, is a small advanced-technology research UAV, developed by BAE Systems in conjunction with a number of UK universities over a period of several years, and culminating in a first flight late in 2010. The FLAVIIR ([Buonanno, 2009](#)) programme was jointly funded by BAE Systems and the UK Engineering and Physical Sciences Research Council. The School of Engineering at Cranfield University performed the lead design role for the project.

The Demon was developed to demonstrate a number of advanced technologies—in particular, to demonstrate the application of flapless flight control in which conventional flap control surfaces are replaced with circulation control devices. This was found to provide a significant design

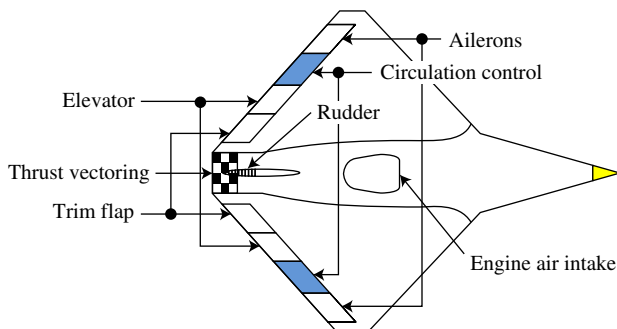


FIGURE 15.4 Demon UAV plan view.

challenge, and early flights of the vehicle were made with a mix of conventional and fluidic controls. The fluidic controls are indicated in the trailing edge of the wing in Fig. 15.4. The Demon has a take-off mass of approximately 44 kg, a wing span of 2.2 m, and a maximum speed of about 100 knots. Propulsive power is provided by a small gas turbine the exhaust of which is vectored in pitch by blown fluidic control means. Since the blown controls require high flow rates of high-pressure air, this is provided by a secondary gas turbine mounted in the nose of the vehicle. The flight control system of the vehicle is configured to allow both remote manual and fully autonomous control using various combinations of conventional and blown effectors. Initial flights have been made using remote manual control only.

In order to create simulation models of the Demon, aerodynamic and other data were developed using theoretical and empirical methods, and by static and dynamic wind tunnel testing at reduced scale. A description of some aspects of this work may be found in Buonanno (2009), and the linearised equations of motion were obtained from the simulation model developed by Saban (2006). The equations of motion relate to an early representation of the Demon and are known to be of doubtful accuracy in some aspects of the aerodynamic description. However, the equations of motion are sufficient for the present purpose and have been adjusted to ensure consistency of units.

The longitudinal equations of motion corresponding with a flight speed of 45 m/s at an altitude of 1000 m are given in concise state form:

$$\dot{\mathbf{x}} = \mathbf{Ax} + \mathbf{Bu}$$

where

$$\mathbf{x}^T = [u \quad w \quad q \quad \theta] \quad \mathbf{u}^T = [\eta \quad \tau]$$

$$\mathbf{A} = \begin{bmatrix} -0.0324 & 0.137 & -2.2382 & -9.7972 \\ -0.252 & -3.7906 & 44.4781 & -0.5006 \\ 0.0291 & -0.7668 & -0.2658 & -0.132 \\ 0 & 0 & 1 & 0 \end{bmatrix} \quad \mathbf{B} = \begin{bmatrix} 0.4126 & 2.5267 \\ -22.1866 & 0 \\ -37.99 & -0.1134 \\ 0 & 0 \end{bmatrix}$$

The variables u, w have units m/s, q has units rad/s, θ and η have units rad, and thrust τ has units N.

The engine control lag has a time constant $T_\tau = 0.334$ s and is given by the transfer function

$$\frac{\tau(s)}{\tau_d(s)} = \frac{1}{(1 + 0.334s)}$$

with corresponding time domain equation $\dot{\tau} = -2.994\tau + 2.994\tau_d$.

The “elevator” control actuator is a typical model aircraft control servo and is represented by the second order transfer function

$$\frac{\eta(s)}{\eta_d(s)} = \frac{625}{(s^2 + 30s + 625)}$$

with corresponding state equation

$$\begin{bmatrix} \dot{\eta} \\ \dot{v}_\eta \end{bmatrix} = \begin{bmatrix} 0 & 1 \\ -625 & -30 \end{bmatrix} \begin{bmatrix} \eta \\ v_n \end{bmatrix} + \begin{bmatrix} 0 \\ 625 \end{bmatrix} \eta_d$$

15.6.2 The design requirements

A typical structure for the PFCS is shown in Fig. 15.5, in which longitudinal control of the aircraft is effected by independent control of speed, or thrust, and pitch attitude.

The requirement is to design appropriate values for the system gains and command path filters to give the controlled aircraft flying qualities compatible with the flight dynamics of the airframe. Common standard flying qualities requirements are not generally available for UAVs, so it is useful, but not essential, to refer to piloted aircraft requirements for guidance. It is probably prudent to seek higher levels of stability in a UAV, but it must be remembered that higher system gains will demand a higher power-bandwidth capability of the FCS and an acceptable design compromise must be found. The design should seek to achieve the following;

- Good step response characteristics: 1:1 relationship between steady-state command and response—little or no overshoot; short settling time—no intrusive lag effects.
- A closed-loop engine lag time constant that must not be allowed to become too long.
- Closed-loop elevator actuator properties that must not be allowed to diverge too far from their open-loop properties.
- Avoidance of closed-loop thrust and elevator demand saturation during normal operation.
- Avoidance of intrusive oscillatory response characteristics.
- Optional command path filtering that may be used for closed-loop response shaping.

The following points offer some guidance on the solution of the assignment.

- It is important to appreciate the flight dynamics characteristics of the basic airframe and to maintain close attention to the changes in the characteristics at each step of the design process. It is not good design practice to seek system performance beyond the capabilities of the airframe, engine, and actuator.
- The closure of three feedback loops will cause favourable and unfavourable interactions on the overall system performance. It is essential to understand the effects of each loop closure (guidance may be found in Chapter 11).

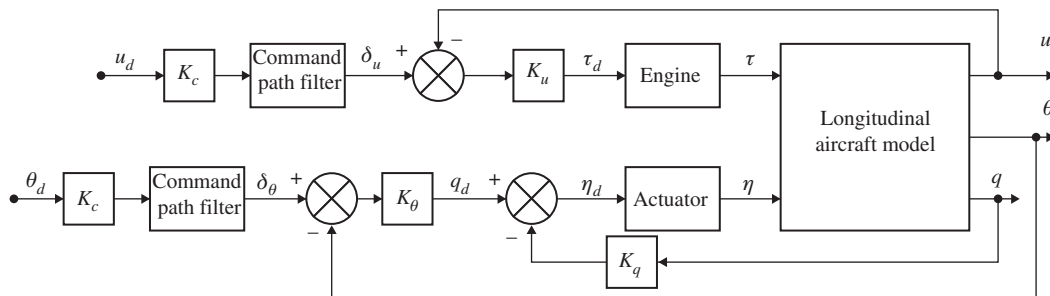


FIGURE 15.5 Typical PFCS controller architecture.

- Both controlled variables are dominant in phugoid dynamics, and control loop interactions may be expected. It is preferable, but not necessary, to design the speed control loop first to fix the closed-loop phugoid dynamics as desired. The pitch control loops are then more easily designed with the speed control loop closed.
- Trial and error solutions using tools such as Simulink are not acceptable. Do not be tempted to repeat each design step many times in an effort to achieve a “good” result. It is far better to produce a carefully explained coherent PFCS solution, even if its performance is not perfect. However, some limited trial and error investigations will be necessary in order to properly appreciate the interactions between control loops.

15.6.3 The assignment tasks

Solving the equations of motion

Solve the two input state equation and write out all eight of the response transfer functions. Evaluate the stability characteristics of the aircraft and the steady gain of each of the transfer functions. Decide on the desired stability properties of the aircraft with PFCS; justify and explain your choices. Review and comment on the control sensitivity of the aircraft with respect to the response variables of interest.

Designing the speed control loop

To facilitate the design of the speed controller, simplify the open-loop state equation to include the single thrust control input only. Augment the state equation to include the engine dynamics. With the aid of a properly annotated root locus plot, assess the effect of the feedback gain K_u on the closed-loop stability characteristics of the controller. State and justify your choice of feedback gain value. Calculate the closed-loop state equation, and solve and list the closed-loop transfer functions. Comment on the closed-loop stability properties and the steady-state gains of the transfer functions.

Assessing the performance of the speed controller

Using the closed-loop transfer function u/δ_u , describe and assess the unit step response. Explain the response shape and, if appropriate, design a first-order command path filter to refine the response shape. Adjust the command path gain K_c to obtain $u/u_d = 1.0$ in the steady state. Show a unit step response for the aircraft with your completed speed controller and comment on its ability to meet the general design requirements.

Re-arranging the system state model with speed loop closed

To design the pitch controller, it is first necessary to rearrange the model, with the speed control loop closed, and to enable the single elevator input only. Using the state equation with speed feedback loop closed, replace the thrust/speed input terms with the elevator input terms from the open-loop model equations of motion. Augment the state equation to include the elevator actuator model—the state equation should now be seventh-order. Solve the resulting state equation and write out all seven transfer functions. Identify and evaluate all of the stability modes and the steady gain of each of the transfer functions. Decide on your strategy for designing the pitch controller, and justify and explain your approach.

Designing the pitch rate control loop

With the aid of a properly annotated root locus plot using the transfer function q/η_d from the previous task, assess the effect of feedback gain K_q on the closed-loop stability characteristics. Similarly, construct a root locus plot using the transfer function θ/η_d from the previous task and assess the effect of feedback gain K_θ on the closed-loop stability characteristics. In the context of the design requirements, compare the effects of these assessments and hence decide on a suitable value for K_q . Calculate the closed-loop state equation by closing the pitch rate q feedback loop using your designed value of K_q . Solve the new closed-loop state equation and list all seven response transfer functions.

Designing the pitch attitude control loop

Finally, to complete the design of the pitch attitude control loop, create a root locus plot using the response transfer function θ/q_d from the previous task. Choose a suitable value for K_θ , paying particular attention to the closed-loop stability modes, engine lag, and elevator actuator characteristics. Calculate the closed-loop state equation with both q and θ loops closed using your designed gain values. Solve and obtain the closed-loop response transfer functions. Comment on the closed-loop stability properties and the steady-state gains of the transfer functions.

Assessing the performance of the pitch attitude controller

Using the closed-loop transfer function θ/δ_θ , describe and assess the unit step response. Explain the response shape and, if appropriate, design a first-order command path filter to refine the response shape. Adjust the command path gain K_c to obtain $\theta/\theta_d = 1.0$ in the steady state. Show a unit step response for the aircraft with your completed pitch attitude controller and comment on its ability to meet the general design requirements.

References

- Buonanno, A. (2009). *Aerodynamic circulation control for flapless flight control of an unmanned air vehicle*. Cranfield, Bedfordshire: Cranfield University, PhD diss.
- Flapless Aerial Vehicle Integrated Interdisciplinary Research programme (FLAVIIR). (2004) <www.flaviir.com>. (Numerous additional information sources and photographic images can also be found on the Internet.)
- Heffley, R. K., & Jewell, W. F. (1972). *Aircraft handling qualities data*. Washington, DC: National Aeronautics and Space Administration, NASA Contractor Report NASA CR-2144.
- Saban, D. (2006). *Flight control system design for the “demon” vehicle*. Cranfield, Bedfordshire: Cranfield University, MSc thesis.
- Teper, G. L. (1969). *Aircraft stability and control data*. Hawthorne, CA: Systems Technology, Inc., STI Technical Report 176-1.

Appendix 1: AeroTrim: A Symmetric Trim Calculator for Subsonic Flight Conditions

A Mathcad Program Written by M. V. Cook, Version Date 1 September 2012

Given the operating condition and some basic geometric and aerodynamic data for a conventional aircraft, this programme calculates an estimate of the symmetric trim state of the aircraft for a chosen airspeed range. The programme is limited to subsonic flight in the troposphere; however, it may be developed easily for application to a wider range of operating conditions and aircraft configurations. Data given are best estimates for the Cranfield Jetstream laboratory aircraft.

1. Aircraft Flight Condition

(Insert values to define aircraft operating condition)

<i>Altitude (ft)</i>	ht := 6562	<i>Convert to m</i>	ht := 0.3048 · ht
<i>Aircraft mass (kg)</i>	m := 6300		
<i>cg position (%c)</i>	h := 0.29		
<i>Flight path angle (deg)</i>	$\gamma_e := 0$	<i>Convert to rad</i>	$\gamma_e := \frac{\gamma_e}{57.3}$
<i>Gravity constant (m/s²)</i>	g := 9.81		

2. Air Density Calculation

Valid for troposphere only—up to 36,000 ft

<i>Gas constant (Nm/kgK)</i>	R := 287.05	
<i>Lapse rate (K/m)</i>	lr := -0.0065	
<i>Temperature (K)</i>	Temp := 288.16 + lr · ht	
<i>Air density (kg/m³)</i>	$\rho := 1.225 \cdot \left(\frac{\text{Temp}}{288.16} \right)^{-\left[\left(\frac{g}{R} \right) + 1 \right]}$	<i>Check results</i>
<i>Density ratio</i>	$\sigma := \frac{\rho}{1.225}$	Temp = 275.15 $\rho = 1.006$ $\sigma = 0.822$

3. Set up Velocity Range for Computations

Note that true airspeed is assumed unless otherwise stated

<i>Counter</i>	i := 0..10
----------------	------------

(set counter to number of velocity test points required)

<i>True airspeed range (knots)</i>	$V_{\text{knots}_i} := 100 + 15 \cdot i$
------------------------------------	--

(set initial velocity and velocity increment as required)

<i>True airspeed (m/s)</i>	$V_i := V_{\text{knots}_i} \cdot 0.515$
----------------------------	---

<i>Equivalent airspeed (knots)</i>	$V_{\text{eas}_i} := V_{\text{knots}_i} \cdot \sqrt{\sigma}$
------------------------------------	--

4. Aircraft Geometry—Constant*(Insert values defined by aircraft geometry)****Wing Geometry***

<i>Wing area (m²)</i>	S := 25.08	
<i>Wing span (m)</i>	b := 15.85	
<i>Wing mean chord (m)</i>	c _w := 1.716	
<i>Sweep 1/4c_w (deg)</i>	$\Lambda := 0$	
<i>z coordinate of 1/4c_w point above (−ve) or below (+ve) ox body axis (m)</i>	$z_w := 0.45$	
<i>Wing rigging angle (deg)</i>	$\alpha_{wr} := 1.0$	<i>Convert to rad</i> $\alpha_{wr} := \frac{\alpha_{wr}}{57.3}$

Tailplane Geometry

<i>Tailplane area (m²)</i>	S _T := 7.79	
<i>Tailplane span (m)</i>	b _T := 6.6	
<i>Tail arm, 1/4c_w to 1/4c_t (m)</i>	l _t := 6.184	
<i>z coordinate of 1/4c_w point above (−ve) or below (+ve) ox body axis (m)</i>	$z_T := -1.435$	
<i>Tail setting angle (deg)</i>	$\eta_T := 1.5$	<i>Convert to rad</i> $\eta_T := \frac{\eta_T}{57.3}$
<i>Fuselage diameter or width (m)</i>	F _d := 1.981	

Engine Installation

<i>Thrust line z coordinate above (−ve) or below (+ve) ox body axis (m)</i>	$z_\tau := 0.312$	
<i>Engine thrust line angle (deg) relative to ox body axis (+nose up)</i>	$\kappa := 0$	<i>Convert to rad</i> $\kappa := \frac{\kappa}{57.3}$

5. Wing-Body Aerodynamics*(Insert values defined by the installed wing aerodynamic design)*

<i>Wing-body C_L-α (per rad)</i>	a := 5.19	
<i>Maximum lift coefficient</i>	C _{Lmax} := 1.37	
<i>Zero lift pitching moment</i>	C _{m0} := −0.0711	
<i>Zero lift drag coefficient</i>	C _{D0} := 0.03	
<i>Zero lift angle of attack (deg)</i>	$\alpha_{w0} := -2$	<i>Convert to rad</i> $\alpha_{w0} := \frac{\alpha_{w0}}{57.3}$
<i>Wing-body aero centre</i>	$h_0 := -0.08$	

6. Tailplane Aerodynamics

(Insert values defined by the tailplane aerodynamic design)

Tail plane $C_L\cdot\alpha$ (per rad)

$$a_1 := 3.2$$

Elevator $C_L\cdot\eta$ (per rad)

$$a_2 := 2.414$$

Zero lift downwash angle (deg)

$$\varepsilon_0 := 2.0$$

$$\text{Convert to rad } \varepsilon_0 := \frac{\varepsilon_0}{57.3}$$

7. Wing and Tailplane Calculations

Aspect ratio $Ar := \frac{b^2}{S}$

Wing semi-span (m) $s := \frac{b}{2}$

Check results

$$Ar = 10.017$$

Tail arm, cg to $1/4c_t$ (m) $l_T := l_t - c_w \cdot (h - 0.25)$

$$s = 7.925$$

Tail volume $V_T := \frac{S_T \cdot l_T}{S \cdot c_w}$

$$l_T = 6.115$$

$$V_T = 1.107$$

8. Downwash at TailRef:-*Stribling, C.B. "Basic Aerodynamics", Butterworth Ltd., 1984.***Tail position relative to wing (% of span)**

$$x := \frac{l_t}{b} \quad z := \frac{z_w - z_T}{b}$$

$$d_{\varepsilon\alpha} := \frac{a}{\pi^2 \cdot Ar} \sum_{fi=5}^{85} \frac{0.5 \cdot \cos\left(\frac{fi \cdot \pi}{180}\right)^2}{\sqrt{x^2 + \left(0.5 \cdot \cos\left(\frac{fi \cdot \pi}{180}\right)\right)^2 + z^2}} \cdot \left[\frac{\left[x + \sqrt{x^2 + \left(0.5 \cdot \cos\left(\frac{fi \cdot \pi}{180}\right)\right)^2 + z^2} \right]}{\left(0.5 \cdot \cos\left(\frac{fi \cdot \pi}{180}\right)\right)^2 + z^2} + \frac{x}{(x^2 + z^2)} \right] \cdot \frac{\pi}{180}$$

Check result $d_{\varepsilon\alpha} = 0.279$

9. Induced Drag FactorRef:- *Shevell, R.S. "Fundamentals of Flight", 2nd edition, Prentice Hall Inc., 1983.*Drag polar is defined, $C_D = C_{D0} + KC_L^2$, where K is the induced drag factor.

Fuselage drag factor $S_d := 0.9998 + 0.0421 \cdot \left(\frac{F_d}{b}\right) - 2.6286 \cdot \left(\frac{F_d}{b}\right)^2 + 2.000 \cdot \left(\frac{F_d}{b}\right)^3$

Empirical constant $k_D := -3.333 \cdot 10^{-4} \cdot \Lambda^2 + 6.667 \cdot 10^{-5} \cdot \Lambda + 0.38$

<i>Oswald efficiency factor</i>	$e := \frac{1}{\pi \cdot A_r \cdot k_D \cdot C_{D0} + \frac{1}{(0.99 \cdot s_d)}}$	<i>Check result</i>
<i>Induced drag factor</i>	$K := \frac{1}{\pi \cdot A_r \cdot e}$	$s_d = 0.968$ $k_D = 0.38$ $e = 0.713$ $K = 0.045$

10. Basic Performance Parameters

<i>Minimum drag speed (knots)</i>	$V_{md} := \left[\left(\sqrt{\frac{2 \cdot m \cdot g}{\rho \cdot S}} \right) \cdot \left(\frac{K}{C_{D0}} \right)^{0.25} \right] \cdot \frac{1}{0.515}$
<i>Equivalent minimum drag speed (knots)</i>	$V_{mdeas} := V_{md} \cdot \sqrt{\sigma}$
<i>Stall speed (knots)</i>	$V_{stall} := \sqrt{\frac{2 \cdot m \cdot g}{\rho \cdot S \cdot C_{Lmax}}} \cdot \frac{1}{0.515}$
<i>Equivalent stall speed (knots)</i>	$V_{stalleas} := V_{stall} \cdot \sqrt{\sigma}$
<i>Neutral point—controls fixed</i>	$h_n := h_0 + V_T \cdot \frac{a_l}{a} \cdot (1 - d_{e\alpha})$
<i>Static margin—controls fixed</i>	$K_n := h_n - h$

11. Trim Calculation

The trim computation finds the trim condition for each speed defined in the speed range table and for the flight condition defined in [Section 1](#).

Initial seed values for solve block

$$C_L := 0.7 \quad C_{LW} := 0.5 \quad C_D := 0.02 \quad C_\tau := 0.4 \quad \alpha_e := 0.1 \quad C_{LT} := 0.1$$

Trim solve block

Given

$$\begin{aligned} \text{Total normal force} \\ (\text{oz body axis}) \end{aligned} \quad 2 \cdot \frac{m \cdot g}{\rho \cdot (V)^2 \cdot S} \cdot \cos(\alpha_e + \gamma_e) = C_L \cdot \cos(\alpha_e) + C_D \cdot \sin(\alpha_e) + C_\tau \cdot \sin(\kappa)$$

$$\begin{aligned} \text{Total axial force} \\ (\text{ox body axis}) \end{aligned} \quad 2 \cdot \frac{m \cdot g}{\rho \cdot (V)^2 \cdot S} \cdot \sin(\alpha_e + \gamma_e) = C_\tau \cdot \cos(\kappa) - C_D \cdot \cos(\alpha_e) + C_L \cdot \sin(\alpha_e)$$

$$\text{Total drag coefficient} \quad C_D = C_{D0} + K \cdot C_L^2$$

$$\text{Wing-body lift coefficient} \quad C_{LW} = a \cdot (\alpha_e + \alpha_{wr} - \alpha_{w0})$$

**Pitching moment
(about cg)**

$$0 = [C_{m0} + (h - h_0) \cdot C_{Lw}] - V_T \cdot C_{LT} + C_\tau \cdot \frac{Z_\tau}{c_w}$$

Tail lift coefficient

$$C_{LT} = (C_L + C_{LW}) \cdot \frac{S}{S_T}$$

Trim(V) := Find(α_e , C_τ , C_D , C_{LT} , C_{LW} , C_L)

End of trim solve block

12. Trim Variables Calculation

$$\alpha_{e_i} := \text{Trim}(V_i)_0$$

$$C_{\tau_i} := \text{Trim}(V_i)_1$$

$$C_{D_i} := \text{Trim}(V_i)_2$$

$$C_{LT_i} := \text{Trim}(V_i)_3$$

$$C_{LW_i} := \text{Trim}(V_i)_4$$

$$C_{L_i} := \text{Trim}(V_i)_5$$

Wing incidence

$$\alpha_{w_i} := \alpha_{e_i} + \alpha_{w_r}$$

Trim elevator angle

$$\eta_{e_i} := \frac{C_{LT_i}}{a_2} - \frac{a_1}{a_2} \cdot [\alpha_{w_i} \cdot (1 - d_{\varepsilon\alpha}) + \eta_T - \alpha_{wr} - \varepsilon_0]$$

Pitch attitude

$$\theta_{e_i} := \gamma_e + \alpha_{w_i} - \alpha_{w_r}$$

Tail angle of attack

$$\alpha_{T_i} := \alpha_{w_i} \cdot (1 - d_{\varepsilon\alpha}) + \eta_T - \varepsilon_0 - \alpha_{wr}$$

Lift to drag ratio

$$L_{D_i} := \frac{C_{LW_i}}{C_{D_i}}$$

13. Conversions of Angles to Degrees

$$\alpha_{w_i} := \alpha_{w_i} \cdot 57.3$$

$$\alpha_{e_i} := \alpha_{e_i} \cdot 57.3$$

$$\theta_{e_i} := \theta_{e_i} \cdot 57.3$$

$$\alpha_{T_i} := \alpha_{T_i} \cdot 57.3$$

$$\eta_{e_i} := \eta_{e_i} \cdot 57.3$$

$$\gamma_e := \gamma_e \cdot 57.3$$

14. Total Trim Forces Acting on Aircraft

Total lift force (N)

$$L_i := 0.5 \cdot \rho \cdot (V_i)^2 \cdot S \cdot C_{L_i}$$

Total drag force(N)

$$D_i := 0.5 \cdot \rho \cdot (V_i)^2 \cdot S \cdot C_{D_i}$$

Total thrust (N)

$$T_i := 0.5 \cdot \rho \cdot (V_i)^2 \cdot S \cdot C_{\tau_i}$$

SUMMARY RESULTS OF TRIM CALCULATION

15. Definition of Flight Condition

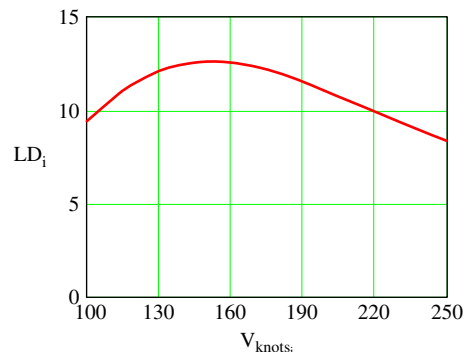
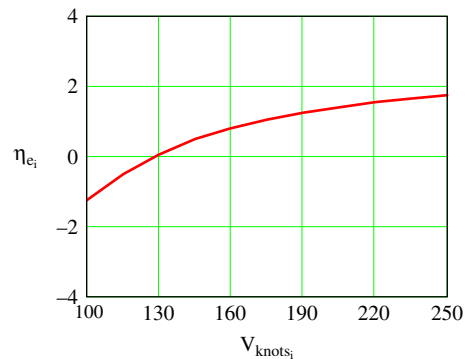
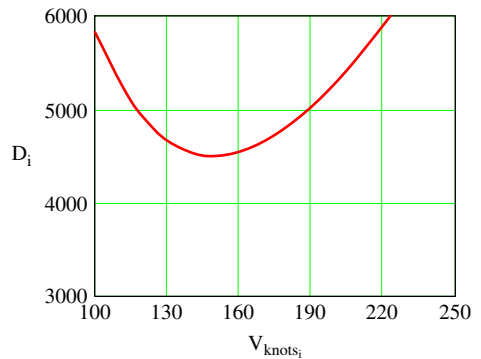
<i>Aircraft weight (N)</i>	$m \cdot g = 6.18 \cdot 10^4$	<i>Minimum drag speed (knots)</i>	$V_{md} = 155.307$
<i>Altitude (ft)</i>	$ht \cdot 3.281 = 6.562 \cdot 10^3$	<i>Equivalent minimum drag speed (knots)</i>	$V_{mdeas} = 140.769$
<i>Flight path angle (deg)</i>	$\gamma_e = 0$	<i>Stall speed (knots)</i>	$V_{stall} = 116.092$
<i>cg position (%c_w)</i>	$h = 0.29$	<i>Equivalent stall speed (knots)</i>	$V_{stalleas} = 105.225$
<i>Neutral point —controls fixed</i>	$h_n = 0.412$	<i>Static margin-controls fixed</i>	$K_n = 0.122$

16. Trim Conditions as a Function of Aircraft Velocity

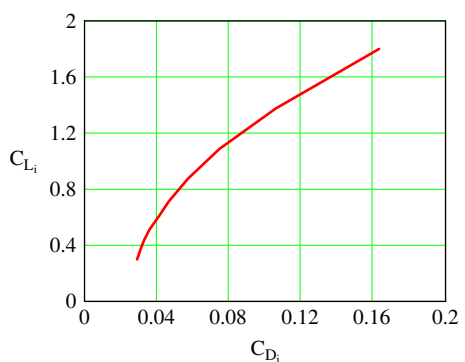
Angles in degrees, velocity in m/s, forces in N unless indicated otherwise.

V_{knots_i}	V_i	C_{L_i}	C_{D_i}	C_{Lw_i}	C_{LT_i}	LD_i	C_{τ_i}	α_{w_i}	α_{c_i}	θ_{e_i}	α_{T_i}	η_{e_i}
100	51.5	1.799	0.174	1.64	0.514	9.409	0.181	16.105	15.105	15.105	10.107	-1.208
115	59.225	1.374	0.114	1.258	0.375	11.017	0.116	11.885	10.885	10.885	7.066	-0.46
130	66.95	1.081	0.082	0.994	0.282	12.106	0.083	8.97	7.97	7.97	4.965	0.1
145	74.675	0.872	0.064	0.805	0.215	12.603	0.064	6.885	5.885	5.885	3.462	0.521
160	82.4	0.717	0.053	0.665	0.167	12.573	0.053	5.346	4.346	4.346	2.353	0.842
175	90.125	0.6	0.046	0.56	0.13	12.154	0.046	4.181	3.181	3.181	1.513	1.091
190	97.85	0.51	0.042	0.478	0.102	11.496	0.042	3.277	2.277	2.277	0.862	1.287
205	105.575	0.438	0.039	0.413	0.08	10.72	0.039	2.564	1.564	1.564	0.348	1.444
220	113.3	0.381	0.036	0.361	0.063	9.912	0.036	1.99	0.99	0.99	-0.066	1.572
235	121.025	0.334	0.035	0.319	0.048	9.123	0.035	1.523	0.523	0.523	-0.403	1.677
250	128.75	0.295	0.034	0.284	0.036	8.383	0.034	1.136	0.136	0.136	-0.681	1.764

V_{knots_i}	V_i	L_i	D_i	T_i
100	51.5	$6.023 \cdot 10^4$	$5.834 \cdot 10^3$	$6.042 \cdot 10^3$
115	59.225	$6.083 \cdot 10^4$	$5.053 \cdot 10^3$	$5.146 \cdot 10^3$
130	66.95	$6.115 \cdot 10^4$	$4.643 \cdot 10^3$	$4.688 \cdot 10^3$
145	74.675	$6.134 \cdot 10^4$	$4.494 \cdot 10^3$	$4.518 \cdot 10^3$
160	82.4	$6.146 \cdot 10^4$	$4.535 \cdot 10^3$	$4.548 \cdot 10^3$
175	90.125	$6.154 \cdot 10^4$	$4.722 \cdot 10^3$	$4.729 \cdot 10^3$
190	97.85	$6.16 \cdot 10^4$	$5.025 \cdot 10^3$	$5.029 \cdot 10^3$
205	105.575	$6.165 \cdot 10^4$	$5.424 \cdot 10^3$	$5.426 \cdot 10^3$
220	113.3	$6.17 \cdot 10^4$	$5.907 \cdot 10^3$	$5.908 \cdot 10^3$
235	121.025	$6.174 \cdot 10^4$	$5.465 \cdot 10^3$	$6.465 \cdot 10^3$
250	128.75	$6.179 \cdot 10^4$	$5.089 \cdot 10^3$	$7.089 \cdot 10^3$

17. Some Useful Trim Plots***Lift to drag ratio with true airspeed.******Elevator angle (deg) to trim with true airspeed.******Total drag (N) variation with true airspeed.***

Drag polar.



- End of program -

Appendix 2: Definitions of Aerodynamic Stability and Control Derivatives

A2.1 Notes

The derivatives given in [Tables A2.5 through A2.8](#) are referred to **generalised body axes**; $U_e = V_0 \cos \theta_e$ and $W_e = V_0 \sin \theta_e$. In the particular case when the derivatives are referred to wind axes, $\theta_e = 0$ and the following simplifications can be made: $U_e = V_0$, $W_e = 0$, $\sin \theta_e = 0$ and $\cos \theta_e = 1$. The equivalent algebraic expressions in [Tables A2.5 to A2.8](#) were derived with the aid of the computer program Mathcad, which includes a facility for symbolic calculation. In [Tables A2.5, A2.6, A2.7, and A2.8](#) normalised mass and inertias are used. They are defined as follows:

$$m' = \frac{m}{\frac{1}{2}\rho V_0 S}$$

$$I'_x = \frac{I_x}{\frac{1}{2}\rho V_0 S b}$$

$$I'_y = \frac{I_y}{\frac{1}{2}\rho V_0 S \bar{c}}$$

$$I'_z = \frac{I_z}{\frac{1}{2}\rho V_0 S b}$$

$$I'_{xz} = \frac{I_{xz}}{\frac{1}{2}\rho V_0 S b}$$

Table A2.1 Longitudinal Aerodynamic Stability Derivatives

Dimensionless	Multiplier	Dimensional
X_u	$\frac{1}{2}\rho V_0 S$	$\overset{\circ}{X}_u$
X_w	$\frac{1}{2}\rho V_0 S$	$\overset{\circ}{X}_w$
$X_{\dot{w}}$	$\frac{1}{2}\rho S \bar{c}$	$\overset{\circ}{X}_{\dot{w}}$
X_q	$\frac{1}{2}\rho V_0 S \bar{c}$	$\overset{\circ}{X}_q$
Z_u	$\frac{1}{2}\rho V_0 S$	$\overset{\circ}{Z}_u$
Z_w	$\frac{1}{2}\rho V_0 S$	$\overset{\circ}{Z}_w$
$Z_{\dot{w}}$	$\frac{1}{2}\rho S \bar{c}$	$\overset{\circ}{Z}_{\dot{w}}$
Z_q	$\frac{1}{2}\rho V_0 S \bar{c}$	$\overset{\circ}{Z}_q$
M_u	$\frac{1}{2}\rho V_0 S \bar{c}$	$\overset{\circ}{M}_u$
M_w	$\frac{1}{2}\rho V_0 S \bar{c}$	$\overset{\circ}{M}_w$
$M_{\dot{w}}$	$\frac{1}{2}\rho S \bar{c}^2$	$\overset{\circ}{M}_{\dot{w}}$
M_q	$\frac{1}{2}\rho V_0 S \bar{c}^2$	$\overset{\circ}{M}_q$

Table A2.2 Longitudinal Control Derivatives

Dimensionless	Multiplier	Dimensional
X_η	$\frac{1}{2}\rho V_0^2 S$	$\overset{\circ}{X}_\eta$
Z_η	$\frac{1}{2}\rho V_0^2 S$	$\overset{\circ}{Z}_\eta$
M_η	$\frac{1}{2}\rho V_0^2 S \bar{c}$	$\overset{\circ}{M}_\eta$
X_τ	1	$\overset{\circ}{X}_\tau$
Z_τ	1	$\overset{\circ}{Z}_\tau$
M_τ	\bar{c}	$\overset{\circ}{M}_\tau$

Table A2.3 Lateral-Directional Aerodynamic Stability Derivatives

Dimensionless	Multiplier	Dimensional
Y_v	$\frac{1}{2}\rho V_0 S$	$\overset{\circ}{Y}_v$
Y_p	$\frac{1}{2}\rho V_0 Sb$	$\overset{\circ}{Y}_p$
Y_r	$\frac{1}{2}\rho V_0 Sb$	$\overset{\circ}{Y}_r$
L_v	$\frac{1}{2}\rho V_0 Sb$	$\overset{\circ}{L}_v$
L_p	$\frac{1}{2}\rho V_0 Sb^2$	$\overset{\circ}{L}_p$
L_r	$\frac{1}{2}\rho V_0 Sb^2$	$\overset{\circ}{L}_r$
N_v	$\frac{1}{2}\rho V_0 Sb$	$\overset{\circ}{N}_v$
N_p	$\frac{1}{2}\rho V_0 Sb^2$	$\overset{\circ}{N}_p$
N_r	$\frac{1}{2}\rho V_0 Sb^2$	$\overset{\circ}{N}_r$

Table A2.4 Lateral-Directional Aerodynamic Control Derivatives

Dimensionless	Multiplier	Dimensional
Y_ξ	$\frac{1}{2}\rho V_0^2 S$	$\overset{\circ}{Y}_\xi$
L_ξ	$\frac{1}{2}\rho V_0^2 Sb$	$\overset{\circ}{L}_\xi$
N_ξ	$\frac{1}{2}\rho V_0^2 Sb$	$\overset{\circ}{N}_\xi$
Y_ζ	$\frac{1}{2}\rho V_0^2 S$	$\overset{\circ}{Y}_\zeta$
L_ζ	$\frac{1}{2}\rho V_0^2 Sb$	$\overset{\circ}{L}_\zeta$
N_ζ	$\frac{1}{2}\rho V_0^2 Sb$	$\overset{\circ}{N}_\zeta$

Table A2.5 Concise Longitudinal Aerodynamic Stability Derivatives**Equivalent Expressions**

Concise Derivative	In Terms of Dimensional Derivatives	In Terms of Dimensionless Derivatives
x_u	$\frac{\dot{X}_u}{m} + \frac{\dot{X}_{\dot{w}} \dot{Z}_u}{m(m - \dot{Z}_{\dot{w}})}$	$\frac{X_u}{m'} + \frac{\frac{\bar{C}}{V_0} X_{\dot{w}} Z_u}{m' \left(m' - \frac{\bar{C}}{V_0} Z_{\dot{w}} \right)}$
z_u	$\frac{\dot{Z}_u}{m - \dot{Z}_{\dot{w}}}$	$\frac{Z_u}{m' - \frac{\bar{C}}{V_0} Z_{\dot{w}}}$
m_u	$\frac{\dot{M}_u}{I_y} + \frac{\dot{Z}_u \dot{M}_{\dot{w}}}{I_y(m - \dot{Z}_{\dot{w}})}$	$\frac{M_u}{I'_y} + \frac{\frac{\bar{C}}{V_0} M_{\dot{w}} Z_u}{I'_y \left(m' - \frac{\bar{C}}{V_0} Z_{\dot{w}} \right)}$
x_w	$\frac{\dot{X}_w}{m} + \frac{\dot{X}_{\dot{w}} \dot{Z}_w}{m(m - \dot{Z}_{\dot{w}})}$	$\frac{X_w}{m'} + \frac{\frac{\bar{C}}{V_0} X_{\dot{w}} Z_w}{m' \left(m' - \frac{\bar{C}}{V_0} Z_{\dot{w}} \right)}$
z_w	$\frac{\dot{Z}_w}{m - \dot{Z}_{\dot{w}}}$	$\frac{Z_w}{m' - \frac{\bar{C}}{V_0} Z_{\dot{w}}}$
m_w	$\frac{\dot{M}_w}{I_y} + \frac{\dot{Z}_w \dot{M}_{\dot{w}}}{I_y(m - \dot{Z}_{\dot{w}})}$	$\frac{M_w}{I'_y} + \frac{\frac{\bar{C}}{V_0} M_{\dot{w}} Z_w}{I'_y \left(m' - \frac{\bar{C}}{V_0} Z_{\dot{w}} \right)}$
x_q	$\frac{\dot{X}_q - mW_e}{m} + \frac{\left(\dot{Z}_q + mU_e \right) \dot{X}_{\dot{w}}}{m(m - \dot{Z}_{\dot{w}})}$	$\frac{\bar{C}X_q - m'W_e}{m'} + \frac{(\bar{C}Z_q + m'U_e) \frac{\bar{C}}{V_0} X_{\dot{w}}}{m' \left(m' - \frac{\bar{C}}{V_0} Z_{\dot{w}} \right)}$
z_q	$\frac{\dot{Z}_q + mU_e}{m - \dot{Z}_{\dot{w}}}$	$\frac{\bar{C}Z_q + m'U_e}{m' - \frac{\bar{C}}{V_0} Z_{\dot{w}}}$
m_q	$\frac{\dot{M}_q}{I_y} + \frac{\left(\dot{Z}_q + mU_e \right) \dot{M}_{\dot{w}}}{I_y(m - \dot{Z}_{\dot{w}})}$	$\frac{\bar{C}M_q}{I'_y} + \frac{(\bar{C}Z_q + m'U_e) \frac{\bar{C}}{V_0} M_{\dot{w}}}{I'_y \left(m' - \frac{\bar{C}}{V_0} Z_{\dot{w}} \right)}$
x_θ	$-g \cos\theta_e - \frac{\dot{X}_{\dot{w}} g \sin\theta_e}{m - \dot{Z}_{\dot{w}}}$	$-g \cos\theta_e - \frac{\frac{\bar{C}}{V_0} X_{\dot{w}} g \sin\theta_e}{m' - \frac{\bar{C}}{V_0} Z_{\dot{w}}}$
z_θ	$-\frac{mg \sin\theta_e}{m - \dot{Z}_{\dot{w}}}$	$-\frac{m'g \sin\theta_e}{m' - \frac{\bar{C}}{V_0} Z_{\dot{w}}}$
m_θ	$-\frac{\dot{M}_{\dot{w}} mg \sin\theta_e}{I_y(m - \dot{Z}_{\dot{w}})}$	$-\frac{\frac{\bar{C}}{V_0} M_{\dot{w}} m' g \sin\theta_e}{I'_y \left(m' - \frac{\bar{C}}{V_0} Z_{\dot{w}} \right)}$

Table A2.6 Concise Longitudinal Control Derivatives

Equivalent Expressions		
Concise Derivative	In Terms of Dimensional Derivatives	In Terms of Dimensionless Derivatives
x_η	$\frac{\overset{\circ}{X}_\eta}{m} + \frac{\overset{\circ}{X}_{\dot{w}} \overset{\circ}{Z}_\eta}{m(m - \overset{\circ}{Z}_{\dot{w}})}$	$\frac{V_0 X_\eta}{m'} + \frac{\frac{\bar{\bar{C}}}{V_0} X_{\dot{w}} Z_\eta}{m'(m' - \frac{\bar{\bar{C}}}{V_0} Z_{\dot{w}})}$
z_η	$\frac{\overset{\circ}{Z}_\eta}{m - \overset{\circ}{Z}_{\dot{w}}}$	$\frac{V_0 Z_\eta}{m' - \frac{\bar{\bar{C}}}{V_0} Z_{\dot{w}}}$
m_η	$\frac{\overset{\circ}{M}_\eta}{I_y} + \frac{\overset{\circ}{M}_{\dot{w}} \overset{\circ}{Z}_\eta}{I_y(m - \overset{\circ}{Z}_{\dot{w}})}$	$\frac{V_0 M_\eta}{I'_y} + \frac{\bar{\bar{C}} M_{\dot{w}} Z_\eta}{I'_y(m' - \frac{\bar{\bar{C}}}{V_0} Z_{\dot{w}})}$
x_τ	$\frac{\overset{\circ}{X}_\tau}{m} + \frac{\overset{\circ}{X}_{\dot{w}} \overset{\circ}{Z}_\tau}{m(m - \overset{\circ}{Z}_{\dot{w}})}$	$\frac{V_0 X_\tau}{m'} + \frac{\frac{\bar{\bar{C}}}{V_0} X_{\dot{w}} Z_\tau}{m'(m' - \frac{\bar{\bar{C}}}{V_0} Z_{\dot{w}})}$
z_τ	$\frac{\overset{\circ}{Z}_\tau}{m - \overset{\circ}{Z}_{\dot{w}}}$	$\frac{V_0 Z_\tau}{m' - \frac{\bar{\bar{C}}}{V_0} Z_{\dot{w}}}$
m_τ	$\frac{\overset{\circ}{M}_\tau}{I_y} + \frac{\overset{\circ}{M}_{\dot{w}} \overset{\circ}{Z}_\tau}{I_y(m - \overset{\circ}{Z}_{\dot{w}})}$	$\frac{V_0 M_\tau}{I'_y} + \frac{\bar{\bar{C}} M_{\dot{w}} Z_\tau}{I'_y(m' - \frac{\bar{\bar{C}}}{V_0} Z_{\dot{w}})}$

Table A2.7 Concise Lateral-Directional Aerodynamic Stability Derivatives

Equivalent Expressions		
Concise Derivative	In Terms of Dimensional Derivatives	In Terms of Dimensionless Derivatives
y_v	$\frac{\overset{\circ}{Y}_v}{m}$	$\frac{Y_v}{m'}$
y_p	$\frac{\left(\overset{\circ}{Y}_p + mW_e\right)}{m}$	$\frac{(bY_p + m'W_e)}{m'}$
y_r	$\frac{\left(\overset{\circ}{Y}_r - mU_e\right)}{m}$	$\frac{(bY_r - m'U_e)}{m'}$
y_ϕ	$g \cos\theta_e$	$g \cos\theta_e$
y_ψ	$g \sin\theta_e$	$g \sin\theta_e$
l_v	$\frac{\left(I_z \overset{\circ}{L}_v + I_{xz} \overset{\circ}{N}_v\right)}{(I_x I_z - I_{xz}^2)}$	$\frac{(I'_z L_v + I'_{xz} N_v)}{(I'_x I'_z - I'_{xz}^2)}$
l_p	$\frac{\left(I_z \overset{\circ}{L}_p + I_{xz} \overset{\circ}{N}_p\right)}{(I_x I_z - I_{xz}^2)}$	$\frac{(I'_z L_p + I'_{xz} N_p)b}{(I'_x I'_z - I'_{xz}^2)}$
l_r	$\frac{\left(I_z \overset{\circ}{L}_r + I_{xz} \overset{\circ}{N}_r\right)}{(I_x I_z - I_{xz}^2)}$	$\frac{(I'_z L_r + I'_{xz} N_r)b}{(I'_x I'_z - I'_{xz}^2)}$
l_ϕ	0	0
l_ψ	0	0
n_v	$\frac{\left(I_x \overset{\circ}{N}_v + I_{xz} \overset{\circ}{L}_v\right)}{(I_x I_z - I_{xz}^2)}$	$\frac{(I'_x N_v + I'_{xz} L_v)}{(I'_x I'_z - I'_{xz}^2)}$
n_p	$\frac{\left(I_x \overset{\circ}{N}_p + I_{xz} \overset{\circ}{L}_p\right)}{(I_x I_z - I_{xz}^2)}$	$\frac{(I'_x N_p + I'_{xz} L_p)b}{(I'_x I'_z - I'_{xz}^2)}$
n_r	$\frac{\left(I_x \overset{\circ}{N}_r + I_{xz} \overset{\circ}{L}_r\right)}{(I_x I_z - I_{xz}^2)}$	$\frac{(I'_x N_r + I'_{xz} L_r)b}{(I'_x I'_z - I'_{xz}^2)}$
n_ϕ	0	0
n_ψ	0	0

Table A2.8 Concise Lateral-Directional Control Derivatives

Equivalent Expressions		
Concise Derivative	In Terms of Dimensional Derivatives	In Terms of Dimensionless Derivatives
y_ξ	$\frac{\overset{\circ}{Y}_\xi}{m}$	$\frac{V_0 Y_\xi}{m'}$
l_ξ	$\frac{(I_z \overset{\circ}{L}_\xi + I_{xz} \overset{\circ}{N}_\xi)}{(I_x I_z - I_{xz}^2)}$	$\frac{V_0 (I'_z L_\xi + I'_{xz} N_\xi)}{(I'_x I'_z - I'_{xz}^2)}$
n_ξ	$\frac{(I_x \overset{\circ}{N}_\xi + I_{xz} \overset{\circ}{L}_\xi)}{(I_x I_z - I_{xz}^2)}$	$\frac{V_0 (I'_x N_\xi + I'_{xz} L_\xi)}{(I'_x I'_z - I'_{xz}^2)}$
y_ζ	$\frac{\overset{\circ}{Y}_\zeta}{m}$	$\frac{V_0 Y_\zeta}{m'}$
l_ζ	$\frac{(I_z \overset{\circ}{L}_\zeta + I_{xz} \overset{\circ}{N}_\zeta)}{(I_x I_z - I_{xz}^2)}$	$\frac{V_0 (I'_z L_\zeta + I'_{xz} N_\zeta)}{(I'_x I'_z - I'_{xz}^2)}$
n_ζ	$\frac{(I_x \overset{\circ}{N}_\zeta + I_{xz} \overset{\circ}{L}_\zeta)}{(I_x I_z - I_{xz}^2)}$	$\frac{V_0 (I'_x N_\zeta + I'_{xz} L_\zeta)}{(I'_x I'_z - I'_{xz}^2)}$

Appendix 3: Aircraft Response Transfer Functions Referred to Aircraft Body Axes

A3.1 Longitudinal Response Transfer Functions in Terms of Dimensional Derivatives

The following longitudinal numerator polynomials describe the motion of the aircraft in response to elevator η input. To obtain the numerators describing the response to engine thrust input, it is simply necessary to replace the subscript η with τ .

Common Denominator Polynomial

$$\Delta(s) = as^4 + bs^3 + cs^2 + ds + e$$

$$a = mI_y \left(m - \dot{Z}_{\dot{w}} \right)$$

$$b = I_y \left(\ddot{X}_u \dot{Z}_{\dot{w}} - \dot{X}_{\dot{w}} \dot{Z}_u \right) - mI_y \left(\ddot{X}_u + \dot{Z}_w \right) - mM_w \left(\dot{Z}_q + mU_e \right) - m\dot{M}_q \left(m - \dot{Z}_{\dot{w}} \right)$$

$$\begin{aligned} c = & I_y \left(\ddot{X}_u \dot{Z}_w - \dot{X}_w \dot{Z}_u \right) + \left(\ddot{X}_u \dot{M}_{\dot{w}} - \dot{X}_{\dot{w}} \dot{M}_u \right) \left(\dot{Z}_q + mU_e \right) \\ & + \dot{Z}_u \left(\dot{X}_{\dot{w}} \dot{M}_q - \dot{X}_q \dot{M}_{\dot{w}} \right) + \left(\dot{X}_u \dot{M}_q - \dot{X}_q \dot{M}_u \right) \left(m - \dot{Z}_{\dot{w}} \right) \\ & + m \left(\dot{M}_q \dot{Z}_w - \dot{M}_w \dot{Z}_q \right) + mW_e \left(\dot{M}_{\dot{w}} \dot{Z}_u - \dot{M}_u \dot{Z}_{\dot{w}} \right) \\ & + m^2 \left(\dot{M}_{\dot{w}} g \sin \theta_e + W_e \dot{M}_u - U_e \dot{M}_w \right) \end{aligned}$$

$$\begin{aligned} d = & \left(\ddot{X}_u \dot{M}_w - \dot{X}_w \dot{M}_u \right) \left(\dot{Z}_q + mU_e \right) \\ & + \left(\dot{M}_u \dot{Z}_w - \dot{M}_w \dot{Z}_u \right) \left(\dot{X}_q - mW_e \right) + \dot{M}_q \left(\dot{X}_w \dot{Z}_u - \dot{X}_u \dot{Z}_w \right) \\ & + mg \cos \theta_e \left(\dot{M}_{\dot{w}} \dot{Z}_u + \dot{M}_u \left(m - \dot{Z}_{\dot{w}} \right) \right) + mg \sin \theta_e \left(\dot{X}_{\dot{w}} \dot{M}_u - \dot{X}_u \dot{M}_{\dot{w}} + m \dot{M}_w \right) \end{aligned}$$

$$e = mg \sin \theta_e \left(\dot{X}_w \dot{M}_u - \dot{X}_u \dot{M}_w \right) + mg \cos \theta_e \left(\dot{M}_w \dot{Z}_u - \dot{M}_u \dot{Z}_w \right)$$

Numerator Polynomial

$$N_\eta^u(s) = as^3 + bs^2 + cs + d$$

$$a \quad I_y \left(\dot{X}_w \dot{Z}_\eta + \dot{X}_\eta \left(m - \dot{Z}_w \right) \right)$$

$$b \quad \begin{aligned} & \dot{X}_\eta \left(-I_y \dot{Z}_w - M_w \left(\dot{Z}_q + mU_e \right) - \dot{M}_q \left(m - \dot{Z}_w \right) \right) \\ & + \dot{Z}_\eta \left(I_y \dot{X}_w - \dot{X}_w \dot{M}_q + \dot{M}_w \left(\dot{X}_q - mW_e \right) \right) \\ & + \dot{M}_\eta \left(\left(\dot{X}_q - mW_e \right) \left(m - \dot{Z}_w \right) + \dot{X}_w \left(\dot{Z}_q + mU_e \right) \right) \end{aligned}$$

$$c \quad \begin{aligned} & \dot{X}_\eta \left(\dot{Z}_w \dot{M}_q - \dot{M}_w \left(\dot{Z}_q + mU_e \right) + mg \sin \theta_e \dot{M}_w \right) \\ & + \dot{Z}_\eta \left(\dot{M}_w \left(\dot{X}_q - mW_e \right) - \dot{X}_w \dot{M}_q - mg \cos \theta_e \dot{M}_w \right) \\ & + \dot{M}_\eta \left(\dot{X}_w \left(\dot{Z}_q + mU_e \right) - \dot{Z}_w \left(\dot{X}_q - mW_e \right) - mg \cos \theta_e \left(m - \dot{Z}_w \right) - mg \sin \theta_e \dot{X}_w \right) \end{aligned}$$

$$d \quad \dot{X}_\eta \dot{M}_w mg \sin \theta_e - \dot{Z}_\eta \dot{M}_w mg \cos \theta_e + \dot{M}_\eta \left(\dot{Z}_w mg \cos \theta_e - \dot{X}_w mg \sin \theta_e \right)$$

Numerator Polynomial

$$N_\eta^w(s) = as^3 + bs^2 + cs + d$$

$$a \quad mI_y \dot{Z}_\eta$$

$$b \quad \begin{aligned} & I_y \dot{X}_u \dot{Z}_u - \dot{Z}_\eta \left(I_y \dot{X}_u + m \dot{M}_q \right) + m \dot{M}_\eta \left(\dot{Z}_q + mU_e \right) \\ & \dot{X}_\eta \left(\dot{M}_u \left(\dot{Z}_q + mU_e \right) - \dot{Z}_u \dot{M}_q \right) + \dot{Z}_\eta \left(\dot{X}_u \dot{M}_q - \dot{M}_u \left(\dot{X}_q - mW_e \right) \right) \end{aligned}$$

$$c \quad + \dot{M}_\eta \left(\dot{Z}_u \left(\dot{X}_q - mW_e \right) - \dot{X}_u \left(\dot{Z}_q + mU_e \right) - m^2 g \sin \theta_e \right)$$

$$d \quad - \dot{X}_\eta \dot{M}_u mg \sin \theta_e + \dot{Z}_\eta \dot{M}_u mg \cos \theta_e + \dot{M}_\eta \left(\dot{X}_u mg \sin \theta_e - \dot{Z}_u mg \cos \theta_e \right)$$

Numerator Polynomials

$$N_\eta^q(s) = s(as^2 + bs + c) \text{ and } N_\eta^\theta(s) = as^2 + bs + c$$

$$a \quad m \dot{Z}_\eta \dot{M}_w + m \dot{M}_\eta \left(m - \dot{Z}_w \right)$$

$$b \quad \begin{aligned} & \dot{X}_\eta \left(\dot{Z}_u \dot{M}_w + \dot{M}_u \left(m - \dot{Z}_w \right) \right) + \dot{Z}_\eta \left(m \dot{M}_w - \dot{X}_u \dot{M}_w + \dot{M}_u \dot{X}_w \right) \\ & + \dot{M}_\eta \left(-\dot{X}_u \left(m - \dot{Z}_w \right) - \dot{Z}_u \dot{X}_w - m \dot{Z}_w \right) \end{aligned}$$

$$c \quad \dot{X}_\eta \left(\dot{Z}_u \dot{M}_w - \dot{M}_u \dot{Z}_w \right) + \dot{Z}_\eta \left(\dot{X}_w \dot{M}_u - \dot{M}_w \dot{X}_u \right) + \dot{M}_\eta \left(\dot{X}_u \dot{Z}_w - \dot{Z}_u \dot{X}_w \right)$$

A3.2 Lateral-Directional Response Transfer Functions in Terms of Dimensional Derivatives

The following lateral-directional numerator polynomials describe the motion of the aircraft in response to aileron ξ input. To obtain the numerators describing the response to rudder input, it is simply necessary to replace the subscript ξ with ζ .

Common Denominator Polynomial

$$\begin{aligned}\Delta(s) &= s(as^4 + bs^3 + cs^2 + ds + e) \\ a &= m(I_x I_z - I_{xz}^2) \\ b &= -\dot{Y}_v(I_x I_z - I_{xz}^2) - m(I_x \dot{N}_r + I_{xz} \dot{L}_r) - m(I_z \dot{L}_p + I_{xz} \dot{N}_p) \\ c &= \dot{Y}_v(I_x \dot{N}_r + I_{xz} \dot{L}_r) + \dot{Y}_v(I_z \dot{L}_p + I_{xz} \dot{N}_p) - (\dot{Y}_p + mW_e)(I_z \dot{L}_v + I_{xz} \dot{N}_v) \\ &\quad - (\dot{Y}_r - mU_e)(I_x \dot{N}_v + I_{xz} \dot{L}_v) + m(\dot{L}_p \dot{N}_r - \dot{L}_r \dot{N}_p) \\ d &= \dot{Y}_v(\dot{L}_r \dot{N}_p - \dot{L}_p \dot{N}_r) + (\dot{Y}_p + mW_e)(\dot{L}_v \dot{N}_r - \dot{L}_r \dot{N}_v) \\ &\quad + (\dot{Y}_r - mU_e)(\dot{L}_p \dot{N}_v - \dot{L}_v \dot{N}_p) \\ &\quad - mg \cos \theta_e(I_z \dot{L}_v + I_{xz} \dot{N}_v) - mg \sin \theta_e(I_x \dot{N}_v + I_{xz} \dot{L}_v) \\ e &= mg \cos \theta_e(\dot{L}_v \dot{N}_r - \dot{L}_r \dot{N}_v) + mg \sin \theta_e(\dot{L}_p \dot{N}_v - \dot{L}_v \dot{N}_p)\end{aligned}$$

Numerator Polynomial

$$\begin{aligned}N_\xi^y(s) &= s(as^3 + bs^2 + cs + d) \\ a &= \dot{Y}_\xi(I_x I_z - I_{xz}^2) \\ b &= \dot{Y}_\xi(-I_x \dot{N}_r - I_z \dot{L}_p - I_{xz}(\dot{L}_r + \dot{N}_p)) + \dot{L}_\xi(I_z(\dot{Y}_p + mW_e) + I_{xz}(\dot{Y}_r - mU_e)) \\ &\quad + \dot{N}_\xi(I_x(\dot{Y}_r - mU_e) + I_{xz}(\dot{Y}_p + mW_e)) \\ c &= \dot{Y}_\xi(\dot{L}_p \dot{N}_r - \dot{L}_r \dot{N}_p) \\ &\quad + \dot{L}_\xi(\dot{N}_p(\dot{Y}_r - mU_e) - \dot{N}_r(\dot{Y}_p + mW_e) + mg(I_z \cos \theta_e + I_{xz} \sin \theta_e)) \\ &\quad + \dot{N}_\xi(\dot{L}_r(\dot{Y}_p + mW_e) - \dot{L}_p(\dot{Y}_r - mU_e) + mg(I_x \sin \theta_e + I_{xz} \cos \theta_e)) \\ d &= \dot{L}_\xi(\dot{N}_p mg \sin \theta_e - \dot{N}_r mg \cos \theta_e) + \dot{N}_\xi(\dot{L}_r mg \cos \theta_e - \dot{L}_p mg \sin \theta_e)\end{aligned}$$

Numerator Polynomials

$$N_\xi^p(s) = s(as^3 + bs^2 + cs + d) \text{ and } N_\xi^\phi(s) = as^3 + bs^2 + cs + d$$

$$a \quad m(I_z \dot{L}_\xi + I_{xz} \dot{N}_\xi)$$

$$b \quad \dot{Y}_\xi \left(I_z \dot{L}_v + I_{xz} \dot{N}_v \right) + \dot{L}_\xi \left(-I_z \dot{Y}_v - m \dot{N}_r \right) + \dot{N}_\xi \left(m \dot{L}_r - I_{xz} \dot{Y}_v \right)$$

$$c \quad \dot{Y}_\xi \left(\dot{L}_r \dot{N}_v - \dot{L}_v \dot{N}_r \right) + \dot{L}_\xi \left(\dot{N}_r \dot{Y}_v - \dot{N}_v \dot{Y}_r + mU_e \dot{N}_v \right) \\ + \dot{N}_\xi \left(\dot{L}_v \dot{Y}_r - \dot{L}_r \dot{Y}_v - mU_e \dot{L}_v \right)$$

$$d \quad mg \sin \theta_e \left(\dot{L}_v \dot{N}_\xi - \dot{L}_\xi \dot{N}_v \right)$$

Numerator Polynomials

$$N_\xi^r(s) = s(as^3 + bs^2 + cs + d) \text{ and } N_\xi^\psi(s) = as^3 + bs^2 + cs + d$$

$$a \quad m(I_x \dot{N}_\xi + I_{xz} \dot{L}_\xi)$$

$$b \quad \dot{Y}_\xi \left(I_x \dot{N}_v + I_{xz} \dot{L}_v \right) + \dot{L}_\xi \left(m \dot{N}_p - I_{xz} \dot{Y}_v \right) - \dot{N}_\xi \left(I_x \dot{Y}_v + m \dot{L}_p \right)$$

$$c \quad \dot{Y}_\xi \left(\dot{L}_v \dot{N}_p - \dot{L}_p \dot{N}_v \right) + \dot{L}_\xi \left(\dot{N}_v \dot{Y}_p - \dot{N}_p \dot{Y}_v + mW_e \dot{N}_v \right) \\ + \dot{N}_\xi \left(\dot{L}_p \dot{Y}_v - \dot{L}_v \dot{Y}_p - mW_e \dot{L}_v \right)$$

$$d \quad mg \cos \theta_e \left(\dot{L}_\xi \dot{N}_v - \dot{L}_v \dot{N}_\xi \right)$$

A3.3 Longitudinal Response Transfer Functions in Terms of Concise Derivatives

Again, the longitudinal numerator polynomials describe the motion of the aircraft in response to elevator η input. To obtain the numerators describing the response to engine thrust input, it is simply necessary to replace the subscript η with τ .

Common Denominator Polynomial

$$\Delta(s) = as^4 + bs^3 + cs^2 + ds + e$$

$$a \quad 1$$

$$b \quad -(m_q + x_u + z_w)$$

$$c \quad (m_q z_w - m_w z_q) + (m_q x_u - m_u x_q) + (x_u z_w - x_w z_u) - m_\theta$$

$$d \quad (m_\theta x_u - m_u x_\theta) + (m_\theta z_w - m_w z_\theta) + m_q (x_w z_u - x_u z_w) + x_q (m_u z_w - m_w z_u) + z_q (m_w x_u - m_u x_w)$$

$$e \quad m_\theta (x_w z_u - x_u z_w) + x_\theta (m_u z_w - m_w z_u) + z_\theta (m_w x_u - m_u x_w)$$

Numerator Polynomial

$$N_{\eta}^u(s) = as^3 + bs^2 + cs + d$$

$$a \quad x_{\eta}$$

$$b \quad m_{\eta}x_q - x_{\eta}(m_q + z_w) + z_{\eta}x_w$$

$$c \quad m_{\eta}(x_wz_q - x_qz_w + x_{\theta}) + x_{\eta}(m_qz_w - m_wz_q - m_{\theta}) + z_{\eta}(m_wx_q - m_qx_w)$$

$$d \quad m_{\eta}(x_wz_{\theta} - x_{\theta}z_w) + x_{\eta}(m_{\theta}z_w - m_wz_{\theta}) + z_{\eta}(m_wx_{\theta} - m_{\theta}x_w)$$

Numerator Polynomial

$$N_{\eta}^w(s) = as^3 + bs^2 + cs + d$$

$$a \quad z_{\eta}$$

$$b \quad m_{\eta}z_q + x_{\eta}z_u - z_{\eta}(m_q + x_u)$$

$$c \quad m_{\eta}(x_qz_u - x_uz_q + z_{\theta}) + x_{\eta}(m_uz_q - m_qz_u) + z_{\eta}(m_qx_u - m_ux_q - m_{\theta})$$

$$d \quad m_{\eta}(x_{\theta}z_u - x_uz_{\theta}) + x_{\eta}(m_uz_{\theta} - m_{\theta}z_u) + z_{\eta}(m_{\theta}x_u - m_ux_{\theta})$$

Numerator Polynomials

$$N_{\eta}^q(s) = s(as^2 + bs + c) \text{ and } N_{\eta}^{\theta}(s) = as^2 + bs + c$$

$$a \quad m_{\eta}$$

$$b \quad -m_{\eta}(x_u + z_w) + x_{\eta}m_u + z_{\eta}m_w$$

$$c \quad m_{\eta}(x_uz_w - x_wz_u) + x_{\eta}(m_wz_u - m_uz_w) + z_{\eta}(m_ux_w - m_wx_u)$$

A3.4 Lateral-Directional Response Transfer Functions in Terms of Concise Derivatives

As before, the lateral-directional numerator polynomials describe the motion of the aircraft in response to aileron ξ input. To obtain the numerators describing the response to rudder input, it is simply necessary to replace the subscript ξ with ζ .

Common Denominator Polynomial

$$\Delta(s) = as^5 + bs^4 + cs^3 + ds^2 + es + f$$

$$a \quad 1$$

$$b \quad -(l_p + n_r + y_v)$$

$$c \quad (l_pn_r - l_rn_p) + (n_ry_v - n_vy_r) + (l_py_v - l_vy_p) - (l_{\phi} + n_{\psi})$$

$$d \quad (l_pn_{\psi} - l_{\psi}n_p) + (l_{\phi}n_r - l_rn_{\phi}) + l_v(n_ry_p - n_py_r - y_{\phi}) + n_v(l_py_r - l_ry_p - y_{\psi}) + y_v(l_rn_p - l_pn_r + l_{\phi} + n_{\psi})$$

$$e \quad (l_{\phi}n_{\psi} - l_{\psi}n_{\phi}) + l_v((n_ry_{\phi} - n_{\phi}y_r) + (n_{\psi}y_p - n_py_{\psi})) + n_v((l_{\phi}y_r - l_ry_{\phi}) + (l_py_{\psi} - l_{\psi}y_p)) + y_v((l_rn_{\phi} - l_{\phi}n_r) + (l_{\psi}n_p - l_pn_{\psi}))$$

$$f \quad l_v(n_{\psi}y_{\phi} - n_{\phi}y_{\psi}) + n_v(l_{\phi}y_{\psi} - l_{\psi}y_{\phi}) + y_v(l_{\psi}n_{\phi} - l_{\phi}n_{\psi})$$

Numerator Polynomial

$$N_\xi^v(s) = as^4 + bs^4 + cs^2 + ds + e$$

$$a \quad y_\xi$$

$$b \quad l_\xi y_p + n_\xi y_r - y_\xi(l_p + n_r)$$

$$c \quad l_\xi(n_p y_r - n_r y_p + y_\phi) + n_\xi(l_r y_p - l_p y_r + y_\psi) + y_\xi(l_p n_r - l_r n_p - l_\phi - n_\psi)$$

$$d \quad l_\xi(n_\phi y_r - n_r y_\phi + n_p y_\psi - n_\psi y_p) + n_\xi(l_r y_\phi - l_\phi y_r + l_\psi y_p - l_p y_\psi) + y_\xi(l_\phi n_r - l_r n_\phi + l_p n_\psi - l_\psi n_p)$$

$$e \quad l_\xi(n_\phi y_\psi - n_\psi y_\phi) + n_\xi(l_\psi y_\phi - l_\phi y_\psi) + y_\xi(l_\phi n_\psi - l_\psi n_\phi)$$

Numerator Polynomials

$$N_\xi^p(s) = s(as^3 + bs^2 + cs + d) \text{ and } N_\xi^\phi(s) = as^3 + bs^2 + cs + d$$

$$a \quad l_\xi$$

$$b \quad -l_\xi(n_r + y_v) + n_\xi l_r + y_\xi l_v$$

$$c \quad l_\xi(n_r y_v - n_v y_r - n_\psi) + n_\xi(l_v y_r - l_r y_v + l_\psi) + y_\xi(l_r n_v - l_v n_r)$$

$$d \quad l_\xi(n_\psi y_v - n_v y_\psi) + n_\xi(l_v y_\psi - l_\psi y_v) + y_\xi(l_\psi n_v - l_v n_\psi)$$

Numerator Polynomials

$$N_\xi^r(s) = s(as^3 + bs^2 + cs + d) \text{ and } N_\xi^\psi(s) = as^3 + bs^2 + cs + d$$

$$a \quad n_\xi$$

$$b \quad l_\xi n_p - n_\xi(l_p + y_v) + y_\xi n_v$$

$$c \quad l_\xi(n_v y_p - n_p y_v + n_\phi) + n_\xi(l_p y_v - l_v y_p - l_\phi) + y_\xi(l_v n_p - l_p n_v)$$

$$d \quad l_\xi(n_\psi y_\phi - n_\phi y_\psi) + n_\xi(l_\phi y_v - l_v y_\phi) + y_\xi(l_v n_\phi - l_\phi n_v)$$

Appendix 4: Units, Conversions, and Constants

Table A4.1 Factors for Conversion from Imperial to SI Units

Parameter	Symbol	Imperial Unit	Equivalent SI Unit
Mass	m	1 slug	14.594 kg
Length	l	1 ft	0.3048 m
Velocity	V	1 ft/s	0.3048 m/s
Acceleration	a	1 ft/s ²	0.3048 m/s ²
Force	F	1 Lb	4.448 N
Moment	M	1 Lbft	1.356 Nm
Density	ρ	1 slug/ft ³	515.383 kg/m ³
Inertia	I	1 slugft ²	1.3558 kgm ²

Table A4.2 Useful Constants

Constant	Symbol	Imperial Unit	SI Unit
1 knot	kt	1.689 ft/s	0.515 m/s
Sea level air density	ρ_0	0.00238 slug/ft ³	1.225 kg/m ³
Speed of sound at sea level	a_0	1116.44 ft/s	340.29 m/s
Radian	rad	57.3 deg	57.3 deg
Gravitational acceleration	g	32.17 ft/s ²	9.81 m/s ²

Appendix 5: A Very Short Table of Laplace Transforms

	$F(t)$	$f(s)$
1	1	$\frac{1}{s}$
2	e^{at}	$\frac{1}{s-a}$
3	$\sin kt$	$\frac{k}{s^2 + k^2}$
4	$\cos kt$	$\frac{s}{s^2 + k^2}$
5	$e^{-at} \sin kt$	$\frac{k}{(s+a)^2 + k^2}$
6	$e^{-at} \cos kt$	$\frac{(s+a)}{(s+a)^2 + k^2}$

Appendix 6: The Dynamics of a Linear Second Order System

The solution of the linearised small-perturbation equations of motion of an aircraft contains recognisable classical second order system terms. A review of the dynamics of a second order system is therefore useful as an aid to the correct interpretation of the solution of these equations.

Consider the classical mass-spring-damper system whose motion is described by the equation of motion

$$m\ddot{x}(t) + c\dot{x}(t) + kx(t) = f(t) \quad (\text{A6.1})$$

where $x(t)$ is the displacement of the mass and $f(t)$ is the forcing function. The constants of the system comprise the mass m , the viscous damping c , and the spring stiffness k .

Classical unforced motion results when the forcing $f(t)$ is made zero and the mass is displaced by, say, A and then released. [Equation \(A6.1\)](#) may then be written as

$$m\ddot{x}(t) + c\dot{x}(t) + kx(t) = 0 \quad (\text{A6.2})$$

and the initial conditions are defined: $\dot{x}(0) = 0$ and $x(0) = A$. The time response of the motion of the mass may be found by solving [equation \(A6.2\)](#) subject to the constraints imposed by the initial conditions. This is readily achieved with the aid of the Laplace transform.

Thus,

$$\begin{aligned} L\{m\ddot{x}(t) + c\dot{x}(t) + kx(t)\} &= m(s^2x(s) - sx(0) - \dot{x}(0)) + c(sx(s) - x(0)) + kx(s) \\ &= m(s^2x(s) - sA) + c(sx(s) - A) + kx(s) = 0 \end{aligned}$$

which after some rearrangement may be written as

$$x(s) = \frac{A(ms + c)}{(ms^2 + cs + k)} \quad (\text{A6.3})$$

or, alternatively,

$$x(s) = \frac{A(s + 2\zeta\omega)}{(s^2 + 2\zeta\omega s + \omega^2)} \quad (\text{A6.4})$$

where

$$\begin{aligned} 2\zeta\omega &= \frac{c}{m} \\ \omega^2 &= \frac{k}{m} \end{aligned} \quad (\text{A6.5})$$

ζ = system damping ratio

ω = system undamped natural frequency

The time response $x(t)$ may be obtained by determining the inverse Laplace transform of [equation \(A6.4\)](#), and the form of the solution obviously depends on the magnitudes of the physical constants of the system: m , c , and k . The characteristic equation of the system is given by equating the denominator of [equation \(A6.3\)](#) or [\(A6.4\)](#) to zero:

$$ms^2 + cs + k = 0 \quad (\text{A6.6})$$

or, equivalently,

$$s^2 + 2\zeta\omega s + \omega^2 = 0 \quad (\text{A6.7})$$

To facilitate the determination of the inverse Laplace transform of [equation \(A6.4\)](#), the denominator is first factorised and the expression on the right-hand side is split into partial fractions. Whence

$$\begin{aligned} x(s) &= \frac{A(s + 2\zeta\omega)}{(s + \omega(\zeta + \sqrt{\zeta^2 - 1}))(s + \omega(\zeta - \sqrt{\zeta^2 - 1}))} \\ &= \frac{A}{2} \left(\frac{\left(1 + \frac{\zeta}{\sqrt{\zeta^2 - 1}}\right)}{(s + \omega(\zeta + \sqrt{\zeta^2 - 1}))} + \frac{\left(1 - \frac{\zeta}{\sqrt{\zeta^2 - 1}}\right)}{(s + \omega(\zeta - \sqrt{\zeta^2 - 1}))} \right) \end{aligned} \quad (\text{A6.8})$$

With reference to the table of transform pairs given in [Appendix 5](#), transform pair 2, the inverse Laplace transform of [equation \(A6.8\)](#) is readily obtained:

$$x(t) = \frac{Ae^{-\omega\zeta t}}{2} \left(\left(1 + \frac{\zeta}{\sqrt{\zeta^2 - 1}}\right)e^{-\omega t\sqrt{\zeta^2 - 1}} + \left(1 - \frac{\zeta}{\sqrt{\zeta^2 - 1}}\right)e^{\omega t\sqrt{\zeta^2 - 1}} \right) \quad (\text{A6.9})$$

[Equation \(A6.9\)](#) is the general solution describing the unforced motion of the mass, and the type of response depends on the value of the damping ratio.

- When $\zeta = 0$, [equation \(A6.9\)](#) reduces to

$$x(t) = \frac{A}{2}(e^{-j\omega t} + e^{j\omega t}) = A \cos \omega t \quad (\text{A6.10})$$

which describes undamped harmonic motion or, alternatively, a neutrally stable system.

- When $0 < \zeta < 1$, [equation \(A6.9\)](#) may be modified by writing

$$\omega_n = \omega\sqrt{1 - \zeta^2}$$

where ω_n is the damped natural frequency. Thus the solution is given by

$$\begin{aligned} x(t) &= \frac{Ae^{-\omega\zeta t}}{2} \left(\left(1 + \frac{j\zeta}{\sqrt{1-\zeta^2}} \right) e^{-j\omega_n t} + \left(1 - \frac{j\zeta}{\sqrt{1-\zeta^2}} \right) e^{j\omega_n t} \right) \\ &= Ae^{-\omega\zeta t} \left(\cos \omega_n t - \frac{\omega\zeta}{\omega_n} \sin \omega_n t \right) \end{aligned} \quad (\text{A6.11})$$

which describes damped harmonic motion.

- When $\zeta = 1$, the coefficients of the exponential terms in [equation \(A6.9\)](#) become infinite. However, by expressing the exponentials as series and by letting $\zeta \rightarrow 1$, it may be shown that the damped natural frequency ω_n tends to zero and the solution is given by

$$x(t) = Ae^{-\omega t}(1 - \omega t) \quad (\text{A6.12})$$

- When $\zeta > 1$, the solution is given by [equation \(A6.9\)](#) directly and so is a function of a number of exponential terms. The motion thus described is non-oscillatory and is exponentially convergent.

Typical response time histories for a range of values of damping ratio are shown in [Fig. A6.1](#).

It is important to note that the type of response is governed entirely by the damping ratio and the undamped natural frequency, which in turn determine the roots of the characteristic [equation, \(A6.6\) or \(A6.7\)](#). Thus the dynamic properties of the system may be directly attributed to its physical properties. Consequently, the type of unforced response may be ascertained simply by inspection of the characteristic equation. A summary of these observations for a stable system are given in the following table.

Summary of a Stable System		
Damping Ratio	Roots of Characteristic Equation	Type of Response
$\zeta = 0$	$(s + j\omega)(s - j\omega) = 0$ Complex with zero real part	Undamped sinusoidal oscillation with frequency ω
$0 < \zeta < 1$	$(s + \omega\zeta + j\omega_n)(s + \omega\zeta - j\omega_n) = 0$ Complex with non-zero real part	Damped sinusoidal oscillation with frequency $\omega_n = \omega\sqrt{1 - \zeta^2}$
$\zeta = 1$	$(s + \omega)^2 = 0$ Repeated real roots	Exponential convergence of form $e^{-\omega t}(1 - \omega t)$
$\zeta > 1$	$(s + r_1)(s + r_2) = 0$ Real roots, where $r_1 = \omega(\zeta + \sqrt{\zeta^2 - 1})$ $r_2 = \omega(\zeta - \sqrt{\zeta^2 - 1})$	Exponential convergence of general form $k_1 e^{-r_1 t} + k_2 e^{-r_2 t}$

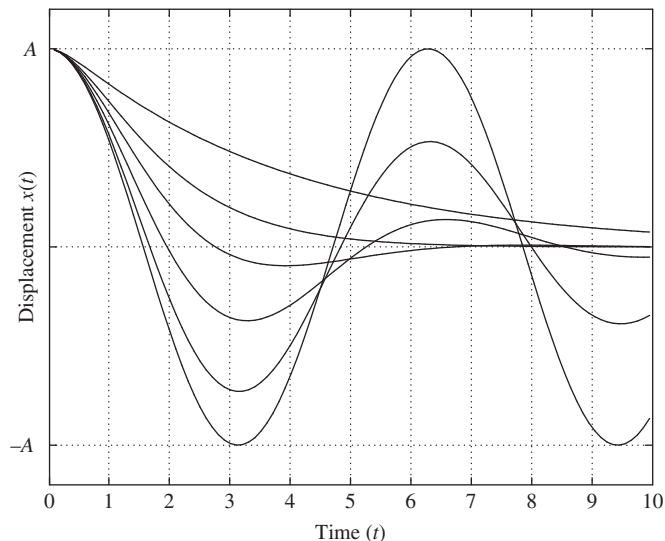


FIGURE A6.1 Typical second-order system responses.

The classical mass-spring-damper system is always stable. However, for rather more general systems which demonstrate similar properties this may not necessarily be so. For a more general interpretation, including unstable systems in which $\zeta < 0$, it is sufficient only to note that the solutions are similar except that the motion they describe is divergent rather than convergent. Aeroplanes typically demonstrate both stable and unstable characteristics, both of which are conveniently described by this simple linear second order model.

Appendix 7: North American Aerodynamic Derivative Notation

Table A7.1 Longitudinal Normalised Derivatives

Dimensionless Coefficient	Multiplier	Dimensional
$C_{x_u} = -(M_0 C_{D_M} + 2C_D)$	$\rho V_0 S / 2m$	X_u
$C_{x_u}^* = -(M_0 C_{D_M} + 2C_D) + M_0 C_{\tau_M} \cos \kappa$	$\rho V_0 S / 2m$	X_u^*
$C_{x_{\dot{w}}} = C_{x_{\dot{\alpha}}}$	$\rho S \bar{C} / 4m$	$X_{\dot{w}}$
$C_{x_w} = C_L - C_{D_\alpha}$	$\rho V_0 S / 2m$	X_w
C_{x_q}	$\rho V_0 S \bar{C} / 4m$	X_q
C_{x_δ}	$\rho V_0^2 S / 2m$	X_δ
$C_{z_u} = -(M_0 C_{L_M} + 2C_L)$	$\rho V_0 S / 2m$	Z_u
$C_{z_u}^* = -(M_0 C_{L_M} + 2C_L) - M_0 C_{\tau_M} \sin \kappa$	$\rho V_0 S / 2m$	Z_u^*
$C_{z_{\dot{w}}} = C_{z_{\dot{\alpha}}}$	$\rho S \bar{C} / 4m$	$Z_{\dot{w}}$
$C_{z_w} = -(C_D + C_{L_\alpha})$	$\rho V_0 S / 2m$	Z_w
C_{z_q}	$\rho V_0 S \bar{C} / 4m$	Z_q
C_{z_δ}	$\rho V_0^2 S / 2m$	Z_δ
$C_{m_u} = M_0 C_{m_M}$	$\rho V_0 S \bar{C} / 2I_y$	M_u
$C_{m_u}^* = M_0 C_{m_M} + M_0 \frac{z_\tau}{\bar{C}} C_{\tau_M} \cos \kappa$	$\rho V_0 S \bar{C} / 2I_y$	M_u^*
$C_{m_{\dot{w}}} = C_{m_{\dot{\alpha}}}$	$\rho S \bar{C} / 4I_y$	$M_{\dot{w}}$
$C_{m_w} = C_{m_\alpha}$	$\rho V_0 S \bar{C} / 2I_y$	M_w
C_{m_q}	$\rho V_0 S \bar{C}^2 / 4I_y$	M_q
C_{m_δ}	$\rho V_0^2 S \bar{C} / 2I_y$	M_δ

Notes: Thrust coefficient is defined as $C_\tau = \tau / \frac{1}{2} \rho V_0^2 S$. In the notational style, $C_{\tau_M} = \partial C_\tau / \partial M$; κ is the (upward) inclination of the thrust line with respect to the x axis; z_τ is the normal offset of the thrust line from the cg. It is assumed that x_τ , the axial offset of the thrust line from the cg, is negligibly small.

Table A7.2 Longitudinal Dimensionless Derivative Equivalents

American	British	American	British
C_{x_u}		C_{z_α}	Z_w
$C_{x_u}^*$	X_u	C_{z_q}	$2Z_q$
$C_{x_{\dot{\alpha}}}$	$2X_{\dot{w}}$	C_{z_δ}	$Z_{\eta\tau}$
C_{x_α}	X_w	C_{m_u}	
C_{x_q}	$2X_q$	$C_{m_u}^*$	M_u

(Continued)

Table A7.2 (Continued)

American	British	American	British
C_{x_δ}	$X_{\eta, \tau}$	C_{m_α}	$2M_{\dot{w}}$
C_{z_u}		C_{m_α}	M_w
$C_{z_u}^*$	Z_u	C_{m_q}	$2M_q$
C_{z_α}	$2Z_{\dot{w}}$	C_{m_δ}	$M_{\eta, \tau}$

Table A7.3 Lateral-Directional Normalised Derivatives

Dimensionless Coefficient	Multiplier	Dimensional
C_{y_v}	$\rho V_0 S / 2m$	Y_v
C_{y_β}	$\rho V_0^2 S / 2m$	Y_β
C_{y_p}	$\rho V_0 Sb / 4m$	Y_p
C_{y_r}	$\rho V_0 Sb / 4m$	Y_r
C_{y_δ}	$\rho V_0^2 S / 2m$	Y_δ
C_{l_v}	$\rho V_0 Sb / 2I_x$	L_v
C_{l_β}	$\rho V_0^2 Sb / 2I_x$	L_β
C_{l_p}	$\rho V_0 Sb^2 / 4I_x$	L_p
C_{l_r}	$\rho V_0 Sb^2 / 4I_x$	L_r
C_{l_δ}	$\rho V_0^2 Sb / 2I_x$	L_δ
C_{n_v}	$\rho V_0 Sb / 2I_z$	N_v
C_{n_β}	$\rho V_0^2 Sb / 2I_z$	N_β
C_{n_p}	$\rho V_0 Sb^2 / 4I_z$	N_p
C_{n_r}	$\rho V_0 Sb^2 / 4I_z$	N_r
C_{n_δ}	$\rho V_0^2 Sb / 2I_z$	N_δ

Table A7.4 Lateral-Directional Dimensionless Derivative Equivalents

American	British	American	British
C_{y_v}	Y_v	C_{l_r}	$2L_r$
C_{y_β}		C_{l_δ}	$L_{\xi, \zeta}$
C_{y_p}	$2Y_p$	C_{n_v}	N_v
C_{y_r}	$2Y_r$	C_{n_β}	
C_{y_δ}	$Y_{\xi, \zeta}$	C_{n_p}	$2N_p$
C_{l_v}	L_v	C_{n_r}	$2N_r$
C_{l_β}		C_{n_δ}	$N_{\xi, \zeta}$
C_{l_p}	$2L_p$		

Appendix 8: Approximate Expressions for the Dimensionless Aerodynamic Stability and Control Derivatives

Table A8.1 Longitudinal Aerodynamic Stability Derivatives

Small Perturbation Derivatives Referred to Aircraft Wind Axes			
Derivative	Description	Expression	Comments
X_u eq. (13.16)	Axial force due to velocity	$-2C_D - V_0 \frac{\partial C_D}{\partial V} + \frac{1}{\frac{1}{2}\rho V_0 S} \frac{\partial \tau}{\partial V}$	Drag and thrust effects due to velocity perturbation
X_w eq. (13.27)	Axial force due to "incidence"	$C_L - \frac{\partial C_D}{\partial \alpha}$	Lift and drag effects due to incidence perturbation
X_q eq. (13.46)	Axial force due to pitch rate	$-\bar{V}_T \frac{\partial C_{D_T}}{\partial \alpha_T}$	Tailplane drag effect, usually negligible
$X_{\dot{w}}$ eq. (13.68)	Axial force due to downwash lag	$-\bar{V}_T \frac{\partial C_{D_T}}{\partial \alpha_T} \frac{d\varepsilon}{d\alpha} \equiv X_q \frac{d\varepsilon}{d\alpha}$	Tailplane drag due to downwash lag effect (added mass effect)
Z_u eq. (13.21)	Normal force due to velocity	$-2C_L - V_0 \frac{\partial C_L}{\partial V}$	Lift effects due to velocity perturbation
Z_w eq. (13.30)	Normal force due to "incidence"	$-C_D - \frac{\partial C_L}{\partial \alpha}$	Lift and drag effects due to incidence perturbation
Z_q eq. (13.51)	Normal force due to pitch rate	$-\bar{V}_T a_1$	Tailplane lift effect
$Z_{\dot{w}}$ eq. (13.72)	Normal force due to downwash lag	$-\bar{V}_T a_1 \frac{d\varepsilon}{d\alpha} = Z_q \frac{d\varepsilon}{d\alpha}$	Tailplane lift due to downwash lag effect (added mass effect)
M_u eq. (13.34)	Pitching moment due to velocity	$V_0 \frac{\partial C_m}{\partial V}$	Mach dependent, small at low speed
M_w eq. (13.39)	Pitching moment due to "incidence"	$\frac{dC_m}{d\alpha} = -aK_n$	Pitch stiffness, dependent on static margin
M_q eq. (13.55)	Pitching moment due to pitch rate	$-\bar{V}_T a_1 \frac{l_T}{c} \equiv Z_q \frac{l_T}{c}$	Pitch damping, due mainly to tailplane
$M_{\dot{w}}$ eq. (13.76)	Pitching moment due to downwash lag	$-\bar{V}_T a_1 \frac{l_T}{c} \frac{d\varepsilon}{d\alpha} \equiv M_q \frac{d\varepsilon}{d\alpha}$	Pitch damping due to downwash lag effect at tailplane

Table A8.2 Lateral-Directional Aerodynamic Stability Derivatives**Small Perturbation Derivatives Referred to Aircraft Wind Axes**

Derivative	Description	Expression	Comments
Y_v eq. (13.82)	Side force due to sideslip	$\left(\frac{S_B}{S} y_B - \frac{S_F}{S} a_{1F} \right)$	Always negative and hence stabilising
L_v eq. (13.92)	Rolling moment due to sideslip	Wing with dihedral $- \frac{1}{Ss} \int_0^s c_y a_y \Gamma y dy$	Lateral static stability, determined by total dihedral effect; many contributions, most of which are difficult to estimate reliably; most accessible approximate contributions given
eq. (13.105)		Wing with aft sweep $- \frac{2C_L \tan \Lambda_{1/4}}{Ss} \int_0^s c_y y dy$	
eq. (13.108)		Fin contribution $- a_{1F} \bar{V}_F \frac{h_F}{l_F}$	
N_v eq. (13.112)	Yawing moment due to sideslip	Fin contribution $a_{1F} \bar{V}_F$	Natural weathercock stability, dominated by fin effect
Y_p eq. (13.117)	Side force due to roll rate	Fin contribution $- \frac{1}{Sb} \int_0^{H_F} a_h c_h h dh$	Fin effect dominates, often negligible
L_p eq. (13.128)	Rolling moment due to roll rate	Wing contribution $- \frac{1}{2Ss^2} \int_0^s (a_y + C_{Dy}) c_y y^2 dy$	Roll damping; wing effects dominate but fin and tailplane contribute
N_p eq. (13.137)	Yawing moment due to roll rate	Wing contribution $- \frac{1}{2Ss^2} \int_0^s \left(C_{L_y} - \frac{dC_D}{d\alpha_y} \right) c_y y^2 dy$	
Y_r eq. (13.142)	Side force due to yaw rate	Fin contribution $\bar{V}_F a_{1F}$	Many contributions but often negligible
L_r eq. (13.150)	Rolling moment due to yaw rate	Wing contribution $\frac{1}{Ss^2} \int_0^s C_{L_y} c_y y^2 dy$	
eq. (13.155)		Fin contribution $a_{1F} \bar{V}_F \frac{h_F}{b} \equiv - L_{v(fin)} \frac{l_F}{b}$	
N_r eq. (13.162)	Yawing moment due to yaw rate	Wing contribution $- \frac{1}{Ss^2} \int_0^s C_{Dy} c_y y^2 dy$	Yaw damping, for large aspect ratio rectangular wing wing contribution approximately $C_D/6$
eq. (13.167)		Fin contribution $- a_{1F} \bar{V}_F \frac{l_F}{b} = - \frac{l_F}{b} N_{v(fin)}$	

Table A8.3 Longitudinal Aerodynamic Control Derivatives

Small Perturbation Derivatives Referred to Aircraft Wind Axes			
Derivative	Description	Expression	Comments
X_η eq. (13.174)	Axial force due to elevator	$-2 \frac{S_T}{S} k_T C_{L_T} a_2$	Usually insignificantly small
Z_η eq. (13.178)	Normal force due to elevator	$-\frac{S_T}{S} a_2$	
M_η eq. (13.181)	Pitching moment due to elevator	$-\bar{V}_T a_2$	Principal measure of pitch control power

Table A8.4 Lateral-Directional Aerodynamic Control Derivatives

Small Perturbation Derivatives Referred to Aircraft Wind Axes			
Derivative	Description	Expression	Comments
Y_ξ	Side force due to aileron		Insignificant for conventional aeroplanes
L_ξ eq. (13.188)	Rolling moment due to aileron	$-\frac{1}{Ss} a_{2_A} \int_{y_1}^{y_2} c_y dy$	Principal measure of roll control power
N_ξ eq. (13.193)	Yawing moment due to aileron	$\frac{1}{Ss} \int_{y_1}^{y_2} \left(\frac{\partial C_{D_y}}{\partial \xi} \right) c_y dy$	Adverse yaw due to aileron
Y_ζ eq. (13.197)	Side force due to rudder	$\frac{S_F}{S} a_{2_R}$	
L_ζ eq. (13.200)	Rolling moment due to rudder	$\bar{V}_F \frac{h_F}{l_F} a_{2_R}$	Principal measure of yaw control power
N_ζ eq. (13.203)	Yawing moment due to rudder	$-\bar{V}_F a_{2_R}$	Adverse roll due to rudder

Appendix 9: Transformation of Aerodynamic Stability Derivatives from a Body Axes Reference to a Wind Axes Reference

A9.1 Introduction

Aerodynamic stability derivatives are usually quoted with respect to either a system of body axes or a system of wind axes. When the derivatives are quoted with respect to one system, and it is desired to work with the equations of motion referred to a different system, the derivatives must be transformed to the system of interest. Fortunately, the transformation of aerodynamic derivatives from one axis system to another is a relatively straightforward procedure using the transformation relationships discussed in Chapter 2. The procedure for transforming derivatives from a body axes reference to a wind axes reference is illustrated here. However, it can be applied for transforming derivatives between any two systems of reference axes provided their angular relationship is known.

In steady level symmetric flight a system of body axes differs from that of wind axes only by the body incidence α_e , as shown in Fig. 2.2. In the following paragraphs small perturbation force and velocity components, X , Y , Z and u , v , w , respectively, are indicated in the usual way, where the subscript denotes the reference axes. Small perturbation moment and angular velocity components, L , M , N and p , q , r , respectively, are also most conveniently represented by vectors as described in Chapter 2. Again, the subscript denotes the reference axis system.

A9.2 Force and Moment Transformation

The transformation of the aerodynamic force components from a *body axes to a wind axes* reference may be obtained directly by the application of the inverse direction cosine matrix, as given by equation (2.13). Writing $\theta = \alpha_e$ and $\phi = \psi = 0$, since level symmetric flight is assumed, then

$$\begin{bmatrix} X_w \\ Y_w \\ Z_w \end{bmatrix} = \begin{bmatrix} \cos \alpha_e & 0 & \sin \alpha_e \\ 0 & 1 & 0 \\ -\sin \alpha_e & 0 & \cos \alpha_e \end{bmatrix} \begin{bmatrix} X_b \\ Y_b \\ Z_b \end{bmatrix} \quad (\text{A9.1})$$

Similarly, the aerodynamic moments transformation may be written as

$$\begin{bmatrix} L_w \\ M_w \\ N_w \end{bmatrix} = \begin{bmatrix} \cos \alpha_e & 0 & \sin \alpha_e \\ 0 & 1 & 0 \\ -\sin \alpha_e & 0 & \cos \alpha_e \end{bmatrix} \begin{bmatrix} L_b \\ M_b \\ N_b \end{bmatrix} \quad (\text{A9.2})$$

A9.3 Aerodynamic Stability Derivative Transformations

A9.3.1 Force-Velocity Derivatives

Consider the situation when the aerodynamic force components comprise only those terms involving the force-velocity derivatives. Then, referred to wind axes,

$$\begin{bmatrix} \dot{X}_w \\ \dot{Y}_w \\ \dot{Z}_w \end{bmatrix} = \begin{bmatrix} \dot{\bar{X}}_{u_w} & 0 & \dot{\bar{X}}_{w_w} \\ 0 & \dot{\bar{Y}}_{v_w} & 0 \\ \dot{\bar{Z}}_{u_w} & 0 & \dot{\bar{X}}_{w_w} \end{bmatrix} \begin{bmatrix} u_w \\ v_w \\ w_w \end{bmatrix} \quad (\text{A9.3})$$

and referred to body axes,

$$\begin{bmatrix} \dot{X}_b \\ \dot{Y}_b \\ \dot{Z}_b \end{bmatrix} = \begin{bmatrix} \dot{\bar{X}}_{u_b} & 0 & \dot{\bar{X}}_{w_b} \\ 0 & \dot{\bar{Y}}_{v_b} & 0 \\ \dot{\bar{Z}}_{u_b} & 0 & \dot{\bar{X}}_{w_b} \end{bmatrix} \begin{bmatrix} u_b \\ v_b \\ w_b \end{bmatrix} \quad (\text{A9.4})$$

Substitute equations (A9.3) and (A9.4) into equation (A9.1):

$$\begin{bmatrix} \dot{\bar{X}}_{u_w} & 0 & \dot{\bar{X}}_{w_w} \\ 0 & \dot{\bar{Y}}_{v_w} & 0 \\ \dot{\bar{Z}}_{u_w} & 0 & \dot{\bar{X}}_{w_w} \end{bmatrix} \begin{bmatrix} u_w \\ v_w \\ w_w \end{bmatrix} = \begin{bmatrix} \cos \alpha_e & 0 & \sin \alpha_e \\ 0 & 1 & 0 \\ -\sin \alpha_e & 0 & \cos \alpha_e \end{bmatrix} \begin{bmatrix} \dot{\bar{X}}_{u_b} & 0 & \dot{\bar{X}}_{w_b} \\ 0 & \dot{\bar{Y}}_{v_b} & 0 \\ \dot{\bar{Z}}_{u_b} & 0 & \dot{\bar{X}}_{w_b} \end{bmatrix} \begin{bmatrix} u_b \\ v_b \\ w_b \end{bmatrix} \quad (\text{A9.5})$$

Now the transformation of linear velocity components from a *wind axes to a body axes* reference may be obtained directly from the application of the direction cosine matrix, equation (2.12), with the same constraints as previously:

$$\begin{bmatrix} u_b \\ v_b \\ w_b \end{bmatrix} = \begin{bmatrix} \cos \alpha_e & 0 & -\sin \alpha_e \\ 0 & 1 & 0 \\ \sin \alpha_e & 0 & \cos \alpha_e \end{bmatrix} \begin{bmatrix} u_w \\ v_w \\ w_w \end{bmatrix} \quad (\text{A9.6})$$

Substitute the velocity vector referred to body axes, given by equation (A9.6), into equation (A9.5), and cancel the velocity vectors referred to wind axes to obtain

$$\begin{bmatrix} \dot{\bar{X}}_{u_w} & 0 & \dot{\bar{X}}_{w_w} \\ 0 & \dot{\bar{Y}}_{v_w} & 0 \\ \dot{\bar{Z}}_{u_w} & 0 & \dot{\bar{X}}_{w_w} \end{bmatrix} = \begin{bmatrix} \cos \alpha_e & 0 & \sin \alpha_e \\ 0 & 1 & 0 \\ -\sin \alpha_e & 0 & \cos \alpha_e \end{bmatrix} \begin{bmatrix} \dot{\bar{X}}_{u_b} & 0 & \dot{\bar{X}}_{w_b} \\ 0 & \dot{\bar{Y}}_{v_b} & 0 \\ \dot{\bar{Z}}_{u_b} & 0 & \dot{\bar{X}}_{w_b} \end{bmatrix} \begin{bmatrix} \cos \alpha_e & 0 & -\sin \alpha_e \\ 0 & 1 & 0 \\ \sin \alpha_e & 0 & \cos \alpha_e \end{bmatrix}$$

or, after multiplying the matrices on the right hand side, the following transformations are obtained:

$$\begin{aligned} \dot{\bar{X}}_{u_w} &= \dot{\bar{X}}_{u_b} \cos^2 \alpha_e + \dot{\bar{Z}}_{w_b} \sin^2 \alpha_e + (\dot{\bar{X}}_{w_b} + \dot{\bar{Z}}_{u_b}) \sin \alpha_e \cos \alpha_e \\ \dot{\bar{X}}_{w_w} &= \dot{\bar{X}}_{w_b} \cos^2 \alpha_e - \dot{\bar{Z}}_{u_b} \sin^2 \alpha_e - (\dot{\bar{X}}_{u_b} - \dot{\bar{Z}}_{w_b}) \sin \alpha_e \cos \alpha_e \\ \dot{\bar{Y}}_{v_w} &= \dot{\bar{Y}}_{v_b} \\ \dot{\bar{Z}}_{u_w} &= \dot{\bar{Z}}_{u_b} \cos^2 \alpha_e - \dot{\bar{X}}_{w_b} \sin^2 \alpha_e - (\dot{\bar{X}}_{u_b} - \dot{\bar{Z}}_{w_b}) \sin \alpha_e \cos \alpha_e \\ \dot{\bar{Z}}_{w_w} &= \dot{\bar{Z}}_{w_b} \cos^2 \alpha_e + \dot{\bar{X}}_{u_b} \sin^2 \alpha_e - (\dot{\bar{X}}_{w_b} + \dot{\bar{Z}}_{u_b}) \sin \alpha_e \cos \alpha_e \end{aligned} \quad (\text{A9.7})$$

A9.3.2 Moment-Velocity Derivatives

Consider now the situation when the aerodynamic moment components comprise only those terms involving the moment-velocity derivatives. Then, referred to wind axes,

$$\begin{bmatrix} L_w \\ M_w \\ N_w \end{bmatrix} = \begin{bmatrix} 0 & \overset{\circ}{L}_{v_w} & 0 \\ \overset{\circ}{M}_{u_w} & 0 & \overset{\circ}{M}_{w_w} \\ 0 & \overset{\circ}{N}_{v_w} & 0 \end{bmatrix} \begin{bmatrix} u_w \\ v_w \\ w_w \end{bmatrix} \quad (\text{A9.8})$$

and referred to body axes,

$$\begin{bmatrix} L_b \\ M_b \\ N_b \end{bmatrix} = \begin{bmatrix} 0 & \overset{\circ}{L}_{v_b} & 0 \\ \overset{\circ}{M}_{u_b} & 0 & \overset{\circ}{M}_{w_b} \\ 0 & \overset{\circ}{N}_{v_b} & 0 \end{bmatrix} \begin{bmatrix} u_b \\ v_b \\ w_b \end{bmatrix} \quad (\text{A9.9})$$

Substitute equations (A9.8) and (A9.9) into equation (A9.2):

$$\begin{bmatrix} 0 & \overset{\circ}{L}_{v_w} & 0 \\ \overset{\circ}{M}_{u_w} & 0 & \overset{\circ}{M}_{w_w} \\ 0 & \overset{\circ}{N}_{v_w} & 0 \end{bmatrix} \begin{bmatrix} u_w \\ v_w \\ w_w \end{bmatrix} = \begin{bmatrix} \cos \alpha_e & 0 & \sin \alpha_e \\ 0 & 1 & 0 \\ -\sin \alpha_e & 0 & \cos \alpha_e \end{bmatrix} \begin{bmatrix} 0 & \overset{\circ}{L}_{v_b} & 0 \\ \overset{\circ}{M}_{u_b} & 0 & \overset{\circ}{M}_{w_b} \\ 0 & \overset{\circ}{N}_{v_b} & 0 \end{bmatrix} \begin{bmatrix} u_b \\ v_b \\ w_b \end{bmatrix} \quad (\text{A9.10})$$

As before, the transformation of linear velocity components from a *wind axes to a body axes* reference is given by equation (A9.6). Substitute the velocity vector referred to body axes, given by equation (A9.6), into equation (A9.10). Again, the velocity vectors referred to wind axes cancel and, after multiplying the matrices on the right hand side, the following transformations are obtained:

$$\begin{aligned} \overset{\circ}{L}_{v_w} &= \overset{\circ}{L}_{v_b} \cos \alpha_e + \overset{\circ}{N}_{v_b} \sin \alpha_e \\ \overset{\circ}{M}_{u_w} &= \overset{\circ}{M}_{u_b} \cos \alpha_e + \overset{\circ}{M}_{w_b} \sin \alpha_e \\ \overset{\circ}{M}_{w_w} &= \overset{\circ}{M}_{w_b} \cos \alpha_e - \overset{\circ}{M}_{u_b} \sin \alpha_e \\ \overset{\circ}{N}_{v_w} &= \overset{\circ}{N}_{v_b} \cos \alpha_e - \overset{\circ}{L}_{v_b} \sin \alpha_e \end{aligned} \quad (\text{A9.11})$$

A9.3.3 Force-Rotary Derivatives

Consider now the situation in which the aerodynamic force components comprise only those terms involving the force angular velocity derivatives, more commonly referred to as force-rotary derivatives. Then, referred to wind axes,

$$\begin{bmatrix} X_w \\ Y_w \\ Z_w \end{bmatrix} = \begin{bmatrix} 0 & \overset{\circ}{X}_{q_w} & 0 \\ \overset{\circ}{Y}_{p_w} & 0 & \overset{\circ}{Y}_{r_w} \\ 0 & \overset{\circ}{Z}_{q_w} & 0 \end{bmatrix} \begin{bmatrix} p_w \\ q_w \\ r_w \end{bmatrix} \quad (\text{A9.12})$$

and referred to body axes,

$$\begin{bmatrix} X_b \\ Y_b \\ Z_b \end{bmatrix} = \begin{bmatrix} 0 & \dot{X}_{q_b} & 0 \\ \dot{Y}_{p_b} & 0 & \dot{Y}_{r_b} \\ 0 & \dot{Z}_{q_b} & 0 \end{bmatrix} \begin{bmatrix} p_b \\ q_b \\ r_b \end{bmatrix} \quad (\text{A9.13})$$

Substitute equations (A9.12) and (A9.13) into equation (A9.1):

$$\begin{bmatrix} 0 & \dot{X}_{q_w} & 0 \\ \dot{Y}_{p_w} & 0 & \dot{Y}_{r_w} \\ 0 & \dot{Z}_{q_w} & 0 \end{bmatrix} \begin{bmatrix} p_w \\ q_w \\ r_w \end{bmatrix} = \begin{bmatrix} \cos \alpha_e & 0 & \sin \alpha_e \\ 0 & 1 & 0 \\ -\sin \alpha_e & 0 & \cos \alpha_e \end{bmatrix} \begin{bmatrix} 0 & \dot{X}_{q_b} & 0 \\ \dot{Y}_{p_b} & 0 & \dot{Y}_{r_b} \\ 0 & \dot{Z}_{q_b} & 0 \end{bmatrix} \begin{bmatrix} p_b \\ q_b \\ r_b \end{bmatrix} \quad (\text{A9.14})$$

Now, with reference to Chapter 2, the treatment of angular velocity components as vectors enables their transformation from a *wind axes to a body axes* reference to be obtained as before by the direct application of the direction cosine matrix, equation (2.12). Thus, with the same constraints as previously,

$$\begin{bmatrix} p_b \\ q_b \\ r_b \end{bmatrix} = \begin{bmatrix} \cos \alpha_e & 0 & -\sin \alpha_e \\ 0 & 1 & 0 \\ \sin \alpha_e & 0 & \cos \alpha_e \end{bmatrix} \begin{bmatrix} p_w \\ q_w \\ r_w \end{bmatrix} \quad (\text{A9.15})$$

Substitute the angular velocity vector referred to body axes, given by equation (A9.15), into equation (A9.14), and cancel the velocity vectors referred to wind axes to obtain

$$\begin{bmatrix} 0 & \dot{X}_{q_w} & 0 \\ \dot{Y}_{p_w} & 0 & \dot{Y}_{r_w} \\ 0 & \dot{Z}_{q_w} & 0 \end{bmatrix} = \begin{bmatrix} \cos \alpha_e & 0 & \sin \alpha_e \\ 0 & 1 & 0 \\ -\sin \alpha_e & 0 & \cos \alpha_e \end{bmatrix} \begin{bmatrix} 0 & \dot{X}_{q_b} & 0 \\ \dot{Y}_{p_b} & 0 & \dot{Y}_{r_b} \\ 0 & \dot{Z}_{q_b} & 0 \end{bmatrix} \begin{bmatrix} \cos \alpha_e & 0 & -\sin \alpha_e \\ 0 & 1 & 0 \\ \sin \alpha_e & 0 & \cos \alpha_e \end{bmatrix}$$

or, after multiplying the matrices on the right hand side, the following transformations are obtained:

$$\begin{aligned} \dot{X}_{q_w} &= \dot{X}_{q_b} \cos \alpha_e + \dot{Z}_{q_b} \sin \alpha_e \\ \dot{Y}_{p_w} &= \dot{Y}_{p_b} \cos \alpha_e + \dot{Y}_{r_b} \sin \alpha_e \\ \dot{Y}_{r_w} &= \dot{Y}_{r_b} \cos \alpha_e - \dot{Y}_{p_b} \sin \alpha_e \\ \dot{Z}_{q_w} &= \dot{Z}_{q_b} \cos \alpha_e - \dot{X}_{q_b} \sin \alpha_e \end{aligned} \quad (\text{A9.16})$$

A9.3.4 Moment-Rotary Derivatives

Consider now the situation in which the aerodynamic moment components comprise only those terms involving the moment-angular velocity, or moment-rotary, derivatives. Then, referred to wind axes,

$$\begin{bmatrix} \overset{\circ}{L}_w \\ \overset{\circ}{M}_w \\ \overset{\circ}{N}_w \end{bmatrix} = \begin{bmatrix} \overset{\circ}{L}_{p_w} & 0 & \overset{\circ}{L}_{r_w} \\ 0 & \overset{\circ}{M}_{q_w} & 0 \\ \overset{\circ}{N}_{p_w} & 0 & \overset{\circ}{N}_{r_w} \end{bmatrix} \begin{bmatrix} p_w \\ q_w \\ r_w \end{bmatrix} \quad (\text{A9.17})$$

and referred to body axes,

$$\begin{bmatrix} \overset{\circ}{L}_b \\ \overset{\circ}{M}_b \\ \overset{\circ}{N}_b \end{bmatrix} = \begin{bmatrix} \overset{\circ}{L}_{p_b} & 0 & \overset{\circ}{L}_{r_b} \\ 0 & \overset{\circ}{M}_{q_b} & 0 \\ \overset{\circ}{N}_{p_b} & 0 & \overset{\circ}{N}_{r_b} \end{bmatrix} \begin{bmatrix} p_b \\ q_b \\ r_b \end{bmatrix} \quad (\text{A9.18})$$

Substitute equations (A9.17) and (A9.18) into equation (A9.2):

$$\begin{bmatrix} \overset{\circ}{L}_{p_w} & 0 & \overset{\circ}{L}_{r_w} \\ 0 & \overset{\circ}{M}_{q_w} & 0 \\ \overset{\circ}{N}_{p_w} & 0 & \overset{\circ}{N}_{r_w} \end{bmatrix} \begin{bmatrix} p_w \\ q_w \\ r_w \end{bmatrix} = \begin{bmatrix} \cos \alpha_e & 0 & \sin \alpha_e \\ 0 & 1 & 0 \\ -\sin \alpha_e & 0 & \cos \alpha_e \end{bmatrix} \begin{bmatrix} \overset{\circ}{L}_{p_b} & 0 & \overset{\circ}{L}_{r_b} \\ 0 & \overset{\circ}{M}_{q_b} & 0 \\ \overset{\circ}{N}_{p_b} & 0 & \overset{\circ}{N}_{r_b} \end{bmatrix} \begin{bmatrix} p_b \\ q_b \\ r_b \end{bmatrix} \quad (\text{A9.19})$$

As before, the transformation of angular velocity components from a *wind axes to a body axes* reference is given by equation (A9.15). Substitute the angular velocity vector referred to body axes, given by equation (A9.15), into equation (A9.19). Again, the angular velocity vectors referred to wind axes cancel and, after multiplying the matrices on the right hand side, the following transformations are obtained:

$$\begin{aligned} \overset{\circ}{L}_{p_w} &= \overset{\circ}{L}_{p_b} \cos^2 \alpha_e + \overset{\circ}{N}_{r_b} \sin^2 \alpha_e + (\overset{\circ}{L}_{r_b} + \overset{\circ}{N}_{p_b}) \sin \alpha_e \cos \alpha_e \\ \overset{\circ}{L}_{r_w} &= \overset{\circ}{L}_{r_b} \cos^2 \alpha_e - \overset{\circ}{N}_{p_b} \sin^2 \alpha_e - (\overset{\circ}{L}_{p_b} - \overset{\circ}{N}_{r_b}) \sin \alpha_e \cos \alpha_e \\ \overset{\circ}{M}_{q_w} &= \overset{\circ}{M}_{q_b} \\ \overset{\circ}{N}_{p_w} &= \overset{\circ}{N}_{p_b} \cos^2 \alpha_e - \overset{\circ}{L}_{r_b} \sin^2 \alpha_e - (\overset{\circ}{L}_{p_b} - \overset{\circ}{N}_{r_b}) \sin \alpha_e \cos \alpha_e \\ \overset{\circ}{N}_{r_w} &= \overset{\circ}{N}_{r_b} \cos^2 \alpha_e + \overset{\circ}{L}_{p_b} \sin^2 \alpha_e - (\overset{\circ}{L}_{r_b} + \overset{\circ}{N}_{p_b}) \sin \alpha_e \cos \alpha_e \end{aligned} \quad (\text{A9.20})$$

A9.3.5 Force-Acceleration Derivatives

The force-acceleration derivatives are calculated in exactly the same way as the force-velocity derivatives. However, in this case the aerodynamic force components referred to wind axes are given by

$$\begin{bmatrix} X_w \\ Y_w \\ Z_w \end{bmatrix} = \begin{bmatrix} 0 & 0 & \overset{\circ}{X}_{\dot{w}_w} \\ 0 & 0 & 0 \\ 0 & 0 & \overset{\circ}{Z}_{\dot{w}_w} \end{bmatrix} \begin{bmatrix} \dot{u}_w \\ \dot{v}_w \\ \dot{w}_w \end{bmatrix} \quad (\text{A9.21})$$

and referred to body axes are given by

$$\begin{bmatrix} \dot{X}_b \\ \dot{Y}_b \\ \dot{Z}_b \end{bmatrix} = \begin{bmatrix} 0 & 0 & \dot{X}_{\dot{w}_b} \\ 0 & 0 & 0 \\ 0 & 0 & \dot{Z}_{\dot{w}_b} \end{bmatrix} \begin{bmatrix} \dot{u}_b \\ \dot{v}_b \\ \dot{w}_b \end{bmatrix} \quad (\text{A9.22})$$

Equations (A9.21) and (A9.22) are substituted into equation (A9.1), velocity vectors become acceleration vectors, and, after some algebraic manipulation, the following transformations are obtained:

$$\begin{aligned} \ddot{X}_{\dot{w}_w} &= \dot{X}_{\dot{w}_b} \cos^2 \alpha_e + \dot{Z}_{\dot{w}_b} \sin \alpha_e \cos \alpha_e \\ \ddot{Z}_{\dot{w}_w} &= \dot{Z}_{\dot{w}_b} \cos^2 \alpha_e - \dot{X}_{\dot{w}_b} \sin \alpha_e \cos \alpha_e \end{aligned} \quad (\text{A9.23})$$

A9.3.6 Moment-Acceleration Derivatives

The moment-acceleration derivatives are calculated in exactly the same way as the moment-velocity derivatives. However, in this case the aerodynamic moment components referred to wind axes are given by

$$\begin{bmatrix} L_w \\ M_w \\ N_w \end{bmatrix} = \begin{bmatrix} 0 & 0 & 0 \\ 0 & 0 & \dot{M}_{\dot{w}_w} \\ 0 & 0 & 0 \end{bmatrix} \begin{bmatrix} \dot{u}_w \\ \dot{v}_w \\ \dot{w}_w \end{bmatrix} \quad (\text{A9.24})$$

and referred to body axes are given by

$$\begin{bmatrix} L_b \\ M_b \\ N_b \end{bmatrix} = \begin{bmatrix} 0 & 0 & 0 \\ 0 & 0 & \dot{M}_{\dot{w}_b} \\ 0 & 0 & 0 \end{bmatrix} \begin{bmatrix} \dot{u}_b \\ \dot{v}_b \\ \dot{w}_b \end{bmatrix} \quad (\text{A9.25})$$

Equations (A9.24) and (A9.25) are substituted into equation (A9.2), the velocity vectors become acceleration vectors, and, after some algebraic manipulation, the following transformation is obtained:

$$\ddot{M}_{\dot{w}_w} = \dot{M}_{\dot{w}_b} \cos \alpha_e \quad (\text{A9.26})$$

A9.3.7 Aerodynamic Control Derivatives

The aerodynamic control derivatives are most easily dealt with by denoting a general control input δ . The transformation of the control force derivatives from a *body axis* reference to a *wind axes* reference then follows directly from equation (A9.1):

$$\begin{bmatrix} \dot{\bar{X}}_{\delta_w} \\ \dot{\bar{Y}}_{\delta_w} \\ \dot{\bar{Z}}_{\delta_w} \end{bmatrix} \delta = \begin{bmatrix} \cos \alpha_e & 0 & \sin \alpha_e \\ 0 & 1 & 0 \\ -\sin \alpha_e & 0 & \cos \alpha_e \end{bmatrix} \begin{bmatrix} \dot{\bar{X}}_{\delta_b} \\ \dot{\bar{Y}}_{\delta_b} \\ \dot{\bar{Z}}_{\delta_b} \end{bmatrix} \delta \quad (\text{A9.27})$$

The corresponding transformation of the control moment derivatives follows directly from [equation \(A9.2\)](#):

$$\begin{bmatrix} \dot{\bar{L}}_{\delta_w} \\ \dot{\bar{M}}_{\delta_w} \\ \dot{\bar{N}}_{\delta_w} \end{bmatrix} \delta = \begin{bmatrix} \cos \alpha_e & 0 & \sin \alpha_e \\ 0 & 1 & 0 \\ -\sin \alpha_e & 0 & \cos \alpha_e \end{bmatrix} \begin{bmatrix} \dot{\bar{L}}_{\delta_b} \\ \dot{\bar{M}}_{\delta_b} \\ \dot{\bar{N}}_{\delta_b} \end{bmatrix} \delta \quad (\text{A9.28})$$

The specific control derivative transformations are then obtained by substituting elevator angle η , aileron angle ξ , rudder angle ζ , thrust τ , and so on, in place of δ in [equations \(A9.27\) and \(A9.28\)](#). Bearing in mind that the longitudinal and lateral-directional equations of motion are decoupled, it follows that

$$\begin{aligned} \dot{\bar{X}}_{\eta_w} &= \dot{\bar{X}}_{\eta_b} \cos \alpha_e + \dot{\bar{Z}}_{\eta_b} \sin \alpha_e \\ \dot{\bar{Z}}_{\eta_w} &= \dot{\bar{Z}}_{\eta_b} \cos \alpha_e - \dot{\bar{X}}_{\eta_b} \sin \alpha_e \\ \dot{\bar{M}}_{\eta_w} &= \dot{\bar{M}}_{\eta_b} \end{aligned} \quad (\text{A9.29})$$

and

$$\begin{aligned} \dot{\bar{Y}}_{\xi_w} &= \dot{\bar{Y}}_{\xi_b} \\ \dot{\bar{L}}_{\xi_w} &= \dot{\bar{L}}_{\xi_b} \cos \alpha_e + \dot{\bar{N}}_{\xi_b} \sin \alpha_e \\ \dot{\bar{N}}_{\xi_w} &= \dot{\bar{N}}_{\xi_b} \cos \alpha_e - \dot{\bar{L}}_{\xi_b} \sin \alpha_e \end{aligned} \quad (\text{A9.30})$$

By substituting τ for η in [equation \(A9.29\)](#), the thrust control derivative transformations are obtained. Similarly, by substituting ζ for ξ in [equation \(A9.30\)](#), the rudder control derivative transformations are obtained.

A9.4 Summary

The derivative transformations of *body axes to wind axes* described here are summarised in [Table A9.1](#). The transformations from *wind axes to body axes* are easily obtained by the inverse procedure, and these are summarised for convenience in [Table A9.2](#). The corresponding control derivative transformations are summarised in [Tables A9.3 and A9.4](#).

Table A9.1 Body to wind axes derivative transformations

Wind Axes	Body Axes
$\dot{\bar{X}}_{u_w}$	$\dot{\bar{X}}_{u_b} \cos^2 \alpha_e + \dot{\bar{Z}}_{w_b} \sin^2 \alpha_e + (\dot{\bar{X}}_{w_b} + \dot{\bar{Z}}_{u_b}) \sin \alpha_e \cos \alpha_e$
$\dot{\bar{X}}_{w_w}$	$\dot{\bar{X}}_{w_b} \cos^2 \alpha_e - \dot{\bar{Z}}_{u_b} \sin^2 \alpha_e - (\dot{\bar{X}}_{u_b} - \dot{\bar{Z}}_{w_b}) \sin \alpha_e \cos \alpha_e$
$\dot{\bar{Y}}_{v_w}$	$\dot{\bar{Y}}_{v_b}$
$\dot{\bar{Z}}_{u_w}$	$\dot{\bar{Z}}_{u_b} \cos^2 \alpha_e - \dot{\bar{X}}_{w_b} \sin^2 \alpha_e - (\dot{\bar{X}}_{u_b} - \dot{\bar{Z}}_{w_b}) \sin \alpha_e \cos \alpha_e$
$\dot{\bar{Z}}_{w_w}$	$\dot{\bar{Z}}_{w_b} \cos^2 \alpha_e + \dot{\bar{X}}_{u_b} \sin^2 \alpha_e - (\dot{\bar{X}}_{w_b} + \dot{\bar{Z}}_{u_b}) \sin \alpha_e \cos \alpha_e$
$\dot{\bar{L}}_{v_w}$	$\dot{\bar{L}}_{v_b} \cos \alpha_e + \dot{\bar{N}}_{v_b} \sin \alpha_e$
$\dot{\bar{M}}_{u_w}$	$\dot{\bar{M}}_{u_b} \cos \alpha_e + \dot{\bar{M}}_{w_b} \sin \alpha_e$
$\dot{\bar{M}}_{w_w}$	$\dot{\bar{M}}_{w_b} \cos \alpha_e - \dot{\bar{M}}_{u_b} \sin \alpha_e$
$\dot{\bar{N}}_{v_w}$	$\dot{\bar{N}}_{v_b} \cos \alpha_e - \dot{\bar{L}}_{v_b} \sin \alpha_e$
$\dot{\bar{X}}_{q_w}$	$\dot{\bar{X}}_{q_b} \cos \alpha_e + \dot{\bar{Z}}_{q_b} \sin \alpha_e$
$\dot{\bar{Y}}_{p_w}$	$\dot{\bar{Y}}_{p_b} \cos \alpha_e + \dot{\bar{Y}}_{r_b} \sin \alpha_e$
$\dot{\bar{Y}}_{r_w}$	$\dot{\bar{Y}}_{r_b} \cos \alpha_e - \dot{\bar{Y}}_{p_b} \sin \alpha_e$
$\dot{\bar{Z}}_{q_w}$	$\dot{\bar{Z}}_{q_b} \cos \alpha_e - \dot{\bar{X}}_{q_b} \sin \alpha_e$
$\dot{\bar{L}}_{p_w}$	$\dot{\bar{L}}_{p_b} \cos^2 \alpha_e + \dot{\bar{N}}_{r_b} \sin^2 \alpha_e + (\dot{\bar{L}}_{r_b} + \dot{\bar{N}}_{p_b}) \sin \alpha_e \cos \alpha_e$
$\dot{\bar{L}}_{r_w}$	$\dot{\bar{L}}_{r_b} \cos^2 \alpha_e - \dot{\bar{N}}_{p_b} \sin^2 \alpha_e - (\dot{\bar{L}}_{p_b} - \dot{\bar{N}}_{r_b}) \sin \alpha_e \cos \alpha_e$
$\dot{\bar{M}}_{q_w}$	$\dot{\bar{M}}_{q_b}$
$\dot{\bar{N}}_{p_w}$	$\dot{\bar{N}}_{p_b} \cos^2 \alpha_e - \dot{\bar{L}}_{r_b} \sin^2 \alpha_e - (\dot{\bar{L}}_{p_b} - \dot{\bar{N}}_{r_b}) \sin \alpha_e \cos \alpha_e$
$\dot{\bar{N}}_{r_w}$	$\dot{\bar{N}}_{r_b} \cos^2 \alpha_e + \dot{\bar{L}}_{p_b} \sin^2 \alpha_e - (\dot{\bar{L}}_{r_b} + \dot{\bar{N}}_{p_b}) \sin \alpha_e \cos \alpha_e$
$\dot{\bar{X}}_{\dot{w}_w}$	$\dot{\bar{X}}_{\dot{w}_b} \cos^2 \alpha_e + \dot{\bar{Z}}_{\dot{w}_b} \sin \alpha_e \cos \alpha_e$
$\dot{\bar{Z}}_{\dot{w}_w}$	$\dot{\bar{Z}}_{\dot{w}_b} \cos^2 \alpha_e - \dot{\bar{X}}_{\dot{w}_b} \sin \alpha_e \cos \alpha_e$
$\dot{\bar{M}}_{\dot{w}_w}$	$\dot{\bar{M}}_{\dot{w}_b} \cos \alpha_e$

Table A9.2 Wind to body axes derivative transformations

Body Axes	Wind Axes
\dot{X}_{u_b}	$\dot{X}_{u_w} \cos^2 \alpha_e + \dot{Z}_{w_w} \sin^2 \alpha_e - (\dot{X}_{w_w} + \dot{Z}_{u_w}) \sin \alpha_e \cos \alpha_e$
\dot{X}_{w_b}	$\dot{X}_{w_w} \cos^2 \alpha_e - \dot{Z}_{u_w} \sin^2 \alpha_e + (\dot{X}_{u_w} - \dot{Z}_{w_w}) \sin \alpha_e \cos \alpha_e$
\dot{Y}_{v_b}	\dot{Y}_{v_w}
\dot{Z}_{u_b}	$\dot{Z}_{u_w} \cos^2 \alpha_e - \dot{X}_{w_w} \sin^2 \alpha_e + (\dot{X}_{u_w} - \dot{Z}_{w_w}) \sin \alpha_e \cos \alpha_e$
\dot{Z}_{w_b}	$\dot{Z}_{w_w} \cos^2 \alpha_e + \dot{X}_{u_w} \sin^2 \alpha_e + (\dot{X}_{w_w} + \dot{Z}_{u_w}) \sin \alpha_e \cos \alpha_e$
\dot{L}_{v_b}	$\dot{L}_{v_w} \cos \alpha_e - \dot{N}_{v_w} \sin \alpha_e$
\dot{M}_{u_b}	$\dot{M}_{u_w} \cos \alpha_e - \dot{M}_{w_w} \sin \alpha_e$
\dot{M}_{w_b}	$\dot{M}_{w_w} \cos \alpha_e + \dot{M}_{u_w} \sin \alpha_e$
\dot{N}_{v_b}	$\dot{N}_{v_w} \cos \alpha_e + \dot{L}_{v_w} \sin \alpha_e$
\dot{X}_{q_b}	$\dot{X}_{q_w} \cos \alpha_e - \dot{Z}_{q_w} \sin \alpha_e$
\dot{Y}_{p_b}	$\dot{Y}_{p_w} \cos \alpha_e - \dot{Y}_{r_w} \sin \alpha_e$
\dot{Y}_{r_b}	$\dot{Y}_{r_w} \cos \alpha_e + \dot{Y}_{p_w} \sin \alpha_e$
\dot{Z}_{q_b}	$\dot{Z}_{q_w} \cos \alpha_e + \dot{X}_{q_w} \sin \alpha_e$
\dot{L}_{p_b}	$\dot{L}_{p_w} \cos^2 \alpha_e + \dot{N}_{r_w} \sin^2 \alpha_e - (\dot{L}_{r_w} + \dot{N}_{p_w}) \sin \alpha_e \cos \alpha_e$
\dot{L}_{r_b}	$\dot{L}_{r_w} \cos^2 \alpha_e - \dot{N}_{p_w} \sin^2 \alpha_e + (\dot{L}_{p_w} - \dot{N}_{r_w}) \sin \alpha_e \cos \alpha_e$
\dot{M}_{q_b}	\dot{M}_{q_w}
\dot{N}_{p_b}	$\dot{N}_{p_w} \cos^2 \alpha_e - \dot{L}_{r_w} \sin^2 \alpha_e + (\dot{L}_{p_w} - \dot{N}_{r_w}) \sin \alpha_e \cos \alpha_e$
\dot{N}_{r_b}	$\dot{N}_{r_w} \cos^2 \alpha_e + \dot{L}_{p_w} \sin^2 \alpha_e + (\dot{L}_{r_w} + \dot{N}_{p_w}) \sin \alpha_e \cos \alpha_e$
$\dot{X}_{\dot{w}_b}$	$\dot{X}_{\dot{w}_w} \cos^2 \alpha_e - \dot{Z}_{\dot{w}_w} \sin \alpha_e \cos \alpha_e$
$\dot{Z}_{\dot{w}_b}$	$\dot{Z}_{\dot{w}_w} \cos^2 \alpha_e + \dot{X}_{\dot{w}_w} \sin \alpha_e \cos \alpha_e$
$\dot{M}_{\dot{w}_b}$	$\dot{M}_{\dot{w}_w} \cos \alpha_e$

In Tables A9.3 and A9.4, it is simply necessary to write η , τ , ξ , or ζ in place of δ as appropriate.

Table A9.3 Body axes to wind axes control derivative transformations

Wind Axes	Body Axes
\dot{X}_{δ_w}	$\dot{X}_{\delta_b} \cos \alpha_e + \dot{Z}_{\delta_b} \sin \alpha_e$
\dot{Y}_{δ_w}	\dot{Y}_{δ_b}
\dot{Z}_{δ_w}	$\dot{Z}_{\delta_b} \cos \alpha_e - \dot{X}_{\delta_b} \sin \alpha_e$
\dot{L}_{δ_w}	$\dot{L}_{\delta_b} \cos \alpha_e + \dot{N}_{\delta_b} \sin \alpha_e$
\dot{M}_{δ_w}	\dot{M}_{δ_b}
\dot{N}_{δ_w}	$\dot{N}_{\delta_b} \cos \alpha_e - \dot{L}_{\delta_b} \sin \alpha_e$

Table A9.4 Wind axes to body axes control derivative transformations

Body Axes	Wind Axes
\dot{X}_{δ_b}	$\dot{X}_{\delta_w} \cos \alpha_e - \dot{Z}_{\delta_w} \sin \alpha_e$
\dot{Y}_{δ_b}	\dot{Y}_{δ_w}
\dot{Z}_{δ_b}	$\dot{Z}_{\delta_w} \cos \alpha_e + \dot{X}_{\delta_w} \sin \alpha_e$
\dot{L}_{δ_b}	$\dot{L}_{\delta_w} \cos \alpha_e - \dot{N}_{\delta_w} \sin \alpha_e$
\dot{M}_{δ_b}	\dot{M}_{δ_w}
\dot{N}_{δ_b}	$\dot{N}_{\delta_w} \cos \alpha_e + \dot{L}_{\delta_w} \sin \alpha_e$

Appendix 10: Transformation of the Moments and Products of Inertia from a Body Axes Reference to a Wind Axes Reference

A10.1 Introduction

In the same way that it is sometimes necessary to transform the aerodynamic stability and control derivatives from a body axes reference to a wind axes reference and vice versa, it is necessary to transform the corresponding moments and products of inertia. Again, the procedure is very straightforward and makes use of the transformation relationships discussed in Chapter 2. It is assumed that the body axes and wind axes in question have a common origin at the *cg* of the aeroplane, and that the aeroplane is in steady level symmetric flight. Thus the axes differ only by the steady body incidence α_e as shown in Fig. 2.2.

A10.2 Coordinate Transformation

A10.2.1 Body Axes to Wind Axes

A set of coordinates in a body axes system x_b , y_b , z_b may be transformed into the equivalent set in a wind axes system x_w , y_w , z_w by application of the inverse direction cosine matrix given by equation (2.13). Writing $\theta = \alpha_e$ and $\phi = \psi = 0$, since level symmetric flight is assumed,

$$\begin{bmatrix} x_w \\ y_w \\ z_w \end{bmatrix} = \begin{bmatrix} \cos\alpha_e & 0 & \sin\alpha_e \\ 0 & 1 & 0 \\ -\sin\alpha_e & 0 & \cos\alpha_e \end{bmatrix} \begin{bmatrix} x_b \\ y_b \\ z_b \end{bmatrix} \quad (\text{A10.1})$$

or

$$\begin{aligned} x_w &= x_b \cos\alpha_e + z_b \sin\alpha_e \\ y_w &= y_b \\ z_w &= z_b \cos\alpha_e - x_b \sin\alpha_e \end{aligned} \quad (\text{A10.2})$$

A10.2.2 Wind Axes to Body Axes

A set of coordinates in a wind axes system x_w, y_w, z_w may be transformed into the equivalent set in a body axes system x_b, y_b, z_b by application of the direction cosine matrix given by equation (2.12). Again, writing $\theta = \alpha_e$ and $\phi = \psi = 0$, since level symmetric flight is assumed,

$$\begin{bmatrix} x_b \\ y_b \\ z_b \end{bmatrix} = \begin{bmatrix} \cos\alpha_e & 0 & -\sin\alpha_e \\ 0 & 1 & 0 \\ \sin\alpha_e & 0 & \cos\alpha_e \end{bmatrix} \begin{bmatrix} x_w \\ y_w \\ z_w \end{bmatrix} \quad (\text{A10.3})$$

which is simply the inverse of [equation \(A10.1\)](#). Alternatively,

$$\begin{aligned} x_b &= x_w \cos\alpha_e - z_w \sin\alpha_e \\ y_b &= y_w \\ z_b &= z_w \cos\alpha_e + x_w \sin\alpha_e \end{aligned} \quad (\text{A10.4})$$

A10.3 Transformation of the Moment of Inertia in Roll from a Body Axes Reference to a Wind Axes Reference

The moment of inertia in roll is defined in Chapter 4, Table 4.1, and may be written when referenced to wind axes as

$$I_{x_w} = \sum \delta m(y_w^2 + z_w^2) \quad (\text{A10.5})$$

Substitute for y_w and z_w from [equations \(A10.2\)](#) to obtain

$$I_{x_w} = \sum \delta m(y_b^2 + z_b^2) + \sum \delta m(x_b^2 - z_b^2) \sin^2\alpha_e - 2 \sum \delta m x_b z_b \sin\alpha_e \cos\alpha_e \quad (\text{A10.6})$$

Add the following null expression to the right-hand side of [equation \(A10.6\)](#):

$$\sum \delta m(y_b^2 + z_b^2) \sin^2\alpha_e - \sum \delta m(y_b^2 + z_b^2) \sin^2\alpha_e$$

Rearrange to obtain

$$I_{x_w} = \sum \delta m(y_b^2 + z_b^2) \cos^2\alpha_e + \sum \delta m(x_b^2 + y_b^2) \sin^2\alpha_e - 2 \sum \delta m x_b z_b \sin\alpha_e \cos\alpha_e \quad (\text{A10.7})$$

Referring to the definitions of moments and products of inertia in Chapter 4, Table 4.1, [equation \(A10.7\)](#) may be rewritten as

$$I_{x_w} = I_{x_b} \cos^2\alpha_e + I_{z_b} \sin^2\alpha_e - 2 I_{xz_b} \sin\alpha_e \cos\alpha_e \quad (\text{A10.8})$$

[Equation \(A10.8\)](#) therefore describes the inertia transformation from a body axes reference to a wind axes reference.

This simple procedure may be repeated to obtain all transformations of moment and product of inertia from a body axes reference to a wind axes reference. The inverse procedure, using the coordinate transformations given by [equations \(A10.4\)](#), is equally straightforward for obtaining the corresponding transformations from a wind axes reference to a body axes reference.

A10.4 Summary

The *body axes to wind axes* moments and products of inertia transformations are summarised in [Table A10.1](#). The corresponding transformations from *wind axes to body axes* obtained by the inverse procedure are summarised in [Table A10.2](#).

Table A10.1 Moment and Product of Inertia Transformations from a Body Axes Reference to a Wind Axes Reference

Wind Axes	Body Axes
I_{x_w}	$I_{x_b} \cos^2 \alpha_e + I_{z_b} \sin^2 \alpha_e - 2I_{xz_b} \sin \alpha_e \cos \alpha_e$
I_{y_w}	I_{y_b}
I_{z_w}	$I_{z_b} \cos^2 \alpha_e + I_{x_b} \sin^2 \alpha_e + 2I_{xz_b} \sin \alpha_e \cos \alpha_e$
I_{xy_w}	$I_{xy_b} \cos \alpha_e + I_{yz_b} \sin \alpha_e$
I_{xz_w}	$I_{xz_b} (\cos^2 \alpha_e - \sin^2 \alpha_e) + (I_{x_b} - I_{z_b}) \sin \alpha_e \cos \alpha_e$
I_{yz_w}	$I_{yz_b} \cos \alpha_e - I_{xy_b} \sin \alpha_e$

Table A10.2 Moment and Product of Inertia Transformations from a Wind Axes Reference to a Body Axes Reference

Body Axes	Wind Axes
I_{x_b}	$I_{x_w} \cos^2 \alpha_e + I_{z_w} \sin^2 \alpha_e + 2I_{xz_w} \sin \alpha_e \cos \alpha_e$
I_{y_b}	I_{y_w}
I_{z_b}	$I_{z_w} \cos^2 \alpha_e + I_{x_w} \sin^2 \alpha_e - 2I_{xz_w} \sin \alpha_e \cos \alpha_e$
I_{xy_b}	$I_{xy_w} \cos \alpha_e - I_{yz_w} \sin \alpha_e$
I_{xz_b}	$I_{xz_w} (\cos^2 \alpha_e - \sin^2 \alpha_e) + (I_{z_w} - I_{x_w}) \sin \alpha_e \cos \alpha_e$
I_{yz_b}	$I_{yz_w} \cos \alpha_e + I_{xy_w} \sin \alpha_e$

Appendix 11: The Root Locus Plot

A11.1 Mathematical Background

Given the general closed-loop system transfer function

$$\frac{r(s)}{c(s)} = \frac{G(s)}{1 + G(s)H(s)} \quad (\text{A11.1})$$

where r is the response to a command input c , $G(s)$ is the transfer function of the open-loop system, and $H(s)$ is the transfer function of the feedback controller located in the feedback path. The closed-loop characteristic equation is given by the denominator of [equation \(A11.1\)](#):

$$1 + G(s)H(s) = 0 \quad (\text{A11.2})$$

In general, the transfer function product $G(s)H(s)$ will be a transfer function and may be expressed as the ratio of two polynomials:

$$G(s)H(s) = \frac{K_1(1 + sT_1)(1 + sT_3)\dots}{s^n(1 + sT_2)(1 + sT_4)\dots} \quad (\text{A11.3})$$

or, alternatively,

$$G(s)H(s) = \frac{K(s + 1/T_1)(s + 1/T_3)\dots}{s^n(s + 1/T_2)(s + 1/T_4)\dots} \quad (\text{A11.4})$$

where the gain constant is given by

$$K = \frac{K_1 T_1 T_3 \dots}{T_2 T_4 \dots} \quad (\text{A11.5})$$

Each factor in [equation \(A11.4\)](#) may be expressed alternatively in terms of magnitude and phase, assuming sinusoidal command and response such that $s = j\omega$, for example,

$$(s + 1/T_1) = A_1 e^{j\phi_1} \quad (\text{A11.6})$$

whence [equation \(A11.4\)](#) may be written as

$$G(s)H(s) = \frac{KA_1A_3\dots e^{j((\phi_1+\phi_3+\dots)-(n\phi_0+\phi_2+\phi_4+\dots))}}{A_0^n A_2 A_4 \dots} \equiv Ae^{j\phi} \quad (\text{A11.7})$$

where the total magnitude A is given by

$$A = \frac{KA_1A_3\dots}{A_0^n A_2 A_4 \dots} \quad (\text{A11.8})$$

and the total phase is given by

$$\phi = (\phi_1 + \phi_3 + \dots) - (n\phi_0 + \phi_2 + \phi_4 + \dots) \quad (\text{A11.9})$$

Thus the characteristic equation (A11.2) may be written as

$$1 + G(s)H(s) \equiv 1 + Ae^{j\phi} = 0 \quad (\text{A11.10})$$

which has the solution

$$Ae^{j\phi} = -1 \quad (\text{A11.11})$$

For the solution of equation (A11.11) to exist, two conditions must be satisfied:

The *angle condition*:

$$\phi = (\phi_1 + \phi_3 + \dots) - (n\phi_0 + \phi_2 + \phi_4 + \dots) = (2k + 1)180 \text{ deg} \quad (\text{A11.12})$$

where $k = 0, \pm 1, \pm 2, \pm 3, \dots$

The *magnitude condition*:

$$|G(s)H(s)| = A = \frac{KA_1A_3\dots}{A_0^nA_2A_4\dots} = 1 \quad (\text{A11.13})$$

Thus any point in the s -plane where the conditions defined by both equations (A11.12) and (A11.13) are satisfied defines a root of the characteristic equation. By finding all such points in the s -plane, a locus of the roots of the characteristic equation may be constructed. In fact, the root loci may be identified merely by satisfying the angle condition only; the loci may then be *calibrated* by applying the magnitude condition to selected points of interest on the loci.

A11.2. Rules for Constructing a Root Locus Plot

The simple closed-loop system of interest is defined by the structure shown in Fig. A11.1. The object is to establish how the roots of the closed-loop transfer function are governed by the choice of feedback gain K_r . The *open-loop* system transfer function is known at the outset and comprises the product of the transfer functions of all system components in the loop:

$$K_rG(s)H(s) \quad (\text{A11.14})$$

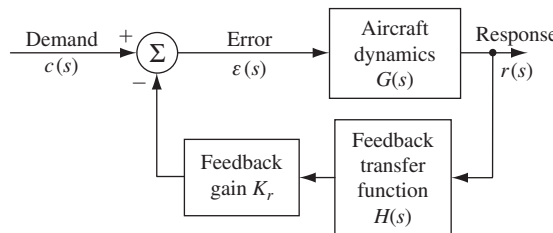


FIGURE A11.1 Simple closed-loop system.

The corresponding *closed-loop* transfer function is

$$\frac{r(s)}{c(s)} = \frac{G(s)}{1 + K_r G(s)H(s)} \quad (\text{A11.15})$$

The root locus plot is constructed from the open-loop transfer function (A11.14) which, for convenience, should be in factorised form. The *zeros* are the numerator roots of (A11.14), and the *poles* are its denominator roots. When plotting the root loci on the s -plane, it is often convenient to choose the same numerical scales for both the real and imaginary axes.

Rule 1

Continuous curves which comprise the branches of the locus start at the poles of $G(s)H(s)$, where the gain $K_r = 0$. The branches of the locus terminate at the zeros of $G(s)H(s)$ or at infinity, where the gain $K_r = \infty$.

Rule 2

The locus includes all points on the real axis to the left of an odd number of poles plus zeros.

Rule 3

As $K_r \rightarrow \infty$, the branches of the locus become asymptotic to straight lines with angles

$$\frac{(2k+1)180}{n_p - n_z} \deg \quad k = 0, \pm 1, \pm 2, \pm 3, \dots$$

where

n_p = number of poles

n_z = number of zeros

Rule 4

The asymptotes radiate from a point on the real axis called the *centre of gravity* (cg) of the plot and are determined by

$$cg = \frac{\sum \text{poles} - \sum \text{zeros}}{n_p - n_z}$$

Rule 5

The loci *break in* to or *break away* from points on the real axis located between pairs of zeros or pairs of poles, respectively. Two methods may be used to estimate the locations of the break-in or break-away points on the real axis. The first is approximate and gives results of acceptable accuracy for the majority of cases. The second is exact and may be used when the first method gives unsatisfactory results.

Method 1

- Select a test point on the real axis in the vicinity of a known break-in or break-away point.
- Measure the distances from the test point to each real axis pole and zero. Assign a negative sign to the pole distances and a positive sign to the zero distances, and calculate the reciprocals of the distances.
- Calculate the sum of the reciprocals for all poles and zeros to the left of the test point and calculate the sum of the reciprocals for all poles and zeros to the right of the test point. The test point is a break-in or brake-away point when the left and right reciprocal sums are equal.
- Choose a new test point and iterate until the break-in or break-away point is obtained with acceptable accuracy.

Note that this method may give inaccurate results when complex poles and zeros lie close to the real axis.

Method 2

- Denote the open-loop transfer function:

$$G(s)H(s) = \frac{A(s)}{B(s)} \quad (\text{A11.16})$$

- Define a function $F(s)$:

$$F(s) = B(s) \frac{dA(s)}{ds} - A(s) \frac{dB(s)}{ds} \quad (\text{A11.17})$$

The roots of $F(s)$ include all the break-in or break-away points.

Rule 6

Loci branching into, or away from, the real axis do so at 90 degrees to the real axis.

Rule 7

The angle of departure of a locus from a complex pole, or the angle of arrival at a complex zero, is given by

$$\phi = \sum(\text{angles to all other zeros}) - \sum(\text{angles to all other poles}) - 180 \text{ deg} \quad (\text{A11.18})$$

An example is illustrated in Fig. A11.2. With reference to that figure, the angle of departure of the locus from complex pole p_1 is given by

$$\phi = (\theta_1 + \theta_3 + \theta_4) - (\theta_2 + \theta_4) - 180 \text{ deg} \quad (\text{A11.19})$$

Rule 8

The total loop gain at any point on a locus is given by

$$\text{Gain} = \frac{\prod(\text{distances from test point to poles})}{\prod(\text{distances from test point to zeros})} \quad (\text{A11.20})$$

Note that, if the system under investigation has no zeros, the denominator of expression (A11.20) is taken to be unity.

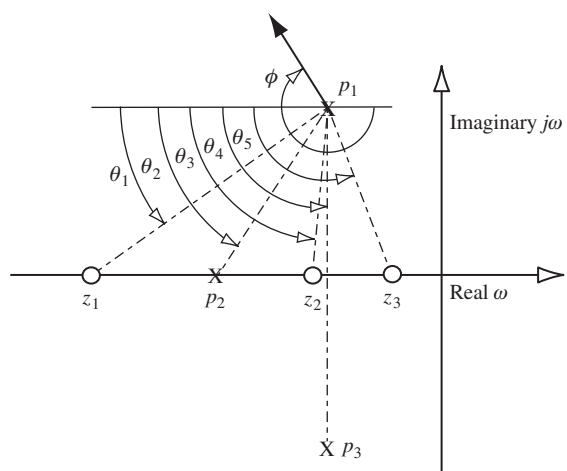


FIGURE A11.2 Example of the locus departure angle from a complex pole.

Index

Note: Page number followed by “*b*”, “*f*” and “*t*” refer to boxes, figures and tables, respectively.

A

- A-7A Corsair II, 150, 165–166, 173, 501*t*, 502*t*
 - velocity frequency response, 173
- Accelerated flight, 221
- Acceleration
 - inertial, 73
 - initial pitch, 281–283
 - normal, 281–283
 - perturbations, derivatives, 382–386
 - response to elevator, 229–230
 - and rotary motion, 75*f*
 - tangential, 75
- Ackeret theory, 365
- Adjustment
 - elevator tab, 52
 - trim tab, 52
- Adverse roll, 189
- Adverse yaw, 192
- Aerobatic aircraft, 76*b*
- Aerodynamic
 - centre, aerofoil, 31
 - coefficients, dimensionless, 90
 - control derivatives, 406–412
 - control terms, 84
 - data, 423*t*
 - drag, 357
 - force, and moment components, 375
 - modelling, 353
 - limitations of, 370
 - operating conditions, 65
 - spring, 197–199
 - stability derivatives, 84
 - longitudinal, 373–386
 - terms, 82–84
- Aerofoil
 - aerodynamic centre, 31–32
 - cambered, 31
 - centre of pressure, 31
- Aerotrim, 69–72
- Agility, 223
- Aileron
 - control geometry, 409*f*
 - derivatives and, 408–411
 - displacements, 30
 - rolling moment due to, 410
 - sideforce due to, 409
 - and yawing moment, 410–411

Aircraft

- classification, 272
- dynamics, and manoeuvring, 235–236
- handling, 222–223
- role, 272–276
- with stability augmentation, 236–243
- Aircraft behaviour
 - like amplifier, 172
 - like attenuator, 172
- Aircraft body fixed axes, 16–20
- Aircraft geometry, 5
- Aircraft gust and turbulence response, 467–486
 - spatial and temporal equivalence, 469–470
 - synthetic turbulence, 470–472
 - variance, power spectral density, and white noise, 467–469
- Aircraft trim condition, 65–72
 - calculation
 - Aerotrim, 69–72
 - controls fixed static stability, 68–69
 - elevator to trim, 67–68
- Airframes
 - configuration, trimmed equilibrium, 36
 - flexibility, 42
- Algorithms
 - Faddeeva, 129–130
 - Generalised Eigenvalue Problem, 129–130
- American Military Specification MIL-F-8785C, 271
- American Military Standard MIL-STD-1797A, 271–272
- Amplifier
 - in aircraft behaviour, 172
- Angle of attack, 31–32
- Angular
 - perturbation, 81–82
 - relationships, symmetric flight, 18–20, 19*f*
 - velocities, 24–27
- Apparent inertia, 382–383
- Apparent mass, 382–383
- Approximations
 - dutch roll mode, 202–206
 - roll mode, 200–201
 - short period mode, 158–161
 - spiral mode, 201–202
- Aspect ratio, 28
- Atmospheric disturbances, 4–5
 - on aircraft flying qualities, 443–444
 - continuous turbulence, 446–447, 448*f*
 - discrete gusts, 446

Atmospheric disturbances (*Continued*)

- evaluation methods, 444–445
- linear aircraft equations of motion, 447–458
- steady wind, 445
- turbulence modelling, 458–464
- wind shear, 446

Atmospheric disturbances on flying qualities, 443–444

Attenuator

- in aircraft behaviour, 172

Attitude, 16, 21

- angles, 21
- constant steady state pitch, 122
- perturbation, 81
- rate, 24

Augmentation, stability, 453–458

- aircraft with, 236–243

Augmentation system, design, 301–304

Augmented state equation, 143

Automatic flight control system (AFCS), 2

Autopilot, stability augmentation system, 296

Axes

- aerodynamic, 17
- body, 16
- choice of, 20
- generalised body, 16–17
- moving, 16–17, 17f
- principal inertia, 79
- stability, 17
- transformations, 21–27
- wind, 17–20

Axial force

- due to axial velocity, 375–376
- due to elevator, 407
- due to normal velocity, 377
- due to pitch rate, 380–381
- due to rate of change of normal velocity, 384–385
- due to velocity, 357–358

Axial velocity

- axial force due to, 375–376
- normal force due to, 376–377
- and pitching moment, 378

B

Balance, 82, 222

Bandwidth, 169

- frequency, 172
- speed of response, 173

Banked turn, 26f

Bode diagram, 170–176, 206–212

- break frequency, 171–172
- gain plot, 170
- interpretation, 172–176

Body axis system, 16–17

- Body rates, angular, 25
- Boeing B-747, 257–258, 258f
- British Civil Airworthiness Requirements (BCARs), 269–270
- British Defence Standard DEF-STAN 00-970, 271–272
- Busemann theory, 365

C

Centre of gravity

- location, 29
- trimmed equilibrium, 36

Centre of pressure, 31

- wings, 31

Chaotic system theory, 246

Characteristic equation, 115, 154–155, 188, 247–248

- augmented, 303, 305
- Douglas DC-8, 204
- lateral-directional, 201, 249–250
- order of, 199–200
- reduced order, 157–168, 199–200
- solution of, 188, 247–248

Characteristic polynomial, 115

Chord

- geometric, 28
- mean aerodynamic, 28
- standard mean, 28

Chordwise strip element on right wing panel, 389f

Civil Aviation Authority (CAA), 269–270

Civil transport aeroplane

- stability and control characteristics, 491–494

Closed loop, 177

- control law, 304–305
- equations of motion, 305
- system analysis, 304–308

Closed-loop system, 177

Cockpit design, 4

Coefficient E, 254–255

Command and stability augmentation system (CSAS), 299–300

Command augmentation, 337–349

- command path filter
- design, 338–340
- to system state model, 341–349

frequency response, of phase compensation filter, 340–341

Command path control, 302

Compressibility, 362–369

Computers, 8–10

- analytical, 8

- flight control, 8–9

- software, 9–10

Concise lateral state equation, 97b

Continuous turbulence, 446–447, 448f

- Control
 augmentation, 6
 derivatives, 7
 Lockheed F-104 Starfighter, 118
 error signal, 302–303
 force, to trim, 35, 53
 gains, 296
 law, 296
 closed loop, 295
 stability augmentation system (SAS), 296, 298–299, 335
 and response, 5
 and stability, 6
 system, closed loop, 295
 terms, aerodynamic, 84
- Control and stability augmentation system (CSAS), 261
- Control anticipation parameter (CAP), 280–283
 definition, 281
- Controllability, 246–247, 261
- Controlled motion, 262
- Controlled system
 multi-input, 333–337
 single input, 333–337
- Controls, 30–31
 aerodynamic, 30
 engine, 30–31
 fixed
 dynamic stability, 179–180
 manoeuvre margin, 160–161, 227–228
 manoeuvre point, 160–161, 227–228
 neutral point, 31–32, 47–48, 50f, 160–161
 stability, 47–50, 227–229
 stability margin, 56, 160–161
 free
 dynamic stability, 179–180
 neutral point, 51–52, 54b, 55f
 stability, 51–56, 230–233
 notation, 30–31
 in pitch, 30
 in roll, 30
 in yaw, 30
- Controls-fixed dynamic stability, 179–180
- Controls-fixed manoeuvre margin, 160–161
- Controls-fixed manoeuvre point, 160–161
- Controls-fixed neutral point, 160–161
- Controls-fixed stability margin, 160–161
- Controls-free dynamic stability, 179–180
- Convair CV-880, 491–492
- Convolution integral, 131
- Cooper–Harper rating scale, 276–277, 277t
- “1-Cosine” gust, 464–465
- Coupling
 aerodynamic, 89, 197–199, 202–203
 dynamic, 177, 189, 213
 mode, 177
- Coursework studies, 487
- Cramer’s rule, 112–116, 119
- Critical damping, 257–259
- Crosswind intensity, 445t
- D**
- Damping, 36–37, 150–154
 angle, 256–257
 ratio, 119, 122, 287–288
 requirements, dutch roll mode, 289–292
- Damping angle
 of *s*-plane, 256–257
- Damping in roll, 195
- Datum-path, earth axes, 16
- Decibels, 170
- Decoupled equations of motion, 87–90
- Definitions
 control anticipation parameter (CAP), 281
 Mach cone, 363
 Mach number, 362
 pitch, 18
 roll, 18
 shock stall, 363
 shock wave, 363
 stability, 245
 subsonic flight, 363
 supersonic flight, 363
 transonic flight, 363
 yaw, 18
- Degrees of freedom, 80, 93, 197
- Demonstration of compliance, 270
 test flights, 271
- Department of Defense (DoD), 269–270
- Derivatives
 acceleration perturbations, 382–386
 aerodynamic, 7, 84, 355
 control, 406–412
 lateral-directional stability, 386–406
 longitudinal stability, 373–386
 aero-normalised, 90–91
 axial force due to velocity, 357–358
 calculation, 359
 concise, 200–201, 496
 dimensionless, 90, 92, 95b, 97b, 254
 due to aileron, 408–411
 due to elevator, 407–408
 due to sideslip, 386–396
 estimation, 358–362

- Derivatives (*Continued*)
 force, 375–378
 high performance aeroplanes, 383
 lateral, McDonnell F-4C Phantom, 97*b*
 magnitudes, 137
 measurement
 flight test, 360–362
 wind tunnel, 359–360
 pitch velocity perturbation, 379–382
 quasi-static, 356–358
 rate of roll, 396–400, 397*f*
 rudder, 411–412
 semi-empirical, 359
 yaw rate, 400–406
 Design modification, 6
 Dihedral effect, 58, 59*f*, 196, 284–285, 388
 Dimensionless
 equations of motion, 90–92
 inertias, 92
 Dimensionless normal acceleration, 281–283
 Dirac delta function, 134
 Direct lift control (DLC), 223
 Direction cosine matrix, 22–23
 Directional
 static stability, 63–65
 weathercock effect, 254–255
 Directional weathercock effect, 254–255
 Discrete gusts, 446, 464–467
 “1-Cosine” gust, 464–465
 maximum gust velocity and horizontal length,
 determination of, 466–467
 Displacement per g, 229–230
 Disturbed body incidence and sideslip, 449–450
 Douglas DC-8, 187, 206
 characteristic equation, 249–250
 frequency response, 206–211
 sideslip angle frequency, 209*f*
 Downwash, 383–384, 383*f*
 field, 45–46, 383*f*
 Downwash angle at tail plane at time, 384
 Downwashlag effect, 383
 Drag
 coefficient, 365–366
 due to lift, 365–366
 lateral, 387–388
 and pitching moment
 subsonic lift, 364–365
 supersonic lift, 365–366
 variation with Mach number, 368*f*
 properties, and Mach number, 367*b*
 skin friction, 365–366
 wave, 365–366
 Drag-velocity plot, 357–358
 Dryden turbulence model, 459–461
 and von Kármán, comparison of, 461
 Dutch roll mode, 197–199, 208, 213, 215–216, 253,
 285, 331
 approximations, 202–206
 damping ratio, 208
 damping requirements, 289–292
 flight recording, 215–216
 frequency, 205
 limiting frequency, 289–292
 McDonnell F-4 Phantom, 289*b*
 oscillatory, 189, 197–199
 Dynamic coupling, 177
 Dynamic models, short term, 262–269
 Dynamics
 lateral-directional, 183
 longitudinal, 147
 short term, 212, 261–262
- E**
- Early aviation, 1
 Earth axes, 15–16, 16*f*
 datum-path, 16
 Effective aspect ratio, 365
 Eigenvalues
 and eigenvectors, 131–132
 matrix, 131
 Eigenvectors
 and eigenvalues, 131–132
 magnitude, 137
 matrix, 192
 Elevator
 angle
 to trim, 46–47
 trimmed equilibrium, 35
 and axial force, 407
 deflection, 89
 and stick force, 234–235
 derivatives and, 407–408
 displacements, 30, 229
 hinge moment, 51, 230–231
 longitudinal response to, 149
 normal acceleration response to, 229–230
 and normal force, 408
 and pitching moment, 408
 pulse duration, 178
 tab
 adjustment, 52
 angle to trim, 47, 53
 transfer function, Lockheed F-104
 Starfighter, 306*b*

- Engine
 control, 30–31
 dynamics, 141–144
- Equations
 aero-normalised, 90–91
 characteristic, 115, 154–155, 188, 249–250
 error method, 361
 generalised force, 77–78
 generalised moment, 78–79
 height, 139
 lateral-directional state, 200
 longitudinal characteristic, 154
 longitudinal state, 140
 modal, 132–133
 of motion, 5–7
 in American normalised form, 99–106
 closed loop, 305
 decoupled, 87–90
 dimensional decoupled, 90
 dimensionless, 90–92
 lateral asymmetric, 89–90
 lateral-directional, 89–90, 105b, 185–186, 452–453
 linear aircraft, 447–458
 disturbed body incidence and sideslip, 449–450
 lateral-directional equations of motion, 452–453
 longitudinal equations of motion, 450–452
 stability augmentation, 453–458
 linearised, 80–87
 longitudinal, 87–91, 103b, 450–452
 McDonnell Douglas DC-8, *see* Douglas DC-8
 McDonnell Douglas F-4C Phantom, 95b, 97b,
 333–334
 open loop, 305
 small perturbations, 85–87
 solving, 111–112
 Laplace transform, 111
 pitching moment, 44–47, 225–227
 reduced order, 157–158
 state space form, 93–99
 steady state, 86
 Equilibrium, trimmed, 17, 35–43
 Euler angles, 21
 Experiments, dynamic, 360
- F**
- Failure transient, 297
 Federal Aviation Administration (FAA), 269–270
 Feed forward path, 302
 Feedback path, 301–302
 Fin
 disturbance, 63–64
 effect, 196–197
- effectiveness, 64
 moment arm, 29–30
 volume ratio, 29–30, 62, 394–395
- Final value theorem, 122, 192–193, 264, 281–283
- Fixed axes, aircraft body, 16–20
- Fixed neutral point
 locating, 367b
 and Mach number, 367b
- Flat earth, 15–16
- Flexibility, airframes, 42
- Flight control system (FCS), 295, 296f
 design, 299–300
 electronic (EFCS), 295
 mechanical elements, 299
- Flight critical stability augmentation, *see* Flight control system (FCS)
- Flight envelopes, 6–7, 273–274, 275b, 276f
 extended, 261
 large, 40
 McDonnell-Douglas A-4D Skyhawk,
 274b, 275f, 276f
 normal load factor, 275b
 operational, 274–276, 274t
 permissible, 273
 service, 274
- Flight in nonsteady atmosphere, 441
- Flight path angle, 18–20
- Flight phase, 272–273
 categories, 273
- Flight test measurement, 360–362
- Flow effects, 42f
- Fly-by-wire (FBW)
 aeroplane, 271
 civil transport aeroplanes, 8–9
 controls, 4
 system, 299–300
 reliability, 300
 unstable airframes, 316
- Flying, and handling, 3–4, 177, 212–213, 261
- Flying qualities
 atmospheric disturbances on, 443–444
 lateral-directional, 283–286
 level of, 273
 longitudinal, 278–281
 McDonnell F-4C Phantom, 289b
 requirements, 269–272
 specification, 268
 on *s*-plane, 286–291, 287f
- Force balance, 35, 37
- Frequency
 phugoid, 119, 154–155, 172, 280, 280t, 288
 response, 168–176, 206–211

Frequency response, of phase compensation filter, 340–341
 Frozen field turbulence, *see* Turbulence: modelling
 Full state feedback, 333, 335*f*
 Functional visibility, 5–6, 262, 301
 Functions
 Dirac delta, 134
 unit impulse, 134

G

Gain
 logarithmic, 170
 margin, 173
 and phase, calculation, 170
 plot, Bode diagram, 170
 Gain plot, 170
 break frequencies, 171–172
 Generalised
 force equations, 77–78
 moment equations, 78–79
 Geometric data, 423*r*
 Gradients, stable, 278, 278*f*
 Gravitational
 force components, 82
 terms, 81–82
 Gust
 “1-cosine,” 464–465
 discrete, 464–467
 Gyration, longitudinal radius of, 283

H

Handley Page Jetstream, 178–179, 213
 elevator angle to trim, 49*f*
 flight test, 49*b*, 54*b*, 178–179
 phugoid response, 179
 roll subsidence mode, 213
 with tailplane, 43*b*
 wind tunnel experiments, 43*b*, 44*f*
 without tailplane, 43*b*
 Handling, 212–213
 and flying, 177, 261
 long term, 262
 pilot's perception, 262
 qualities, 3–4, 4*f*
 criteria, 268
 short term, 261–262
 Harmonisation, of control power, 261
 Height integration, 144
 Height response, 139
 High pass filter, 297
 Hinge moment to trim, 53–56, 54*f*
 Homogeneous response, 131
 Horizontal fuselage datum, 16–17, 67

I

Incidence angle feedback to elevator, 319–320, 319*f*
 Incidence lag, 263, 269
 on pitch response, 269, 270*f*
 Incremental stick force per g, 234
 Inertia
 dimensionless, 92
 moments and products, 79*t*
 Inertial acceleration, 76
 components, 73–77
 Initial value theorem, 122–123
 Inner control loop, 299
 Instability, conditional, 253–254
 Integrated actuation, 299
 Intensity
 crosswind, 445*t*
 turbulence, 463–464

J

Jet engine, exhaust, 41–42
 Joint Aviation Authority, 269–270
 Joint Aviation Requirements (JARs), 269–270

K

Kalman filtering, 361

L

Lag, 172
 Lanchester phugoid model, 161–162
 Laplace transform, 495
 Lateral
 dihedral effect, 254–255
 -directional equations of motion, 89–90, 105*b*
 drag, 387–388, 395–396
 perturbation, sideslip angle, 140–141
 relative density, 92
 response transfer functions, 117–119
 Lateral-directional
 augmentation, 321–331
 control, steady, 283–284
 derivative coefficients, 418–420
 equations of motion, 89–90, 452–453
 modes, 288–291, 288*f*
 stability, 36, 284–285, 386–406
 static stability, 57–65

Lead, 172

Level

 of flying qualities, 273
 Lift coefficient, 43–44, 54*b*, 90
 Lift to drag ratio, 165–168
 Lifting properties, and Mach number, 367*b*
 Lift-to-drag ratio, 165–168

- Limiting frequency, dutch roll mode, 286*t*, 289–292
- Linear aircraft equations of motion, 447–458
- disturbed body incidence and sideslip, 449–450
 - lateral-directional equations of motion, 452–453
 - longitudinal equations of motion, 450–452
 - stability augmentation, 453–458
- Linear system modelling, 206–207
- Linear time invariant (LTI) system, 93
- Ling-Temco-Vought A-7A Corsair II, 150
- Load factor, 281–283
- Lockheed F-104 Starfighter, 118*b*, 143, 312*b*
- control derivatives, 118
 - elevator transfer function, 306*b*
 - lateral-directional handling qualities, 494–499
 - longitudinal equations of motion, 143
 - phugoid stability, 307–308
 - pitch attitude response, 118
 - pitch response, 118
 - root locus plot, 308–314
 - stability, dimensional, 118
- Logarithmic gain, 170
- Longitudinal
- characteristic equation, 154–155
 - derivative coefficients, 414–418
 - equations of motion, 87–89, 103*b*, 450–452
 - manoeuvrability, 227–236, 281, 282*f*
 - modes, 287–288
 - damping ratios, 287–288
 - motion, 253
 - reduced order, 263–267
 - reference geometry, 27*f*
 - relative density, 91, 225
 - response to elevator, 149
 - short period, thumb print criterion, 268, 268*f*
 - stability, 177
 - state equation, 93, 140, 142–144, 165–166
 - decoupled, 140
 - static stability
 - condition for, 47
 - degree of, 39–40, 40*f*
- Low-pass system, 169
- LTV A7-A Corsair aircraft, 500–503
- M**
- Mach cone, definition, 363
- Mach number, 90
- critical, definition, 362
 - definition, 362
 - and drag properties, 367*b*, 368*f*
 - flow, 363–364
 - and lifting properties, 367*b*, 368*f*
 - and pitching moment, 368*f*
- Manoeuvrability
- controls free, 281
 - lateral-directional, 286
 - sideslip excursions, 246
 - longitudinal, 281, 282*f*
- Manoeuvre stability, 222–223
- analysis, 223
 - longitudinal
 - controls fixed, 227–229
 - controls free, 230–233
 - elevator deflection and stick force, 234–235
 - normal acceleration response to elevator, 229–230
 - traditional analysis, 222
- Manoeuvring
- and aircraft dynamics, 235–236
 - aircraft with stability augmentation, 236–243
 - classical theory, 222
 - controls fixed, 227–229
 - controls free, 230–233
 - longitudinal stability, 227–235
 - normal, 221–222
 - steady pull-up, 223–225
 - steady symmetric, 223
 - symmetric pull-up, 224*f*
 - tailplane incidence, 226
 - transient upset, 222
- Mathcad, software, 10, 70–72
- Mathematical models, 5–6
- approximate, 5–6
 - high fidelity, 5–6
- MATLAB, 120–122
- software, 9
- Matrix, 93
- direct, 93
 - eigenvalue, 131–132
 - eigenvector, 131
 - exponential, 130–131, 133
 - identity, 94
 - input, 93
 - mass, 95
 - modal, 131
 - output, 93
 - polynomial, 126
 - state, 93
 - state transition, 130–131
 - transfer function, 125–126
 - lateral, 127–138
 - longitudinal, 127
 - zero, 94
- Maximum likelihood method, 361

- McDonnell F-4C Phantom, 88*b*, 95*b*, 333*b*
 aerodynamic variables, 97*b*
 control characteristics, 289*b*
 dutch roll mode characteristics, 291
 equations of motion, 333–334
 flying qualities, 289*b*
 lateral derivatives, 97*b*
 longitudinal equations of motion, 97*b*
 longitudinal stability modes, 334, 336–337
 stability, 289*b*
- McDonnell-Douglas A-4D Skyhawk, 315*b*
 flight envelopes, 274*b*, 275*f*, 276*f*
 stability mode characteristics, 316
- Measurement
 flight test, 360–362
 wind tunnel, 359–360
- Minimum drag speed, 37, 154
- Minimum phase, 173
- Ministry of Defence (MoD), 269–270
- Modal
 equations, 134
 form, 132
 matrix, 132
- Modelling, pitching behaviour, 44–45
- Modes
 coupling, 177, 192
 dynamic stability, 155–157
 excitation, 177–181, 213–217
 faster, 258
 slow, 258
- Moment components, and aerodynamic force, 375
- Moments, and perturbation forces, 80
- Morane Saulnier MS-760 Paris, 275*b*, 276*f*
- Motion
 cues, 262
 variables, 18*f*
- Multi-input, controlled system, 333–337
- N**
- Natural frequency, 122, 156–157, 165–168, 235
- Navigation, trans-globe, 15
- Navion Aircraft Corporation, Navion/H, 265*b*
- Negative feedback, 295, 323
- Neutral stability, 128–129
- Newton's second law, 73
- Nichols chart, 169
- Non-linear system, 245–246
- Non-minimum phase, 173, 175, 189
- Non-minimum phase effect, 125
- Non-steady atmosphere, flight in, 441
- Normal
 acceleration
- equations, 123
 feedback to elevator, 320–321, 320*f*
 response at cg, 125*f*
- force
 axial velocity, 376–377
 due to elevator, 408
 due to normal velocity, 377–378
 due to pitch rate, 381
 due to rate of change of normal velocity, 385
 load factor, 76*b*, 223–224, 264
 flight envelopes, 273–276
 velocity
 and axial force, 377, 384–385
 and normal force, 377–378, 385
 and pitching moment, 379, 385–386
- North American derivative coefficient notation, 412–436
- North American X-15 hypersonic research aeroplane
 stability augmentation, 490–491
- Northrop T-38 Talon, transfer function data, 322
- Nyquist diagram, 169
- O**
- Open loop, equations of motion, 305
- Operational flight envelopes, 274–276
- Optical signal transmission, 300–301
- Oscillations
 phugoid, 156–157, 161–168, 179
 pilot induced, 173
 in roll response to controls, 286
 short period pitching, 119, 122, 137–138, 151, 155–156,
 156*f*, 158–161, 178, 279–281
- Oscillatory dutch roll mode, 128–129
- Outer control loop, 295–296
- Output response variable, 169
- P**
- Parameter identification, 360, 361*f*
 disadvantages, 362
 equation error method, 361
 maximum likelihood method, 361
 statistical regression method, 361
- PC MATLAB, 138, 146, 153, 170, 192, 293, 489
 root locus plot, 293, 308–314
 software, 9
- Peak roll, to peak yaw ratio, 197–199
- Permissible flight envelopes, 273
- Perturbation forces, and moments, 80
- Perturbations
 about trim, 40–41, 80, 212
 angular, 81–82
 attitude, 81
 height, 24

- small, 7
- variables, 17–18, 19*t*
- velocity, 375–378
- Perturbed wind axes, 374*f*
- Phase margin, 173
- Phase plot, 170
- Phugoid, 119, 156–157
 - damping, 311, 317–318
 - frequency, 169, 280, 280*t*, 317–318
 - Lanchester model, 161–162
 - mode, 177, 179
 - oscillation, 138, 161–168
 - reduced order model, 157–168
 - stability, 151
 - Lockheed F-104 Starfighter, 306
- Pilot opinion, 261
 - rating, 276–277
- Pilot workload, 246–247, 273
- Pilot induced oscillations, 173
- Pitch, 22–23
 - altitude, and elevator, 118, 122, 170, 316–317
 - damper, 313
 - definition, 18
 - motion cue, 269
 - rate, 25
 - and axial force, 380–381
 - feedback, 312*f*
 - to elevator, 317–318, 317*f*
 - and normal force, 381
 - and pitching moment, 381–382
 - and tailplane incidence, 380*f*
 - response, Lockheed F-104 Starfighter, 118*b*
 - stiffness, 321, 379
 - velocity perturbation, 379–382
- Pitching
 - Behaviour, modelling, 44–45
 - due to axial velocity, 378
 - due to elevator, 408
 - due to normal velocity, 379
 - due to pitch rate, 381–382
 - equation, 44–47, 225–227
 - simple development, 44–46
 - moment, 32, 37–38, 38*f*, 40–41, 42*f*
 - due to rate of change of normal velocity, 385–386
 - velocity, 385
- Pole placement method, 332–337
 - application, 332
- Poles, 115
- Power effects
 - indirect, 41
 - stability, 40–42
- Power terms, 84–85
- Prandtl–Glauert rule, 364, 367*b*
- Pressure drag, 365–366
- Primary flight control system (PFCS), for
 - advanced-technology UAV, 503–507
- Program CC, 95*b*, 120–122, 173–174
 - root locus plot, 293
 - software, 9–10
- Q**
 - Q-feel system, 299
- R**
 - Rapid incidence adjustment, 158
 - Rate command, 265*b*
 - Rate of roll, derivatives, 396–400, 397*f*
 - Reduced order
 - models, 157–168, 199–206
 - lateral-directional, 200
 - longitudinal, 263–267, 265*b*
 - longitudinal response, 167*f*
 - phugoid dynamics, 161–168
 - Redundancy, 297–298, 300
 - Reference centres, 31–32, 32*f*
 - Reference geometry, 27–30, 27*f*
 - Resolvent, 130
 - Resonant frequencies, 169
 - Response, 111–112, 114–119
 - to aileron, 186, 189
 - and control, 5
 - to controls, 119–123, 149–155, 185–194
 - to elevator, 149–154, 152*f*
 - homogeneous, 131
 - impulse, 131, 134
 - pitch rate, 166, 265*b*, 314*f*
 - to rudder, 189, 192–193
 - second-order-like, 265*b*
 - shapes, 135–138, 150–154
 - shaping, 301–302
 - steady state, 154
 - step, 114–115, 134–135
 - transfer functions, 111–112, 114–119, 149–150, 170, 199
 - acceleration, 123–125
 - elevator, 114–115, 170, 289*b*
 - flight path angle, 141
 - height, 139
 - improper, 114–115, 125
 - incidence, 140–141
 - lateral, 117–119
 - Ling-Temco-Vought A-7A Corsair II, 150
 - longitudinal, 115–117, 186
 - pitch rate, 118–119
 - proper, 114–115

- Response (*Continued*)

sideslip, 140–141

thrust, 117

unforced, 133

Restoring moment, 39–40, 155–156, 195

Retrimming, 48, 52

Reynolds number, 90

Ride quality, 177

Roll, 21–22

 attitude

 feedback to aileron, 325–326, 326*f*

 feedback to rudder, 330–331, 331*f*

 definition, 18

mode, approximation, 194–195

rate, 25

 and aileron, 114–115, 120–122

 feedback to aileron, 323–324, 324*f*

 feedback to rudder, 328–329, 329*f*

 and rolling moment, 351, 397–399

 and sideforce, 396–397

 and yawing moment, 399–400

response

 to aileron, 200, 204

subsidence mode, 128–129, 188–189, 193–195, 212, 217, 284, 284*t*

 flight recording, 214*f*, 215–216

 Handley Page Jetstream, 179, 214–216

 maximum value, 289

Rolling flight, wing incidence in, 398*f*

Rolling moment

 coefficient, 58–59

 due to aileron, 410

 due to roll rate, 397–400

 due to rudder, 412

 due to sideslip, 388–395

 due to yaw rate, 402–405, 402*f*

 equation, 200

 negative, 58–59

Root locus plot, 257–259, 308–314, 310*f*

 applications, 308–314

 incidence angle feedback to elevator, 319–320, 319*f*

 interpretation, 308–314

 normal acceleration feedback to elevator, 320–321, 320*f*

 pitch attitude feedback to elevator, 316, 316*f*

 pitch rate feedback to elevator, 317–318, 317*f*

 roll attitude feedback to aileron, 325–326, 326*f*

 roll attitude feedback to rudder, 330–331, 331*f*

 roll rate feedback to aileron, 324*f*

 roll rate feedback to rudder, 328–329, 329*f*

 sideslip angle feedback to aileron, 322–323, 323*f*

 sideslip angle feedback to rudder, 327–328, 328*f*

 single variable feedback, 314

velocity feedback to elevator, 318–319, 318*f*

yaw attitude feedback to aileron, 326–327, 327*f*

yaw attitude feedback to rudder, 331, 332*f*

yaw rate feedback to aileron, 324–325, 325*f*

yaw rate feedback to rudder, 329–330, 330*f*

Rotary motion

 and acceleration, 75*f*

 and velocity, 74–75

Routh array, 249

Routh–Hurwitz criterion

 application, 248–252

 special cases, 250–252

 stability, 248–252

Routh's discriminant, 253

Rudder

 derivatives, 411–412

 and rolling moment, 412

 and sideforce, 411

 surface, displacements, 30

 and yawing moment, 412

S

- Safety, 297–298

Scale length, turbulence, 461–463

Service flight envelopes, 274

Setting angle, tailplane, 43*b*

Shear, wind, 446

Shock expansion, 365

Shock stall, definition, 363

Shock wave, definition, 363

Short period mode approximation, 158–161

Short term, dynamic models

 controlled motion and motion cues, 262

 incidence lag, 269

 longitudinal reduced order model, 263–267, 265*b*

 thumb print criterion, 268

Short-period mode damping, 280, 280*t*

Sideforce

 due to aileron, 409

 due to roll rate, 396–397

 due to rudder, 411

 due to sideslip, 387–388, 387*f*

 due to yaw rate, 401–402

Sideslip

 angle, 23

 angle feedback to aileron, 322–323, 323*f*

 angle feedback to rudder, 327–328, 328*f*

 disturbance, 60, 63–64, 386

 disturbed body incidence and, 449–450

 fin lift, 394*f*

 lateral cross flow, 393*f*

 and rolling moment, 388–395

- and sideforce, 387–388, 387*f*
- swept wing in, 390, 391*f*
- on a wing with dihedral, 389*f*
- and yawing moment, 395–396
- Side-stick controller, 299–300
- Similarity transform, 132
- Single input, controlled system, 333–337
- Single variable feedback, root locus plot, 314
- Small perturbations, 7
 - equations of motion, 85–87
- Software
 - Mathcad, 10
 - MATLAB, 9
 - Program CC, 9–10
 - 20-Sim, 10
 - Simulink, 9
- Spatial frequency, of turbulence, 458–459
- Specification, flying qualities, 271
- Spherical coordinates, 15
- Spiral mode, 128–129, 189, 196–197, 212, 214–215, 284–286
 - approximations, 201–202
 - boundary, 288
 - stable, 199, 202
 - time constant, 201
 - unstable, 197, 214–215, 322
- s*-plane
 - complex roots on, 256*f*
 - flying qualities on, 286–291
 - lateral-directional modes on, 288–291, 288*f*
 - longitudinal modes on, 287–288, 287*f*
 - root mapping on, 255–258
- Stability, 189, 261–262
 - aerodynamic, 7
 - augmentation, 6, 236–243, 271, 311, 453–458
 - control law, 313
 - longitudinal, 314–321, 315*f*
 - system, 261, 296, 298–301
 - autopilot, 296
 - control law, 297
 - role of, 299
 - conditions for, 36–39, 37*f*
 - and control, 6
 - controls, 246–247
 - fixed, 47–50, 227–229
 - margin, 47–48
 - static, 230–233
 - fixed dynamic, 179–180, 216–217
 - free, 47, 51–56, 230–233
 - meaning, 51
 - free dynamic, 179–180, 216–217
 - free margin, 51–52
 - definition, 245
 - directional static, 63–65, 196
 - dynamic modes, 155–157, 194–199
 - estimating, 356
 - graphical interpretation, 255–258
 - lateral static, 58–63, 196, 388
 - lateral-directional, 36, 213, 386–406
 - augmentation, 321–331, 322*f*
 - dynamic, 284–285
 - short period, 212
 - longitudinal, 287–288
 - dynamic, 279–280
 - manoeuvring, 227–235
 - margins, 56*f*
 - modes, 177
 - static, 47–56, 278–279
 - manoeuvre, 222
 - margin, 39, 48
 - modes, 115, 189, 257–258
 - non-linear systems, 245–246
 - phugoid, 156–157, 280, 307–308, 317
 - power effects, 40–42, 42*f*
 - quartic, 252–255
 - definition, 252
 - relative sensitivity, 311
 - reversal, 43*f*
 - Routh–Hurwitz criterion, 248–252
 - short period mode, 280
 - static
 - and dynamic, 246
 - longitudinal, 47–56
 - margins, 278–279
 - subsonic, 40
 - supersonic, 40
 - variable, 268
 - variation in, 40–43
 - State space method, 125–138
 - Laplace transform, 130
 - State space model augmentation, 138–144
 - State transition matrix, 130–131
 - Static stability
 - lateral-directional, 57–65
 - longitudinal, 47–56
 - Statistical regression, 361
 - Steady wind, 445
 - Stick displacement, 222
 - Stick force, 234–235, 237
 - Stick force per g, 233–235, 237–243, 281
 - measuring, 235
 - Subsonic flight, definition, 363
 - Subsonic lift, drag and pitching moment, 364–365
 - Supersonic flight, definition, 363

Supersonic lift, drag and pitching moment, 365–366
 Symmetric flight, angular relationships, 18–20
 Symmetry, of airframe, 36
 Synthetic turbulence, 470–472
 System analysis, closed loop, 304–308
 System gain, 169–170
 System realisation, 142–144

T

Tailplane
 lift coefficient, 45–46, 226, 407
 moment arm, 29
 setting angle, 45–46
 volume ratio, 29, 381
 weathercock tendency, 155–156
 Tailplane incidence due to pitch rate, 380f
 Test flights
 demonstration of compliance, 271
 variable stability, 268

Throttle lever angle, 84–85, 142

Thrust, 84–85
 line, 40–41
 trimmed equilibrium, 36
 variation, 89

Thumb print criterion, 268–269
 longitudinal short period, 268, 268f

Time response, 111, 122

Transfer function, 206, 302–303
 angular pitch acceleration, 281–283
 matrix, 125–126
 lateral, 127–138
 Lockheed C-5A, 118b
 longitudinal, 127
 open loop, 317

Transformation
 angular velocities, 24–27
 linear, 22–24

Transonic flight, 278–279, 363

Trim
 change of, 278
 function, electrical, 300
 hands-off, 51–52
 state, 5, 35
 tabs, 35
 adjustment, 52
 elevator, 35

Trimability, 35

Trimmed aircraft, 41, 177, 213

Trimmed equilibrium, 17, 35–43
 airframe configuration, 36
 centre of gravity, 36
 elevator angle, 36

flight path angle, 36
 lateral-directional, 36
 longitudinal, 36
 stable, 37f
 thrust, 36
 weight, 36
 Turbulence
 continuous, 446–447, 448f
 intensity, 463–464
 modelling, 458–464
 Dryden model, 459–461
 scale length, 461–463
 turbulence intensity, 463–464
 von Kármán model, 459, 461
 spatial frequency of, 458–459
 synthetic, 470–472

U

Unforced response, *see* Homogeneous response
 Unit impulse function, 134

V

Variable stability, 40–43
 test flights, 268
 Velocity
 eigenfunctions, 137
 feedback to elevator, 312b, 318f
 linear disturbance, 80–81
 perturbations, moment derivatives, 378–379
 resolution, 23f
 and rotary motion, 75f
 tangential, 74–75
 Virtual inertia, 382–383
 Virtual mass, 382–383
 Von Kármán model, 459
 and Dryden models, comparison of, 461

W

Wake, 41
 Washout filter, 297, 499
 Weathercock, 63, 63f, 155–156, 395
 Weight, trimmed equilibrium, 36
 White noise signal, 469
 Wind, steady, 445
 Wind axes, perturbed, 373, 374f
 Wind shear, 446
 Wind tunnel
 experiments, Handley Page Jetstream, 44f
 measurement, 359–360
 accuracy, 359–360

Wing

area, 27
aspect ratio, 28–29
centre of pressure, 31
incidence, in rolling flight, 398/*f*
mean aerodynamic chord (mac), 28
standard mean chord (smc), 28
sweep back, 42

Y

Yaw, 21–22
adverse, 192
angle, 21, 25
attitude
 feedback to aileron, 326–327, 327/*f*
 feedback to rudder, 331, 332/*f*
definition, 18

rate, 25

derivatives, 400–406
feedback to aileron, 324–325, 325/*f*
feedback to rudder, 329–330, 330/*f*
fin incidence, 401/*f*
and rolling moment, 402–405, 402/*f*, 404/*f*
and sideforce, 401–402
and yawing moment, 404–406, 404/*f*

Yawing moment

about cg, 405
coefficient, 64
due to aileron, 410–411
due to roll rate, 399–400
due to rudder, 412
due to sideslip, 395–396
due to yaw rate, 404, 404, 404, 404/*f*, 405, 405–406